PRESSURE FLUCTUATIONS IN THE PLUNGE POOL OF AN IMPINGING JET SPILLWAY (VOLUME II OF II – TABLES AND FIGURES)

A THESIS ON PLUNGE POOL ENERGY DISSIPATORS FOR THE DEGREE OF DOCTOR OF PHILOSOPHY

BY: WILLIAM JAMES WITHERS
DEPARTMENT OF CIVIL ENGINEERING
UNIVERSITY OF GLASGOW
FEBRUARY 1991

PRESSURE FLUCTUATIONS IN THE PLUNGE POOL
OF AN IMPINGING JET SPILLWAY
(VOLUME II OF II – TABLES AND FIGURES)

ILLUSTRATION LIST

(TABLES AND FIGURES FOR EACH CHAPTER IN MAIN TEXT)

Page

Page

Page

CHAPTER 3:

Page

Page

CHAPTER 7

Page

FIGURES FOR CHAPTER 1

Fig.1·1 VIEW OF MORROW POINT DAM

Fig.1·2 VIEW OF CRYSTAL DAM

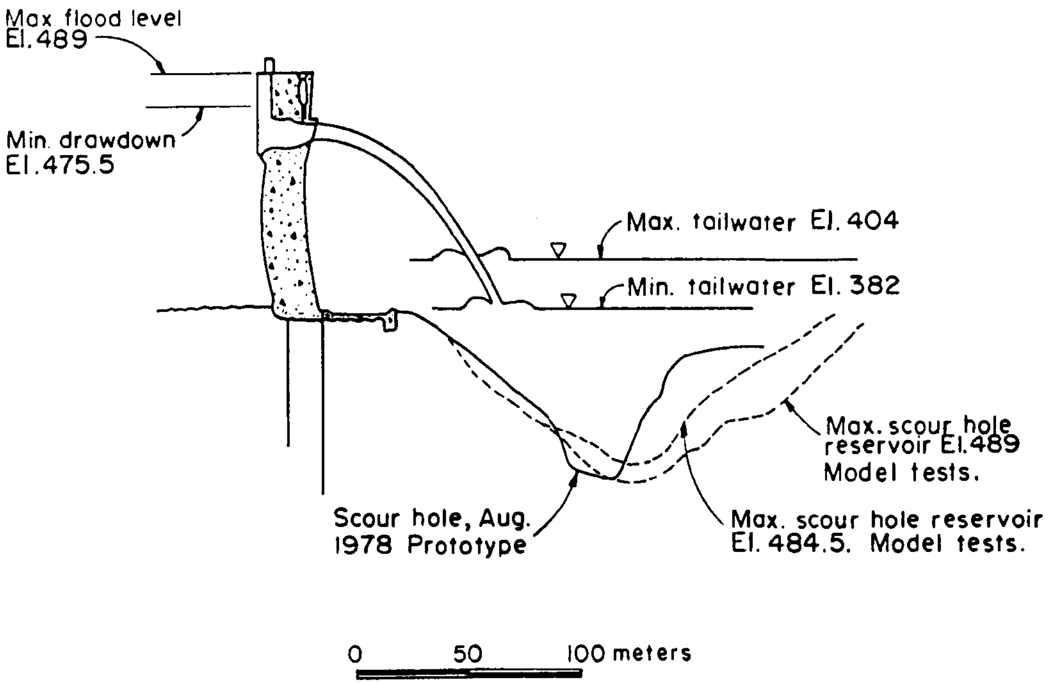

Fig.1·3 SCOUR HOLE AT KARIBA DAM

TABLES & FIGURES FOR CHAPTER 2

Jet turbulence level %	Break-up length - $f(Q_w)$
0.3	LB - 60 Q $W^{0.39}$
3.0	LB - 17.4 Q $W^{0.31}$
8.0	LB - 4.1 Q $W^{0.20}$

Table 2.1 Typical values of jet break-up length for various outlet turbulence levels. (Ervine,McKeogh and Elsway).

Author	Nozzle diameter range mm	Jet length range mm	Jet velocity range m/s	R_{e0} range x 10^4	Nozzle geometry L_0/d_0
Henderson (12)	2.54to12.7	10 - 270	10 - 30	max 20	0,1, 10
van de Sande (38)	1.95 to 10	100-400	3 - 10	max 5	50
Cumming (71)	4.5 to 9	100-800	1.3-8.7	1 to 8	0,5,10,80
van de donk (49)	10 to 100	260-1070	1.5- 11	13 - 40	2.2 - 22
Ervine (69)	6 to 25	0 - 4700	2 - 6	2 - 10	1 - 4
Kumagai (36)	2 to 8	20 - 800	1.2 - 37	0.9 -15	50

Notes: (i) All water/air systems

(ii) R_{e0} - Reynolds number at outlet

(iii) L_0 - length of the cylindrical section of a nozzle.

Table 2.2 Experimental conditions in different authors studies of air entrainment by plunging jets.

Structure	R.M.S. pressure coefficient
Hydraulic jump stilling basin	0.05
Boundary layer on spillway face	0.007
Side walls of bottom outlet	0.06
Baffle blocks in a stilling basin	0.25

Table 2.3 Typical values of Cp' for various hydraulic structures.

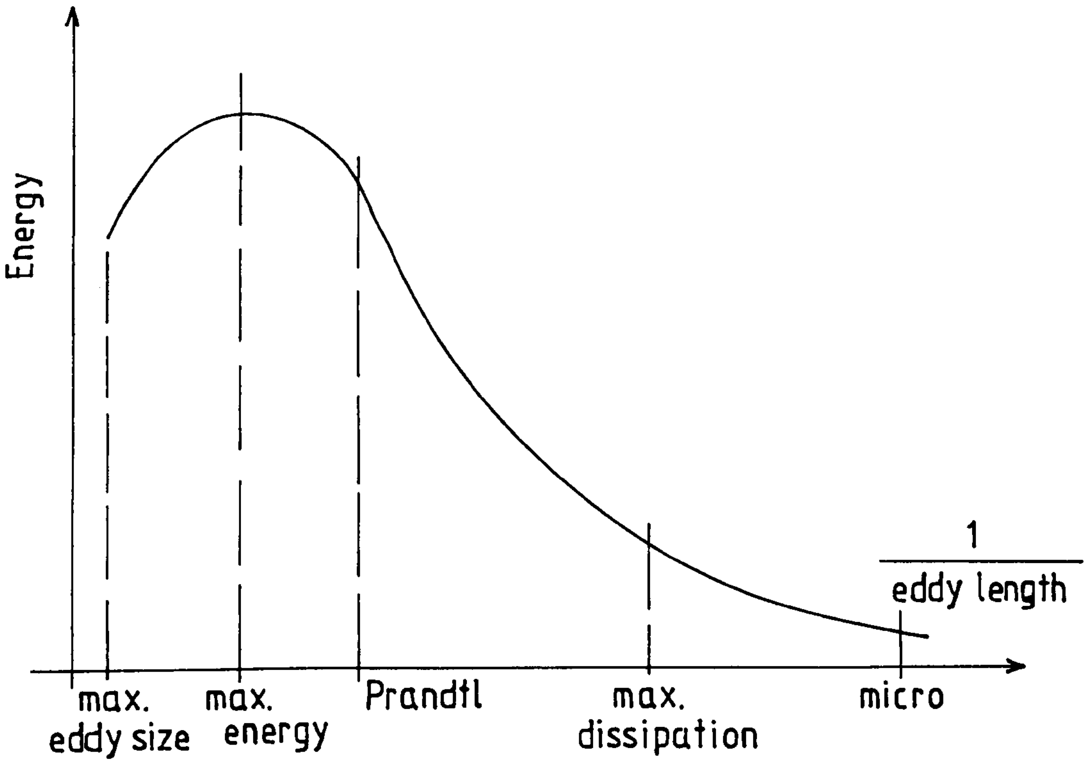

Fig. 2·1(a) TURBULENT ENERGY SPECTRUM

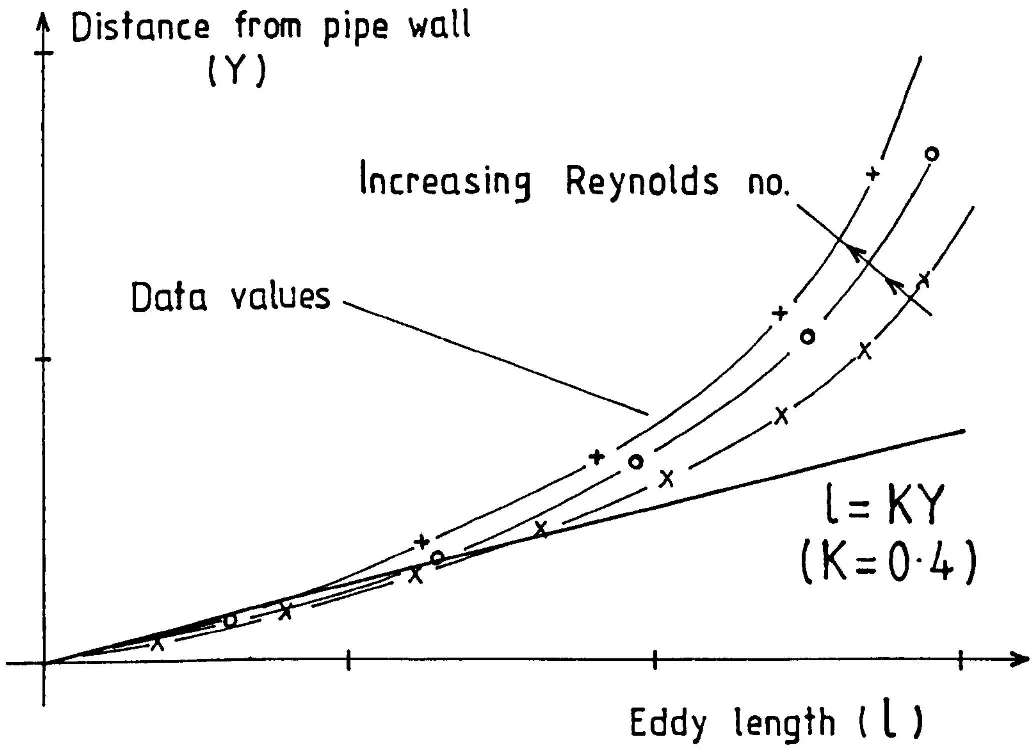

Fig. 2·1(b) COMPARISON OF EDDY LENGTH IN PIPE

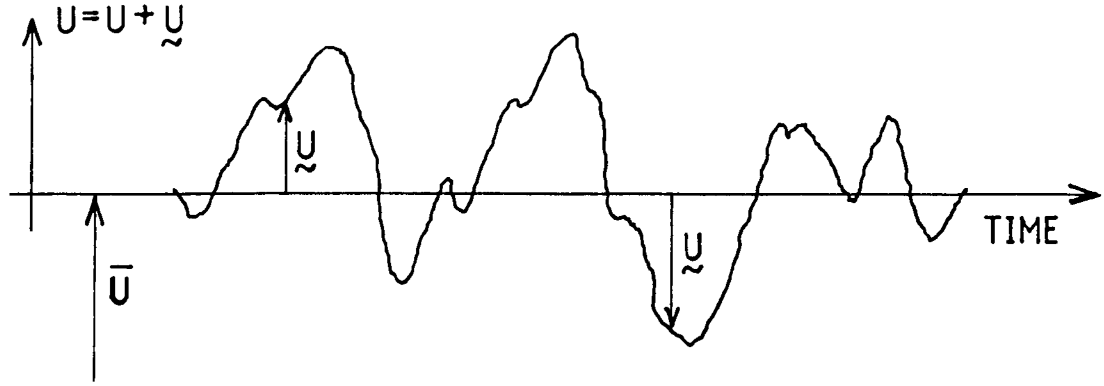

Fig.2·2(a) VELOCITY VARIATION IN X-DIRECTION

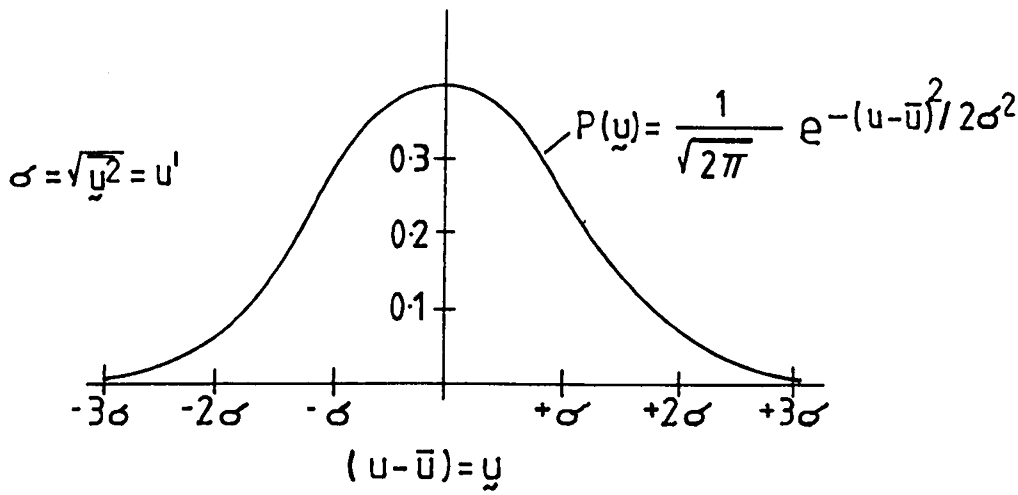

Fig.2·2(b) DISTRIBUTION OF TURBULENT VELOCITY

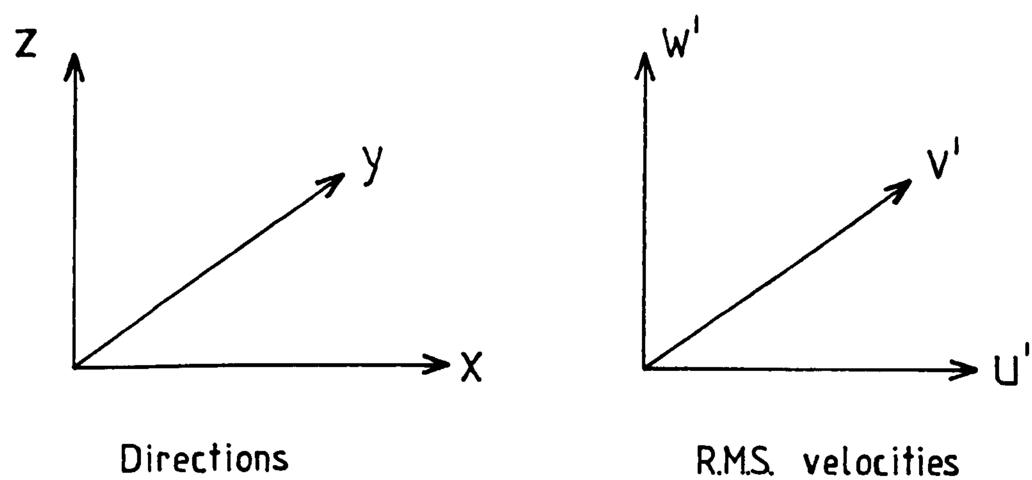

Fig. 2·2(c) CO-ORDINATE SYSTEM FOR FLUCTUATION COMPONENTS (SECTION 2·2 ONLY)

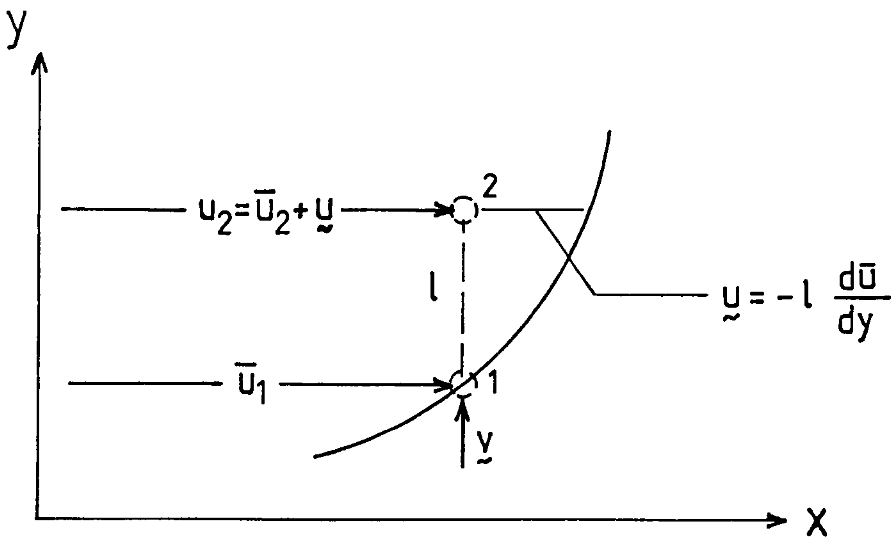

Fig.2·3 TURBULENCE MIXING LENGTH AND VELOCITY FLUCTUATIONS

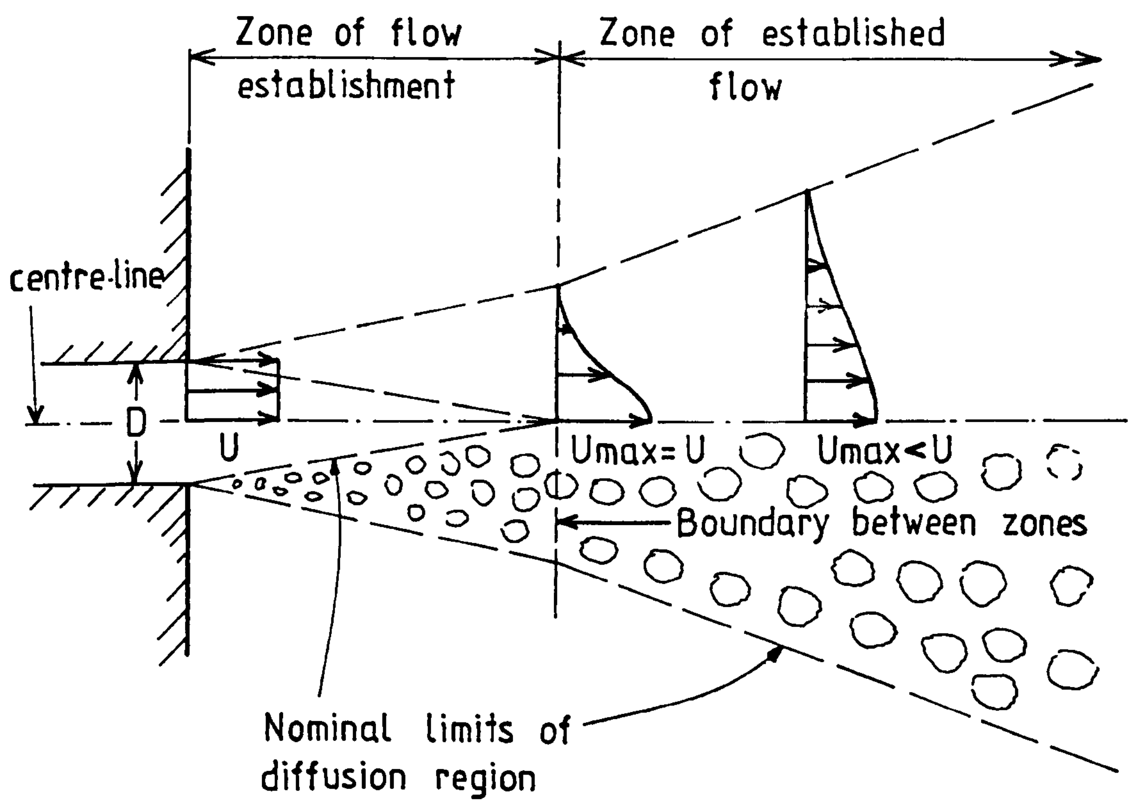

Fig. 2·4 SCHEMATIC REPRESENTATION OF JET DIFFUSION PATTERN (ALBERTSON)

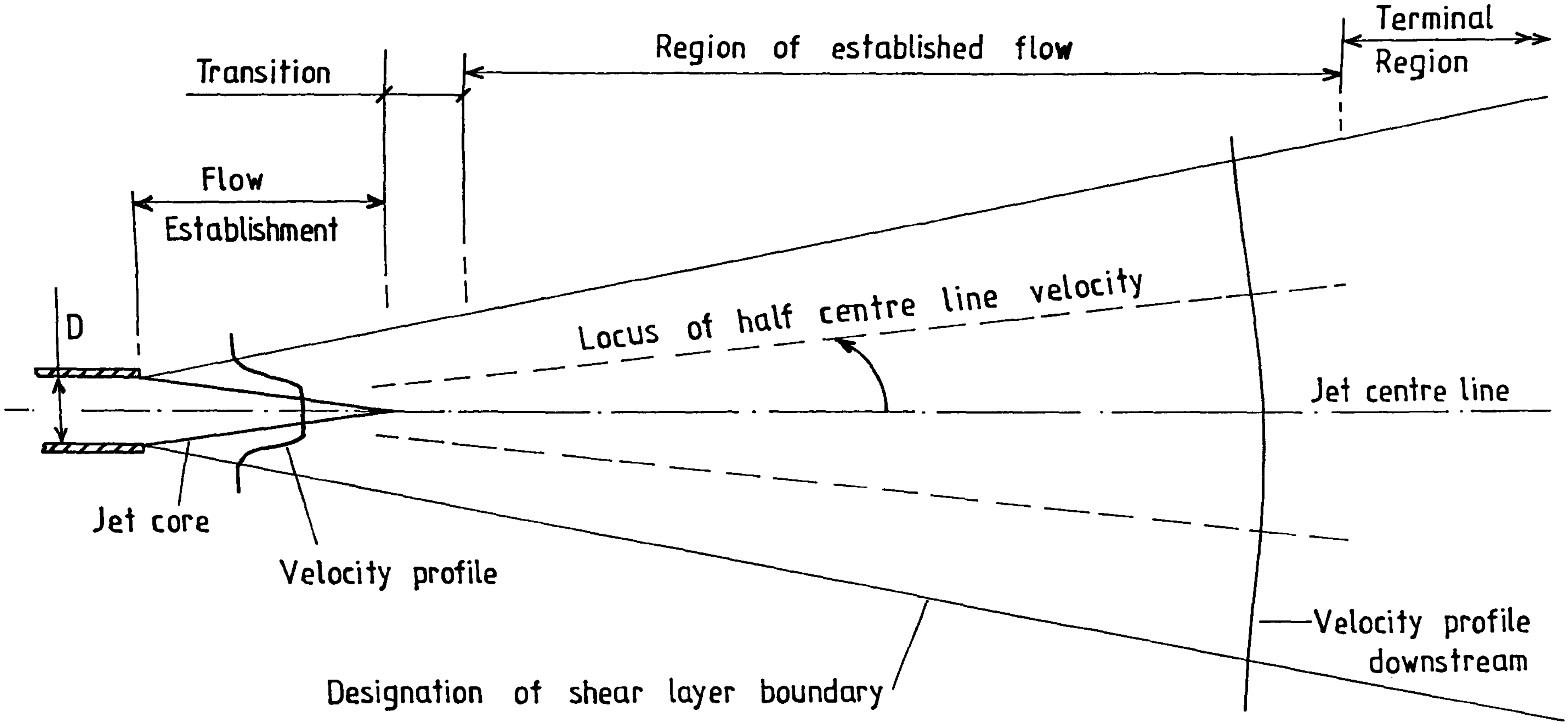

Fig. 2·5 TURBULENT SUBMERGED JET SHOWING TYPICAL VELOCITY PROFILES, FLOW REGIONS AND LOCI OF HALF CENTRE VELOCITIES (DAVIES).

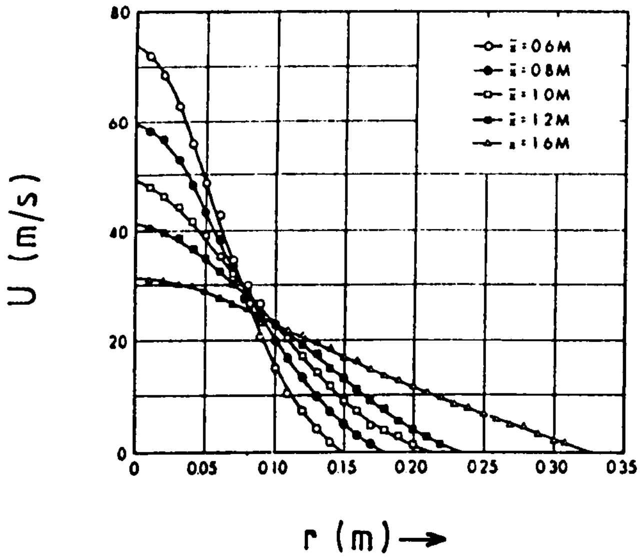

Fig. 2·6 VELOCITY DISTRIBUTION IN CIRCULAR JETS — TRUPEL.
($\overline{x}$ = Axial distance from nozzle outlet)

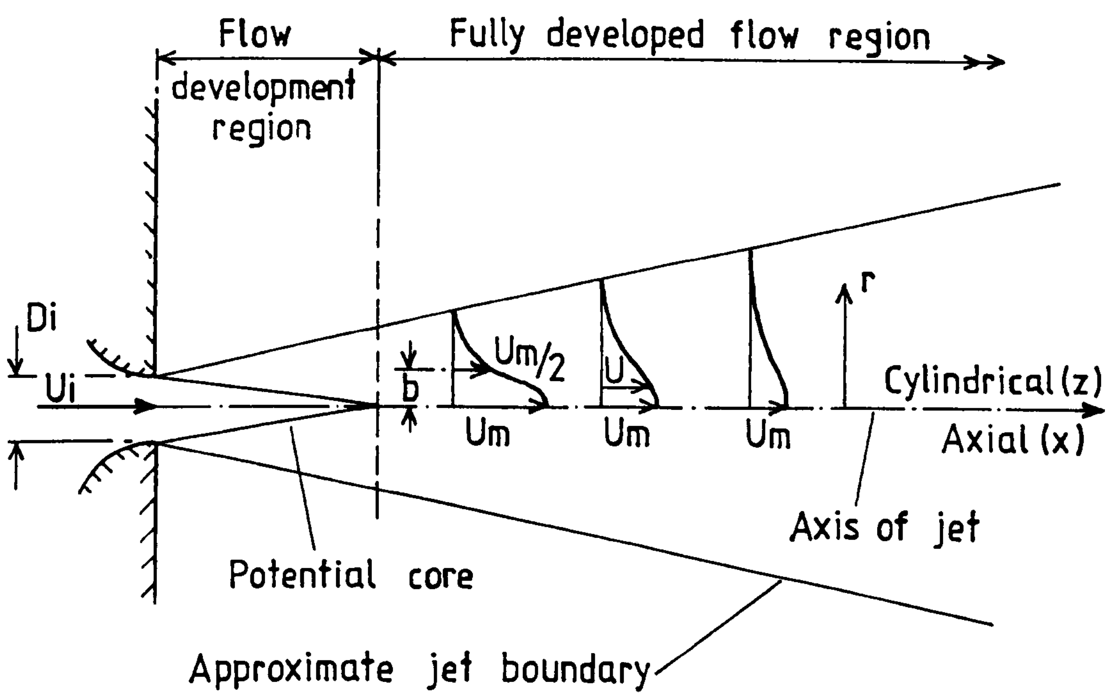

Fig. 2·7 DEFINITION SKETCH OF CIRCULAR TURBULENT JET.

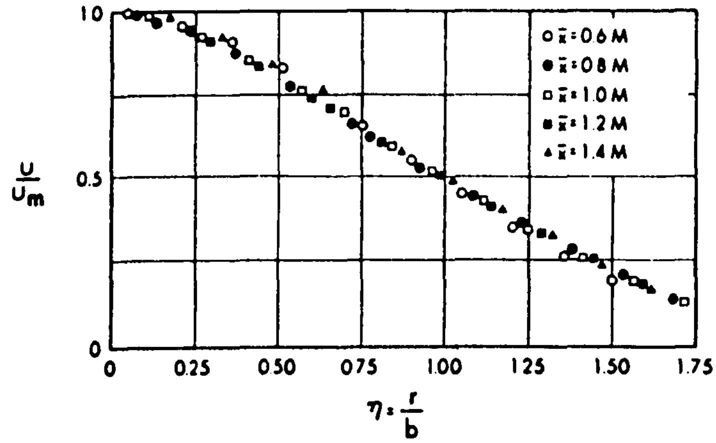

Fig. 2·8 SIMILARITY OF VELOCITY PROFILES

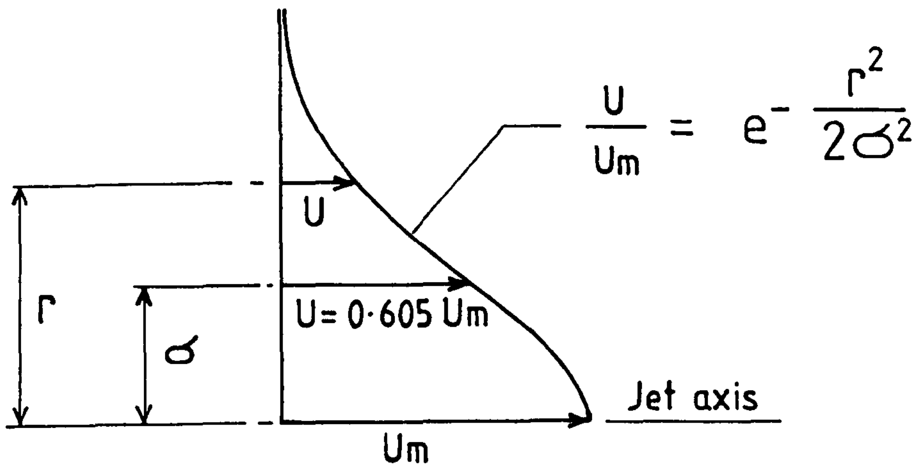

Fig. 2·9 GAUSSIAN NORMAL PROBABILITY VELOCITY DISTRIBUTION

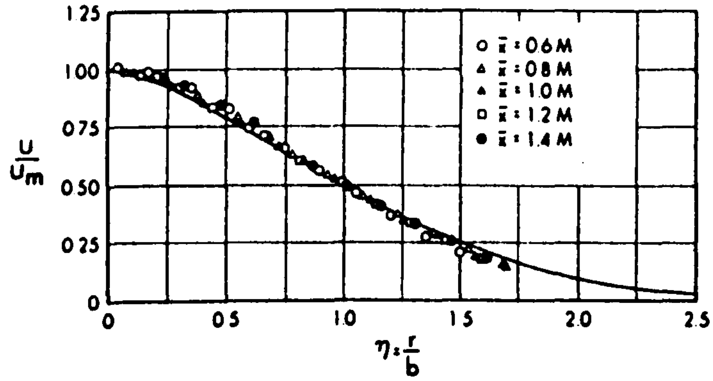

Fig. 2·10 COMPARISON OF TOLLMIEN'S SOLUTION WITH OBSERVATIONS.

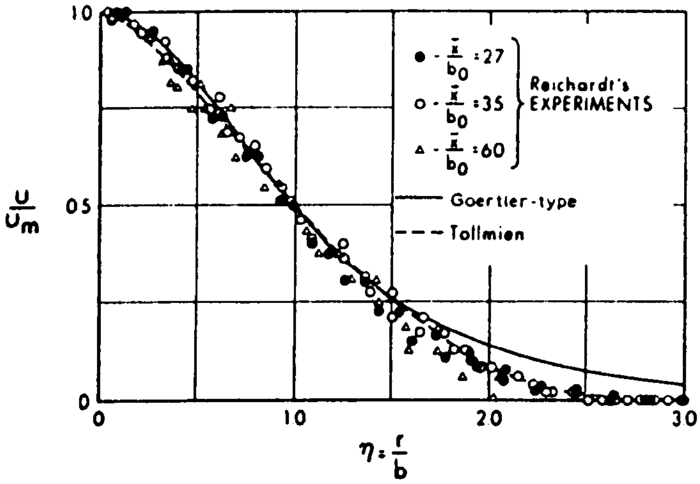

Fig. 2·11 COMPARISON OF GOERTLER AND TOLLMIEN-TYPE SOLUTIONS WITH EXPERIMENTAL RESULTS. (Reichardt:- b_o = Nozzle size)

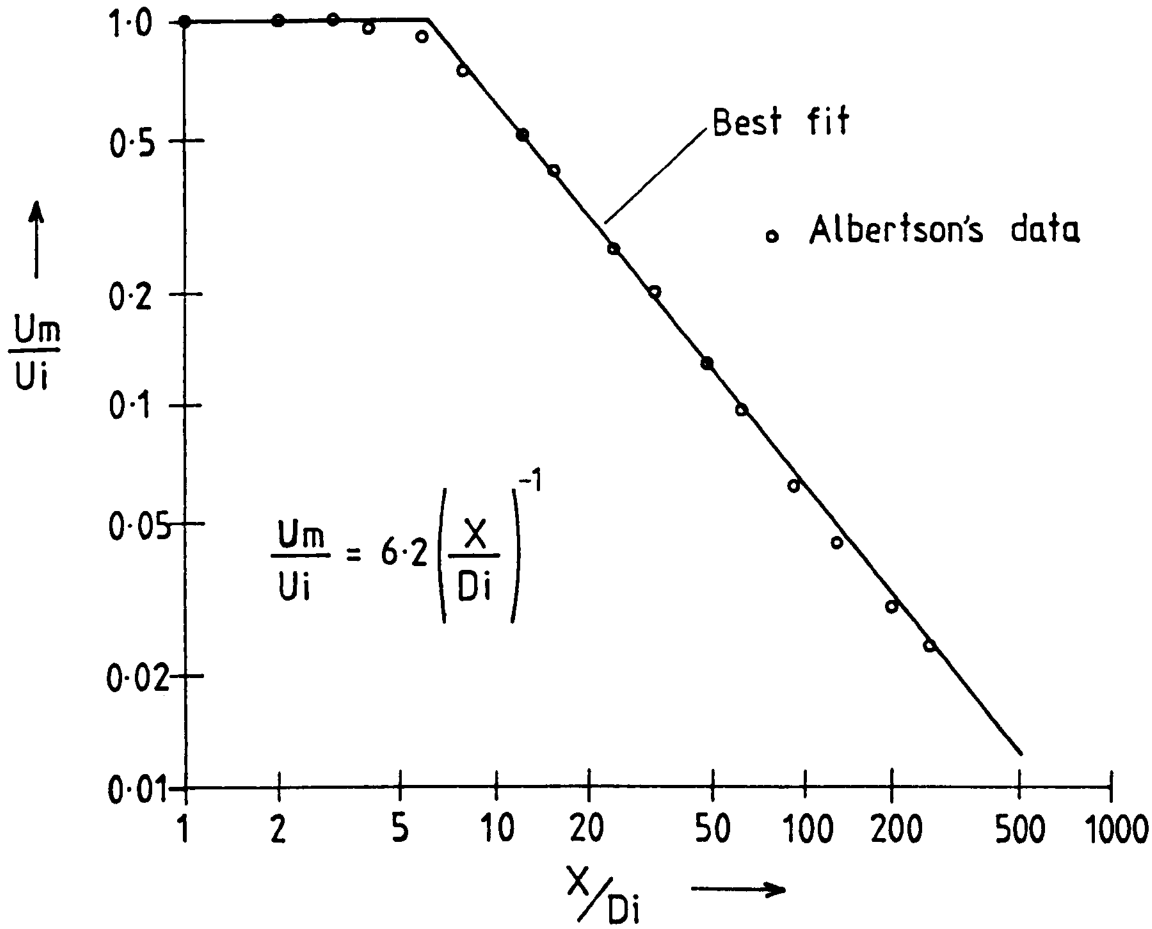

Fig. 2·12 JET CENTRE LINE VELOCITY DECAY (ALBERTSON).

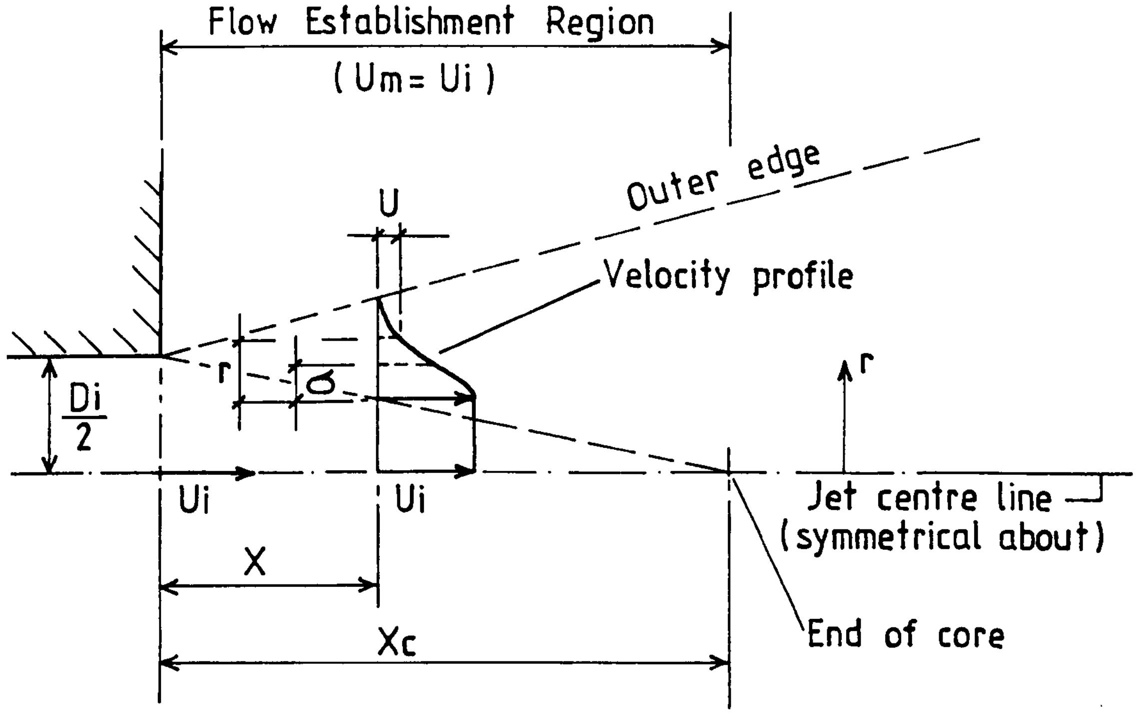

Fig. 2·13 VELOCITY PROFILE IN FLOW ESTABLISHMENT REGION (ALBERTSON).

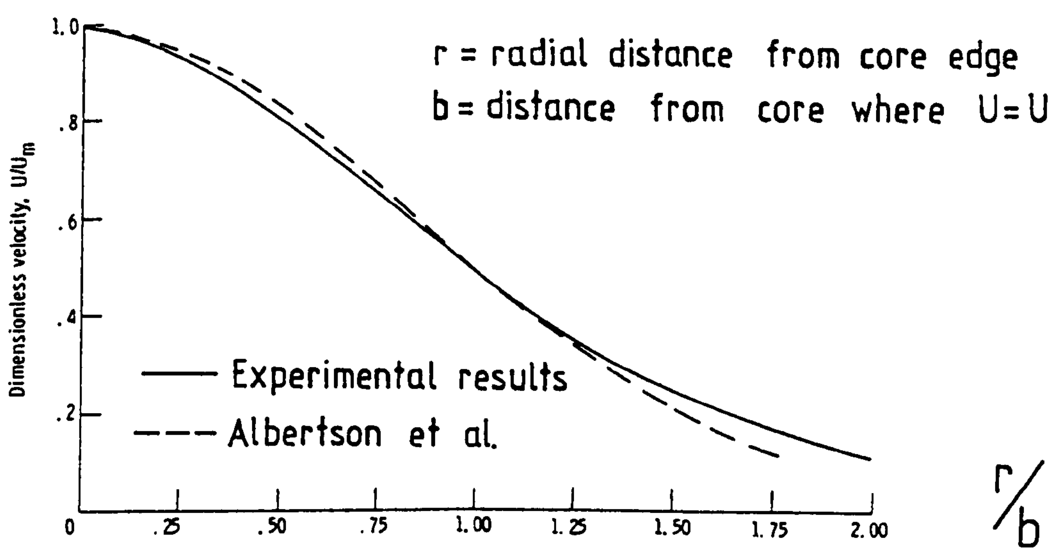

Fig. 2·14 COMPARISON OF EXPERIMENTAL VELOCITY PROFILE THROUGH FLOW ESTABLISHMENT REGION WITH PREDICTION.

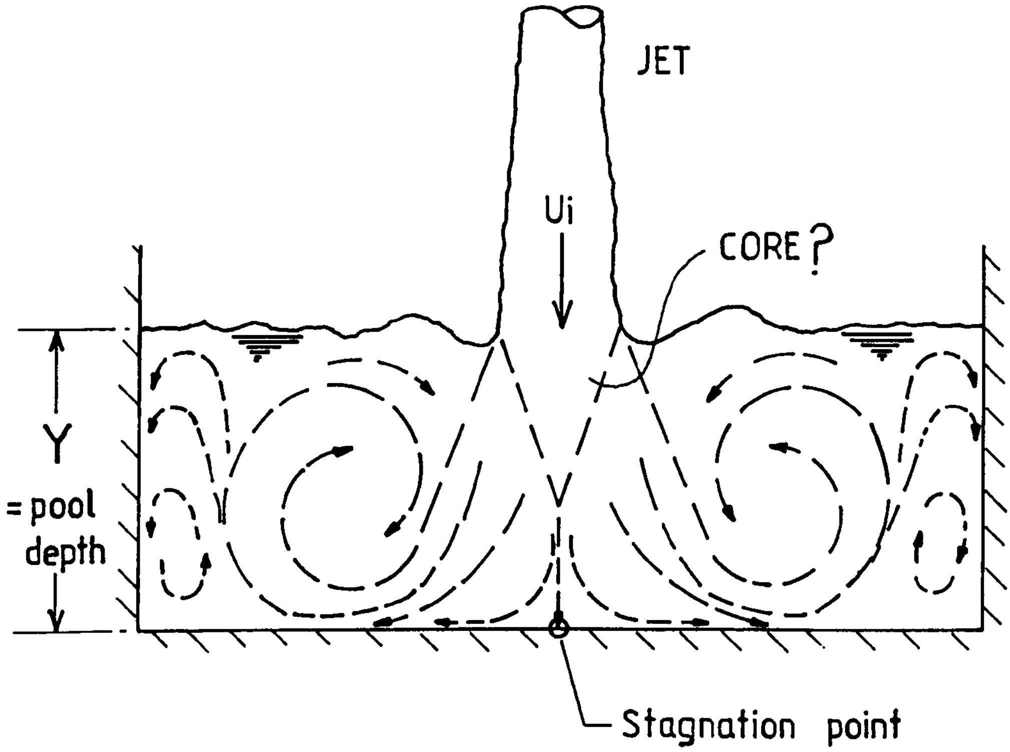

Fig. 2·15 CONFINED JET DIFFUSION — FLOW PATTERN.

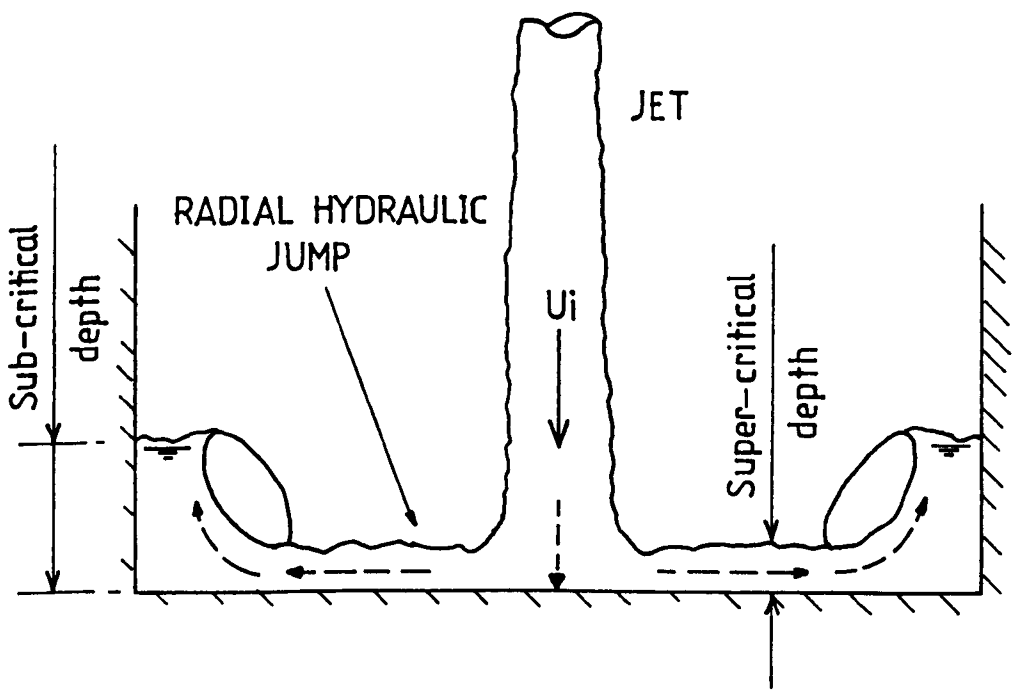

Fig. 2·16 SHALLOW DEPTH IMPINGEMENT — HYDRAULIC JUMP.

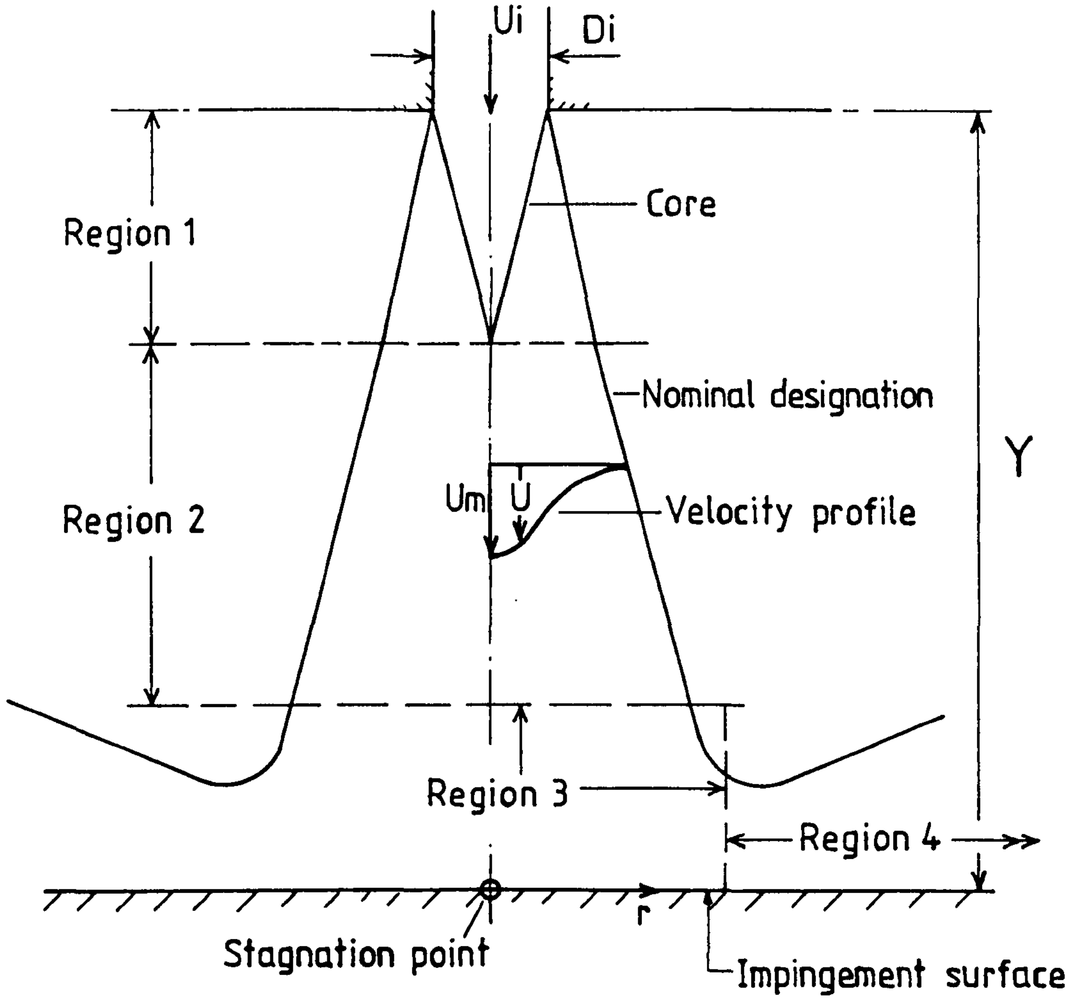

Fig. 2·17 LARGE DEPTH IMPINGEMENT — CHARACTERISTIC FLOW REGIONS.

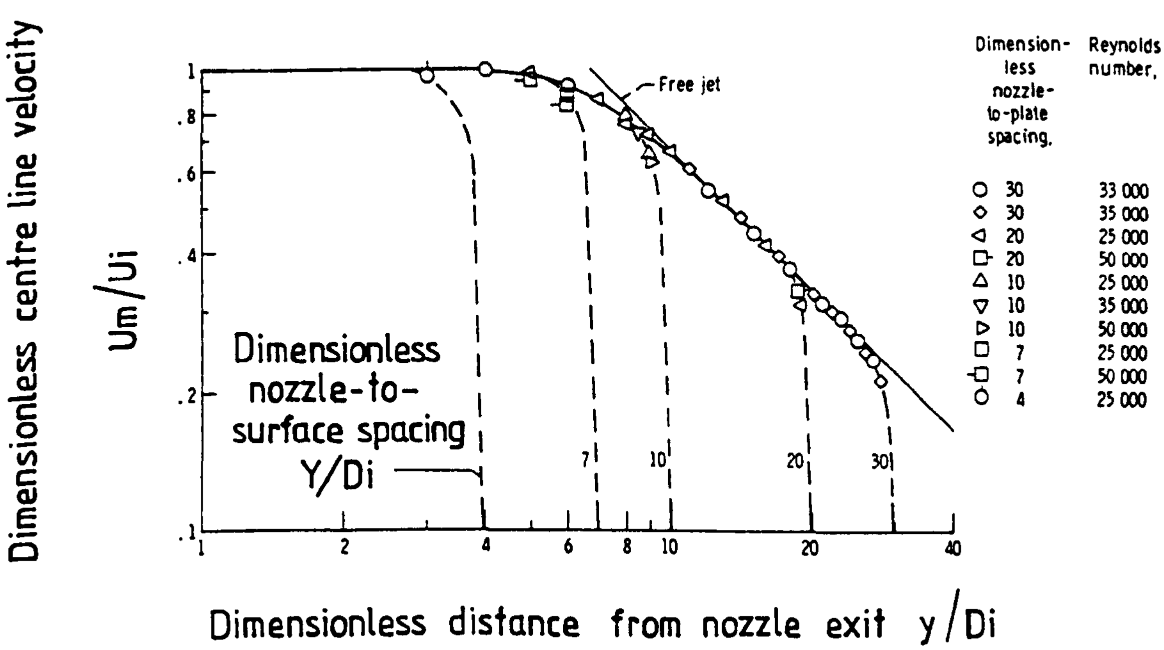

Fig. 2·18 CENTRE LINE VELOCITY DECAY WITH VARIOUS VALUES OF NOZZLE-TO-SURFACE SPACING AND REYNOLDS NUMBER. (Reproduced from N.A.S.A.—TND 5690)

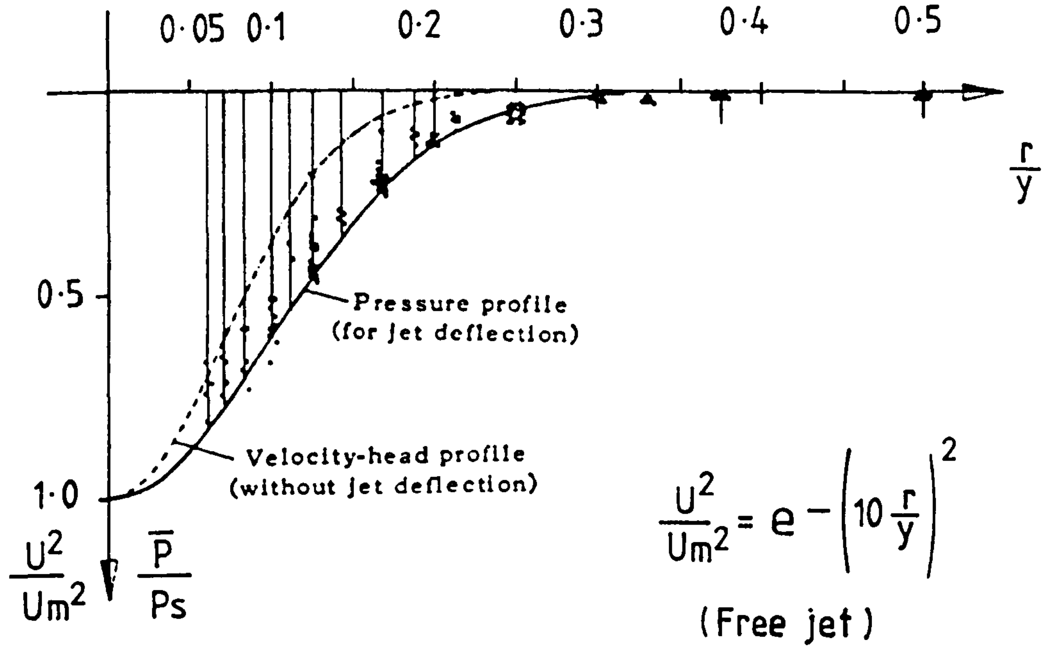

Fig. 2·19 COMPARISON OF MEASURED MEAN PRESSURE DISTRIBUTION WITH FREE JET THEORY (HÄUSLER).

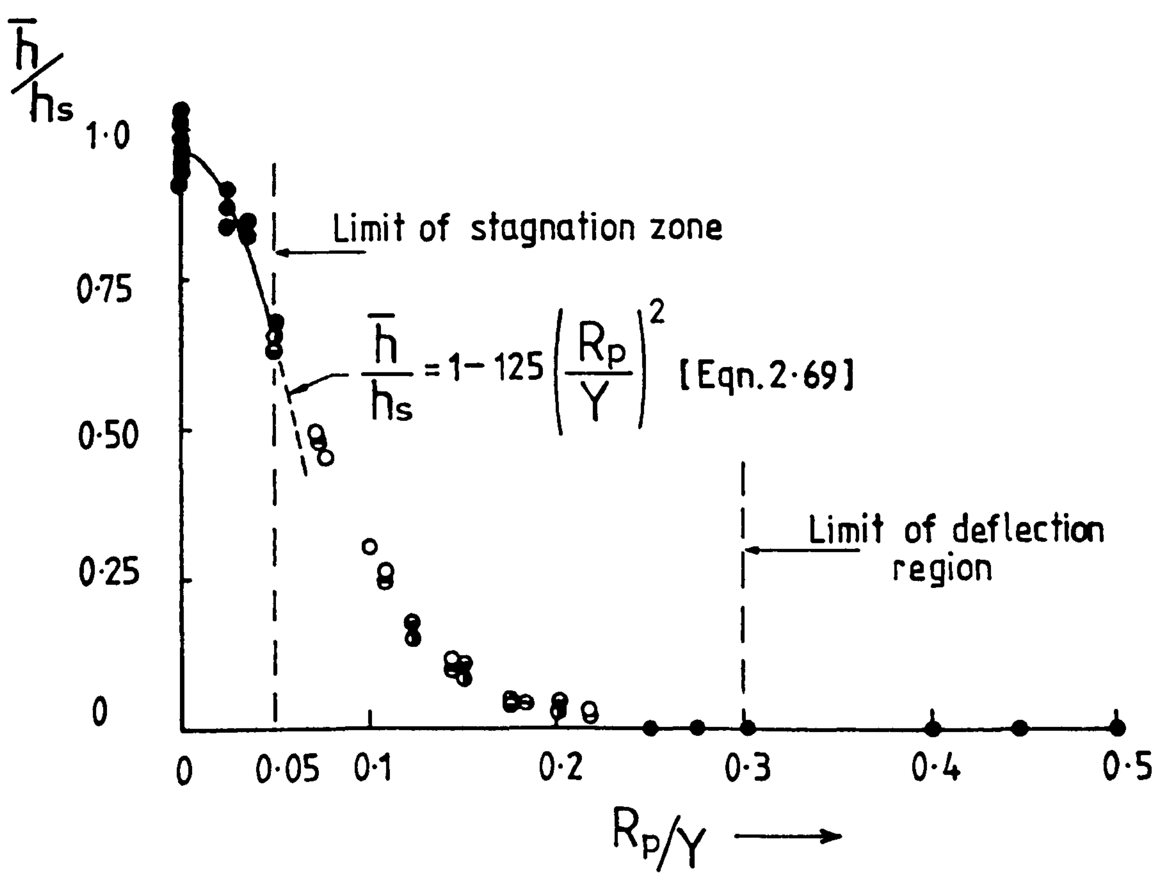

Fig. 2·20 ADDITIONAL PRESSURE HEAD ON BOUNDARY (POREH & CERMAK).

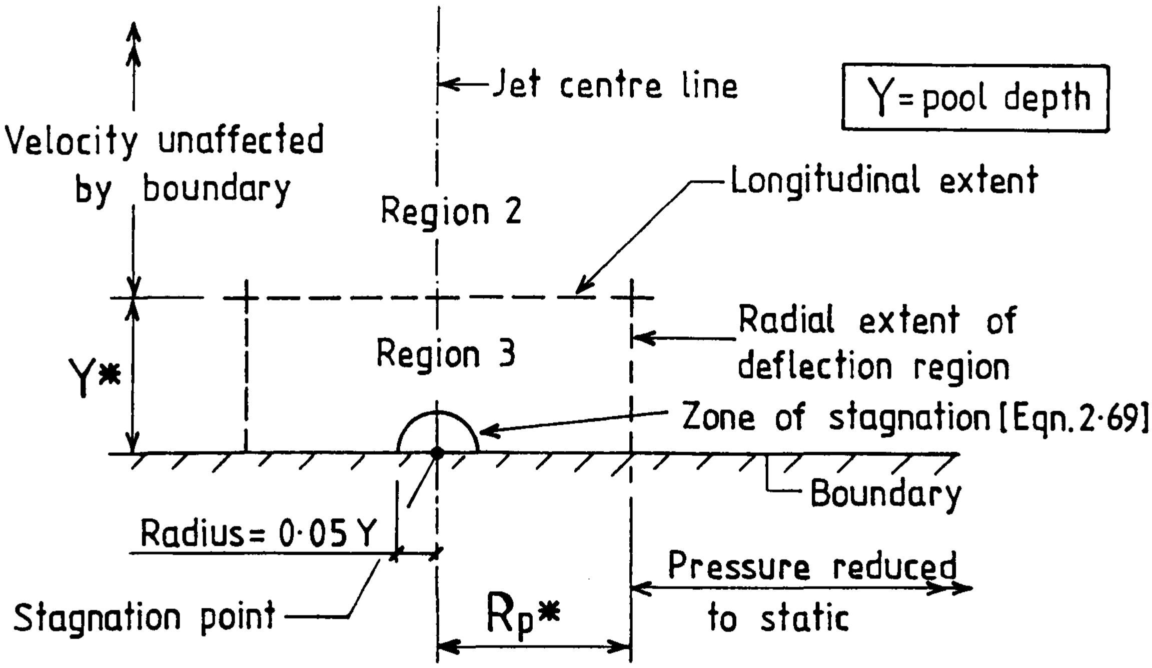

Fig. 2·21 DEFINITION SKETCH OF DEFLECTION REGION AND STAGNATION ZONE.

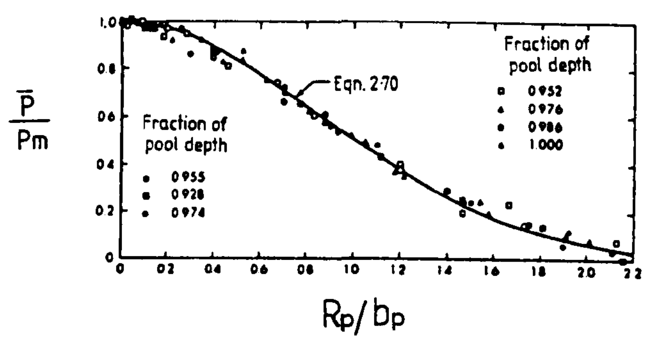

Fig. 2·22 DIMENSIONLESS PRESSURE PROFILES (Beltaos et al.)

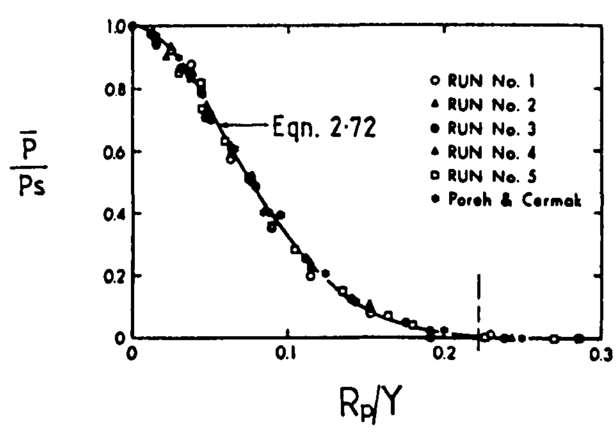

Fig. 2·23 DIMENSIONLESS BOUNDARY-PRESSURE PROFILES.

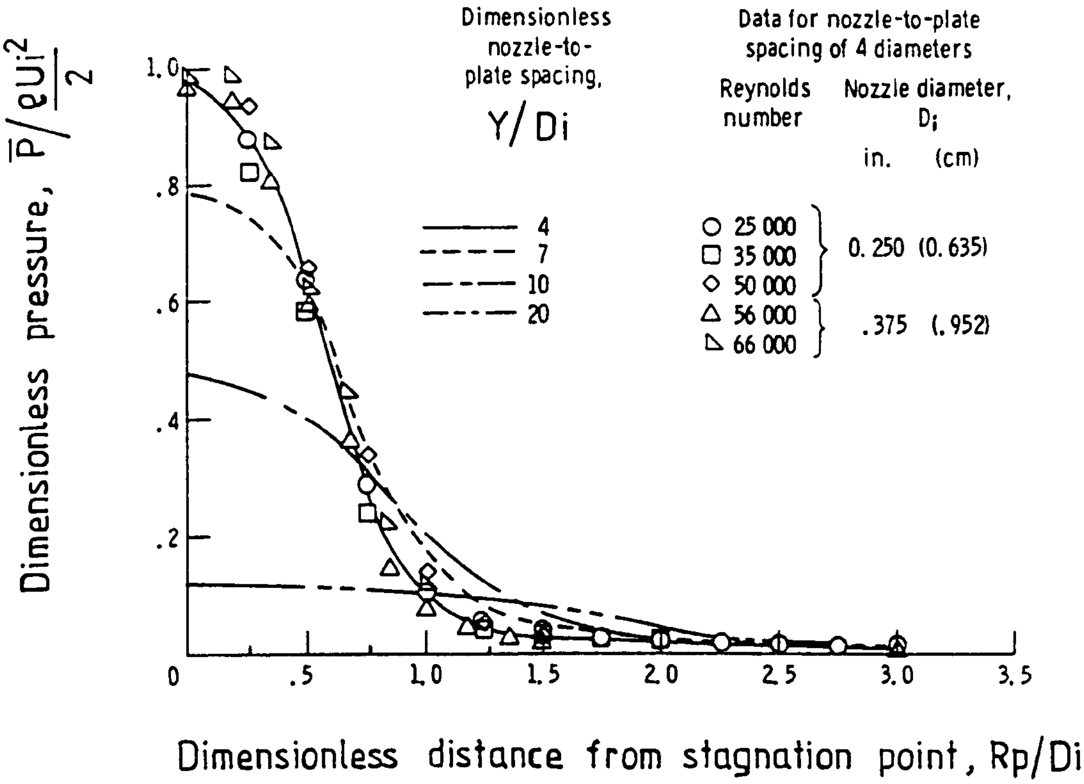

Fig.2·24 PRESSURE DISTRIBUTION ALONG IMPINGEMENT PLATE. (N.A.S.A. TND–5690)

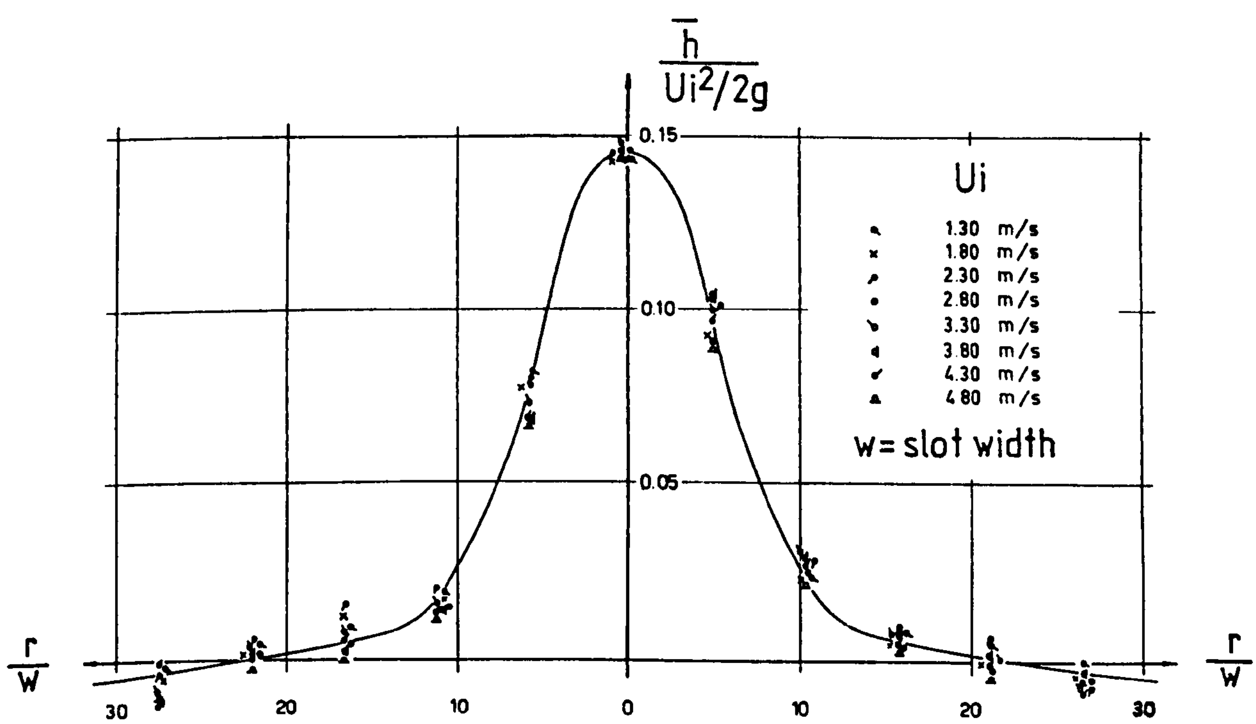

Fig.2·25 DISTRIBUTION OF PRESSURE ON BOTTOM OF BASIN. (Cola)

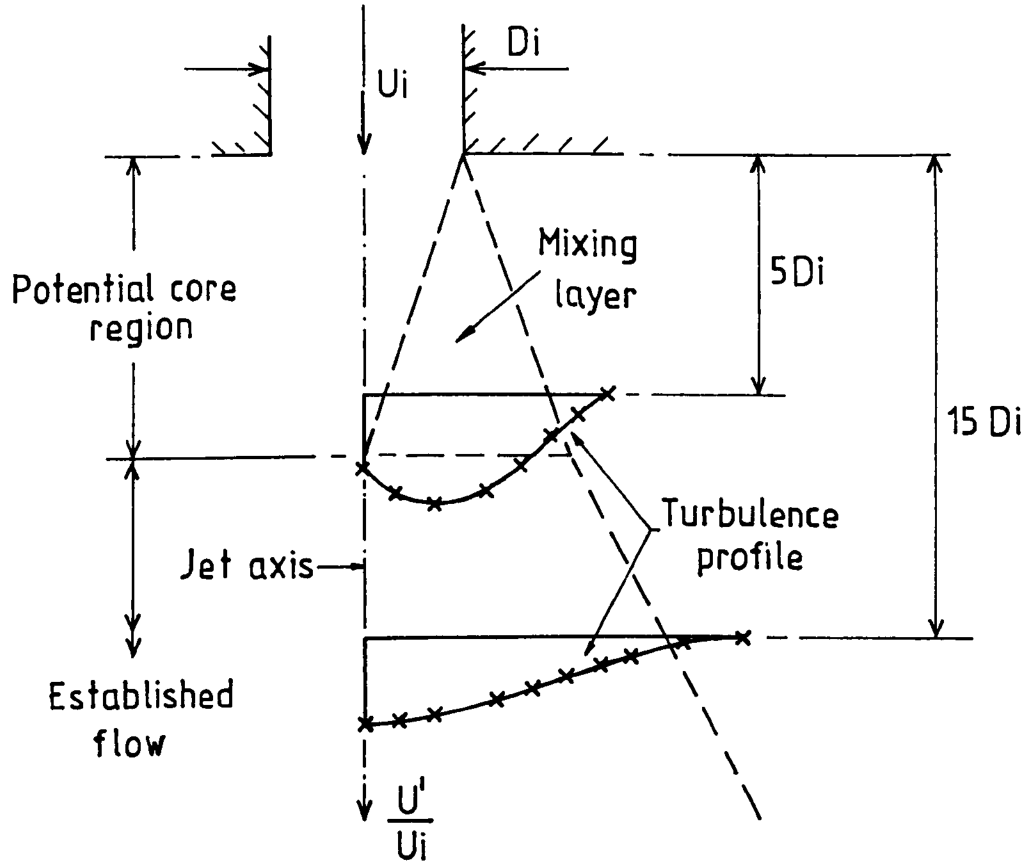

Fig. 2·26 TURBULENCE DEVELOPMENT IN POOL. (Corrsin-Ref.[12])

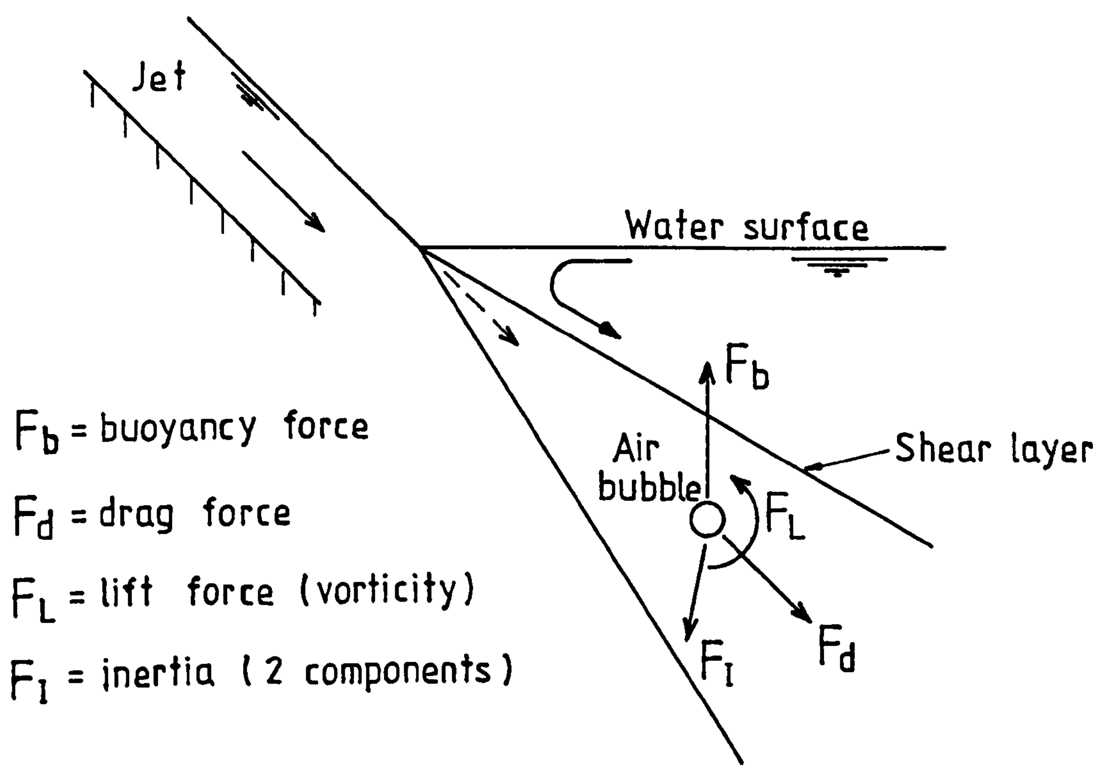

Fig. 2·27 FORCES ON SPHERICAL BUBBLE.

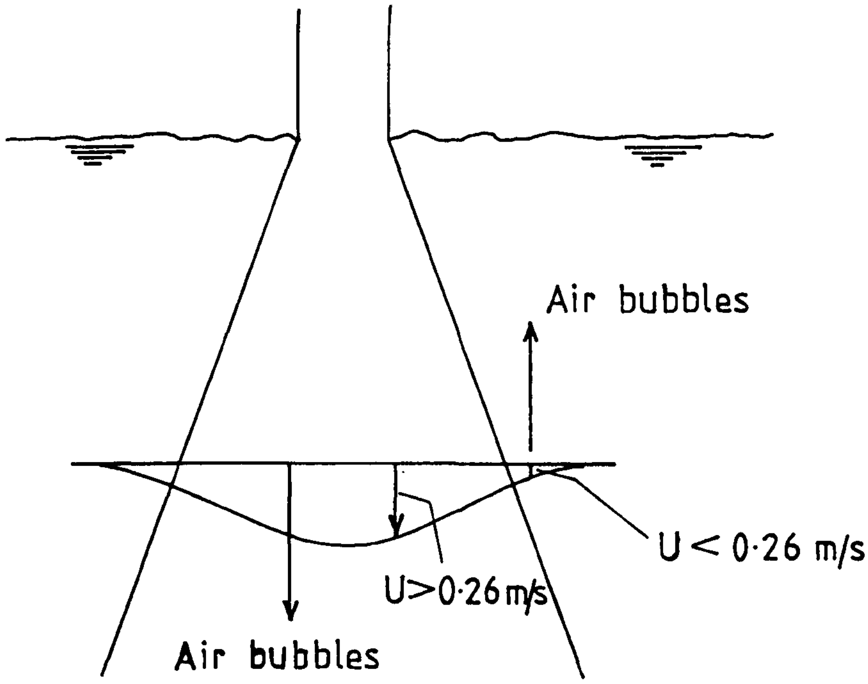

Fig. 2·28 POOL AIR ENTRAINMENT (Smooth turbulent jet).

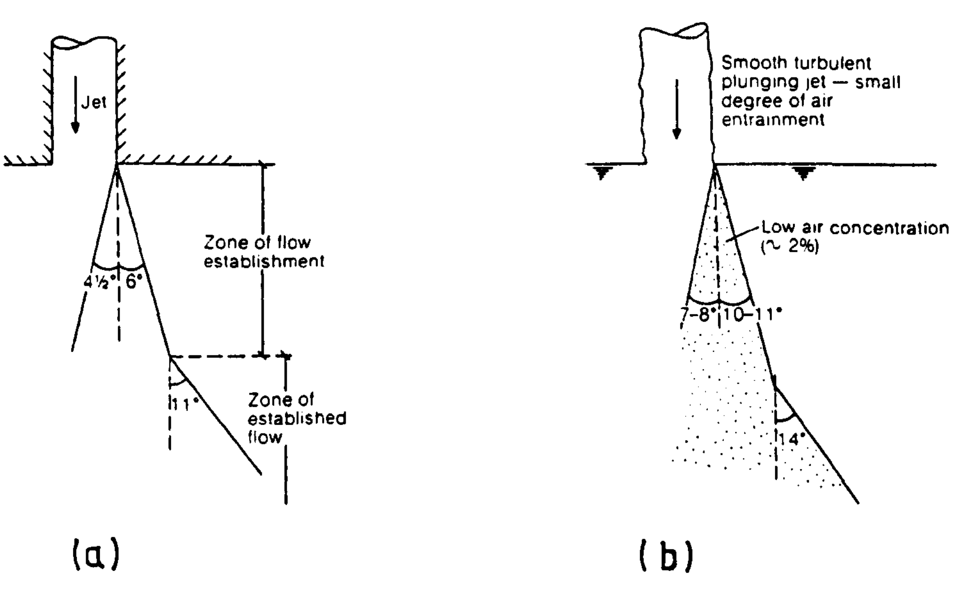

Fig. 2·29 JET DIFFUSION IN THE PLUNGE POOL FOR SINGLE-PHASE AND TWO-PHASE SHEAR LAYERS: (a) Submerged jet (Albertson et al.) ; (b) Smooth turbulent plunging jet (Mckeogh).

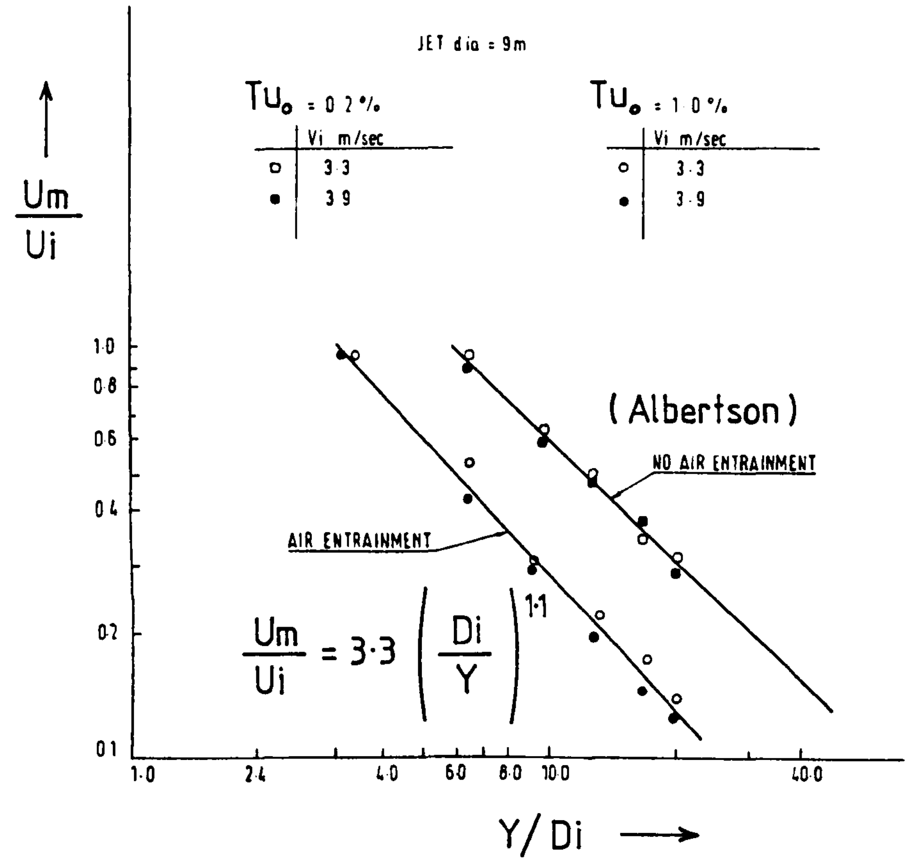

Fig. 2·30 CENTRE LINE VELOCITY DECAY WITH DISTANCE FROM PLUNGE POINT. (McKeogh)

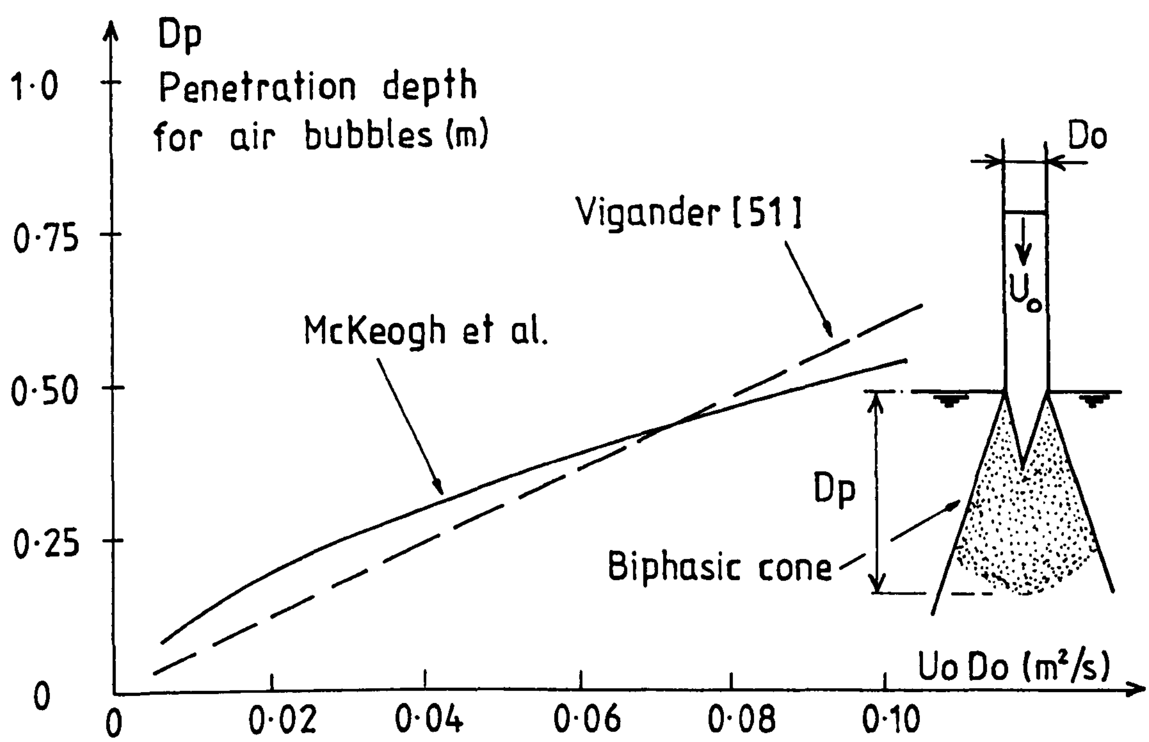

Fig. 2·31 VARIATION OF PENETRATION DEPTH WITH (Uo Do). (Rough turbulent jet, large air entrainment)

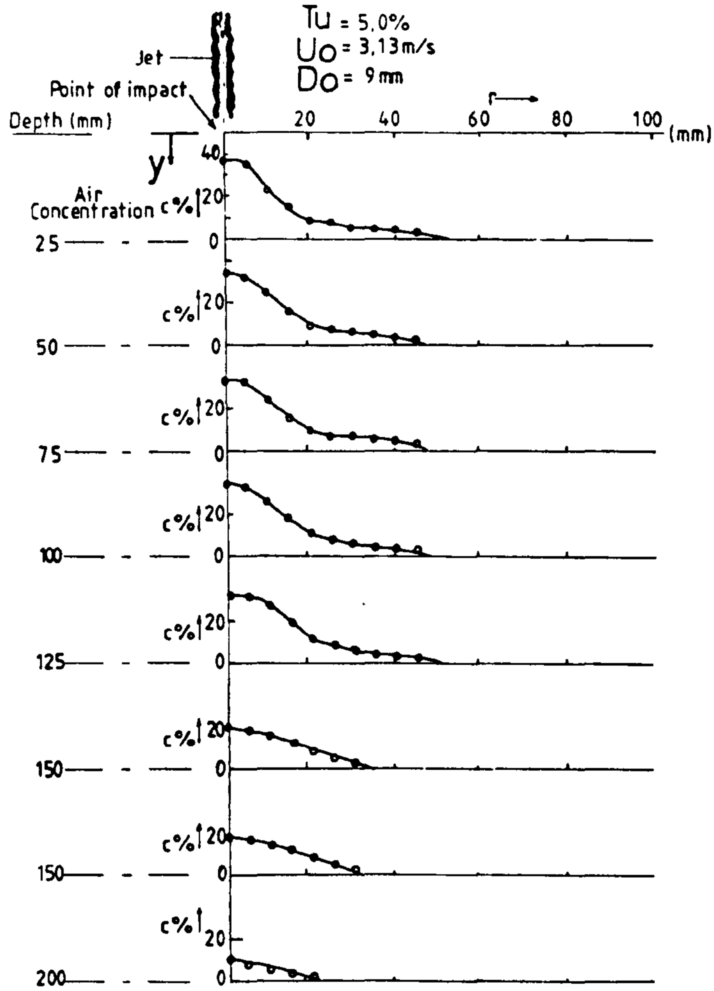

Fig. 2·32 TYPICAL AIR CONCENTRATION PROFILES FOR ROUGH TURBULENT JET.

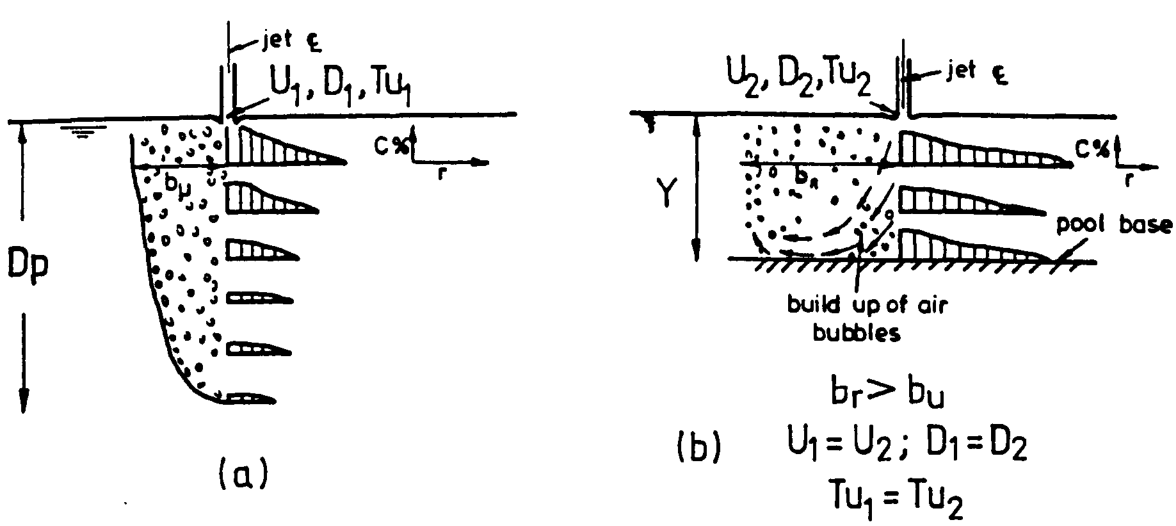

Fig. 2·33 AIR CONCENTRATION PROFILES : (a) Unrestricted ; (b) Restricted jet penetration.

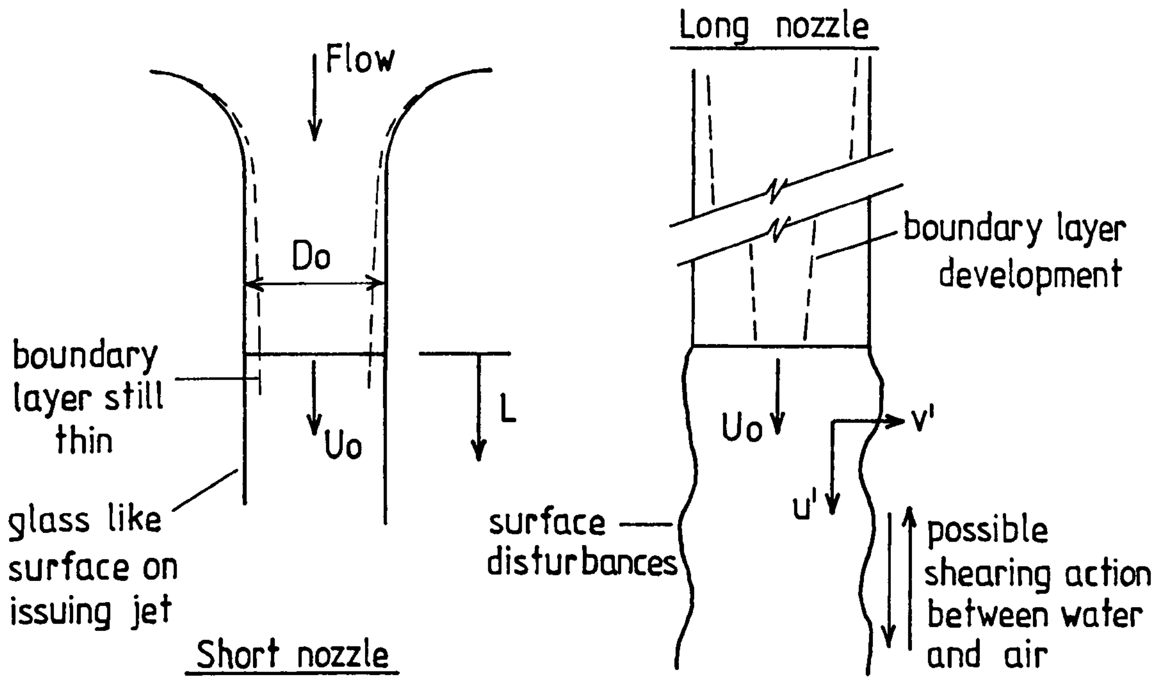

Fig. 2·34 JET ISSUING FROM SHORT / LONG NOZZLE.

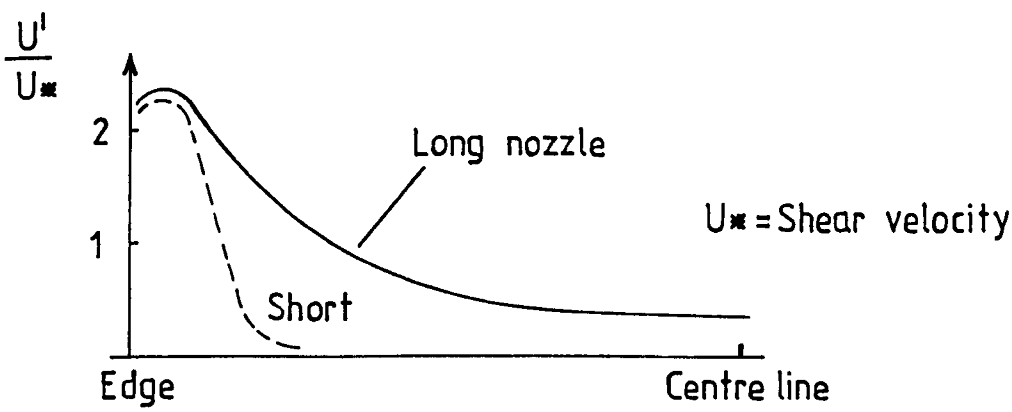

Fig. 2·35 RELATIVE TURBULENCE OF JET ISSUING FROM SHORT / LONG NOZZLE.

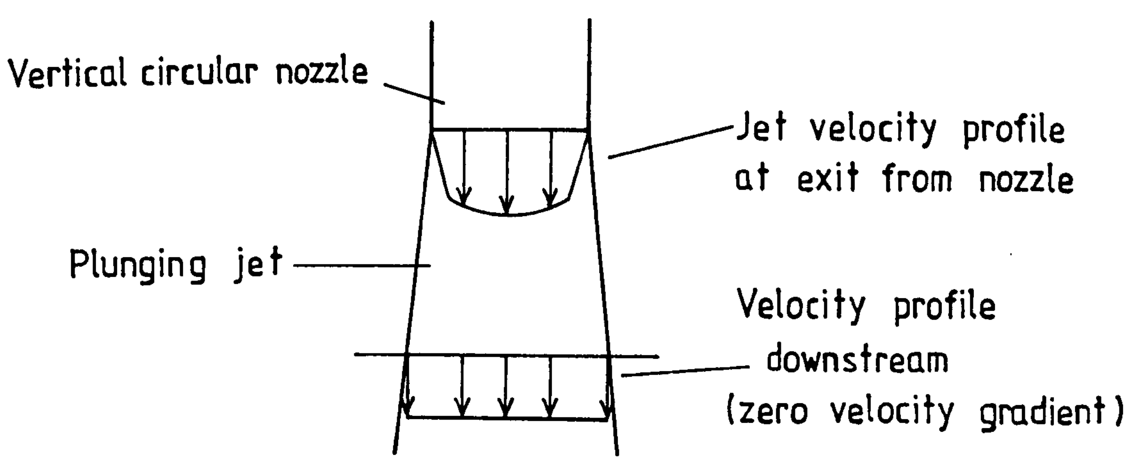

Fig. 2·36 VELOCITY PROFILE ACROSS PLUNGING JET.

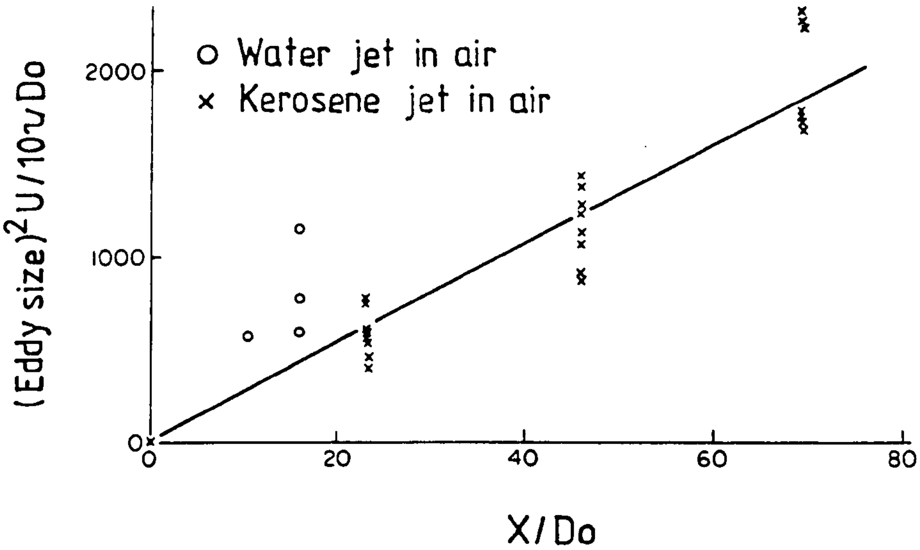

Fig.2·37 PLOT OF (Eddy size)^2 WITH X/Do FOR RESTRAINED TURBULENT JETS. [Davies]

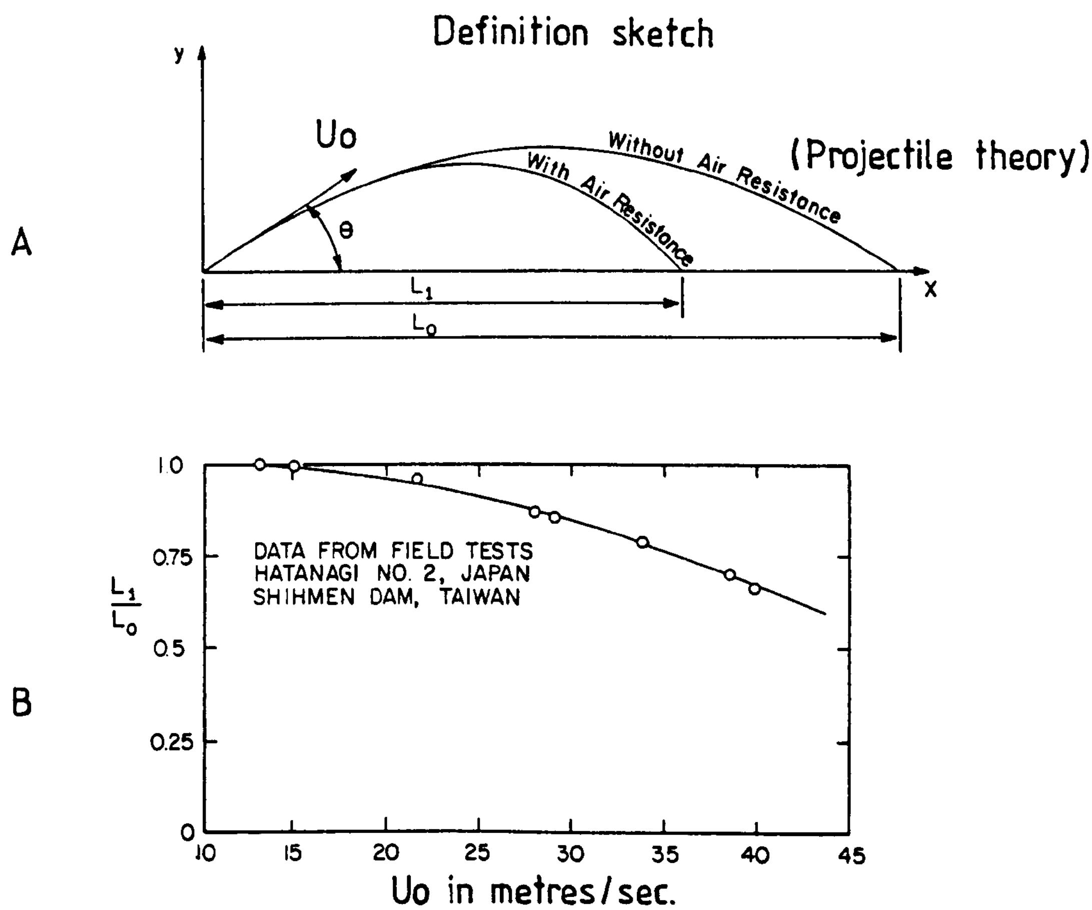

Fig.2·38 JET TRAJECTORY WITH AIR RESISTANCE. [NOVAK]

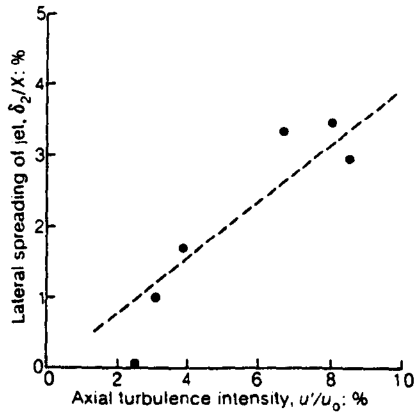

Fig. 2·39(a) LATERAL JET SPREADING WITH TURBULENCE INTENSITY ACTING AT ORIFICE OUTLET. (Ervine and Falvey)

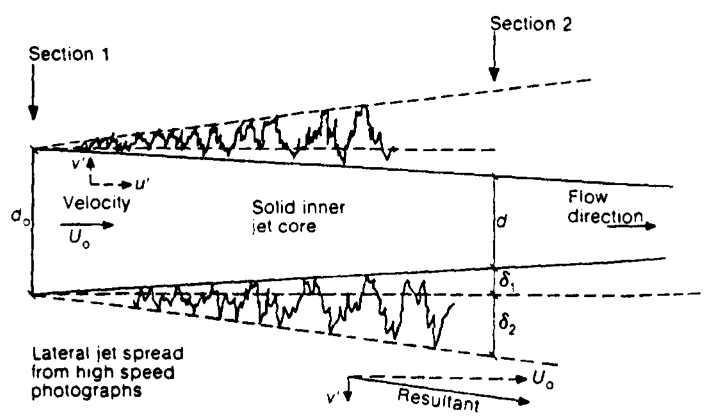

Fig. 2·39(b) SPREADING TURBULENT JET; Total jet diameter at Section 2 is $d_e = d + 2\delta_1 + 2\delta_2$

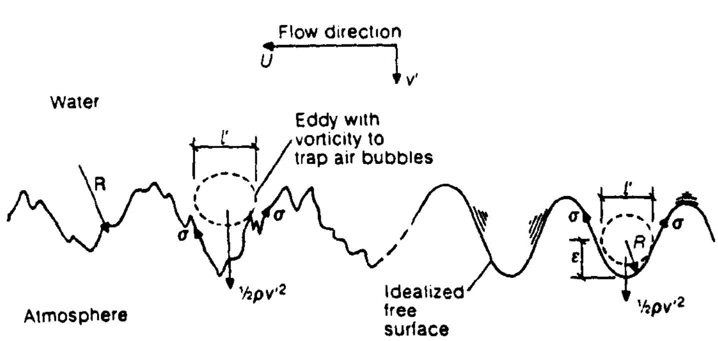

Fig. 2·40 FREE SURFACE WITH DEFINITION OF PHYSICAL PARAMETERS.

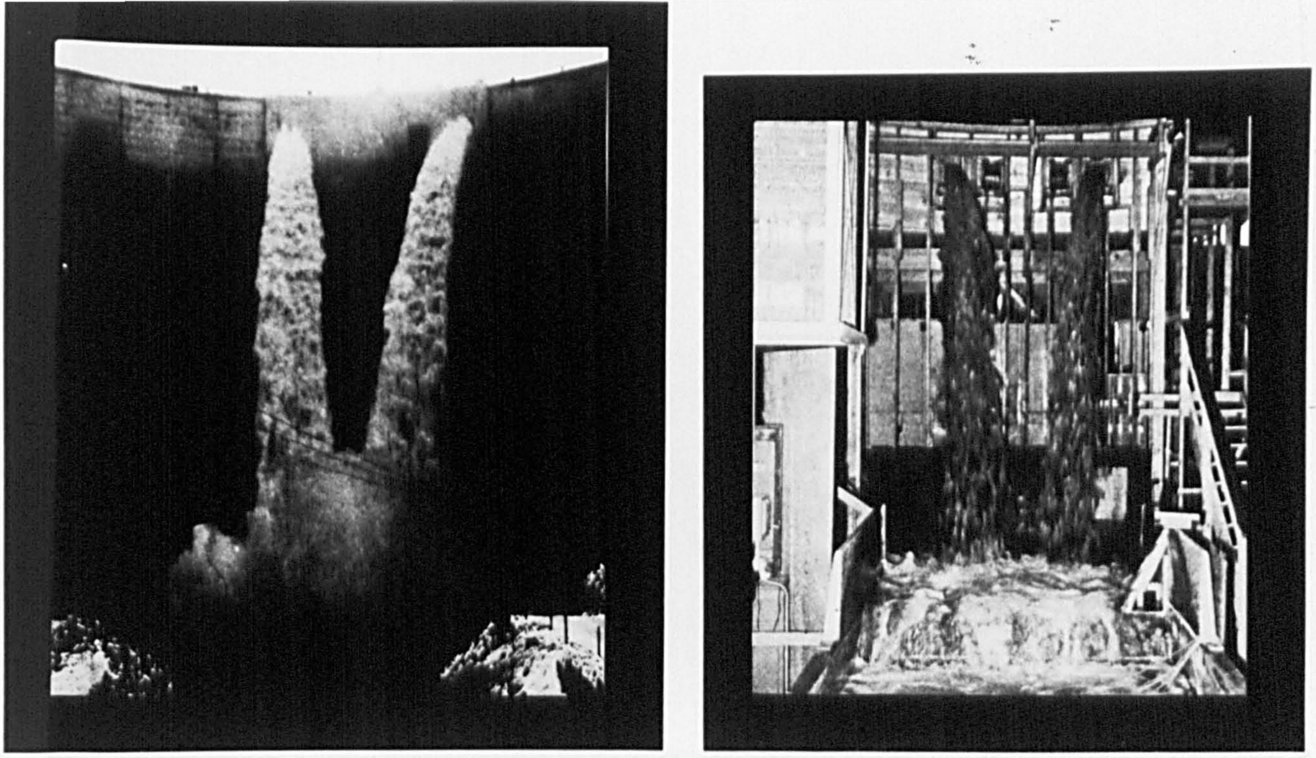

(a) (b)

Fig. 2·41 MORROW POINT DAM : (a) Full-scale jets ; (b) Model jets (1:24 Scale). [U.S.B.R.]

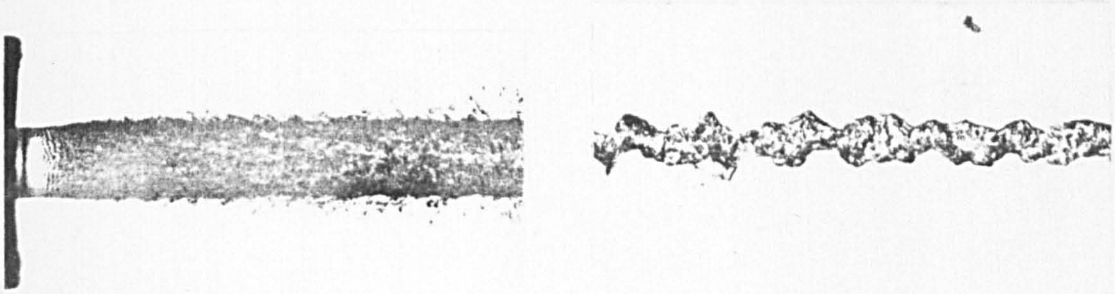

(a) At exit from nozzle (b) 0·9 m from nozzle exit

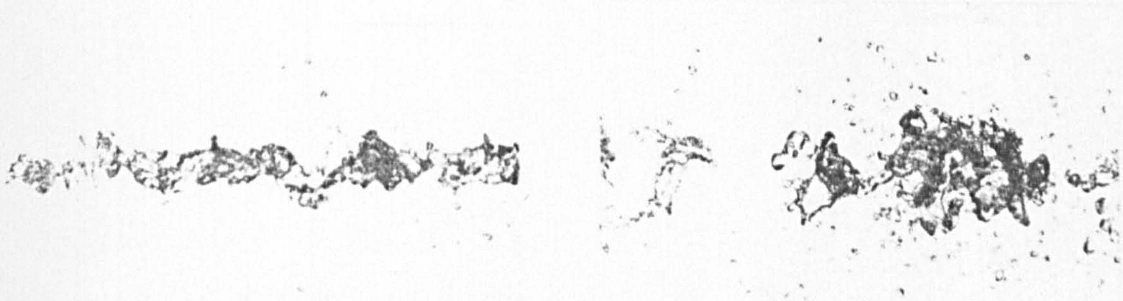

(c) 1·8 m from nozzle exit (d) 2·7 m from nozzle exit

Fig. 2·42 APPEARANCE OF WATER JET FROM 6mm NOZZLE. (Hoyt et al.)

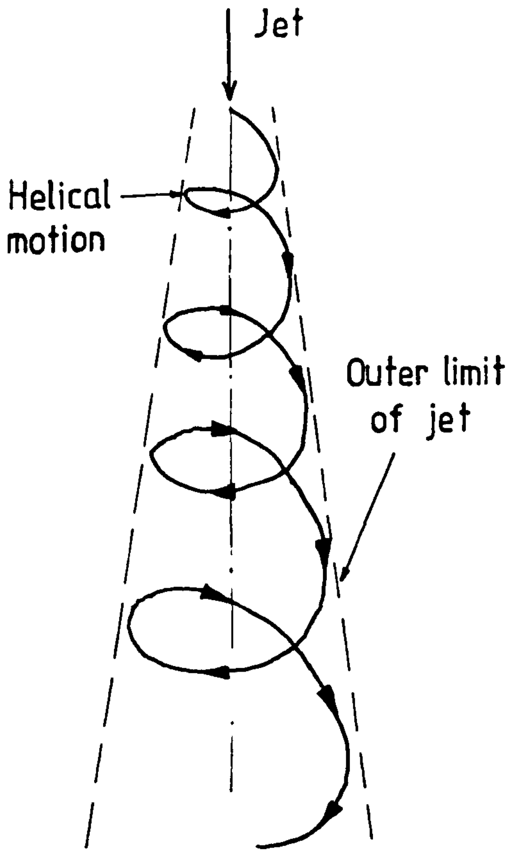

Fig. 2·43 JET AXIAL SWIRL.

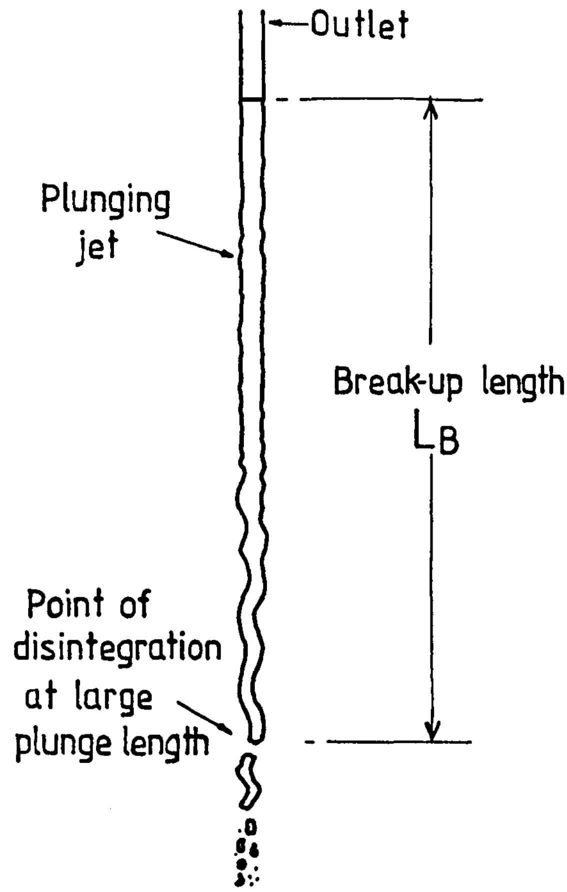

Fig. 2·44 JET BREAK-UP LENGTH.

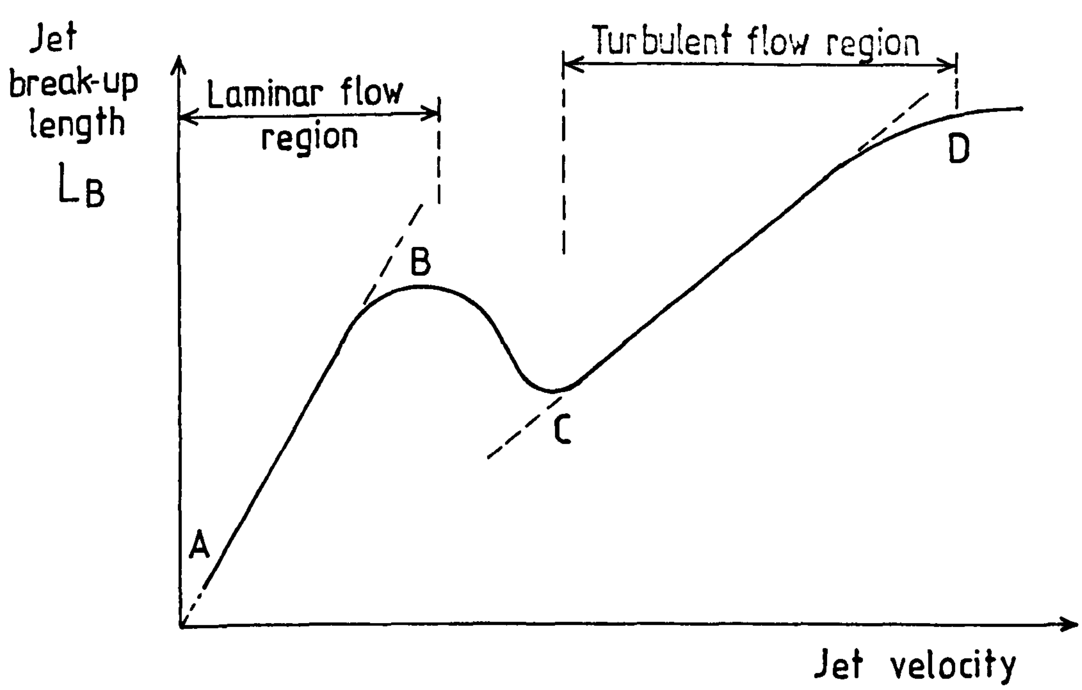

Fig. 2·45 JET STABILITY CURVE (Schematic).

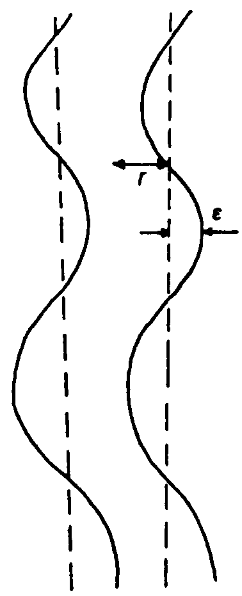

Fig.2·46 Sinuous nature of jet surface just before break-up.(Ervine)

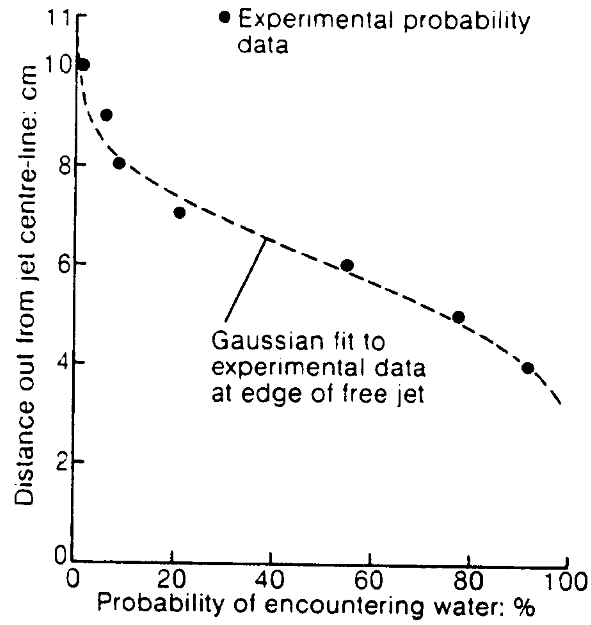

Fig.2·47 Probability of encountering water outside the solid core of a plunging turbulent jet.

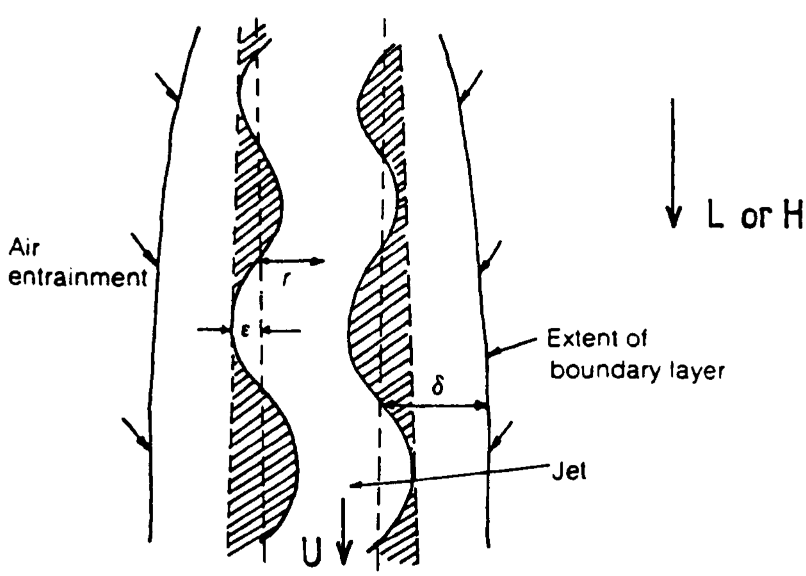

Fig.2·48 Sinuous jet waveform showing boundary layer extent and air entrainment within surface undulations.

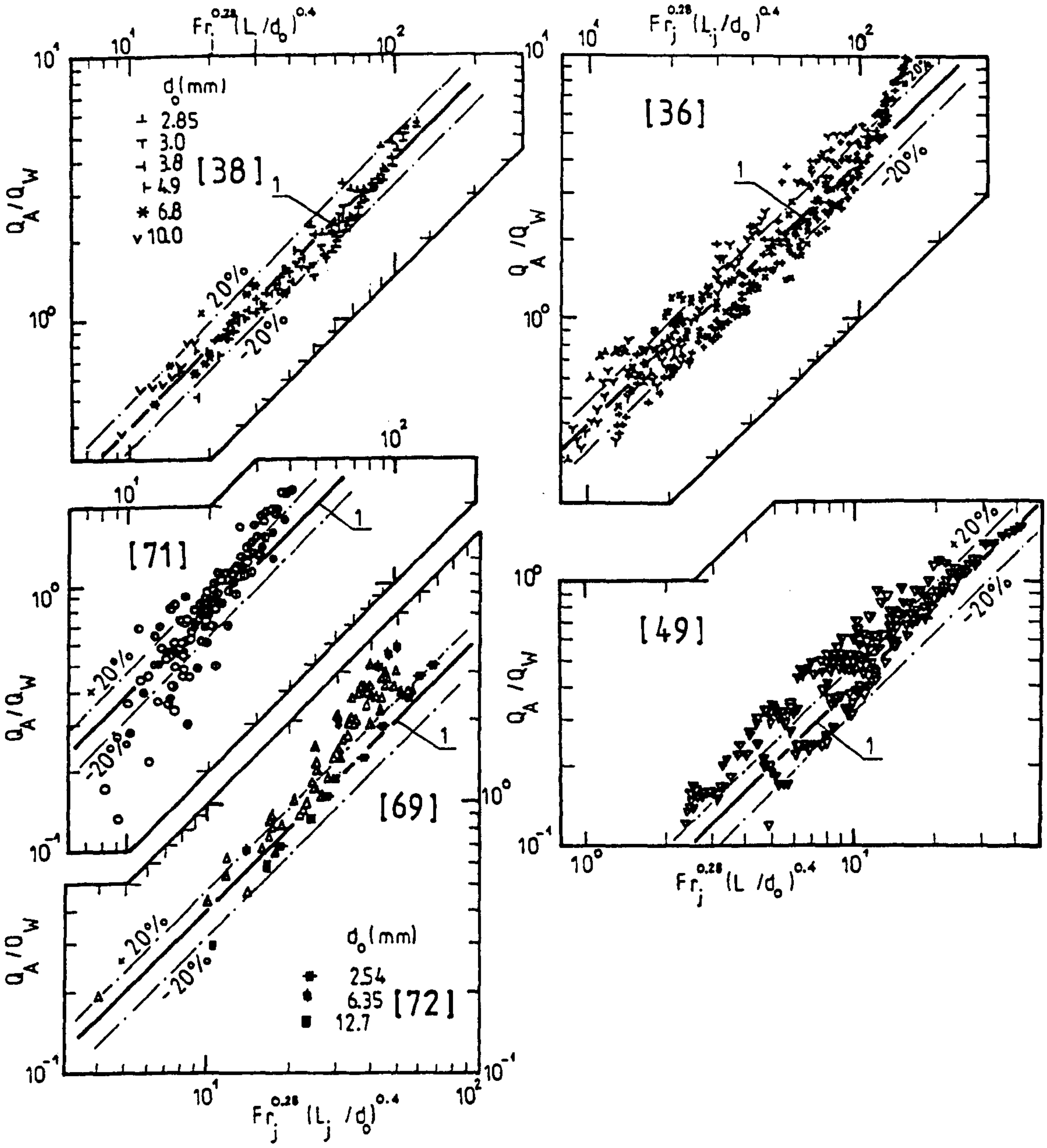

Correlations by Biń [70]

($Fr_j = Ui^2/gd_o$, $L_j = L$)

1— Eqn. 2·108

[ ]— Reference numbers

Fig. 2·49 CORRELATION OF ENTRAINMENT RATIO (Vertical jets).

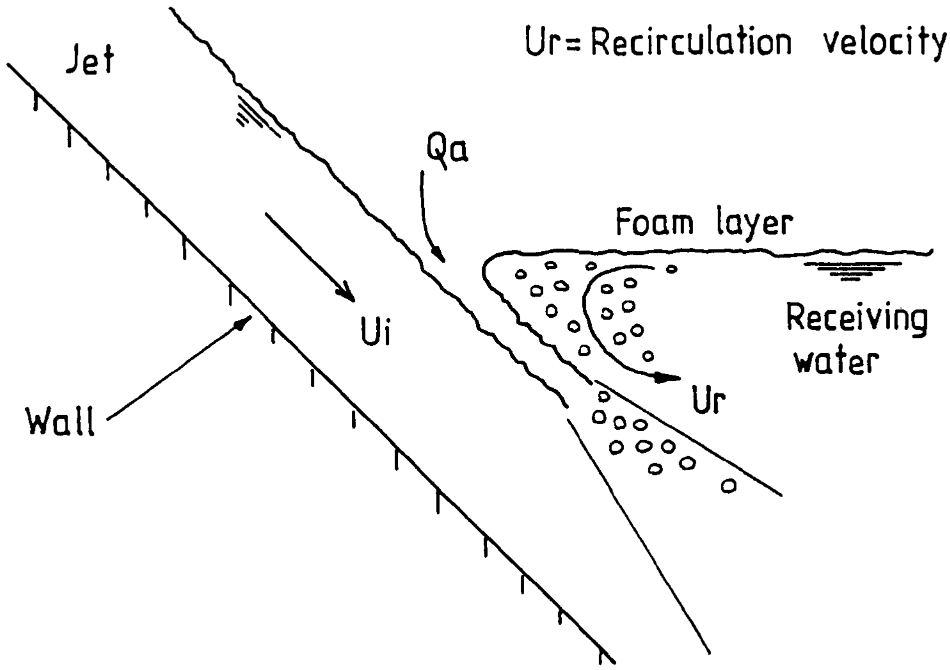

Fig.2·50 AIR ENTRAINMENT OF POOL BY HIGH VELOCITY WALL JET.

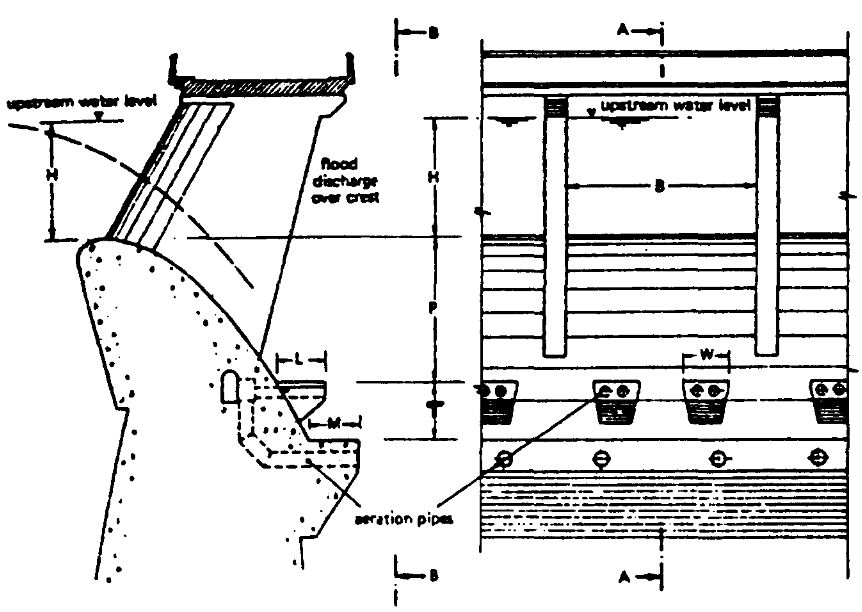

Fig. 2·51 ARRANGEMENT OF CREST SPLITTERS (Mason).

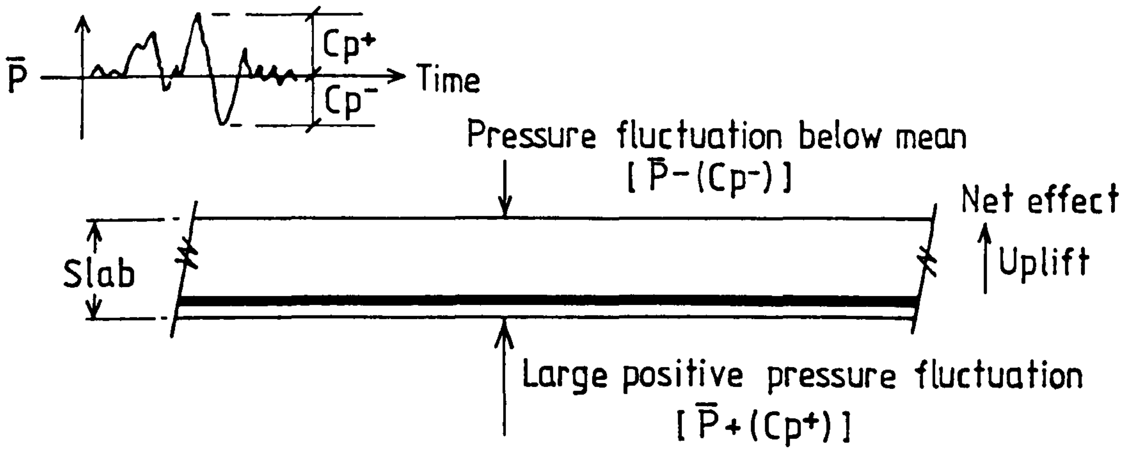

Fig.2·52 POSSIBLE LOADING ON POOL FLOOR SLAB.

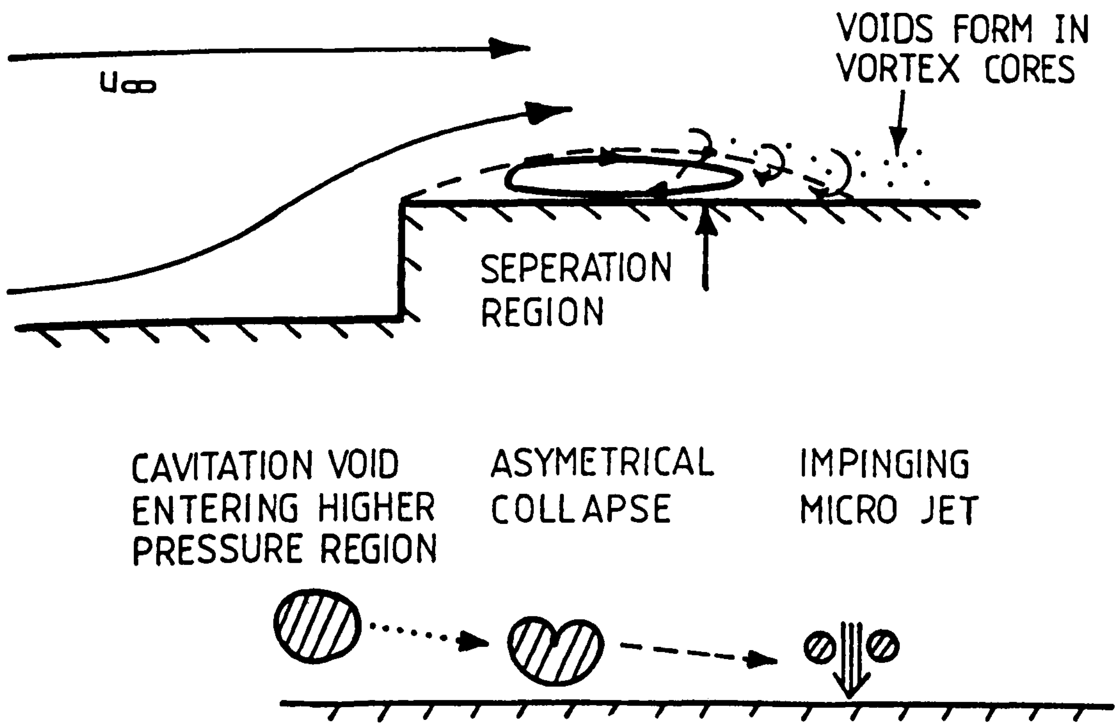

Fig.2·53 FORMATION AND COLLAPSE OF CAVITATION VOID.

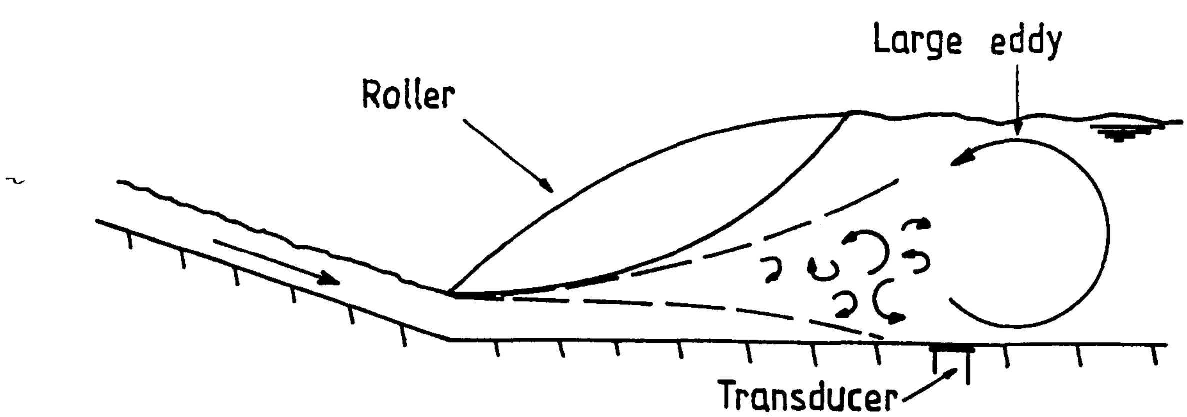

Fig. 2·54 HYDRAULIC JUMP SHOWING EDDY AND TRANSDUCER.

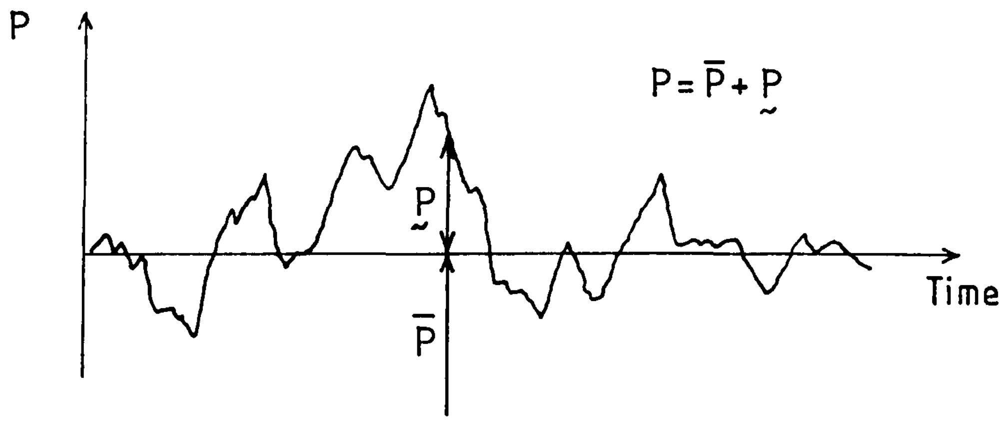

Fig. 2·55 TRACE OF PRESSURE FLUCTUATIONS WITH TIME.

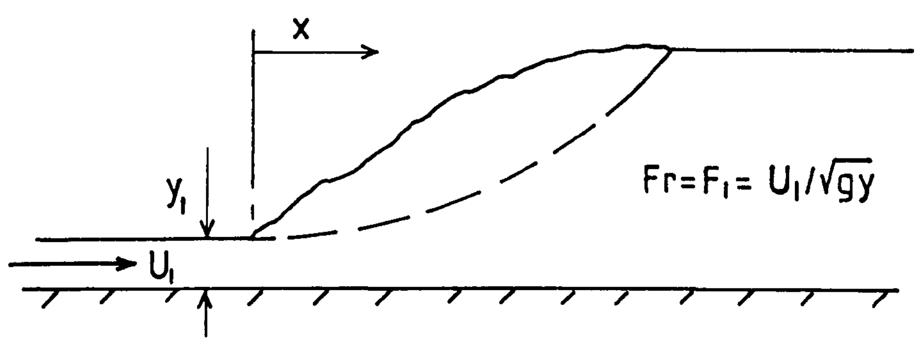

Fig. 2·56(a) DEFINITION SKETCH FOR HYDRAULIC JUMP FIGURES.

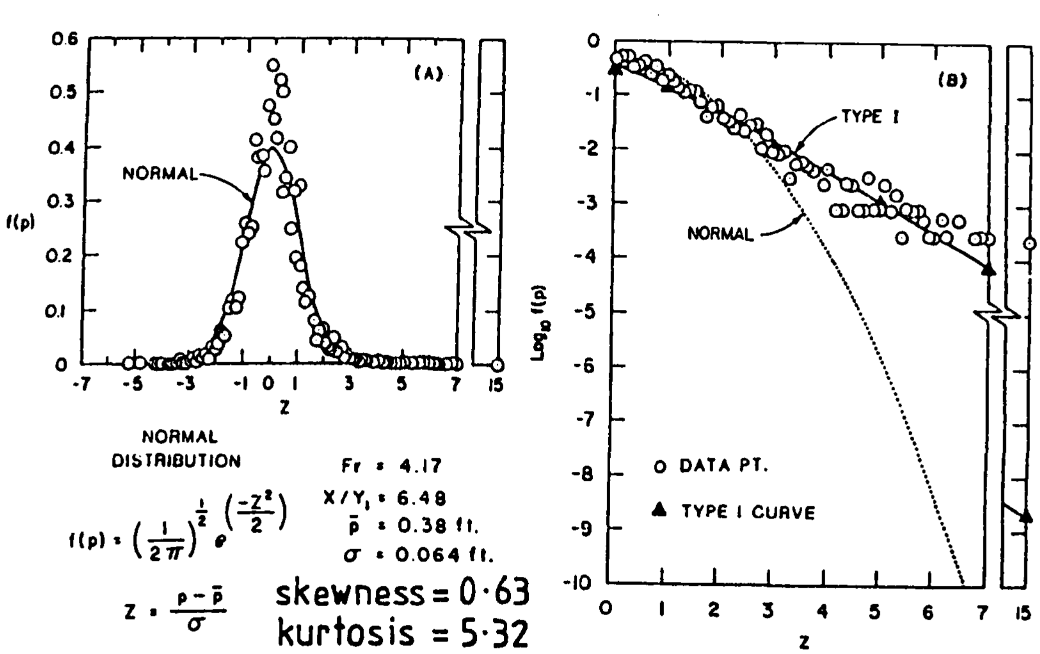

Fig. 2·56(b) PROBABILITY DENSITY FUNCTION OF PRESSURE FLUCTUATIONS BENEATH HYDRAULIC JUMP [Toso].

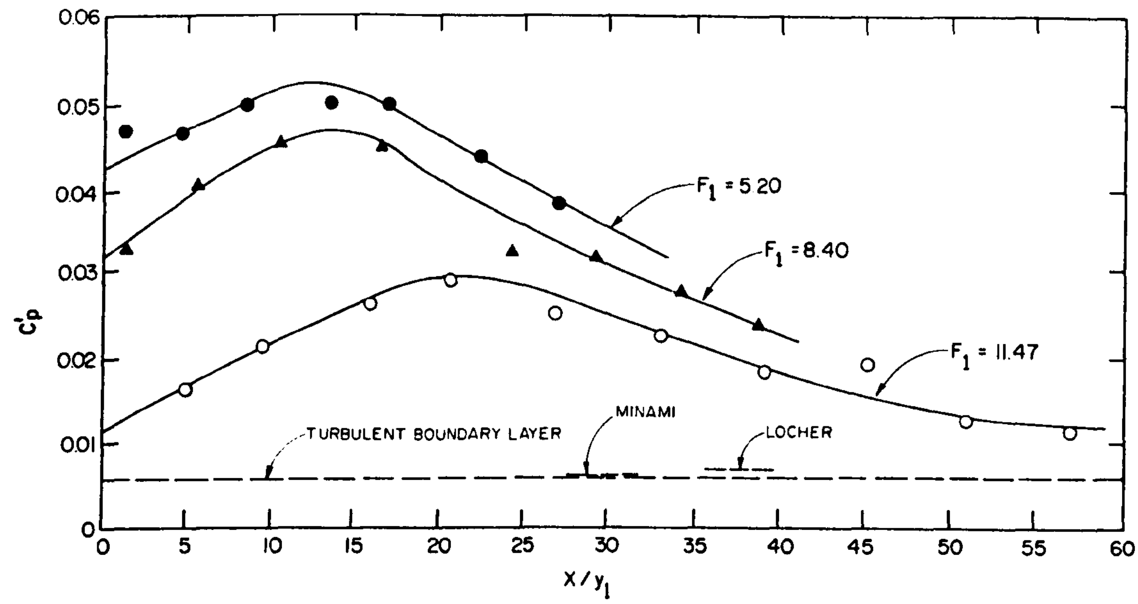

Fig.2·57 PRESSURE FLUCTUATIONS UNDER A FREE HYDRAULIC JUMP (Akbari et al.[83]).

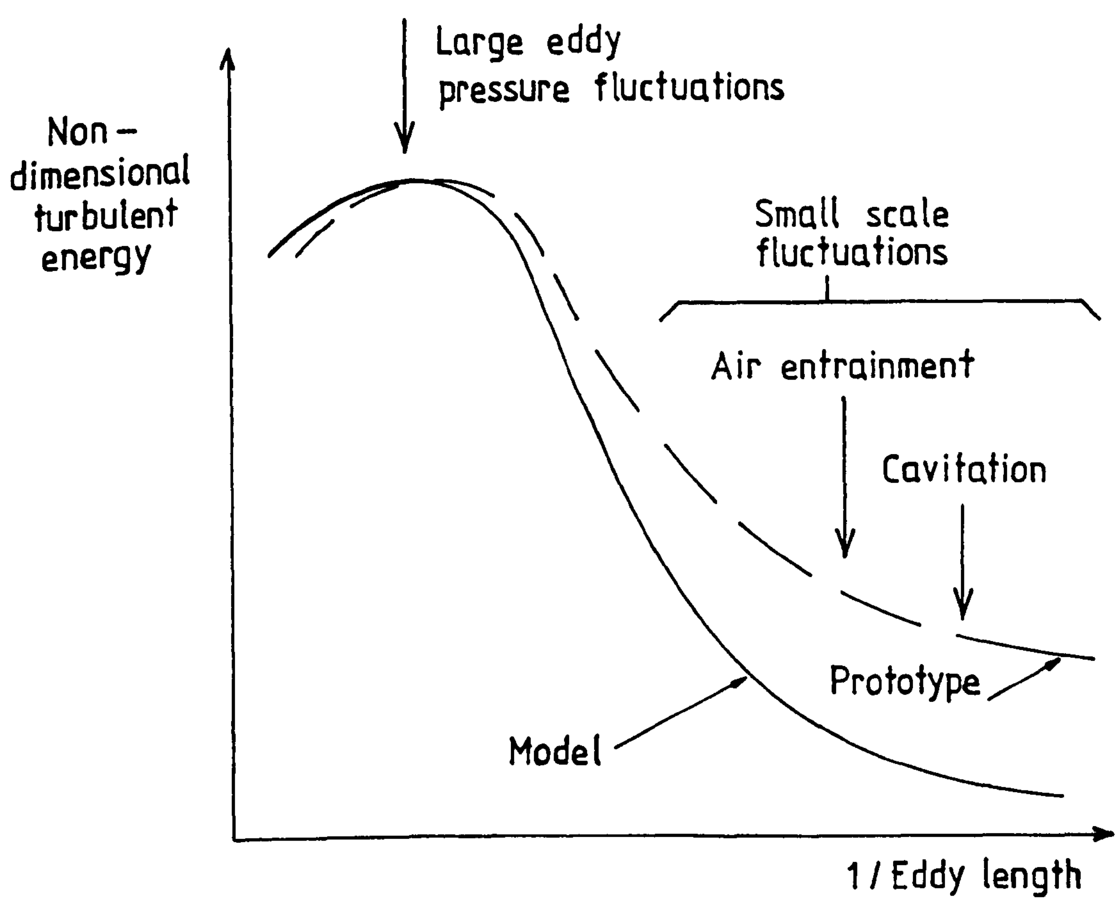

Fig. 2·58 TURBULENT SPECTRUM — MODEL/PROTOTYPE.

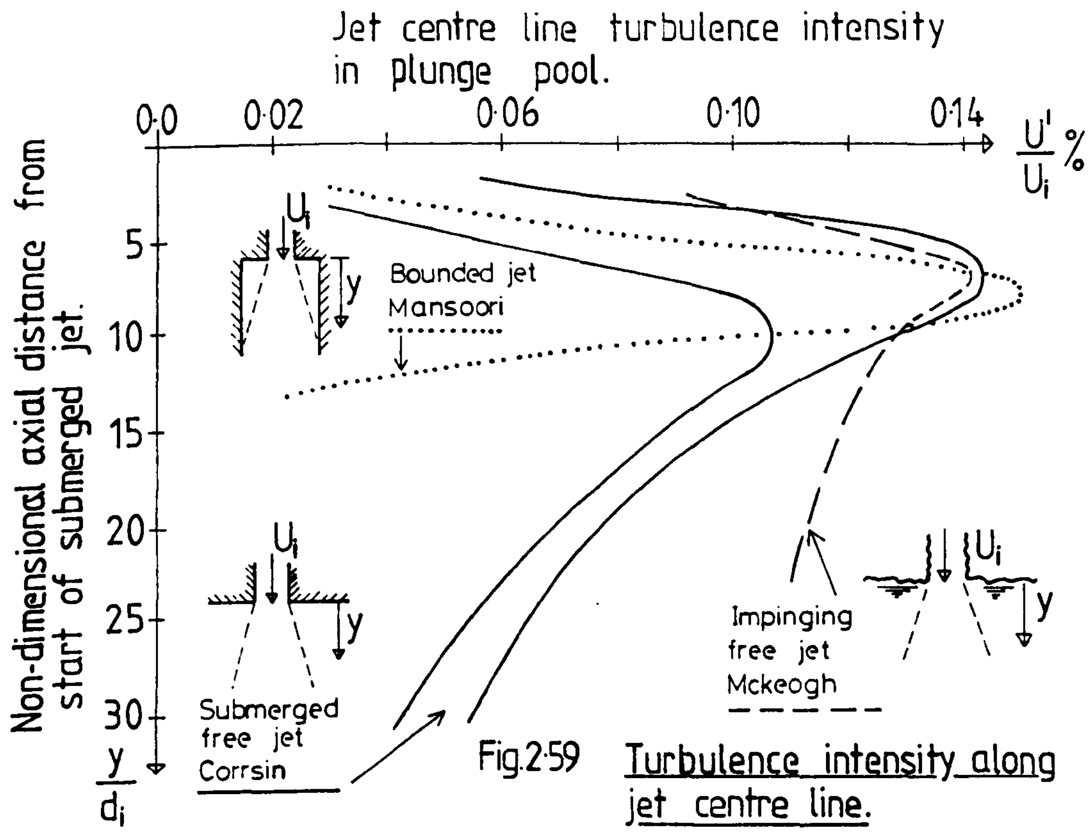

Fig.2.59 Turbulence intensity along jet centre line.

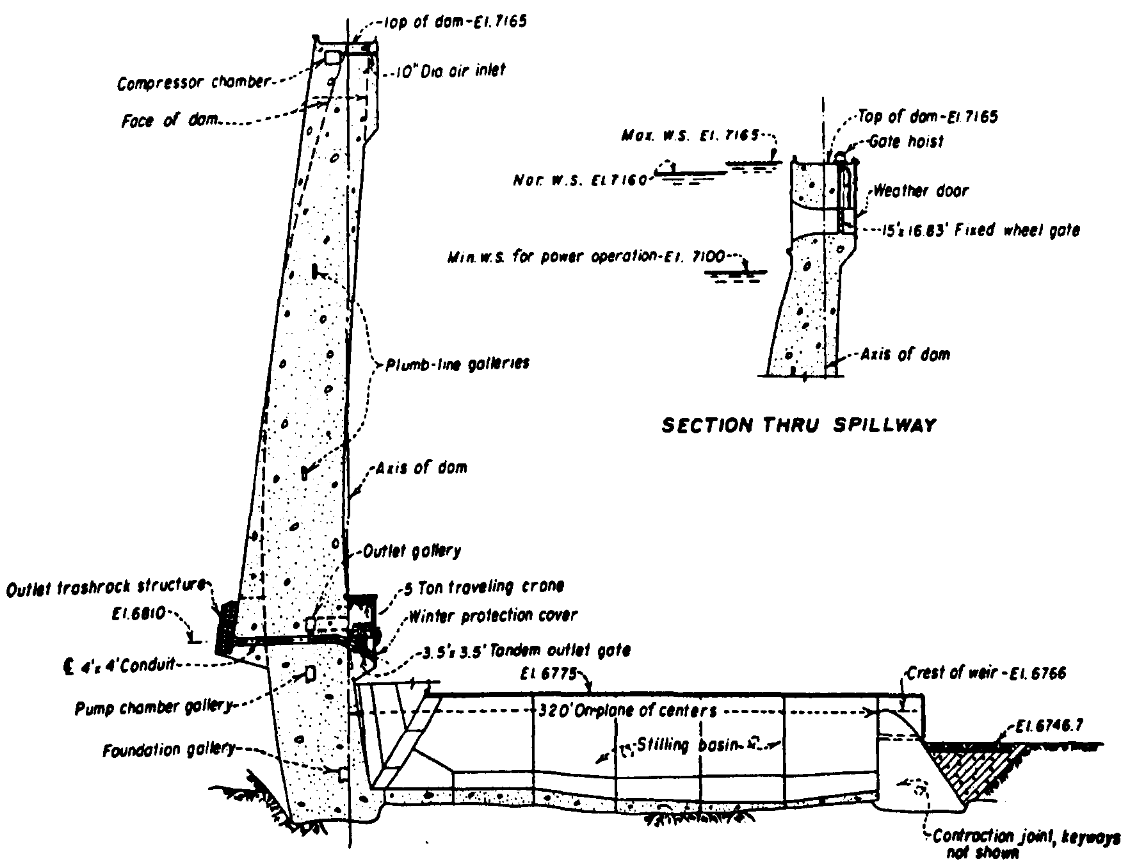

Fig. 2·60 SECTION THROUGH MORROW POINT DAM AND STILLING BASIN.

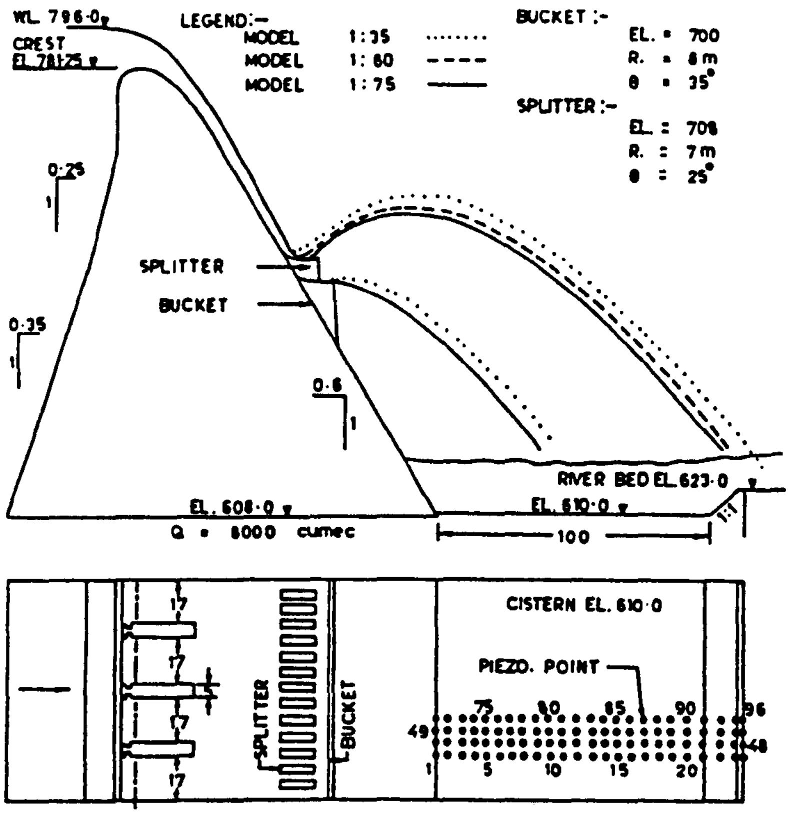

Fig. 2·61 SECTION AND PLAN OF LAKHWAR DAM MODEL.
(Bhargava et al.)

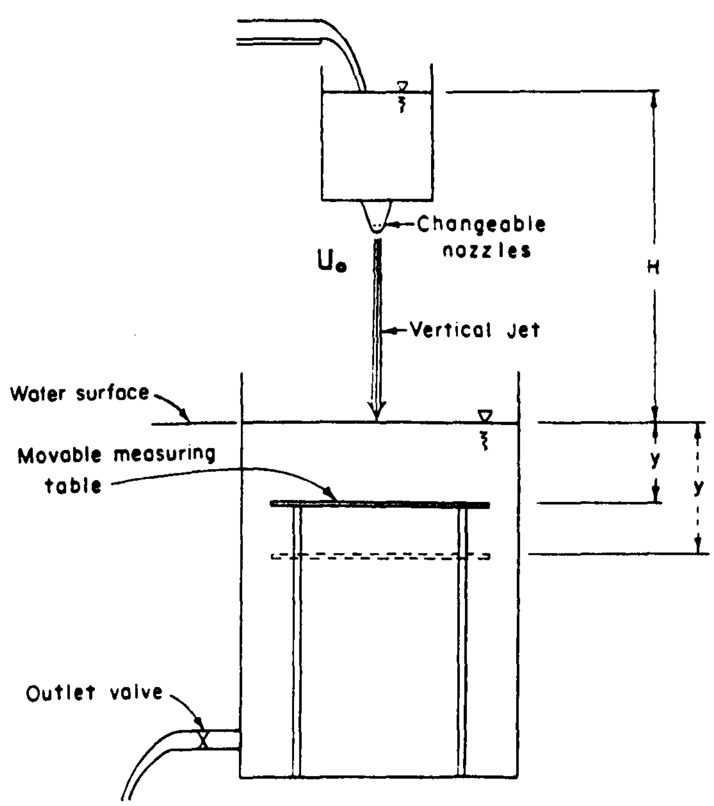

Fig. 2·62 SKETCH OF HÄUSLER'S APPARATUS.

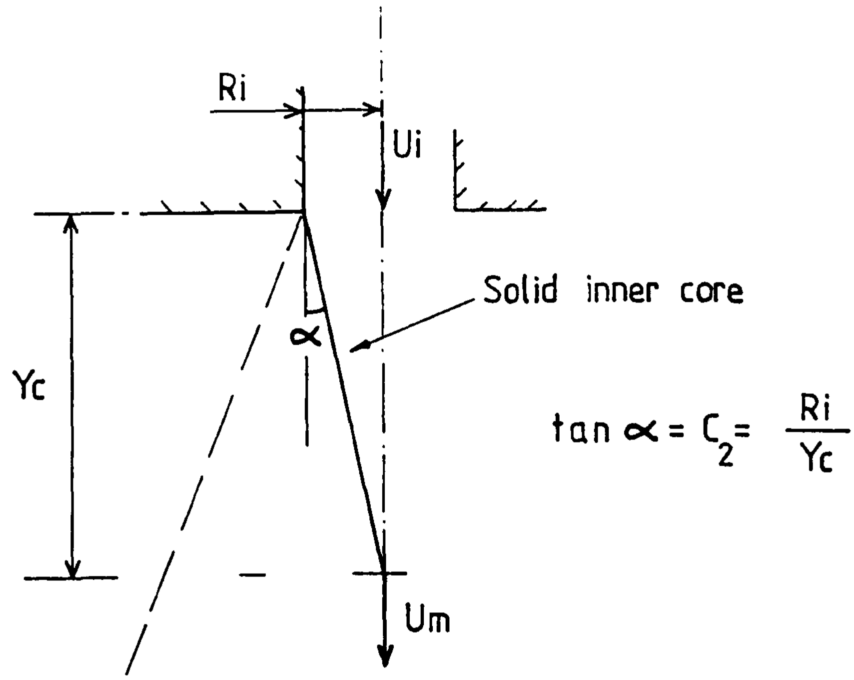

Fig. 2·63 JET CORE LENGTH AND CONVERGENCE ANGLE.

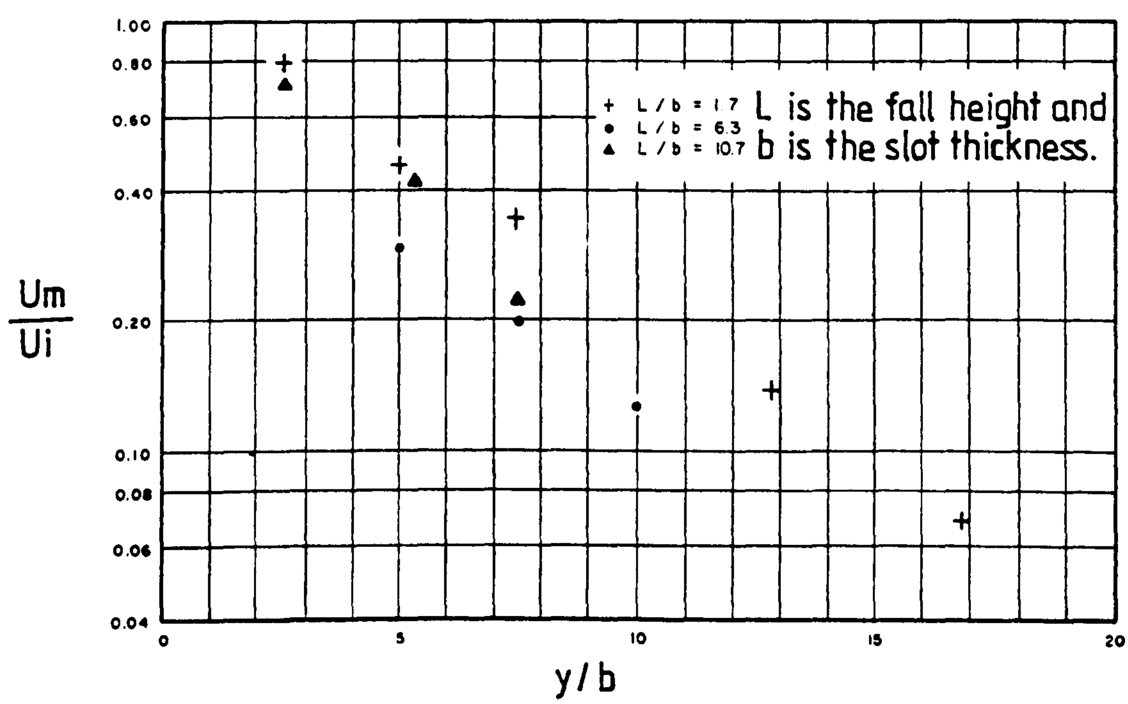

Fig. 2·64 CENTRE LINE VELOCITY DECAY OF JET PLUNGING THROUGH AIR INTO WATER (Lencastre).

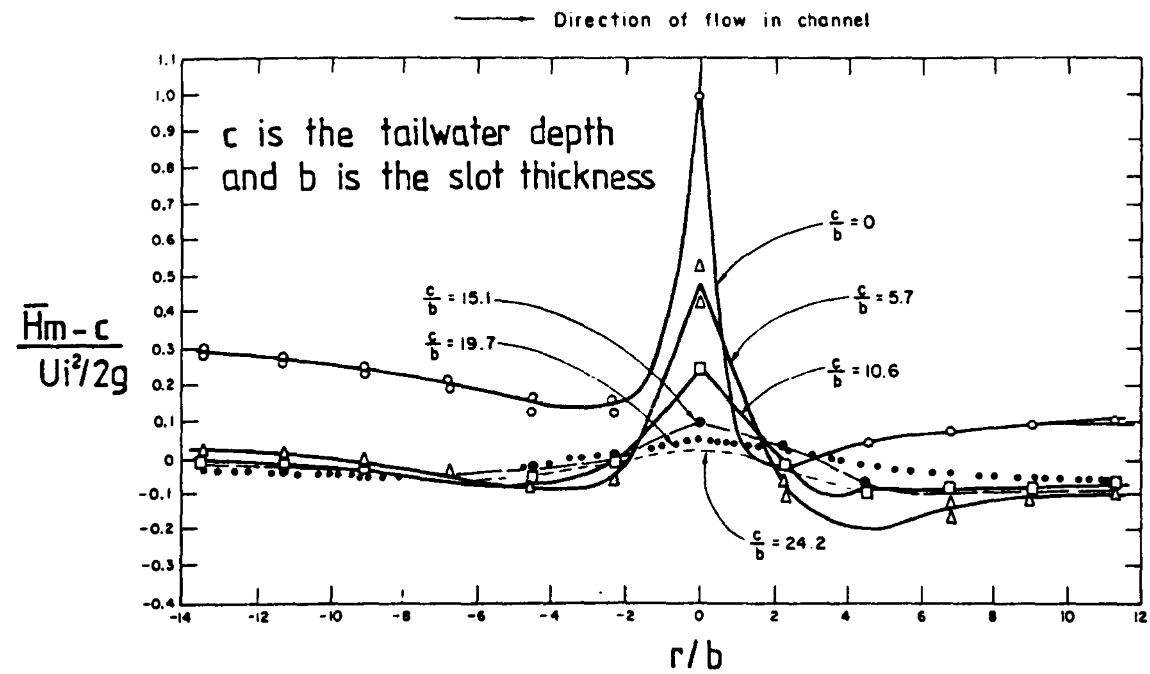

Fig.2·65 DISTRIBUTION OF PRESSURE ON BOTTOM OF PLUNGE BASIN (Lencastre).

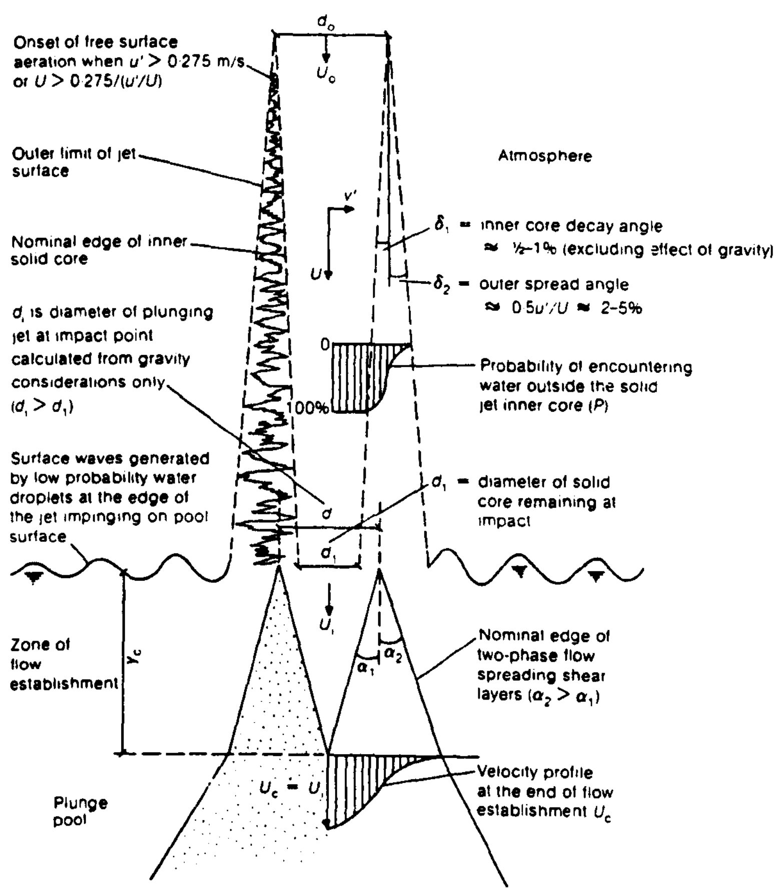

Fig.2·66 JET IN ATMOSPHERE AND IN PLUNGE POOL (Ervine and Falvey).

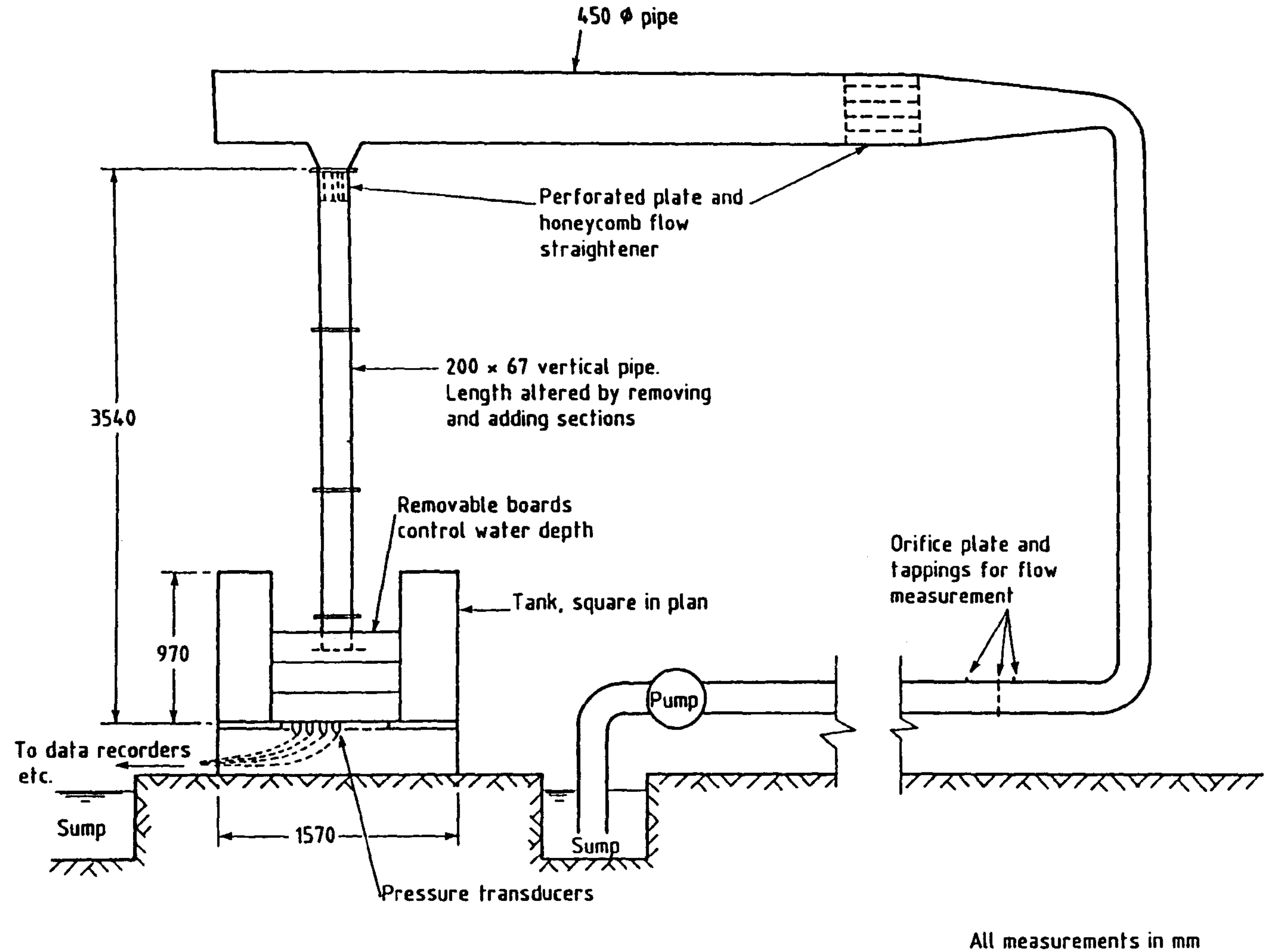

Fig.2·67 LAYOUT OF EXPERIMENTAL RIG (H.R.Ltd)

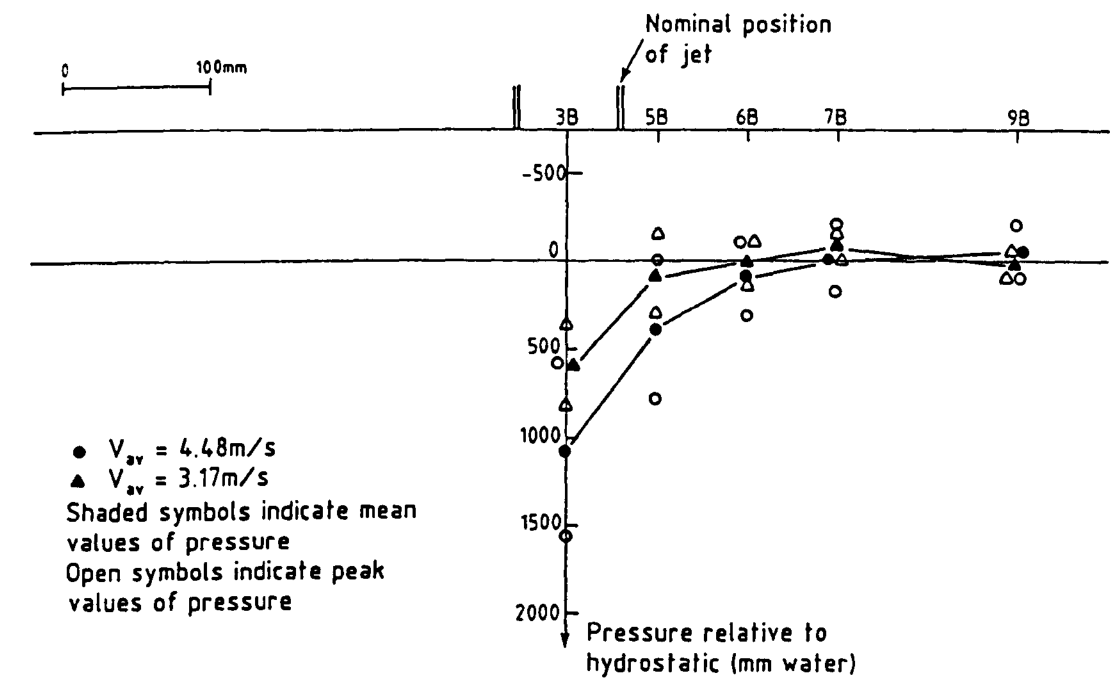

Fig.2·68 DYNAMIC PRESSURES DUE TO SUBMERGED JETS (H.R.Ltd.)

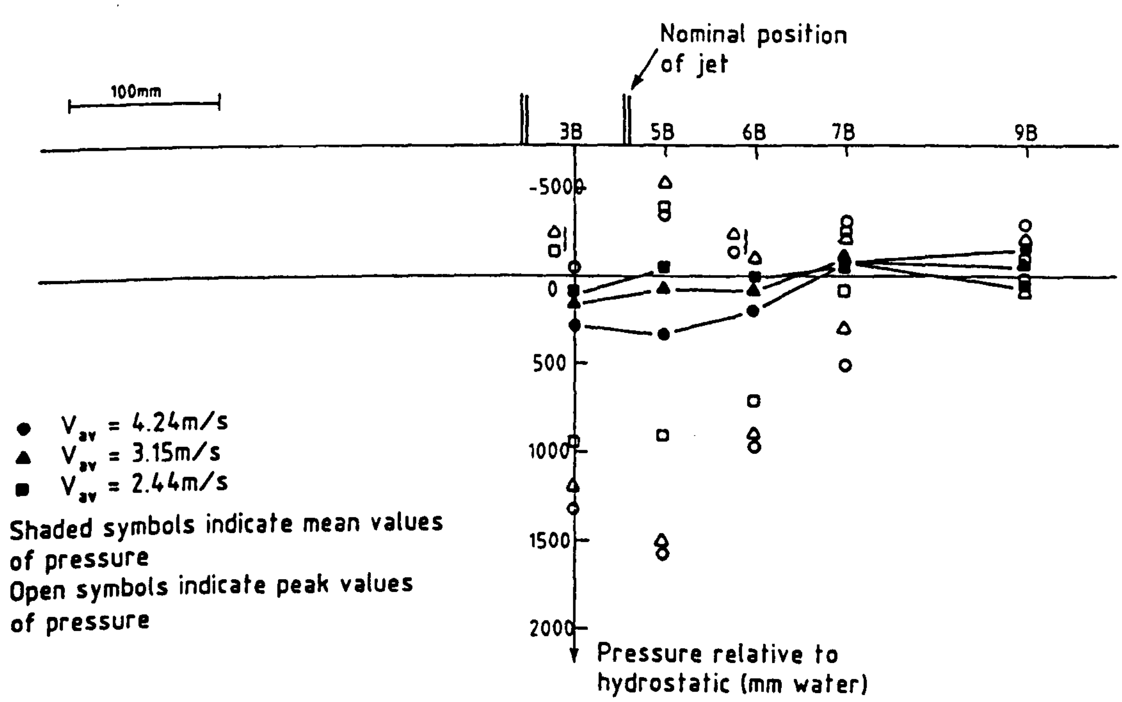

Fig.2·69 DYNAMIC PRESSURES DUE TO PLUNGING JETS (H.R.Ltd.)

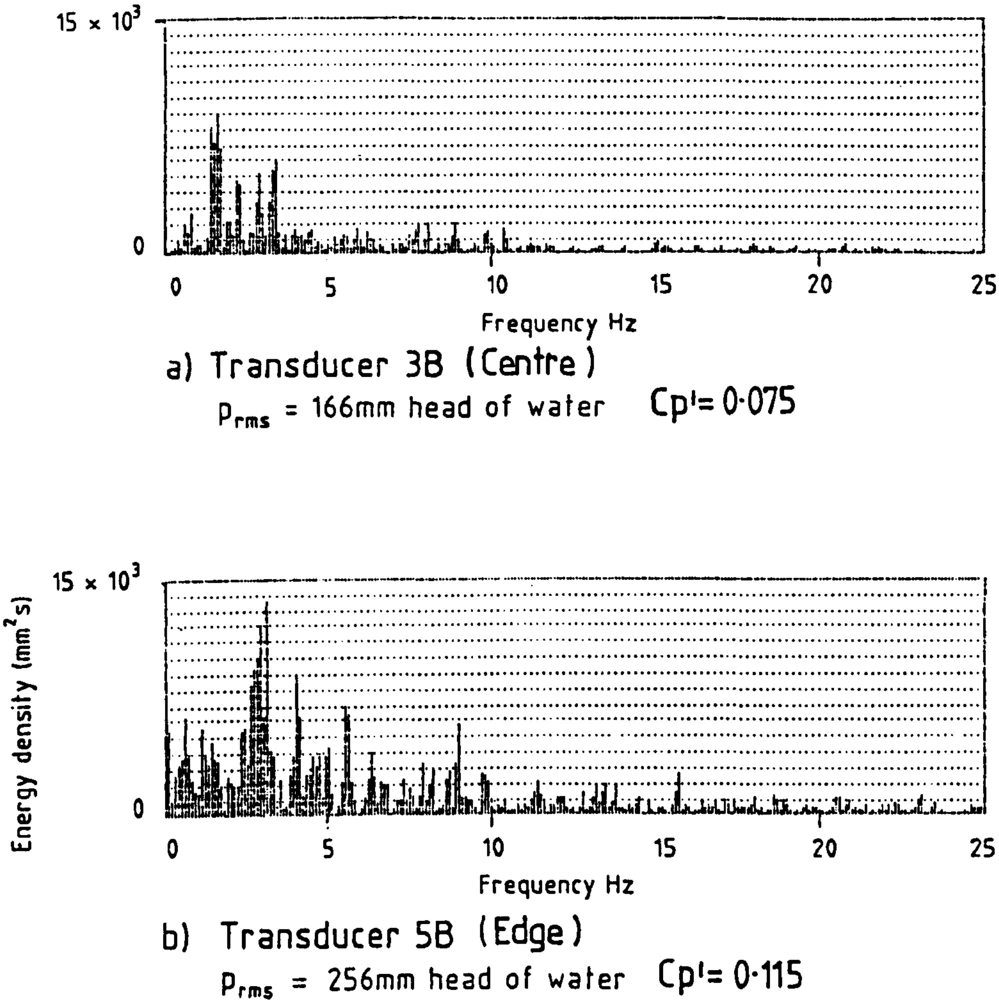

Fig.2·70 DYNAMIC PRESSURE SPECTRA FOR PLUNGING JET, Ui≃6·6m/s

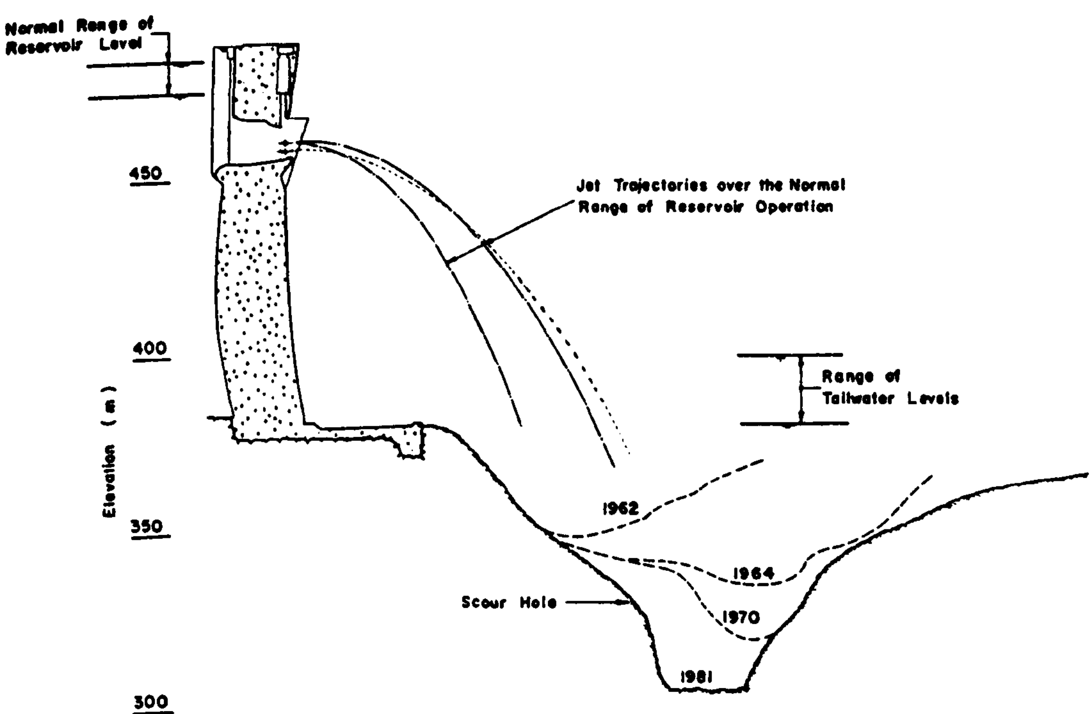

Fig.2·71 DETAIL OF SCOUR HOLE DEVELOPMENT AT KARIBA DAM.

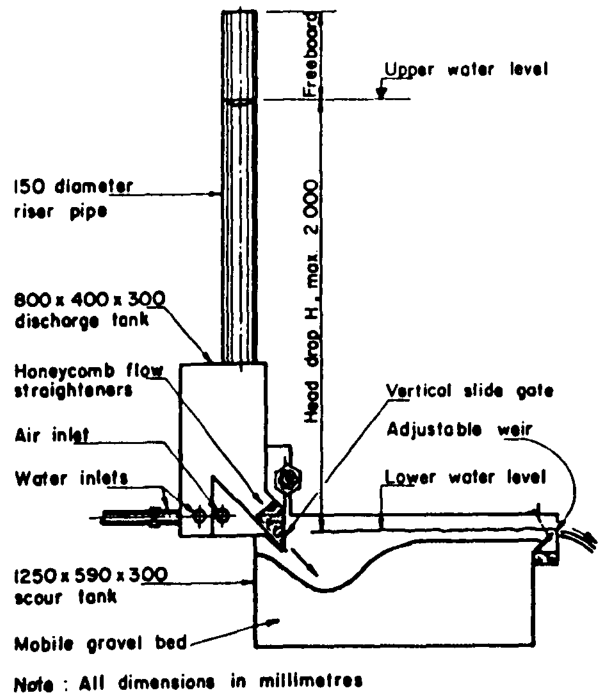

Fig. 2·72 ELEVATION ON PRINCIPAL COMPONENTS OF SCOUR APPARATUS (Mason).

TABLE & FIGURES FOR CHAPTER 3

D_0 (mm)	V_0 m/s	Fro	Reo x 10^5	Weo	L (mm)	L/Do	Y/Do
78	1.5-13	1.7-15	1 - 9.0	50-426	2230-2630	29-34	1.3-6.4
	"	"	"	"	725-1125	9-14	"
52.5	3 - 15	4 - 21	1.4-6.8	81-403	2126-2526	40-48	2-9.5
	"	"	"	"	620-1020	12-19	"
25	3 - 25	6 - 50	0.65-5.0	56-464	2018-2418	81-97	4-20
	"	"	"	"	513-913	21-37	"
orifice 25	"	"	"	"	1020-1420	41-57	"
Approx. Range	1.5-25	1.7-50	0.65-10	50-450	513-2630	9-97	1.3-20

Note : Pool depth (Y) varied from 100 to 500mm in all cases.

Table 3.1 Range of test parameters.

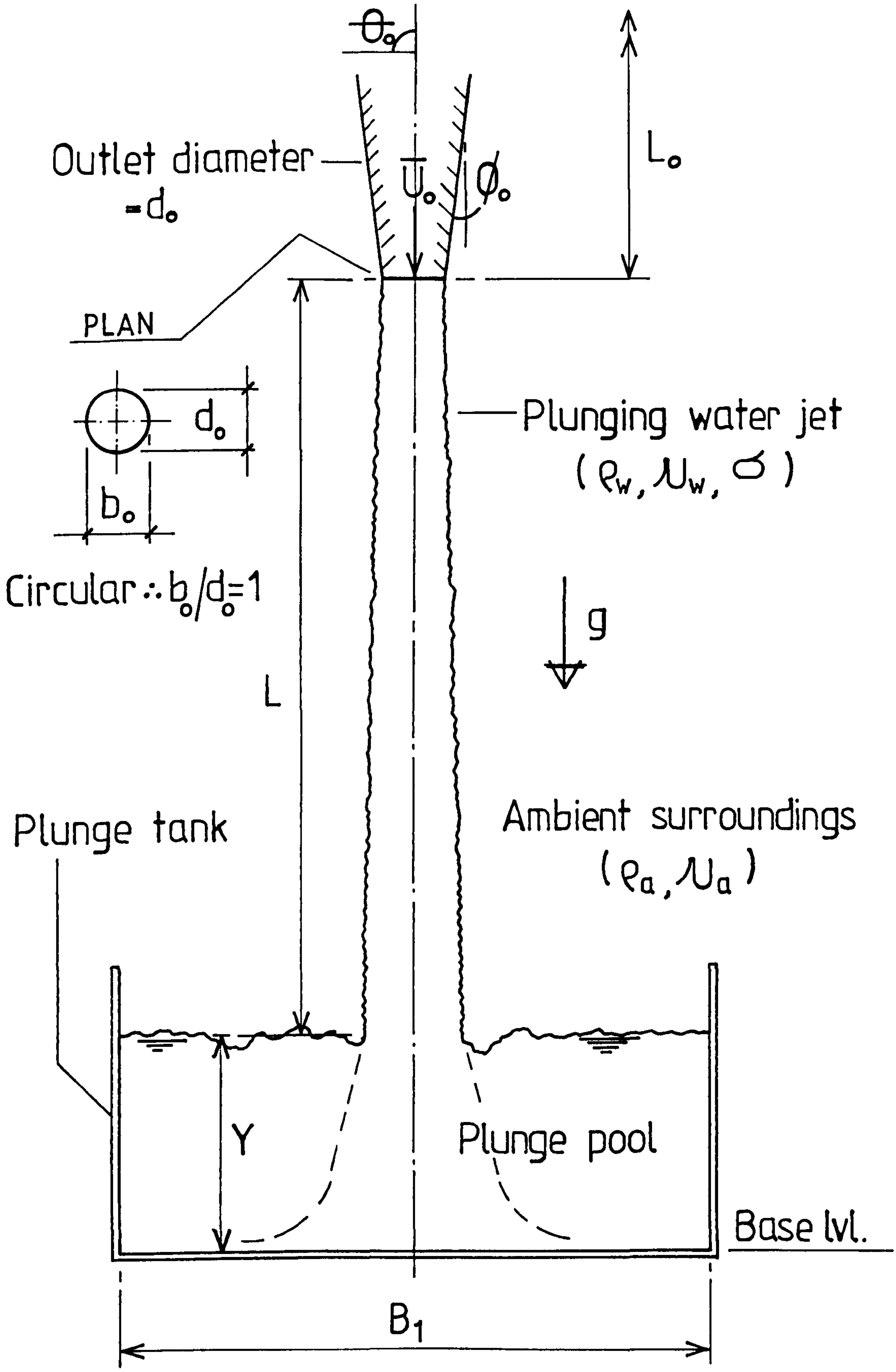

Fig. 3·1 DEFINITION SKETCH OF PHYSICAL PARAMETERS

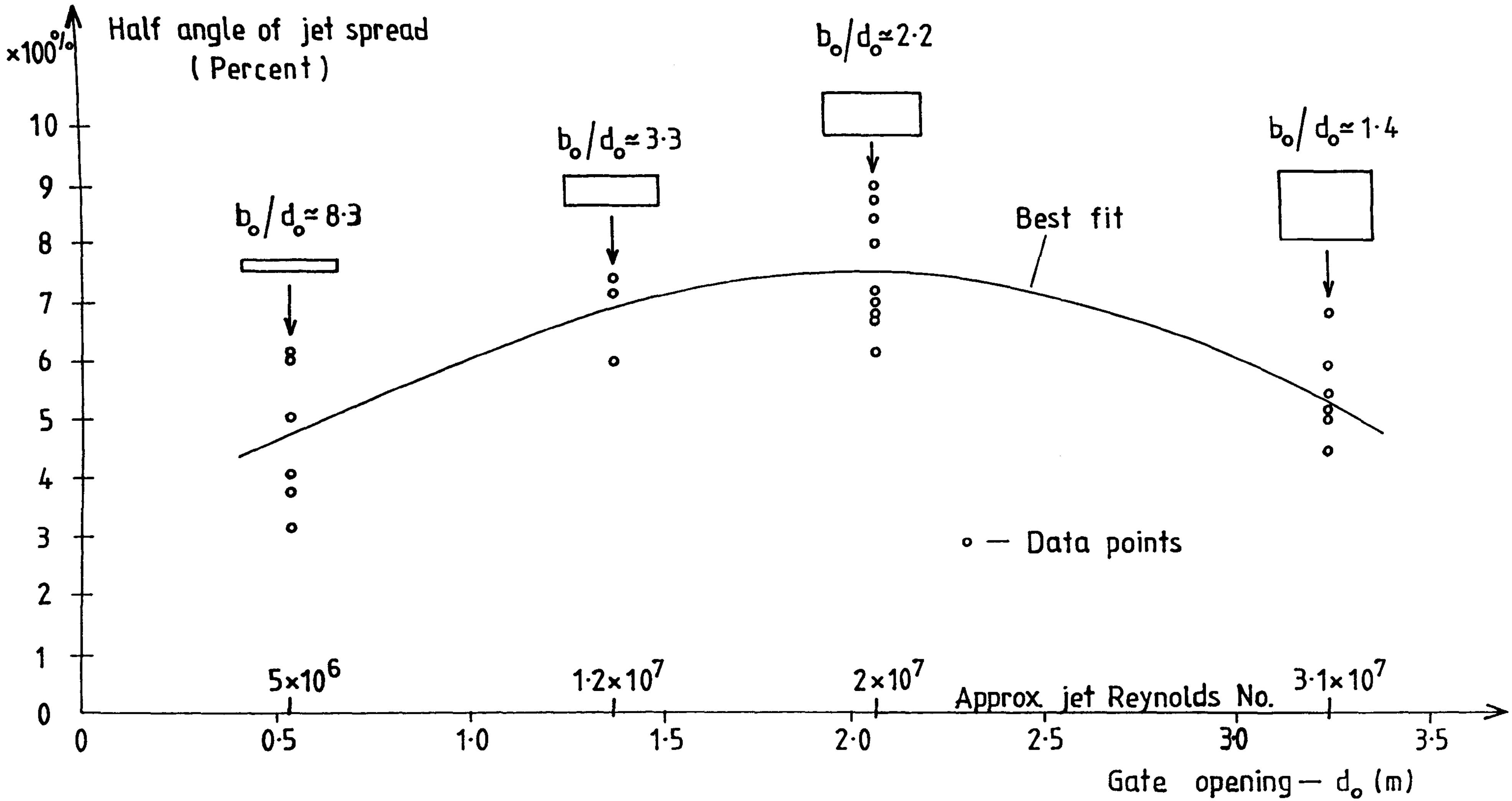

Fig. 3·2 MORROW POINT DAM — APPROX. HALF ANGLE OF SPREAD OF PLUNGING JETS. OUTLET VELOCITY APPROX. CONSTANT ($U_o = 9 \rightarrow 9{\cdot}6$ m/s)

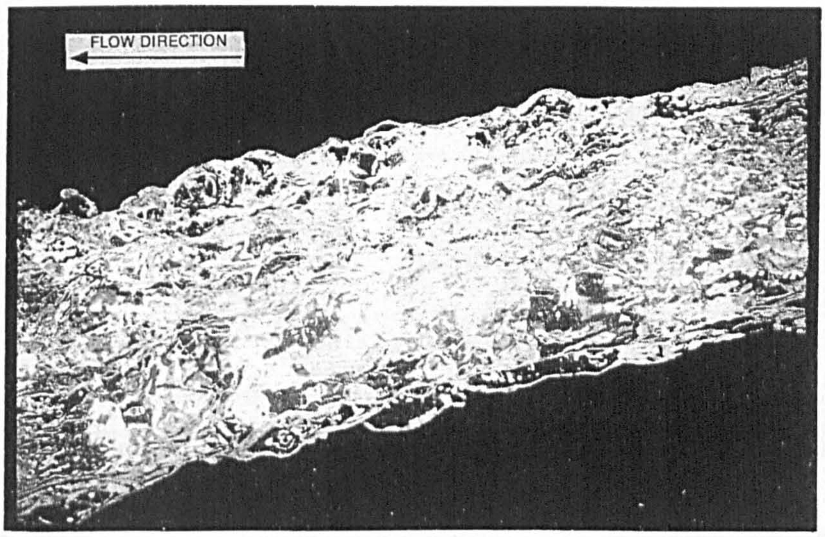

Fig. 3·3 TURBULENT JET : $D_o = 100$ mm, $U = 5$ m/s, $Re = 4 \times 10^5$

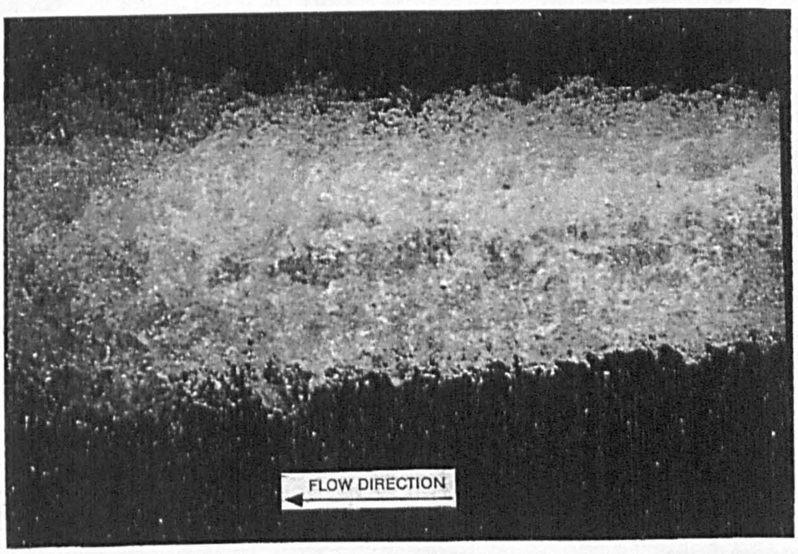

Fig. 3·4 TURBULENT JET : $D_o = 100$ mm, $U = 25$ m/s, $Re = 2 \times 10^6$

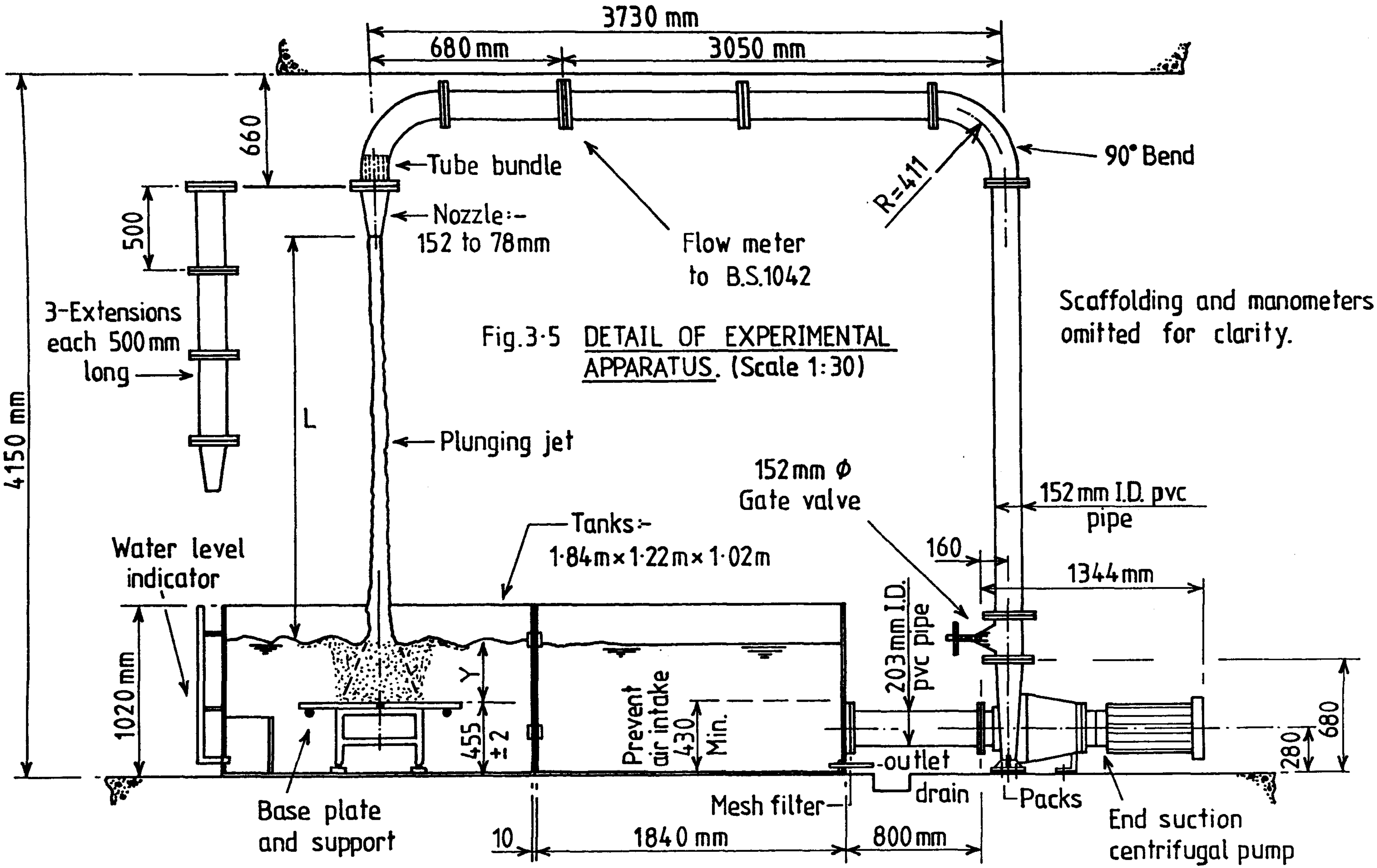

Fig.3·5 DETAIL OF EXPERIMENTAL APPARATUS. (Scale 1:30)

Fig.3·6 END ELEVATION OF EXPERIMENTAL APPARATUS.

Fig.3·7 VIEW OF PUMP, GATE VALVE AND RISING PIPEWORK.

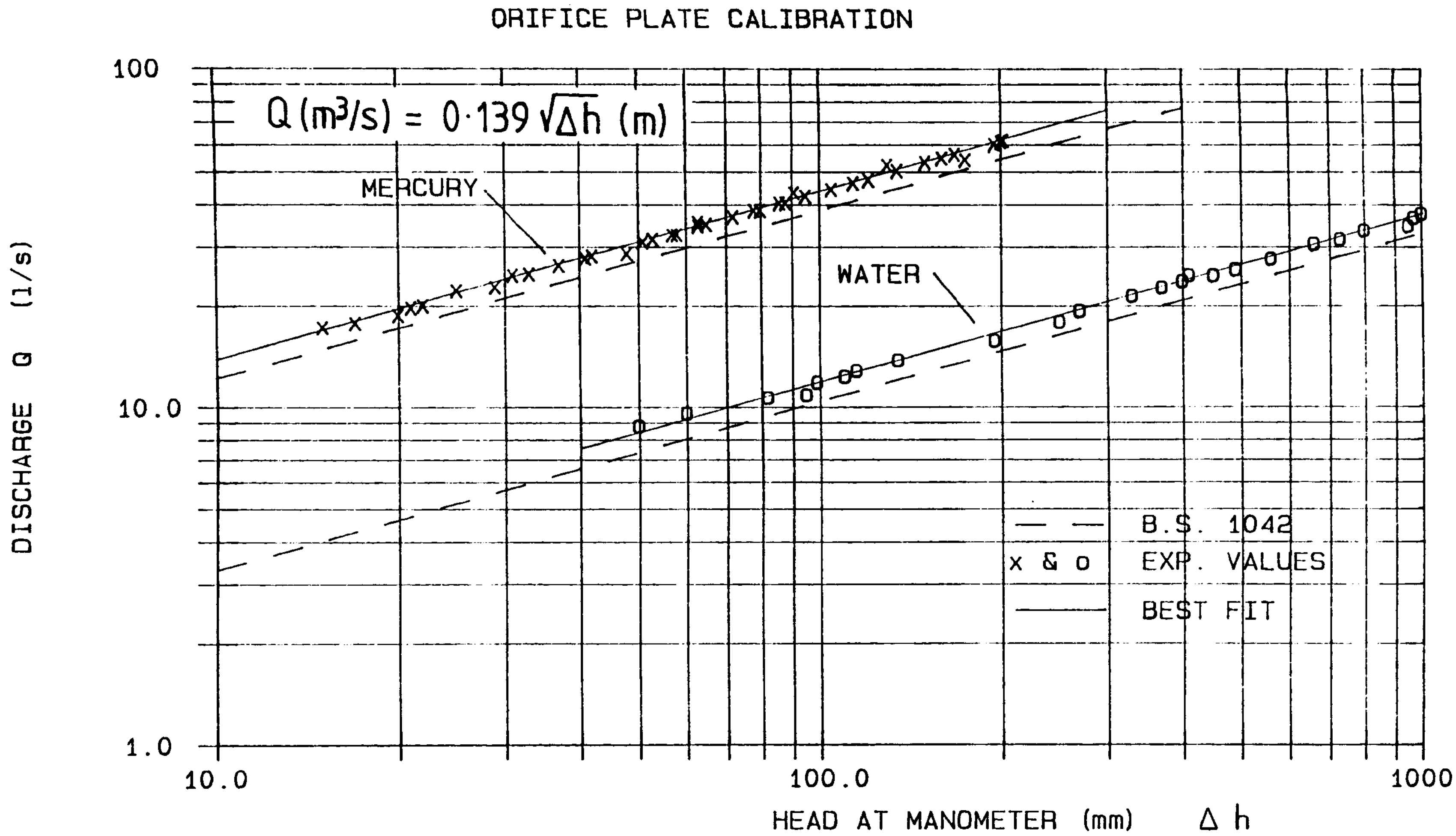

Fig. 3.8 THEORETICAL AND EXPERIMENTAL HEAD-DISCHARGE RELATIONSHIP

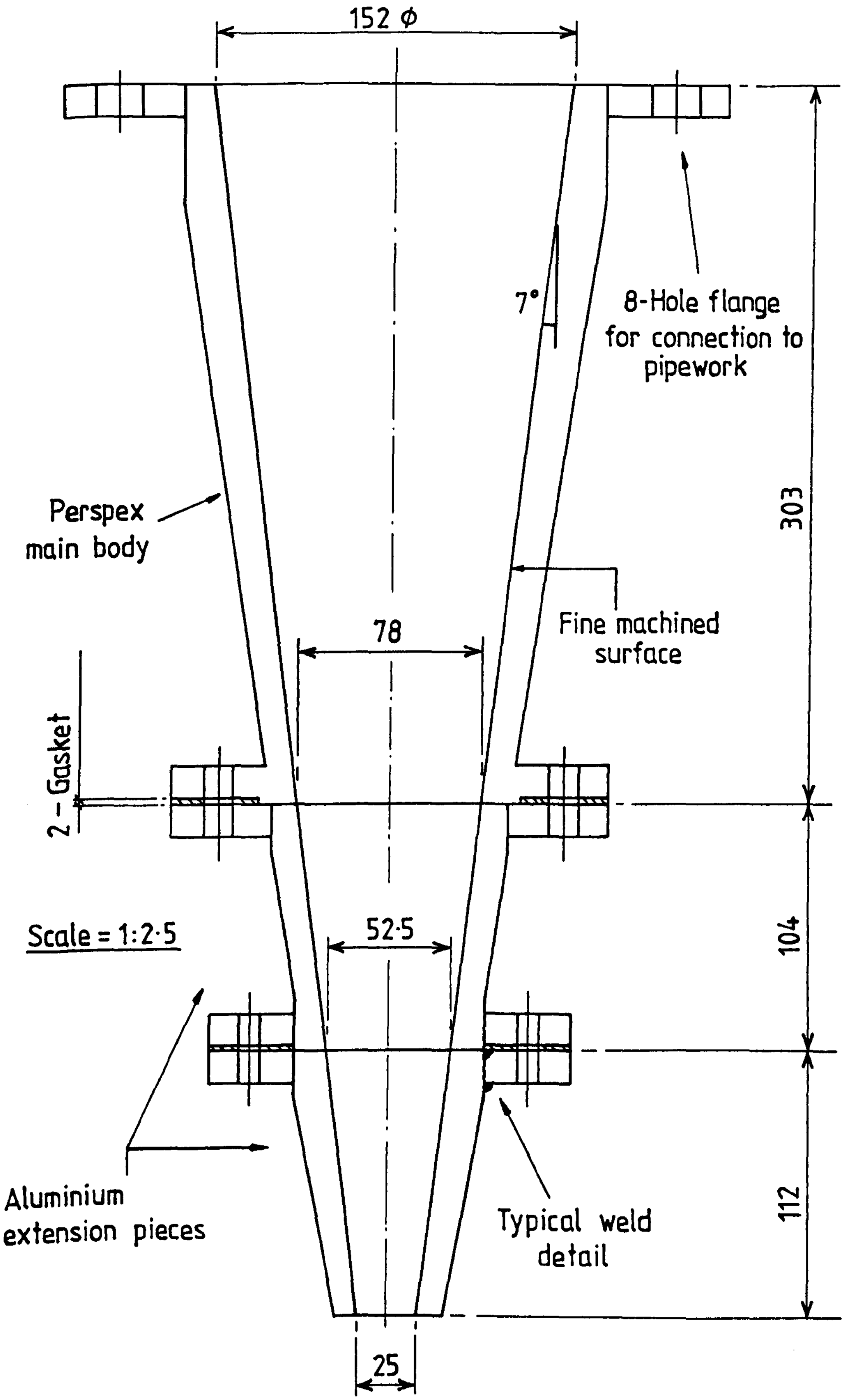

Fig. 3·9 FINAL OUTLET NOZZLE ARRANGEMENT.
(All dimensions in mm.)

Fig.3·10 VIEW OF NOZZLE ATTACHED TO PIPEWORK.

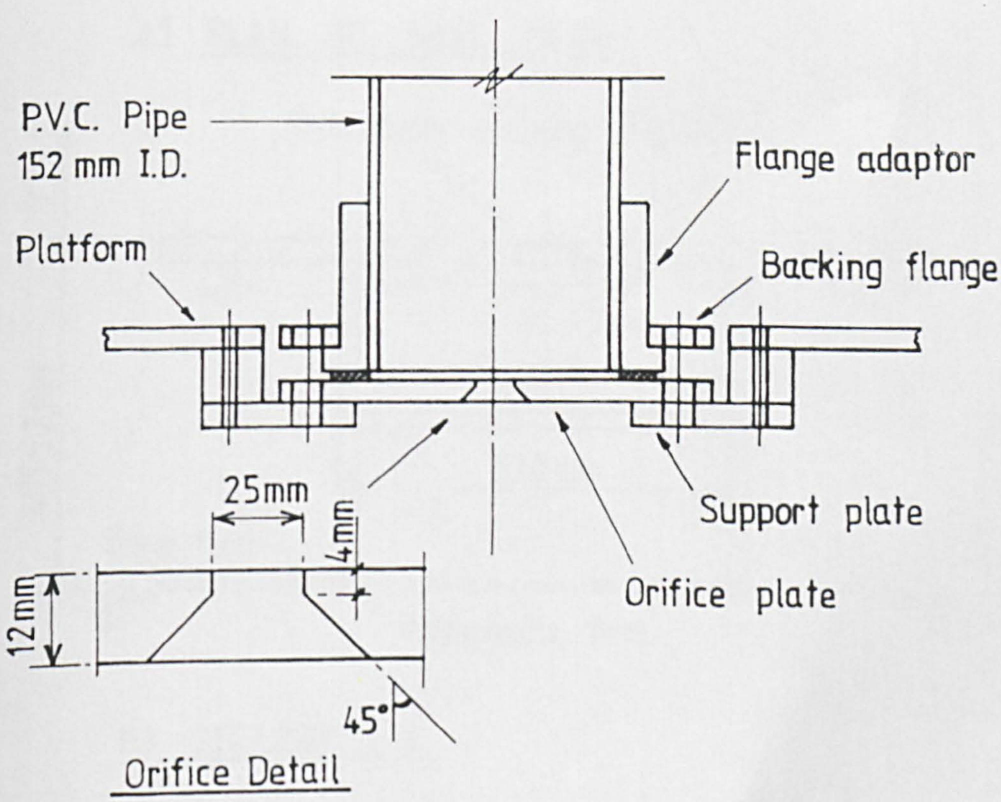

Fig.3·11 SECTION THROUGH ORIFICE AND OUTLET SUPPORT.

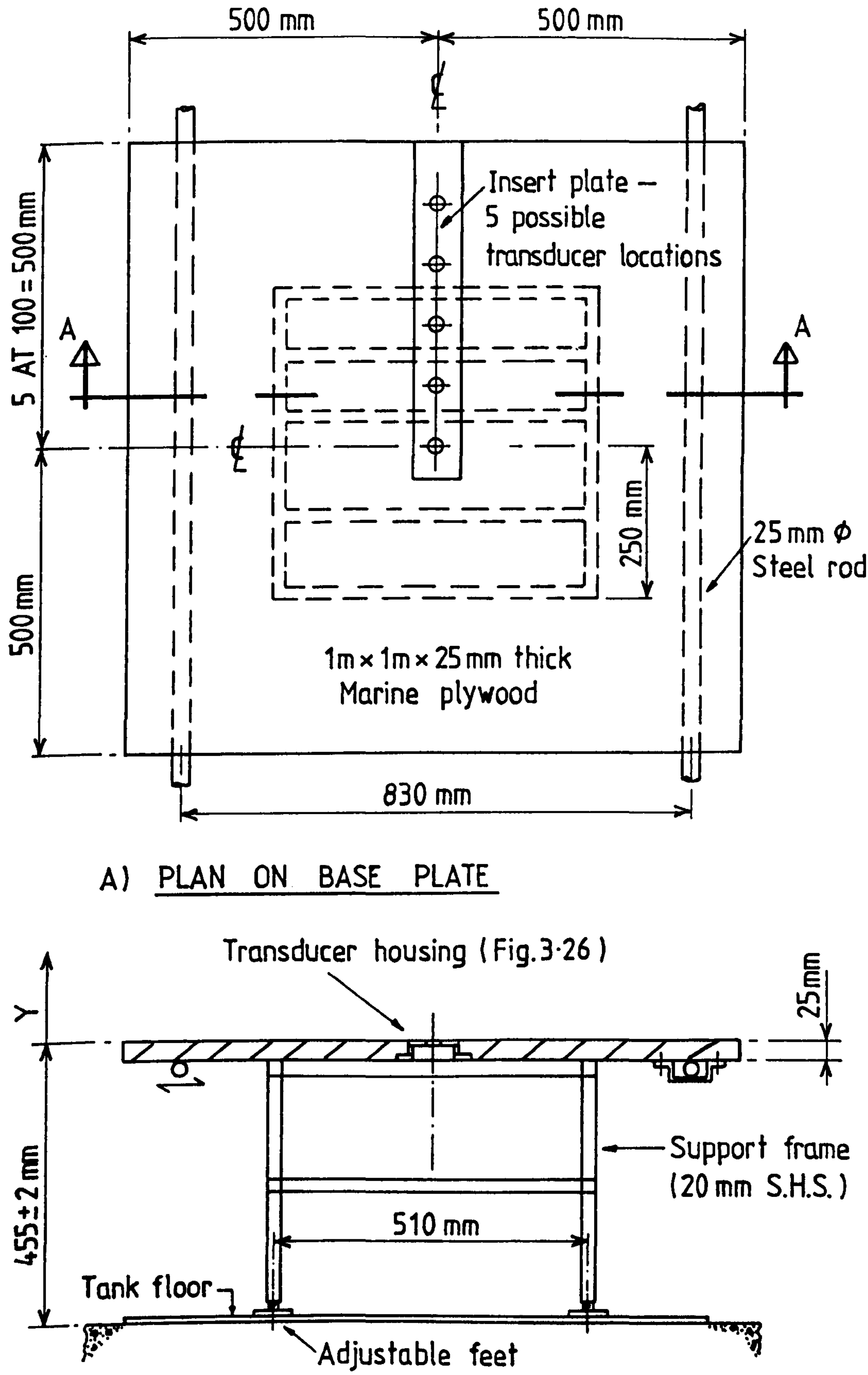

A) PLAN ON BASE PLATE

B) SECTION A-A

Fig. 3·12 PLAN AND SECTION OF PLUNGE TANK BASE PLATE.

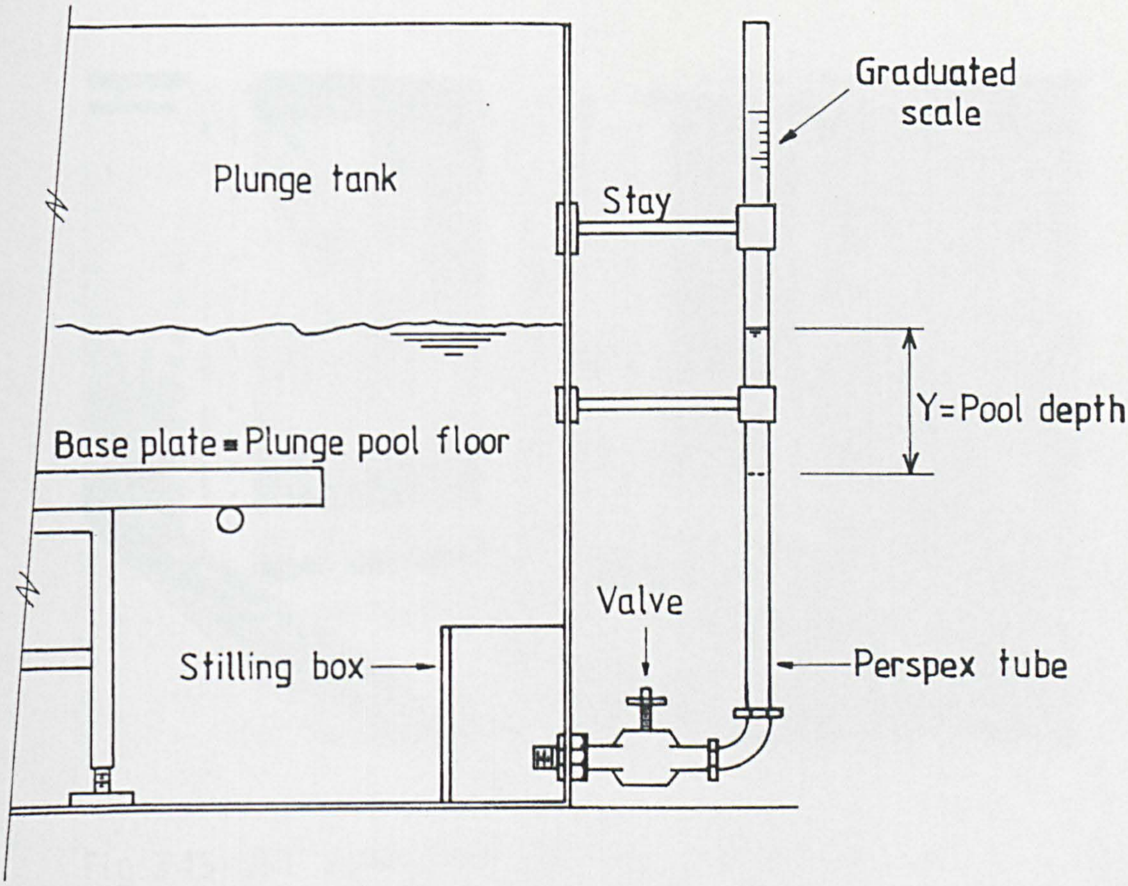

Fig. 3·13 VIEW OF WATER LEVEL INDICATOR.

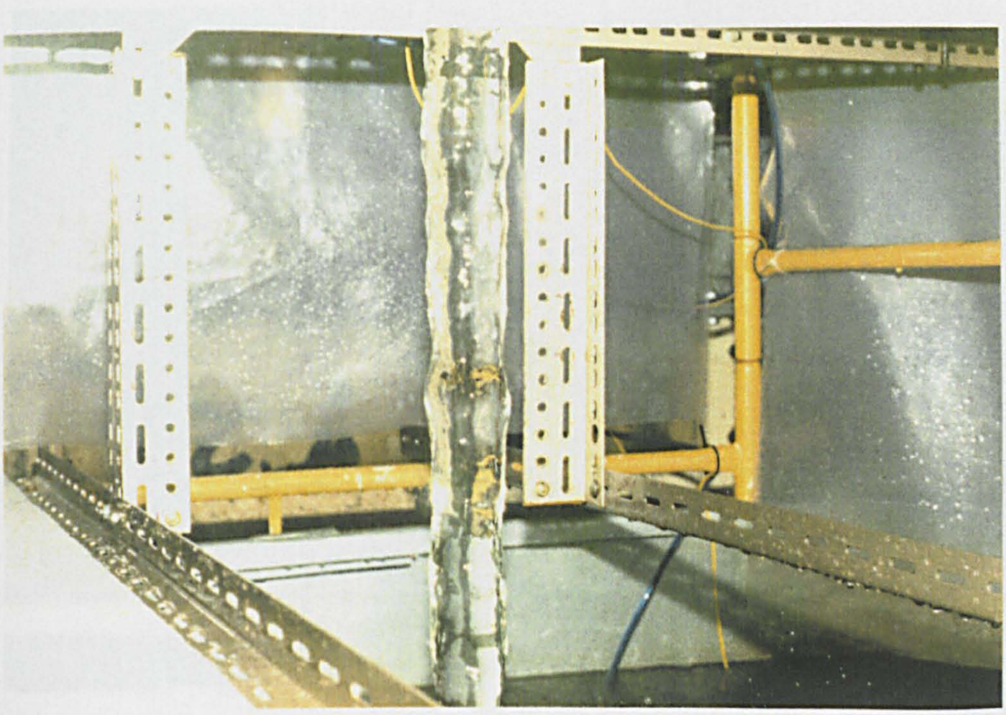

Fig. 3·14 JET CONDITION IN THE ATMOSPHERE.
(Do = 78 mm , Uo ≃ 3 m/s)

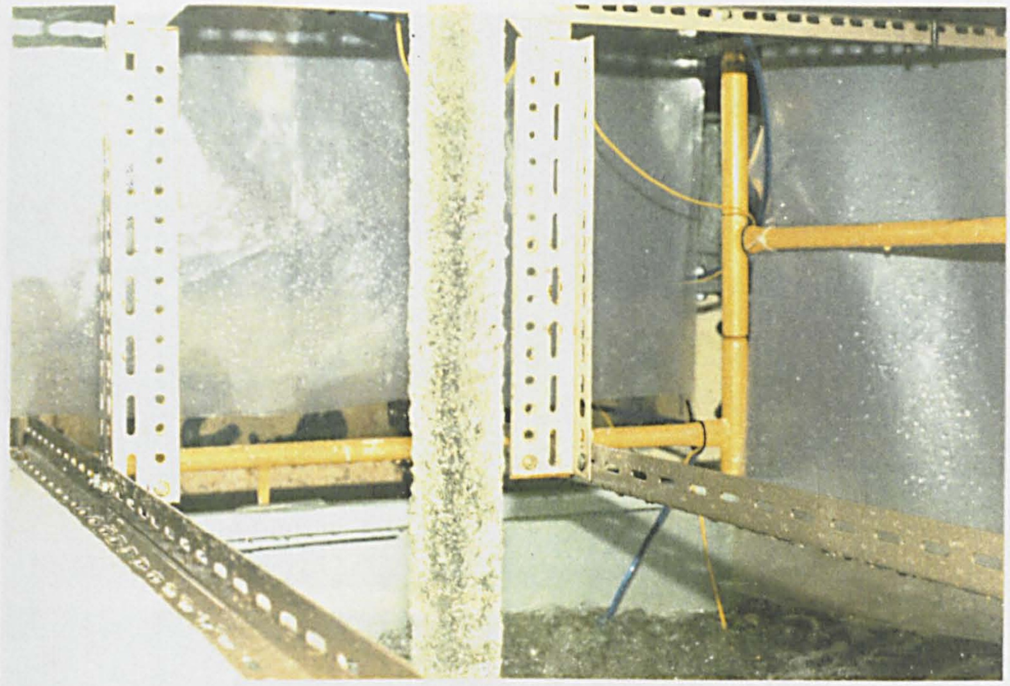

Fig.3·15 JET CONDITION IN THE ATMOSPHERE.
(Do=78 mm , Uo≃ 9 m/s)

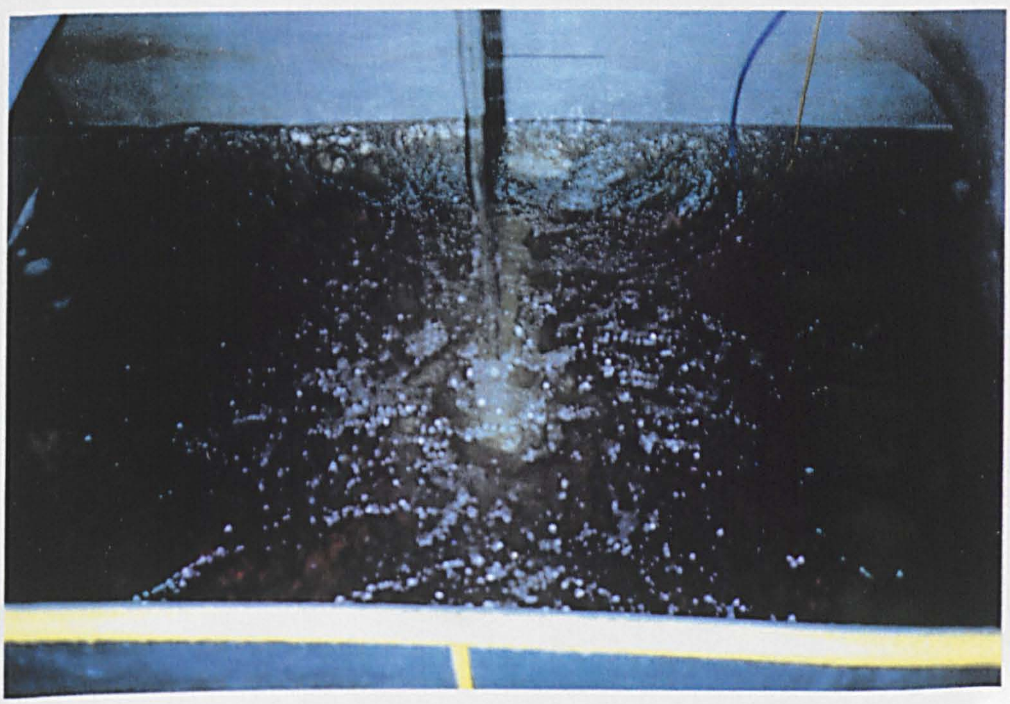

Fig.3·16 PLUNGE POOL DISSIPATION.
(Do=78 mm , Uo≃1·5 m/s , L= 2530 mm, Y= 200 mm)

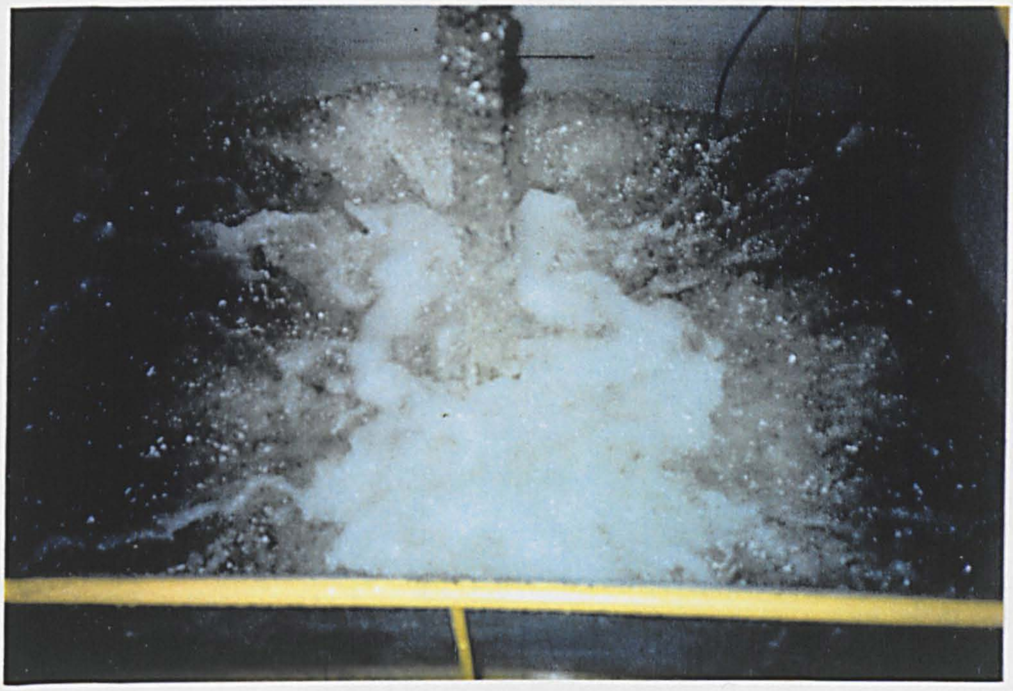

Fig.3·17 PLUNGE POOL DISSIPATION.
(Do=78 mm , Uo≃ 9 m/s , L= 2530 mm , Y = 200 mm)

Fig.3·18 Schematic of experiment and definition of parameters.

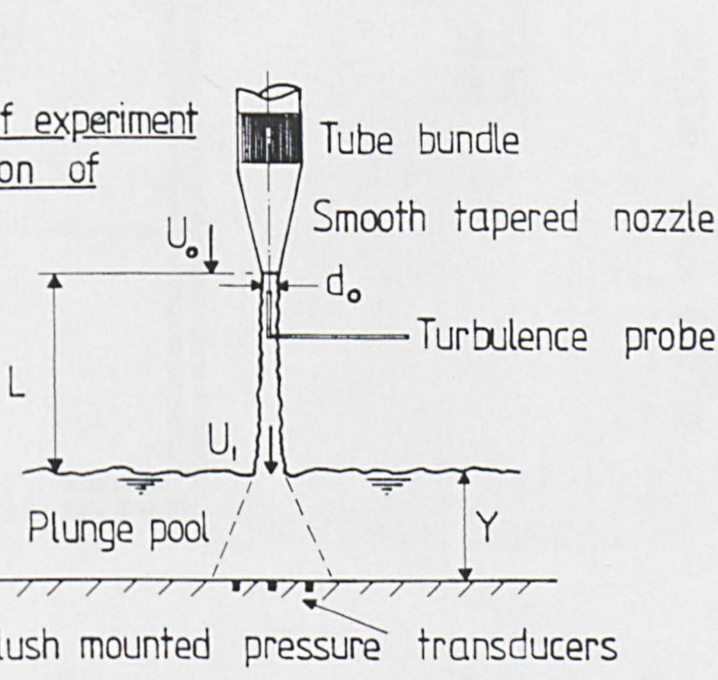

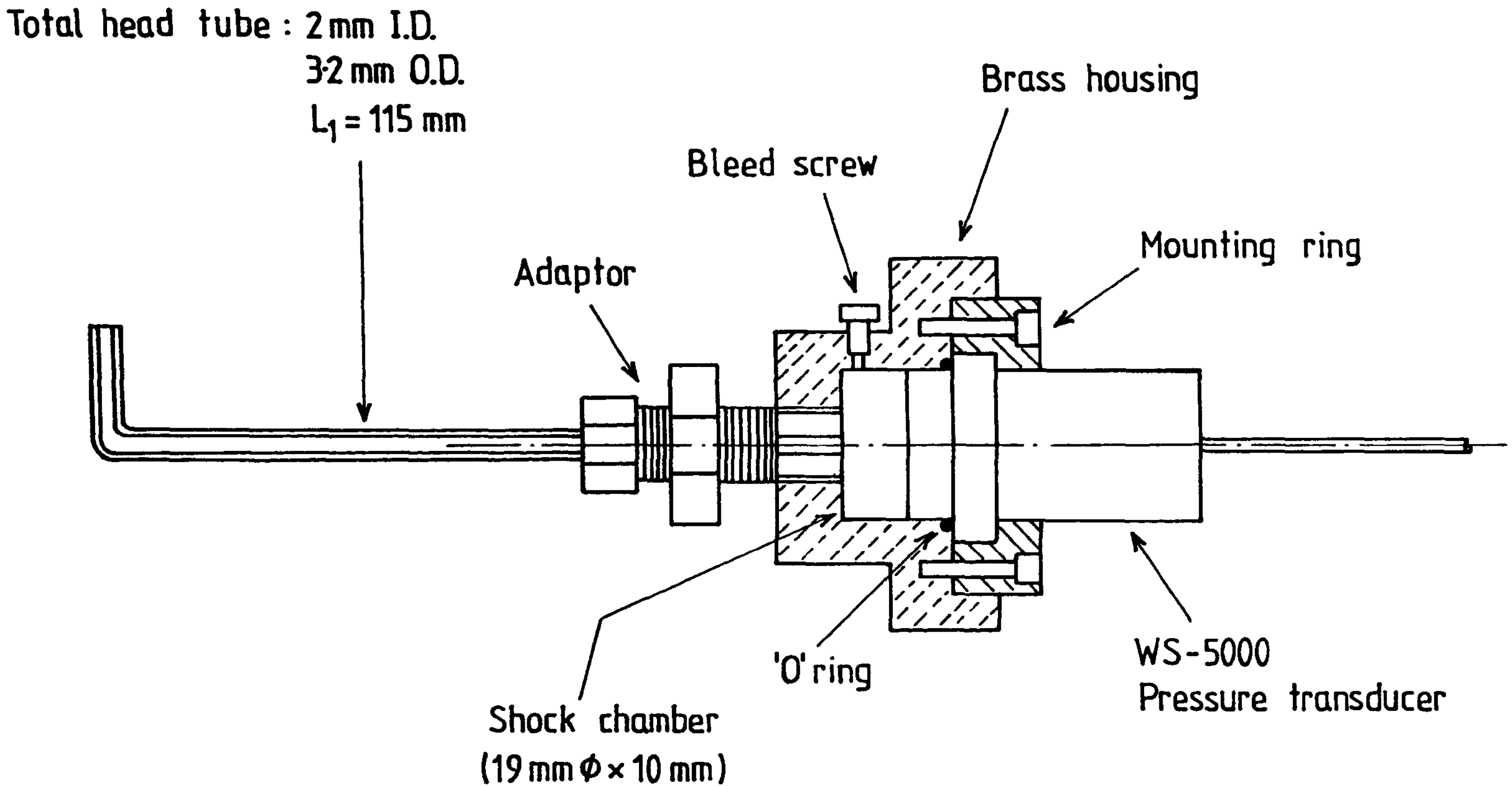

Fig.3·19 FINAL DESIGN OF TURBULENCE TRANSDUCER PROBE.

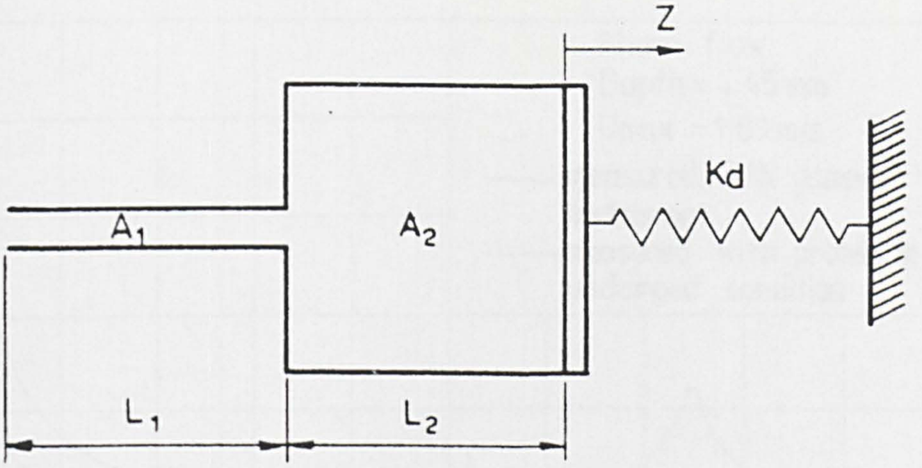

A_1 = Area of total head tube
A_2 = Area of shock chamber
L_1 = Total length of total head tube
L_2 = Length of shock chamber
Z = Deflection of diaphragm
K_d = Spring stiffness

Fig. 3·20 SCHEMATIC REPRESENTATION OF TURBULENCE PROBE.

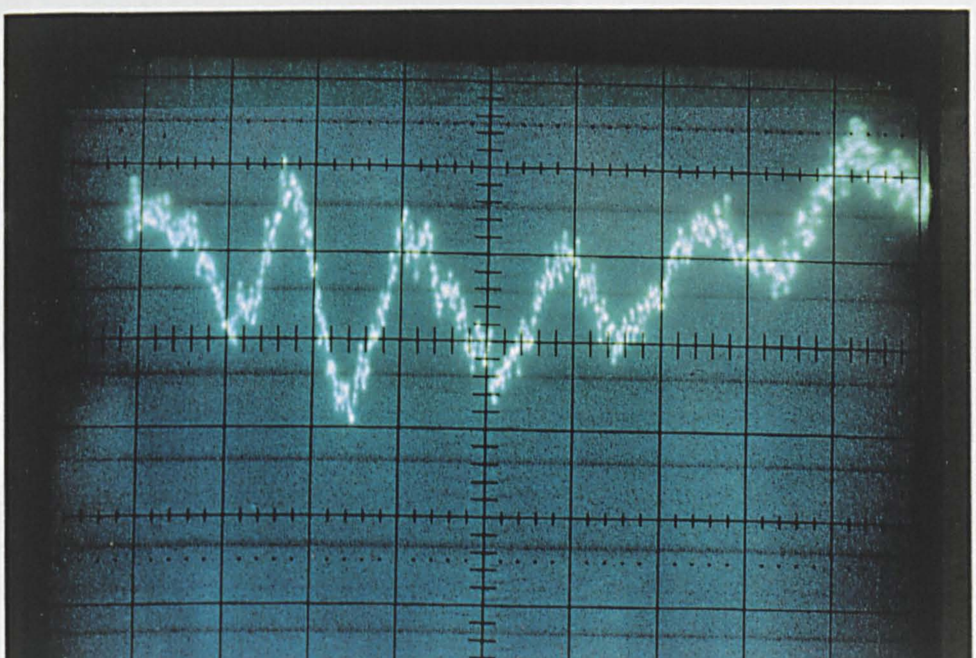

Fig. 3·21 OSCILLOSCOPE TRACE GIVING NATURAL FREQUENCY OF UNDAMPED PROBE. Scan speed = 2·5 millisecs./cm , $f_o \simeq$ 200 Hz.

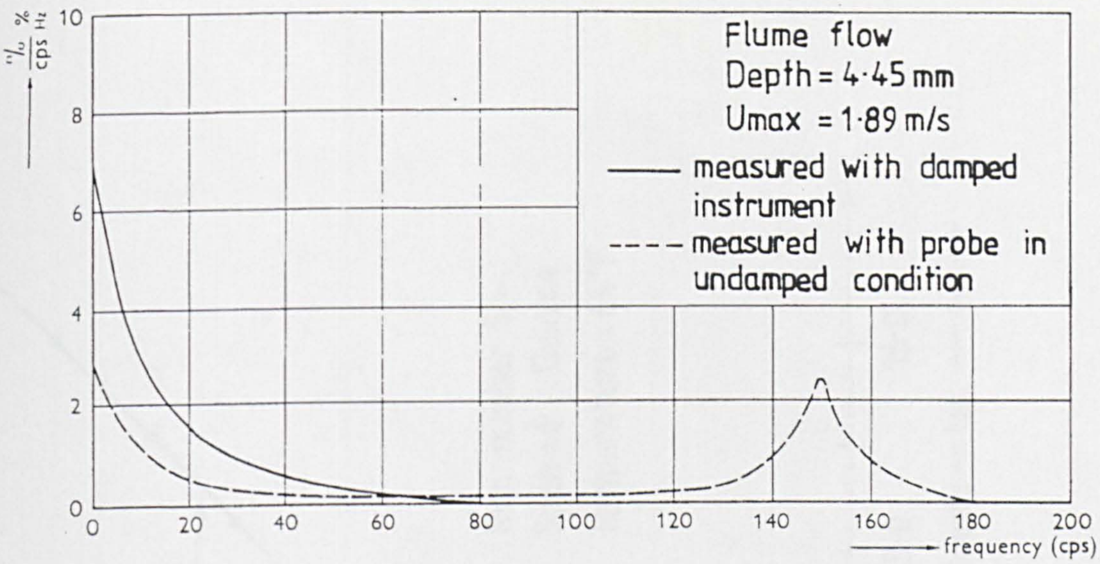

Fig.3·22 TYPICAL ENERGY DENSITY SPECTRA MEASURED WITH TURBULENCE PROBE (f_o = 150 Hz), DAMPED AND UNDAMPED. [Arndt and Ippen]

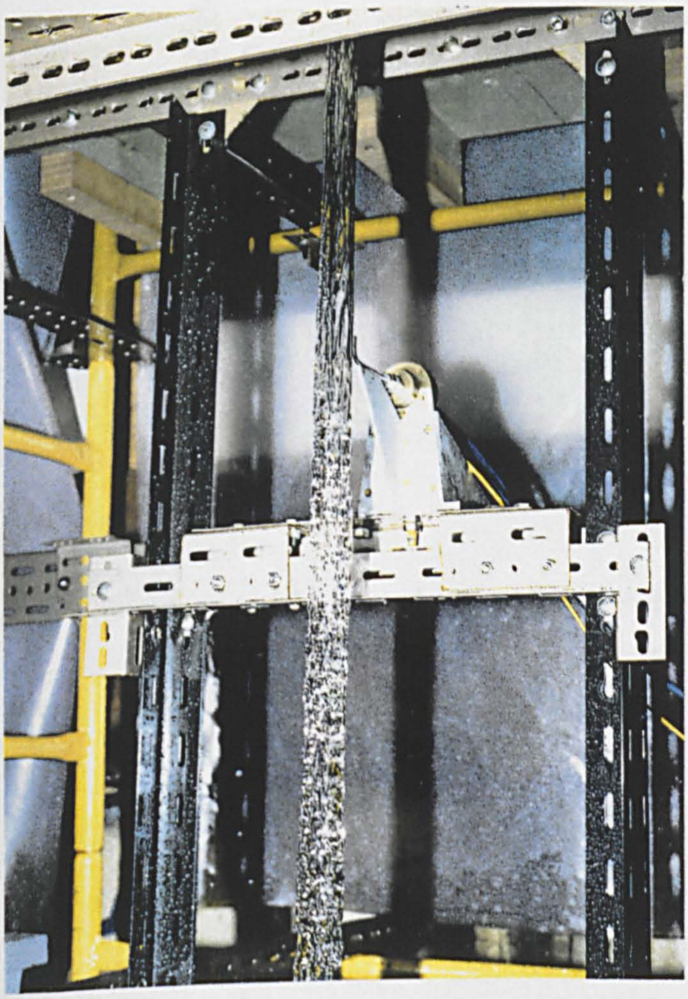

Fig.3·23
TURBULENCE PROBE AND PROBE SUPPORT.

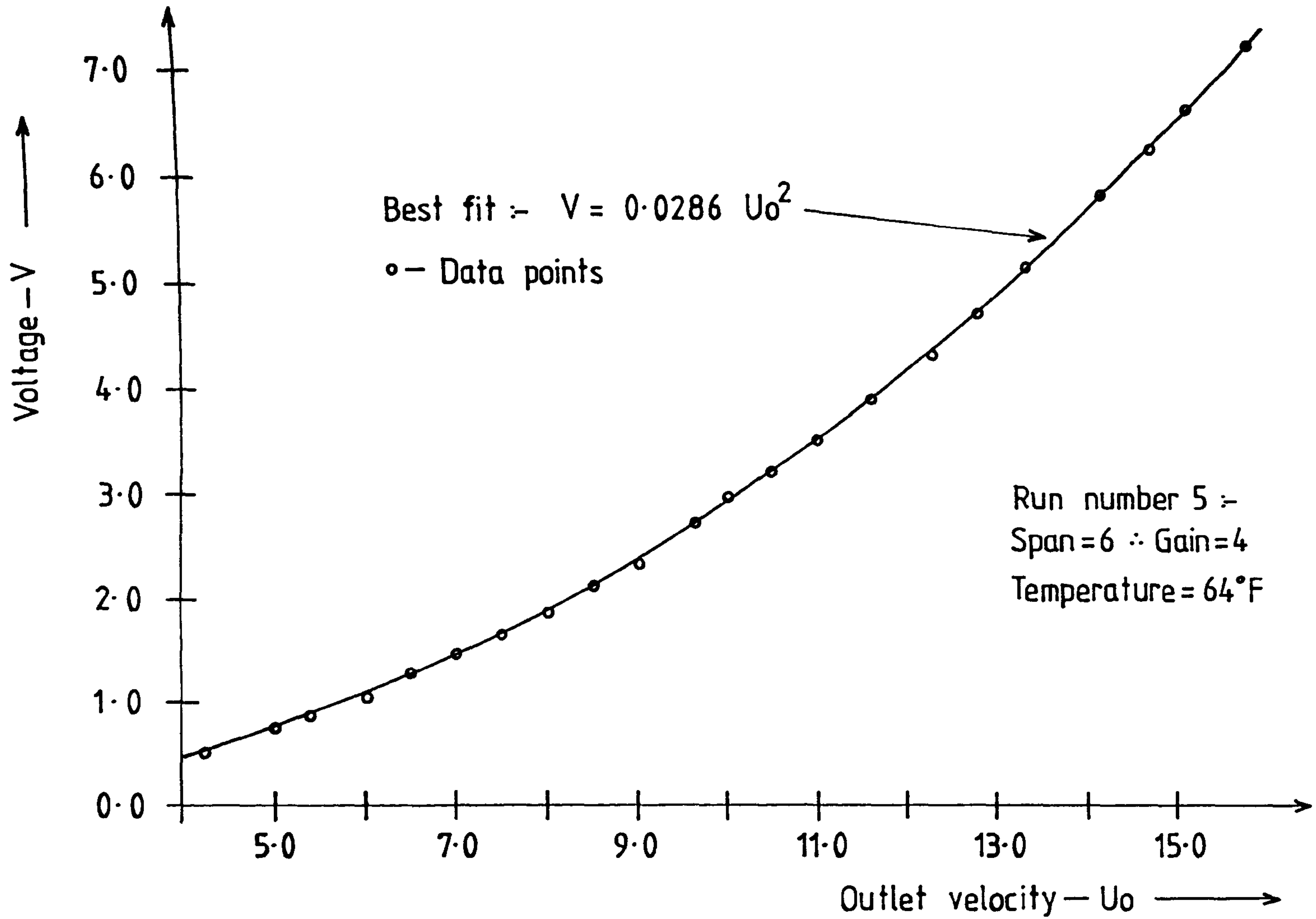

Fig. 3·24 DYNAMIC CALIBRATION OF TURBULENCE PROBE.

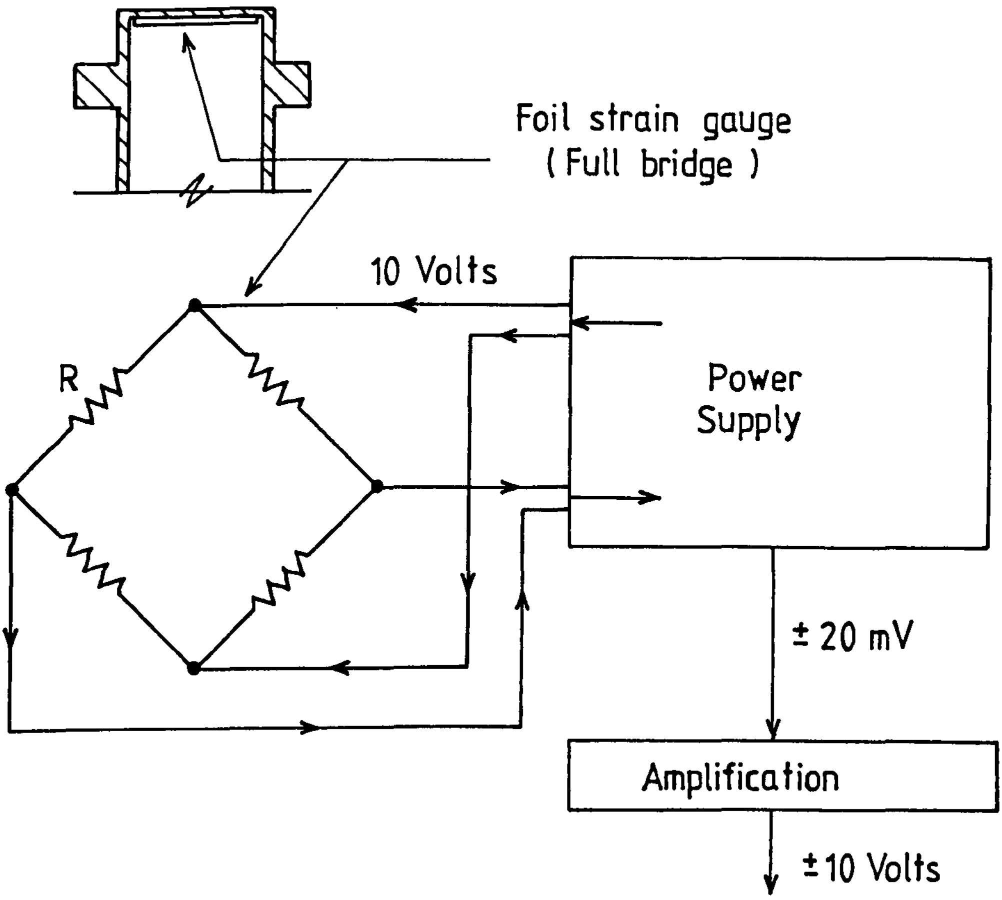

Fig.3·25 SCHEMATIC DIAGRAM OF STRAIN GAUGE ARRANGEMENT.

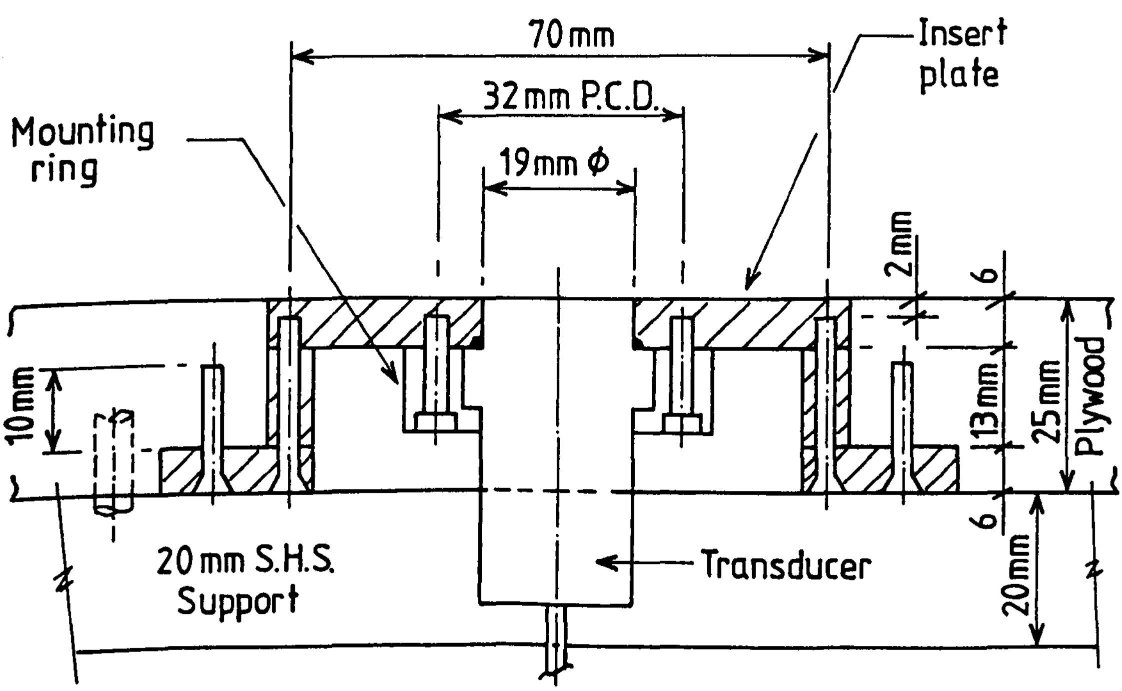

Fig.3·26 TRANSDUCER CONNECTION TO BASE PLATE.

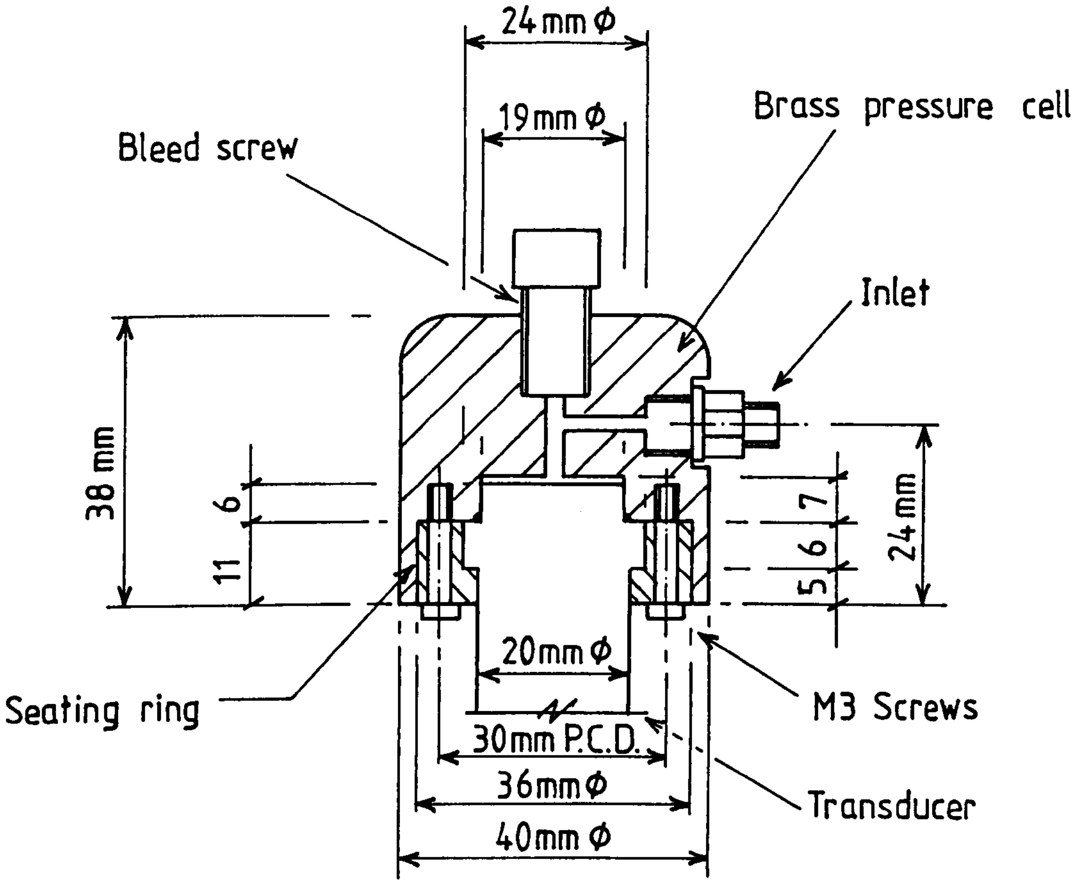

Fig.3·27 BRASS PRESSURE CELL FOR TRANSDUCER CALIBRATION.

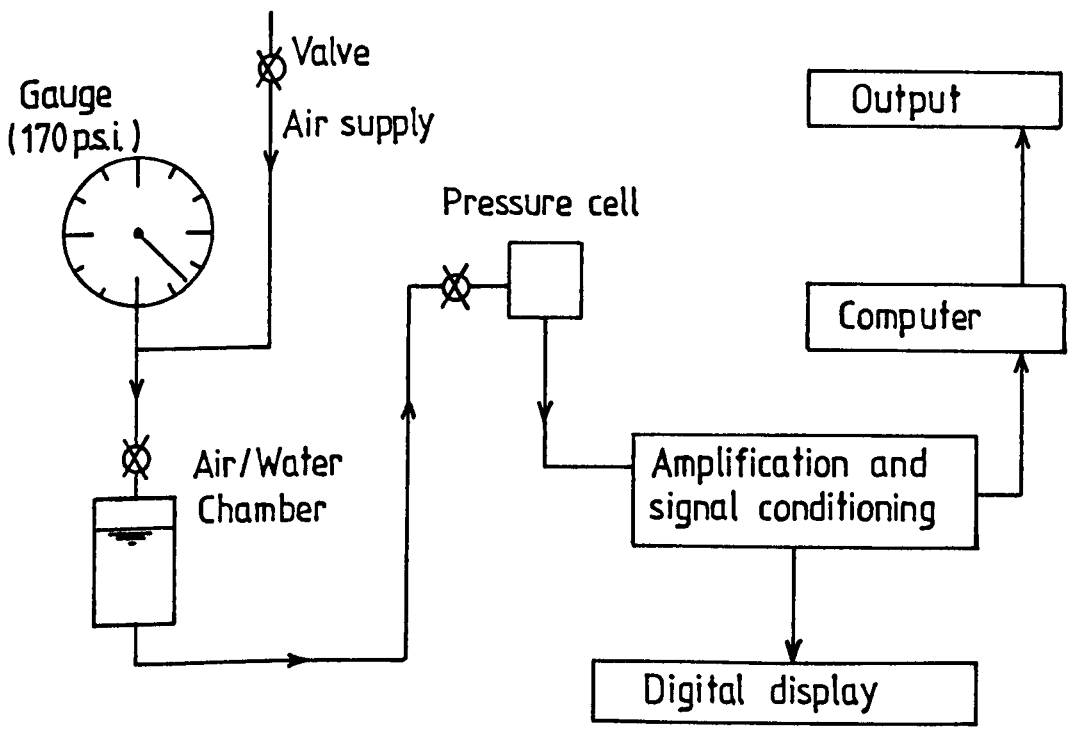

Fig.3·28 SCHEMATIC DIAGRAM OF CALIBRATION RIG.

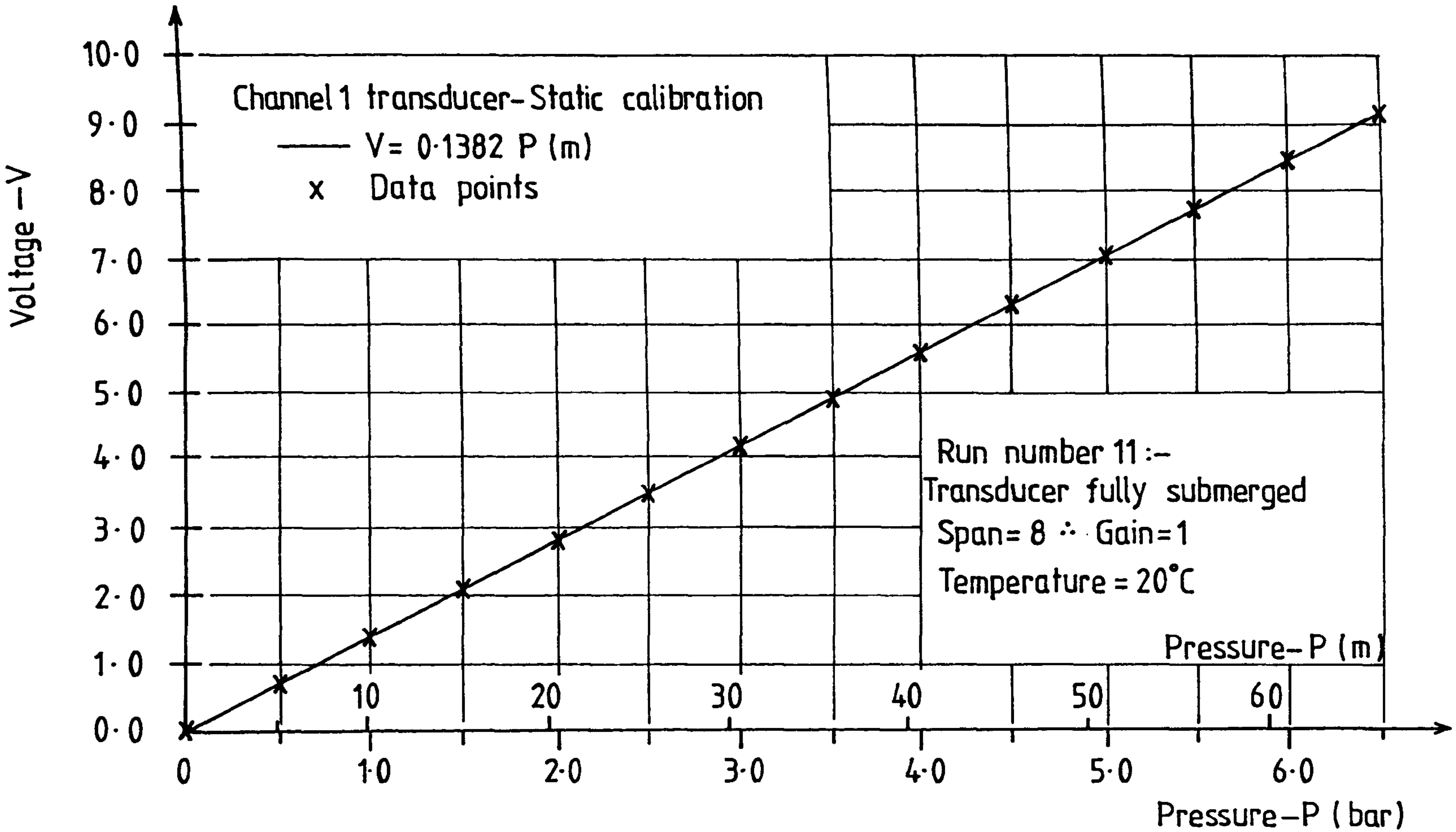

Fig. 3·29 TYPICAL CALIBRATION RELATIONSHIP FOR TRANSDUCER.

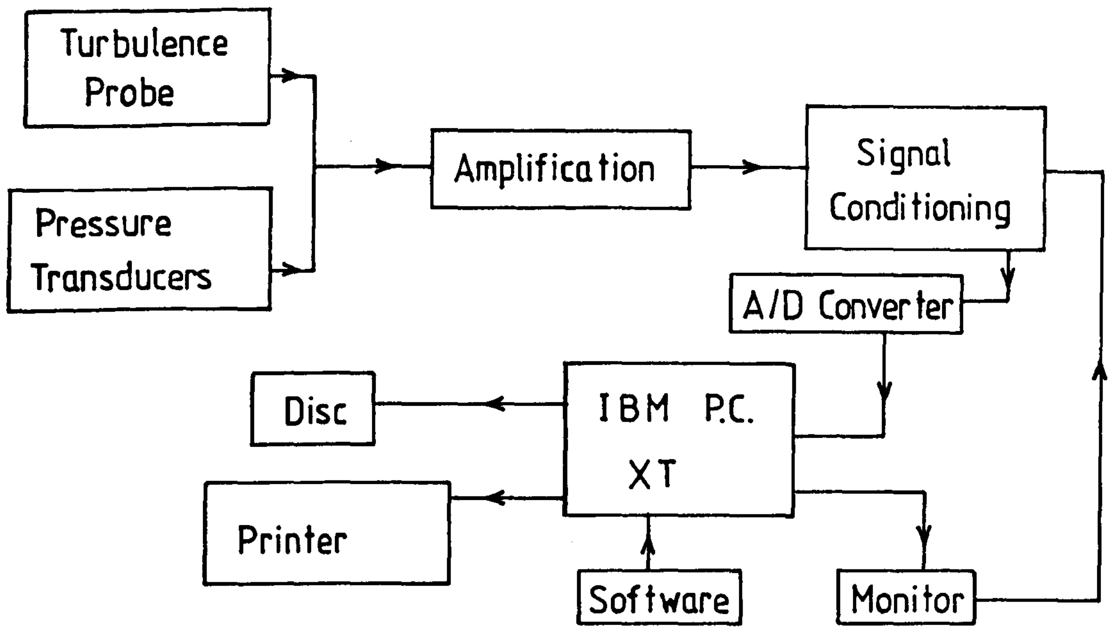

Fig.3·30 METHOD OF DATA COLLECTION.

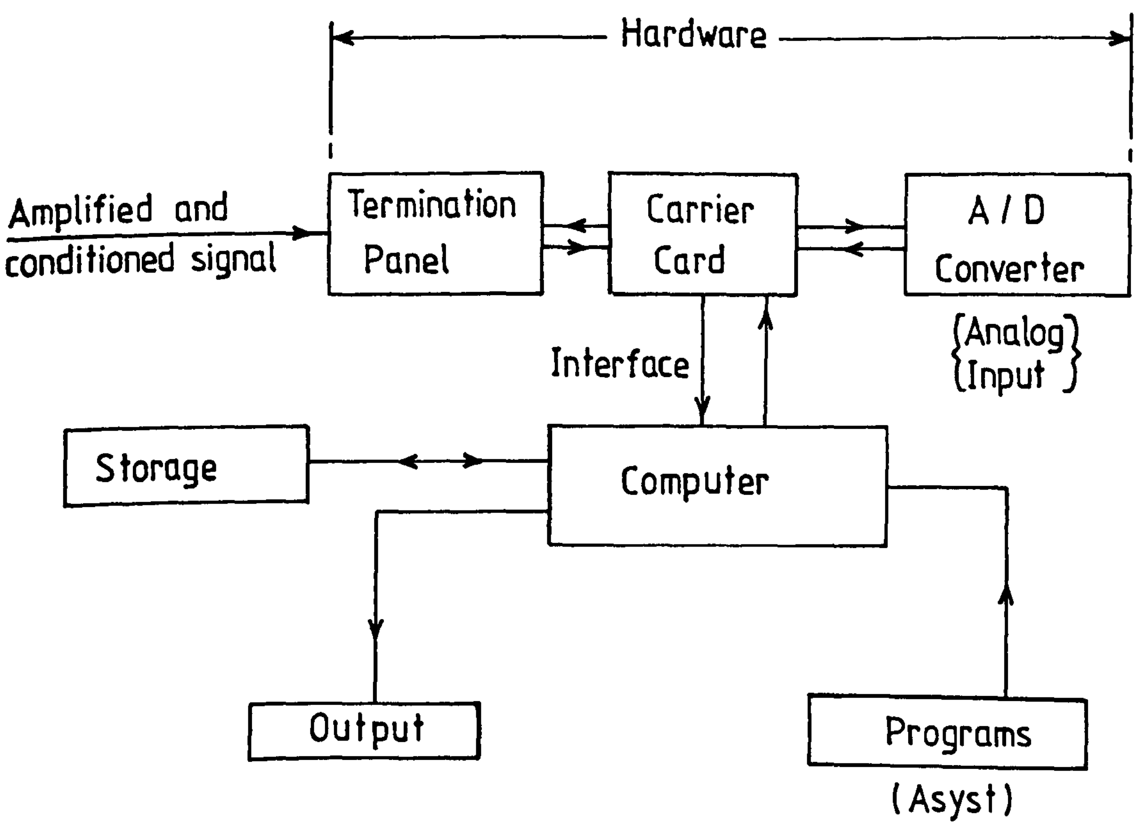

Fig. 3·31 HARDWARE COMPONENTS AND COMPUTER INTERFACE.

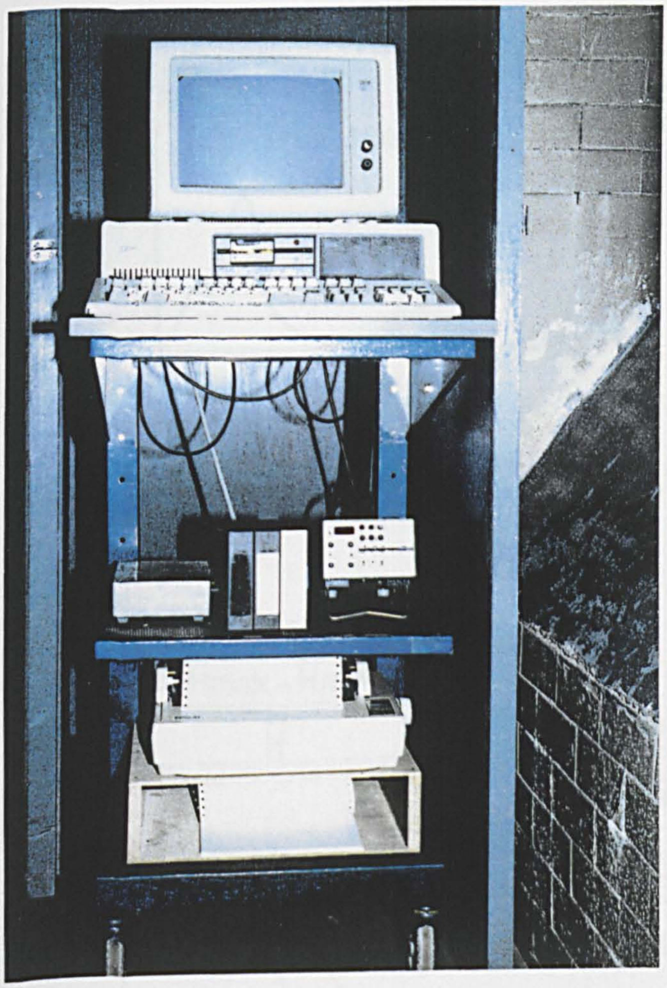

Fig. 3-32

ILLUSTRATION OF COMPUTER SYSTEM AND PERIPHERALS.

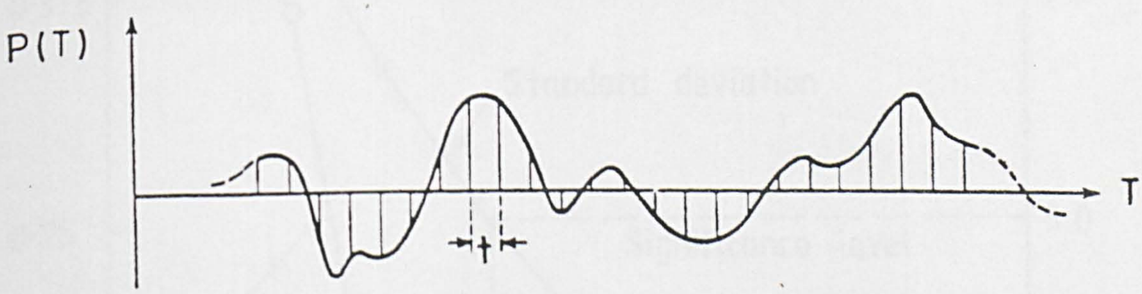

Fig. 3-33 (a) SAMPLING OF CONTINUOUS RECORD.

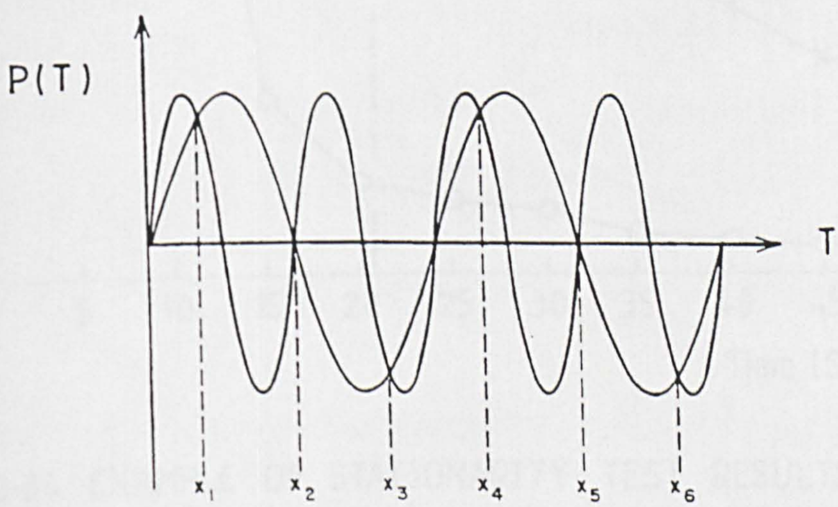

Fig. 3-33 (b) ILLUSTRATION OF ALIASING PROBLEM.

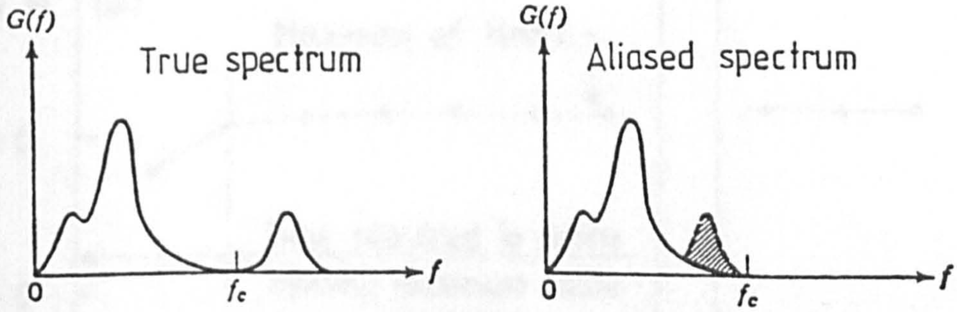

Fig.3·33(c) ALIASED POWER SPECTRUM DUE TO FOLDING.

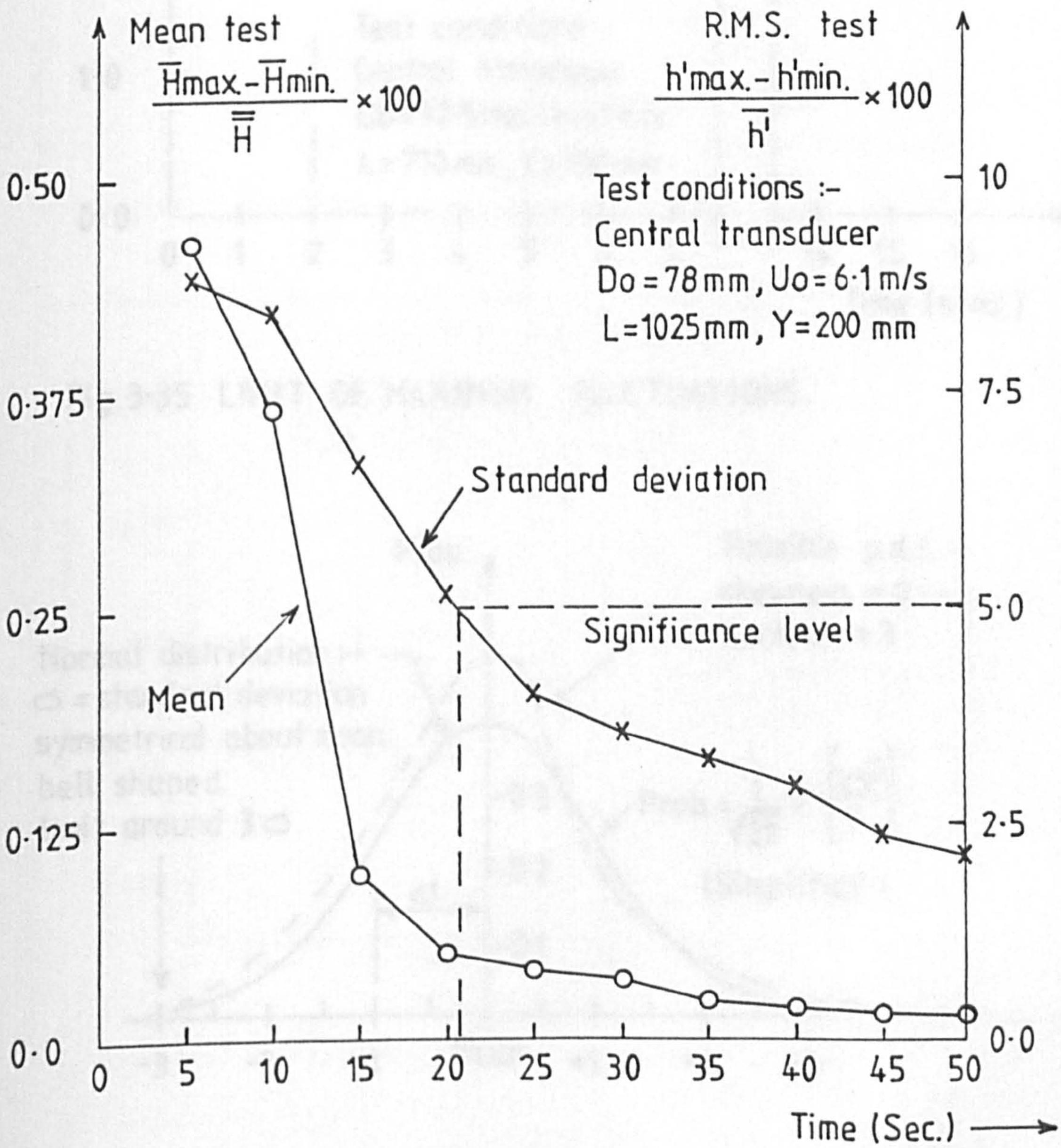

Fig.3·34 EXAMPLE OF STATIONARITY TEST RESULTS.

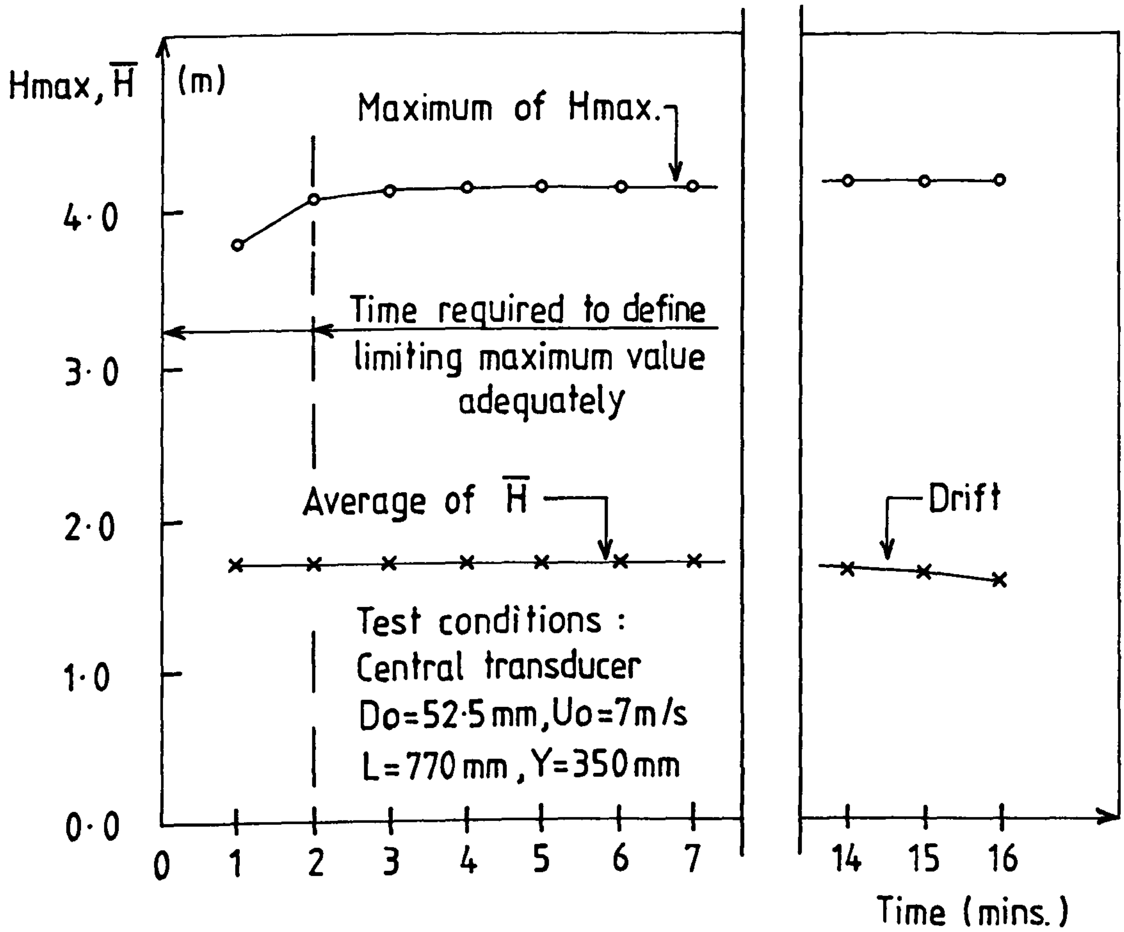

Fig.3·35 LIMIT OF MAXIMUM FLUCTUATIONS.

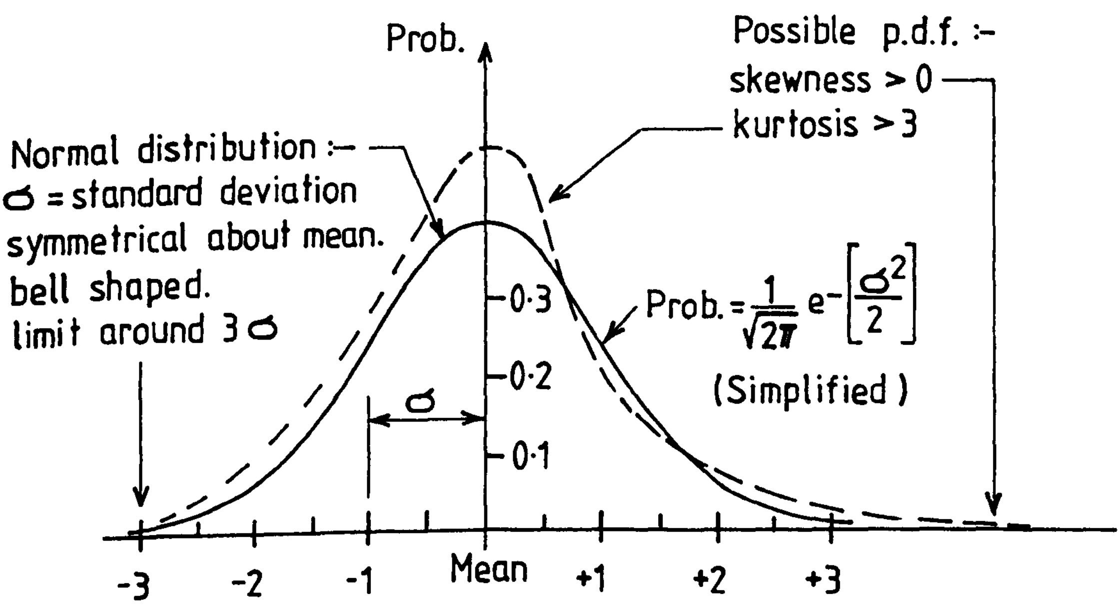

Fig.3·36 MOMENTS OF PROBABILITY DENSITY FUNCTION.

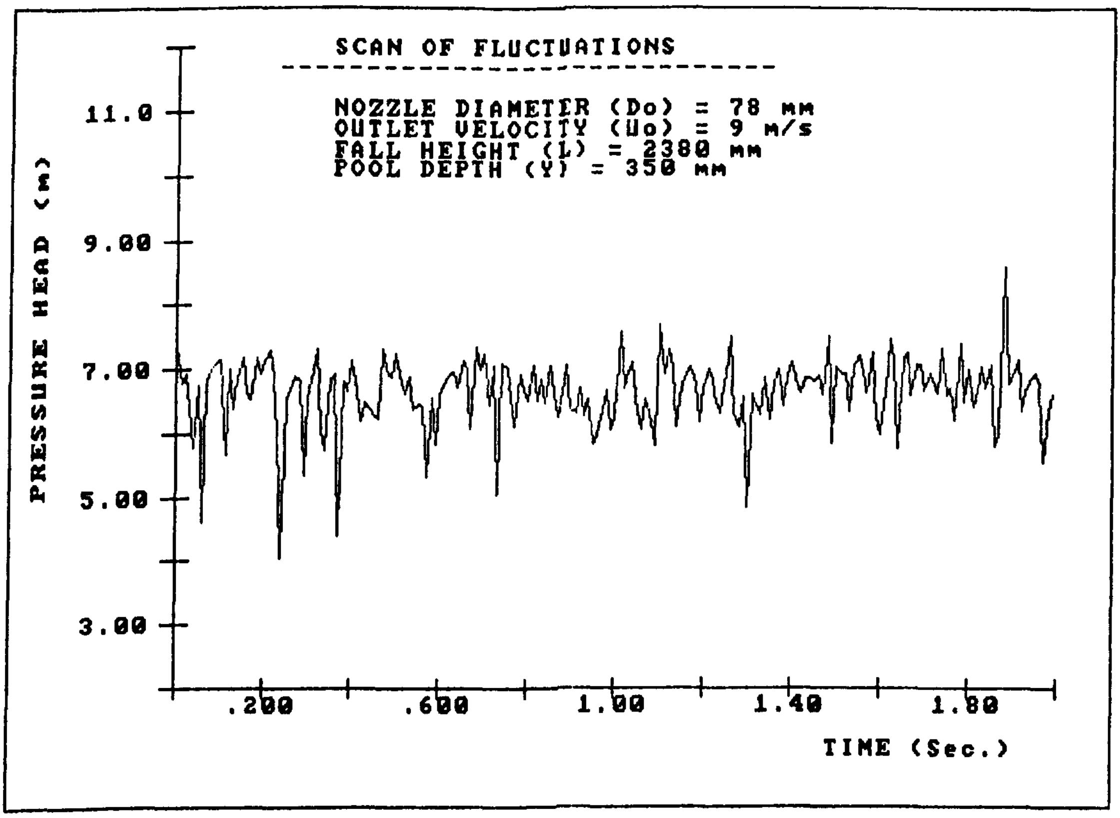

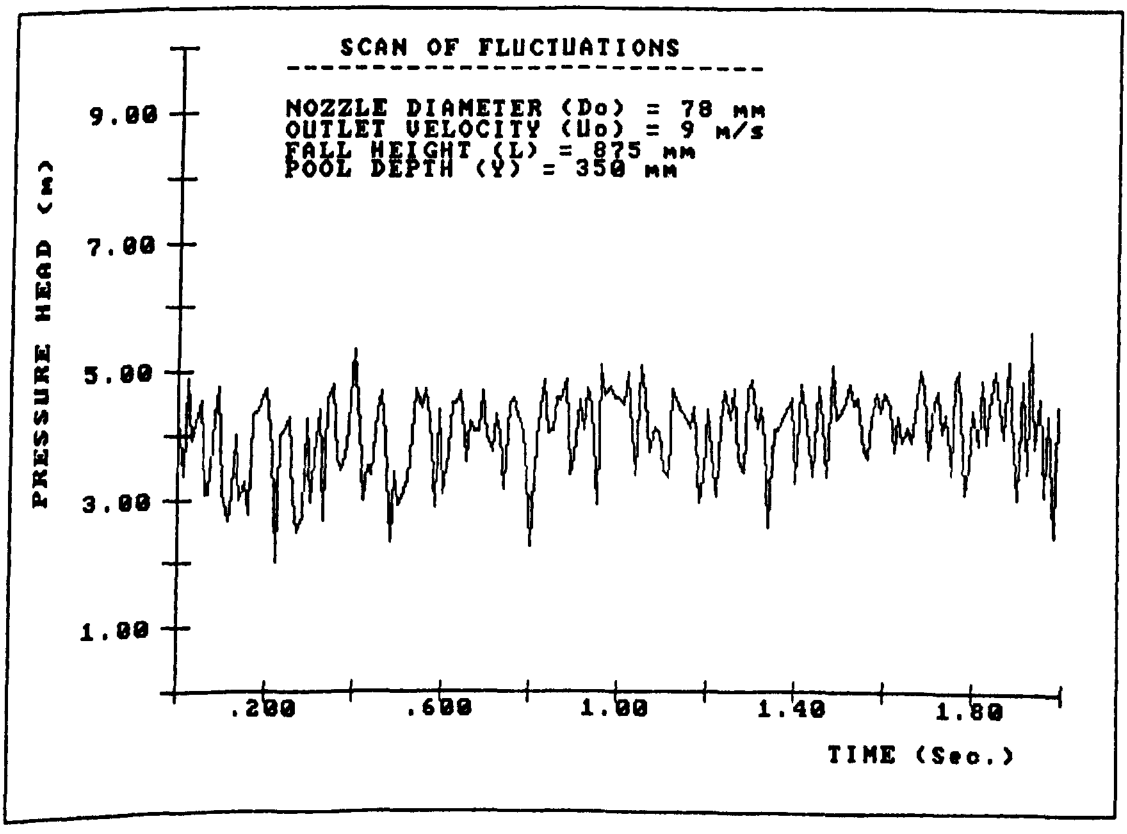

Fig. 3.37 *PRESSURE HEAD RECORD FOR 78 mm DIA. JET AT DIFFERENT FALL LENGTHS*

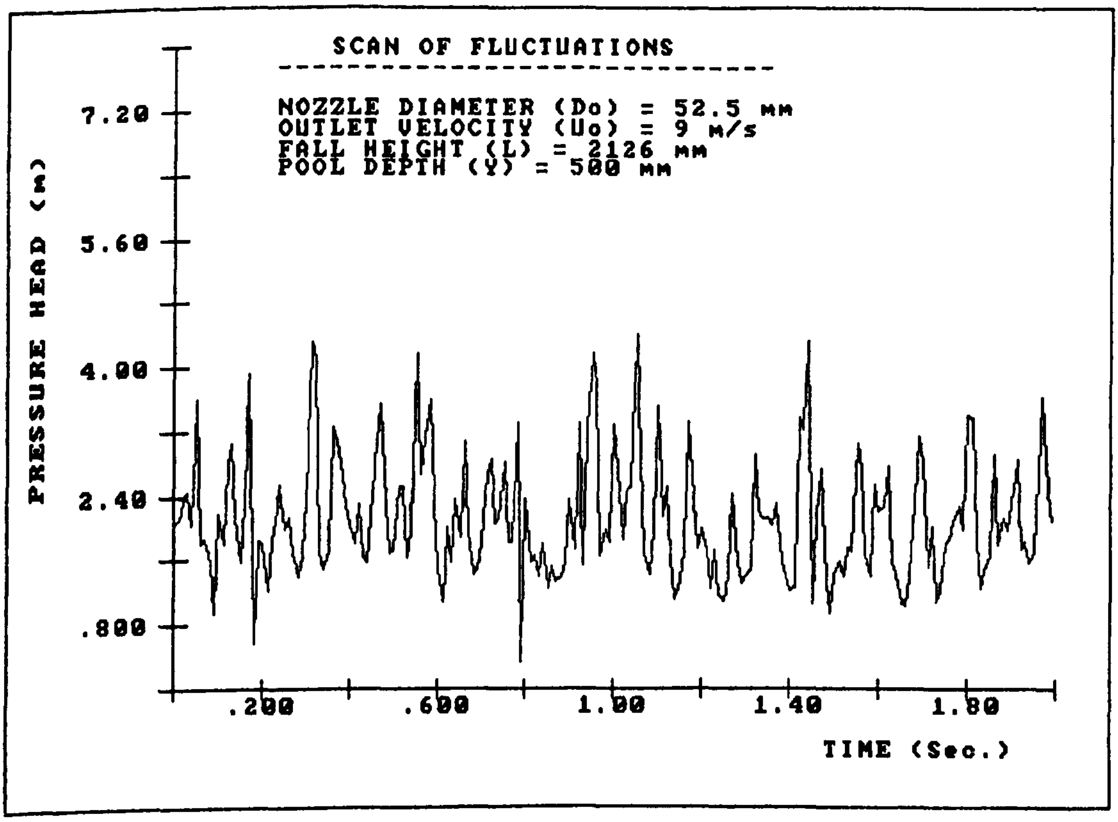

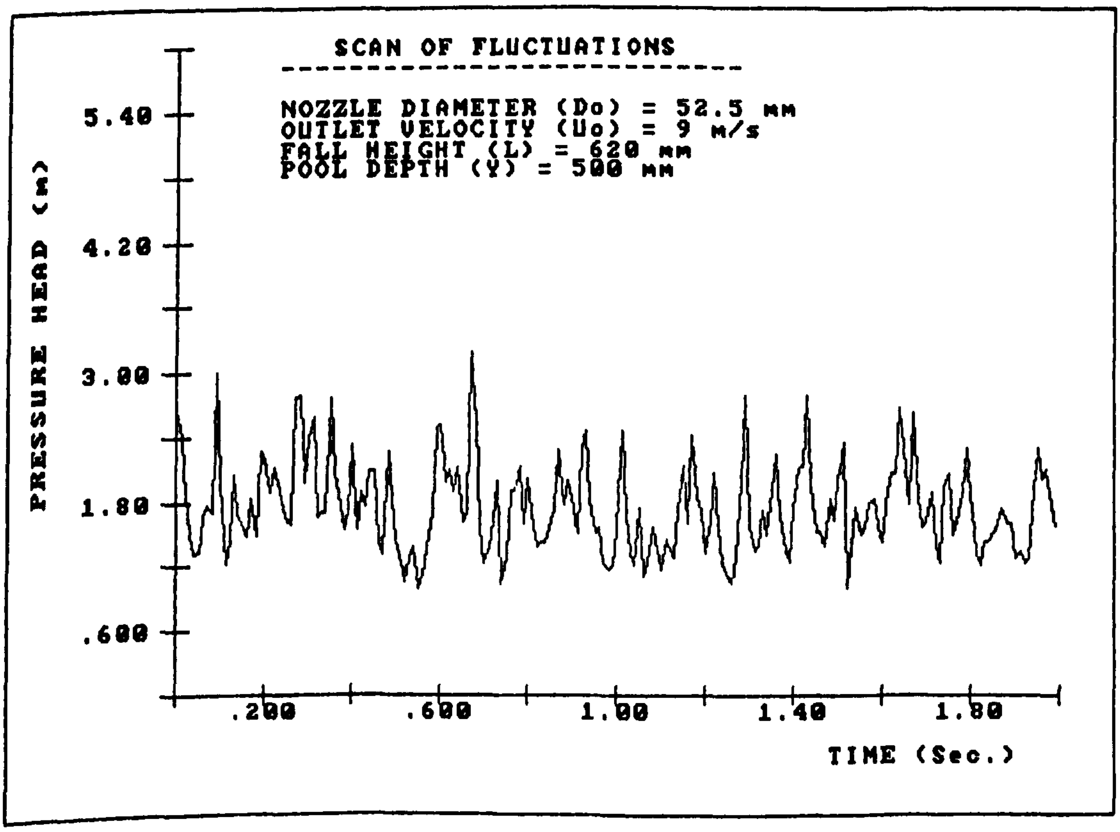

Fig. 3.38 *PRESSURE HEAD RECORD FOR 52.5 mm DIA. JET AT DIFFERENT FALL LENGTHS*

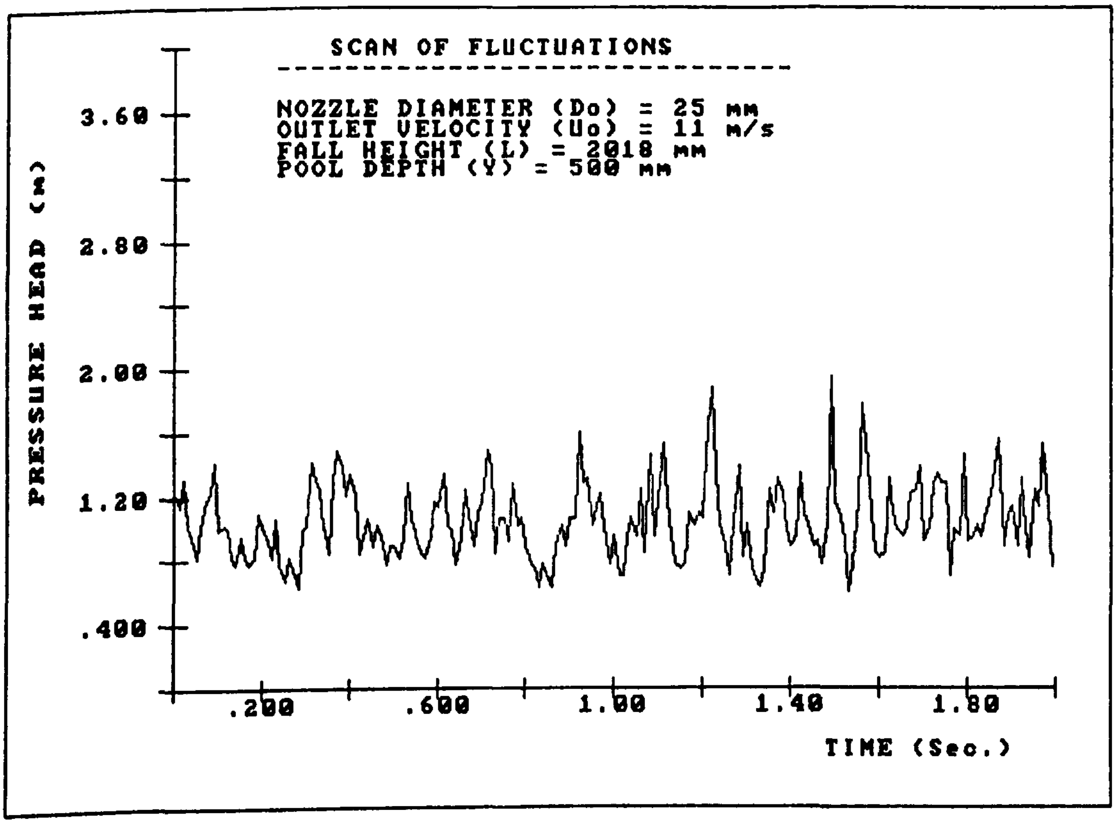

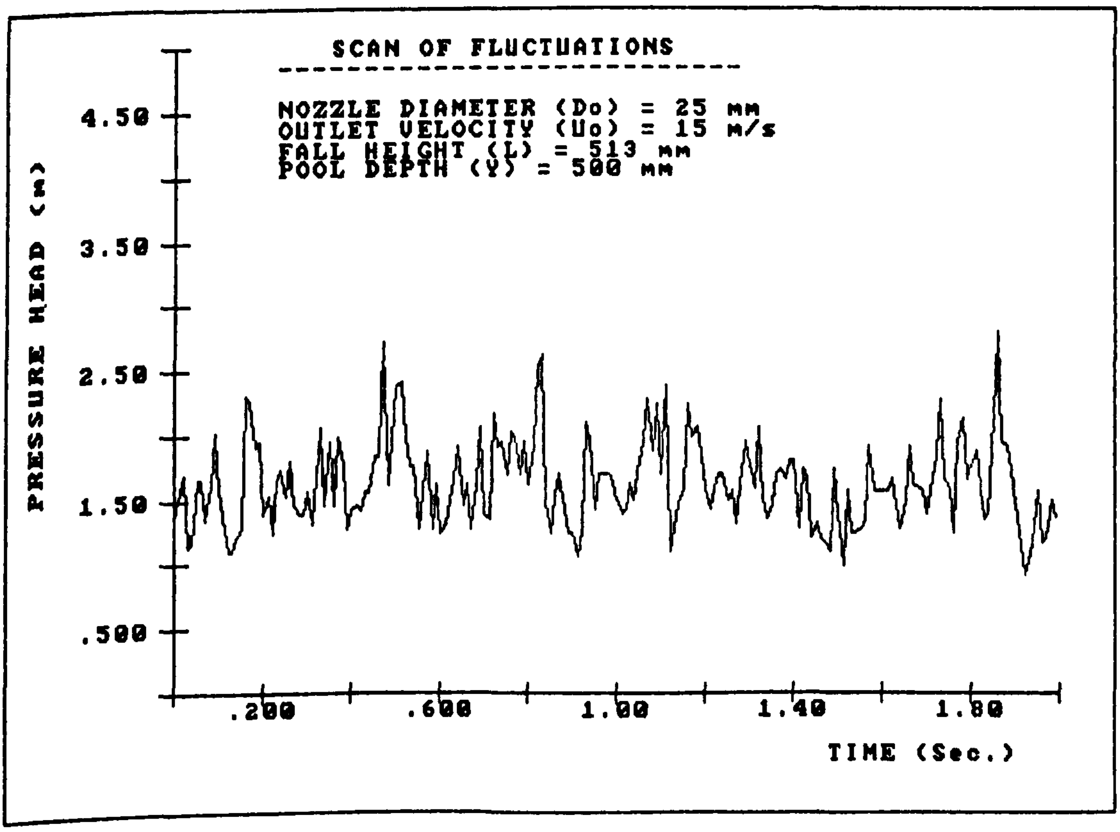

Fig. 3.39 *PRESSURE HEAD RECORD FOR 25 mm NOZZLE DIA. JET AT DIFFERENT VELOCITIES AND FALL LENGTHS*

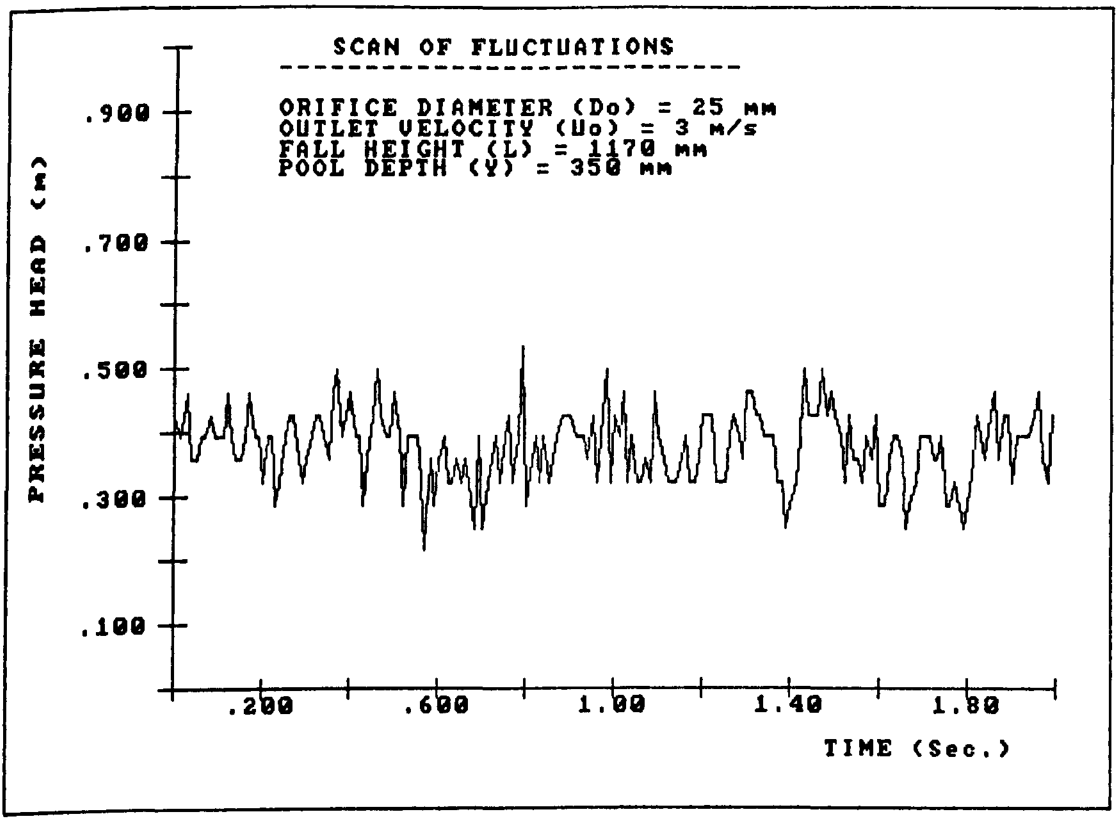

Fig. 3.40 *PRESSURE HEAD RECORD FOR 25 mm ORIFICE DIA. JET*

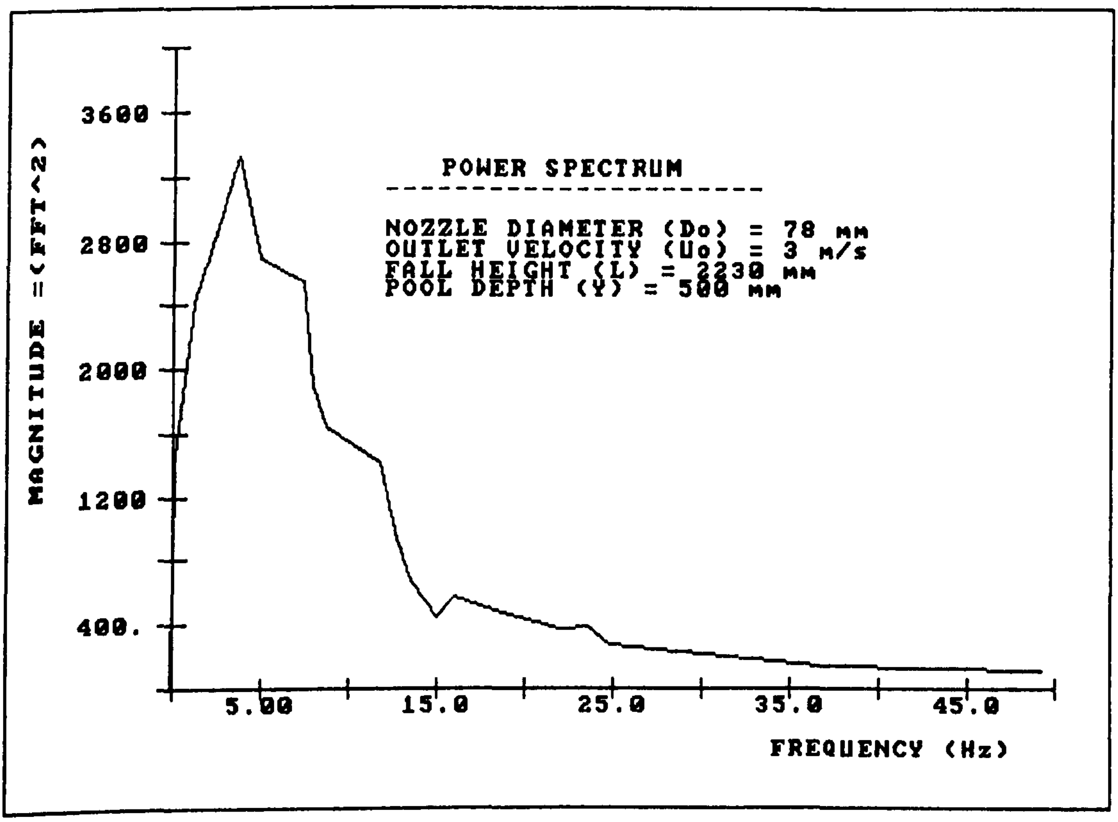

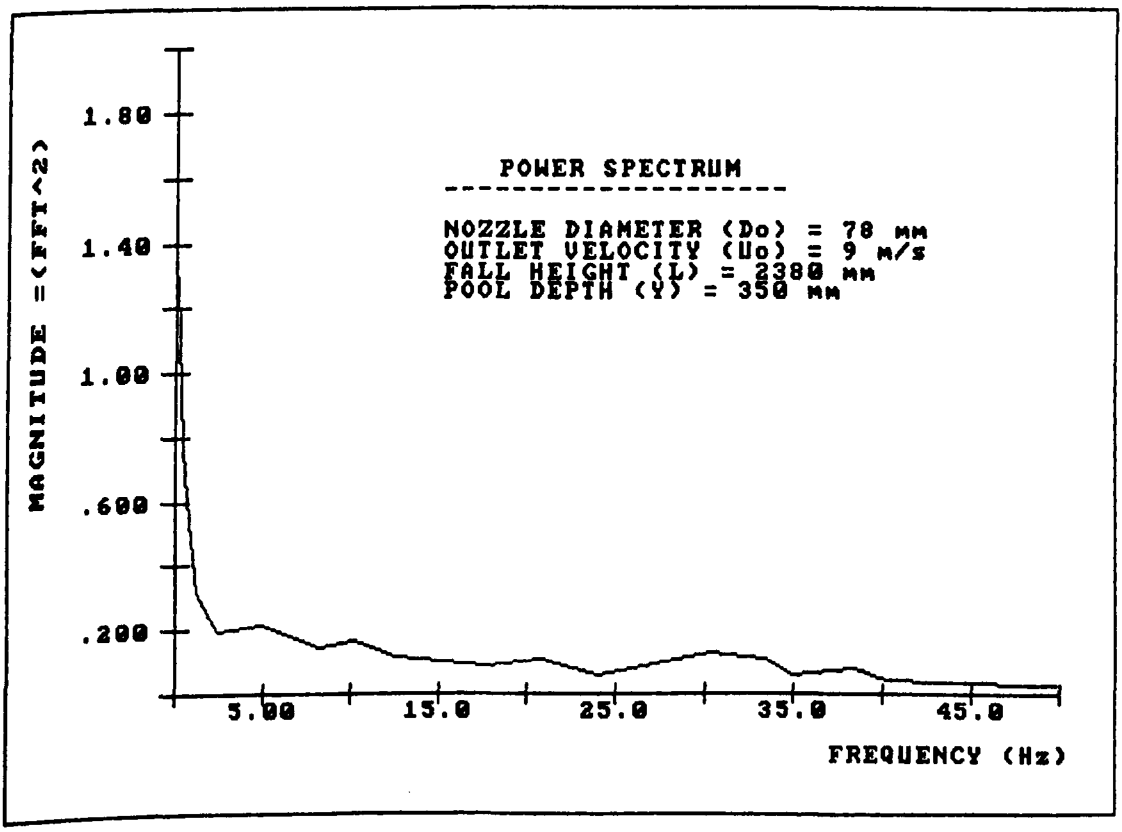

Fig. 3.41 *POWER SPECTRA FOR 78 mm DIA. JET AT DIFFERENT VELOCITIES AND PLUNGE POOL DEPTHS*

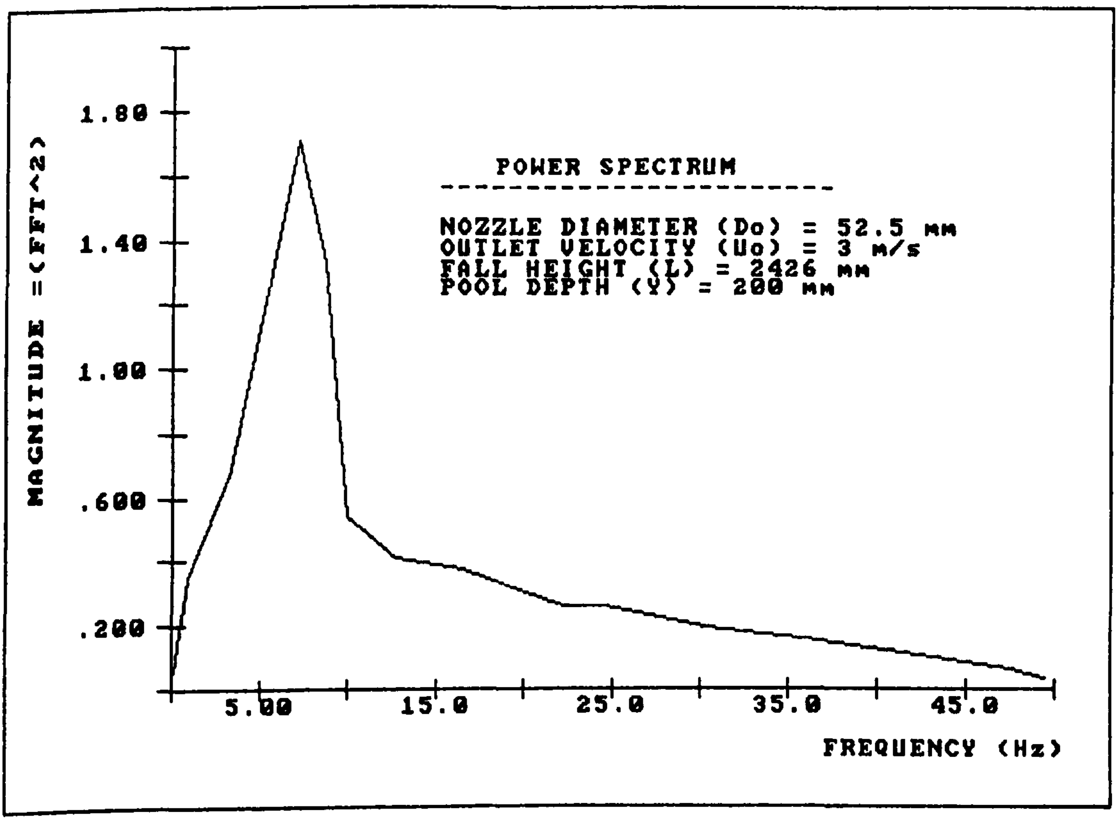

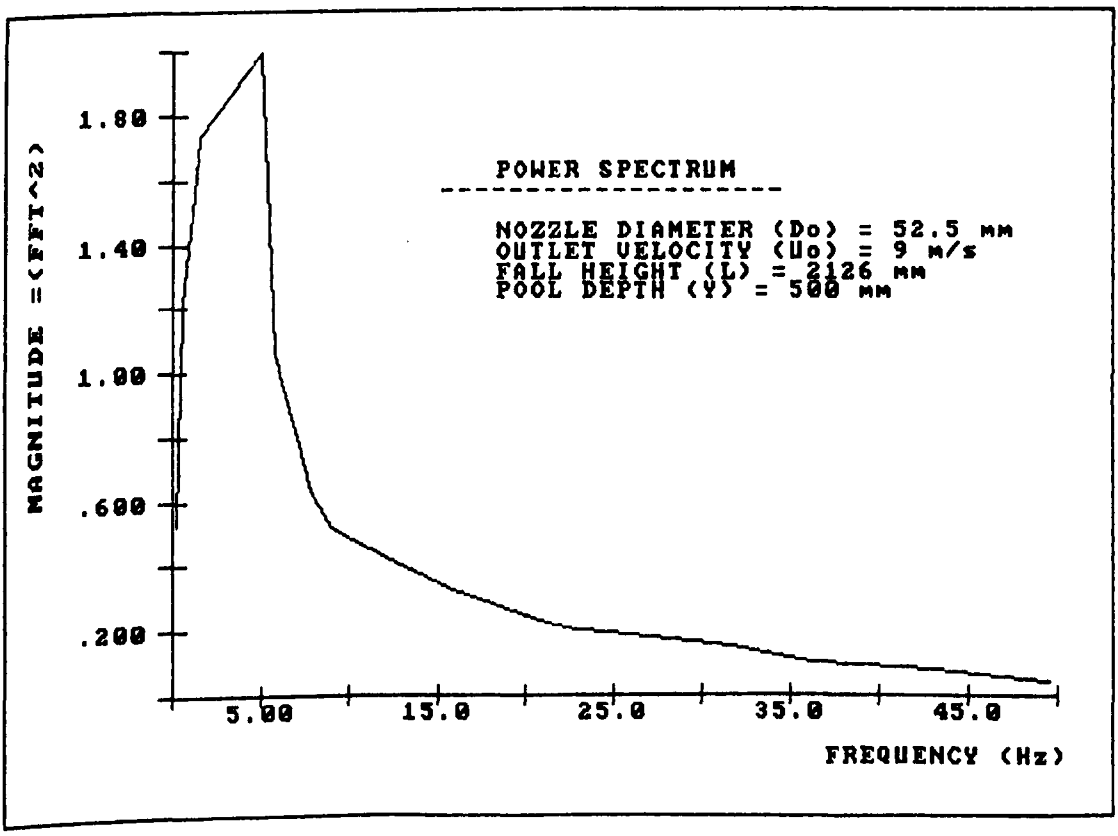

Fig. 3.42 *POWER SPECTRA FOR 52.5 mm DIA. JET AT DIFFERENT VELOCITIES AND PLUNGE POOL DEPTHS*

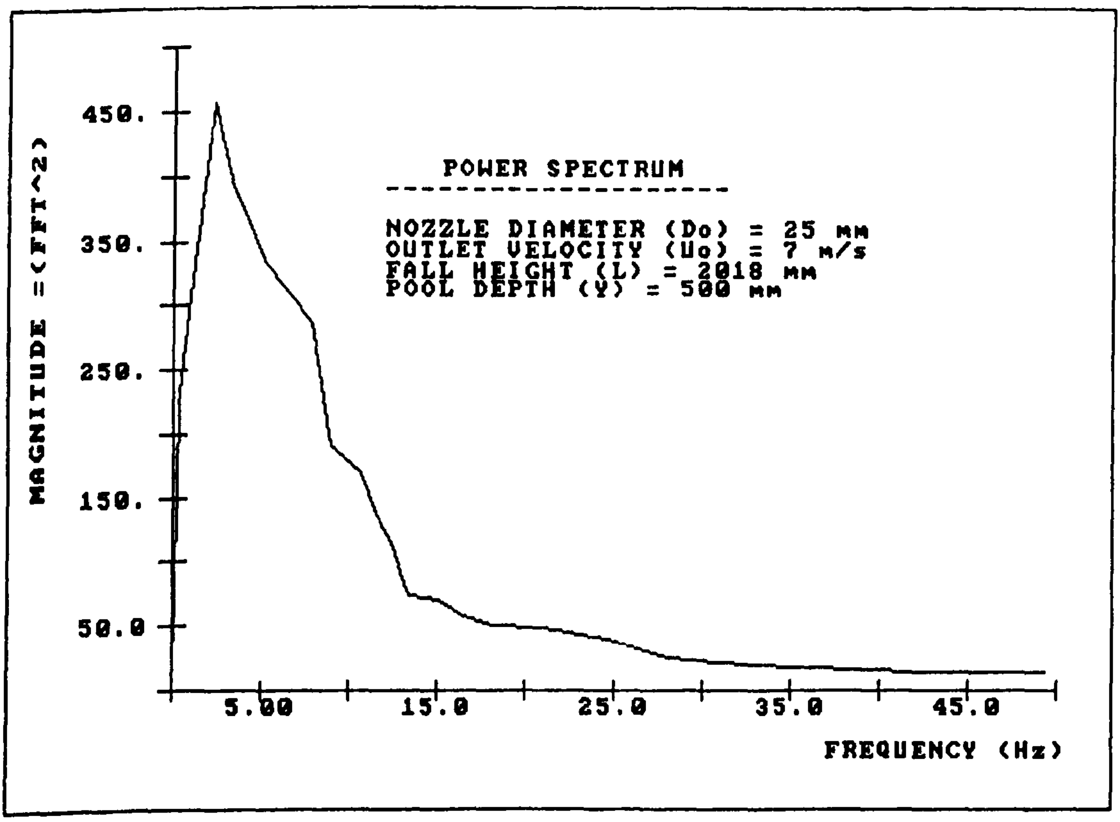

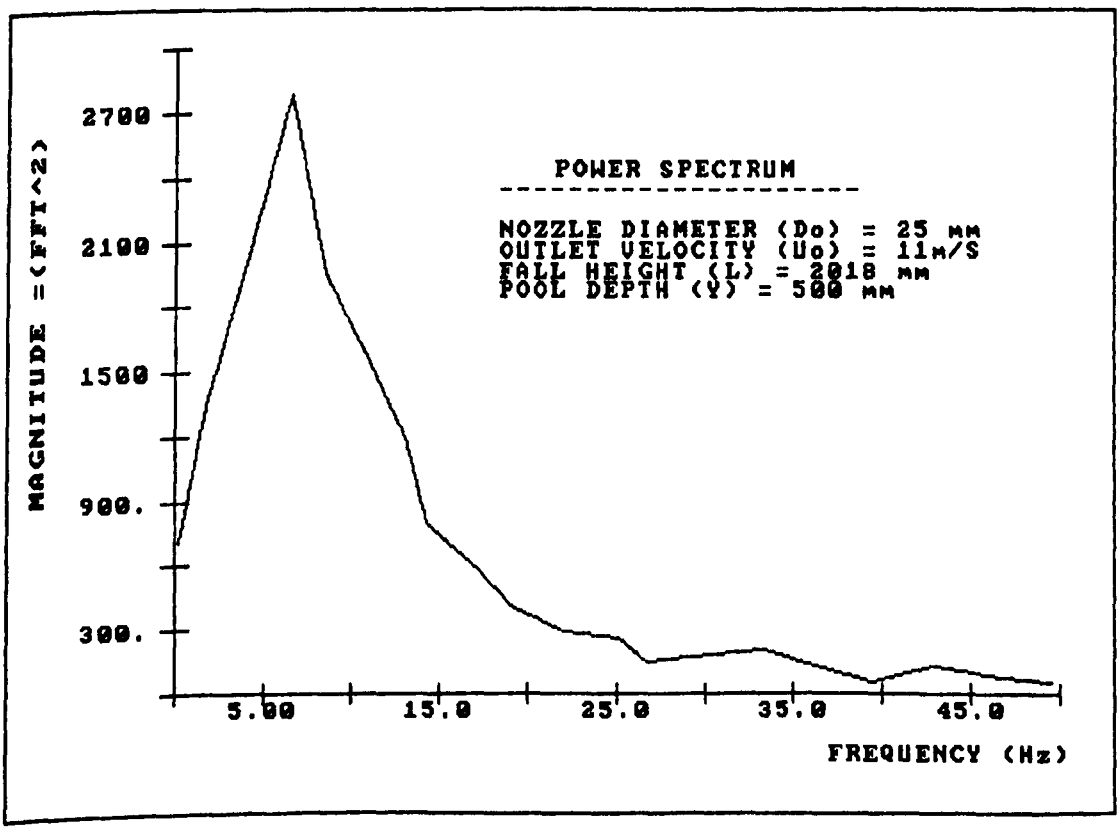

Fig. 3.43 *POWER SPECTRA FOR 25 mm NOZZLE DIA. JET AT DIFFERENT VELOCITIES*

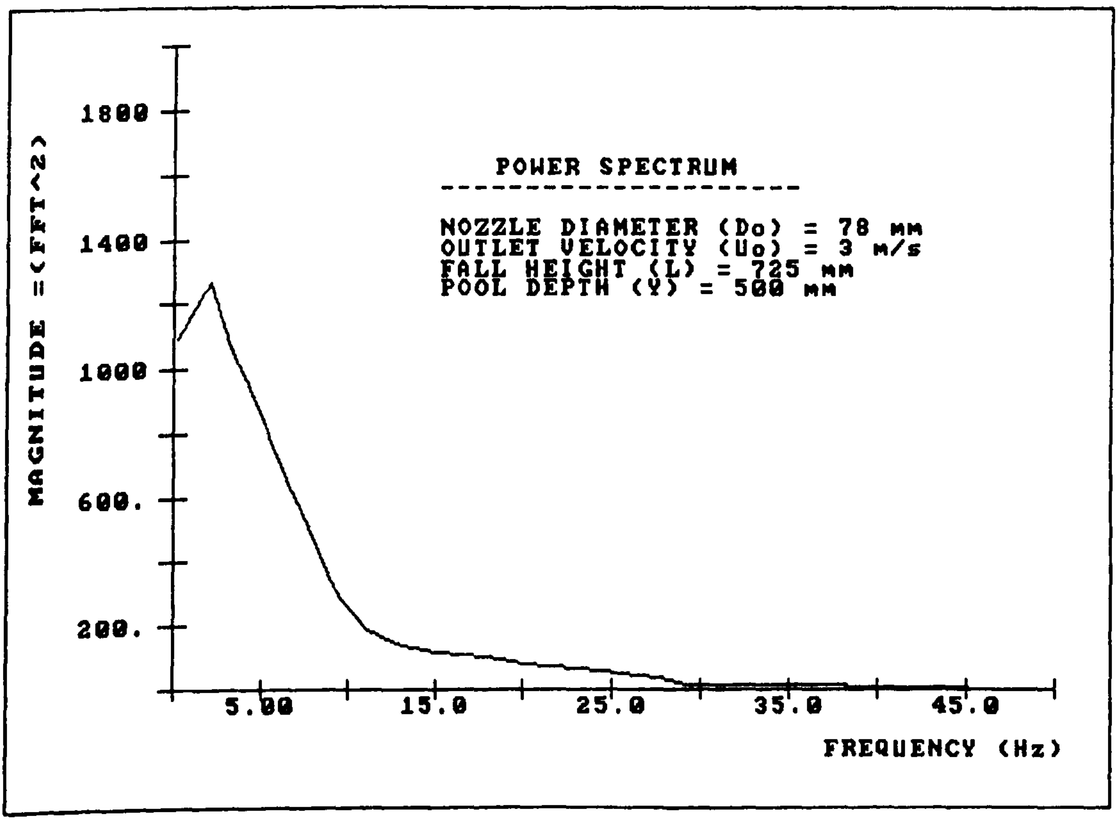

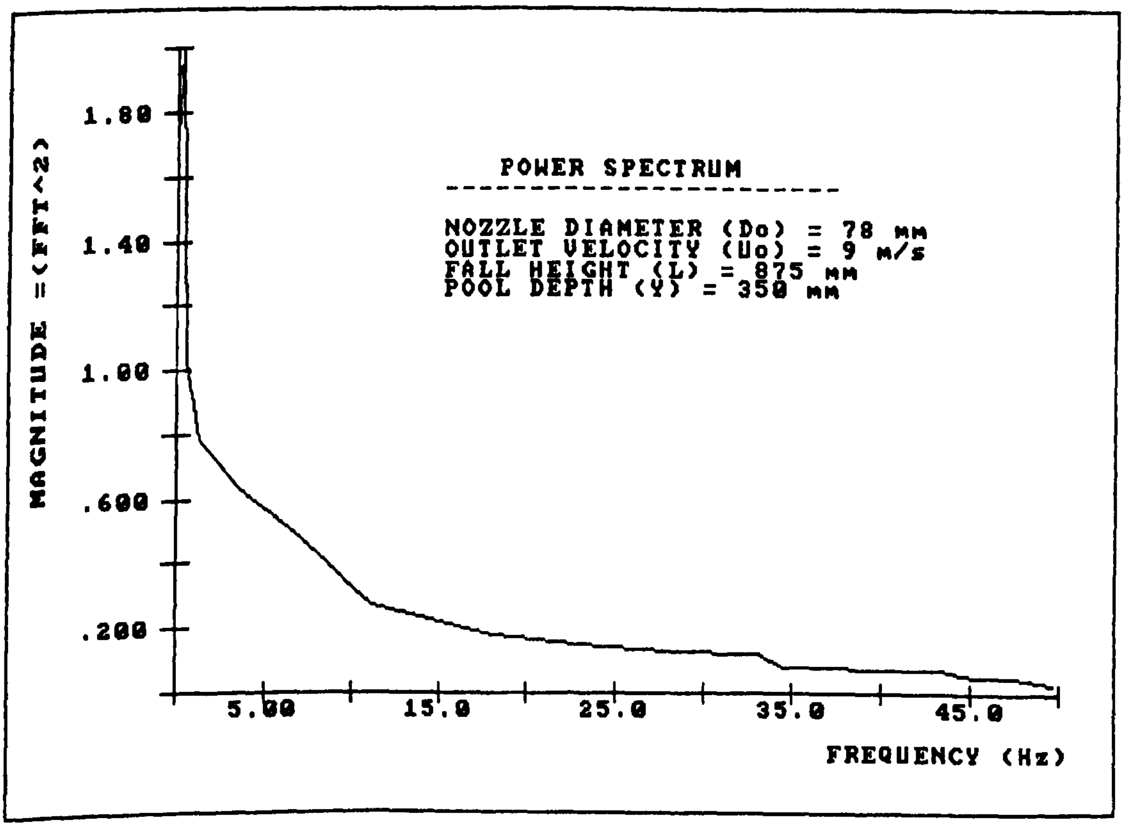

Fig. 3.44 *POWER SPECTRA FOR 78 mm DIA. JET AT DIFFERENT VELOCITIES AND PLUNGE POOL DEPTHS*

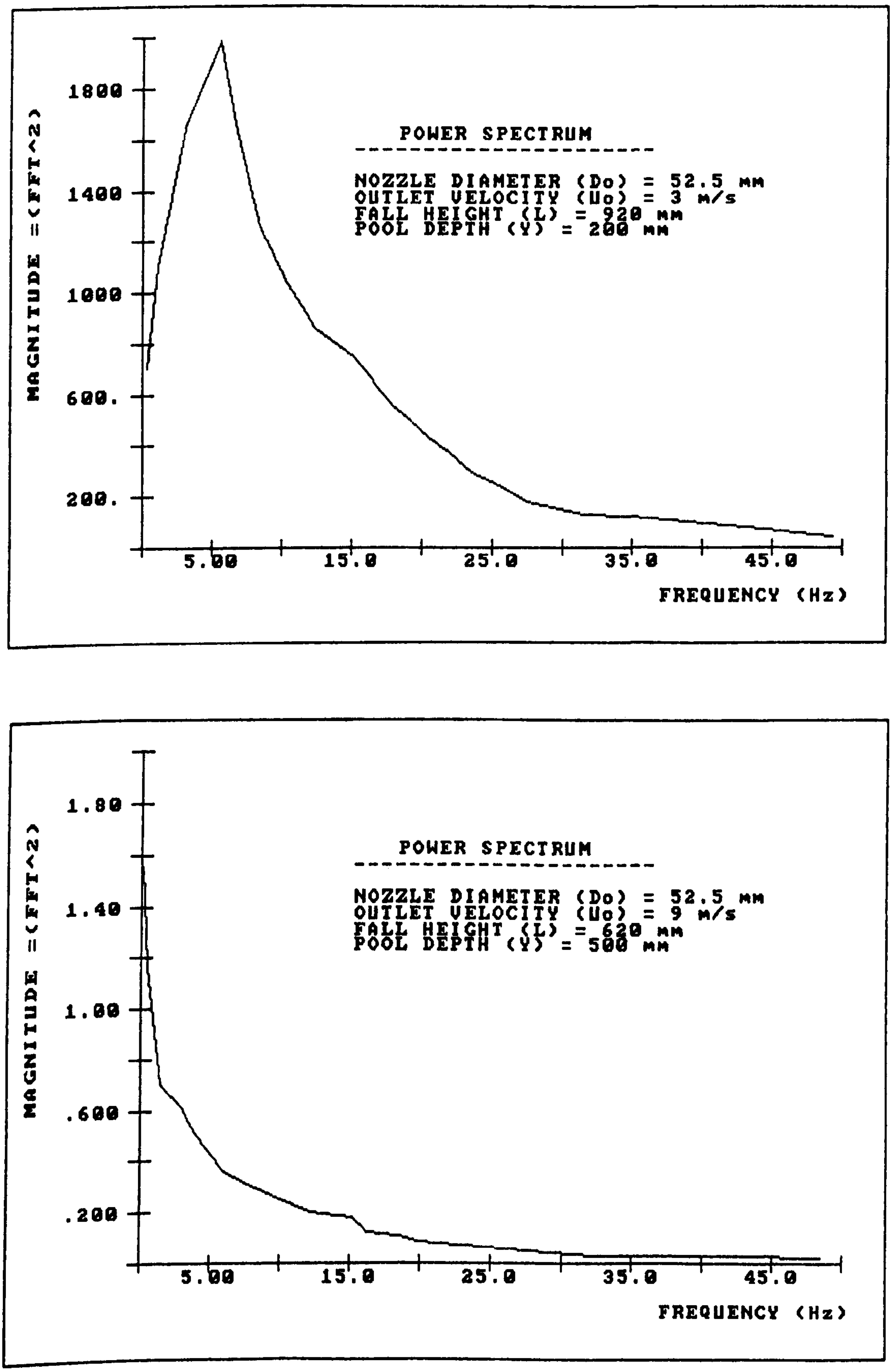

Fig. 3.45 *POWER SPECTRA FOR 52.5 mm DIA. JET AT DIFFERENT VELOCITIES AND PLUNGE POOL DEPTHS*

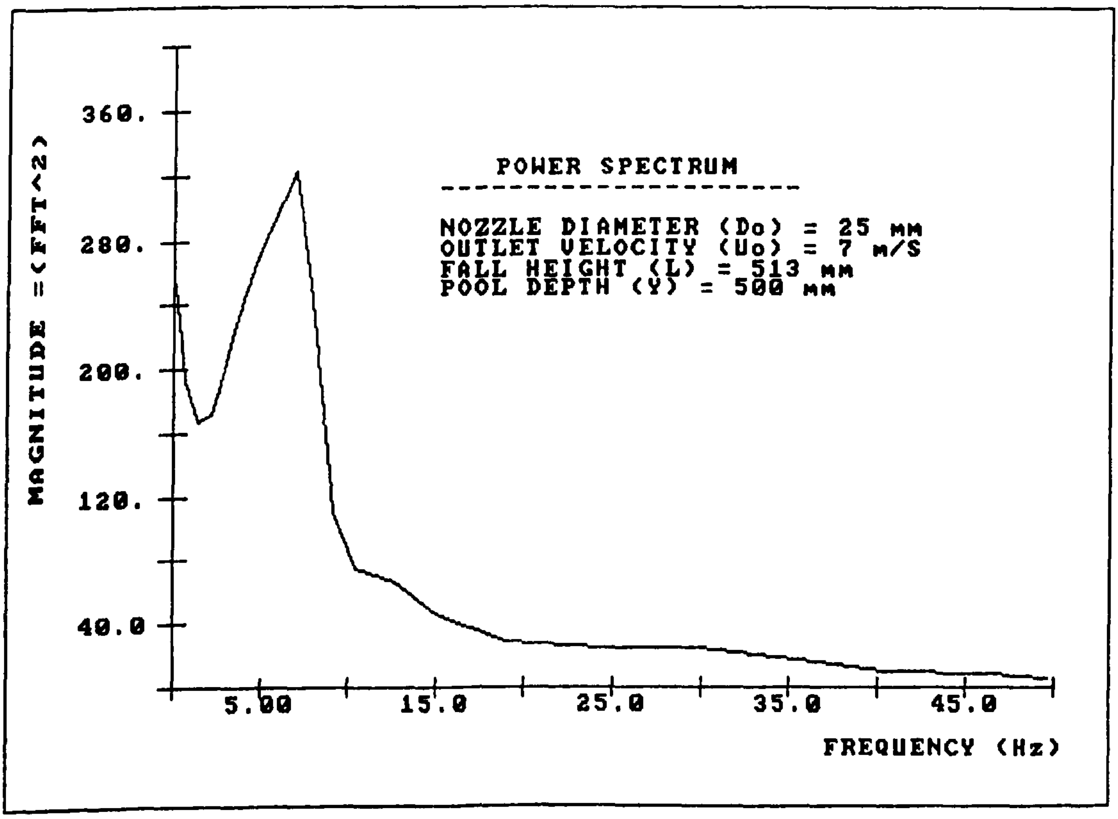

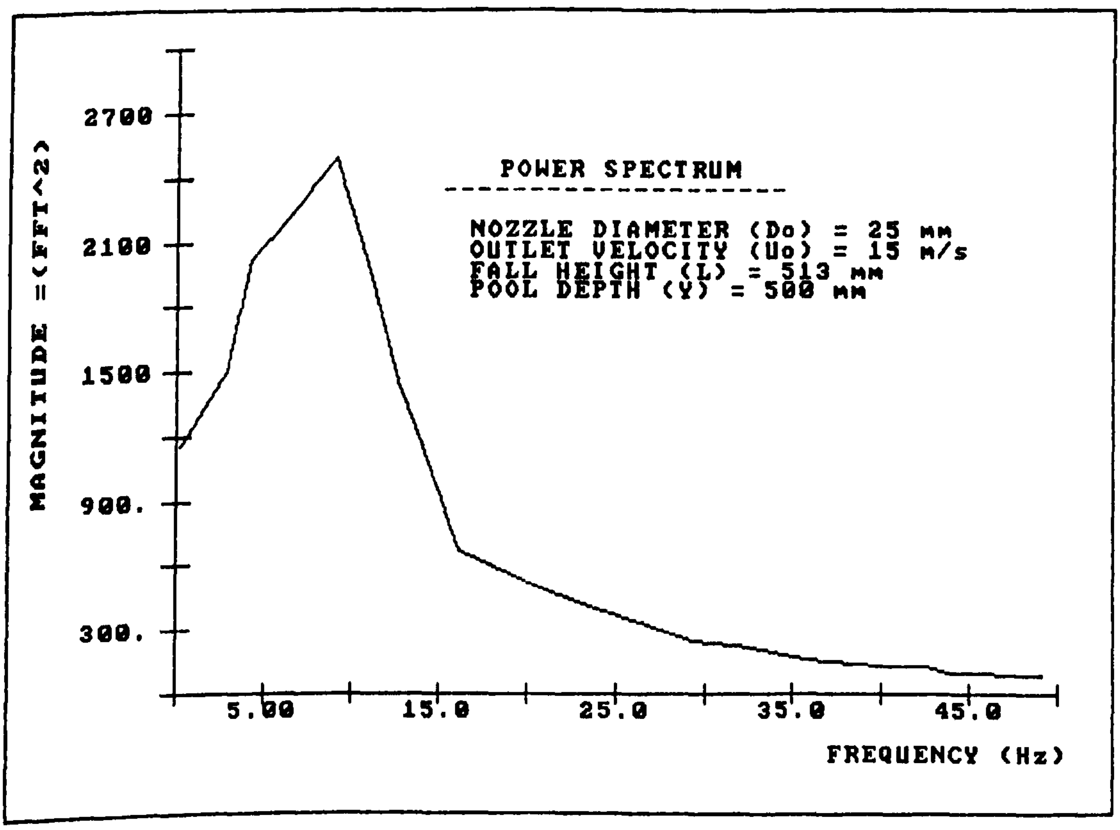

Fig. 3.46 *POWER SPECTRA FOR 25 mm NOZZLE DIA. JET AT DIFFERENT VELOCITIES*

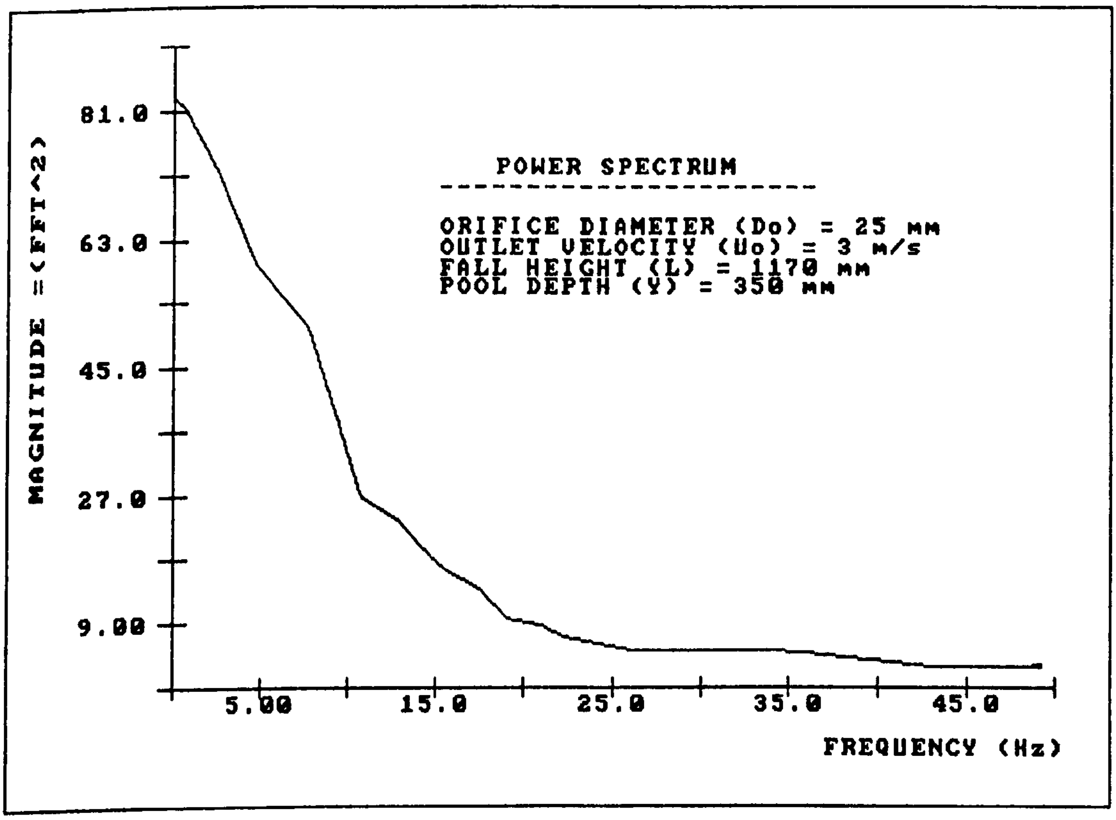

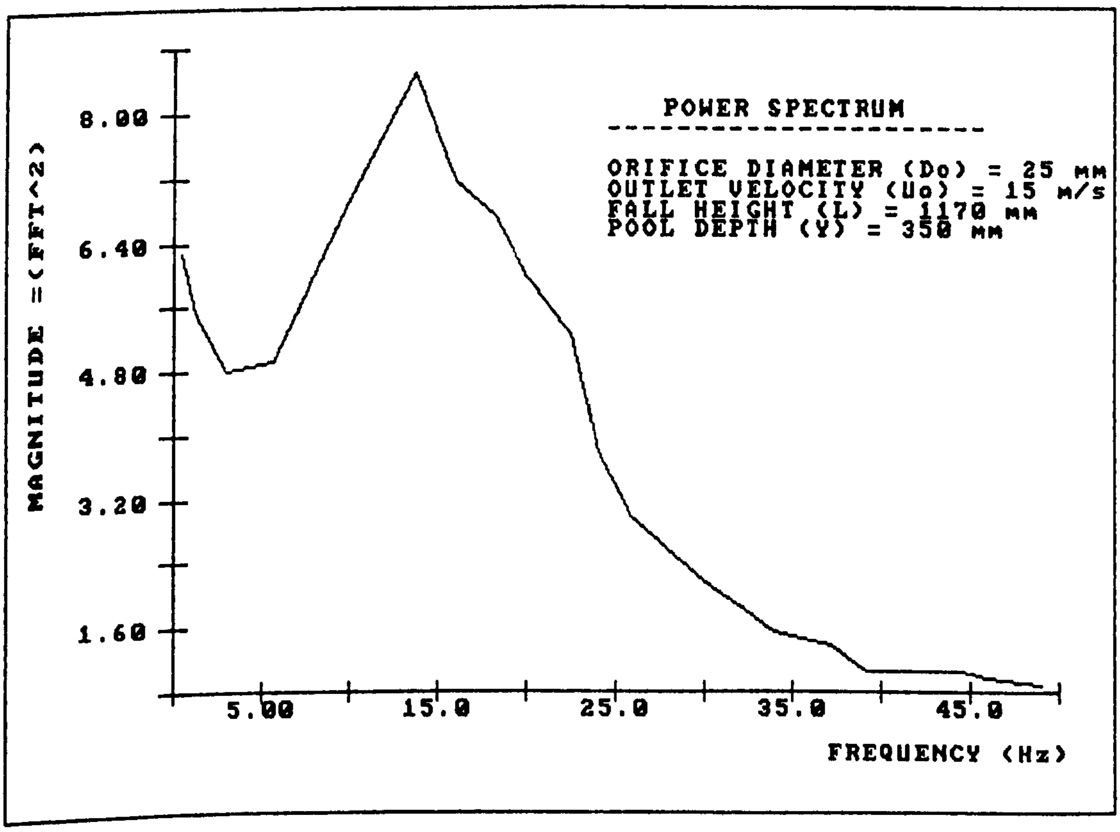

Fig. 3.47 *POWER SPECTRA FOR 25 mm ORIFICE DIA. JET AT DIFFERENT VELOCITIES*

FIGURES FOR CHAPTER 4

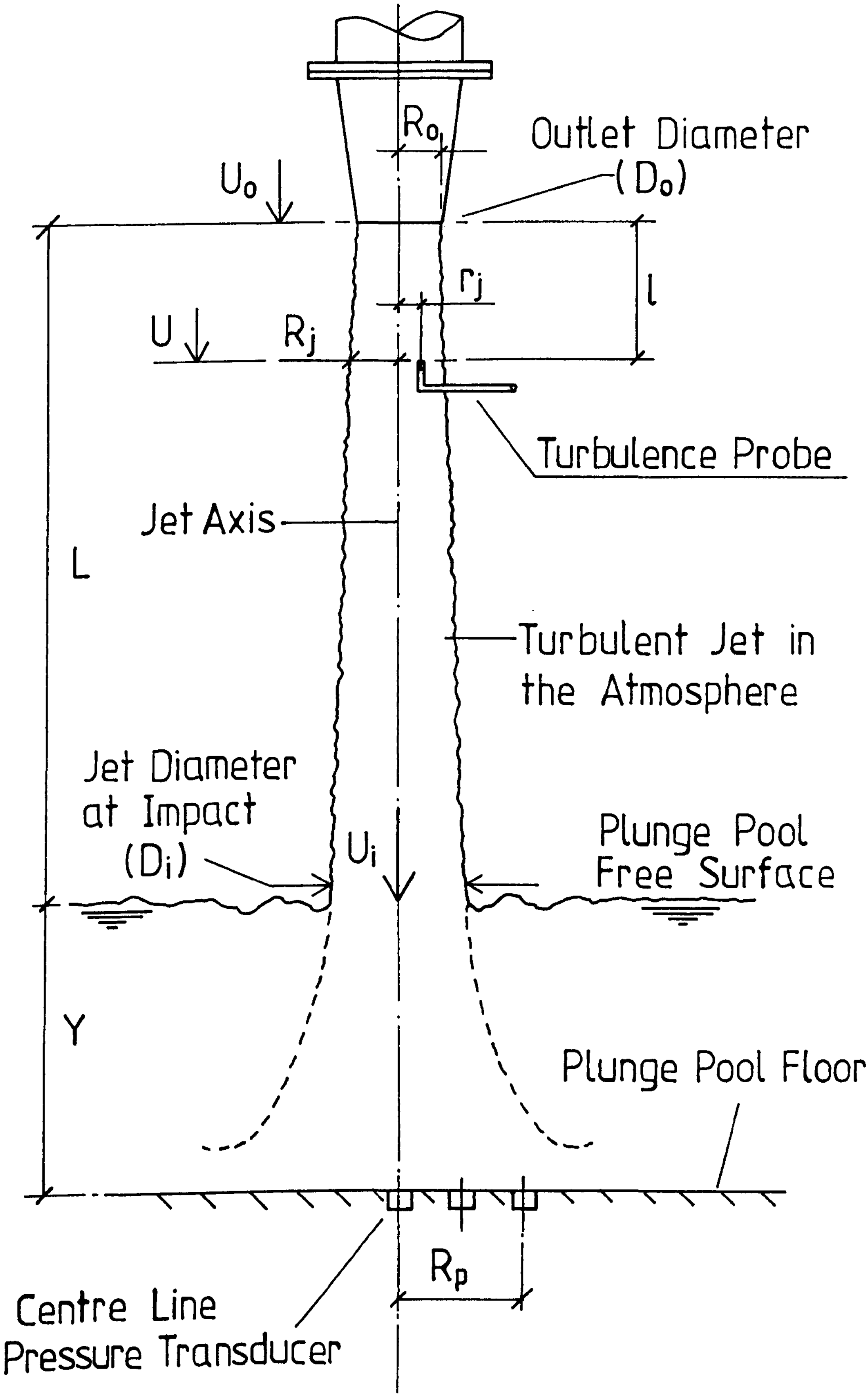

Fig. 4(a) DEFINITION SKETCH FOR TERMS USED IN RESULTS DIAGRAMS.

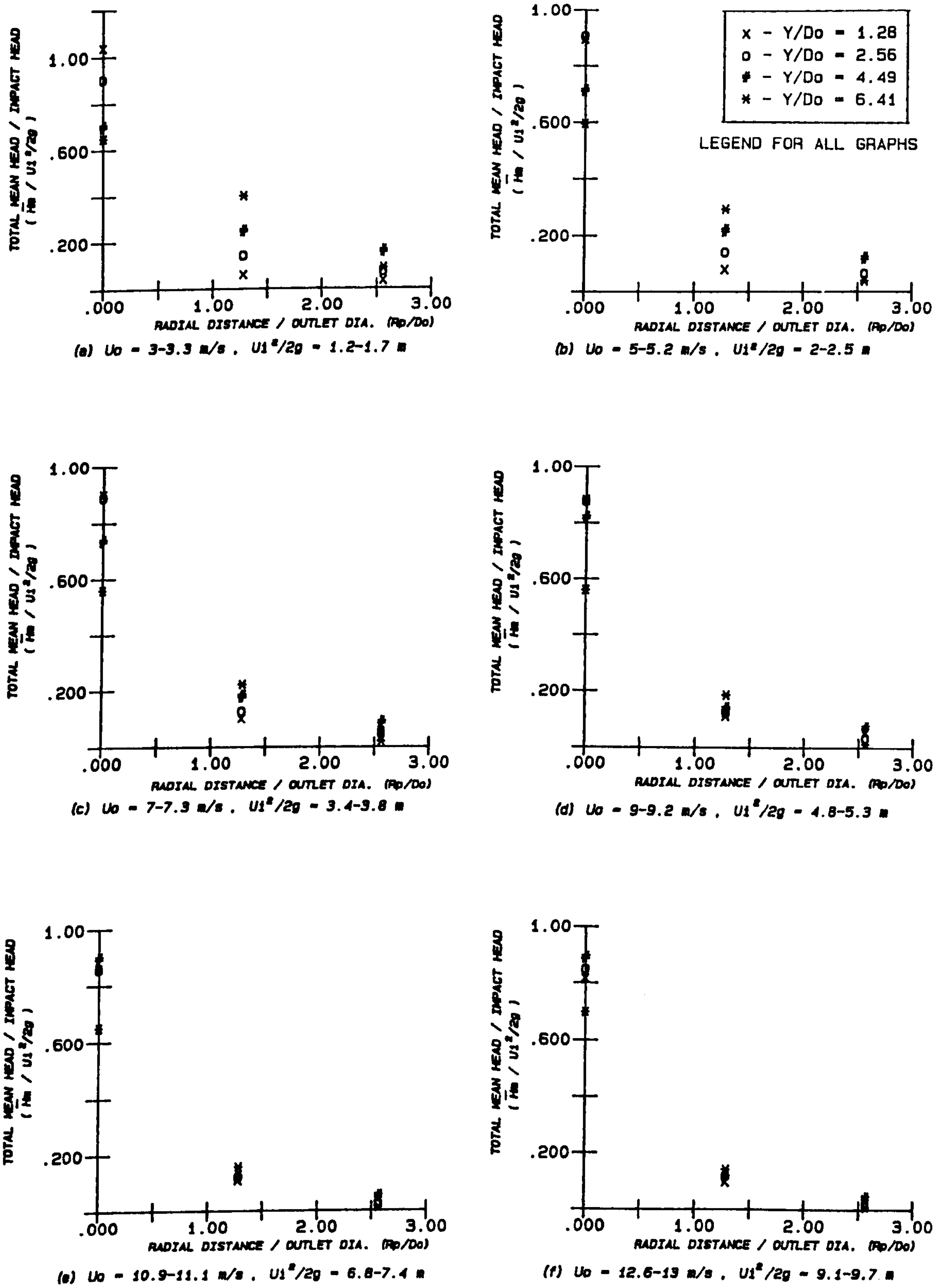

FIG. 4.1 TOTAL MEAN PRESSURE HEAD VARIATION IN RADIAL DIRECTION (Rp/Do) FOR A RANGE OF PLUNGE POOL DEPTHS (Do = 78 mm , L = 725 - 1125 mm)

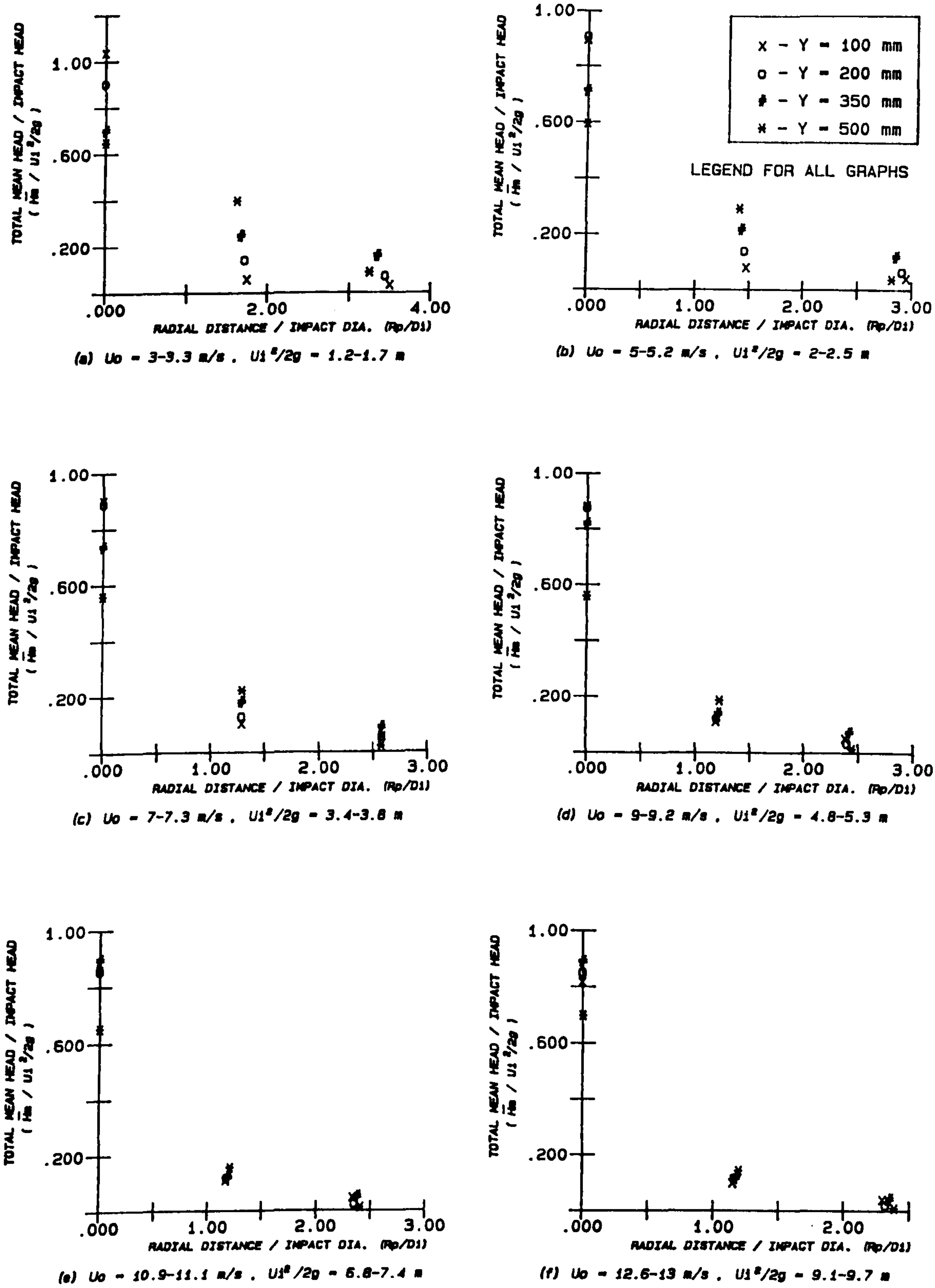

FIG. 4.2 TOTAL MEAN PRESSURE HEAD VARIATION IN RADIAL DIRECTION (Rp/Di) FOR A RANGE OF PLUNGE POOL DEPTHS (Do = 78 mm , L = 725 - 1125 mm)

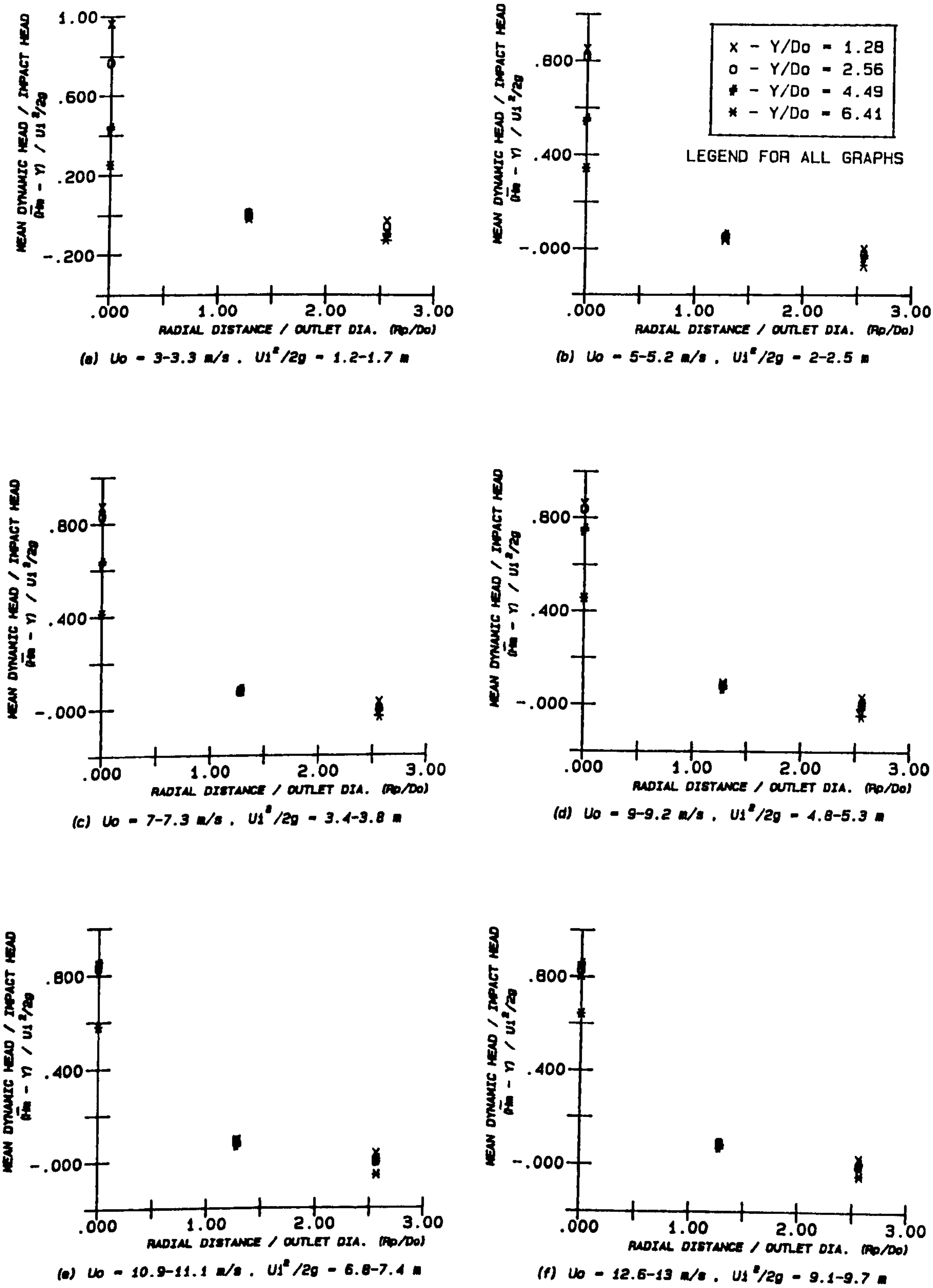

FIG. 4.3 MEAN DYNAMIC PRESSURE HEAD VARIATION IN RADIAL DIRECTION (Rp/Do) FOR A RANGE OF PLUNGE POOL DEPTHS (Do = 78 mm , L = 725 - 1125 mm)

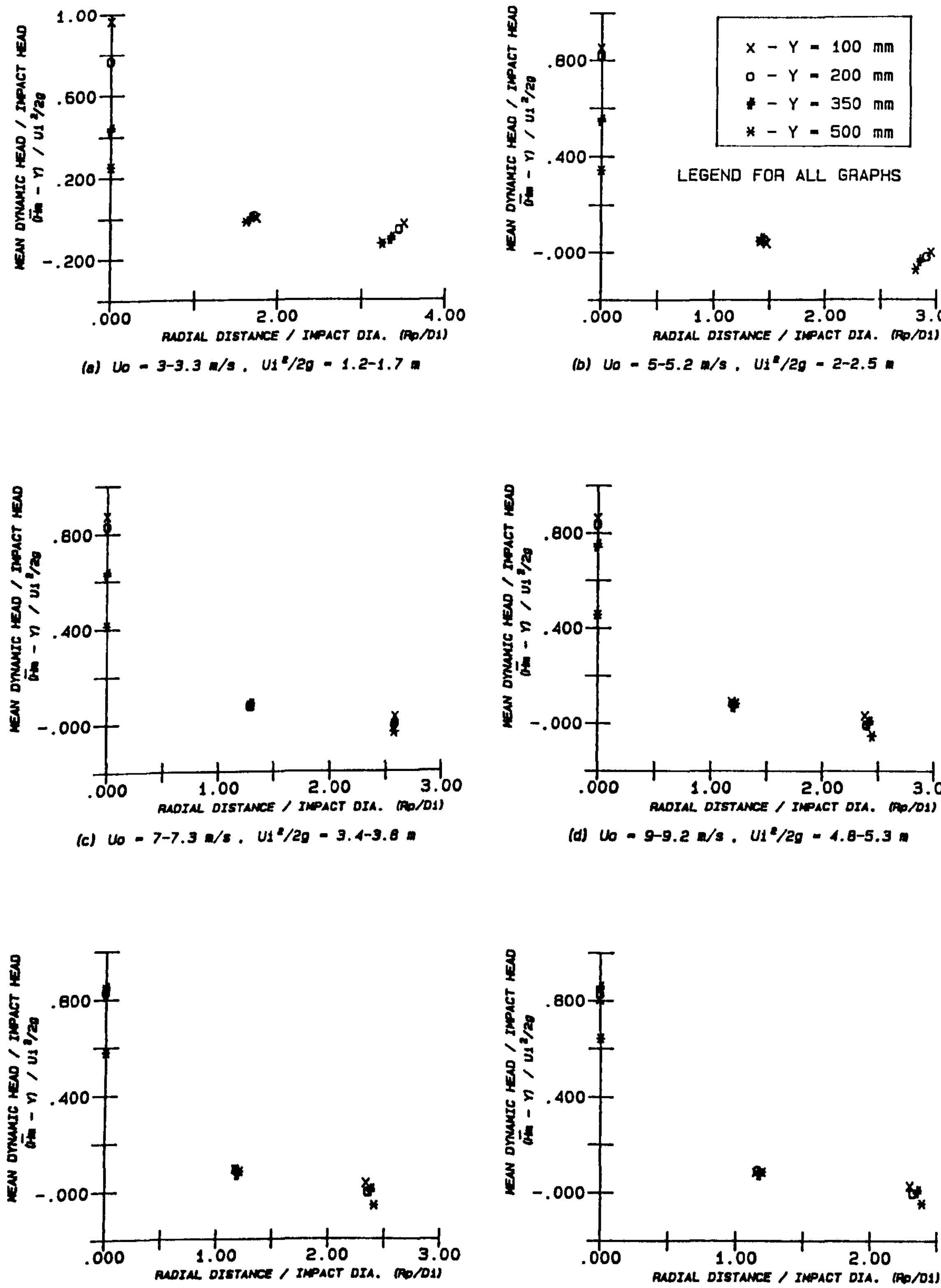

(a) Uo = 3-3.3 m/s , $Ui^2/2g$ = 1.2-1.7 m

(b) Uo = 5-5.2 m/s , $Ui^2/2g$ = 2-2.5 m

(c) Uo = 7-7.3 m/s , $Ui^2/2g$ = 3.4-3.8 m

(d) Uo = 9-9.2 m/s , $Ui^2/2g$ = 4.8-5.3 m

(e) Uo = 10.9-11.1 m/s , $Ui^2/2g$ = 6.8-7.4 m

(f) Uo = 12.6-13 m/s , $Ui^2/2g$ = 9.1-9.7 m

FIG. 4.4 MEAN DYNAMIC PRESSURE HEAD VARIATION IN RADIAL DIRECTION (Rp/Di) FOR A RANGE OF PLUNGE POOL DEPTHS (Do = 78 mm , L = 725 - 1125 mm)

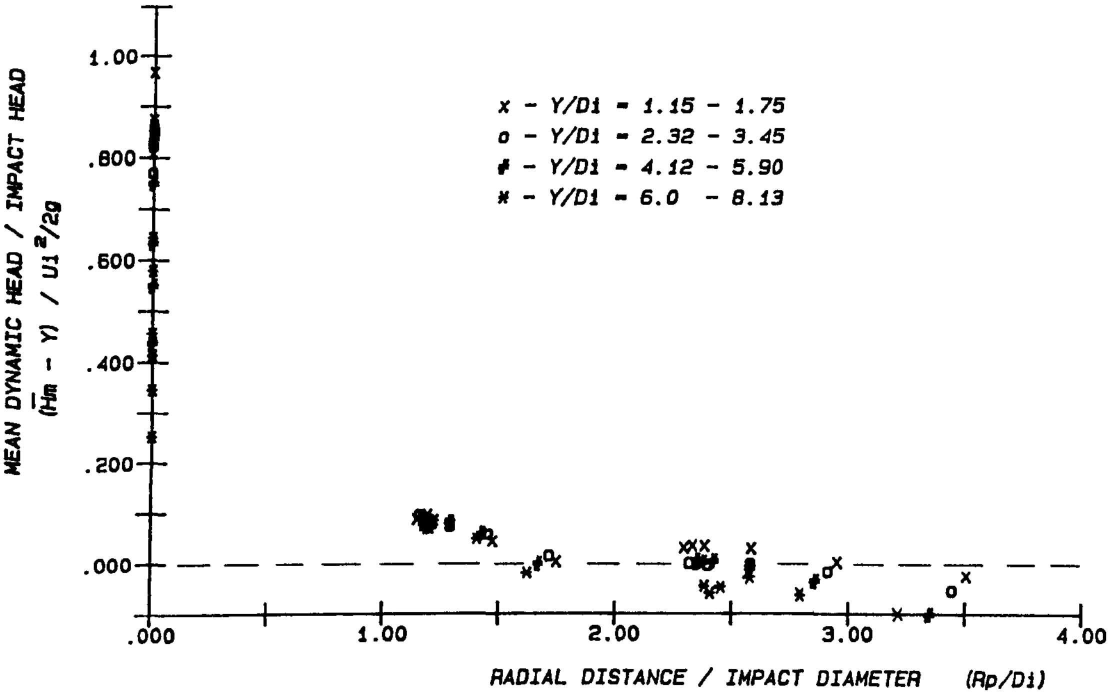

FIG. 4.4 (i) MEAN DYNAMIC PRESSURE HEAD VARIATION IN RADIAL DIRECTION (Rp/Di) FOR ALL RESULTS. (Do = 78 mm , L = 725 - 1125 mm)

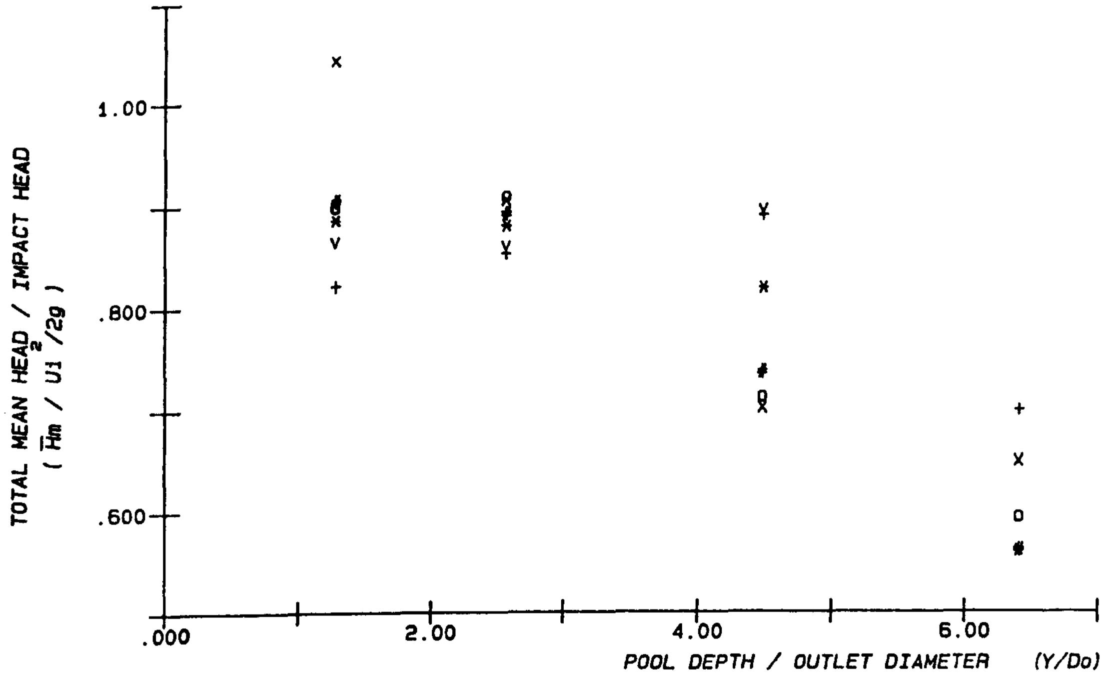

FIG. 4.5 (a) CENTRE LINE TOTAL MEAN PRESSURE HEAD RATIO VERSUS (Y/Do)
(Do = 78 mm , L = 725 - 1125 mm)

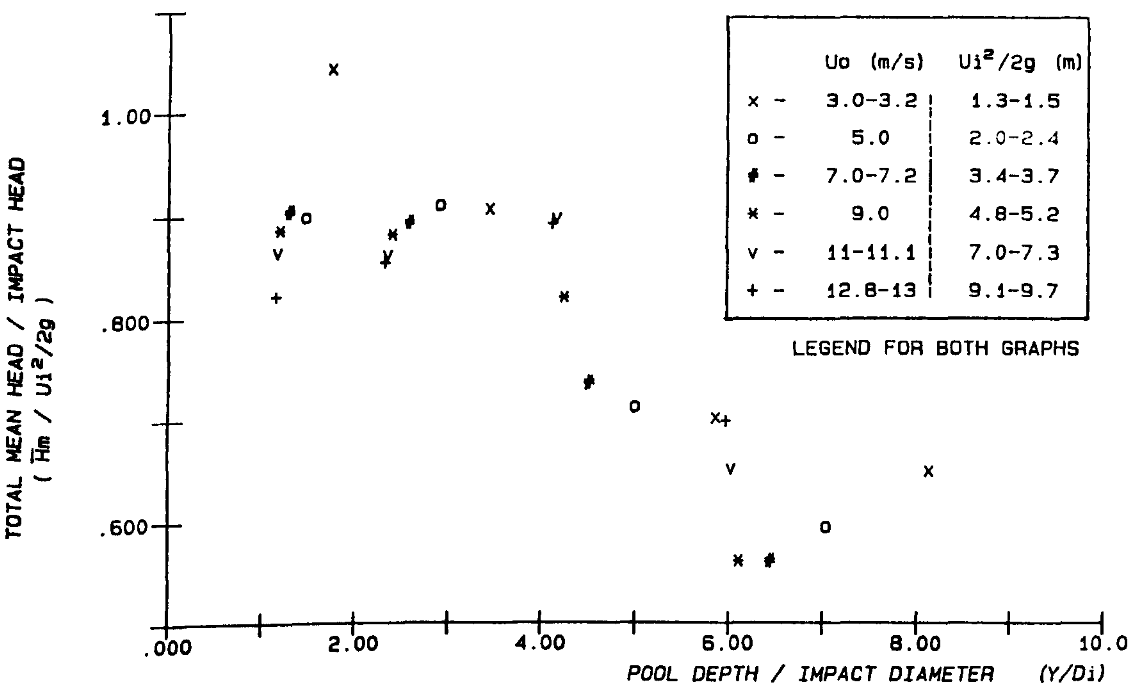

FIG. 4.5 (b) CENTRE LINE TOTAL MEAN PRESSURE HEAD RATIO VERSUS (Y/Di)
(Do = 78 mm , L = 725 - 1125 mm)

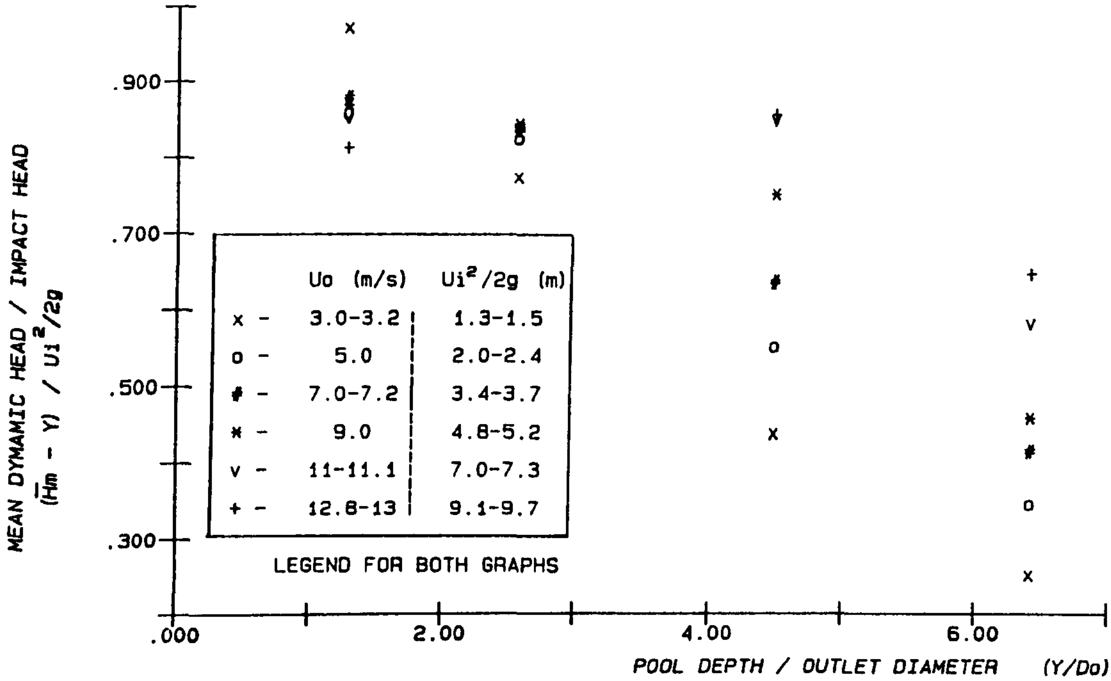

FIG. 4.6 (a) CENTRE LINE MEAN DYNAMIC PRESSURE HEAD RATIO VERSUS (Y/Do)
(Do = 78 mm , L = 725 - 1125 mm)

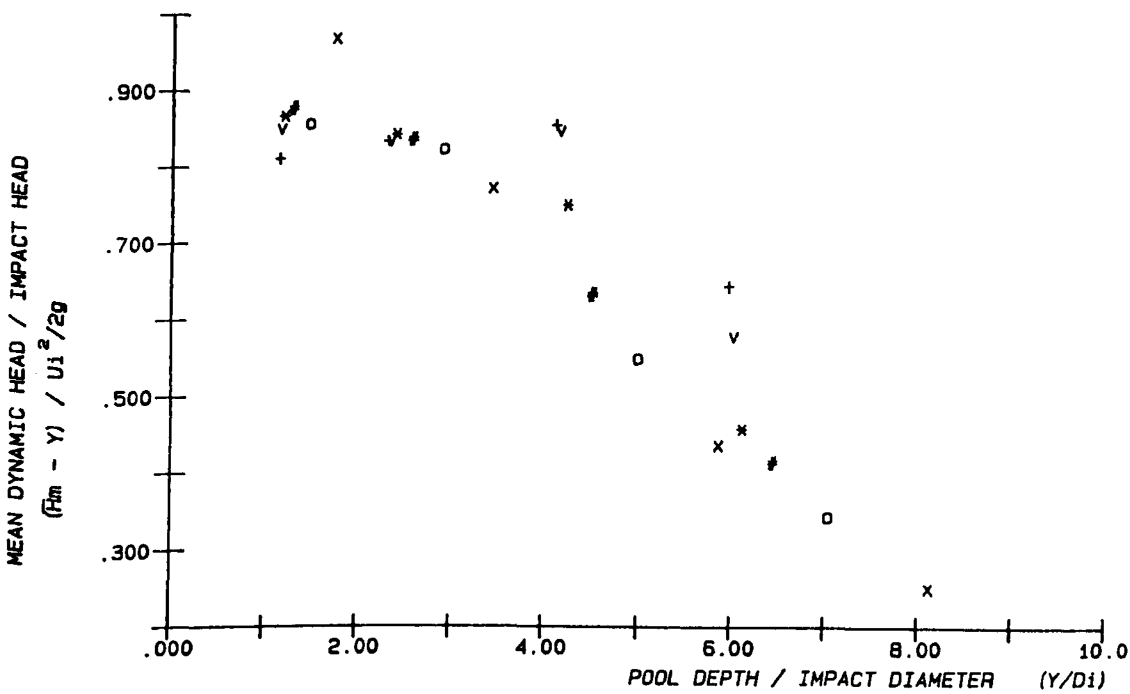

FIG. 4.6 (b) CENTRE LINE MEAN DYNAMIC PRESSURE HEAD RATIO VERSUS (Y/Di)
(Do = 78 mm , L = 725 - 1125 mm)

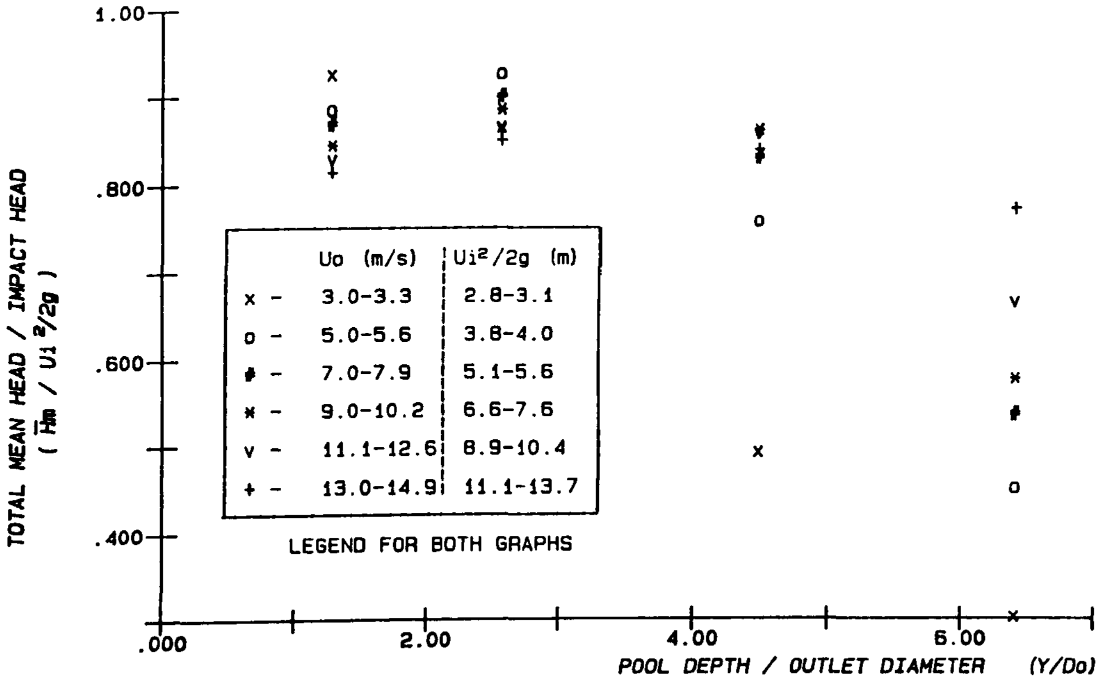

FIG. 4.7(a) CENTRE LINE TOTAL MEAN PRESSURE HEAD RATIO VERSUS (Y/Do)
(Do = 78 mm , L = 2230 - 2630 mm)

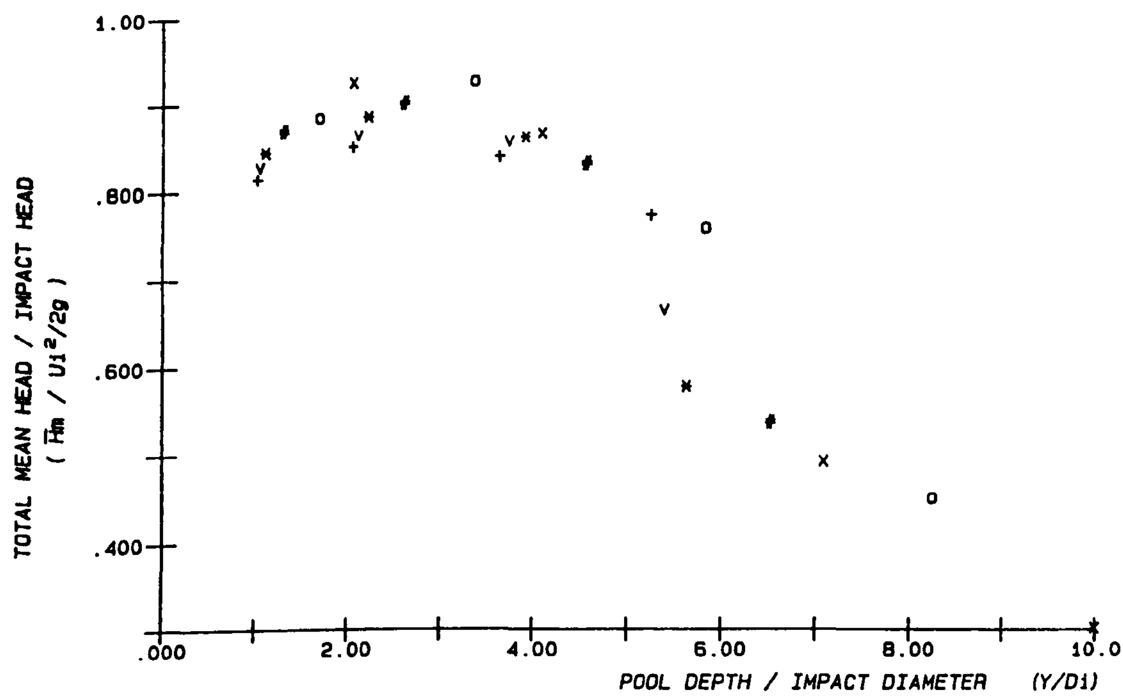

FIG. 4.7(b) CENTRE LINE TOTAL MEAN PRESSURE HEAD RATIO VERSUS (Y/Di)
(Do = 78 mm , L = 2230 - 2630 mm)

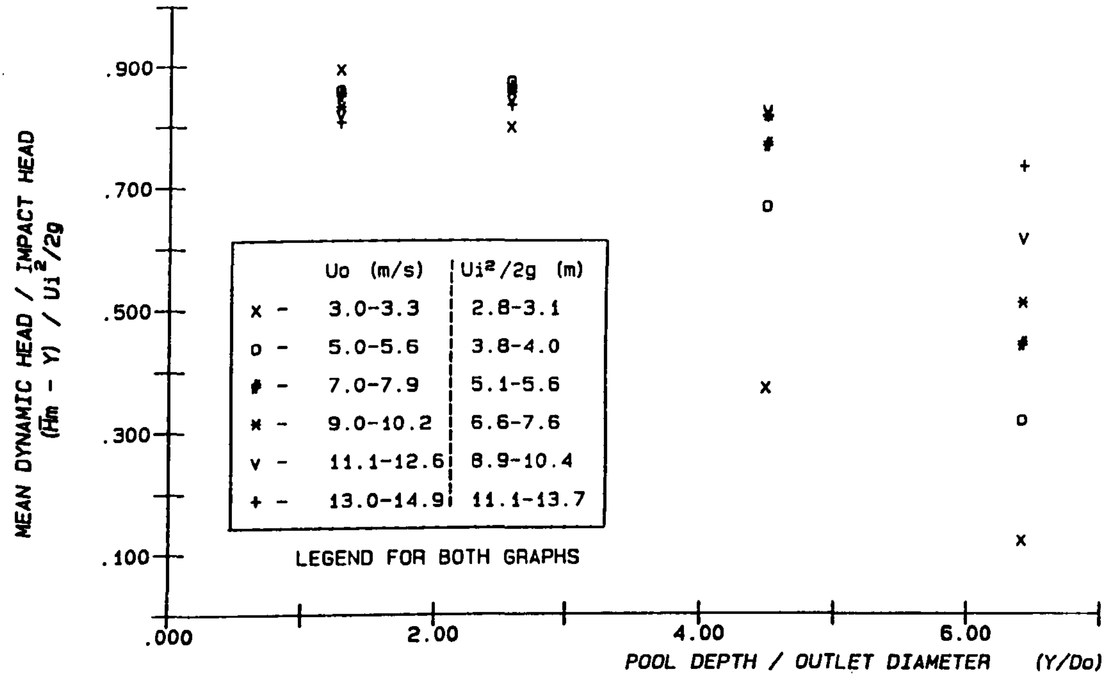

FIG. 4.8 (a) CENTRE LINE MEAN DYNAMIC PRESSURE HEAD RATIO VERSUS (Y/Do)
(Do = 78 mm , L = 2230 - 2630 mm)

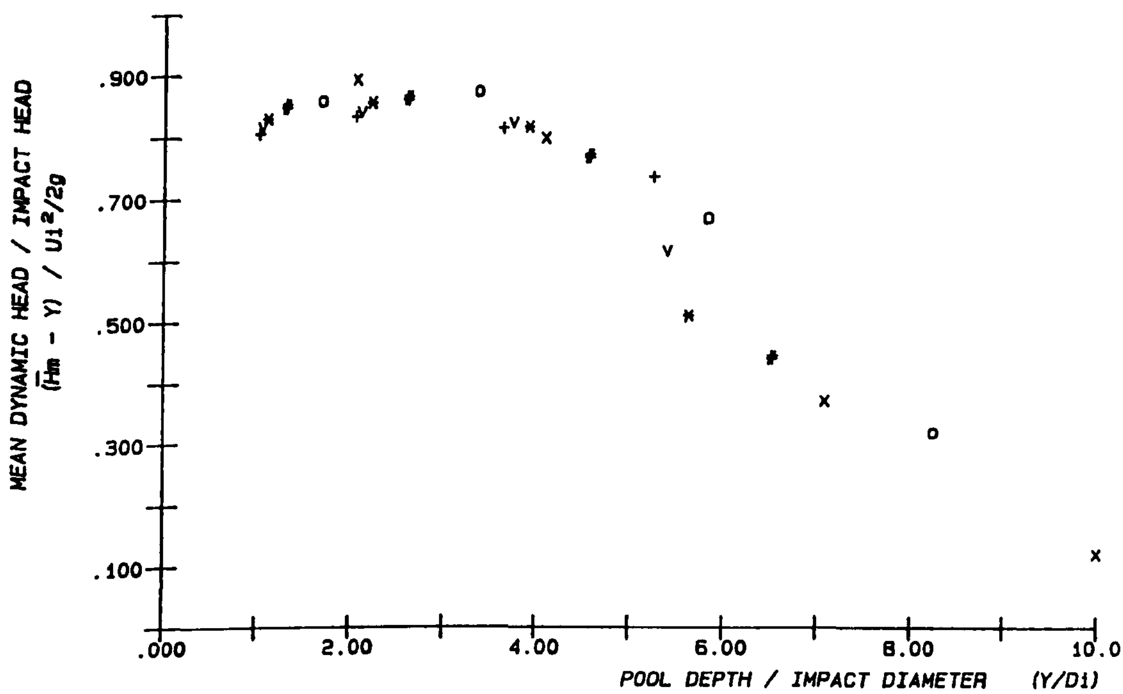

FIG. 4.8 (b) CENTRE LINE MEAN DYNAMIC PRESSURE HEAD RATIO VERSUS (Y/Di)
(Do = 78 mm , L = 2230 - 2630 mm)

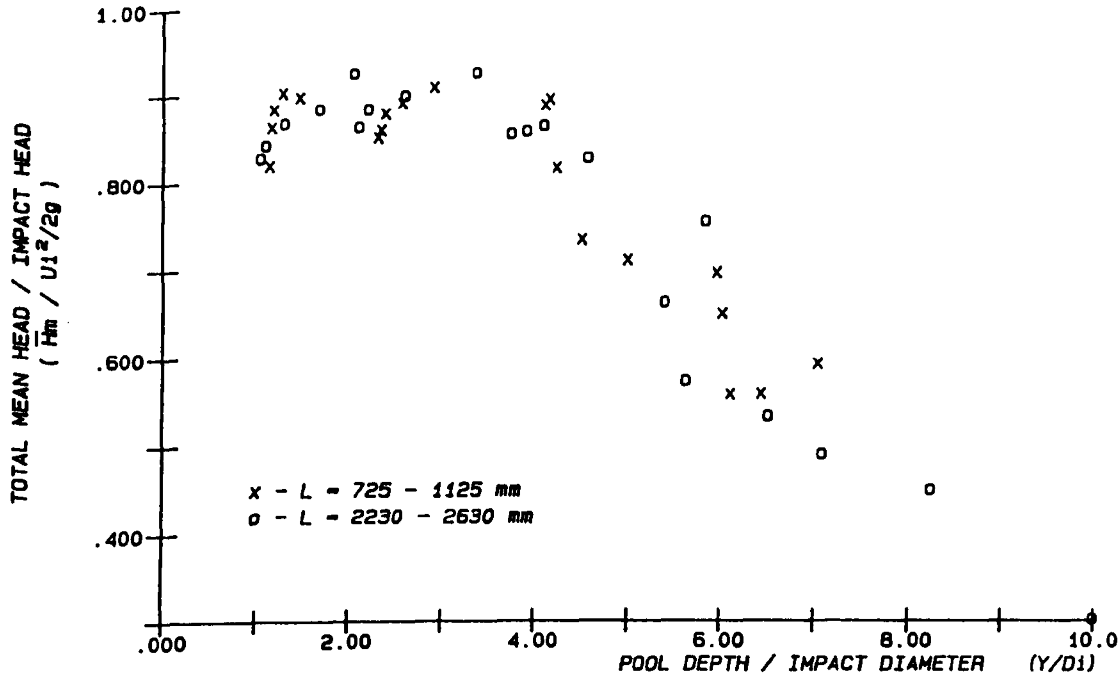

FIG. 4.9 (a) *TOTAL MEAN PRESSURE HEAD AGAINST PLUNGE POOL DEPTH FOR 78 mm NOZZLE FOR THE TWO DIFFERENT FALL LENGTHS*

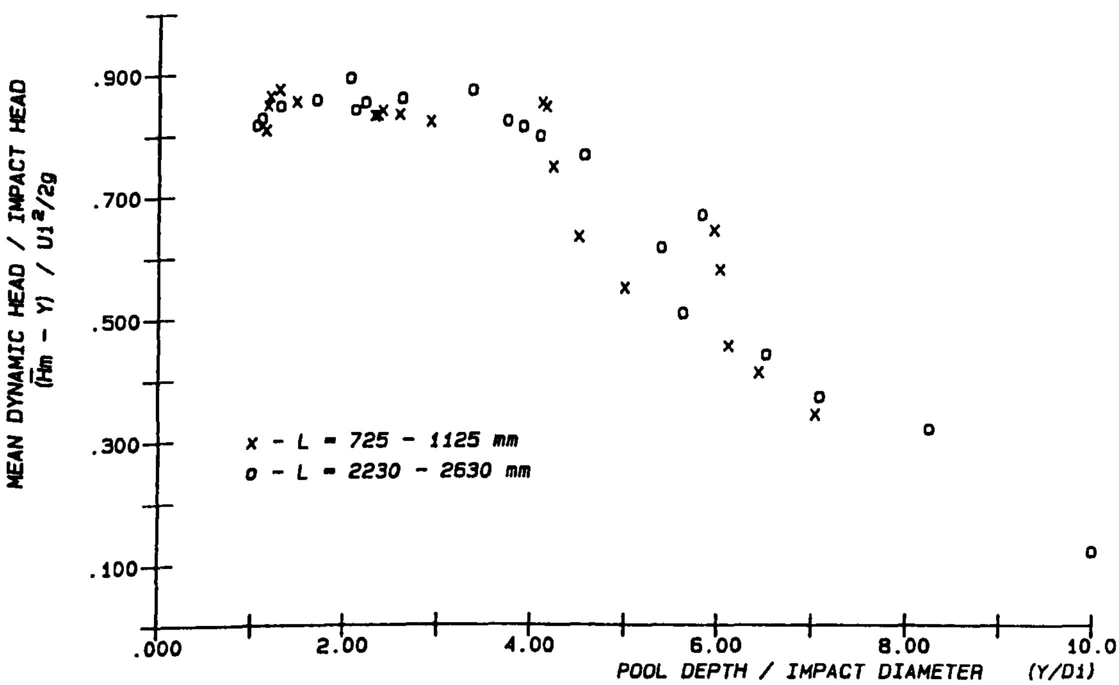

FIG. 4.9 (b) *MEAN DYNAMIC PRESSURE HEAD AGAINST PLUNGE POOL DEPTH FOR 78 mm NOZZLE FOR THE TWO DIFFERENT FALL LENGTHS*

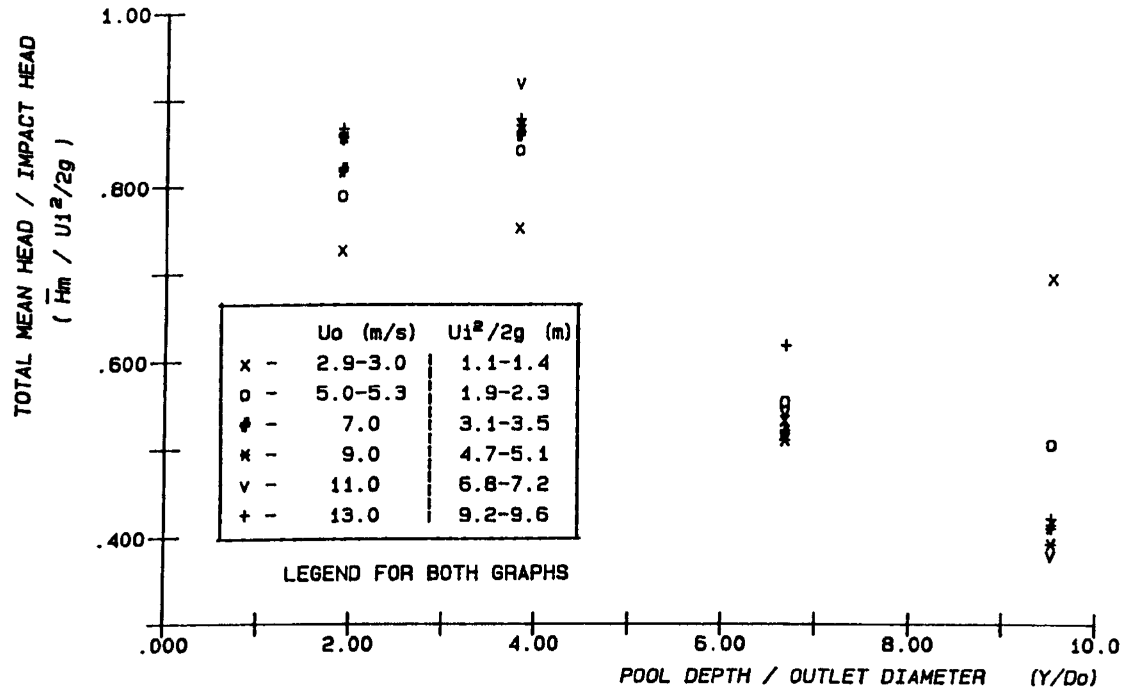

FIG. 4.10 (a) CENTRE LINE TOTAL MEAN PRESSURE HEAD RATIO VERSUS (Y/Do)
(Do = 52.5 mm , L = 620 - 1020 mm)

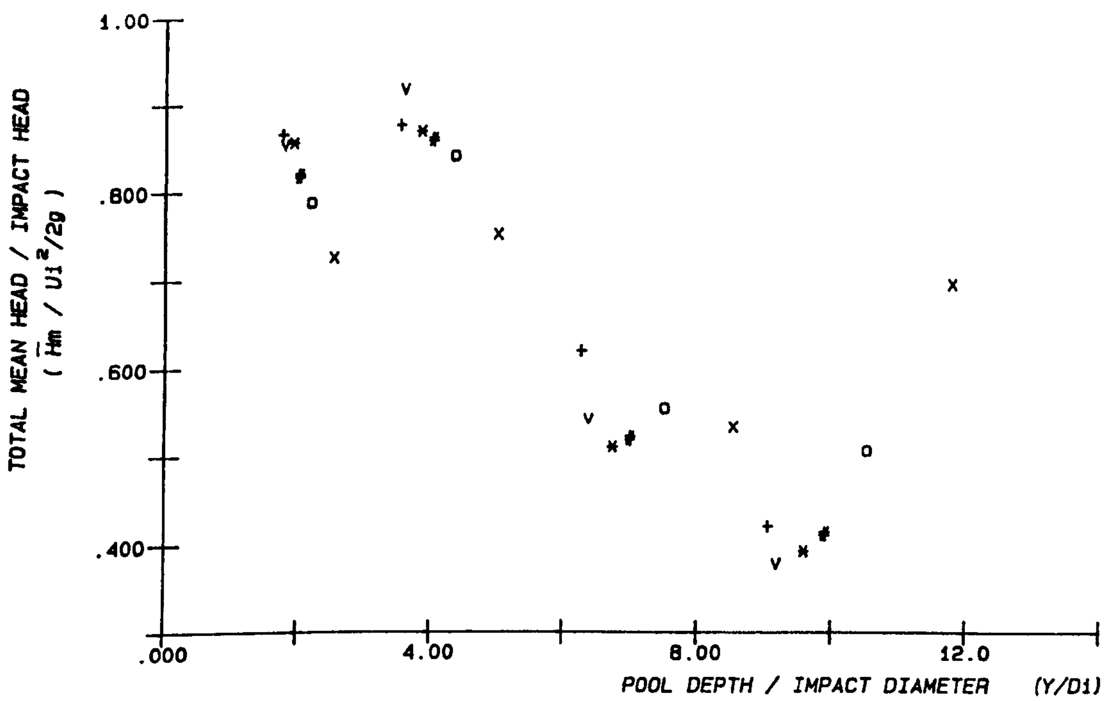

FIG. 4.10 (b) CENTRE LINE TOTAL MEAN PRESSURE HEAD RATIO VERSUS (Y/Di)
(Do = 52.5 mm , L = 620 - 1020 mm)

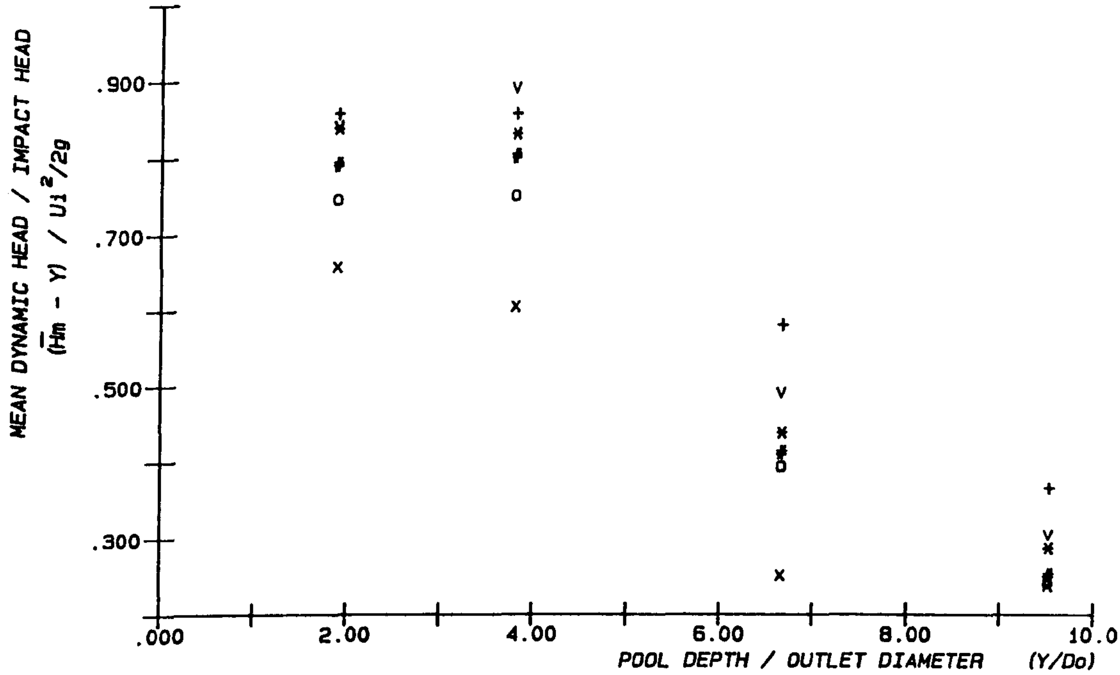

FIG. 4.11 (a) CENTRE LINE MEAN DYNAMIC PRESSURE HEAD RATIO VERSUS (Y/Do)
(Do = 52.5 mm , L = 620 - 1020 mm)

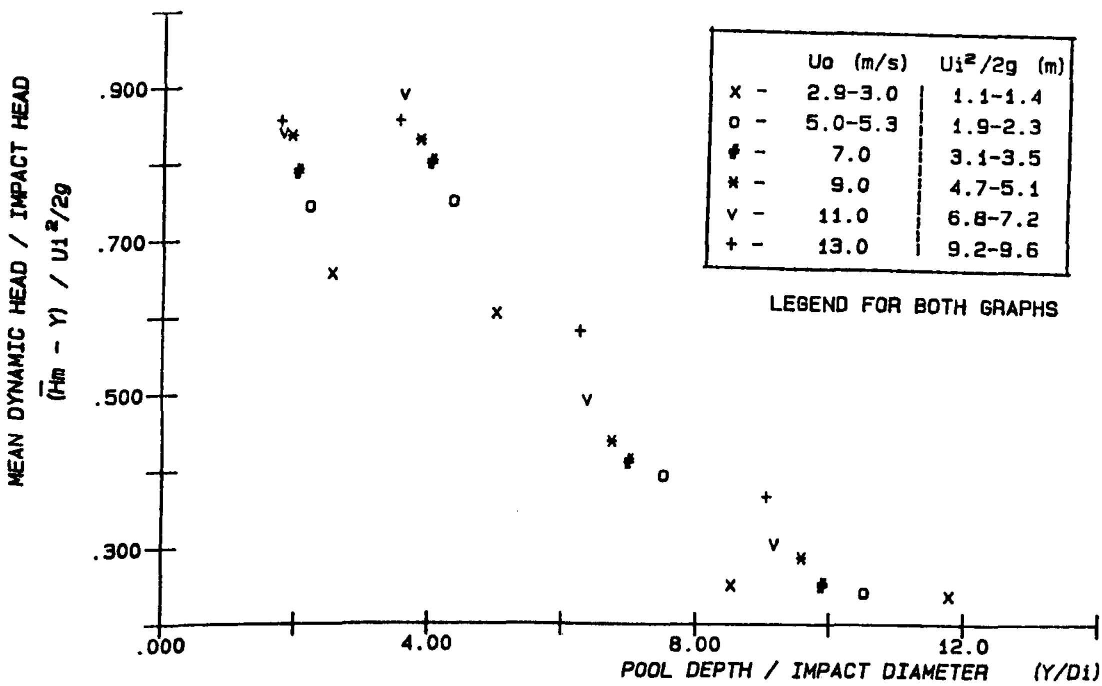

FIG. 4.11 (b) CENTRE LINE MEAN DYNAMIC PRESSURE HEAD RATIO VERSUS (Y/Di)
(Do = 52.5 mm , L = 620 - 1020 mm)

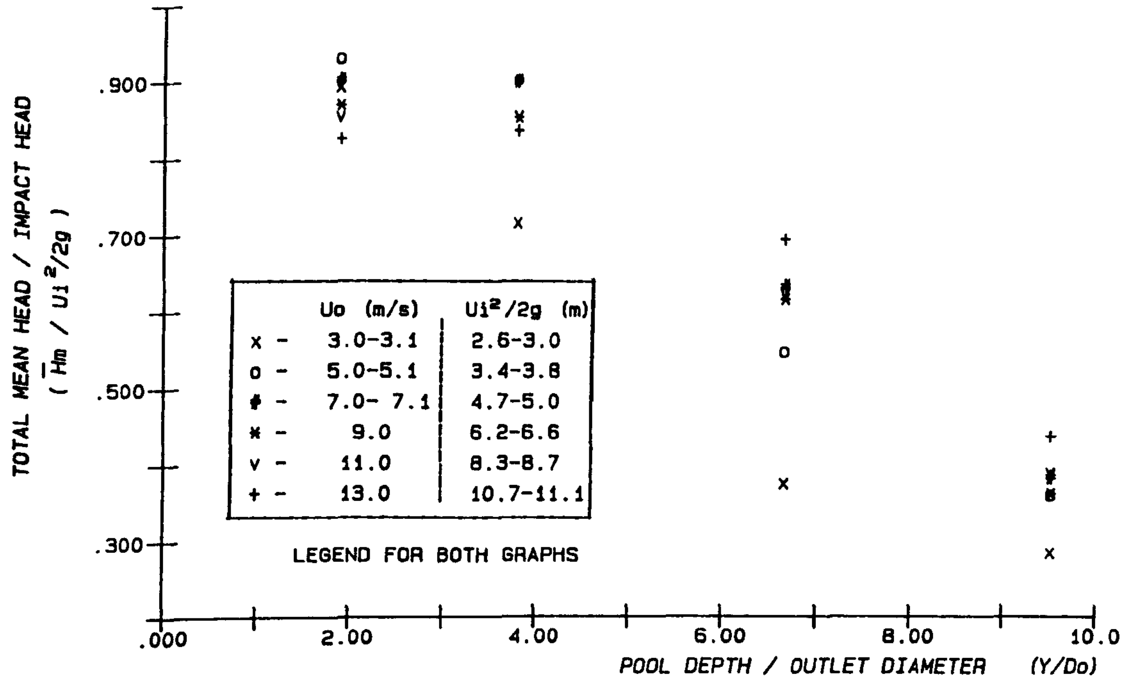

FIG. 4.12(a) CENTRE LINE TOTAL MEAN PRESSURE HEAD RATIO VERSUS (Y/Do)
(Do = 52.5 mm , L = 2126 - 2526 mm)

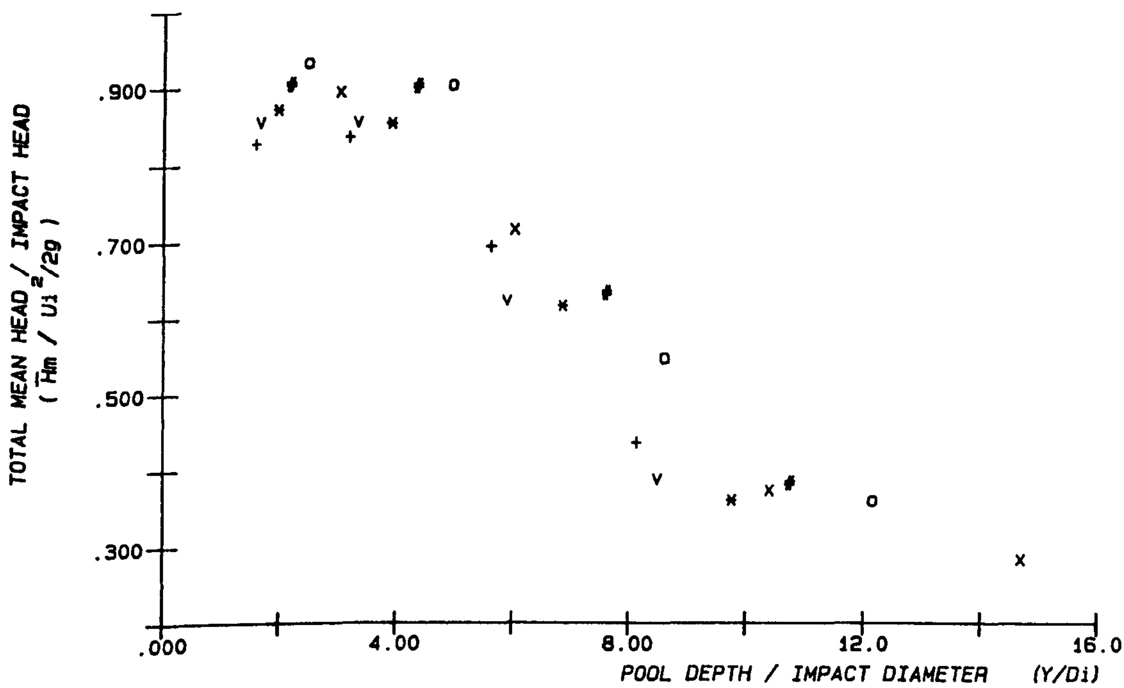

FIG. 4.12(b) CENTRE LINE TOTAL MEAN PRESSURE HEAD RATIO VERSUS (Y/Di)
(Do = 52.5 mm , L = 2126 - 2526 mm)

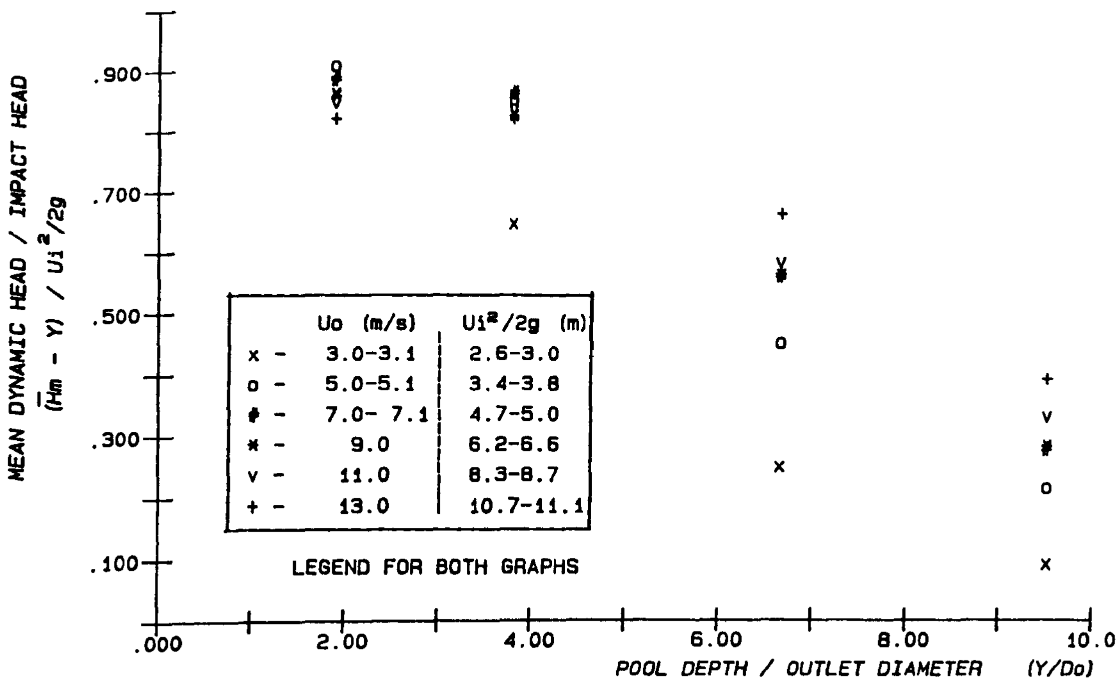

FIG. 4.13 (a) CENTRE LINE MEAN DYNAMIC PRESSURE HEAD RATIO VERSUS (Y/Do)
(Do = 52.5 mm , L = 2126 - 2526 mm)

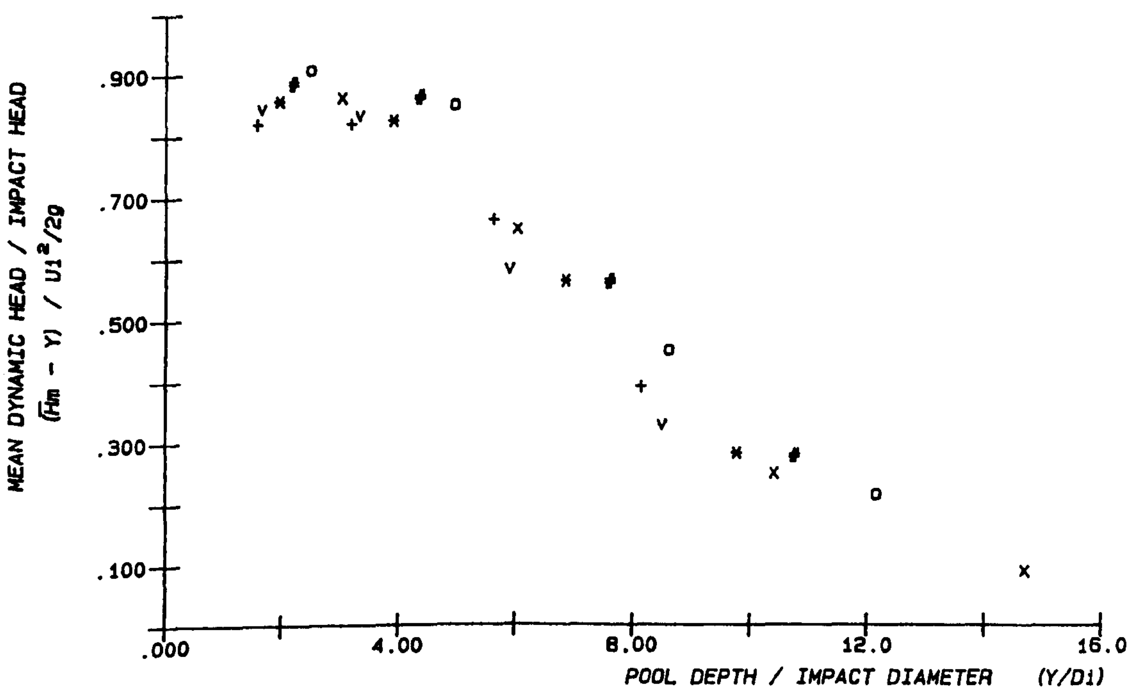

FIG. 4.13 (b) CENTRE LINE MEAN DYNAMIC PRESSURE HEAD RATIO VERSUS (Y/Di)
(Do = 52.5 mm , L = 2126 - 2526 mm)

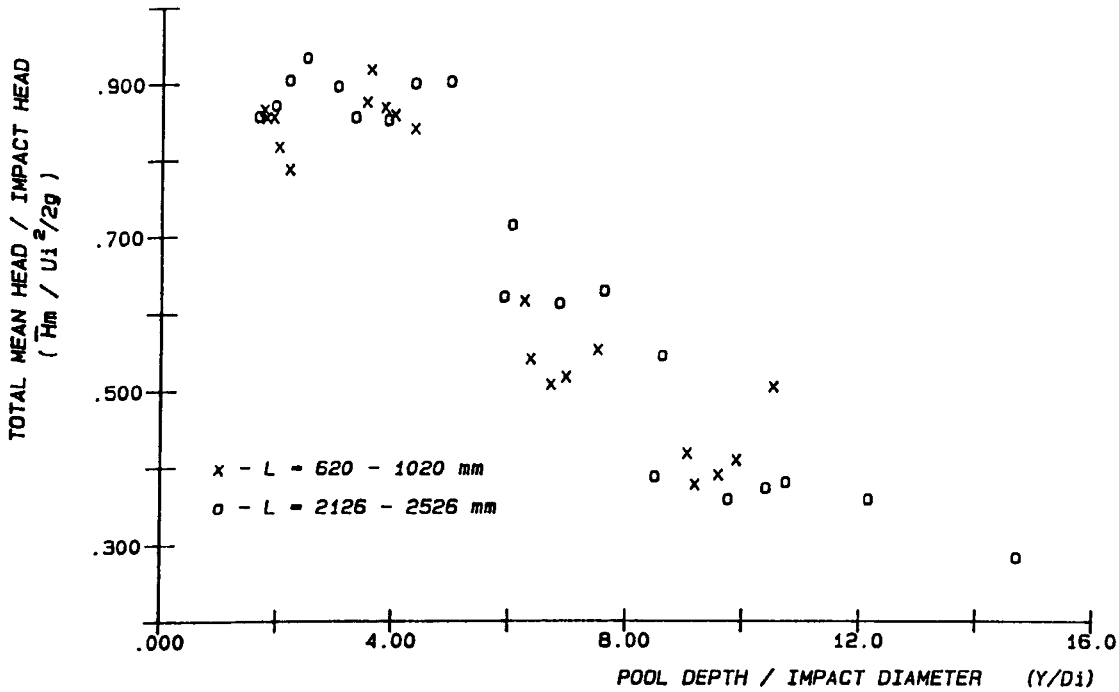

FIG. 4.14(a) TOTAL MEAN PRESSURE HEAD AGAINST PLUNGE POOL DEPTH FOR 52.5 mm NOZZLE FOR THE TWO DIFFERENT FALL LENGTHS

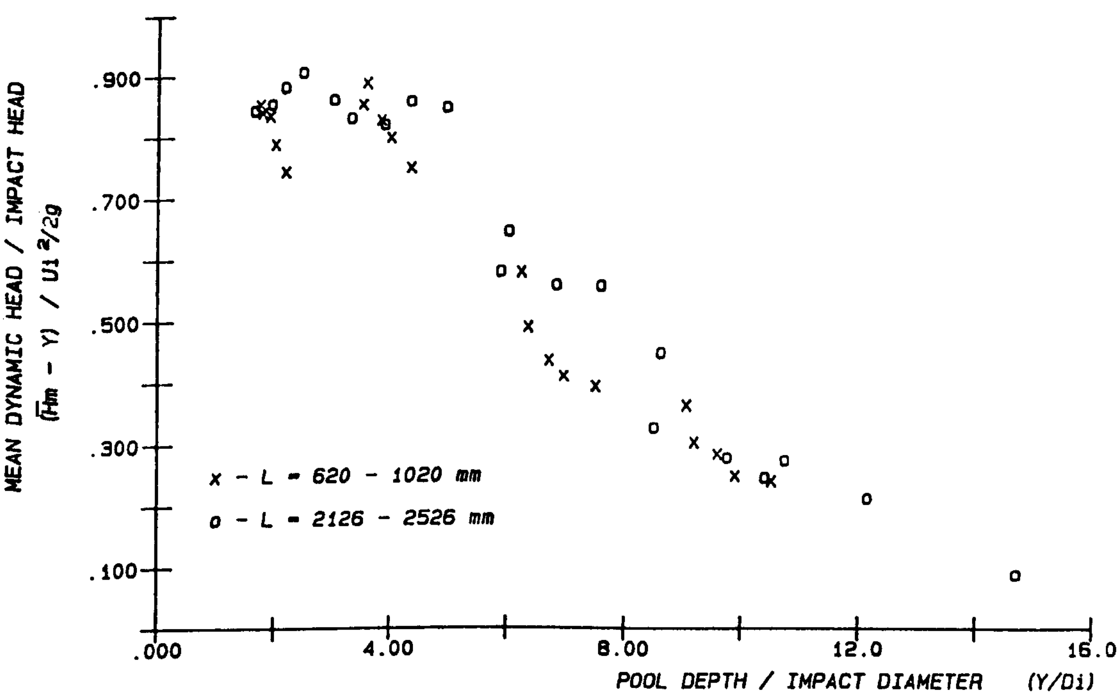

FIG. 4.14(b) MEAN DYNAMIC PRESSURE HEAD AGAINST PLUNGE POOL DEPTH FOR 52.5 mm NOZZLE FOR THE TWO DIFFERENT FALL LENGTHS

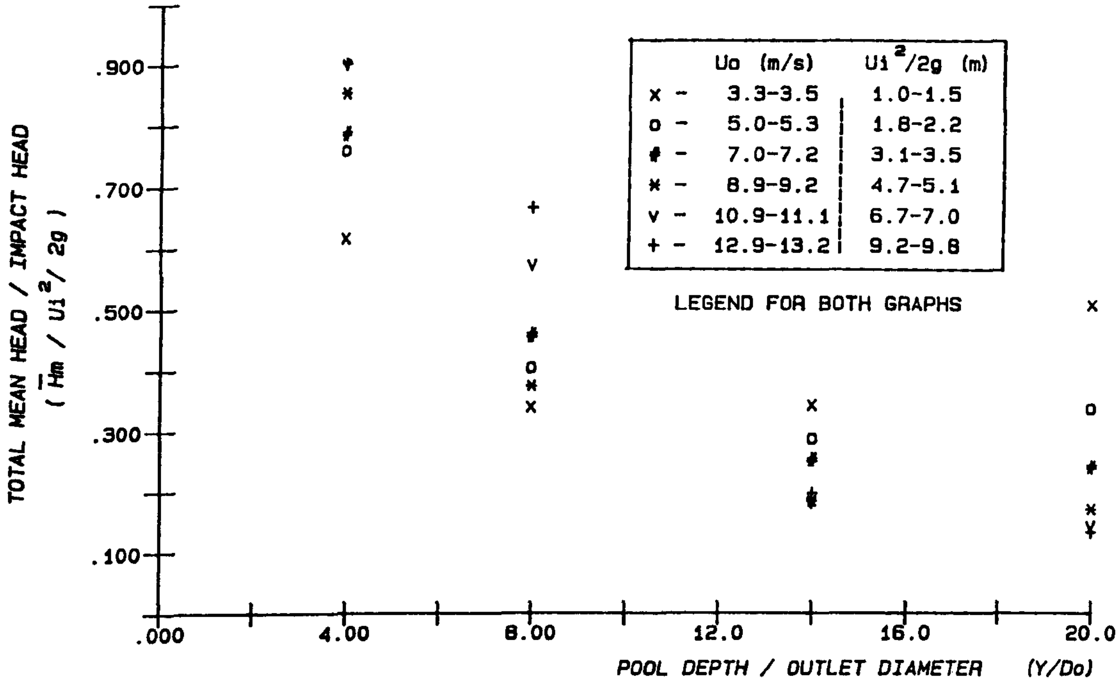

FIG. 4.15 (a) CENTRE LINE TOTAL MEAN PRESSURE HEAD RATIO VERSUS (Y/Do)
(NOZZLE : Do = 25 mm , L = 513 - 913 mm)

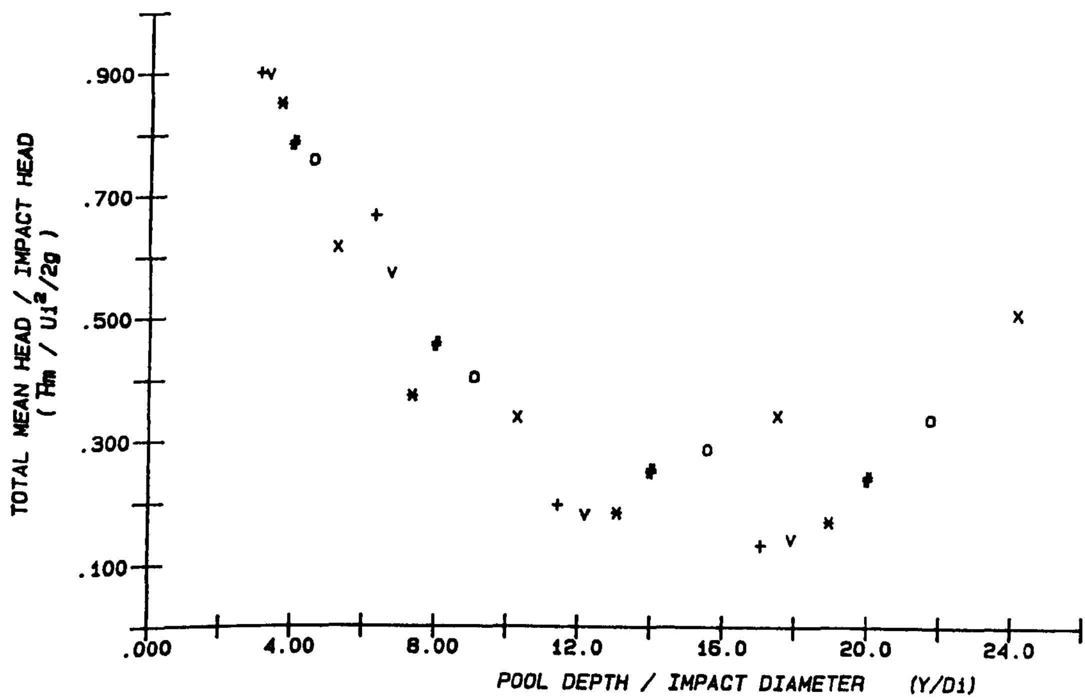

FIG. 4.15 (b) CENTRE LINE TOTAL MEAN PRESSURE HEAD RATIO VERSUS (Y/Di)
(NOZZLE : Do = 25 mm , L = 513 - 913 mm)

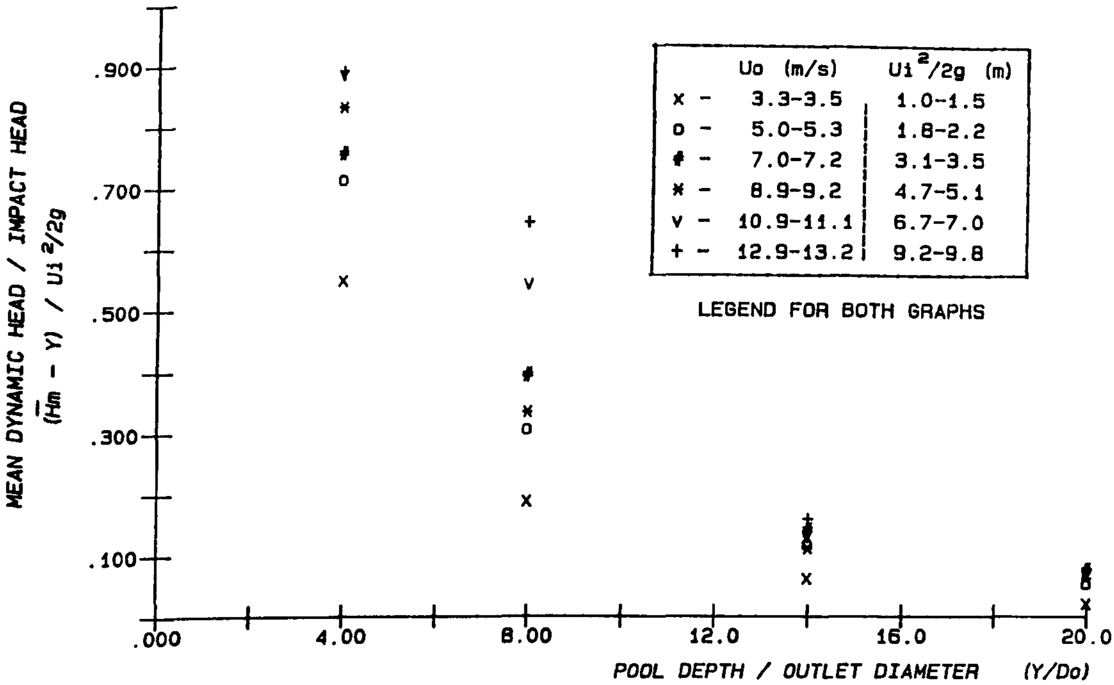

FIG. 4.16 (a) CENTRE LINE MEAN DYNAMIC PRESSURE HEAD RATIO VERSUS (Y/Do)
(NOZZLE : Do = 25 mm , L = 513 - 913 mm)

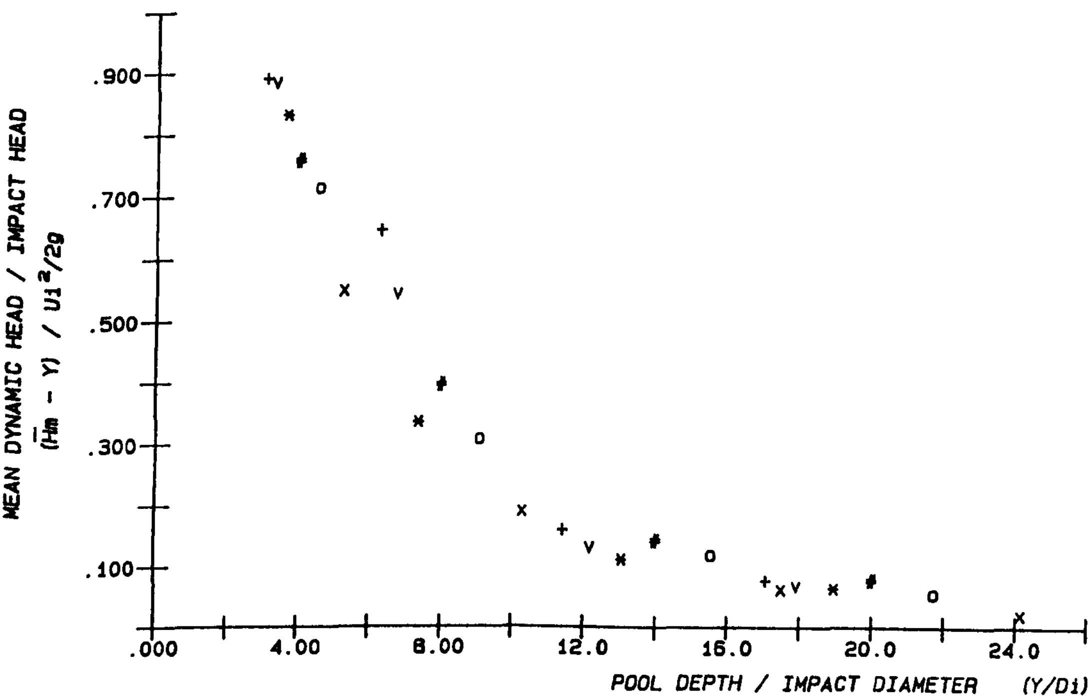

FIG. 4.16 (b) CENTRE LINE MEAN DYNAMIC PRESSURE HEAD RATIO VERSUS (Y/Di)
(NOZZLE : Do = 25 mm , L = 513 - 913 mm)

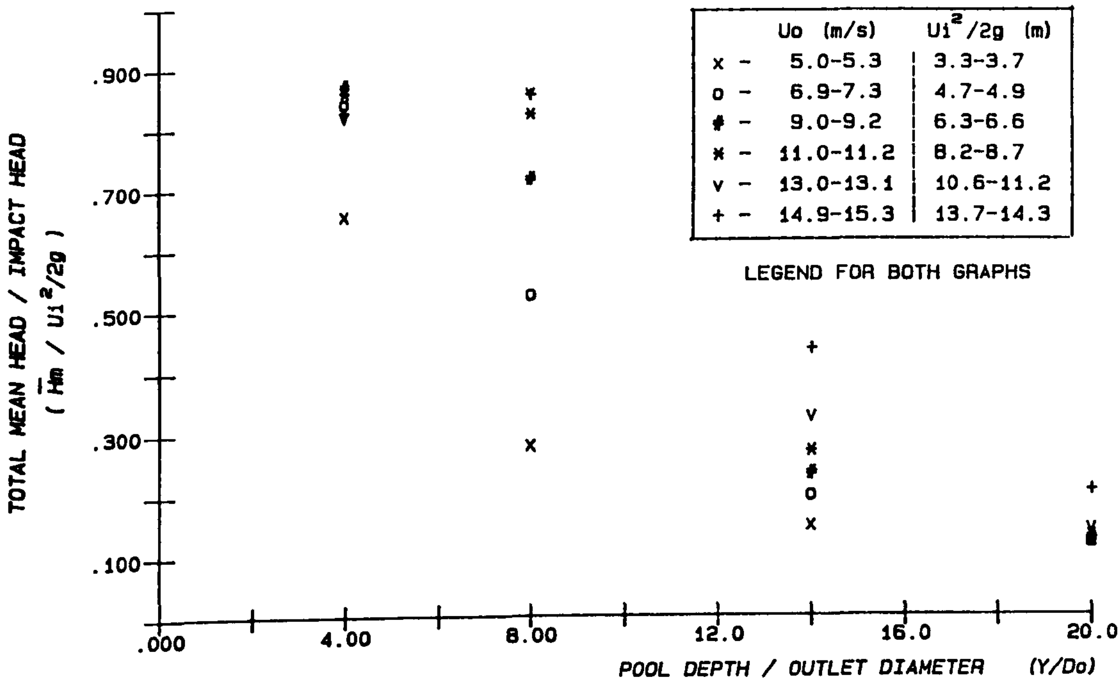

FIG. 4.17 (a) CENTRE LINE TOTAL MEAN PRESSURE HEAD RATIO VERSUS (Y/Do)
(NOZZLE : Do = 25 mm , L = 2018 - 2418 mm)

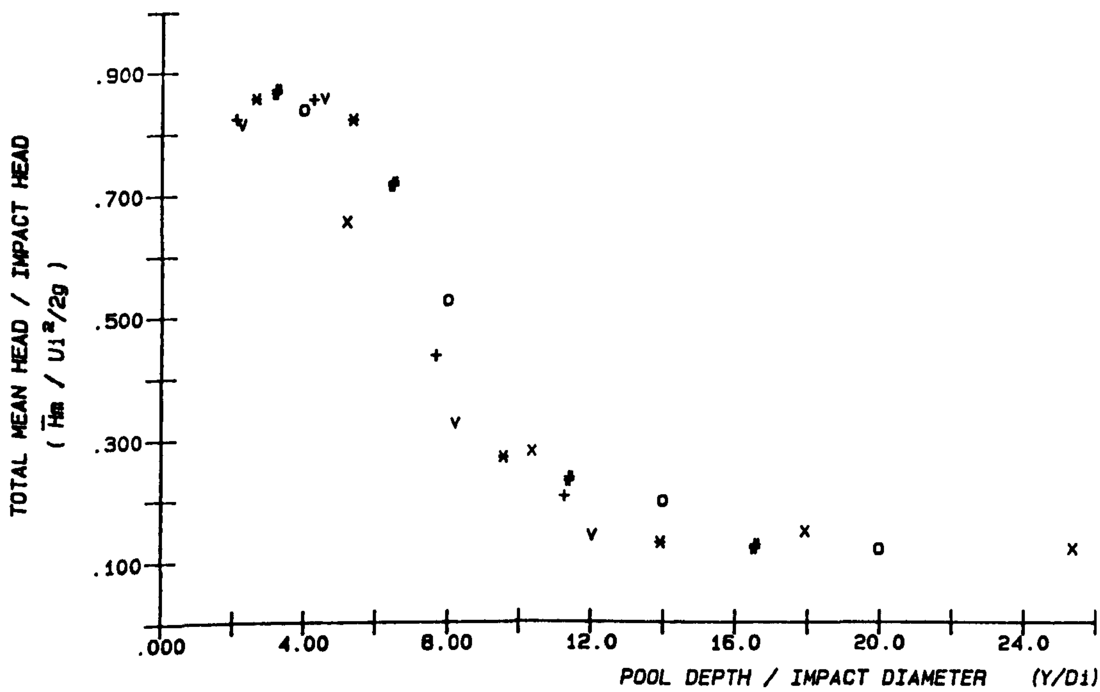

FIG. 4.17 (b) CENTRE LINE TOTAL MEAN PRESSURE HEAD RATIO VERSUS (Y/Di)
(NOZZLE : Do = 25 mm , L = 2018 - 2418 mm)

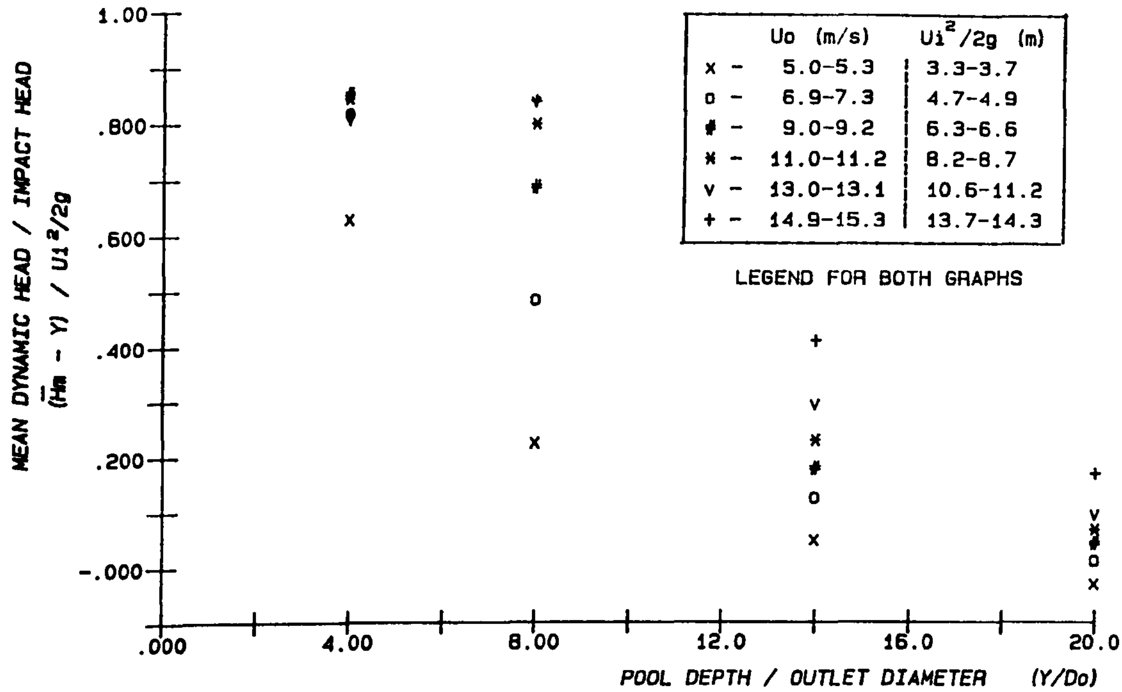

FIG. 4.18 (a) CENTRE LINE MEAN DYNAMIC PRESSURE HEAD RATIO VERSUS (Y/Do)
(NOZZLE : Do = 25 mm , L = 2018 - 2418 mm)

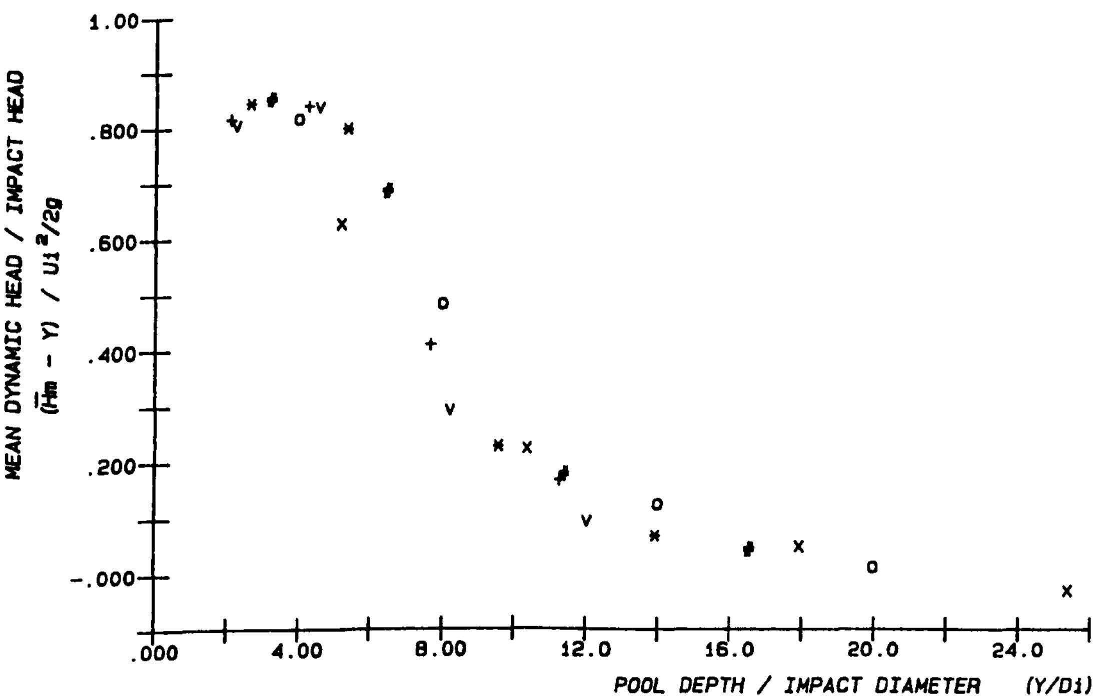

FIG. 4.18 (b) CENTRE LINE MEAN DYNAMIC PRESSURE HEAD RATIO VERSUS (Y/Di)
(NOZZLE : Do = 25 mm , L = 2018 - 2418 mm)

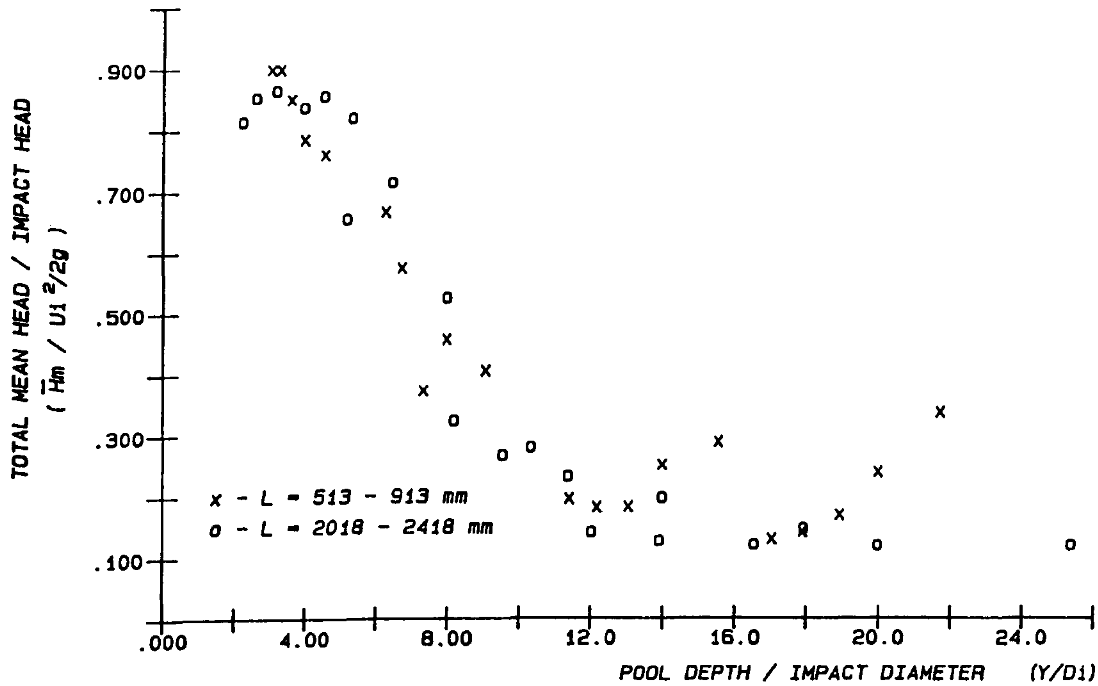

FIG. 4.19 (a) TOTAL MEAN PRESSURE HEAD AGAINST PLUNGE POOL DEPTH FOR 25 mm NOZZLE FOR THE TWO DIFFERENT FALL LENGTHS

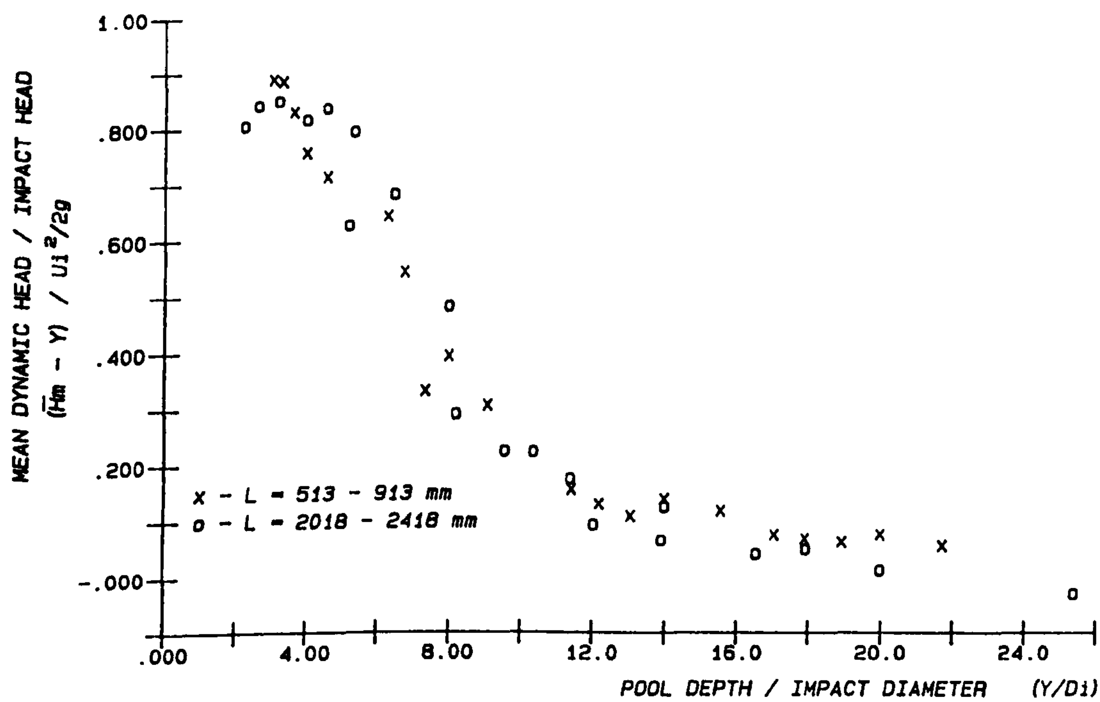

FIG. 4.19 (b) MEAN DYNAMIC PRESSURE HEAD AGAINST PLUNGE POOL DEPTH FOR 25 mm NOZZLE FOR THE TWO DIFFERENT FALL LENGTHS

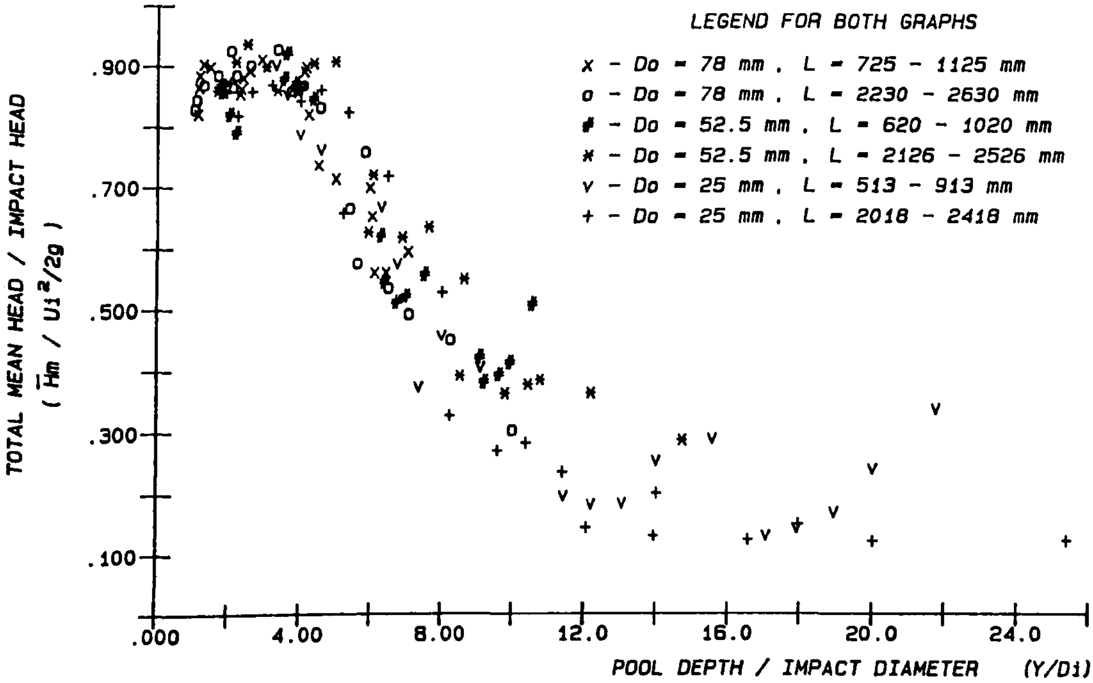

FIG. 4.20 (a) TOTAL MEAN PRESSURE HEAD AGAINST PLUNGE POOL DEPTH FOR ALL NOZZLES AND FALL LENGTHS

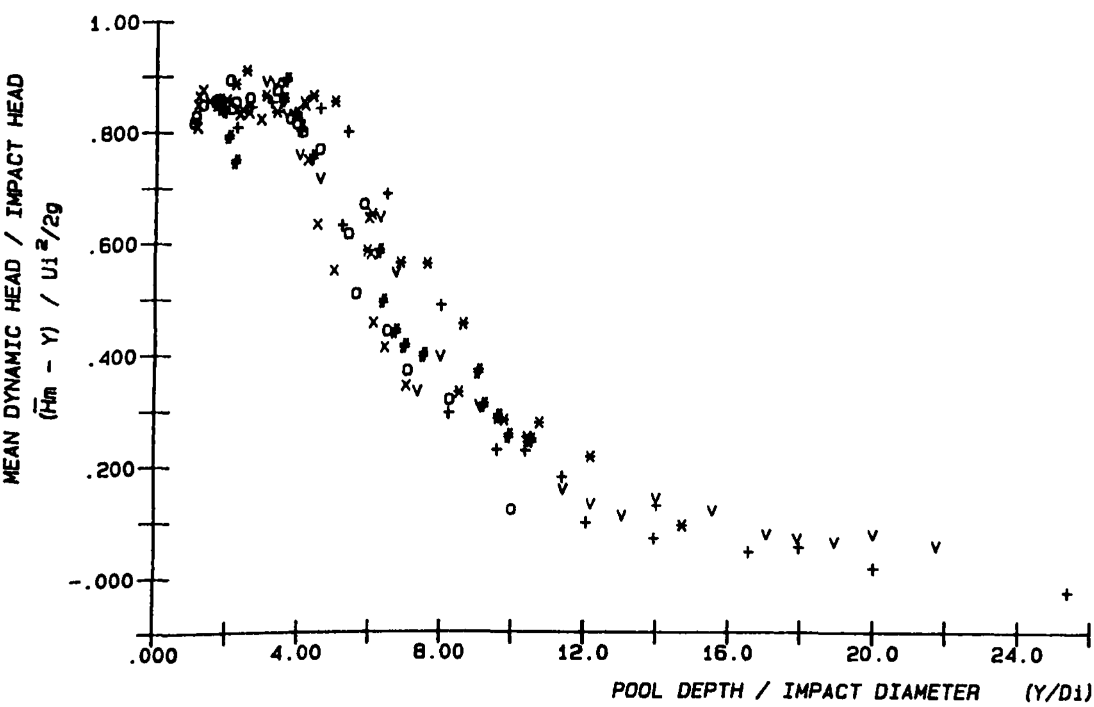

FIG. 4.20 (b) MEAN DYNAMIC PRESSURE HEAD AGAINST PLUNGE POOL DEPTH FOR ALL NOZZLES AND FALL LENGTHS

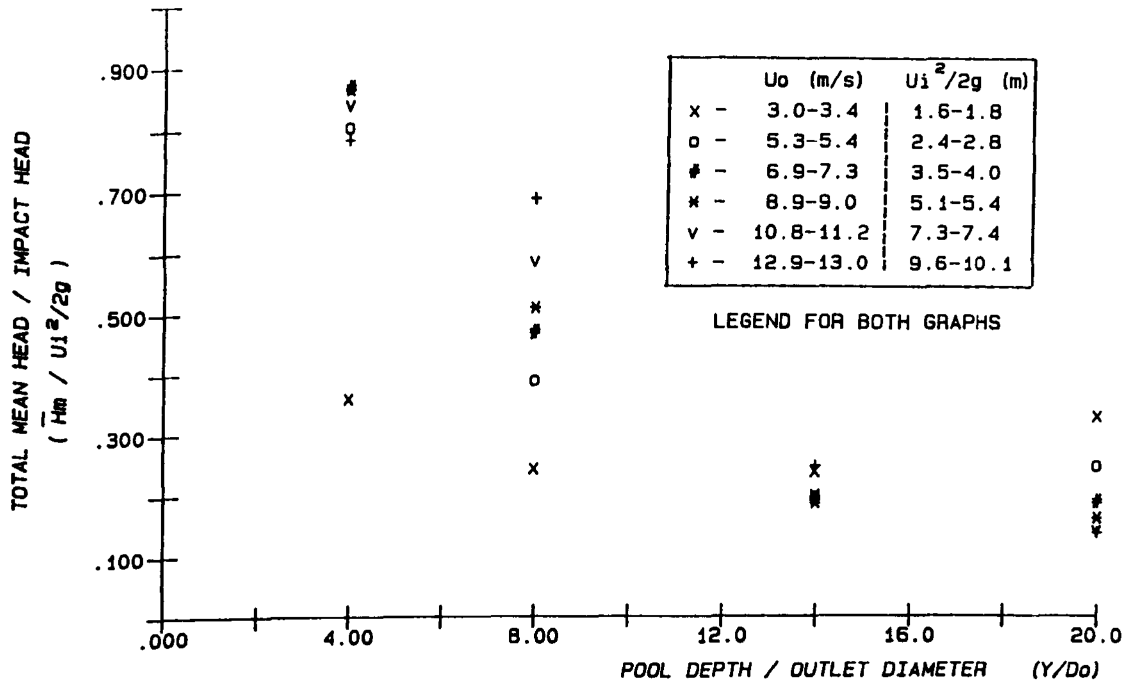

FIG. 4.21 (a) CENTRE LINE TOTAL MEAN PRESSURE HEAD RATIO VERSUS (Y/Do)
(ORIFICE : Do = 25 mm , L = 1020 - 1420 mm)

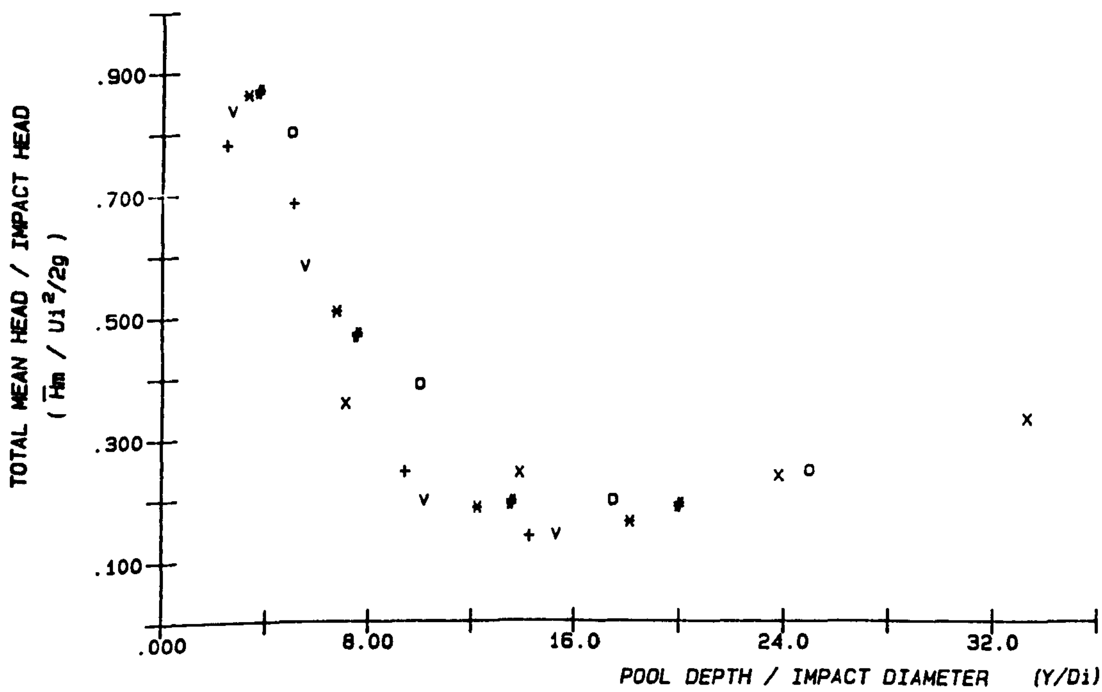

FIG. 4.21 (b) CENTRE LINE TOTAL MEAN PRESSURE HEAD RATIO VERSUS (Y/Di)
(ORIFICE : Do = 25 mm , L = 1020 - 1420 mm)

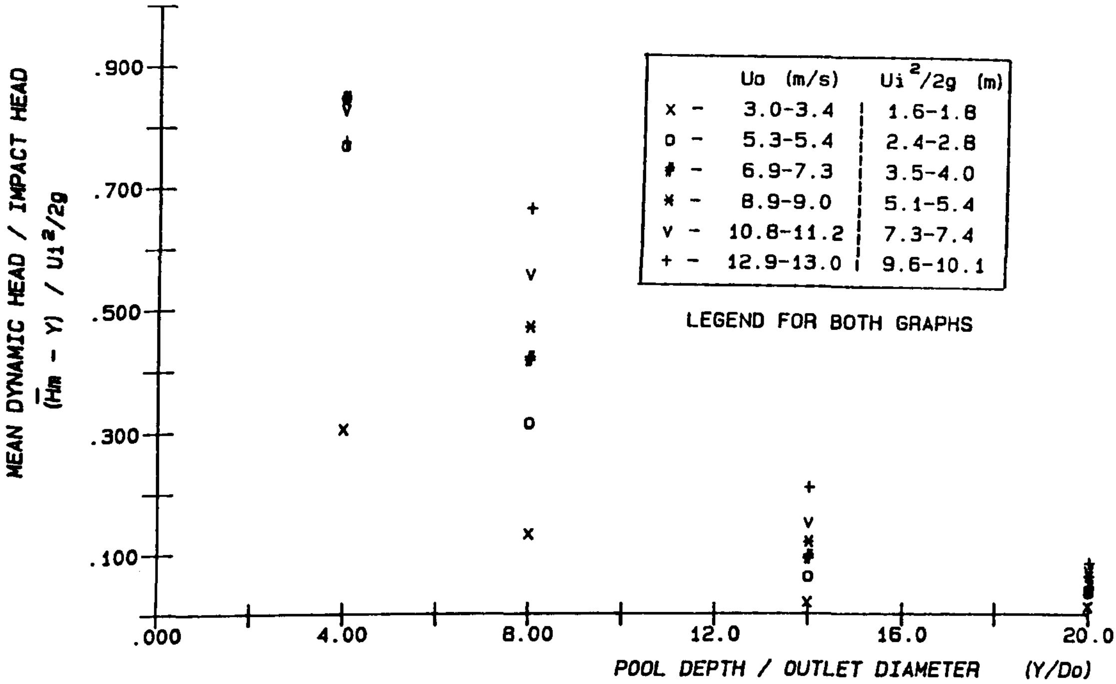

FIG. 4.22 (a) CENTRE LINE MEAN DYNAMIC PRESSURE HEAD RATIO VERSUS (Y/Do)
(ORIFICE : Do = 25 mm , L = 1020 - 1420 mm)

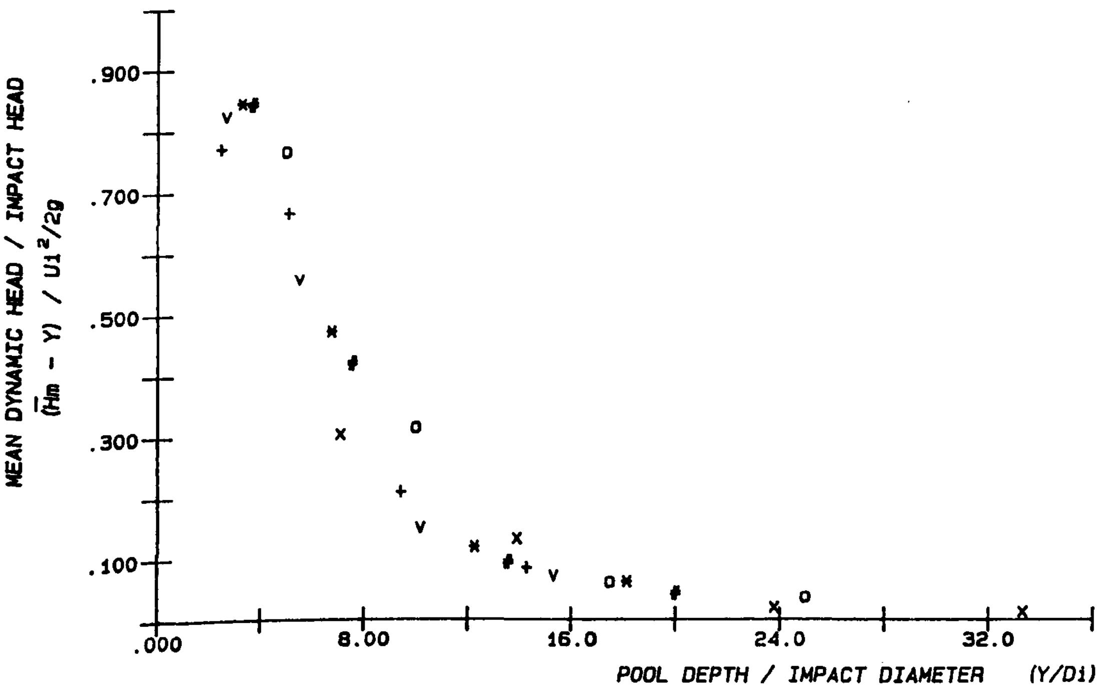

FIG. 4.22 (b) CENTRE LINE MEAN DYNAMIC PRESSURE HEAD RATIO VERSUS (Y/Di)
(ORIFICE : Do = 25 mm , L = 1020 - 1420 mm)

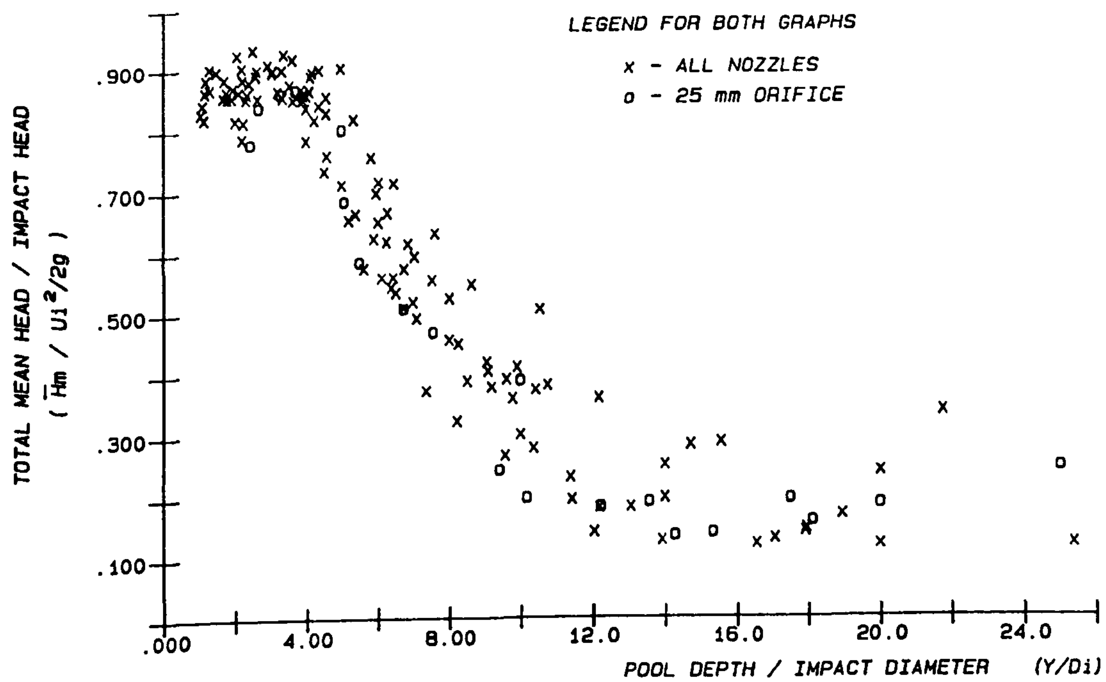

FIG. 4.23(a) COMPARISON OF TOTAL MEAN PRESSURE HEAD AGAINST PLUNGE POOL DEPTH FOR ALL NOZZLES AND 25 mm ORIFICE

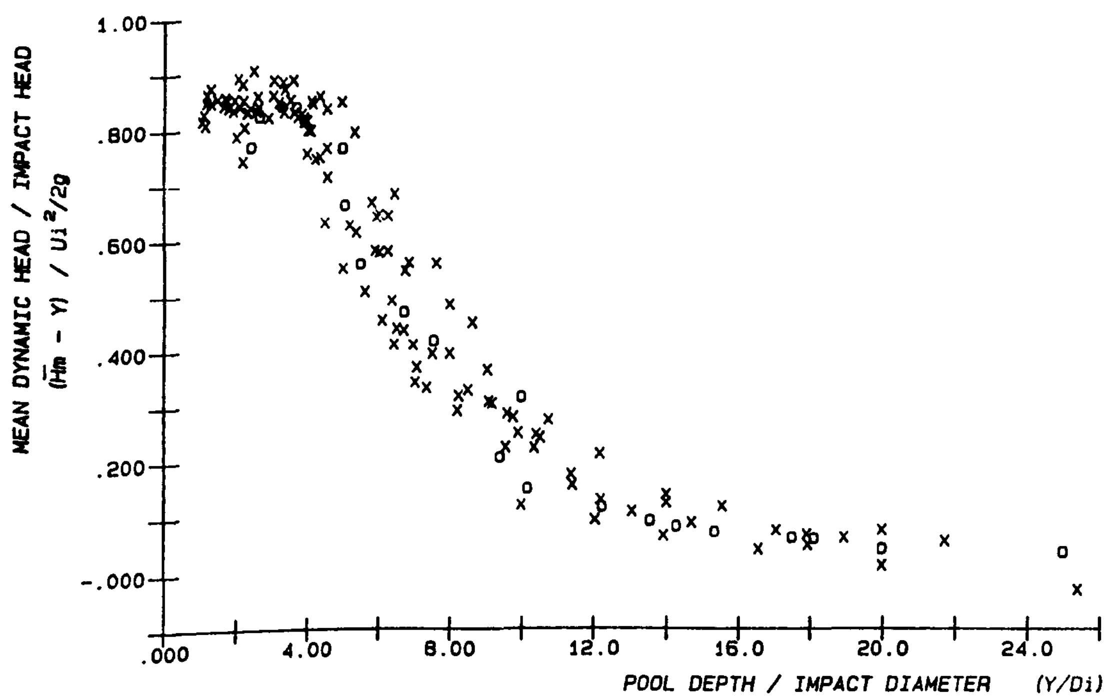

FIG. 4.23(b) COMPARISON OF MEAN DYNAMIC PRESSURE HEAD AGAINST PLUNGE POOL DEPTH FOR ALL NOZZLES AND 25 mm ORIFICE

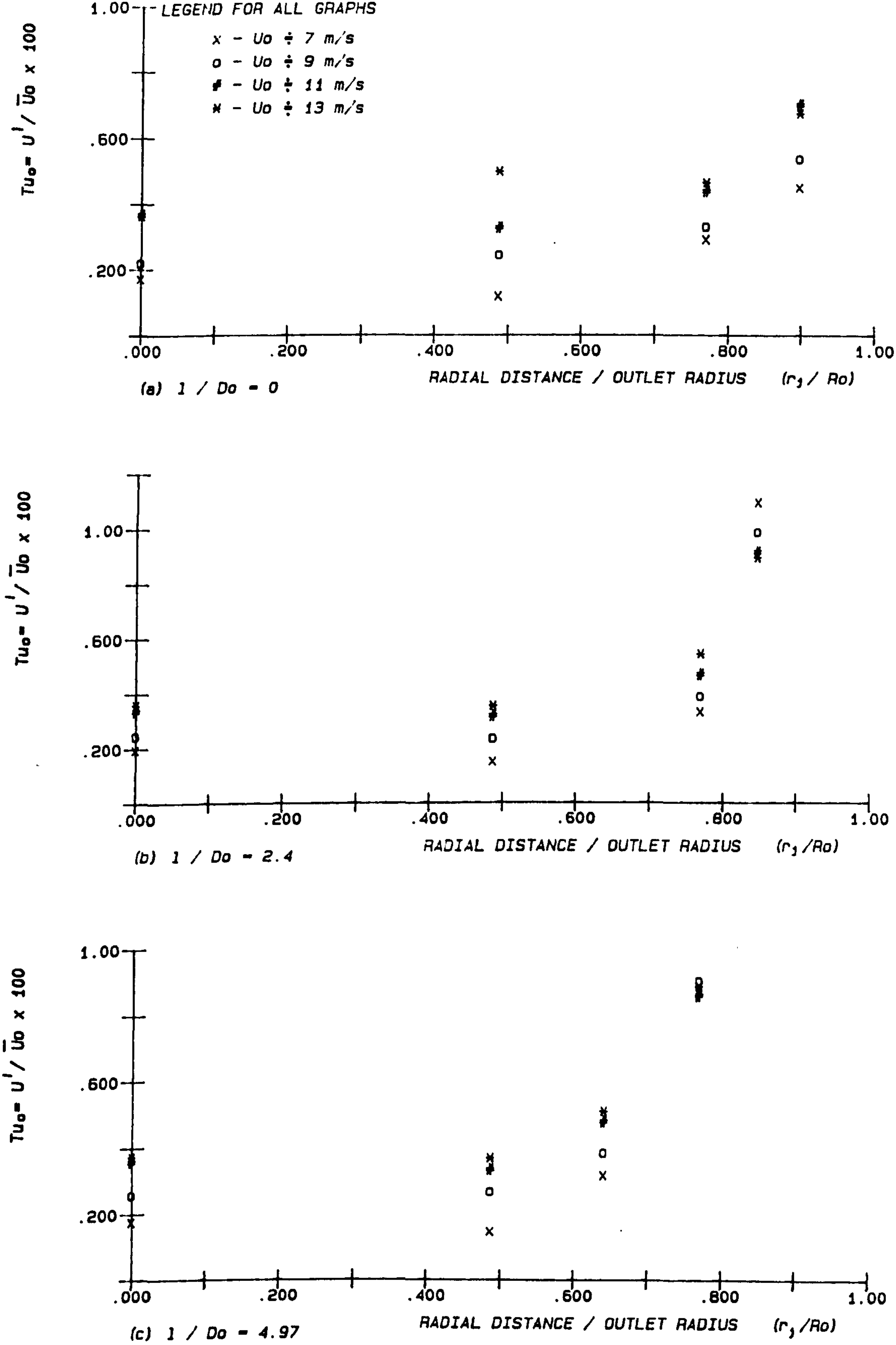

FIG. 4.24 VARIATION OF TURBULENCE INTENSITY (Tu_o%) IN RADIAL DIRECTION (r_1/ Ro). [Do = 78 mm]

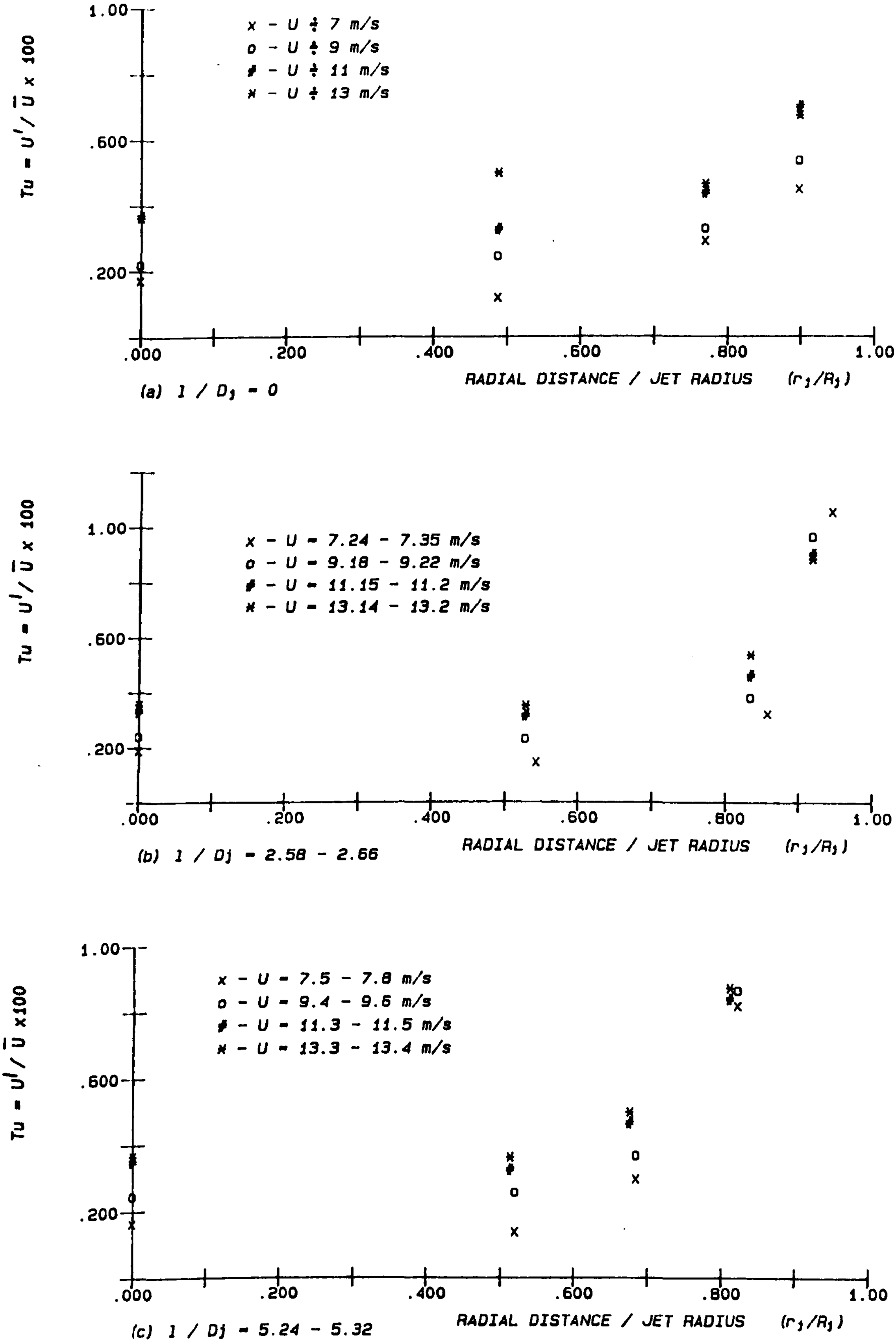

FIG. 4.25 VARIATION OF TURBULENCE INTENSITY (Tu%) IN RADIAL DIRECTION (r_j/R_j). [Do = 78 mm]

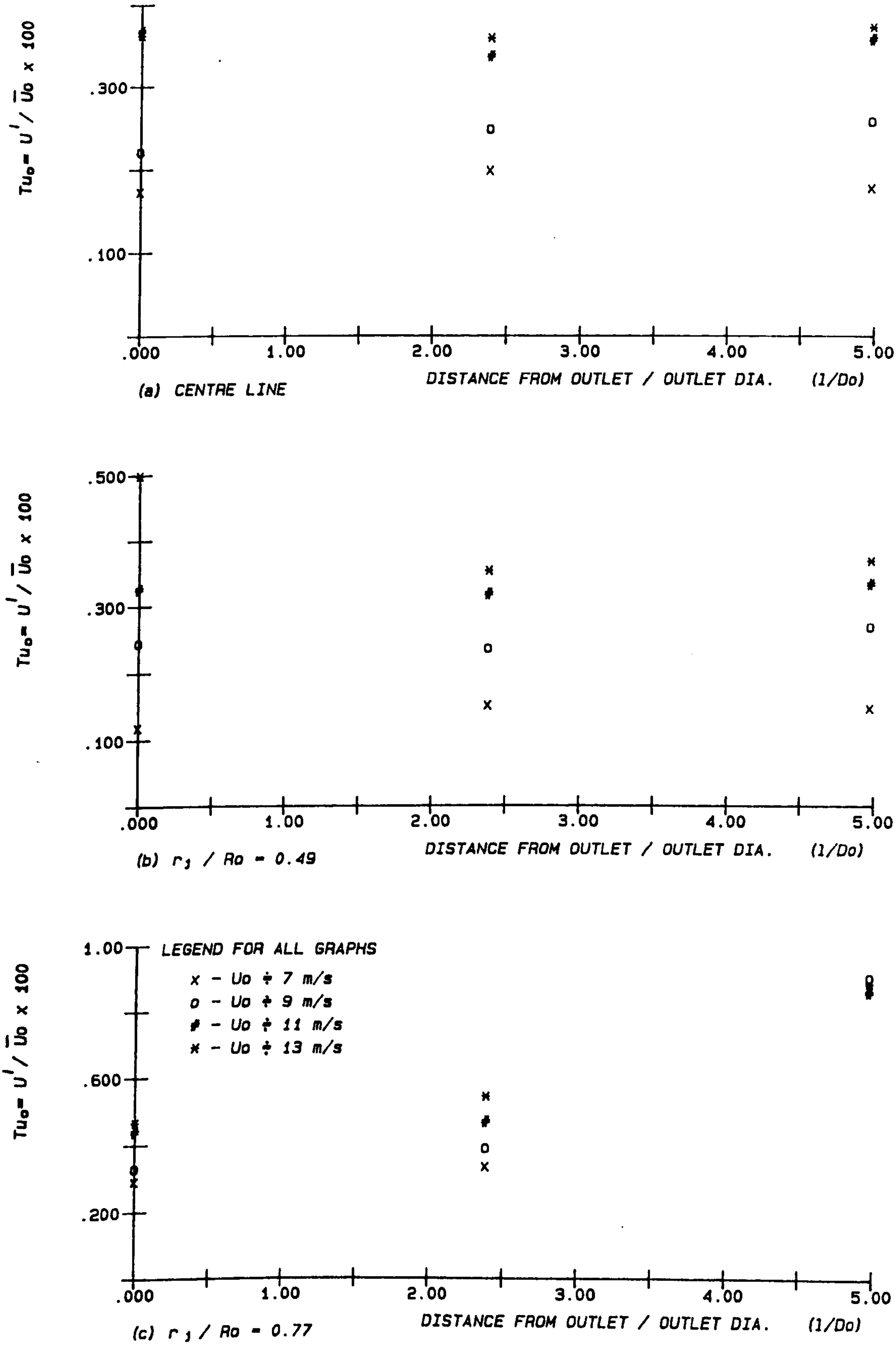

FIG. 4.26 VARIATION OF TURBULENCE INTENSITY (Tu_o%) IN LONGITUDINAL DIRECTION (l / Do). [Do = 78 mm]

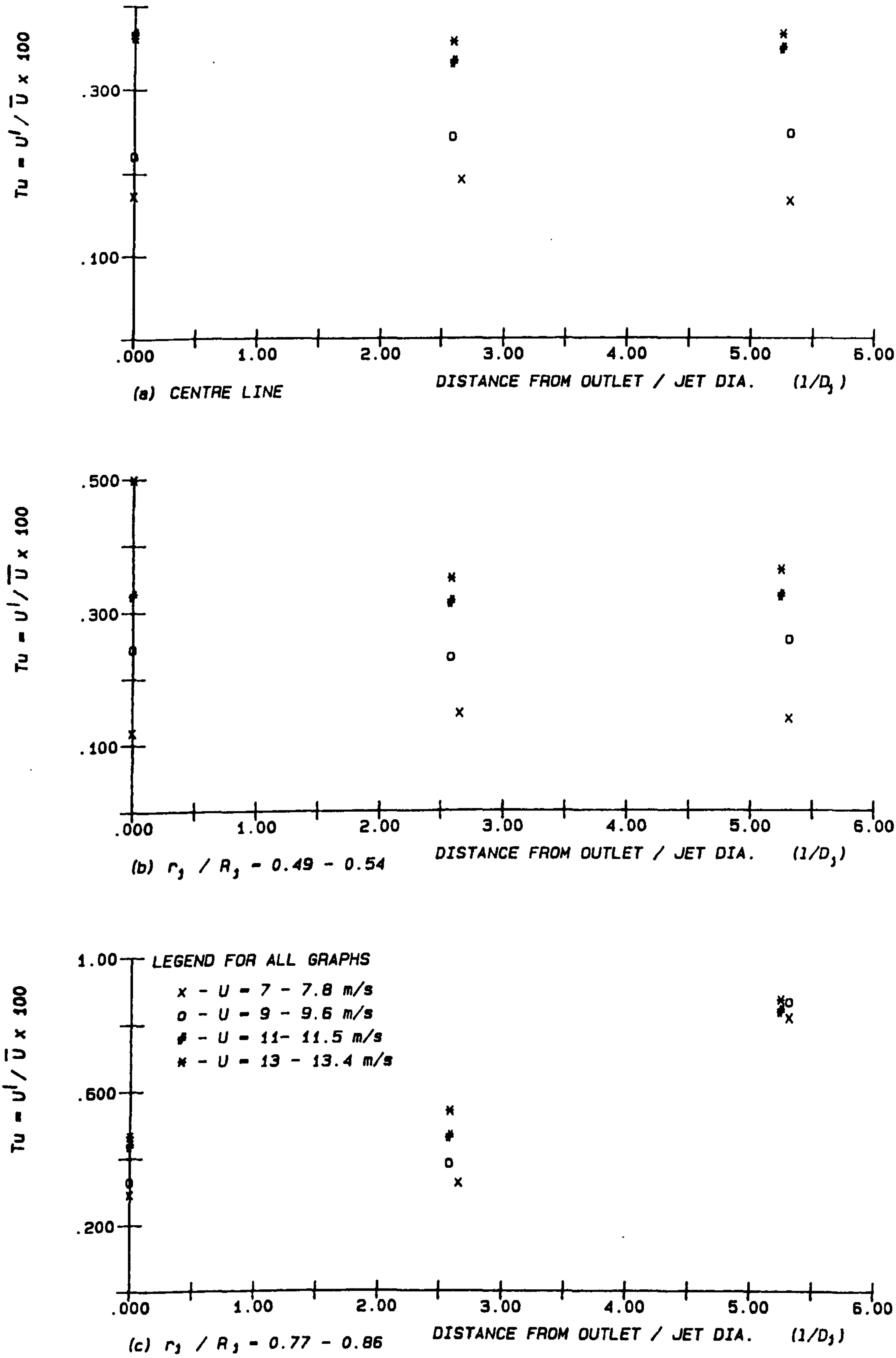

FIG. 4.27 VARIATION OF TURBULENCE INTENSITY (Tu%) IN LONGITUDINAL DIRECTION (l / D_j). [Do = 78 mm]

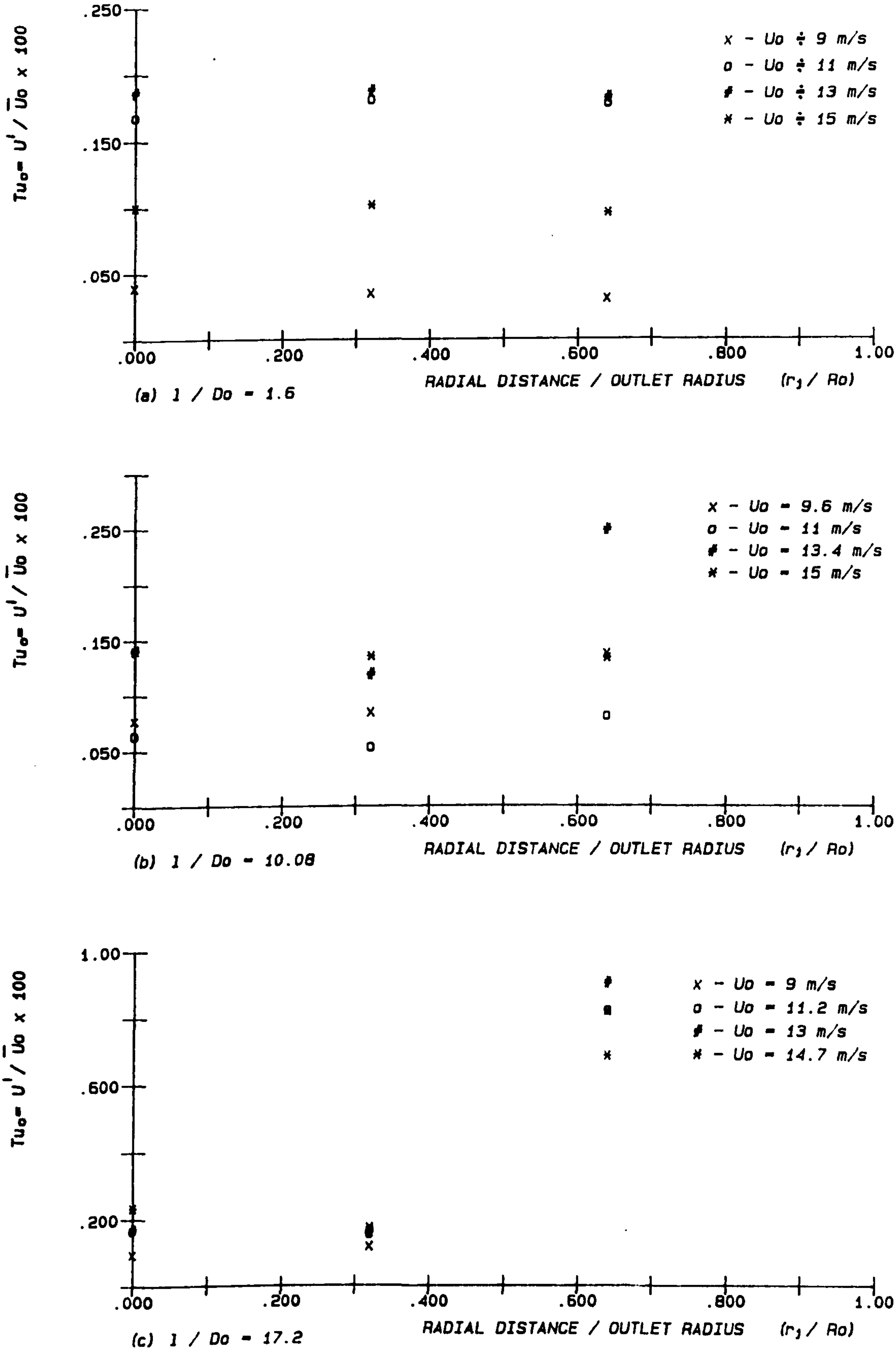

FIG. 4.28 VARIATION OF TURBULENCE INTENSITY (Tu_o%) IN RADIAL DIRECTION (r_j / Ro) . [NOZZLE : Do = 25 mm]

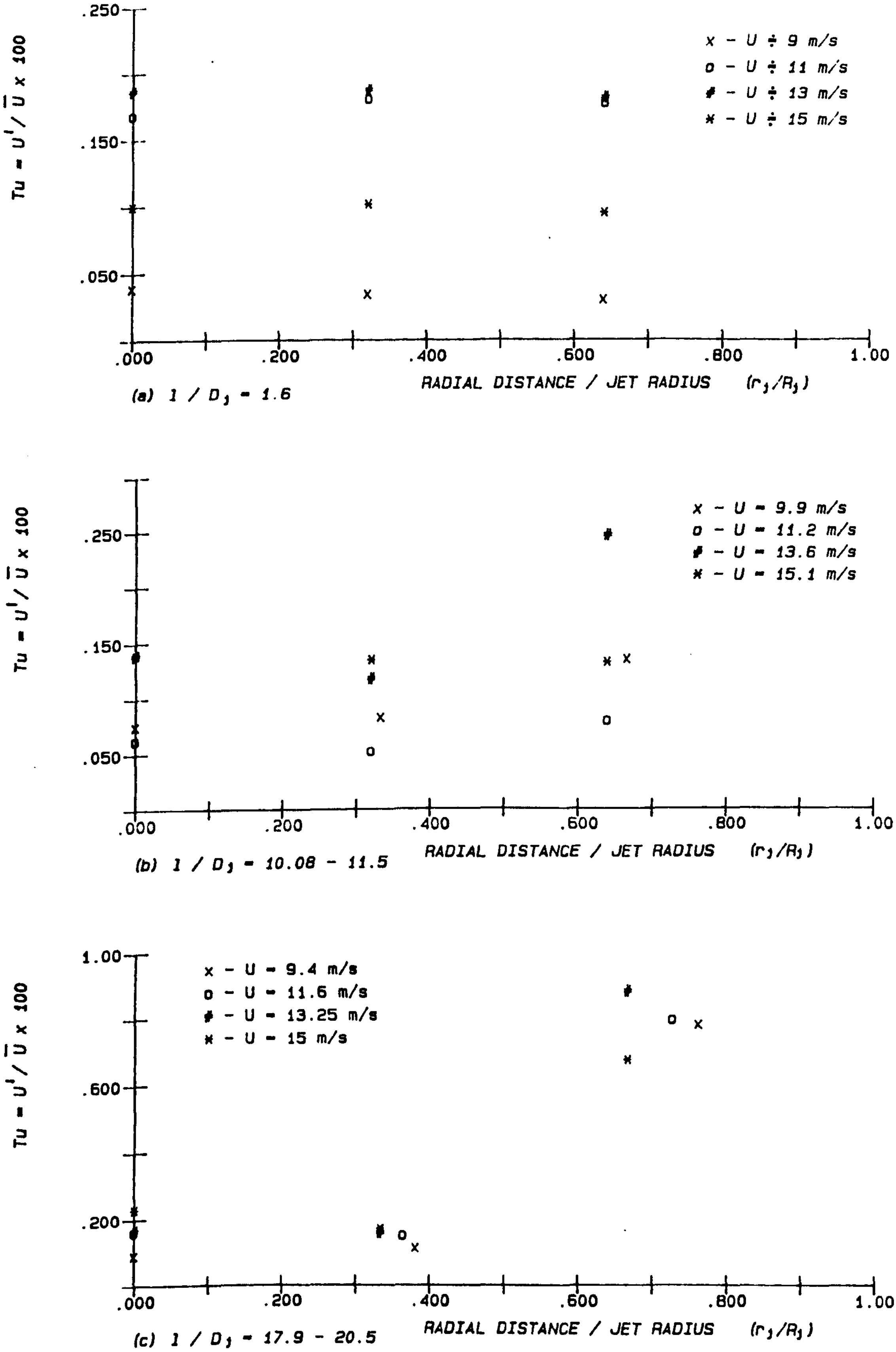

FIG. 4.29 VARIATION OF TURBULENCE INTENSITY (Tu%) IN RADIAL DIRECTION (r_j / R_j). [NOZZLE : Do = 25 mm]

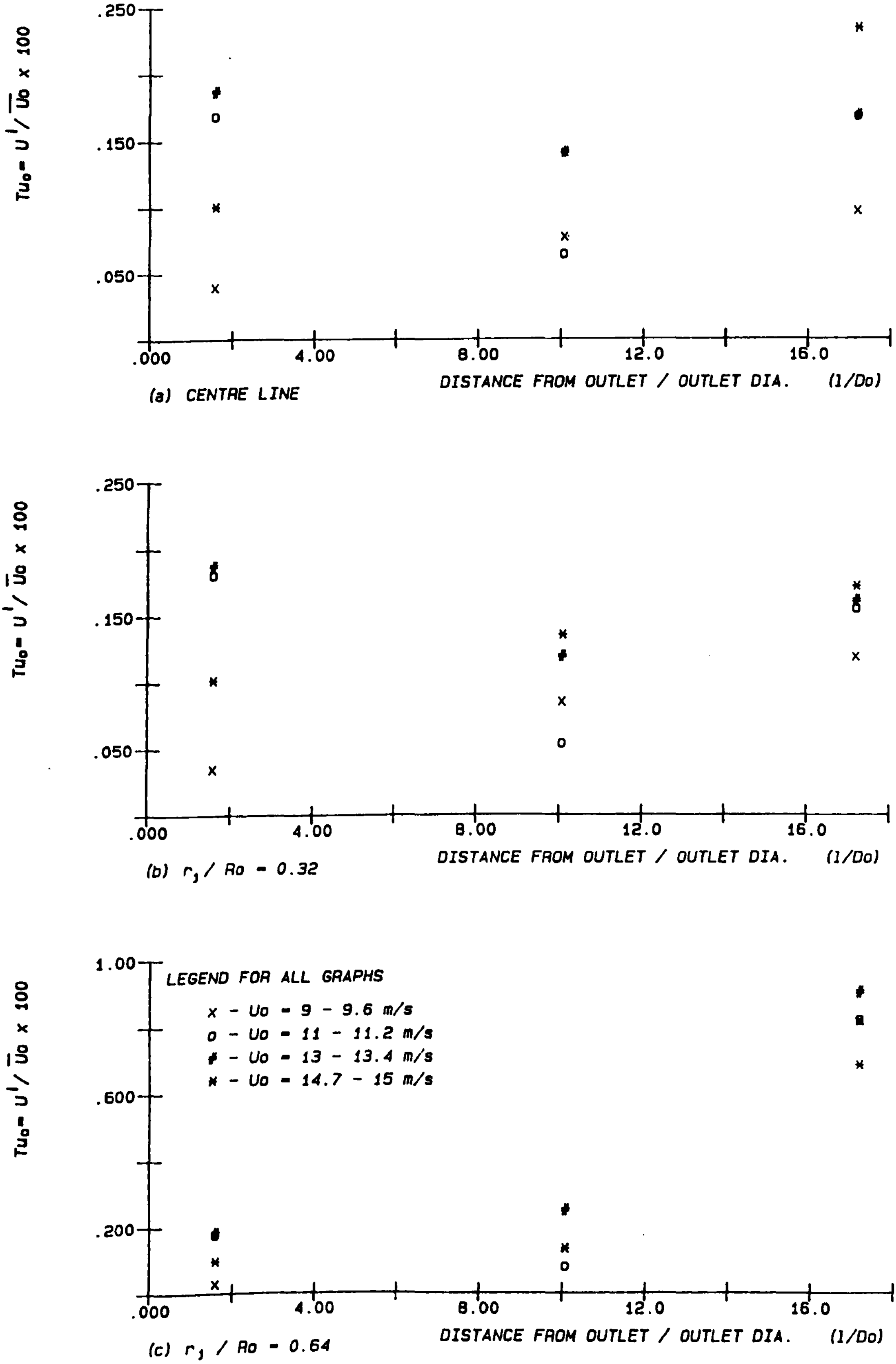

FIG. 4.30 VARIATION OF TURBULENCE INTENSITY (Tu_o%) IN LONGITUDINAL DIRECTION (l / Do). [NOZZLE : Do = 25 mm]

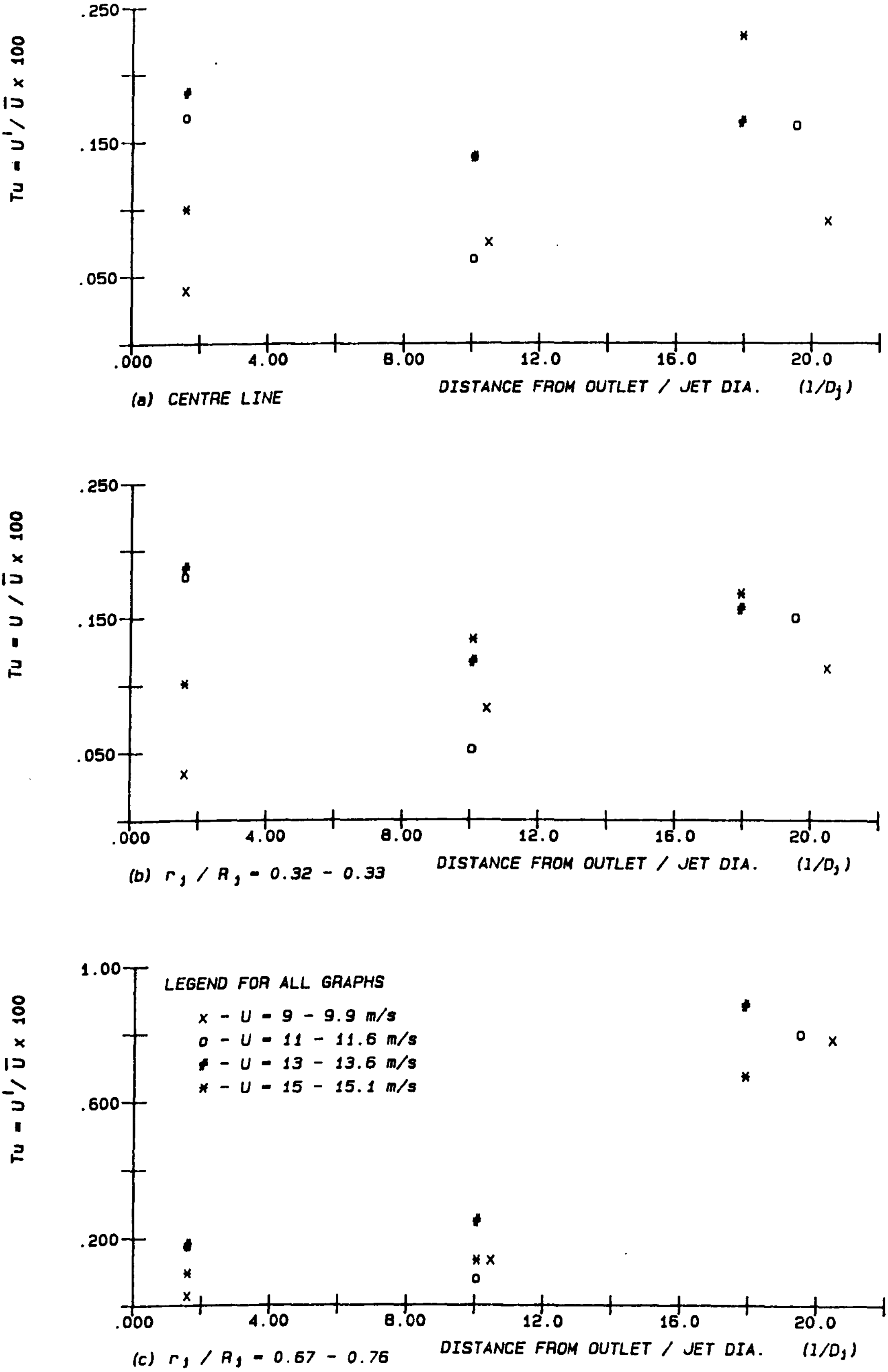

FIG. 4.31 VARIATION OF TURBULENCE INTENSITY (Tu%) IN LONGITUDINAL DIRECTION (l / D_j). [NOZZLE : Do = 25 mm]

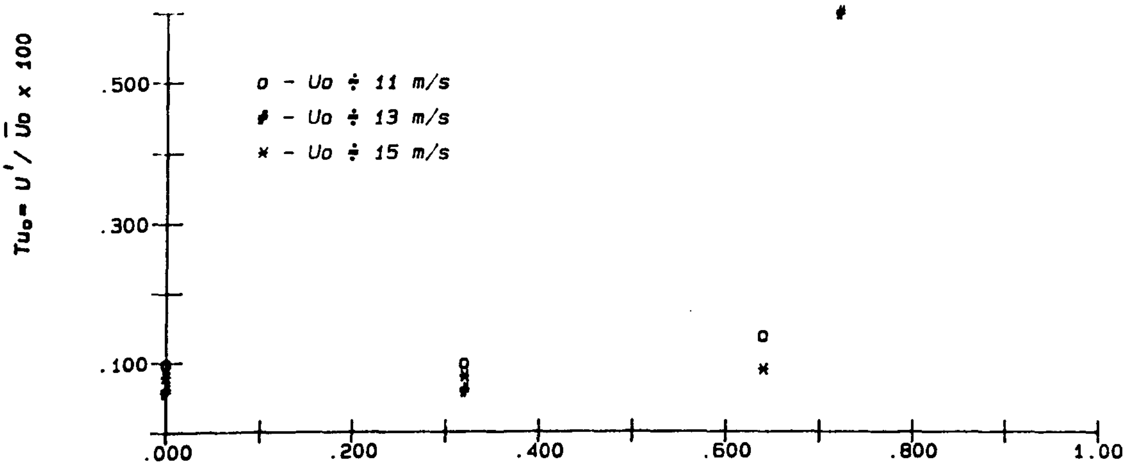

(a) 1 / Do = 2.0

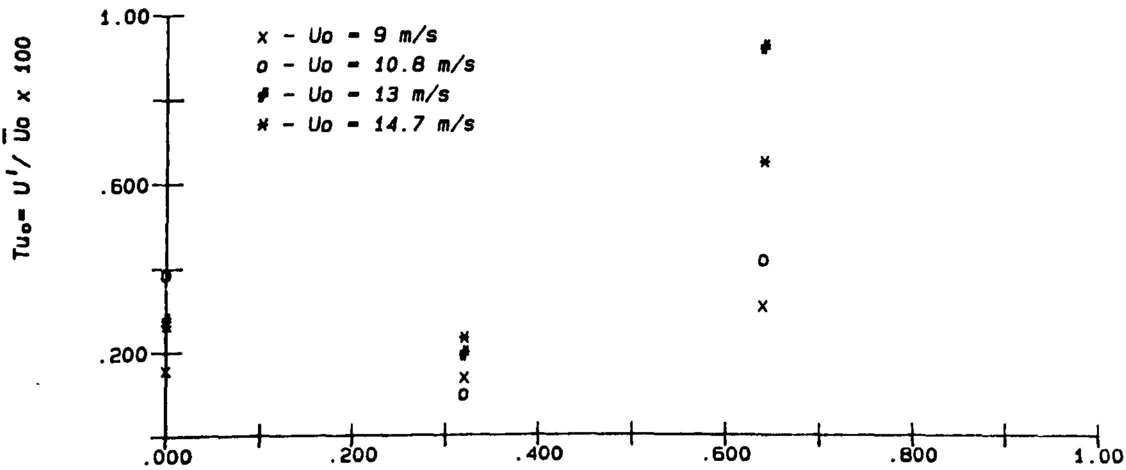

(b) 1 / Do = 4.92

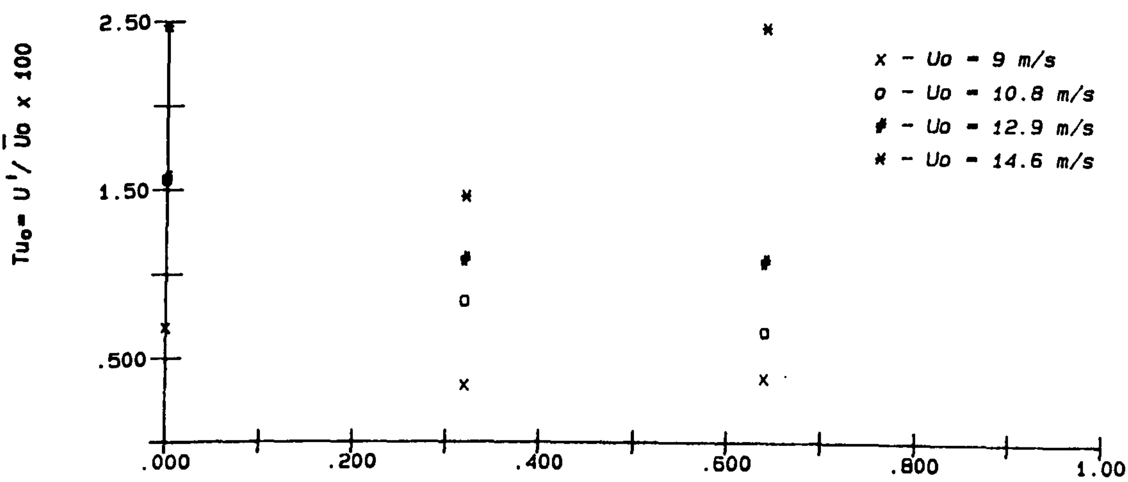

(c) 1 / Do = 10.8

FIG. 4.32 (i) VARIATION OF TURBULENCE INTENSITY (Tu_o%) IN RADIAL DIRECTION (r_j / Ro). [ORIFICE : Do = 25 mm]

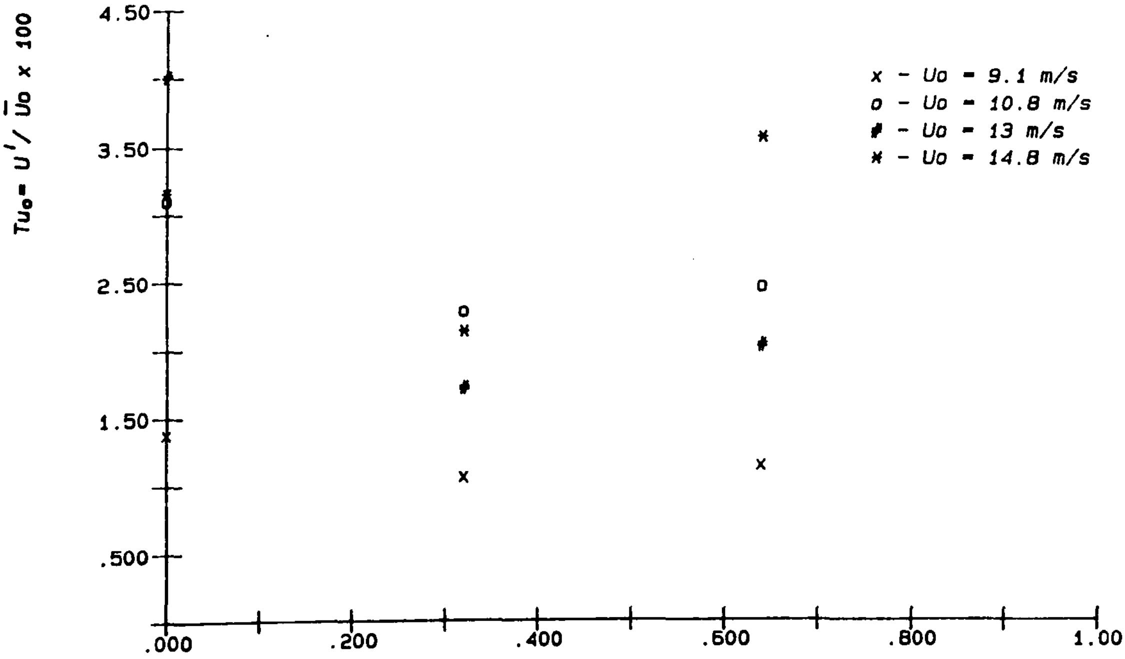

(d) l / Do = 14.4

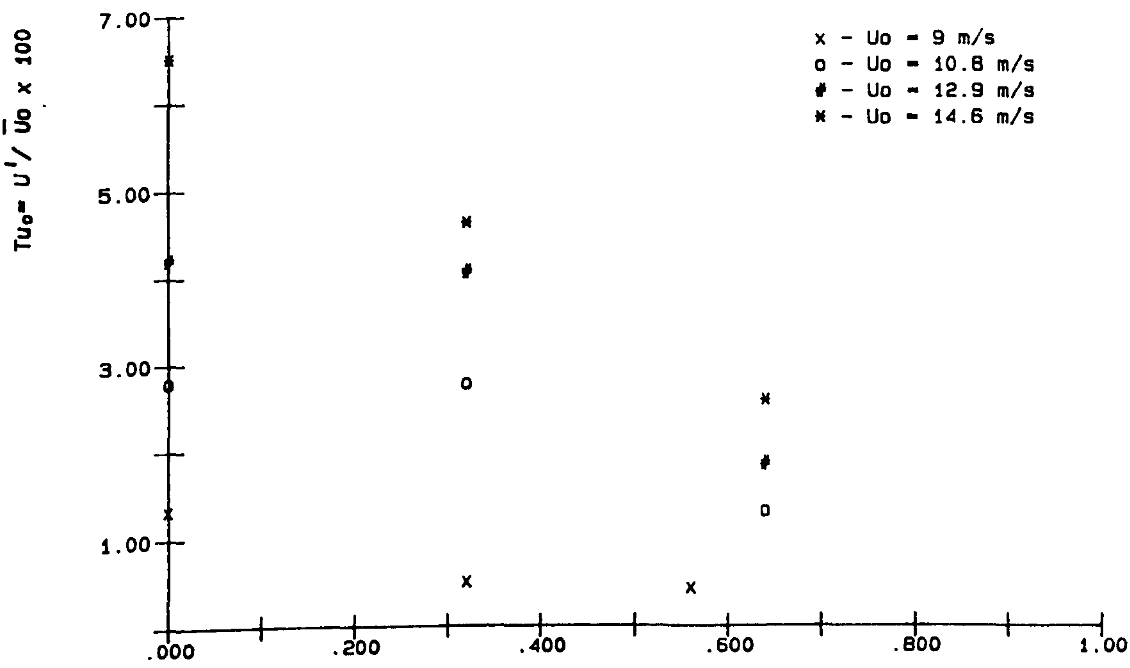

(e) l / Do = 17

FIG. 4.32 (ii) VARIATION OF TURBULENCE INTENSITY (Tu_o%) IN RADIAL DIRECTION (r_j / Ro). [ORIFICE : Do = 25 mm]

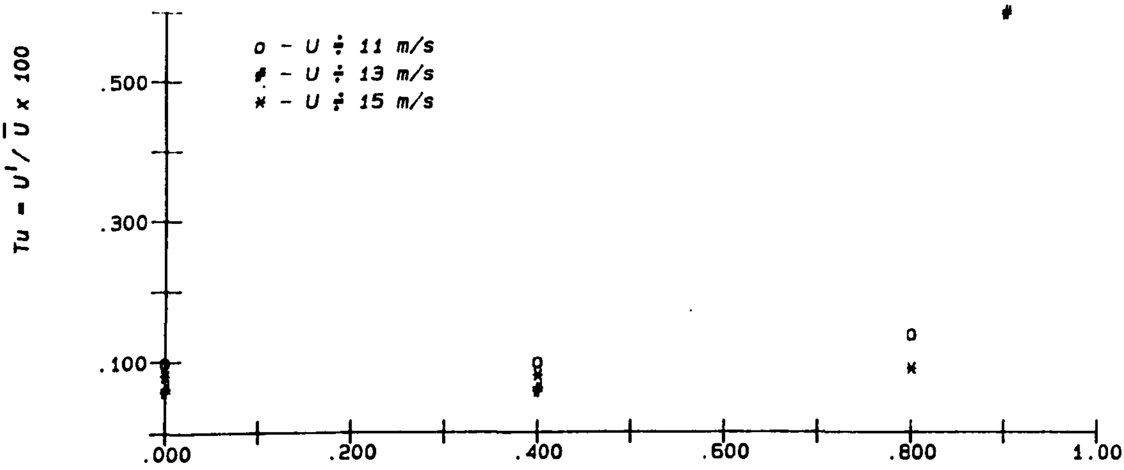

(a) 1 / Dj = 2.5

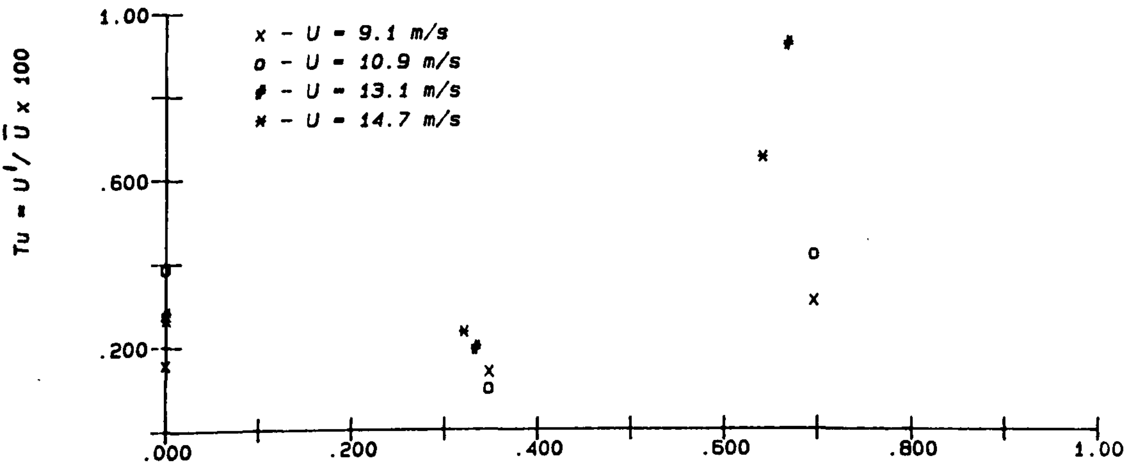

(b) 1 / Dj = 4.92 - 5.35

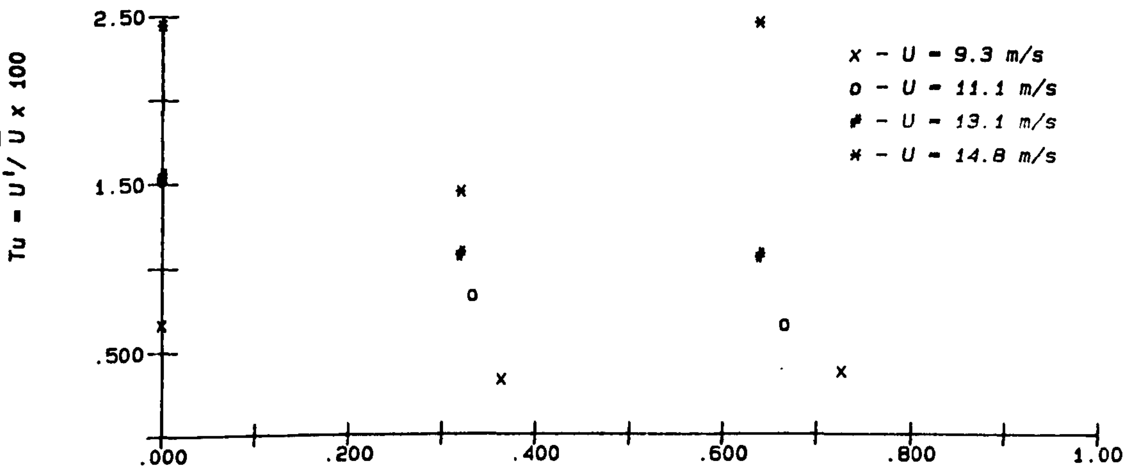

(c) 1 / Dj = 10.8 - 12.3

FIG. 4.33 (i) VARIATION OF TURBULENCE INTENSITY (Tu%) IN RADIAL DIRECTION (r_j / R_j). [ORIFICE : Do = 25 mm]

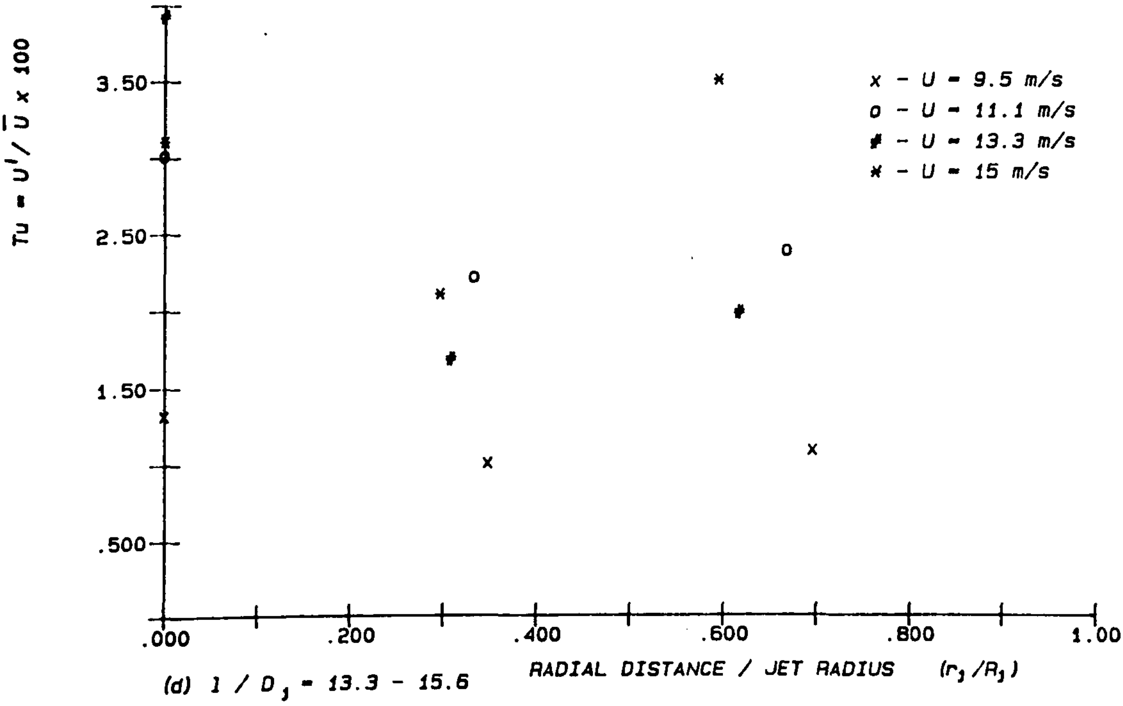

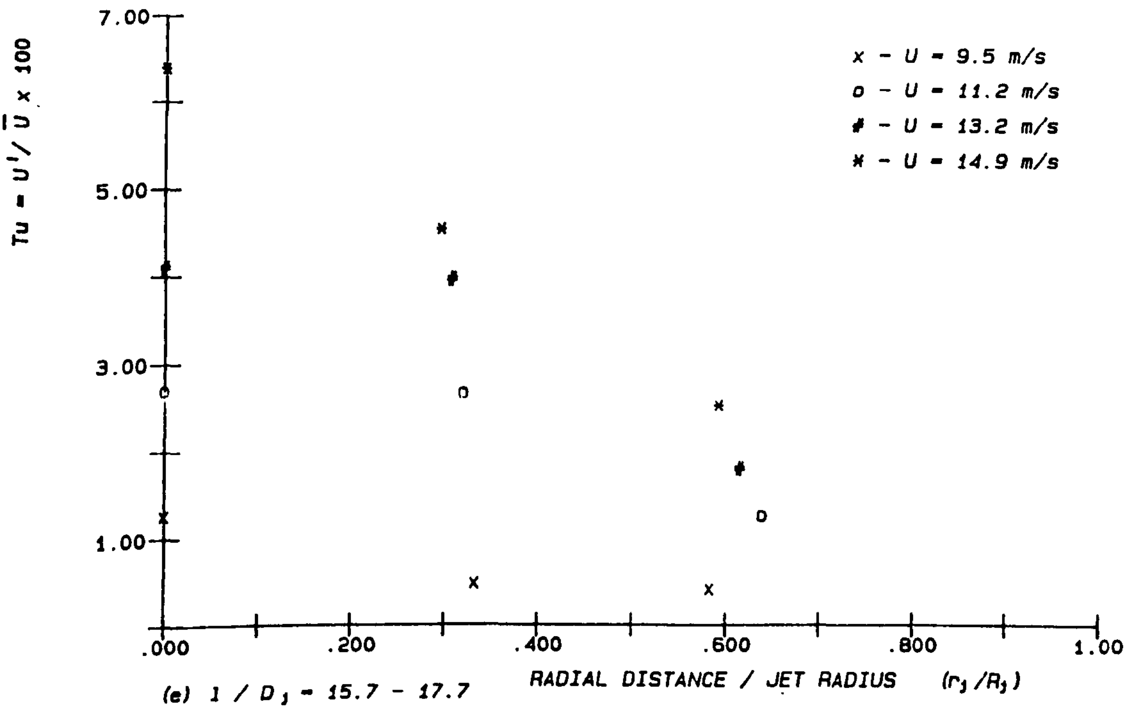

FIG. 4.33 (ii) VARIATION OF TURBULENCE INTENSITY (Tu%) IN RADIAL DIRECTION (r_j / R_j). [ORIFICE : Do = 25 mm]

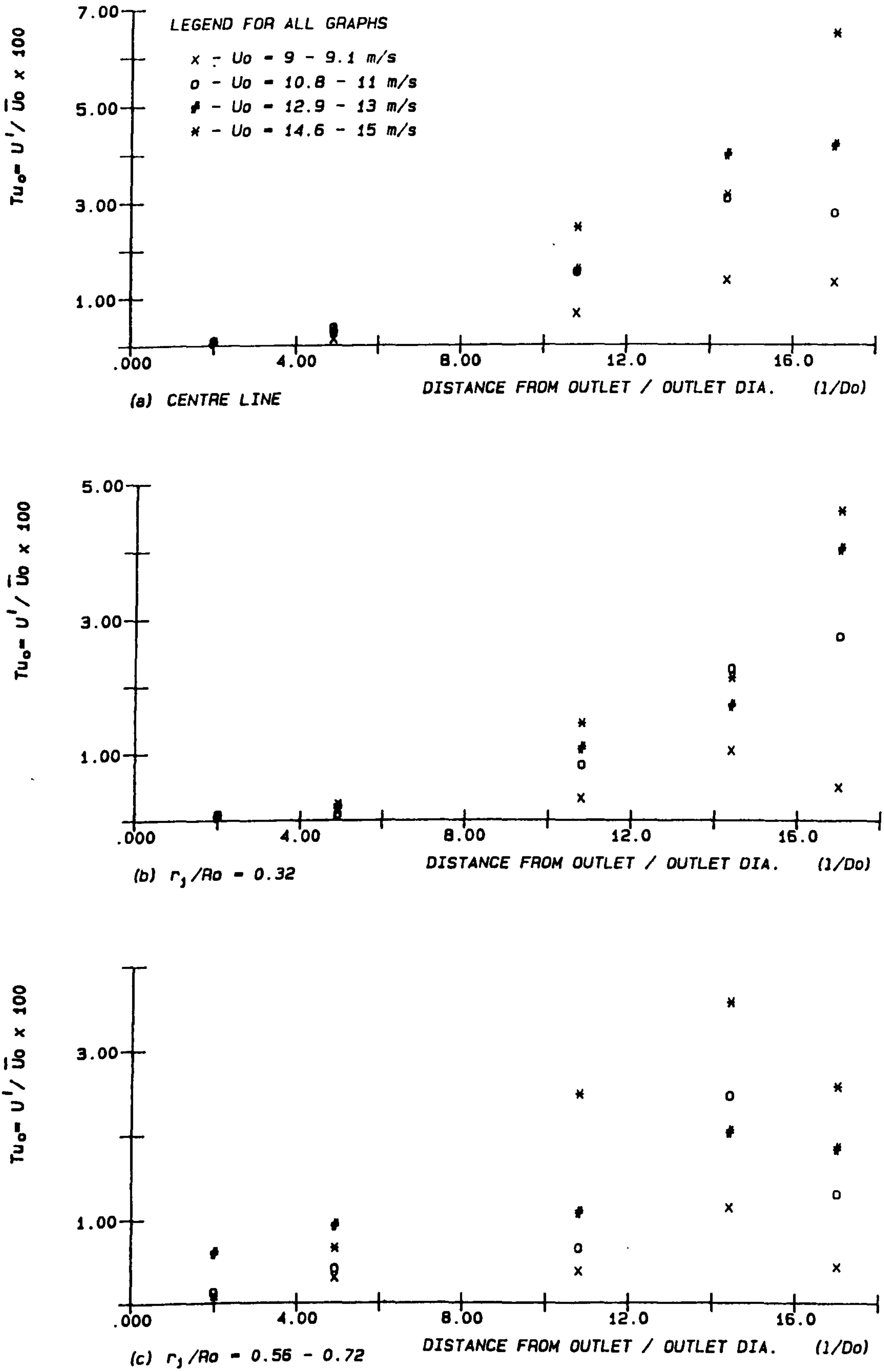

FIG. 4.34 VARIATION OF TURBULENCE INTENSITY (Tu_o%) IN LONGITUDINAL DIRECTION (l / Do). [ORIFICE : Do = 25 mm]

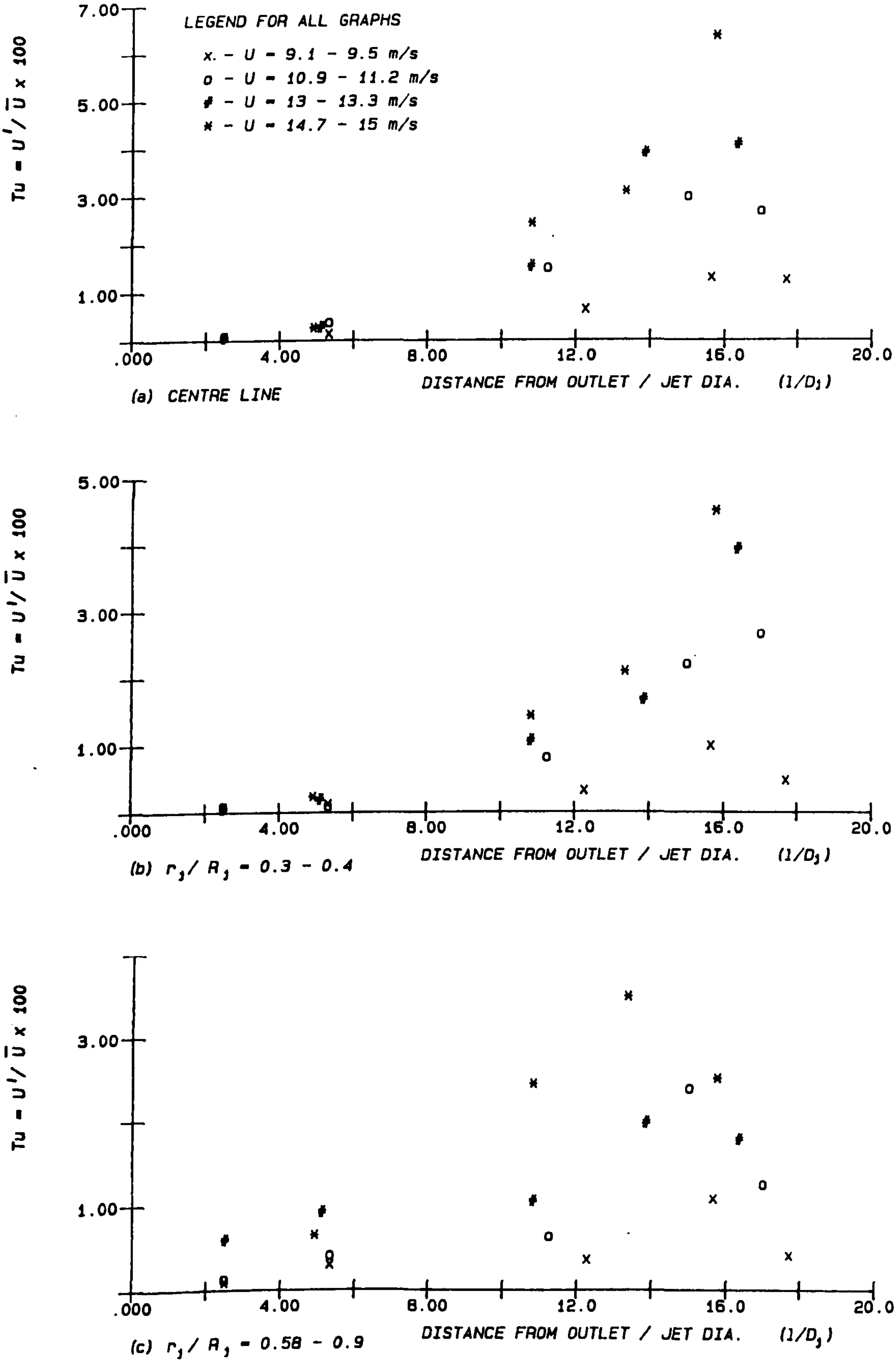

FIG. 4.35 VARIATION OF TURBULENCE INTENSITY (Tu%) IN LONGITUDINAL DIRECTION (1 / D$_j$). [ORIFICE : Do = 25 mm]

FIGURES FOR CHAPTER 5

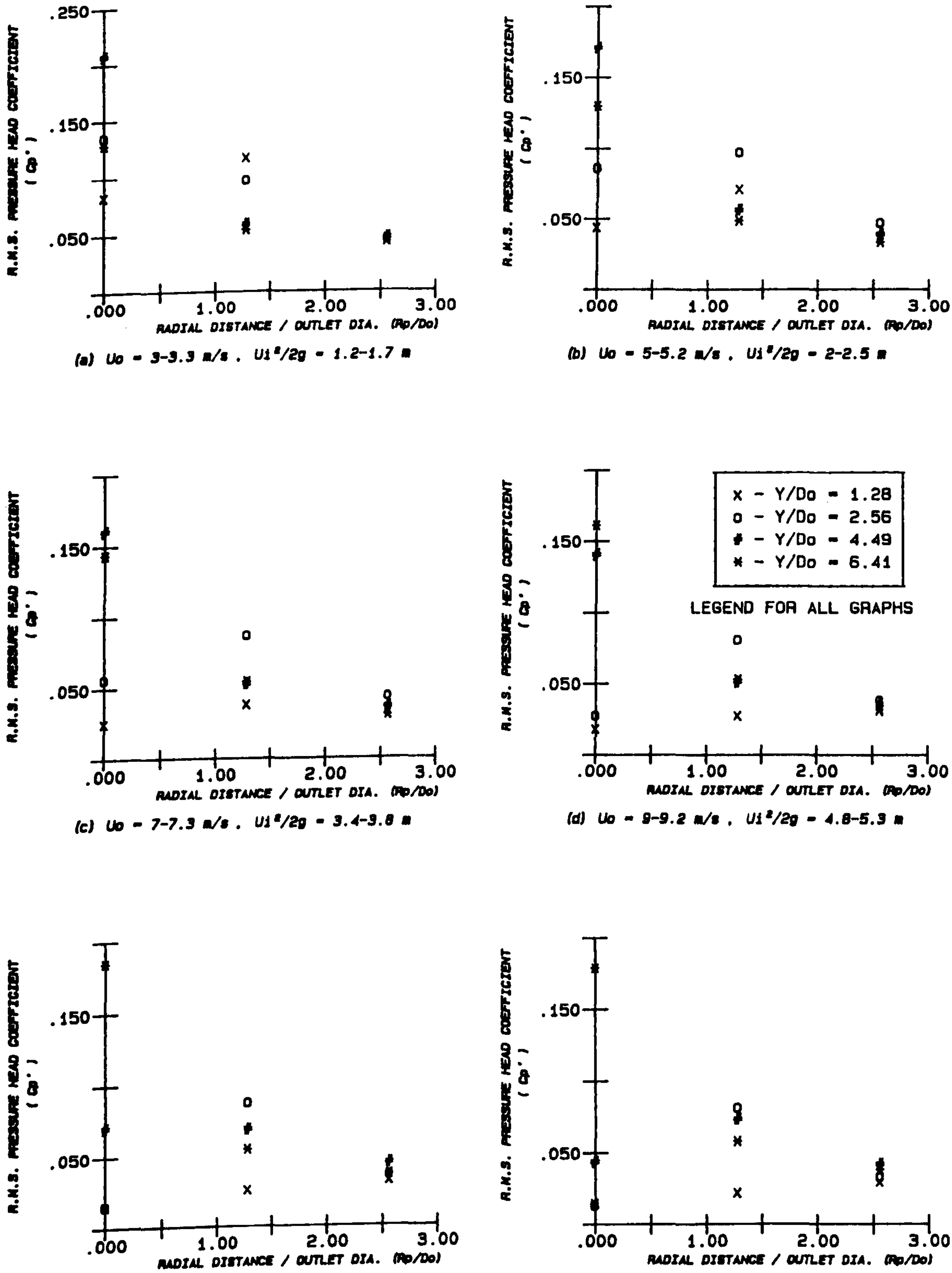

(a) Uo = 3-3.3 m/s , $Ui^2/2g$ = 1.2-1.7 m

(b) Uo = 5-5.2 m/s , $Ui^2/2g$ = 2-2.5 m

(c) Uo = 7-7.3 m/s , $Ui^2/2g$ = 3.4-3.8 m

(d) Uo = 9-9.2 m/s , $Ui^2/2g$ = 4.8-5.3 m

(e) Uo = 10.9-11.1 m/s , $Ui^2/2g$ = 6.8-7.4 m

(f) Uo = 12.6-13 m/s , $Ui^2/2g$ = 9.1-9.7 m

FIG. 5.1 VARIATION OF R.M.S. PRESSURE HEAD COEFFICIENT IN RADIAL DIRECTION (Rp/Do) FOR A RANGE OF PLUNGE POOL DEPTHS (Do = 78 mm , L = 725 - 1125 mm)

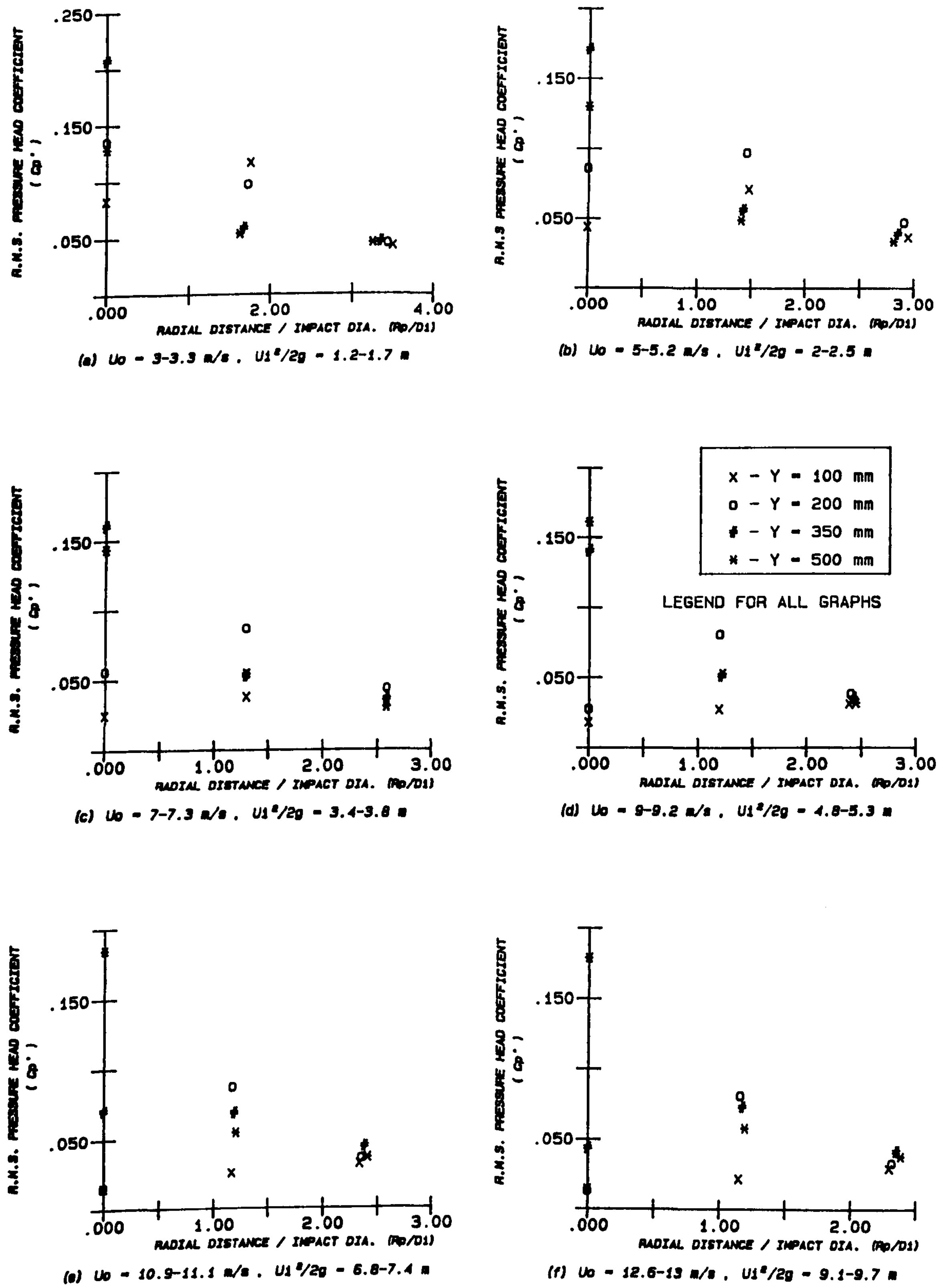

FIG. 5.2 VARIATION OF R.M.S. PRESSURE HEAD COEFFICIENT IN RADIAL DIRECTION (Rp/Di) FOR A RANGE OF PLUNGE POOL DEPTHS (Do = 78 mm , L = 725 - 1125 mm)

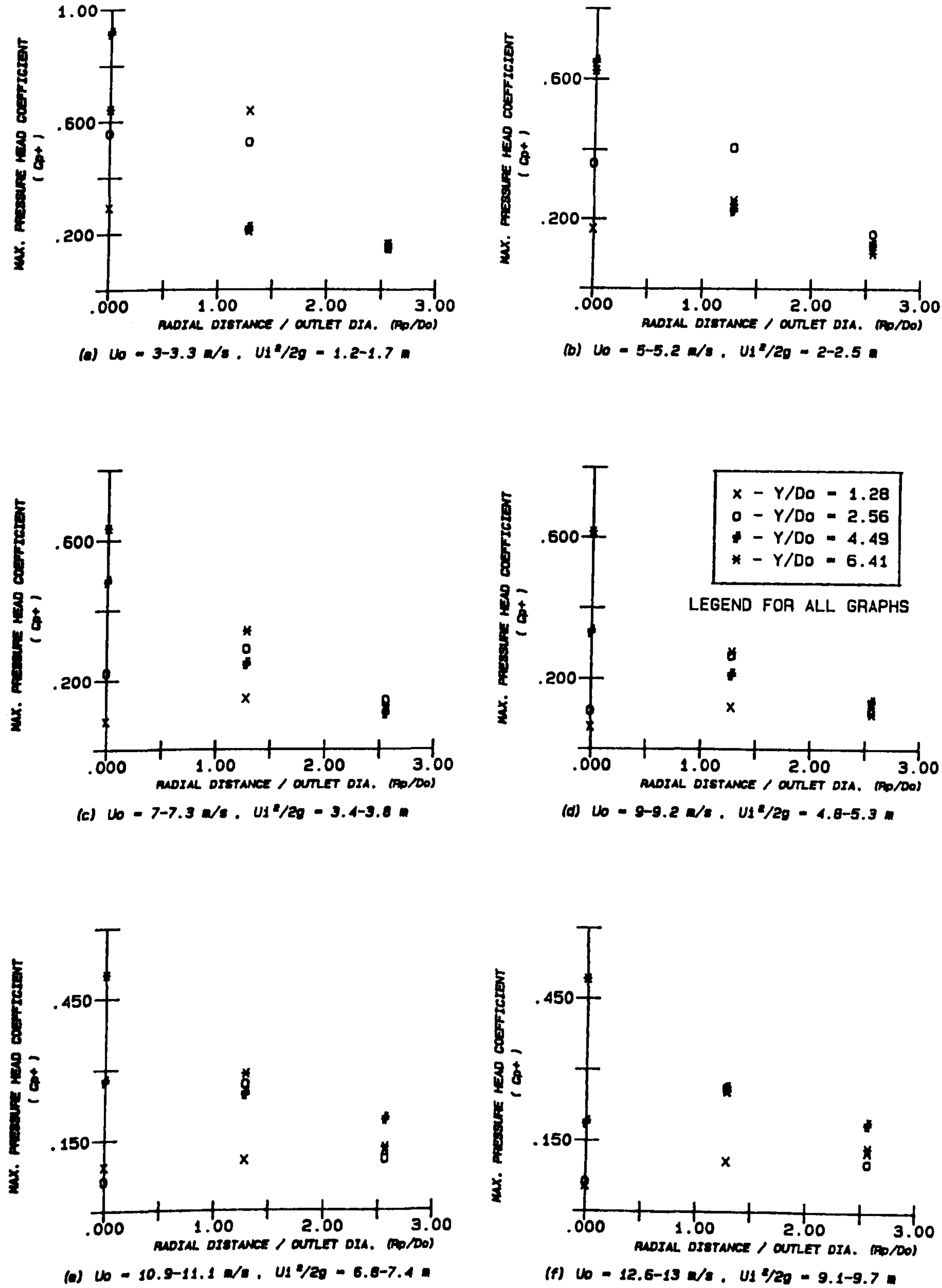

FIG. 5.3 VARIATION OF MAX. PRESSURE HEAD COEFFICIENT IN RADIAL DIRECTION (Rp/Do) FOR A RANGE OF PLUNGE POOL DEPTHS (Do = 78 mm , L = 725 - 1125 mm)

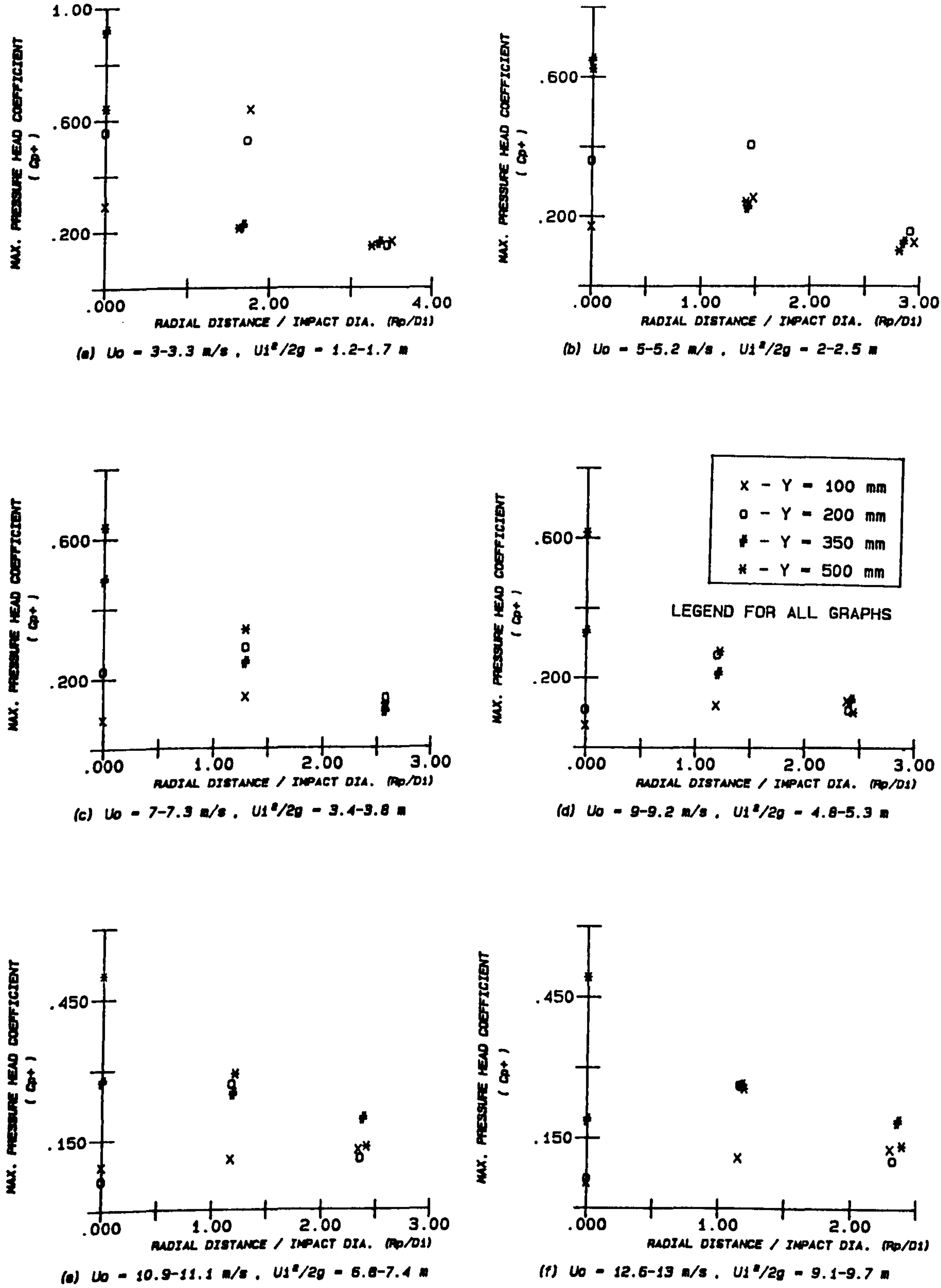

FIG. 5.4 VARIATION OF MAX. PRESSURE HEAD COEFFICIENT IN RADIAL DIRECTION (Rp/Di) FOR A RANGE OF PLUNGE POOL DEPTHS (Do = 78 mm , L = 725 - 1125 mm)

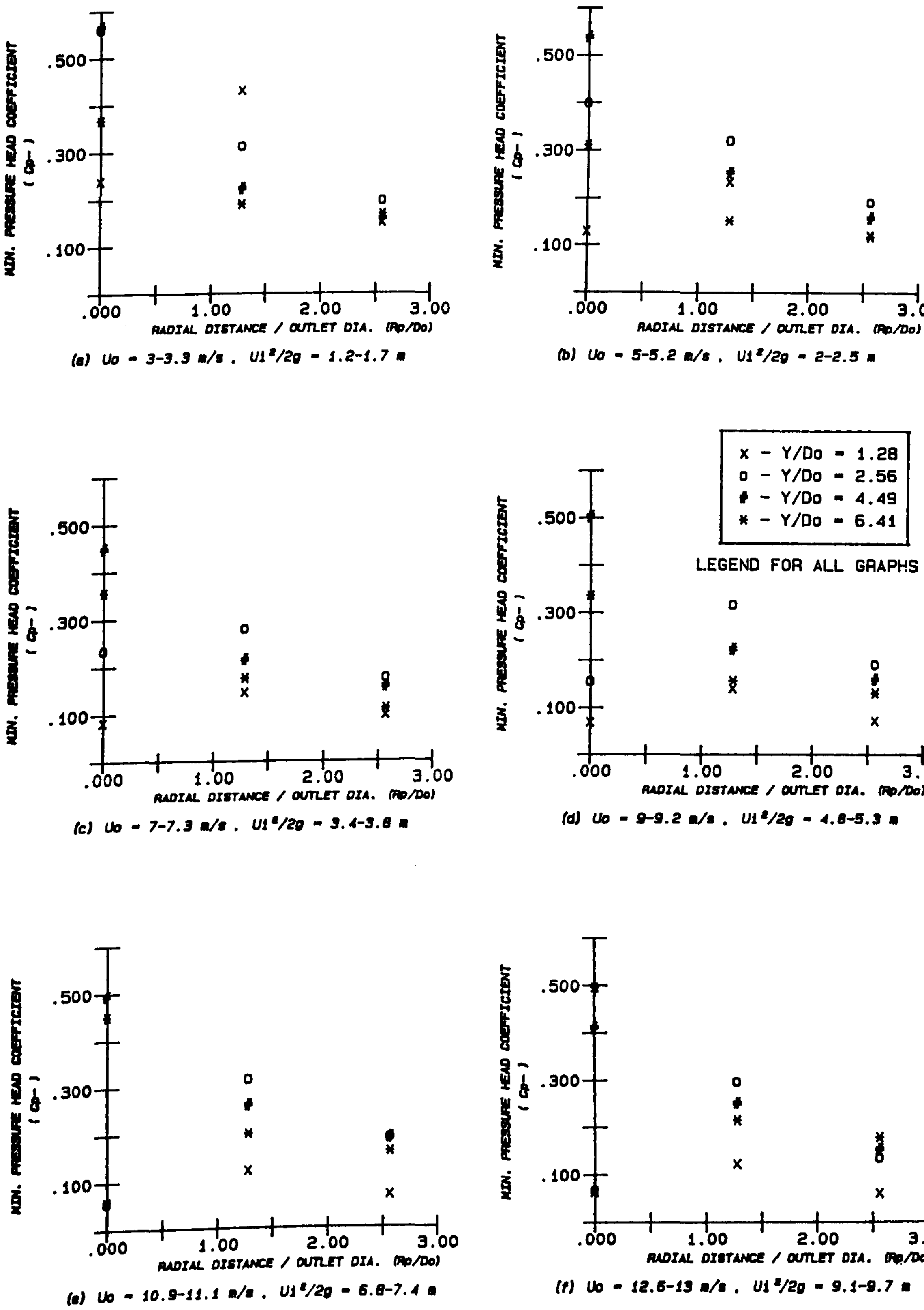

FIG. 5.5 VARIATION OF MIN. PRESSURE HEAD COEFFICIENT IN RADIAL DIRECTION (Rp/Do) FOR A RANGE OF PLUNGE POOL DEPTHS (Do = 78 mm , L = 725 - 1125 mm)

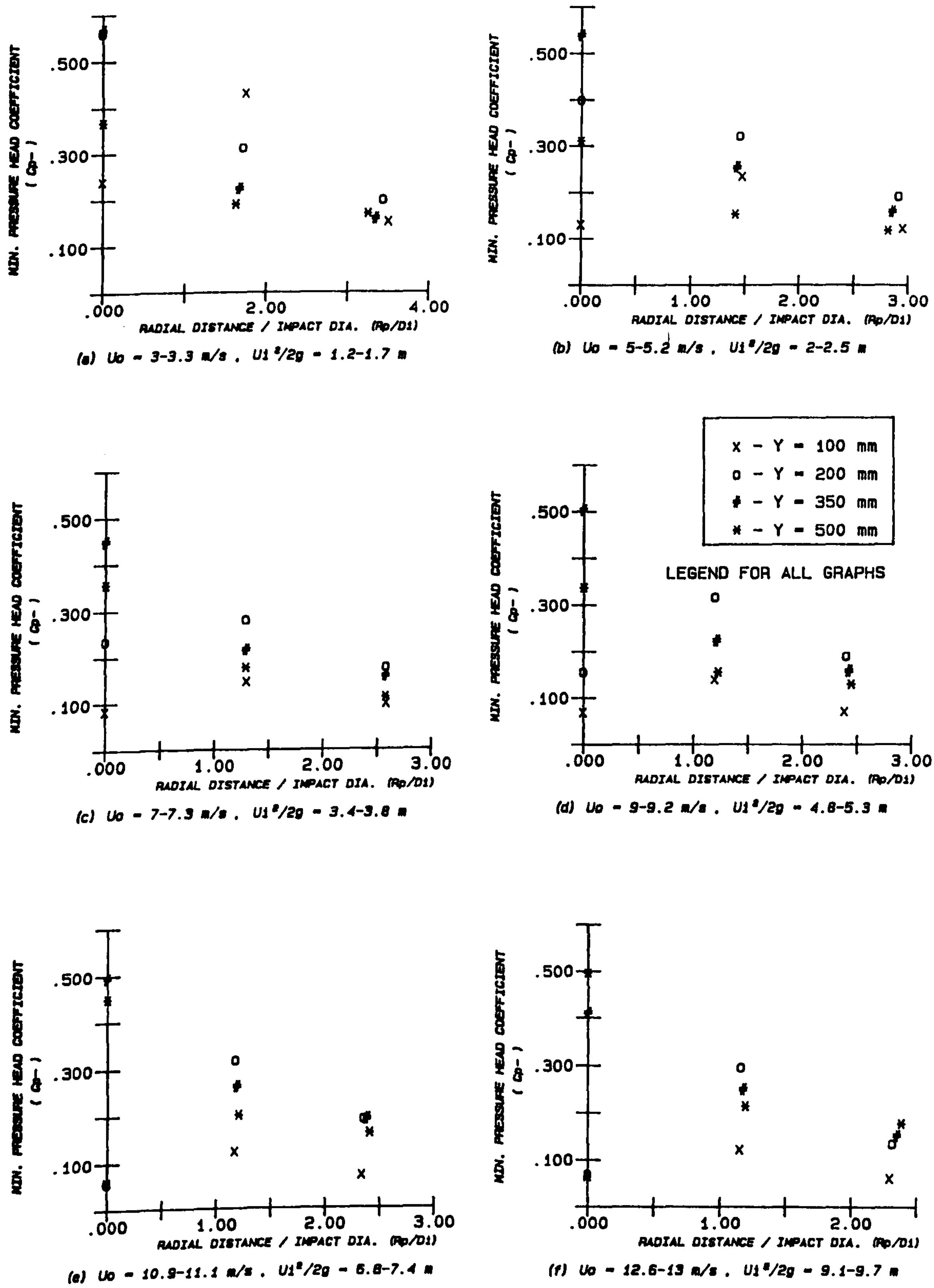

FIG. 5.6 VARIATION OF MIN. PRESSURE HEAD COEFFICIENT IN RADIAL DIRECTION (Rp/Di) FOR A RANGE OF PLUNGE POOL DEPTHS (Do = 78 mm , L = 725 - 1125 mm)

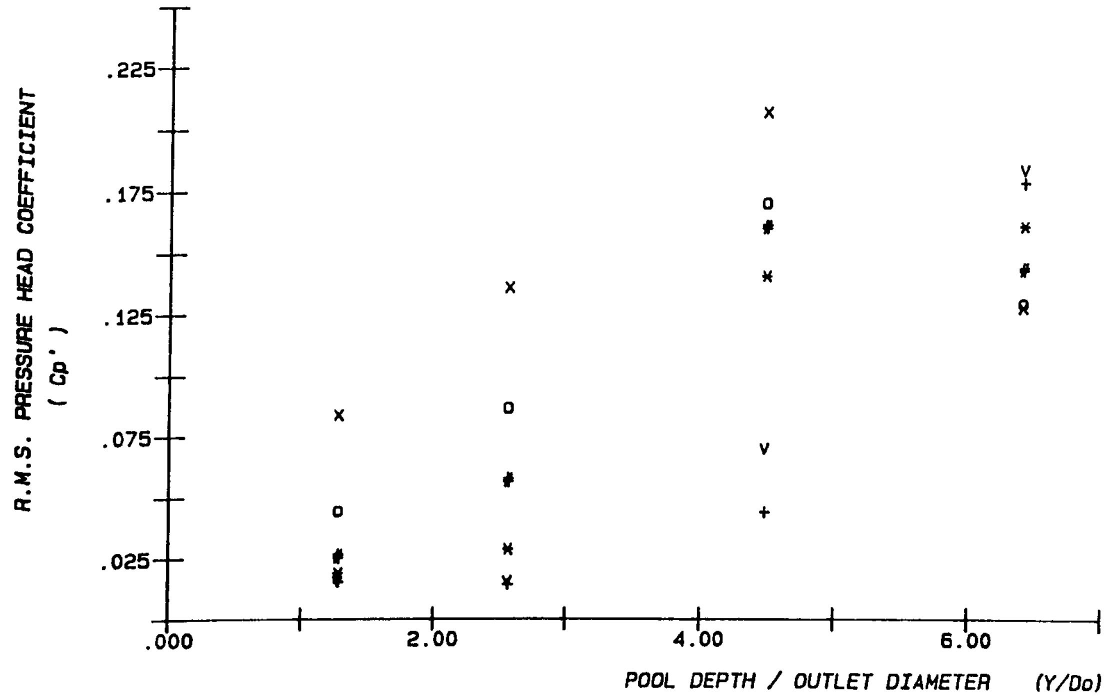

FIG. 5.7(a) CENTRE LINE R.M.S. PRESSURE HEAD COEFFICIENT WITH (Y/Do)
(Do = 78 mm , L = 725 - 1125 mm)

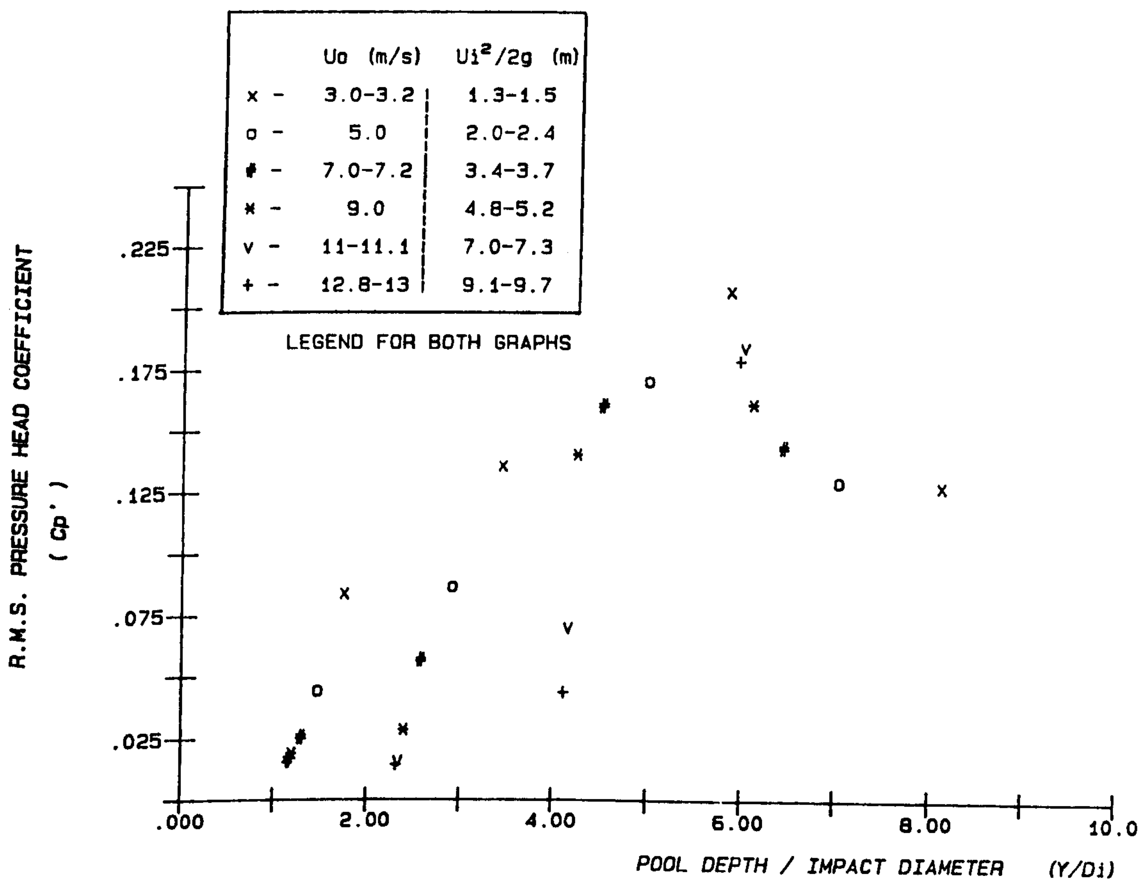

FIG. 5.7(b) CENTRE LINE R.M.S. PRESSURE HEAD COEFFICIENT WITH (Y/Di)
(Do = 78 mm , L = 725 - 1125 mm)

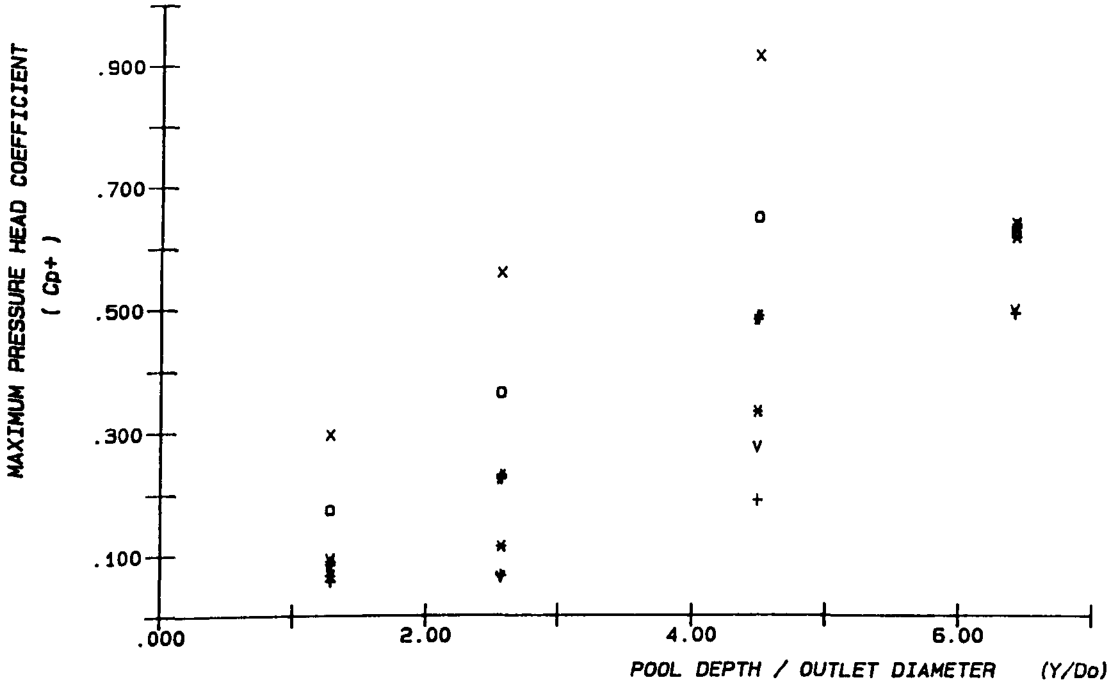

FIG. 5.8 (a) CENTRE LINE MAXIMUM PRESSURE HEAD COEFFICIENT WITH (Y/Do)
(Do = 78 mm , L = 725 - 1125 mm)

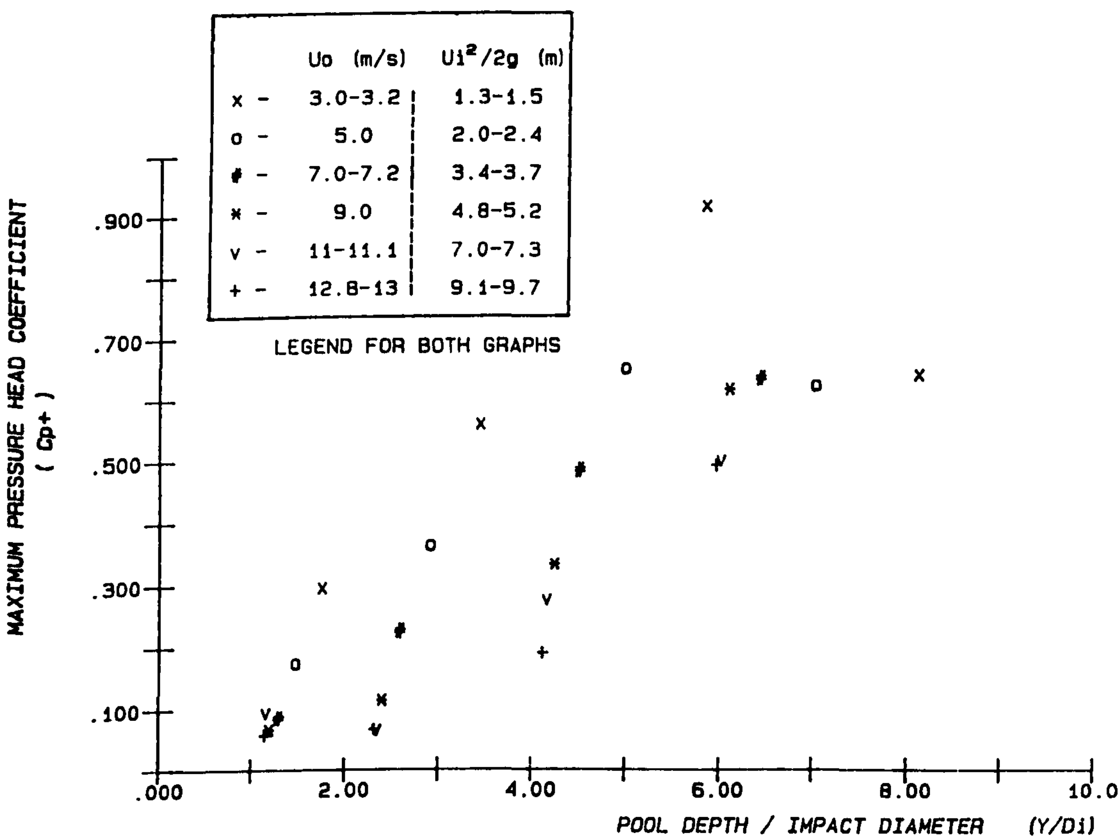

FIG. 5.8 (b) CENTRE LINE MAXIMUM PRESSURE HEAD COEFFICIENT WITH (Y/Di)
(Do = 78 mm , L = 725 - 1125 mm)

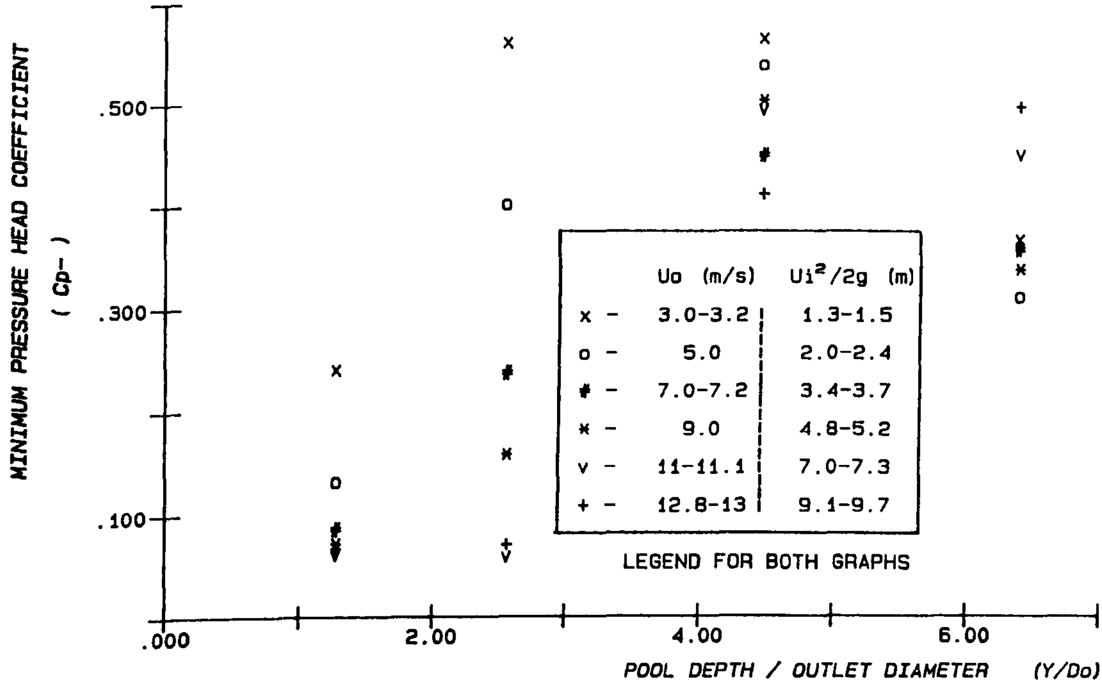

FIG. 5.9(a) CENTRE LINE MINIMUM PRESSURE HEAD COEFFICIENT WITH (Y/Do)
(Do = 78 mm , L = 725 - 1125 mm)

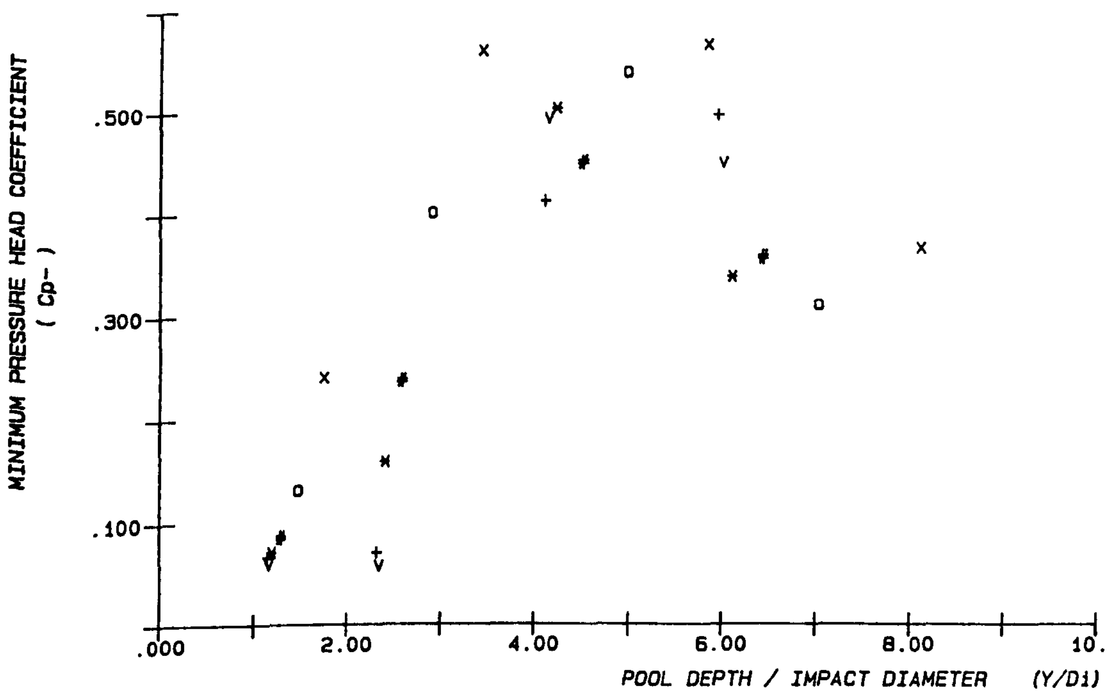

FIG. 5.9(b) CENTRE LINE MINIMUM PRESSURE HEAD COEFFICIENT WITH (Y/Di)
(Do = 78 mm , L = 725 - 1125 mm)

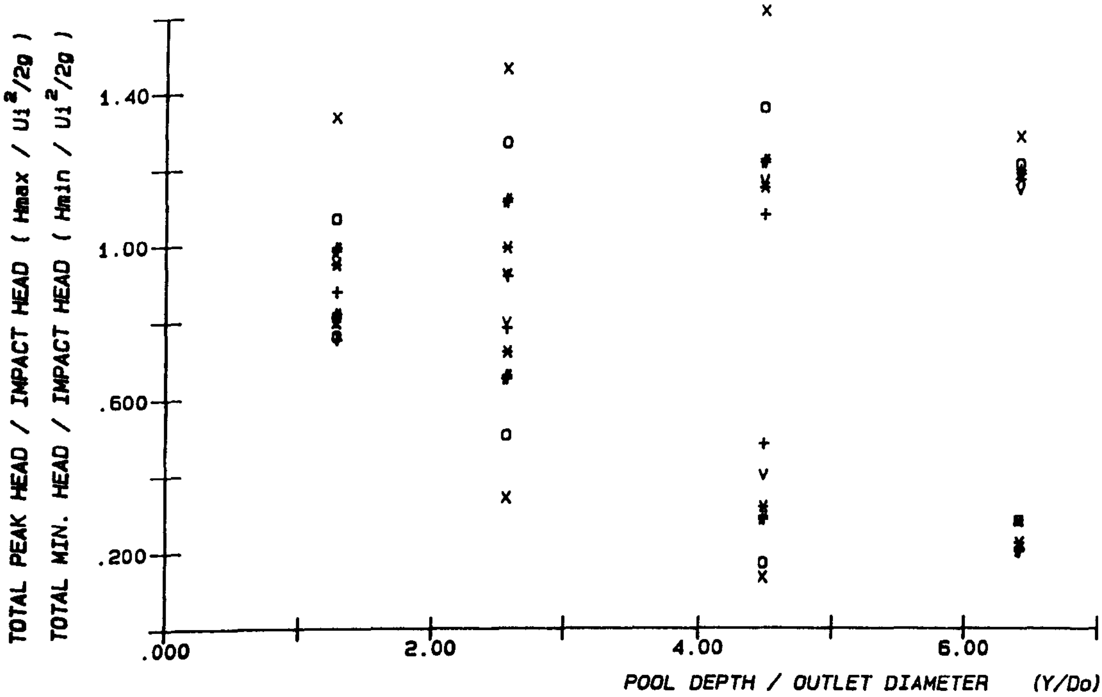

FIG. 5.10 (a) CENTRE LINE TOTAL PEAK AND MINIMUM PRESSURE HEAD RATIO WITH (Y/Do). (Do = 78 mm , L = 725 - 1125 mm)

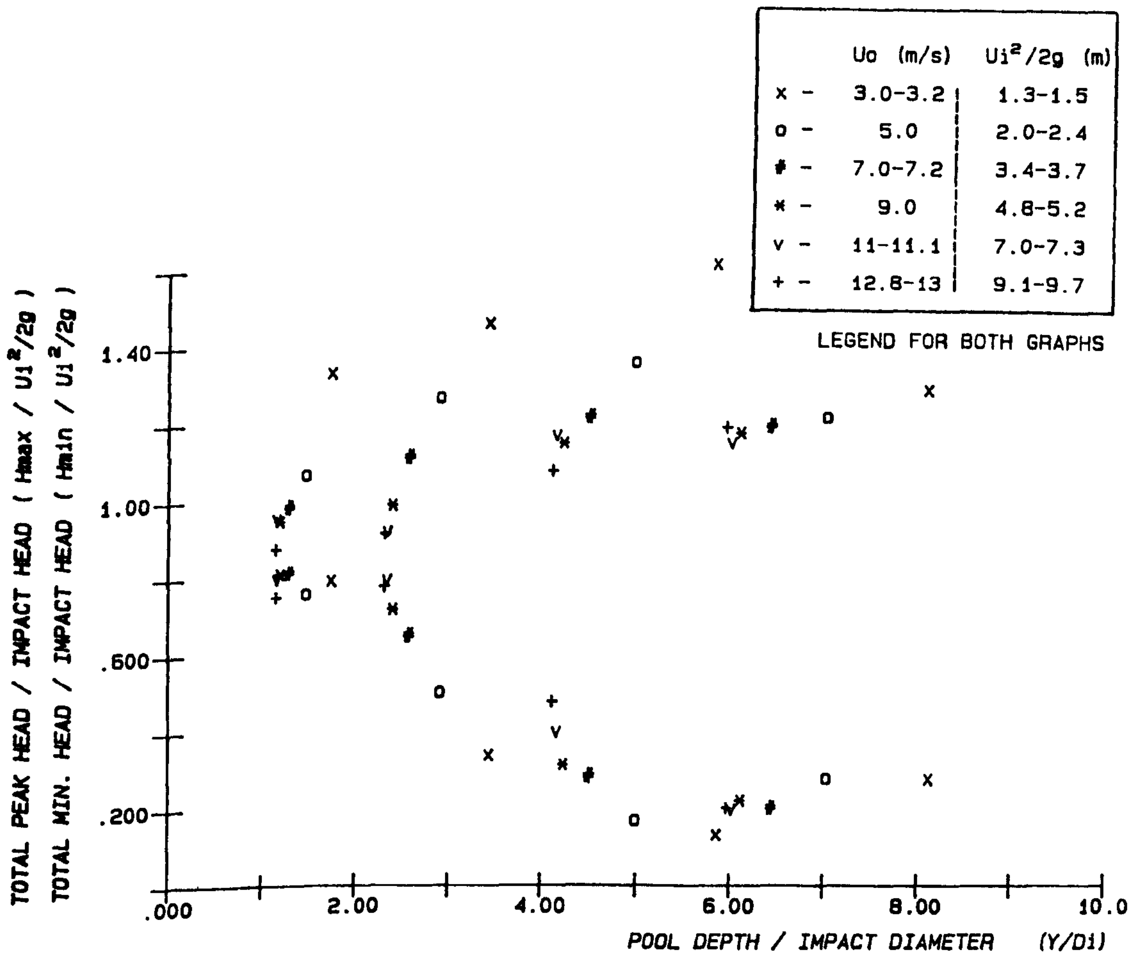

FIG. 5.10 (b) CENTRE LINE TOTAL PEAK AND MINIMUM PRESSURE HEAD RATIO WITH (Y/Di). (Do = 78 mm , L = 725 - 1125 mm)

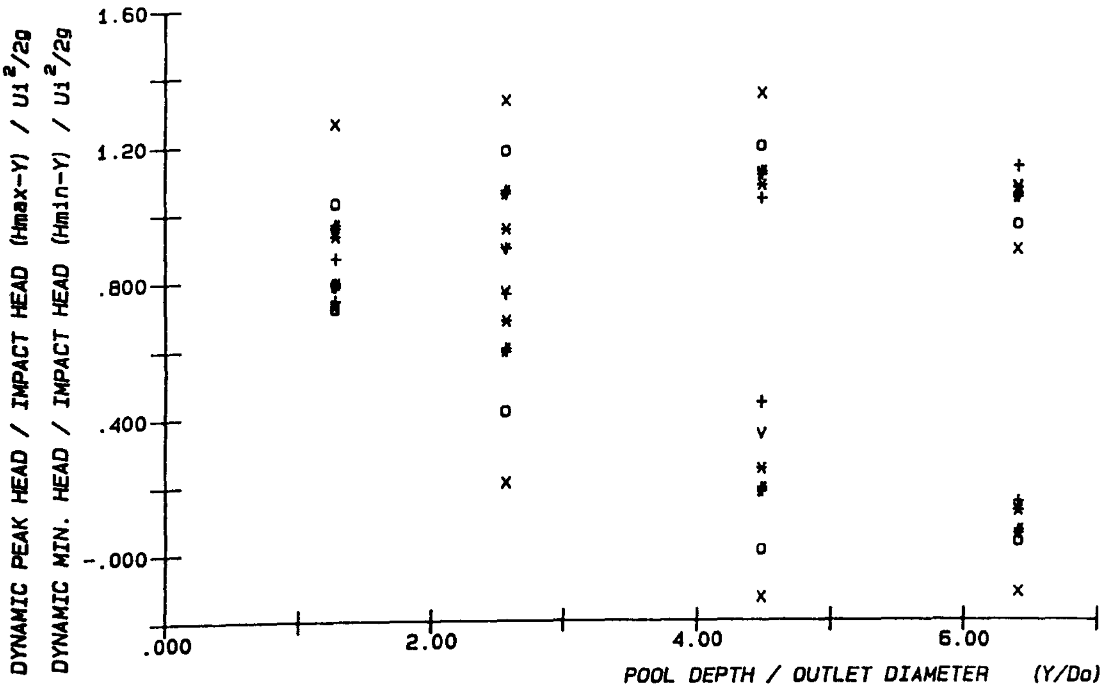

FIG 5.11 (a) CENTRE LINE DYNAMIC PEAK AND MINIMUM PRESSURE HEAD RATIO WITH (Y/Do). (Do = 78 mm , L = 725 - 1125 mm)

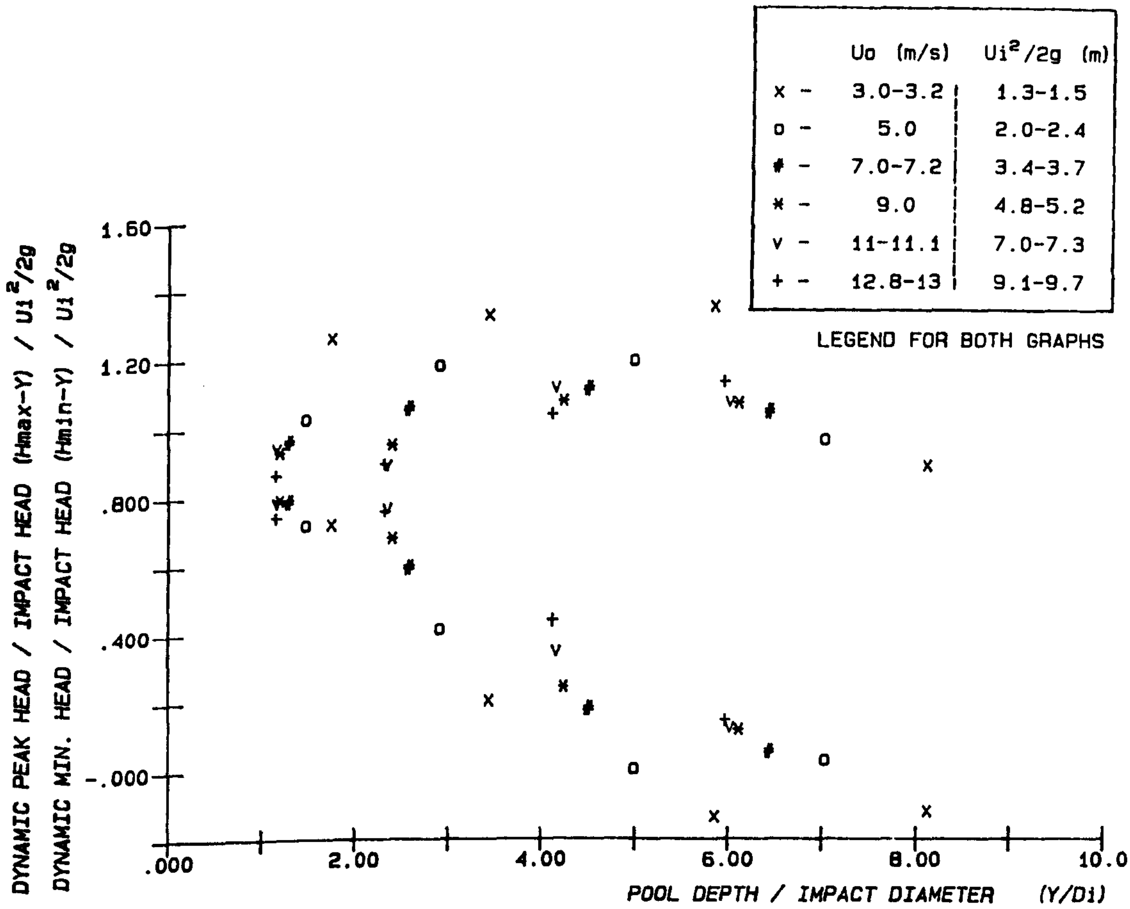

FIG. 5.11 (b) CENTRE LINE DYNAMIC PEAK AND MINIMUM PRESSURE HEAD RATIO WITH (Y/Di). (Do = 78 mm , L = 725 - 1125 mm)

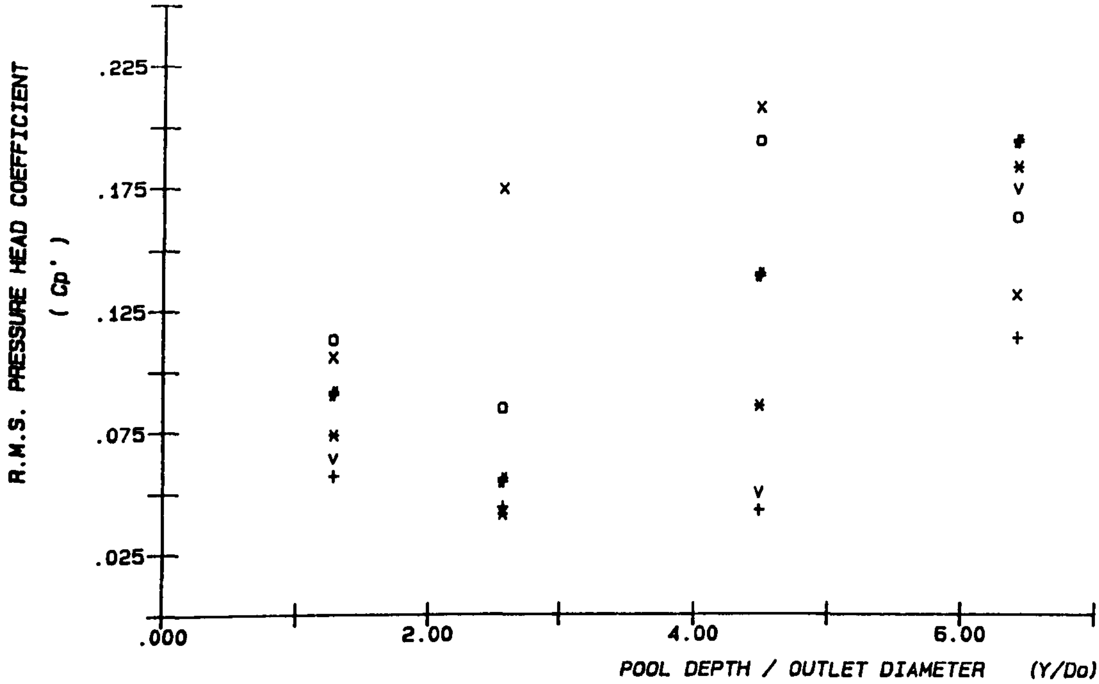

FIG. 5.12(a) CENTRE LINE R.M.S. PRESSURE HEAD COEFFICIENT WITH (Y/Do)
(Do = 78 mm , L = 2230 - 2630 mm)

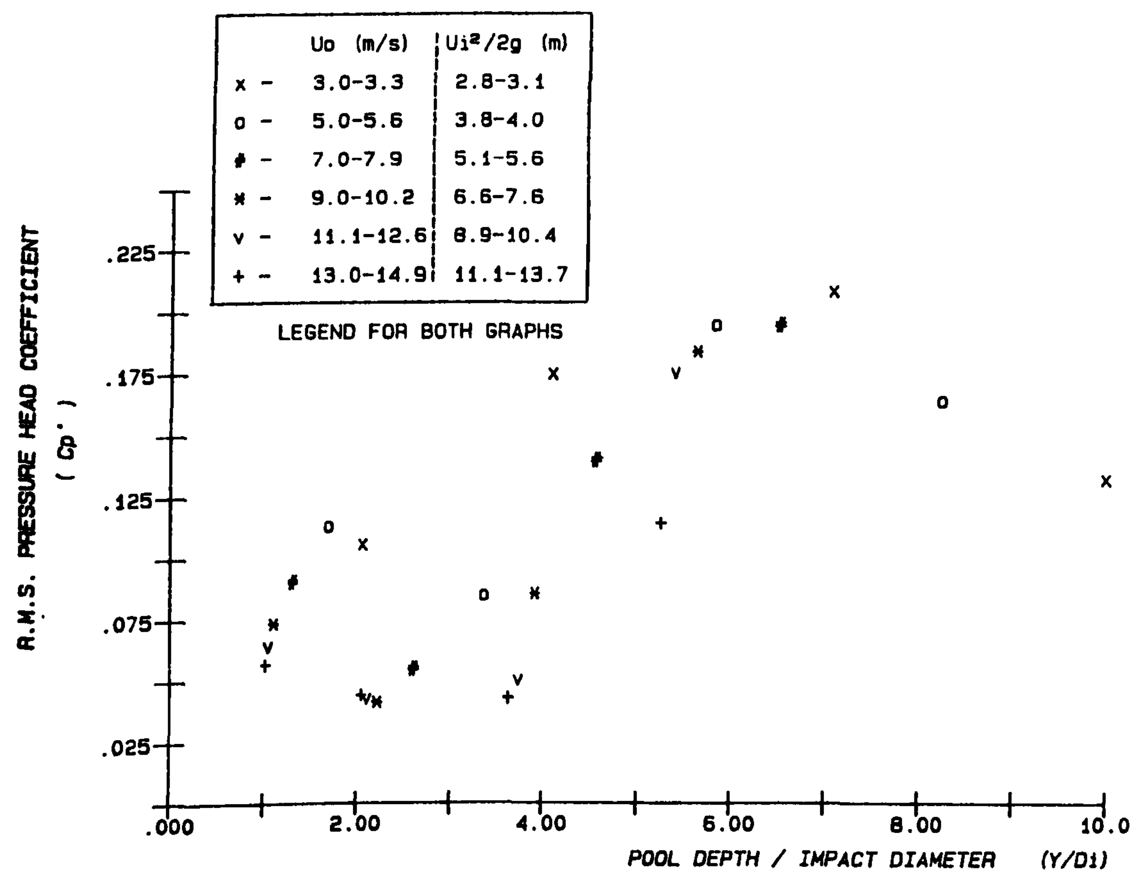

FIG. 5.12(b) CENTRE LINE R.M.S. PRESSURE HEAD COEFFICIENT WITH (Y/Di)
(Do = 78 mm , L = 2230 - 2630 mm)

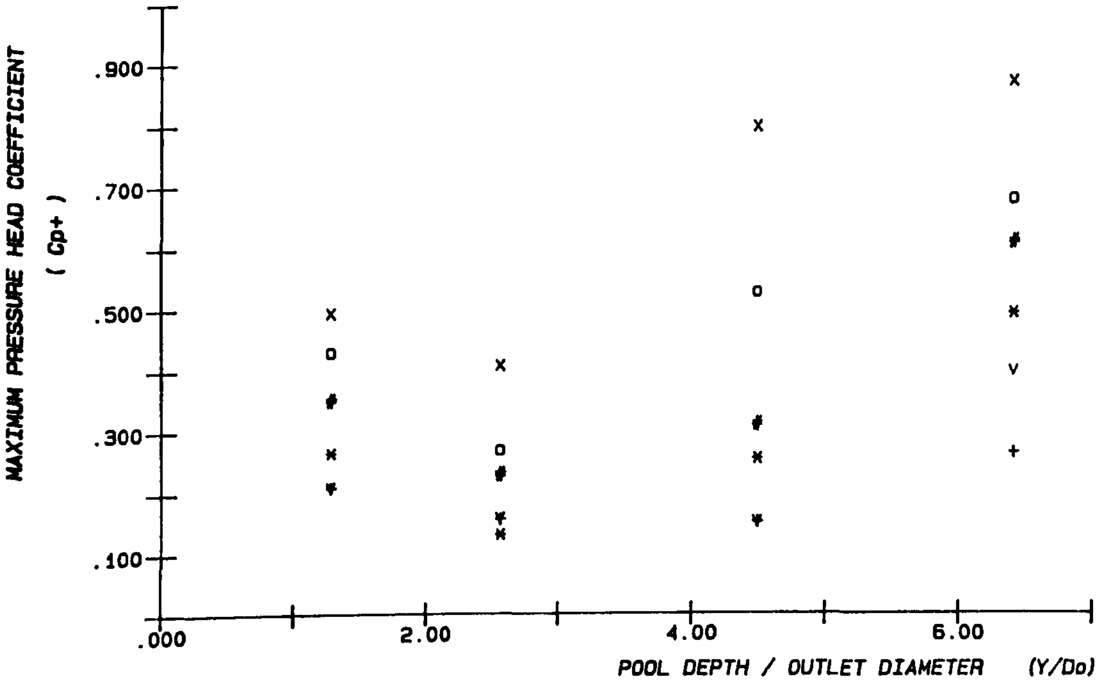

FIG. 5.13(a) CENTRE LINE MAXIMUM PRESSURE HEAD COEFFICIENT WITH (Y/Do)
(Do = 78 mm , L = 2230 - 2630 mm)

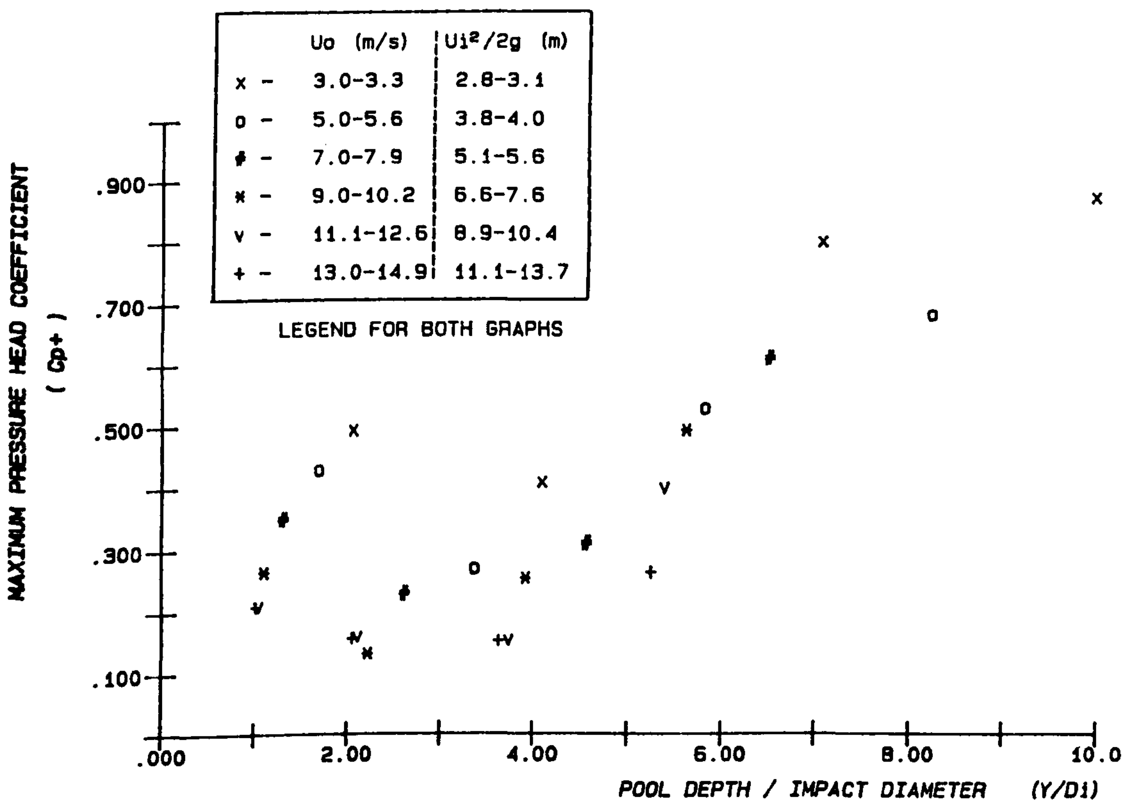

FIG. 5.13(b) CENTRE LINE MAXIMUM PRESSURE HEAD COEFFICIENT WITH (Y/Di)
(Do = 78 mm , L = 2230 - 2630 mm)

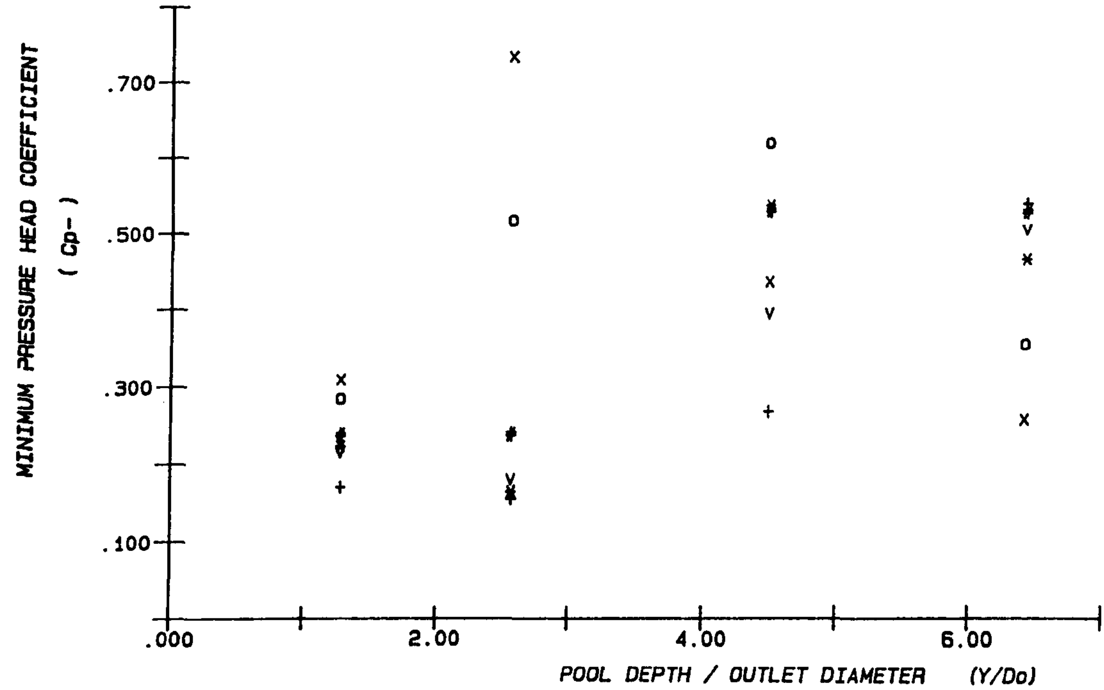

FIG. 5.14 (a) CENTRE LINE MINIMUM PRESSURE HEAD COEFFICIENT WITH (Y/Do)
(Do = 78 mm , L = 2230 - 2630 mm)

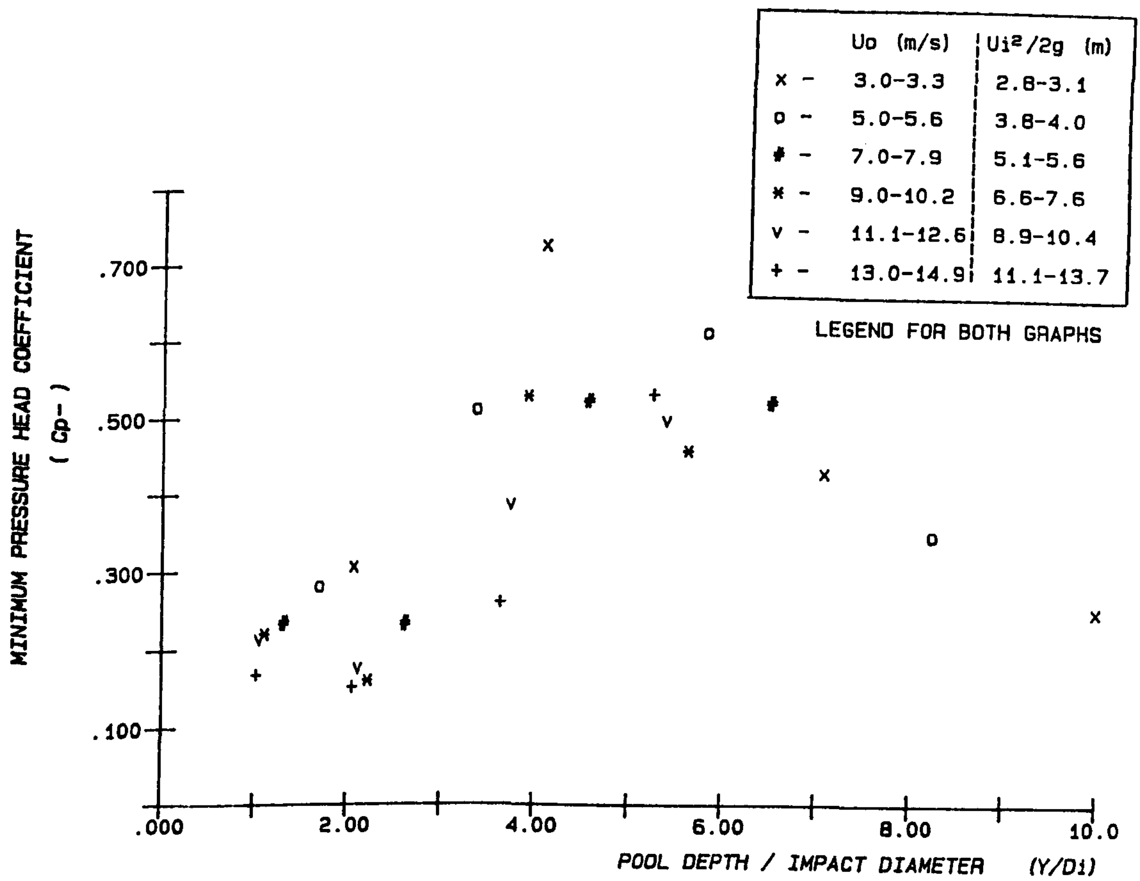

FIG. 5.14 (b) CENTRE LINE MINIMUM PRESSURE HEAD COEFFICIENT WITH (Y/Di)
(Do = 78 mm , L = 2230 - 2630 mm)

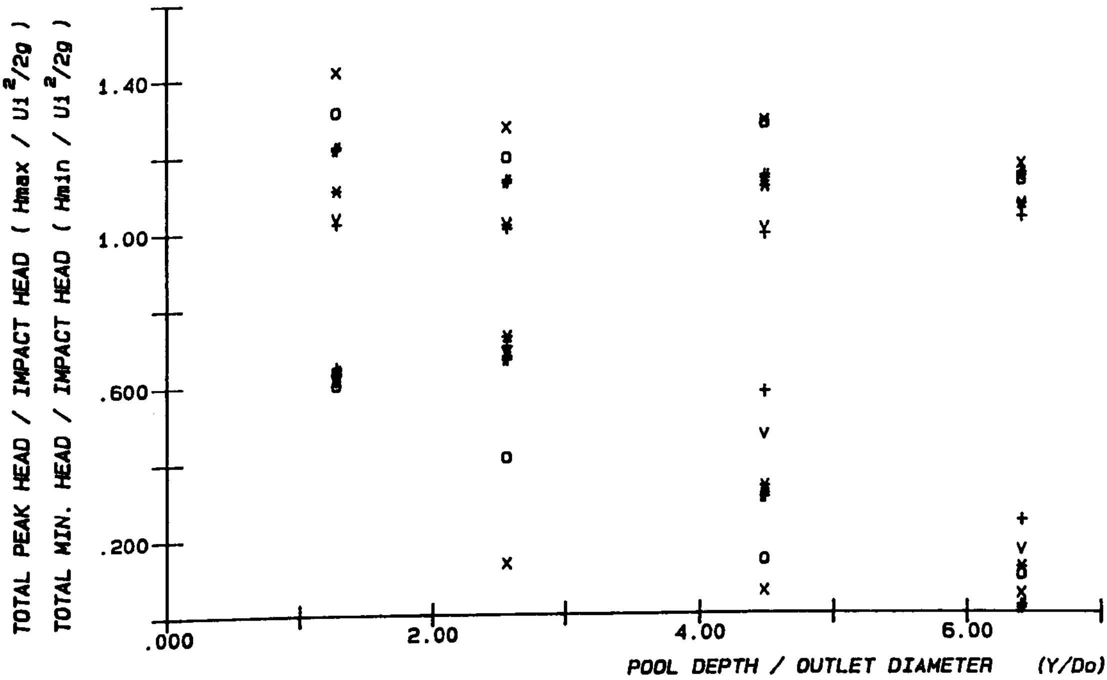

FIG. 5.15(a) CENTRE LINE TOTAL PEAK AND MINIMUM PRESSURE HEAD RATIO WITH (Y/Do). (Do = 78 mm , L = 2230 - 2630)

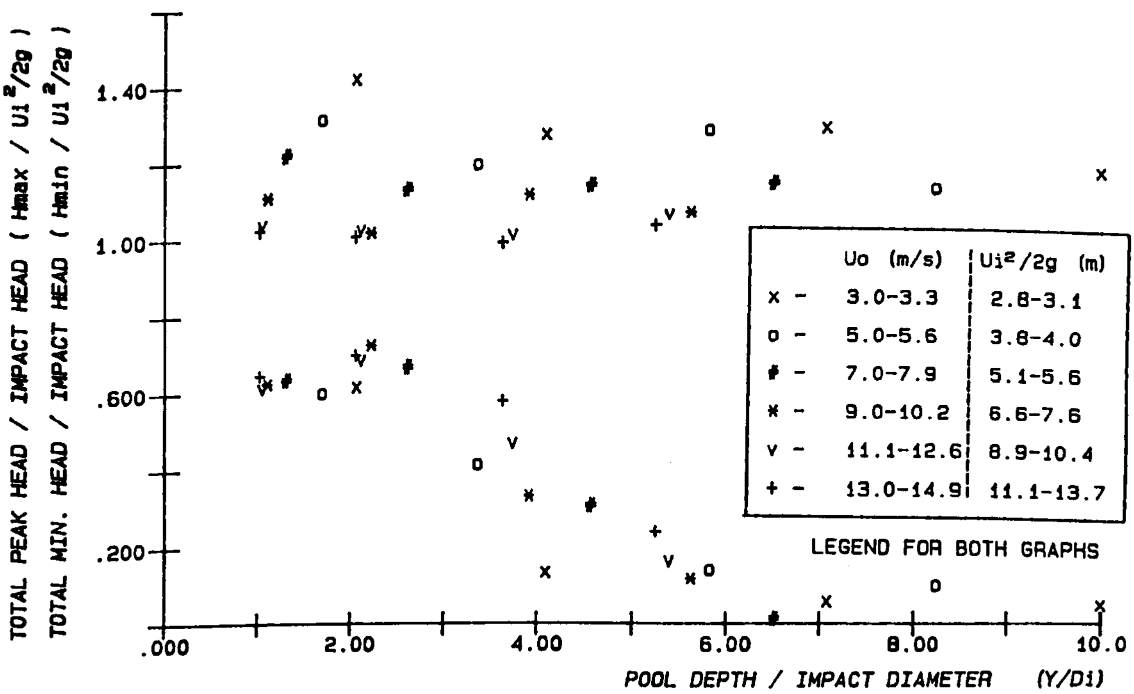

FIG. 5.15(b) CENTRE LINE TOTAL PEAK AND MINIMUM PRESSURE HEAD RATIO WITH (Y/Di). (Do = 78 mm , L = 2230 - 2630 mm)

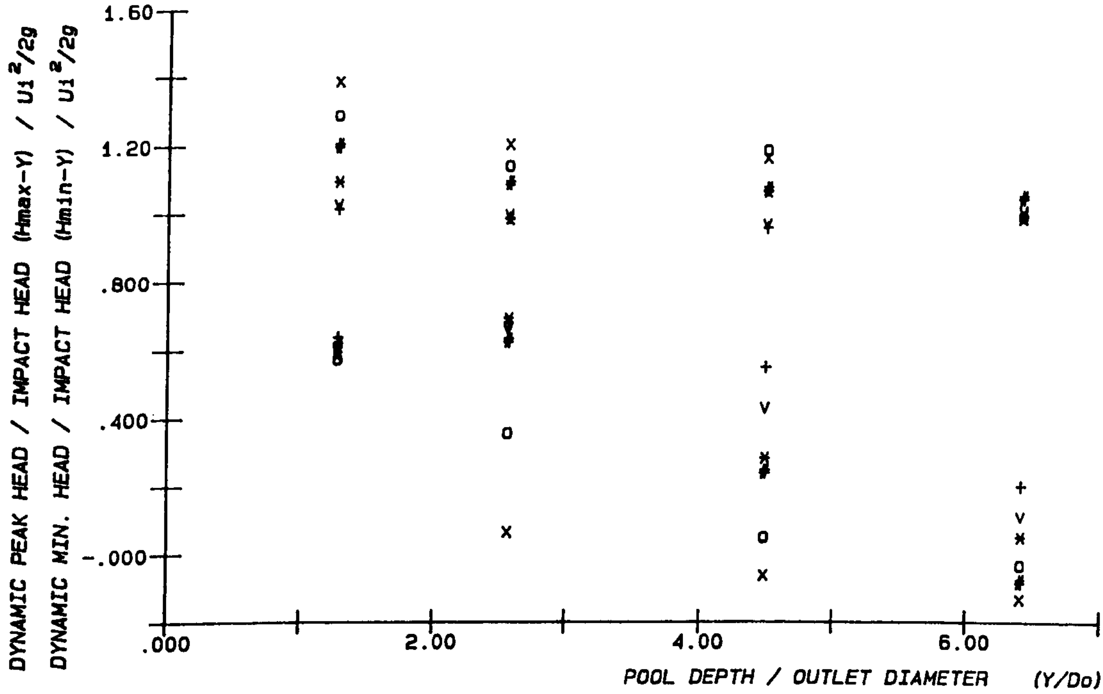

FIG. 5.16(a) CENTRE LINE DYNAMIC PEAK AND MINIMUM PRESSURE HEAD RATIO WITH (Y/Do). (Do = 78 mm , L = 2230 - 2630 mm)

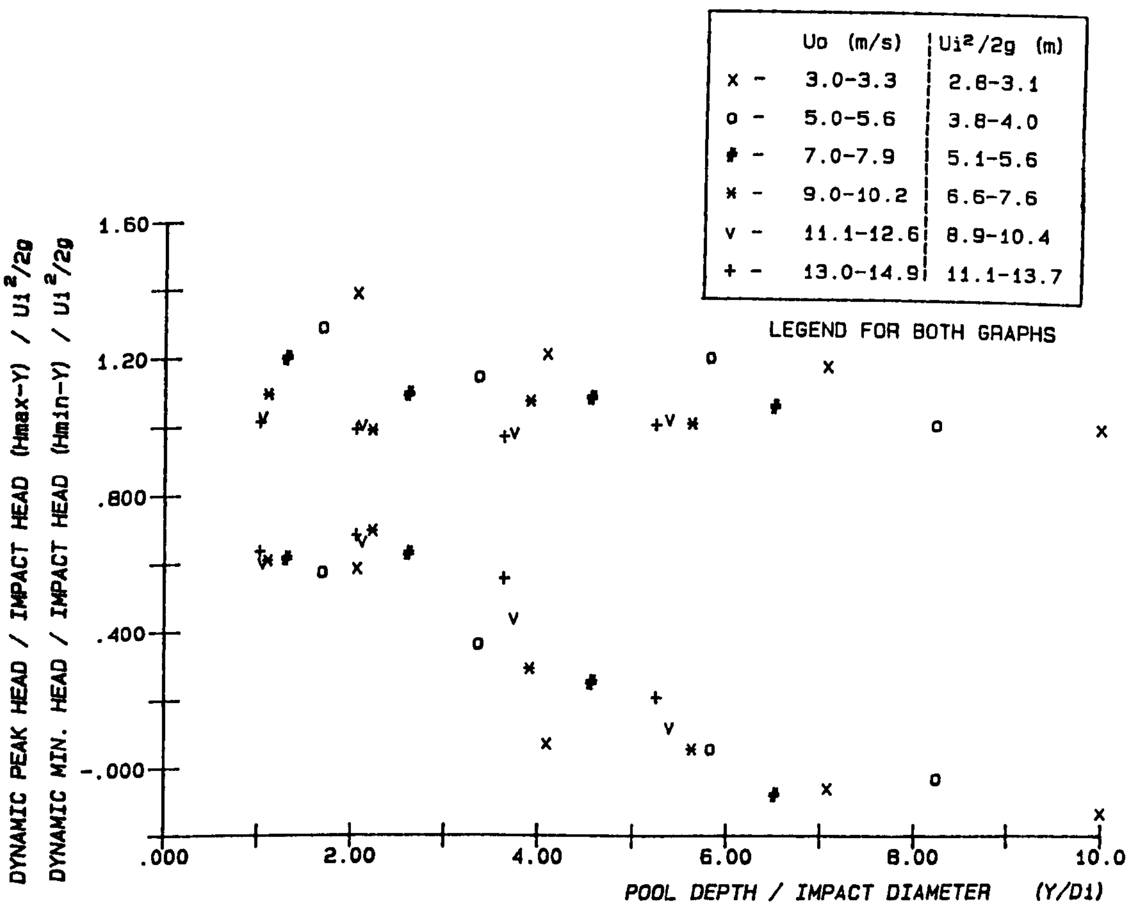

FIG. 5.16(b) CENTRE LINE DYNAMIC PEAK AND MINIMUM PRESSURE HEAD RATIO WITH (Y/Di). (Do = 78 mm , L = 2230 - 2630 mm)

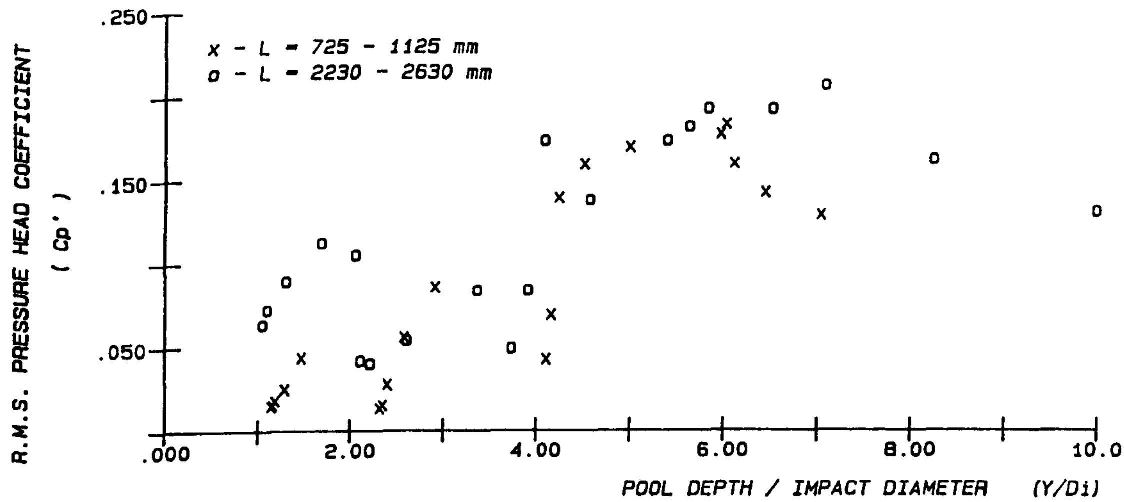

FIG. 5.17(a) R.M.S. PRESSURE HEAD COEFFICIENT AGAINST PLUNGE POOL DEPTH FOR 78 mm NOZZLE FOR THE TWO DIFFERENT FALL LENGTHS

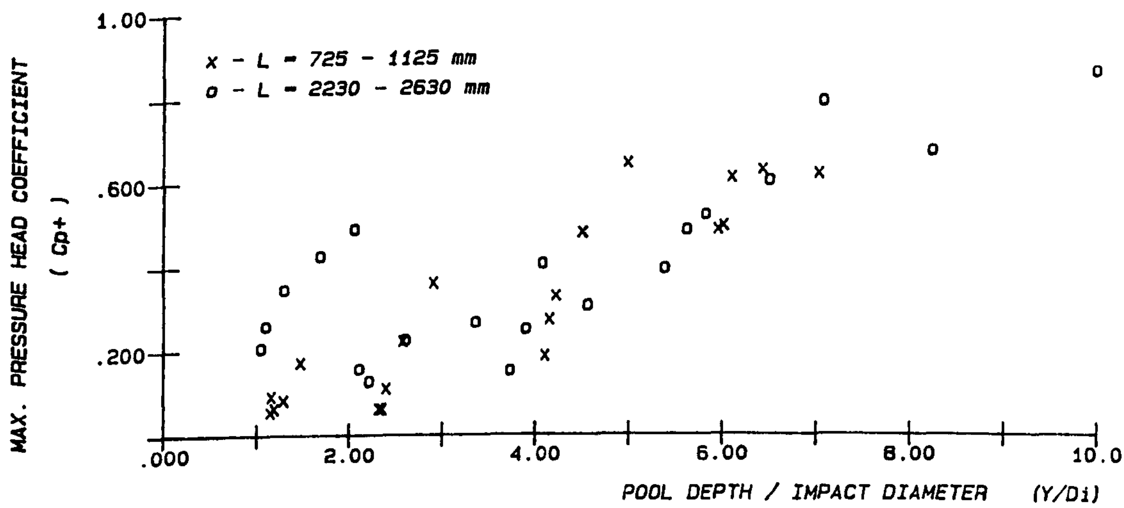

FIG. 5.17(b) MAX. PRESSURE HEAD COEFFICIENT AGAINST PLUNGE POOL DEPTH FOR 78 mm NOZZLE FOR THE TWO DIFFERENT FALL LENGTHS

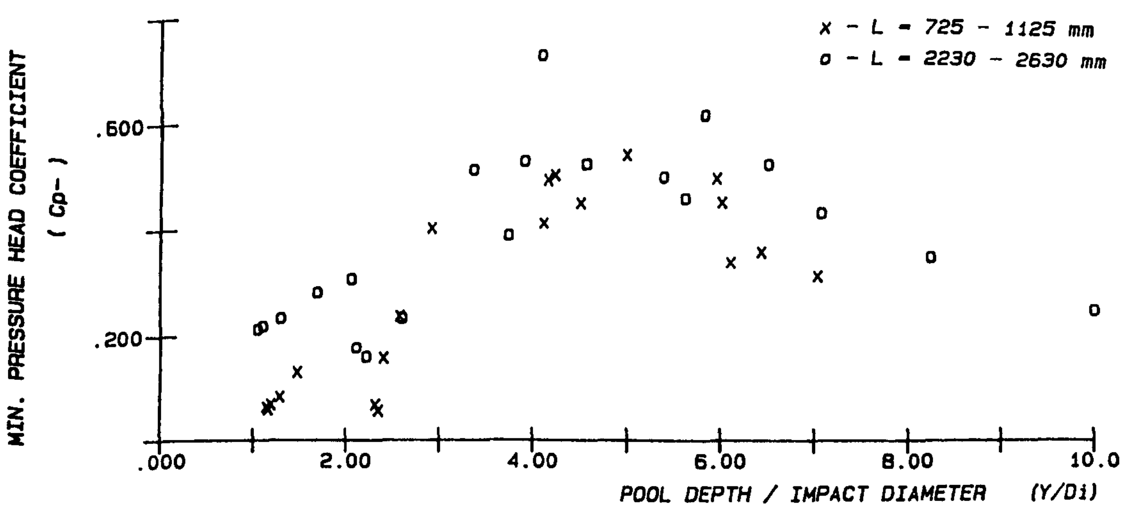

FIG. 5.17(c) MIN. PRESSURE HEAD COEFFICIENT AGAINST PLUNGE POOL DEPTH FOR 78 mm NOZZLE FOR THE TWO DIFFERENT FALL LENGTHS

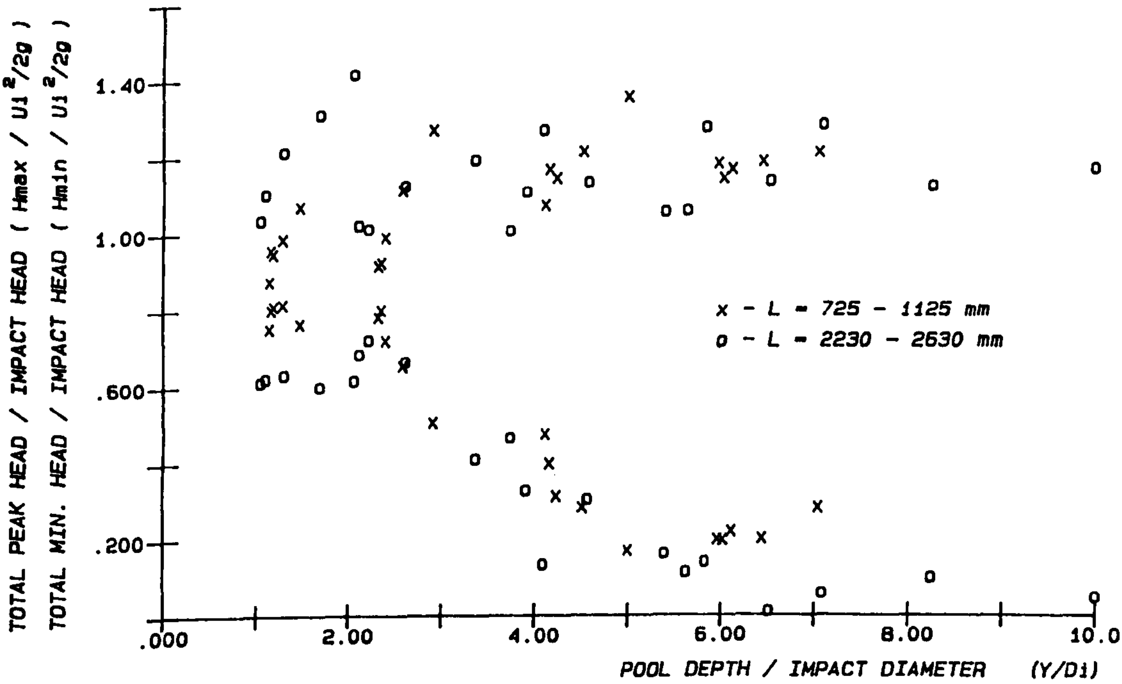

FIG. 5.18(a) TOTAL PEAK AND MINIMUM HEAD AGAINST PLUNGE POOL DEPTH FOR 78 mm NOZZLE FOR THE TWO DIFFERENT FALL LENGTHS

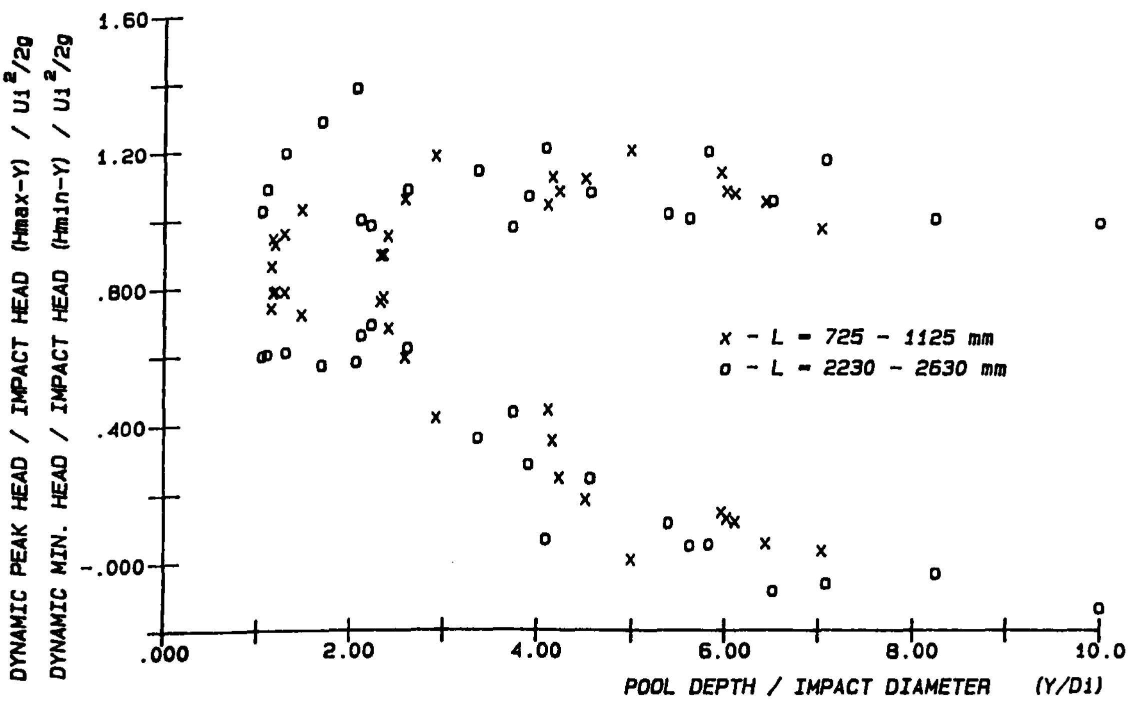

FIG. 5.18(b) DYNAMIC PEAK AND MINIMUM HEAD AGAINST PLUNGE POOL DEPTH FOR 78 mm NOZZLE FOR THE TWO DIFFERENT FALL LENGTHS

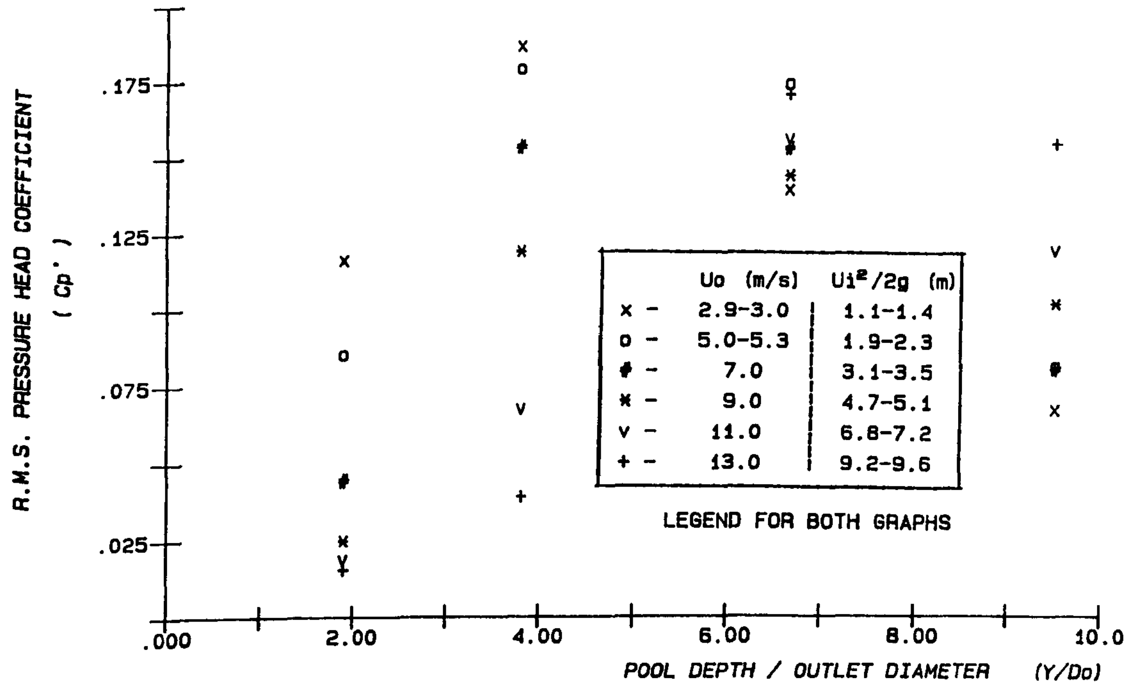

FIG. 5.19 (a) CENTRE LINE R.M.S. PRESSURE HEAD COEFFICIENT WITH (Y/Do)
(Do = 52.5 mm , L = 620 - 1020 mm)

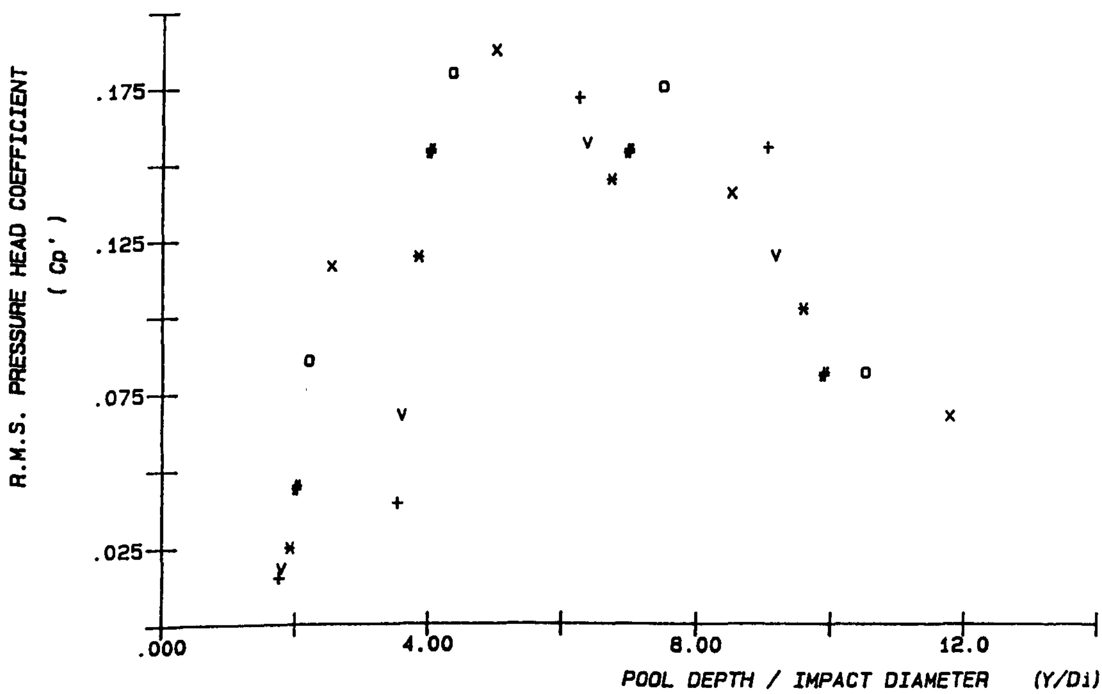

FIG. 5.19 (b) CENTRE LINE R.M.S. PRESSURE HEAD COEFFICIENT WITH (Y/Di)
(Do = 52.5 mm , L = 620 - 1020 mm)

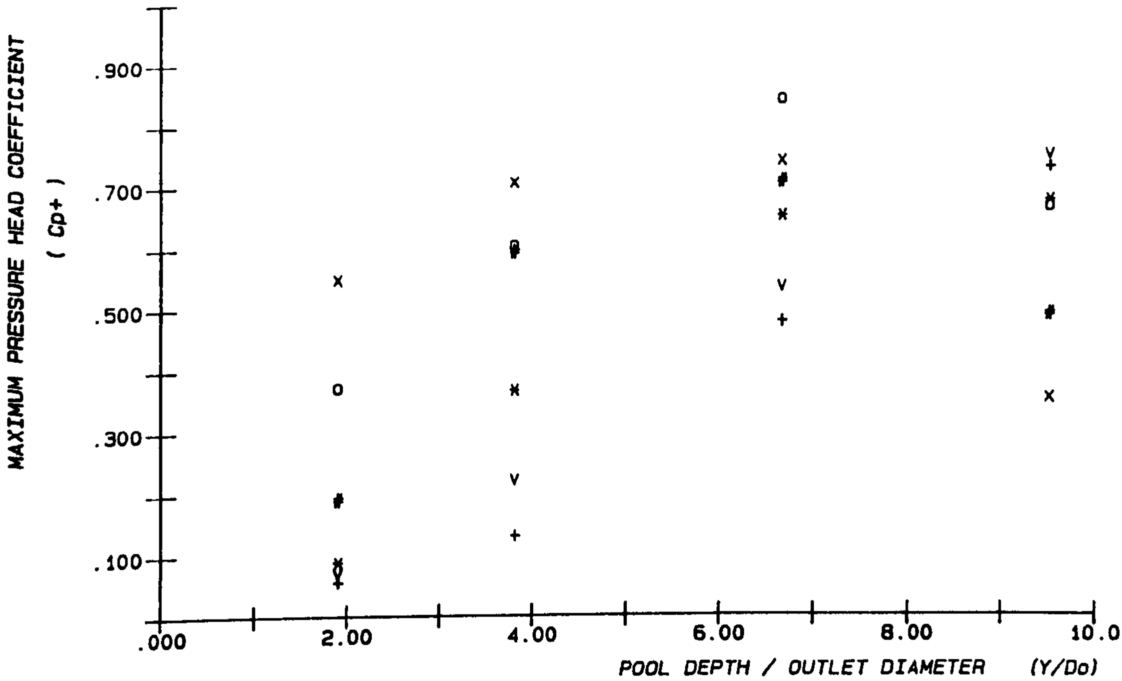

FIG. 5.20 (a) CENTRE LINE MAXIMUM PRESSURE HEAD COEFFICIENT WITH (Y/Do)
(Do = 52.5 mm , L = 620 - 1020 mm)

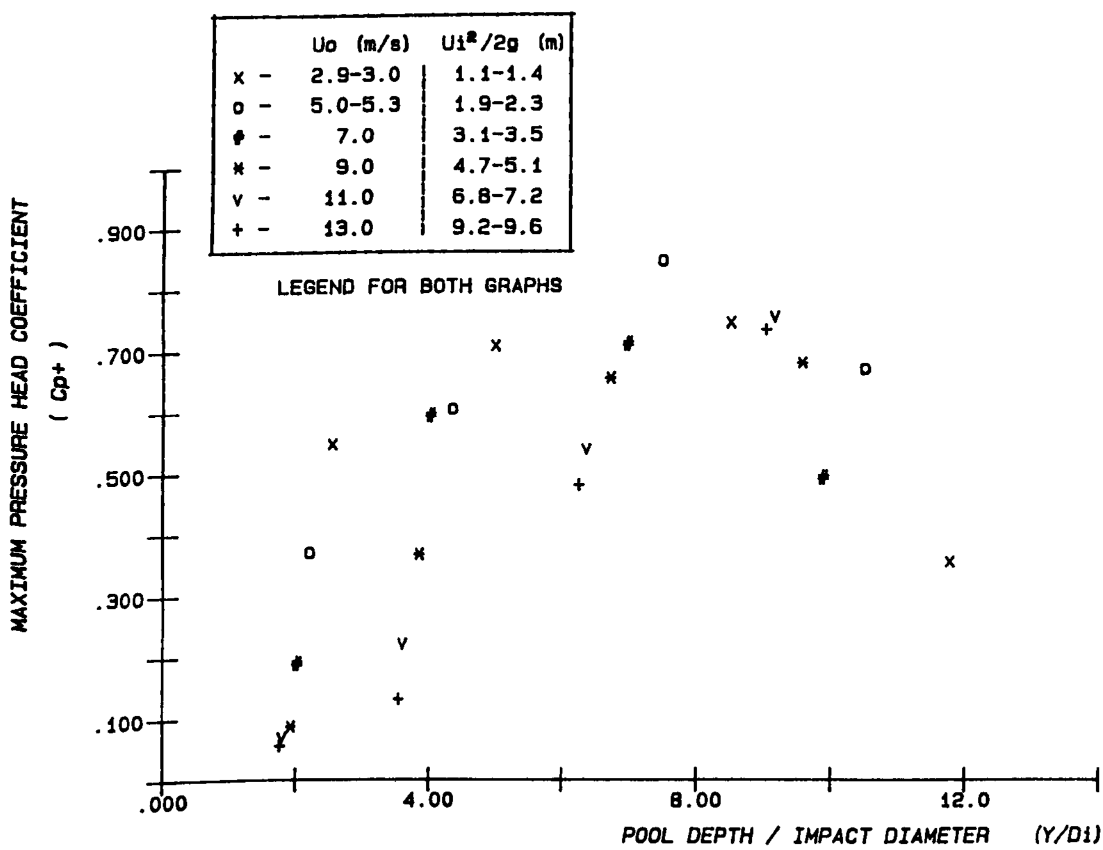

FIG. 5.20 (b) CENTRE LINE MAXIMUM PRESSURE HEAD COEFFICIENT WITH (Y/Di)
(Do = 52.5 mm , L = 620 - 1020 mm)

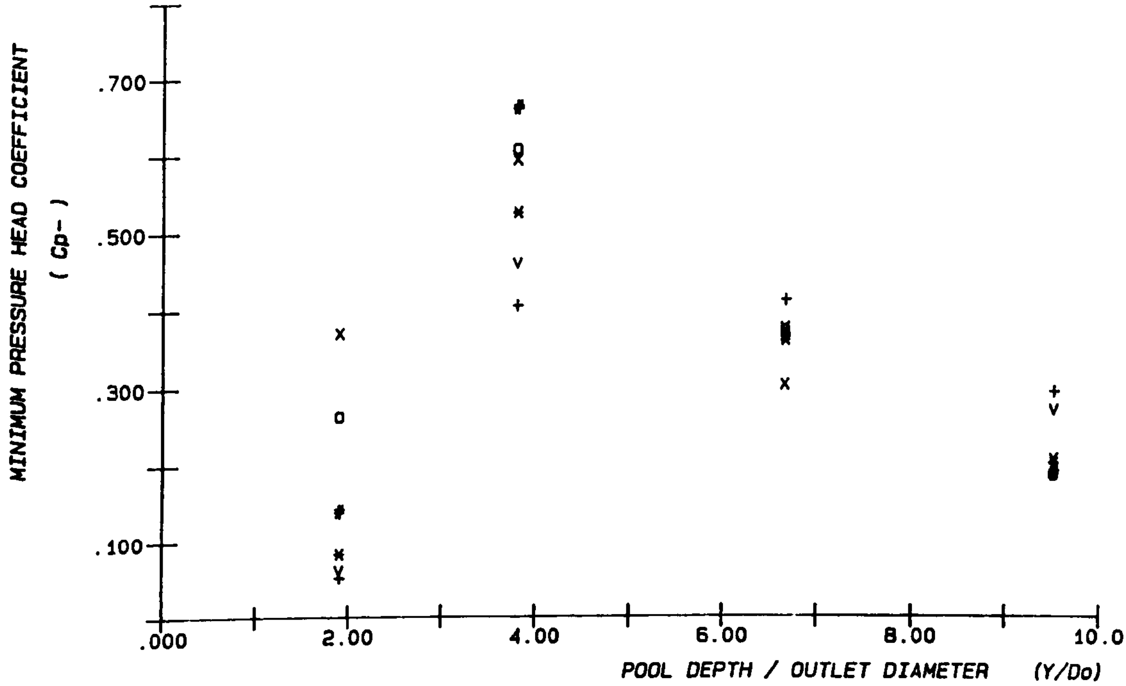

FIG. 5.21 (a) CENTRE LINE MINIMUM PRESSURE HEAD COEFFICIENT WITH (Y/Do)
(Do = 52.5 mm , L = 620 - 1020 mm)

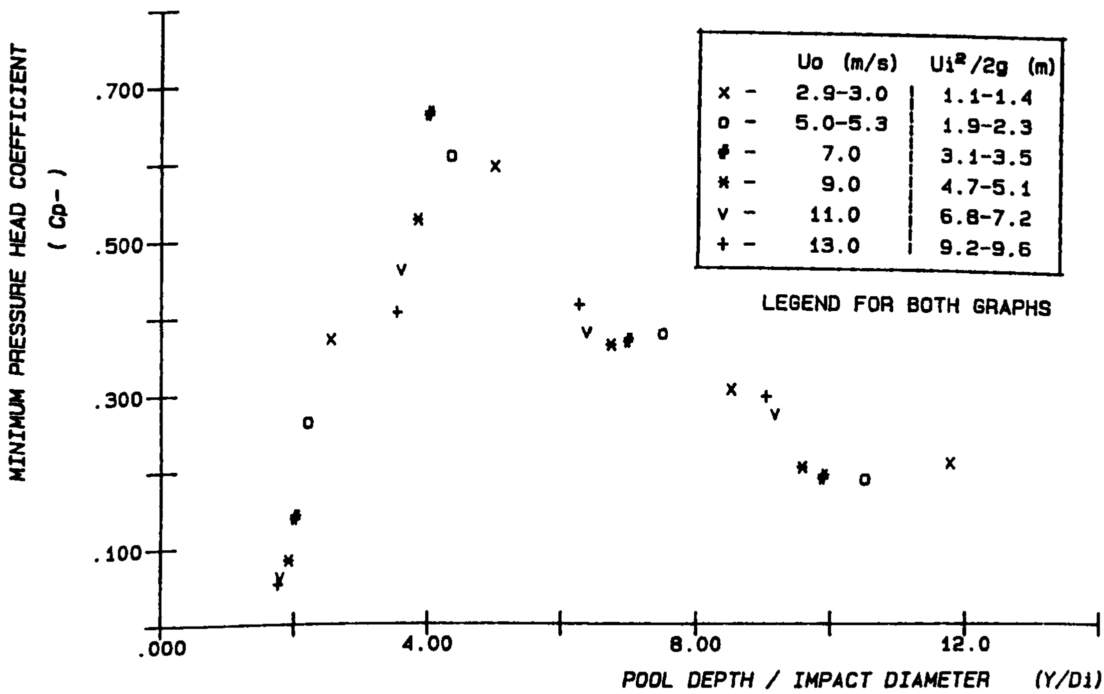

FIG. 5.21 (b) CENTRE LINE MINIMUM PRESSURE HEAD COEFFICIENT WITH (Y/Di)
(Do = 52.5 mm , L = 620 - 1020 mm)

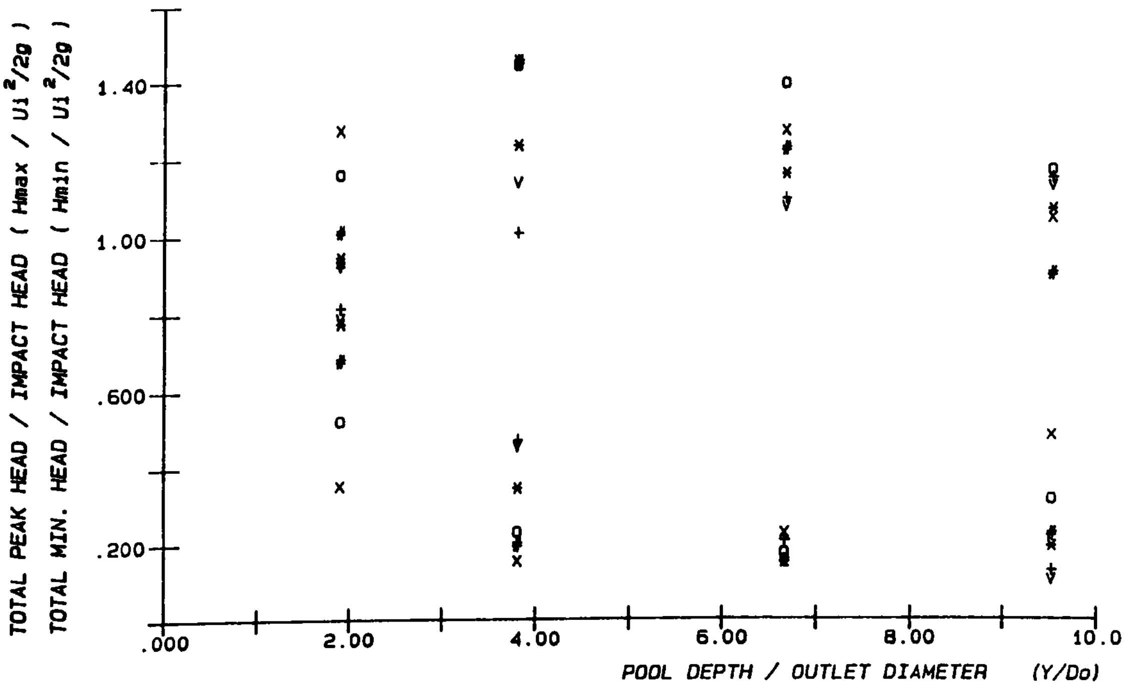

FIG. 5.22(a) CENTRE LINE TOTAL PEAK AND MINIMUM PRESSURE HEAD RATIO WITH (Y/Do). (Do = 52.5 mm , L = 620 - 1020 mm)

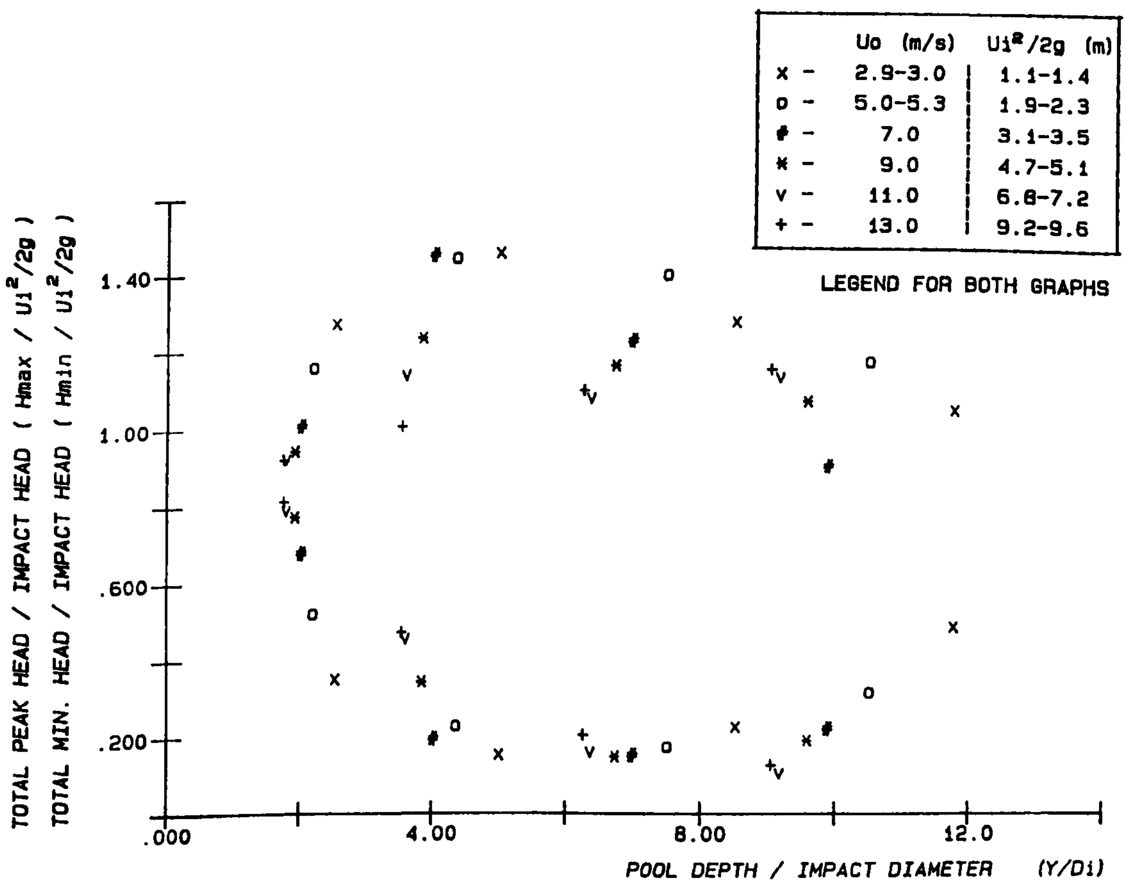

FIG. 5.22(b) CENTRE LINE TOTAL PEAK AND MINIMUM PRESSURE HEAD RATIO WITH (Y/Di). (Do = 52.5 mm , L = 620 - 1020 mm)

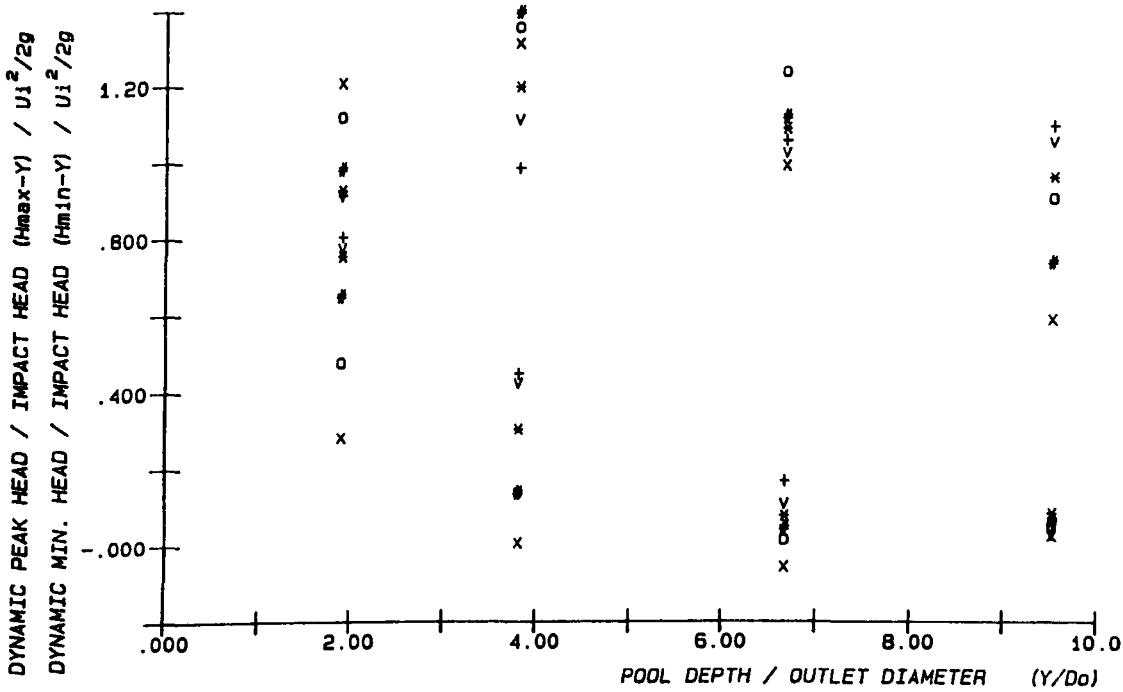

FIG. 5.23(a) CENTRE LINE DYNAMIC PEAK AND MINIMUM PRESSURE HEAD RATIO WITH (Y/Do). (Do = 52.5 mm , L = 620 - 1020 mm)

	Uo (m/s)	$Ui^2/2g$ (m)
x -	2.9-3.0	1.1-1.4
o -	5.0-5.3	1.9-2.3
# -	7.0	3.1-3.5
* -	9.0	4.7-5.1
v -	11.0	6.8-7.2
+ -	13.0	9.2-9.6

LEGEND FOR BOTH GRAPHS

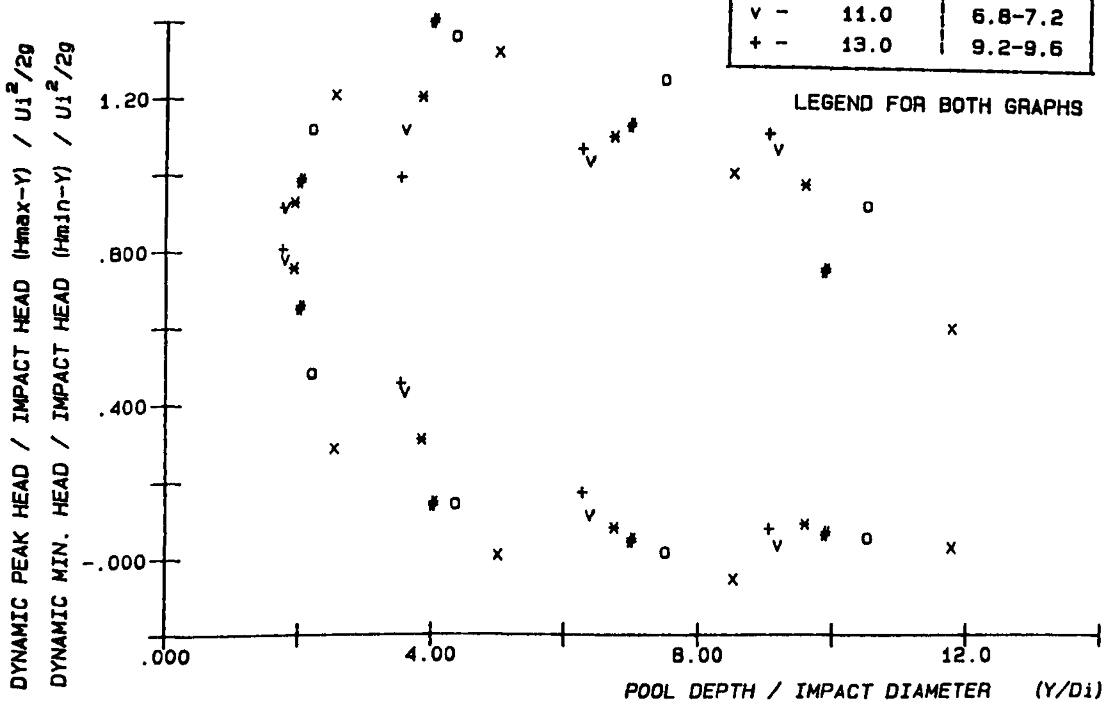

FIG. 5.23(b) CENTRE LINE DYNAMIC PEAK AND MINIMUM PRESSURE HEAD RATIO WITH (Y/Di). (Do = 52.5 mm , L = 620 - 1020 mm)

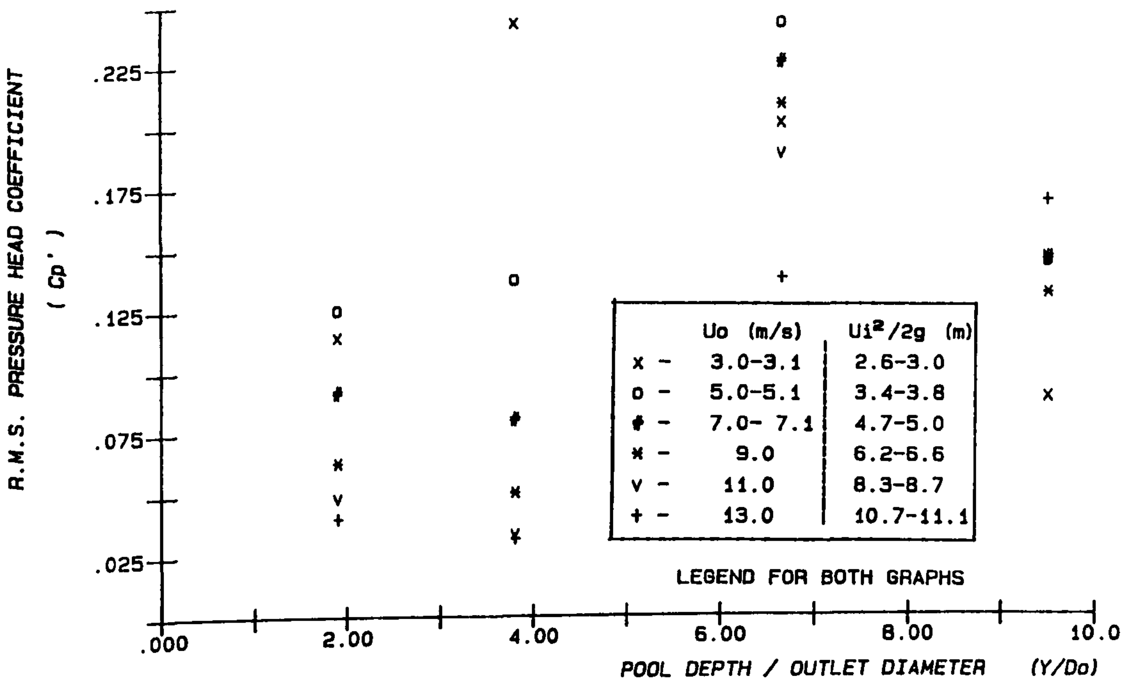

FIG. 5.24(a) CENTRE LINE R.M.S. PRESSURE HEAD COEFFICIENT WITH (Y/Do)
(Do - 52.5 mm , L - 2126 - 2526 mm)

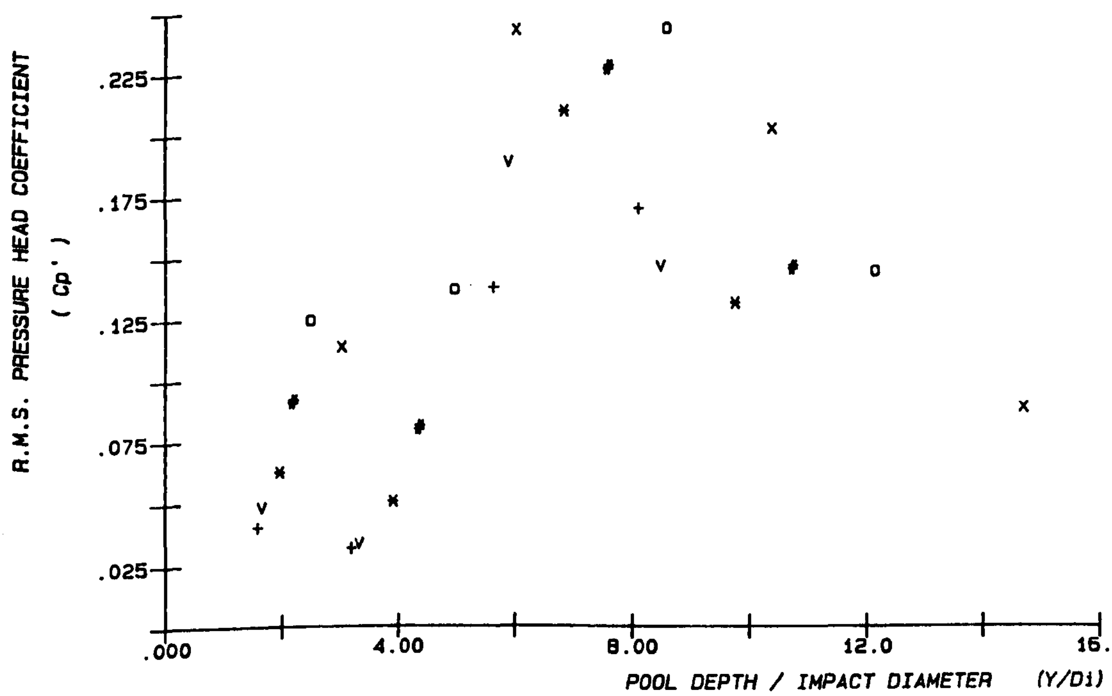

FIG. 5.24(b) CENTRE LINE R.M.S. PRESSURE HEAD COEFFICIENT WITH (Y/Di)
(Do - 52.5 mm , L - 2126 - 2526 mm)

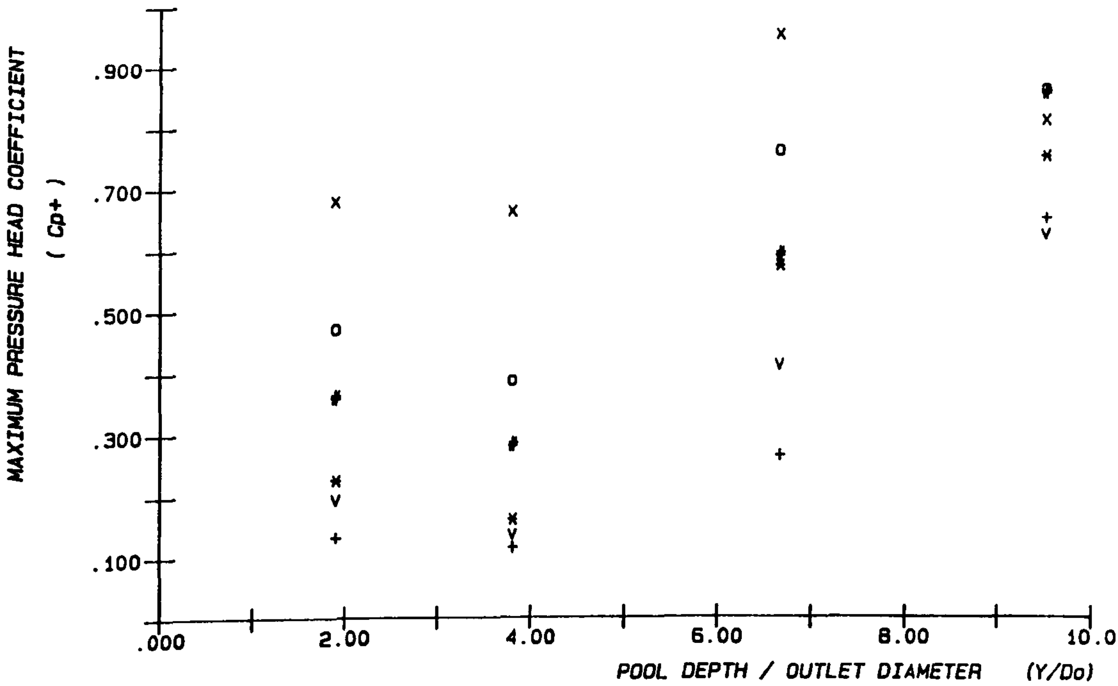

FIG. 5.25(a) CENTRE LINE MAXIMUM PRESSURE HEAD COEFFICIENT WITH (Y/Do)
(Do = 52.5 mm , L = 2126 - 2526 mm)

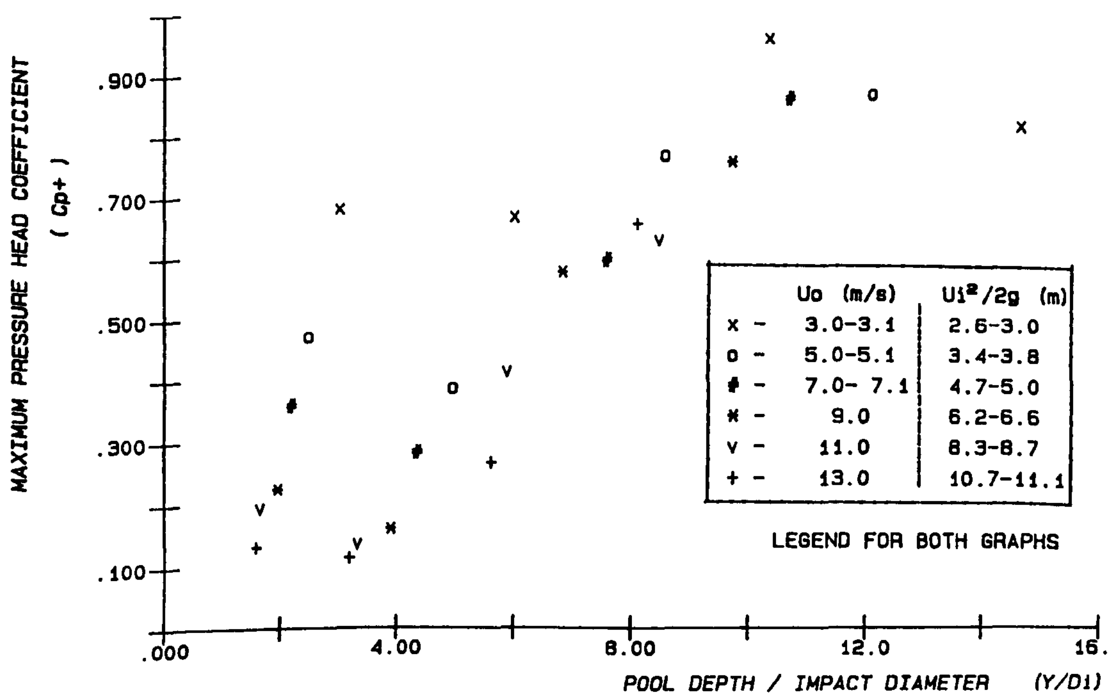

FIG. 5.25(b) CENTRE LINE MAXIMUM PRESSURE HEAD COEFFICIENT WITH (Y/Di)
(Do = 52.5 mm , L = 2126 - 2526 mm)

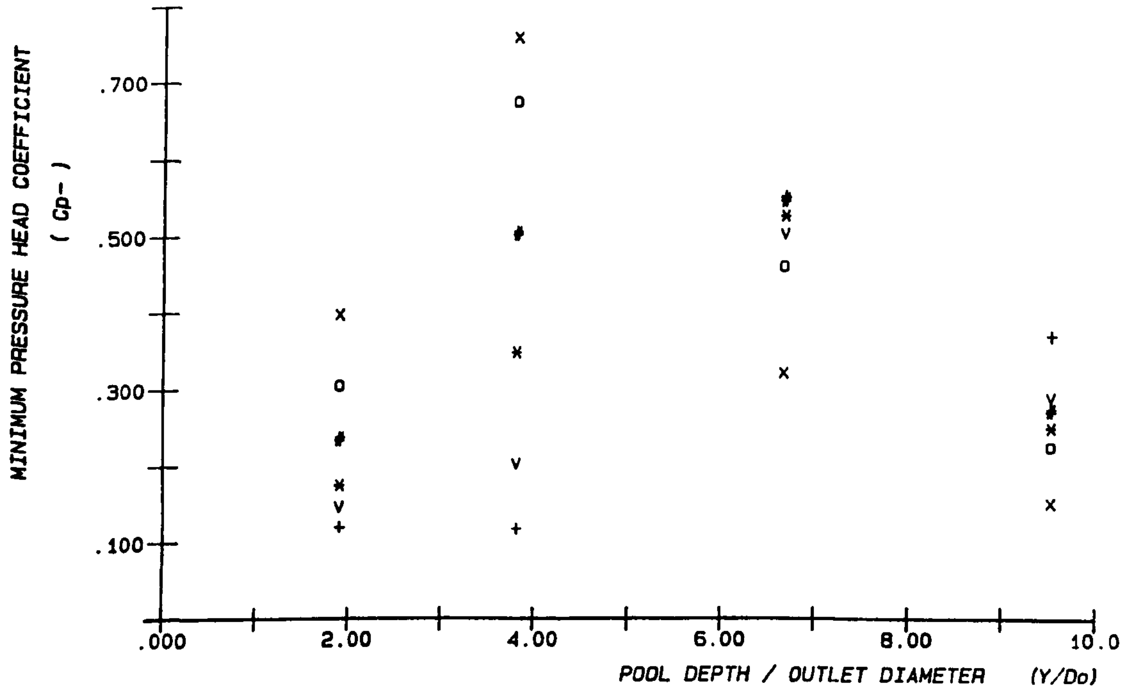

FIG. 5.26 (a) CENTRE LINE MINIMUM PRESSURE HEAD COEFFICIENT WITH (Y/Do)
(Do = 52.5 mm , L = 2126 - 2526 mm)

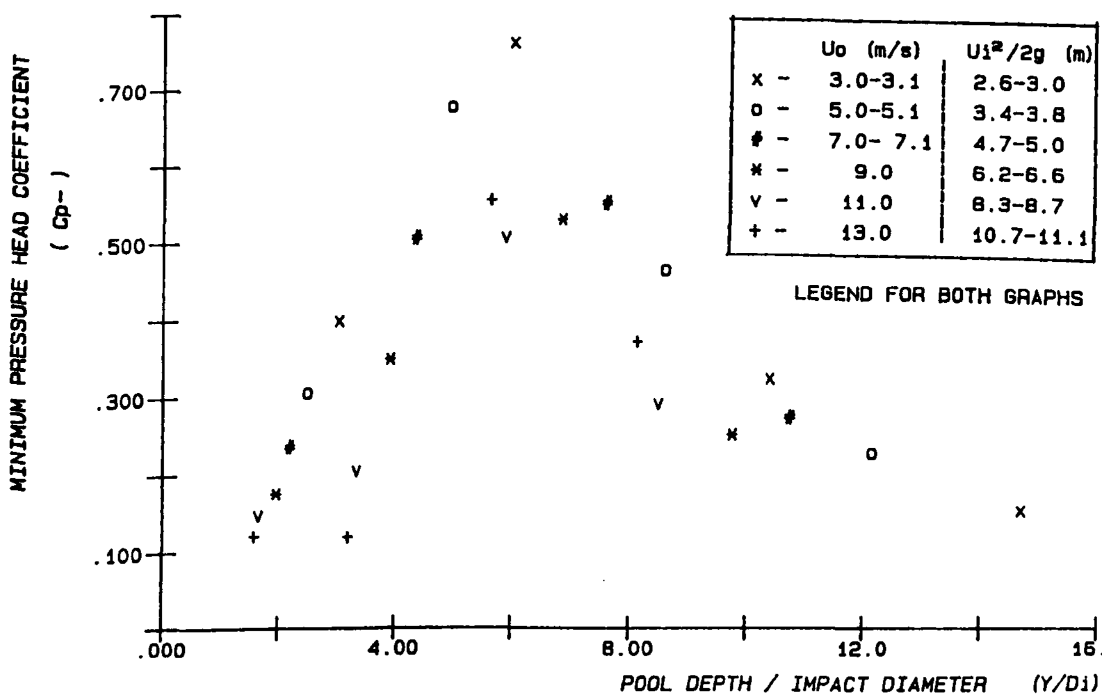

FIG. 5.26 (b) CENTRE LINE MINIMUM PRESSURE HEAD COEFFICIENT WITH (Y/Di)
(Do = 52.5 mm , L = 2126 - 2526 mm)

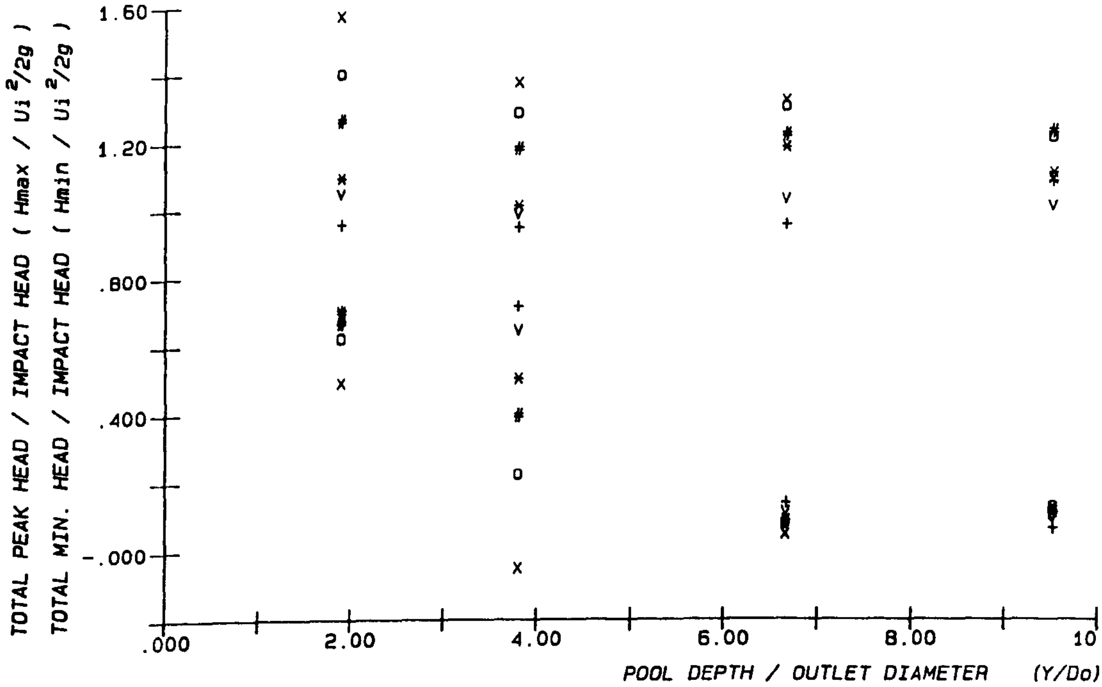

FIG. 5.27(a) CENTRE LINE TOTAL PEAK AND MINIMUM PRESSURE HEAD RATIO WITH (Y/Do). (Do = 52.5 mm , L = 2126 - 2526 mm)

	Uo (m/s)	$Ui^2/2g$ (m)
x -	3.0-3.1	2.6-3.0
o -	5.0-5.1	3.4-3.8
# -	7.0- 7.1	4.7-5.0
* -	9.0	6.2-6.6
v -	11.0	8.3-8.7
+ -	13.0	10.7-11.1

LEGEND FOR BOTH GRAPHS

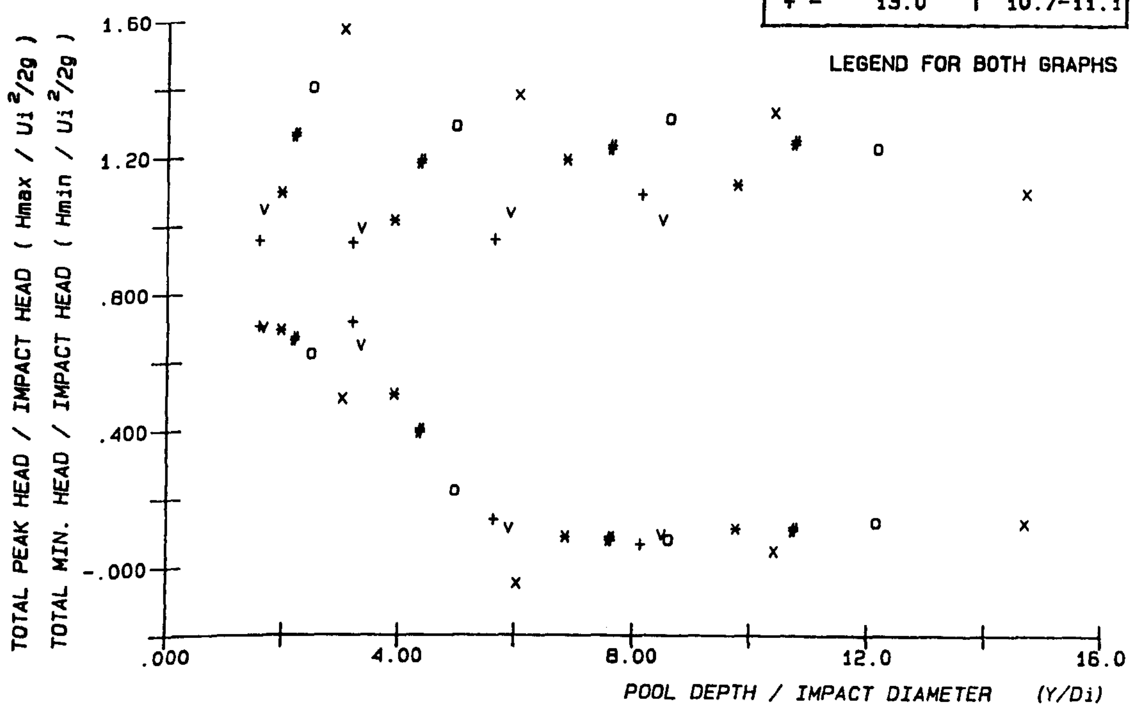

FIG. 5.27(b) CENTRE LINE TOTAL PEAK AND MINIMUM PRESSURE HEAD RATIO WITH (Y/Di). (Do = 52.5 mm , L = 2126 - 2526 mm)

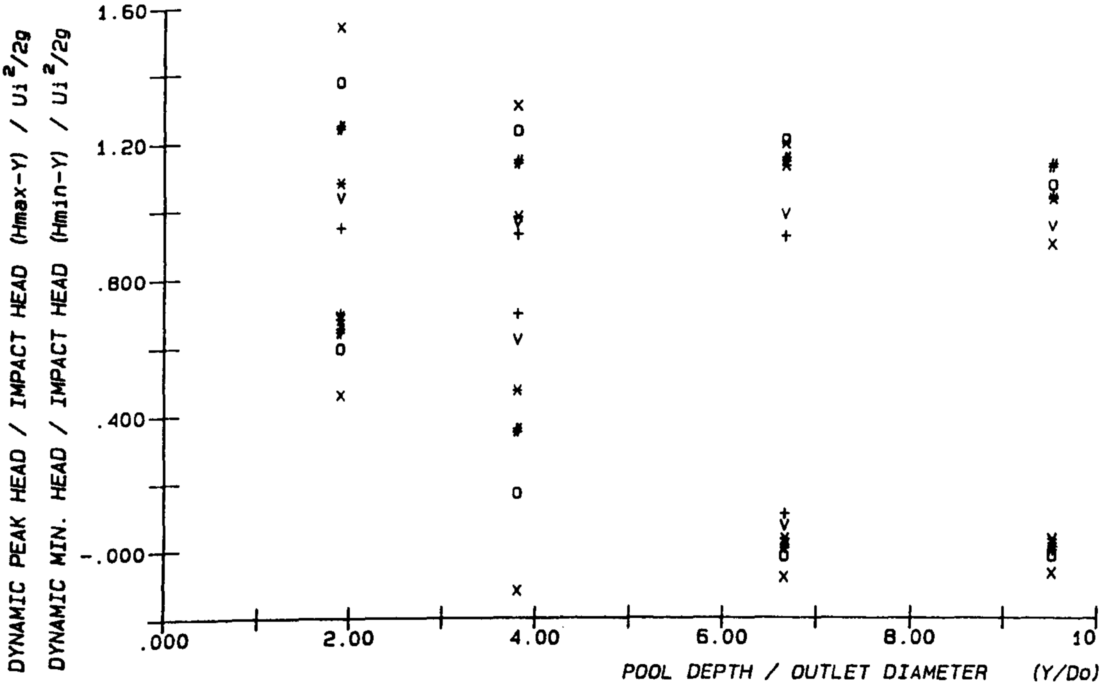

FIG. 5.28(a) CENTRE LINE DYNAMIC PEAK AND MINIMUM PRESSURE HEAD RATIO WITH (Y/Do). (Do = 52.5 mm , L = 2126 - 2526 mm)

	Uo (m/s)	$Ui^2/2g$ (m)
x -	3.0-3.1	2.6-3.0
o -	5.0-5.1	3.4-3.8
# -	7.0- 7.1	4.7-5.0
* -	9.0	6.2-6.6
v -	11.0	8.3-8.7
+ -	13.0	10.7-11.1

LEGEND FOR BOTH GRAPHS

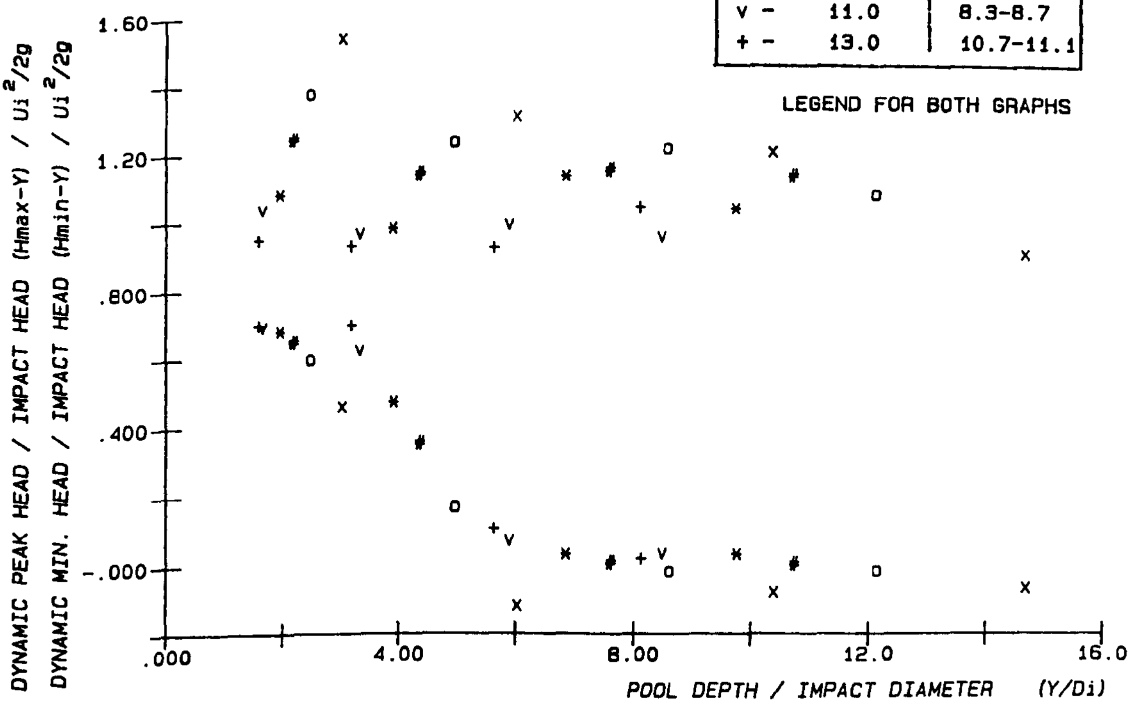

FIG. 5.28(b) CENTRE LINE DYNAMIC PEAK AND MINIMUM PRESSURE HEAD RATIO WITH (Y/Di). (Do = 52.5 mm , L = 2126 - 2526 mm)

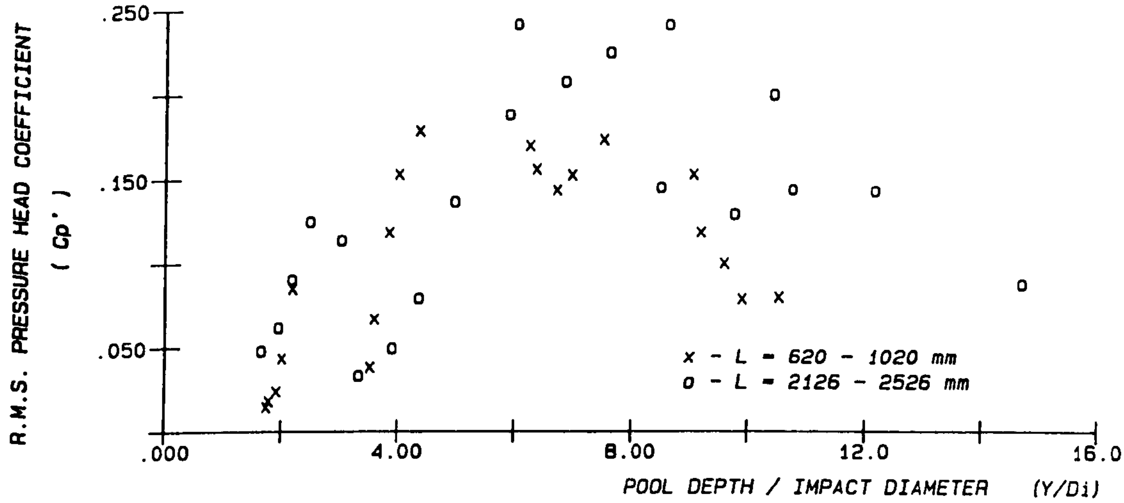

FIG. 5.29 (a) R.M.S. PRESSURE HEAD COEFFICIENT AGAINST PLUNGE POOL DEPTH FOR 52.5 mm NOZZLE FOR THE TWO DIFFERENT FALL LENGTHS

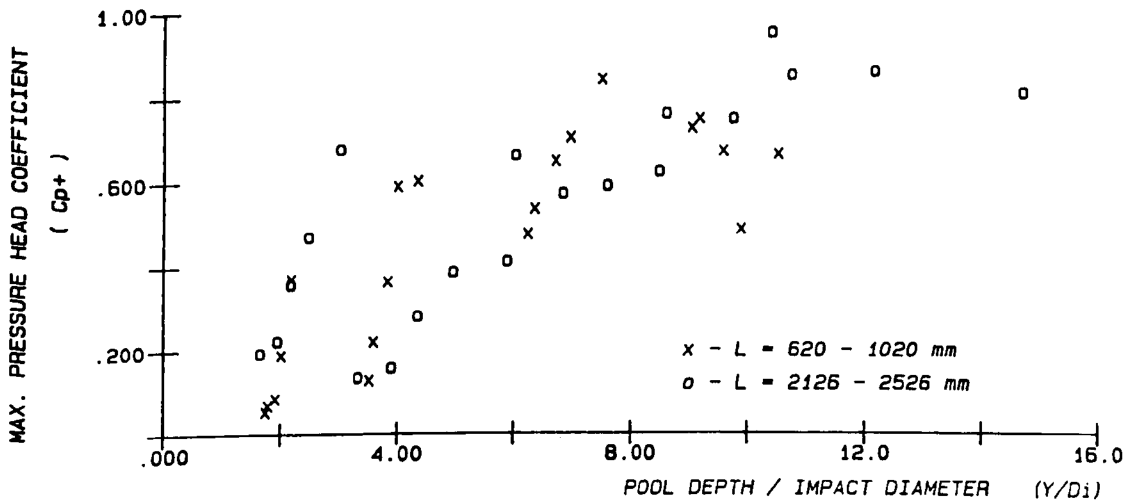

FIG. 5.29 (b) MAX. PRESSURE HEAD COEFFICIENT AGAINST PLUNGE POOL DEPTH FOR 52.5 mm NOZZLE FOR THE TWO DIFFERENT FALL LENGTHS

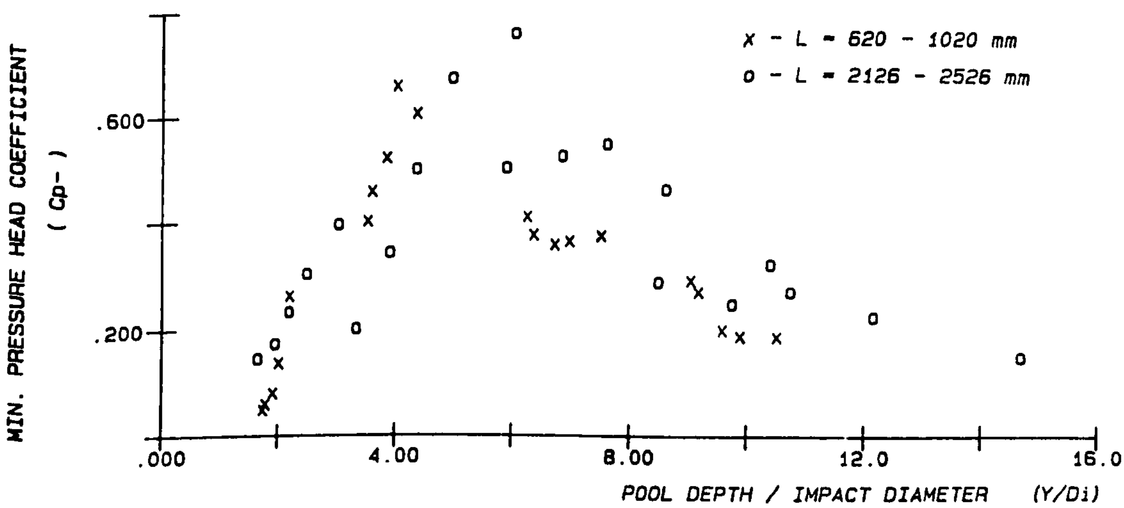

FIG. 5.29 (c) MIN. PRESSURE HEAD COEFFICIENT AGAINST PLUNGE POOL DEPTH FOR 52.5 mm NOZZLE FOR THE TWO DIFFERENT FALL LENGTHS

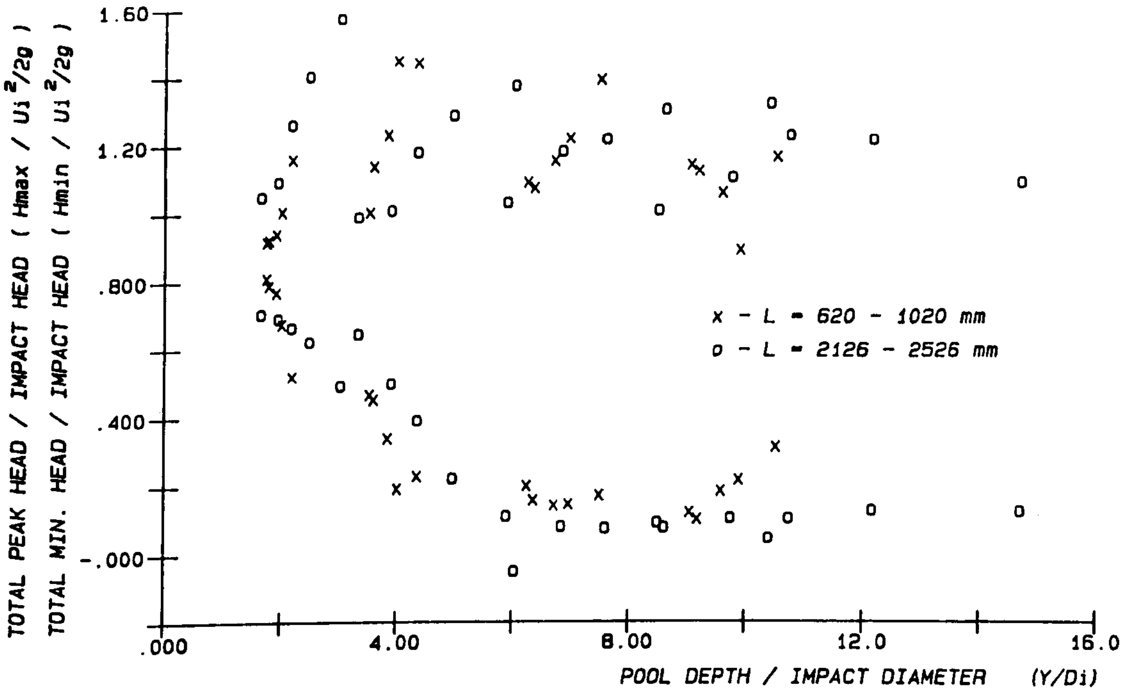

FIG. 5.30 (a) TOTAL PEAK AND MINIMUM HEAD AGAINST PLUNGE POOL DEPTH FOR 52.5 mm NOZZLE FOR THE TWO DIFFERENT FALL LENGTHS

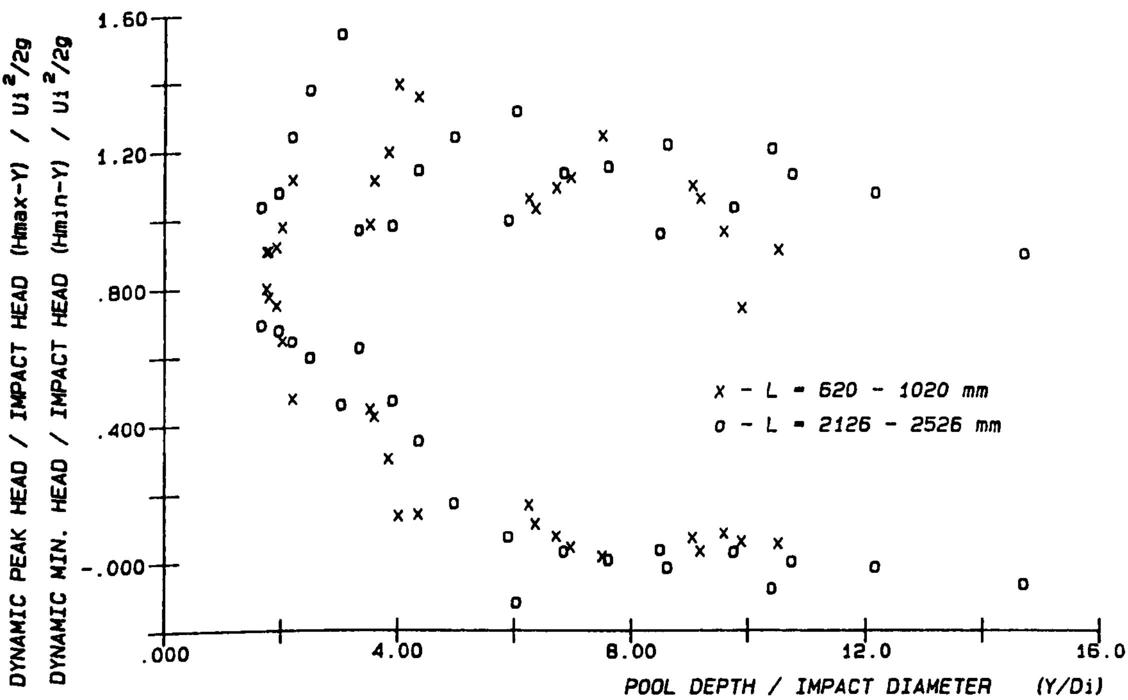

FIG. 5.30 (b) DYNAMIC PEAK AND MINIMUM HEAD AGAINST PLUNGE POOL DEPTH FOR 52.5 mm NOZZLE FOR THE TWO DIFFERENT FALL LENGTHS

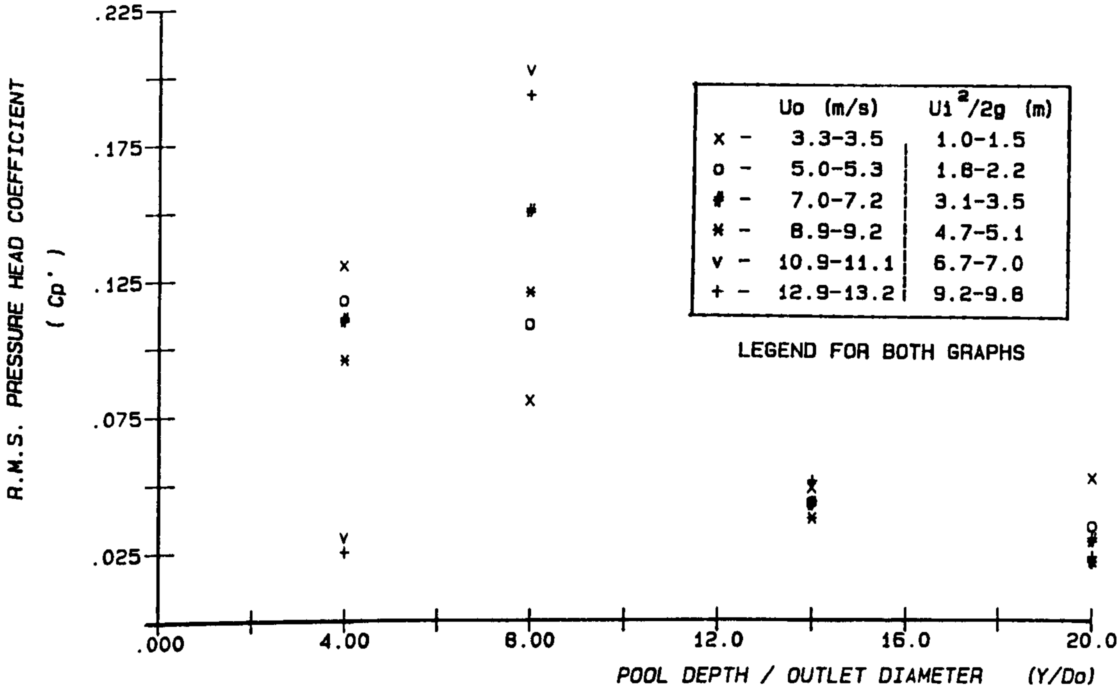

FIG. 5.31 (a) CENTRE LINE R.M.S. PRESSURE HEAD COEFFICIENT WITH (Y/Do)
(NOZZLE : Do = 25 mm , L = 513 - 913 mm)

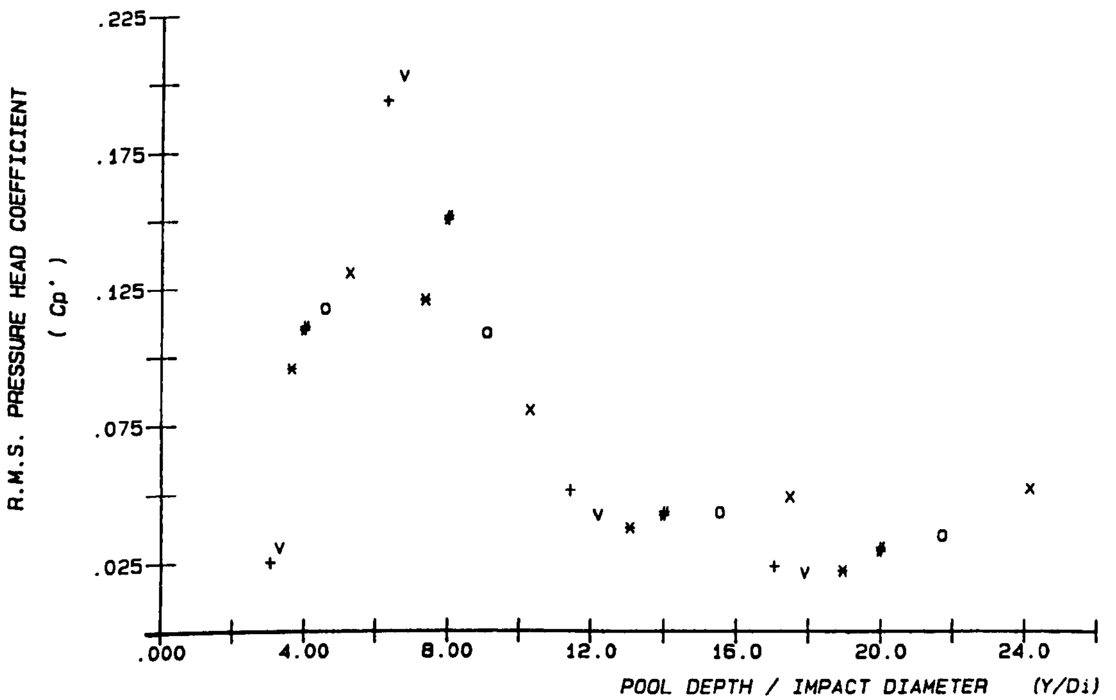

FIG. 5.31 (b) CENTRE LINE R.M.S. PRESSURE HEAD COEFFICIENT WITH (Y/Di)
(NOZZLE : Do = 25 mm , L = 513 - 913 mm)

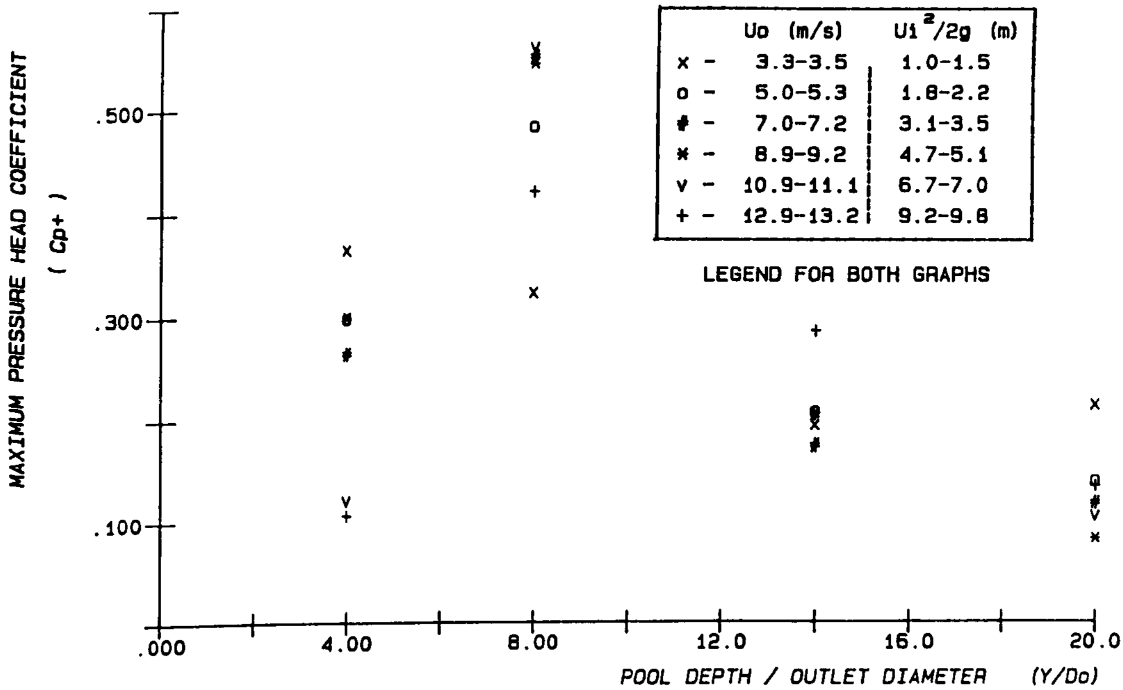

FIG. 5.32 (a) CENTRE LINE MAXIMUM PRESSURE HEAD COEFFICIENT WITH (Y/Do)
(NOZZLE : Do = 25 mm , L = 513 - 913 mm)

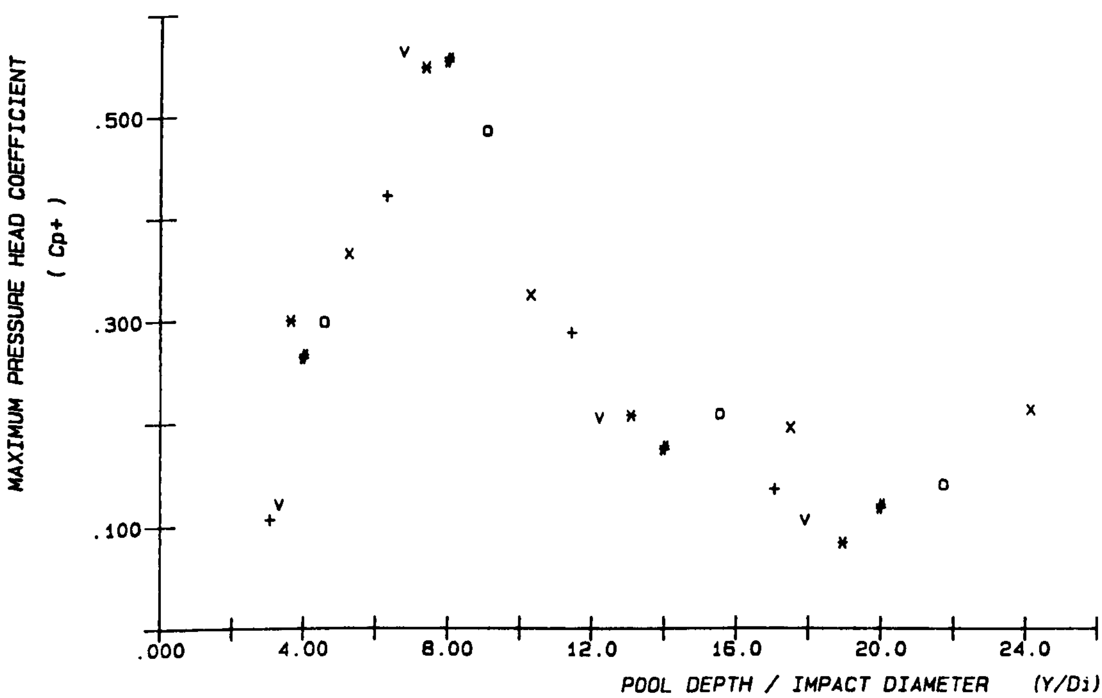

FIG. 5.32 (b) CENTRE LINE MAXIMUM PRESSURE HEAD COEFFICIENT WITH (Y/Di)
(NOZZLE : Do = 25 mm , L = 513 - 913 mm)

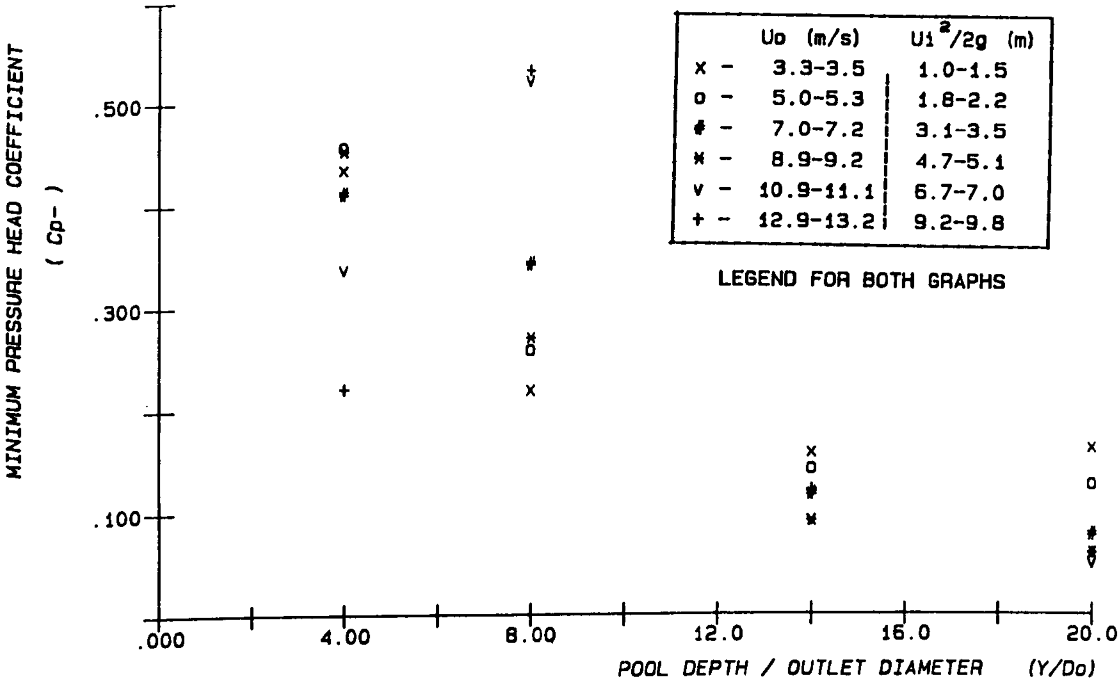

FIG. 5.33 (a) CENTRE LINE MINIMUM PRESSURE HEAD COEFFICIENT WITH (Y/Do)
(NOZZLE : Do = 25 mm , L = 513 - 913 mm)

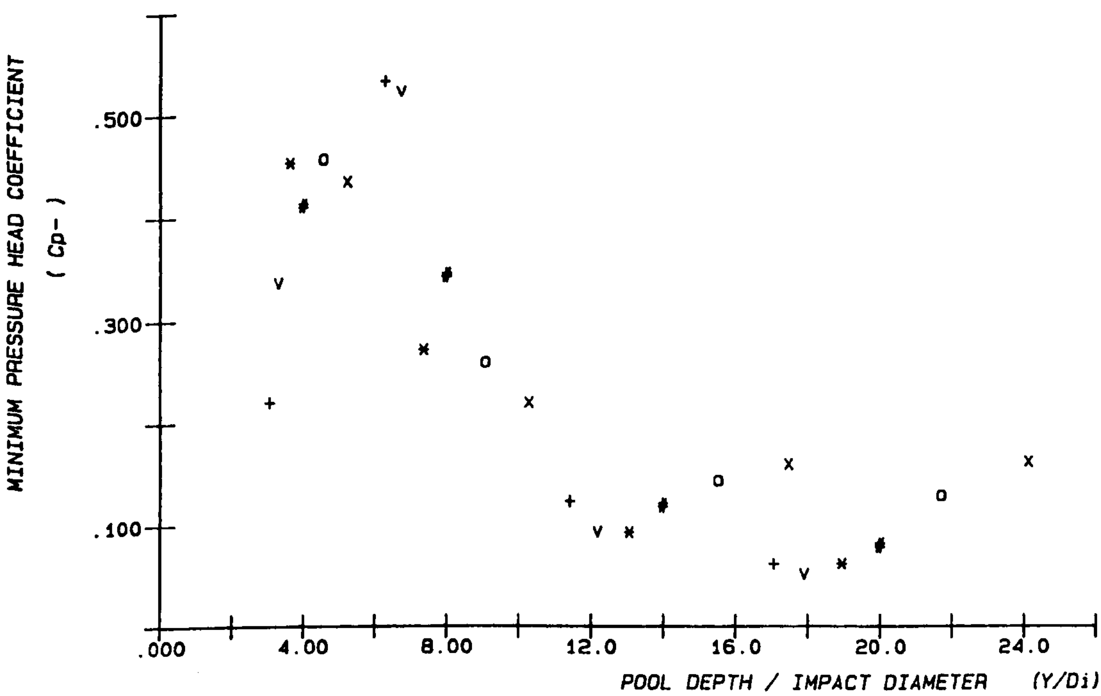

FIG. 5.33 (b) CENTRE LINE MINIMUM PRESSURE HEAD COEFFICIENT WITH (Y/Di)
(NOZZLE : Do = 25 mm , L = 513 - 913 mm)

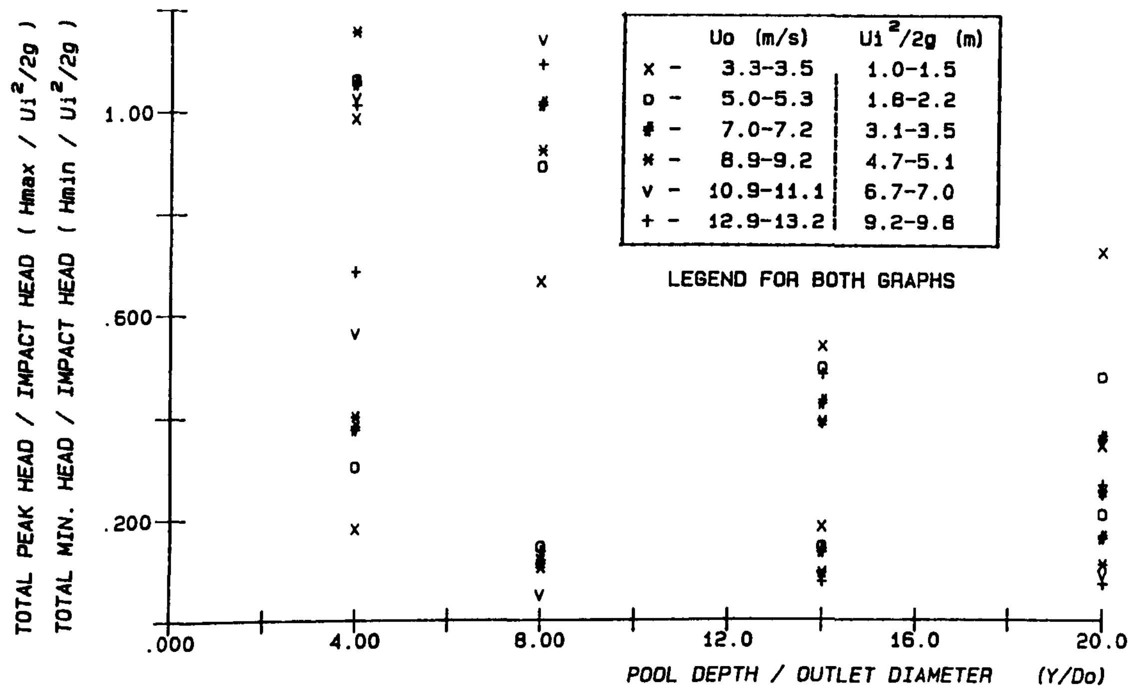

FIG. 5.34 (a) CENTRE LINE TOTAL PEAK AND MINIMUM PRESSURE HEAD RATIO WITH (Y/Do). (NOZZLE : Do = 25 mm , L = 513 - 913 mm)

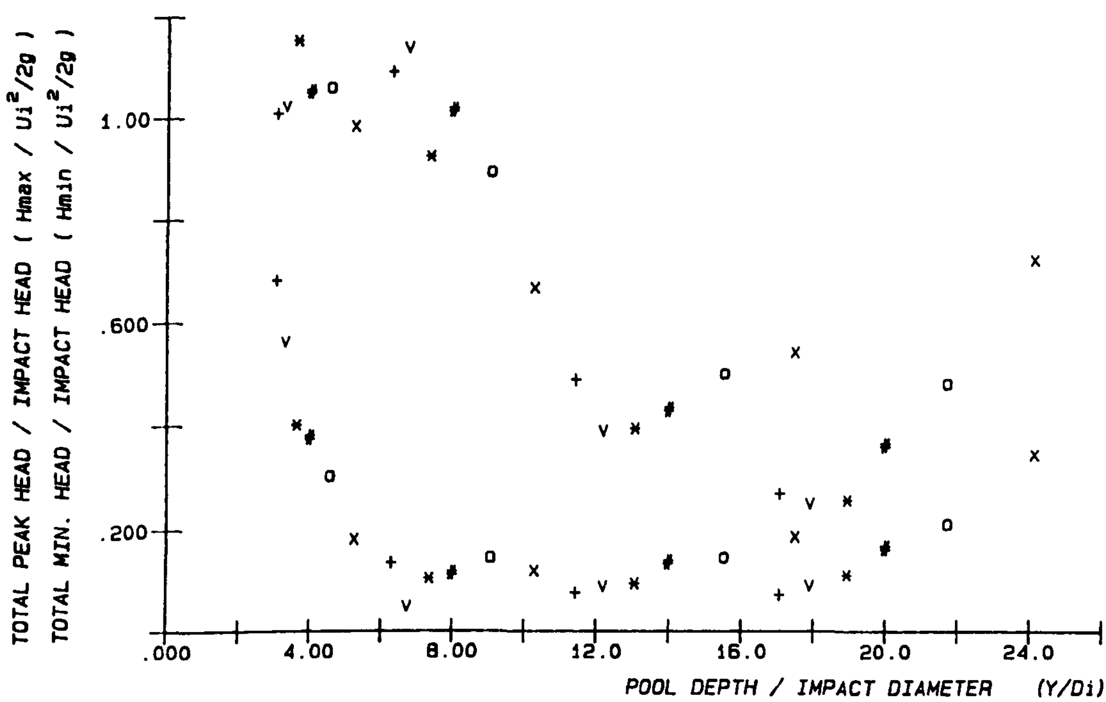

FIG. 5.34 (b) CENTRE LINE TOTAL PEAK AND MINIMUM PRESSURE HEAD RATIO WITH (Y/Di). (NOZZLE : Do = 25 mm , L = 513 - 913 mm)

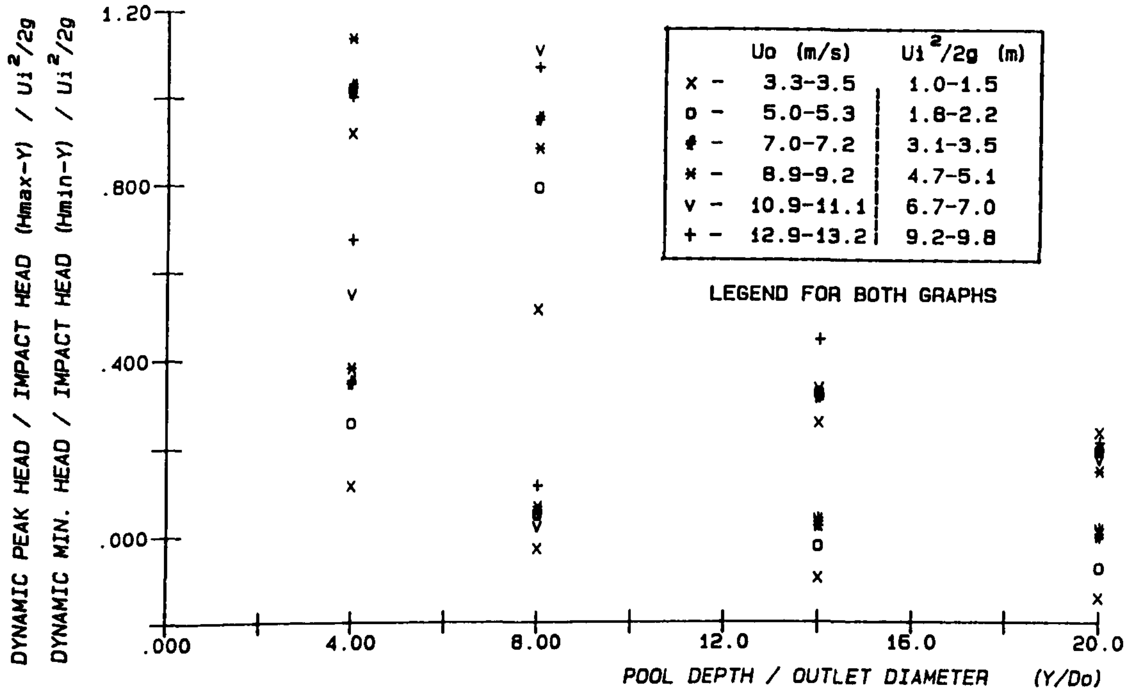

FIG. 5.35(a) CENTRE LINE DYNAMIC PEAK AND MINIMUM PRESSURE HEAD RATIO WITH (Y/Do). (NOZZLE : Do = 25 mm , L = 513 - 913 mm)

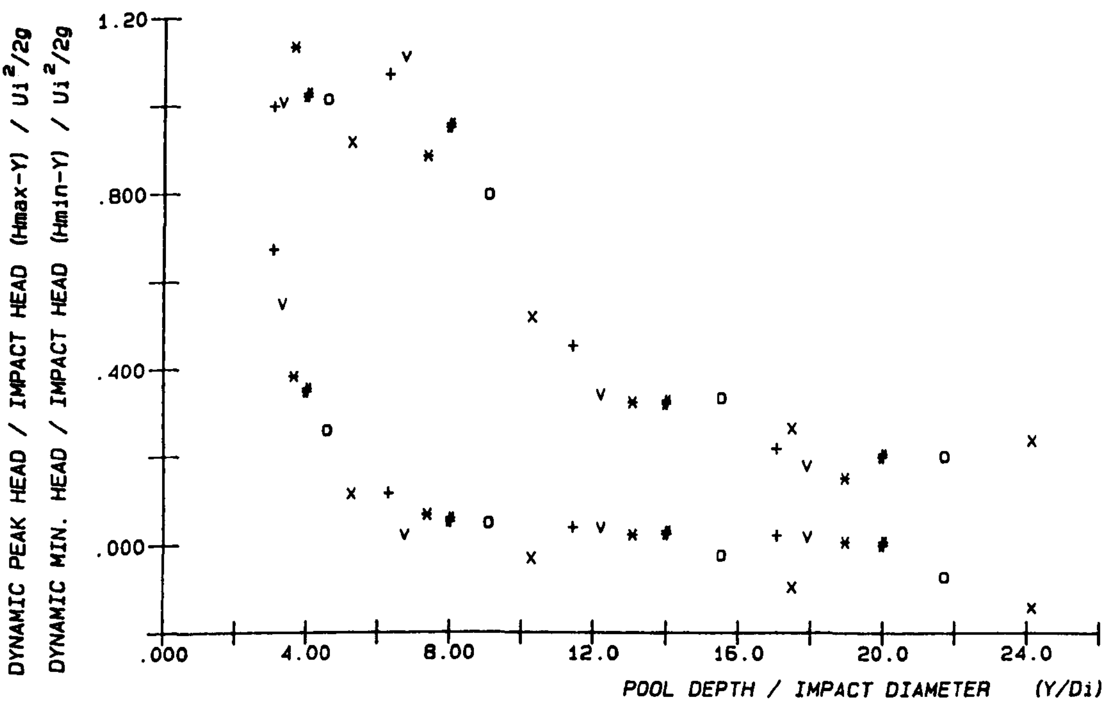

FIG. 5.35(b) CENTRE LINE DYNAMIC PEAK AND MINIMUM PRESSURE HEAD RATIO WITH (Y/Di). (NOZZLE : Do = 25 mm , L = 513 - 913 mm)

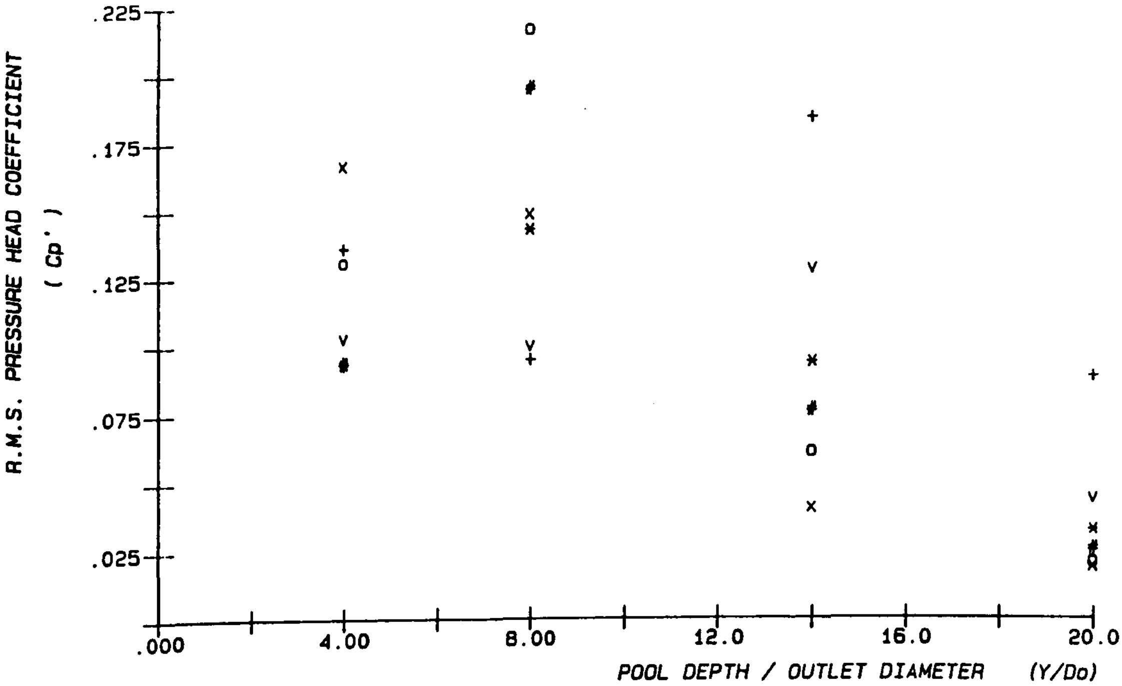

FIG. 5.36 (a) CENTRE LINE R.M.S. PRESSURE HEAD COEFFICIENT WITH (Y/Do)
(NOZZLE : Do = 25 mm , L = 2018 - 2418 mm)

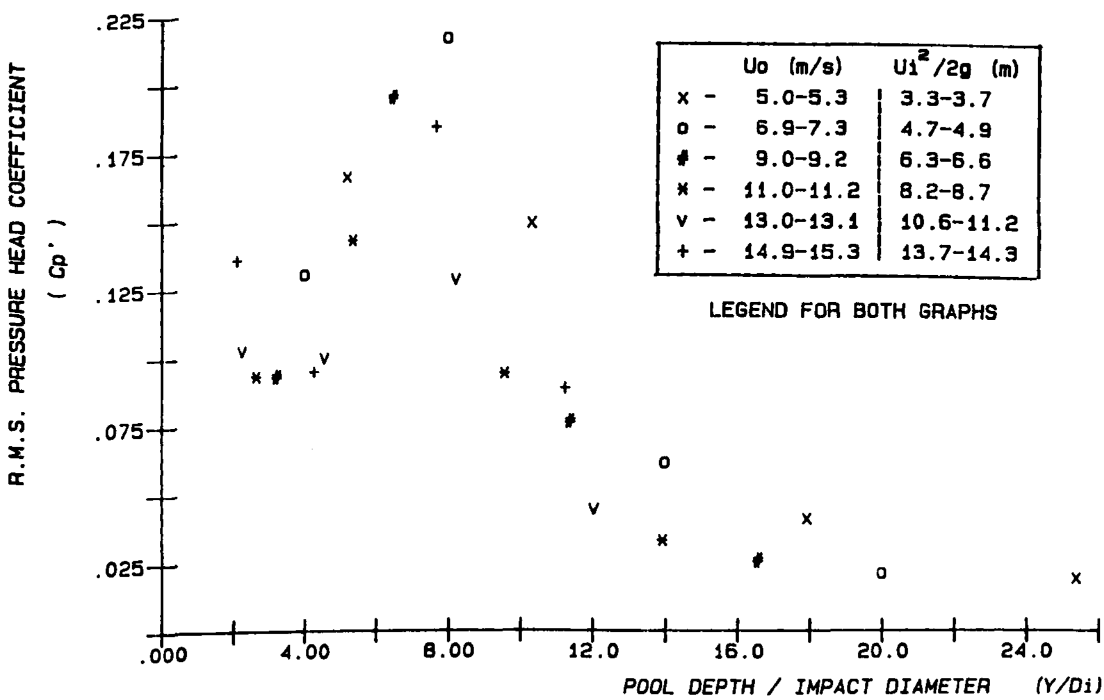

FIG. 5.36 (b) CENTRE LINE R.M.S. PRESSURE HEAD COEFFICIENT WITH (Y/Di)
(NOZZLE : Do = 25 mm , L = 2018 - 2418 mm)

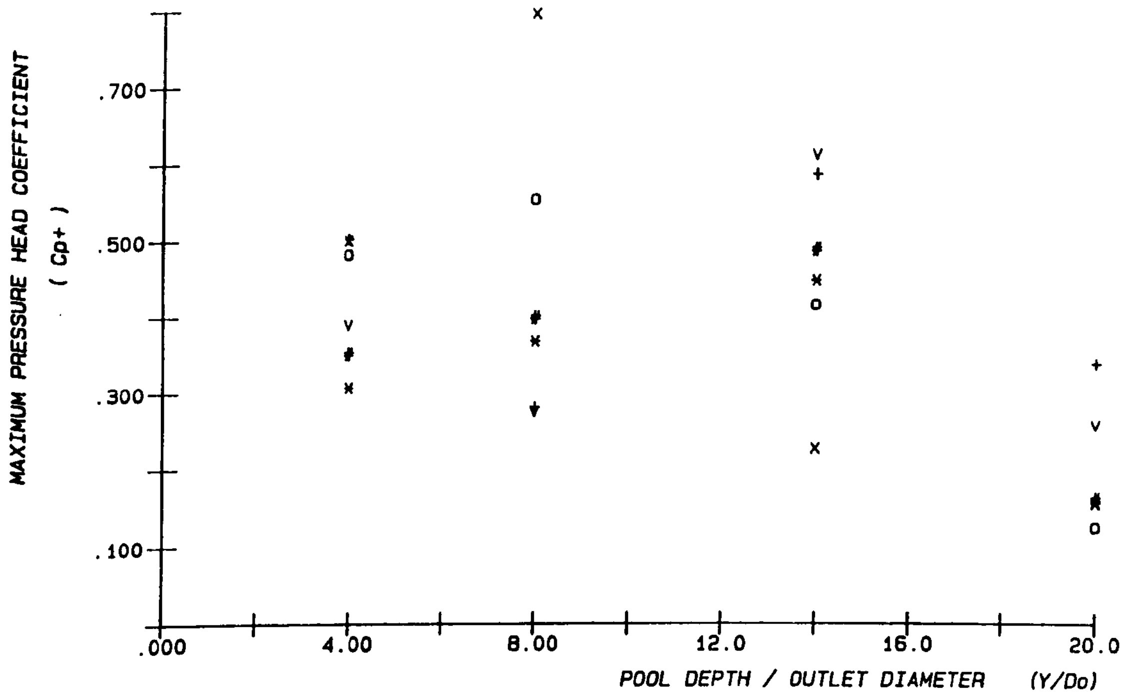

FIG. 5.37 (a) CENTRE LINE MAXIMUM PRESSURE HEAD COEFFICIENT WITH (Y/Do)
(NOZZLE : Do = 25 mm , L = 2018 - 2418 mm)

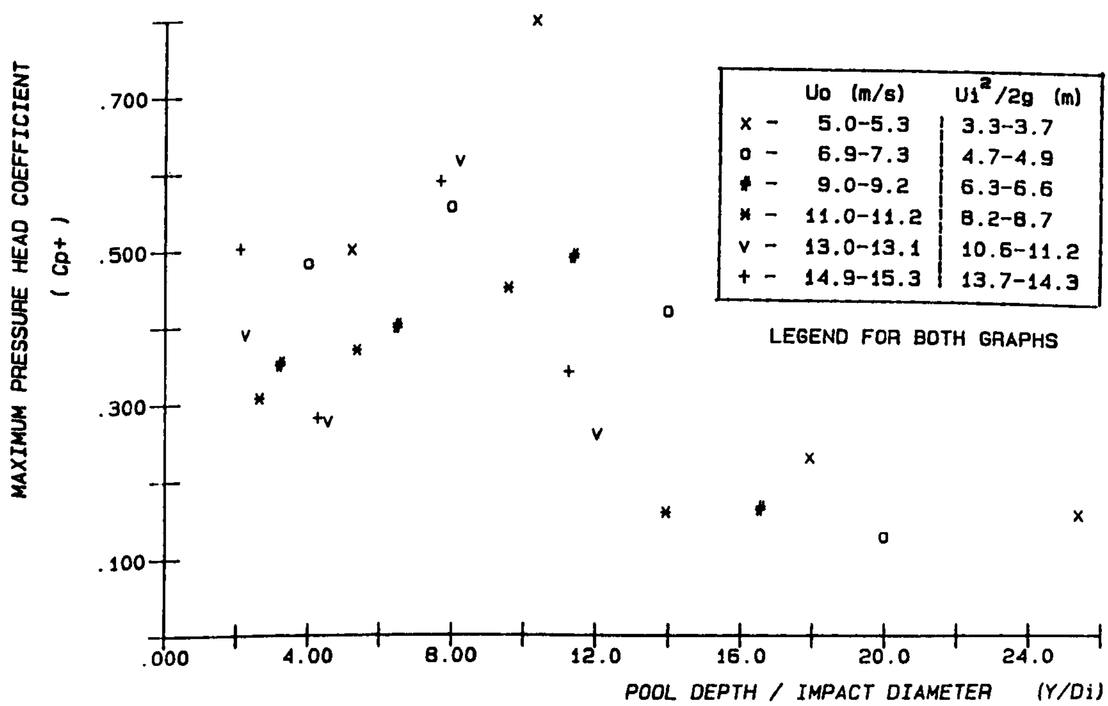

FIG. 5.37 (b) CENTRE LINE MAXIMUM PRESSURE HEAD COEFFICIENT WITH (Y/Di)
(NOZZLE : Do = 25 mm , L = 2018 - 2418 mm)

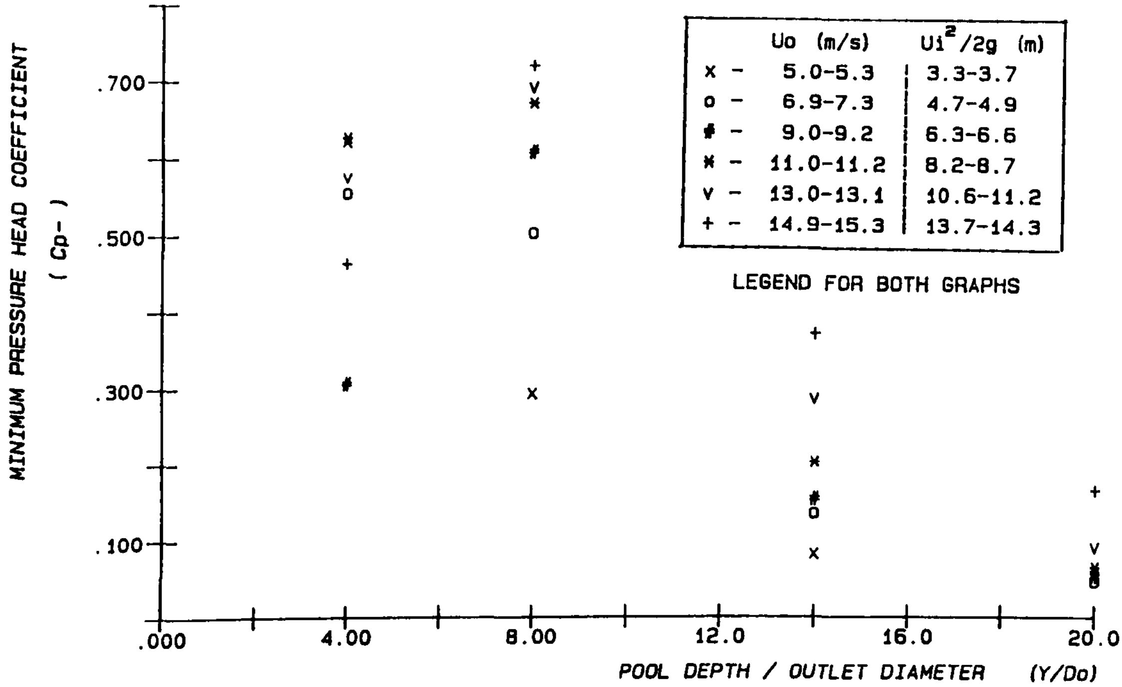

FIG. 5.38(a) CENTRE LINE MINIMUM PRESSURE HEAD COEFFICIENT WITH (Y/Do)
(NOZZLE : Do = 25 mm , L = 2018 - 2418 mm)

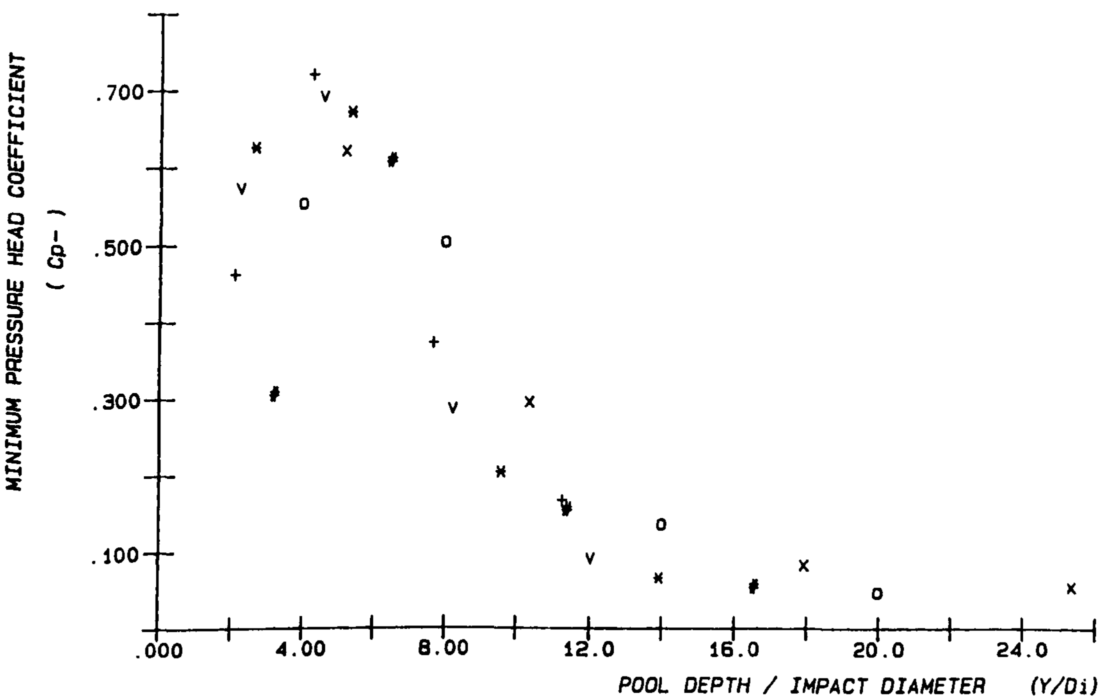

FIG. 5.38(b) CENTRE LINE MINIMUM PRESSURE HEAD COEFFICIENT WITH (Y/Di)
(NOZZLE : Do = 25 mm , L = 2018 - 2418 mm)

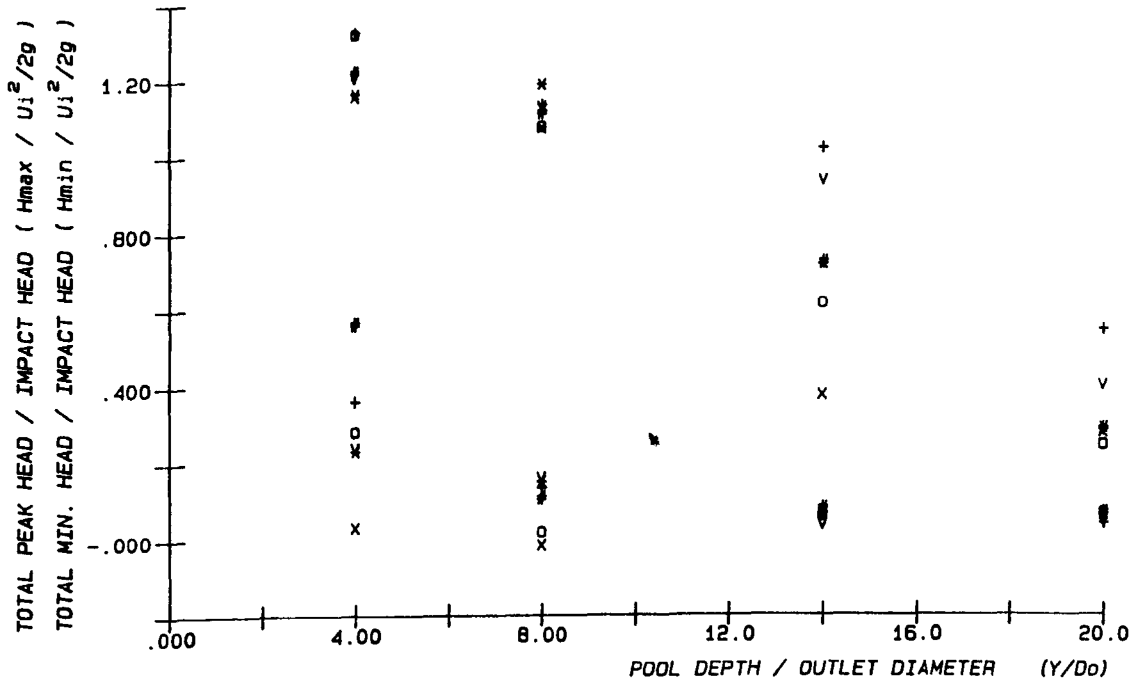

FIG. 5.39(a) CENTRE LINE TOTAL PEAK AND MINIMUM PRESSURE HEAD RATIO WITH (Y/Do). (NOZZLE : Do = 25 mm , L = 2018 - 2418 mm)

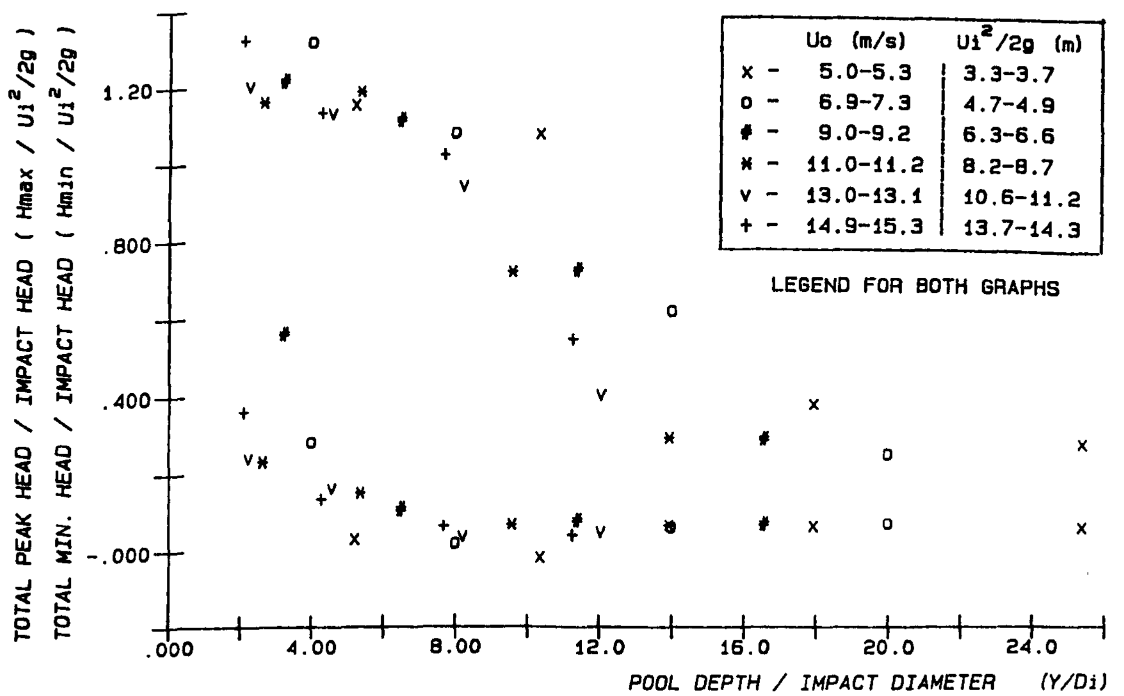

FIG. 5.39(b) CENTRE LINE TOTAL PEAK AND MINIMUM PRESSURE HEAD RATIO WITH (Y/Di). (NOZZLE : Do = 25 mm , L = 2018 - 2418 mm)

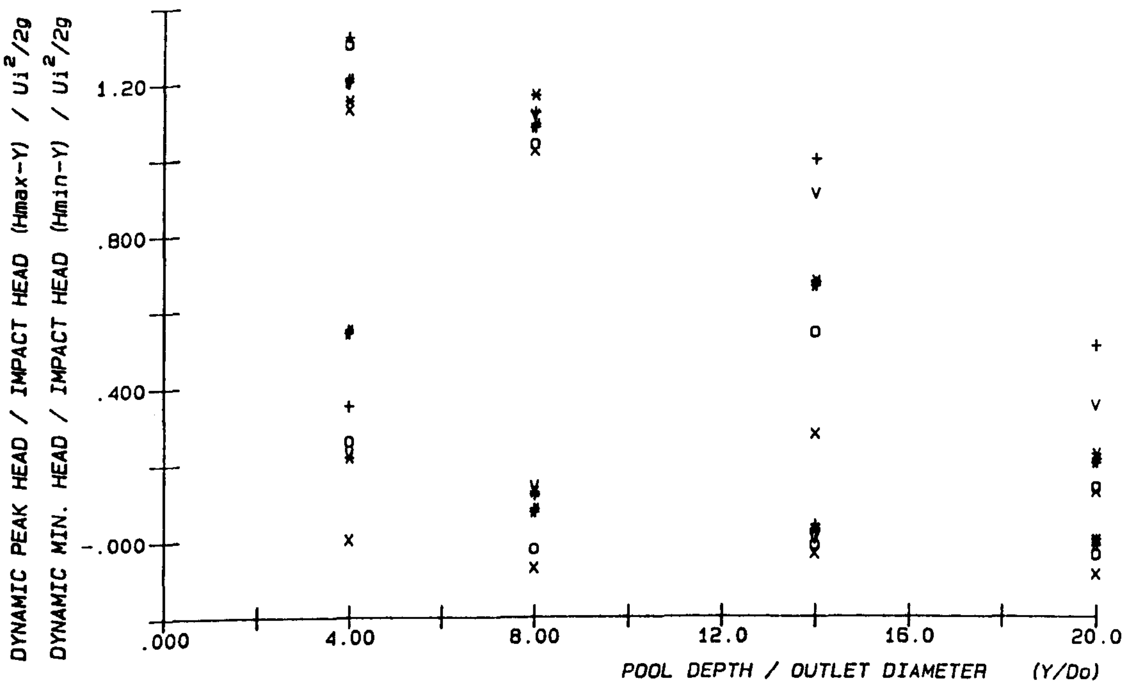

FIG. 5.40 (a) CENTRE LINE DYNAMIC PEAK AND MINIMUM PRESSURE HEAD RATIO WITH (Y/Do). (NOZZLE : Do = 25 mm , L = 2018 - 2418 mm)

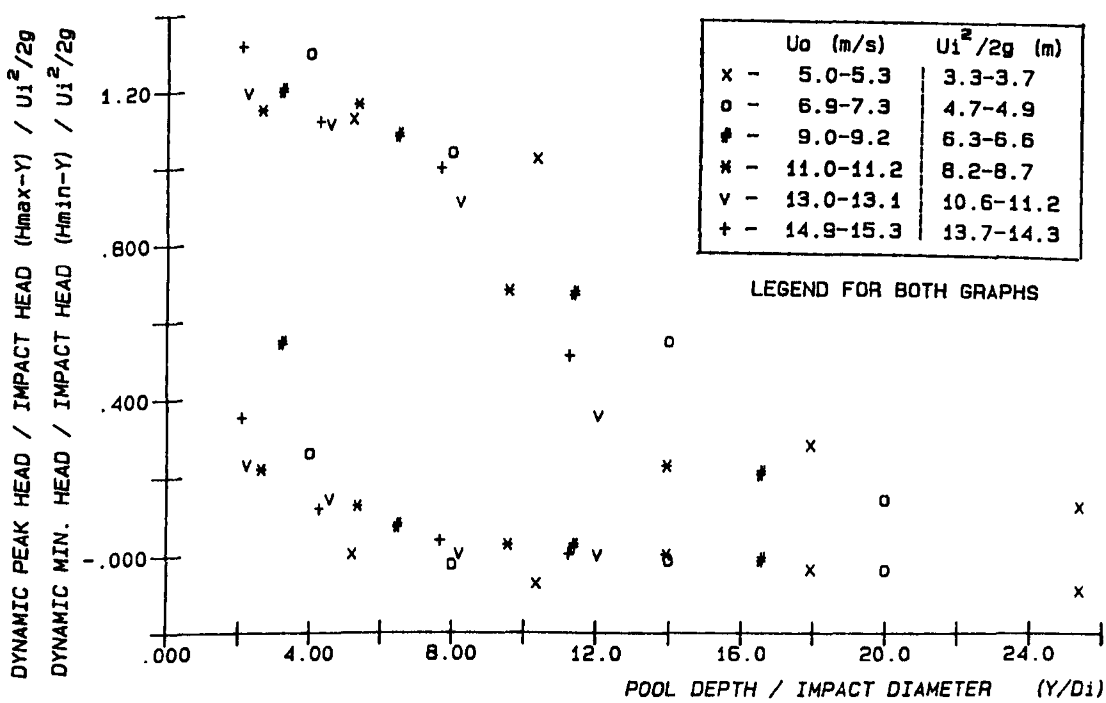

FIG. 5.40 (b) CENTRE LINE DYNAMIC PEAK AND MINIMUM PRESSURE HEAD RATIO WITH (Y/Di). (NOZZLE : Do = 25 mm , L = 2018 - 2418 mm)

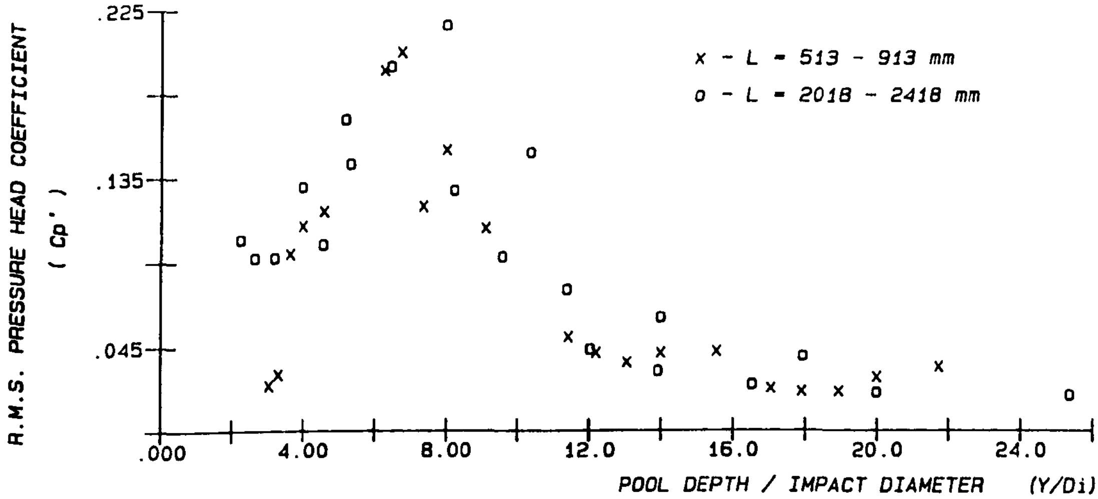

FIG. 5.41 (a) R.M.S. PRESSURE HEAD COEFFICIENT AGAINST PLUNGE POOL DEPTH FOR 25 mm NOZZLE FOR THE TWO DIFFERENT FALL LENGTHS

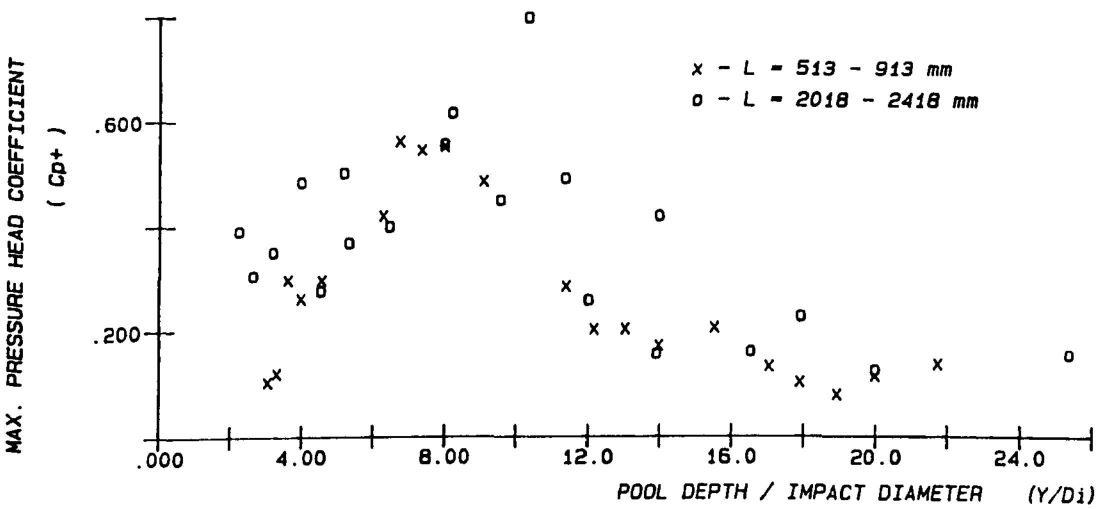

FIG. 5.41 (b) MAX. PRESSURE HEAD COEFFICIENT AGAINST PLUNGE POOL DEPTH FOR 25 mm NOZZLE FOR THE TWO DIFFERENT FALL LENGTHS

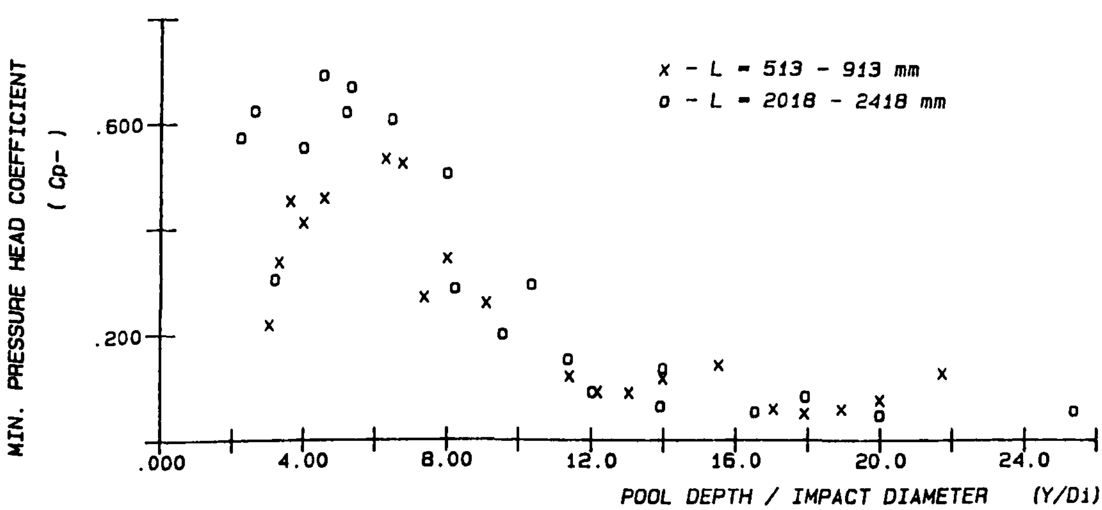

FIG. 5.41 (c) MIN. PRESSURE HEAD COEFFICIENT AGAINST PLUNGE POOL DEPTH FOR 25 mm NOZZLE FOR THE TWO DIFFERENT FALL LENGTHS

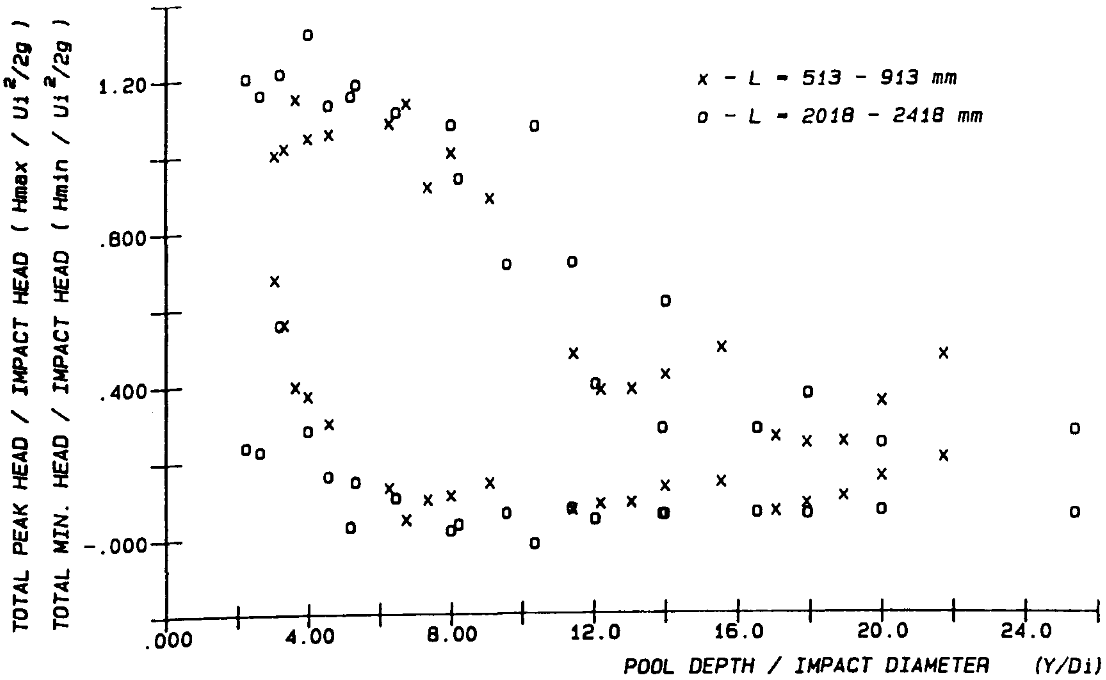

FIG. 5.42 (a) TOTAL PEAK AND MINIMUM HEAD AGAINST PLUNGE POOL DEPTH FOR 25 mm NOZZLE FOR THE TWO DIFFERENT FALL LENGTHS

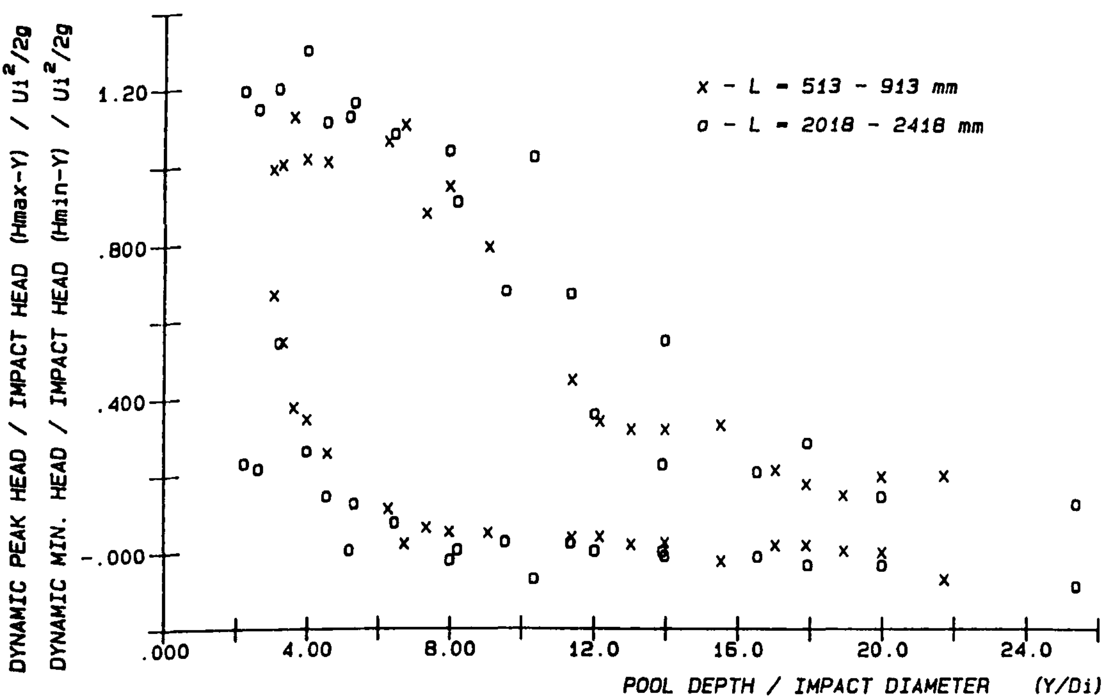

FIG. 5.42 (b) DYNAMIC PEAK AND MINIMUM HEAD AGAINST PLUNGE POOL DEPTH FOR 25 mm NOZZLE FOR THE TWO DIFFERENT FALL LENGTHS

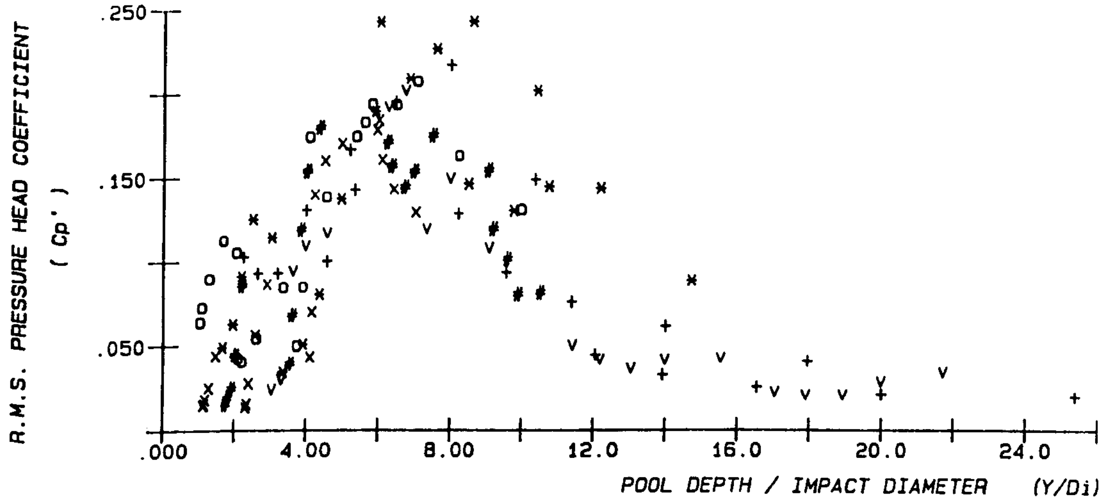

FIG. 5.43(a) R.M.S. PRESSURE HEAD COEFFICIENT AGAINST PLUNGE POOL DEPTH FOR ALL NOZZLES AND FALL LENGTHS

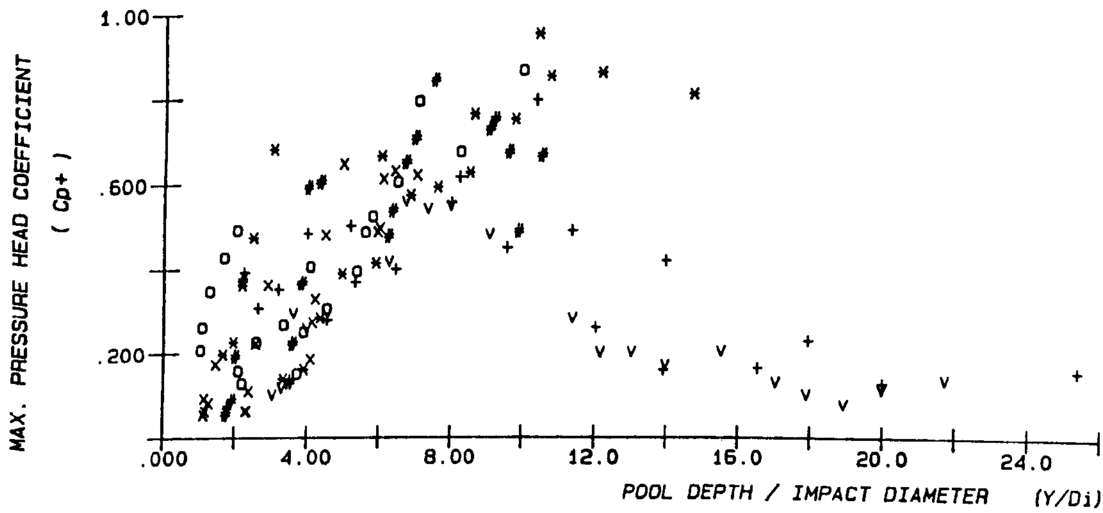

FIG. 5.43(b) MAX. PRESSURE HEAD COEFFICIENT AGAINST PLUNGE POOL DEPTH FOR ALL NOZZLES AND FALL LENGTHS

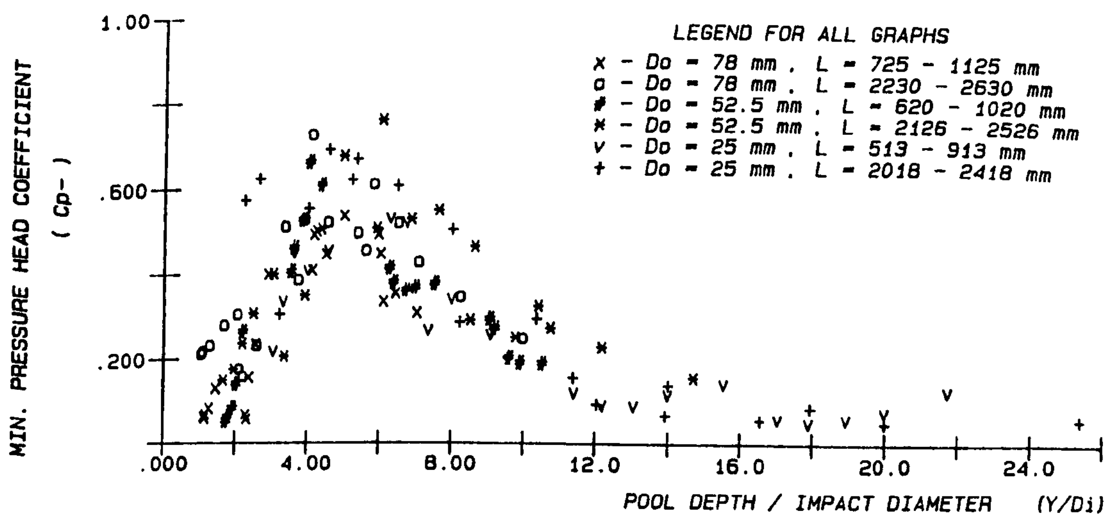

FIG. 5.43(c) MIN. PRESSURE HEAD COEFFICIENT AGAINST PLUNGE POOL DEPTH FOR ALL NOZZLES AND FALL LENGTHS

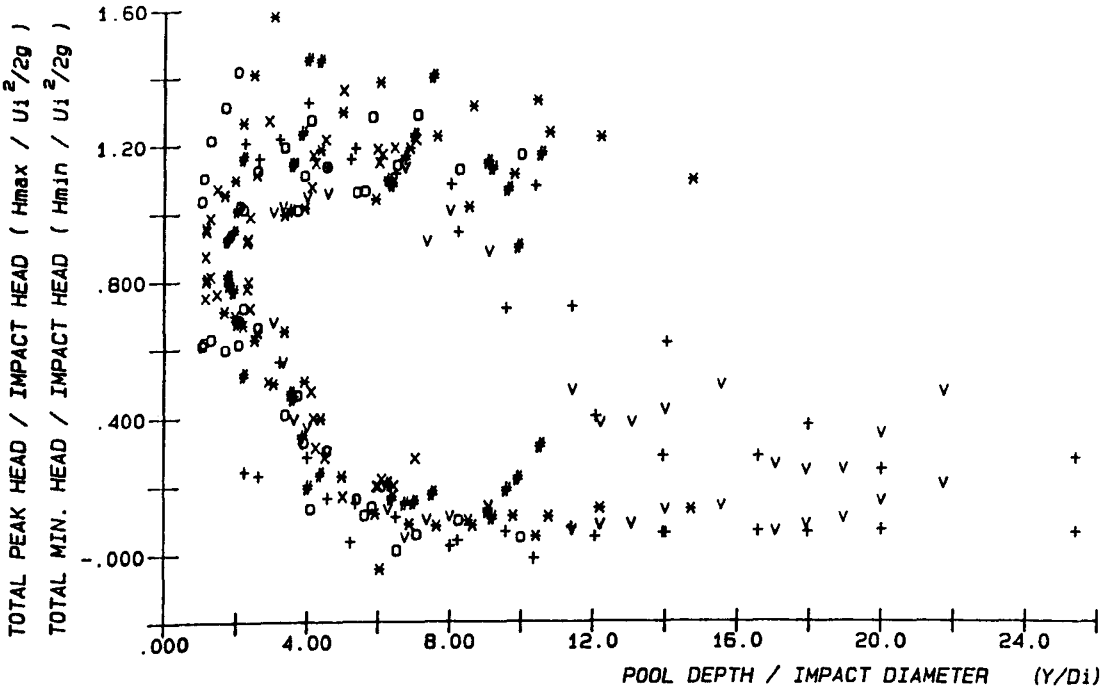

FIG. 5.44 (a) TOTAL PEAK AND MINIMUM HEAD AGAINST PLUNGE POOL DEPTH FOR ALL NOZZLES AND FALL LENGTHS

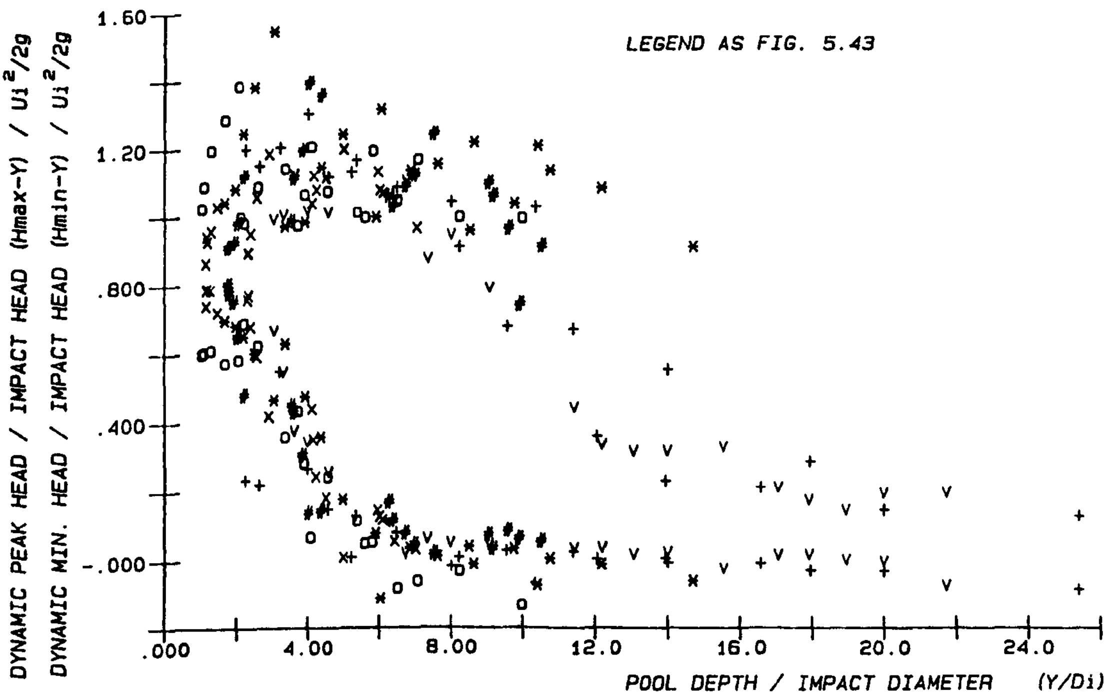

FIG. 5.44 (b) DYNAMIC PEAK AND MINIMUM HEAD AGAINST PLUNGE POOL DEPTH FOR ALL NOZZLES AND FALL LENGTHS

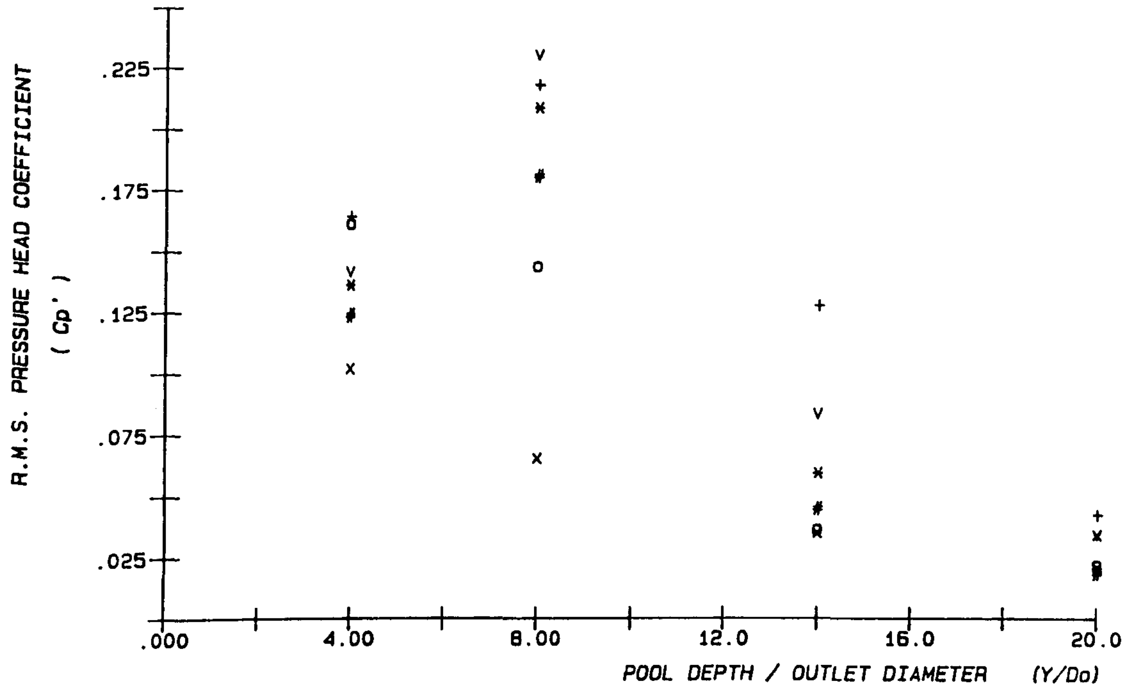

FIG. 5.45 (a) CENTRE LINE R.M.S. PRESSURE HEAD COEFFICIENT WITH (Y/Do)
(ORIFICE : Do = 25 mm , L = 1020 - 1420 mm)

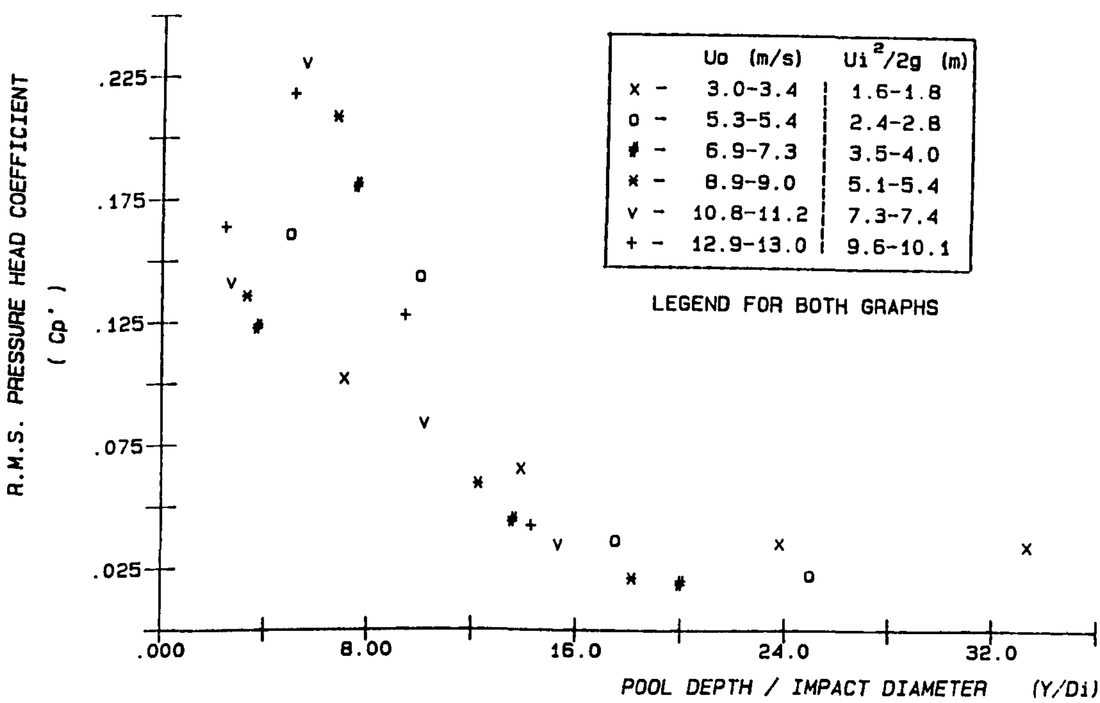

FIG. 5.45 (b) CENTRE LINE R.M.S. PRESSURE HEAD COEFFICIENT WITH (Y/Di)
(ORIFICE : Do = 25 mm , L = 1020 - 1420 mm)

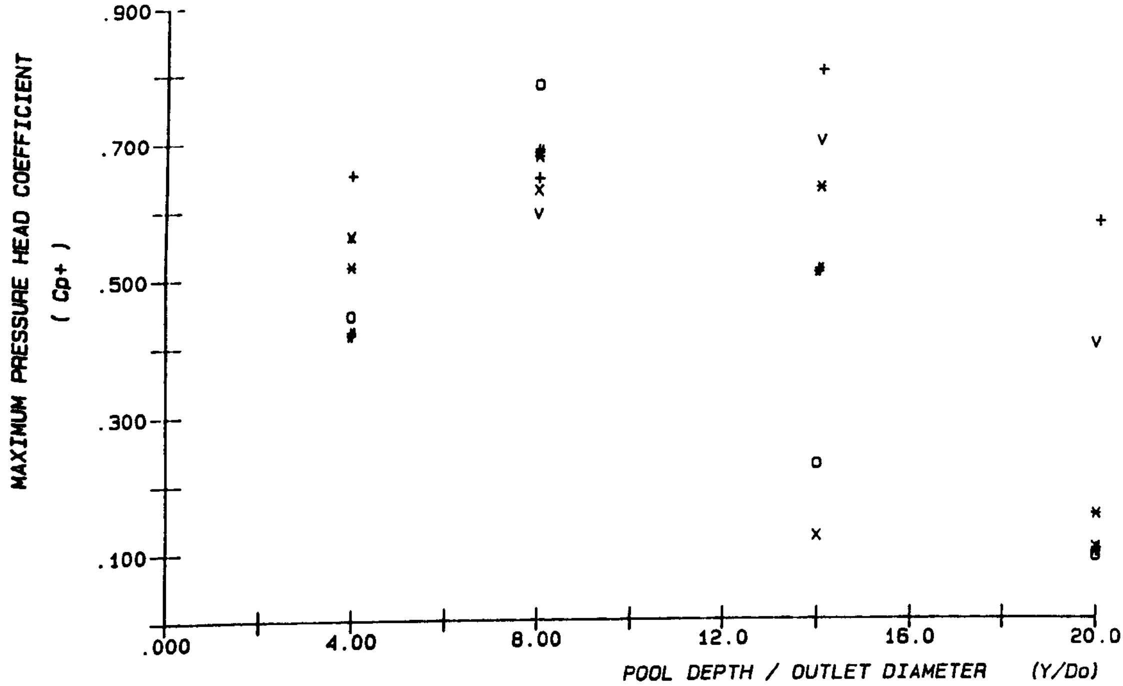

FIG. 5.46 (a) CENTRE LINE MAXIMUM PRESSURE HEAD COEFFICIENT WITH (Y/Do)
(ORIFICE : Do = 25 mm . L = 1020 - 1420 mm)

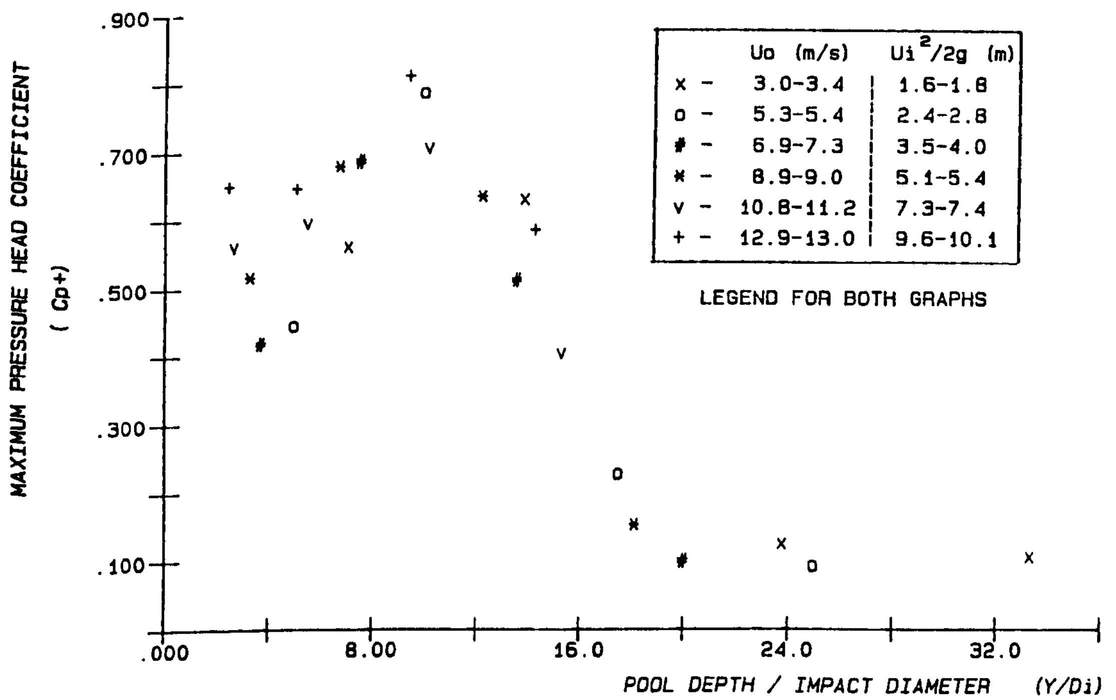

FIG. 5.46 (b) CENTRE LINE MAXIMUM PRESSURE HEAD COEFFICIENT WITH (Y/Di)
(ORIFICE : Do = 25 mm . L = 1020 - 1420 mm)

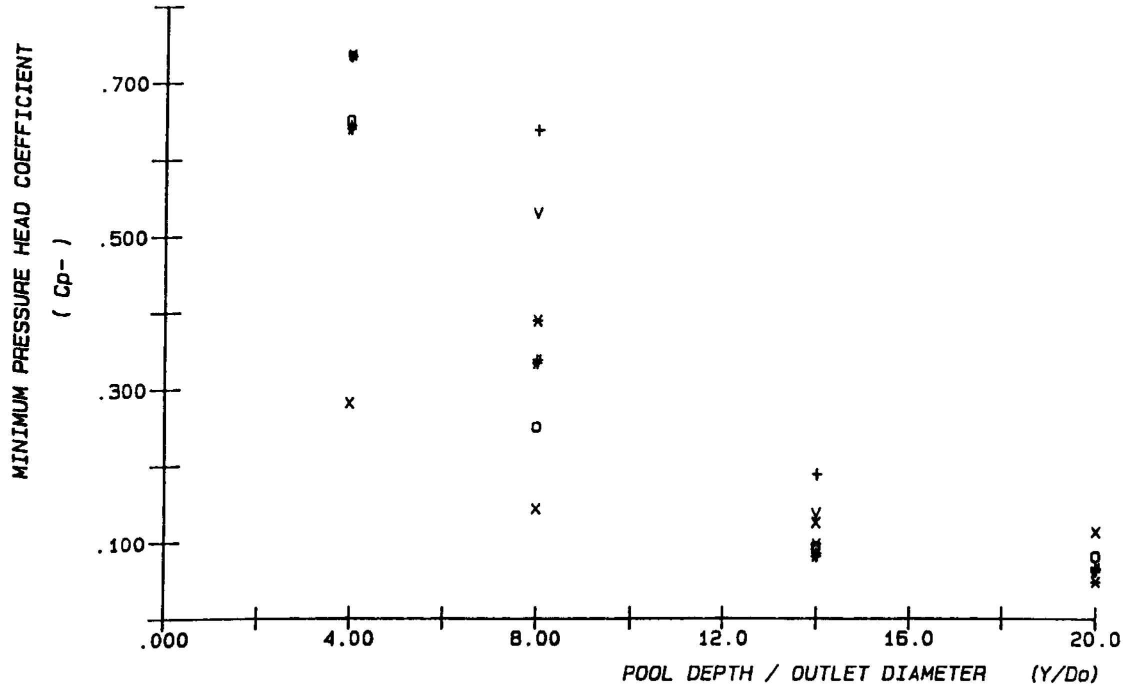

FIG. 5.47(a) CENTRE LINE MINIMUM PRESSURE HEAD COEFFICIENT WITH (Y/Do)
(ORIFICE : Do = 25 mm , L = 1020 - 1420 mm)

	Uo (m/s)	$Ui^2/2g$ (m)
x -	3.0-3.4	1.6-1.8
o -	5.3-5.4	2.4-2.8
# -	6.9-7.3	3.5-4.0
* -	8.9-9.0	5.1-5.4
v -	10.8-11.2	7.3-7.4
+ -	12.9-13.0	9.6-10.1

LEGEND FOR BOTH GRAPHS

FIG. 5.47(b) CENTRE LINE MINIMUM PRESSURE HEAD COEFFICIENT WITH (Y/Di)
(ORIFICE : Do = 25 mm , L = 1020 - 1420 mm)

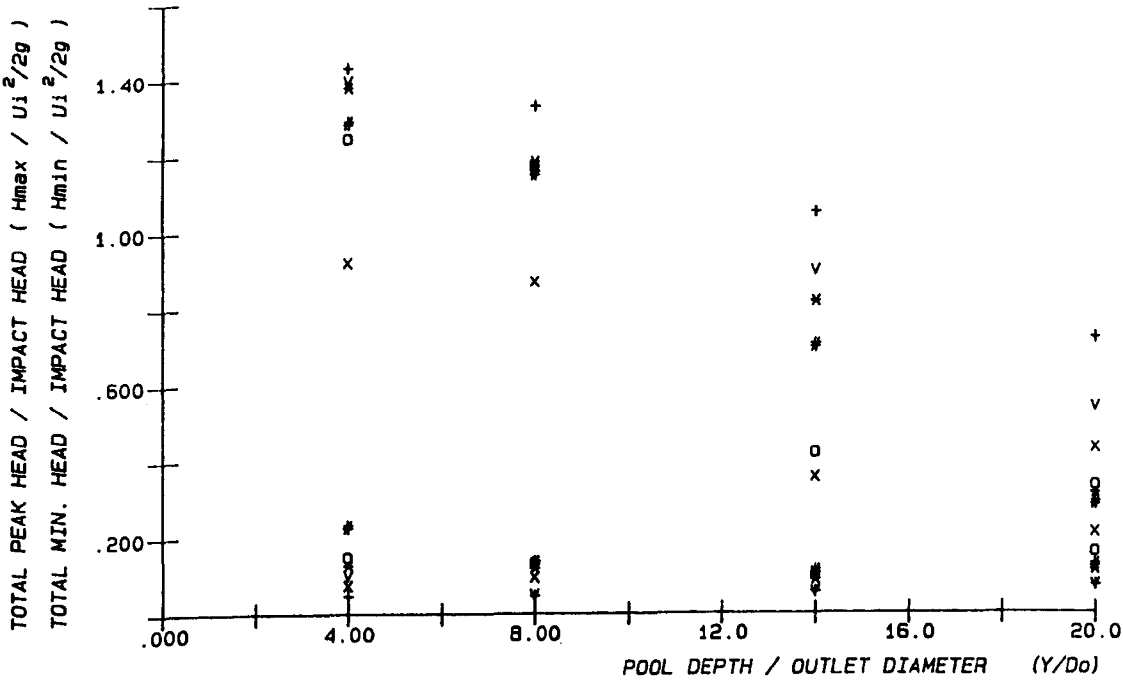

FIG. 5.48 (a) CENTRE LINE TOTAL PEAK AND MINIMUM PRESSURE HEAD RATIO WITH (Y/Do). (ORIFICE : Do = 25 mm , L = 1020 - 1420 mm)

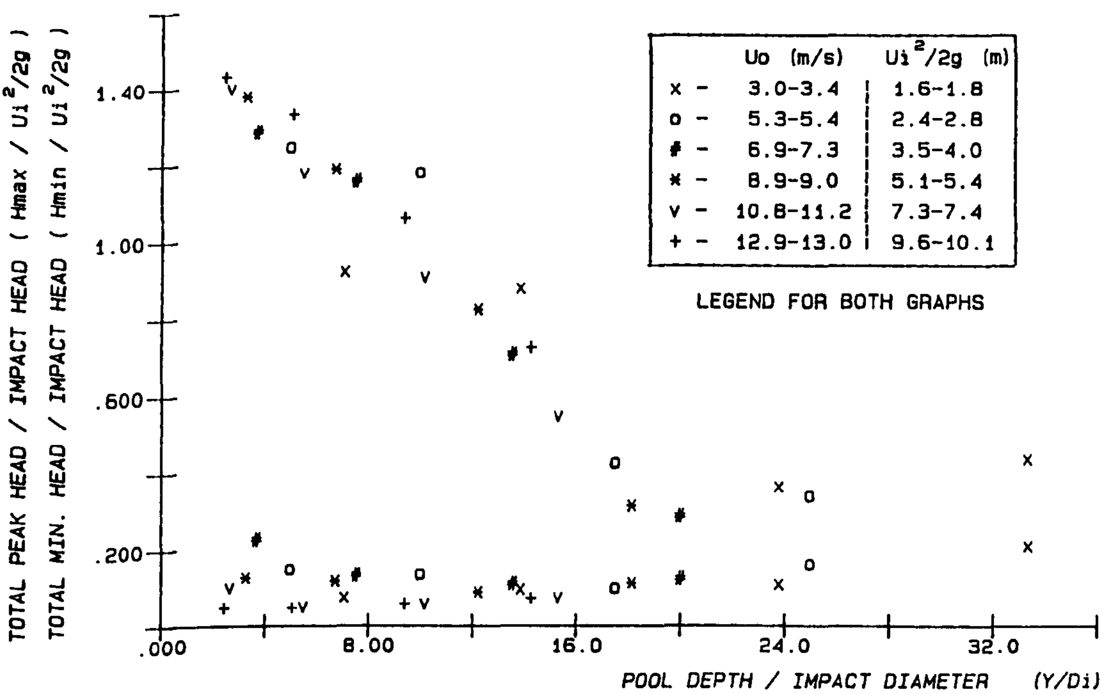

FIG. 5.48 (b) CENTRE LINE TOTAL PEAK AND MINIMUM PRESSURE HEAD RATIO WITH (Y/Di). (ORIFICE : Do = 25 mm , L = 1020 - 1420 mm)

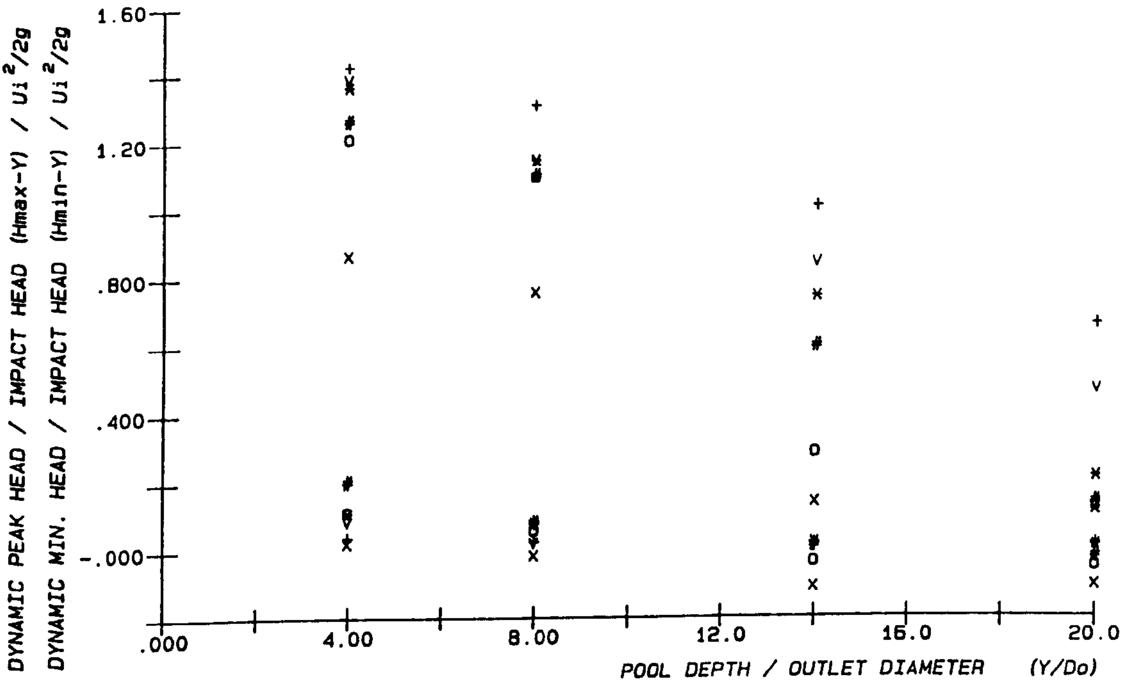

FIG. 5.49(a) CENTRE LINE DYNAMIC PEAK AND MINIMUM PRESSURE HEAD RATIO WITH (Y/Do). (ORIFICE : Do = 25 mm , L = 1020 - 1420 mm)

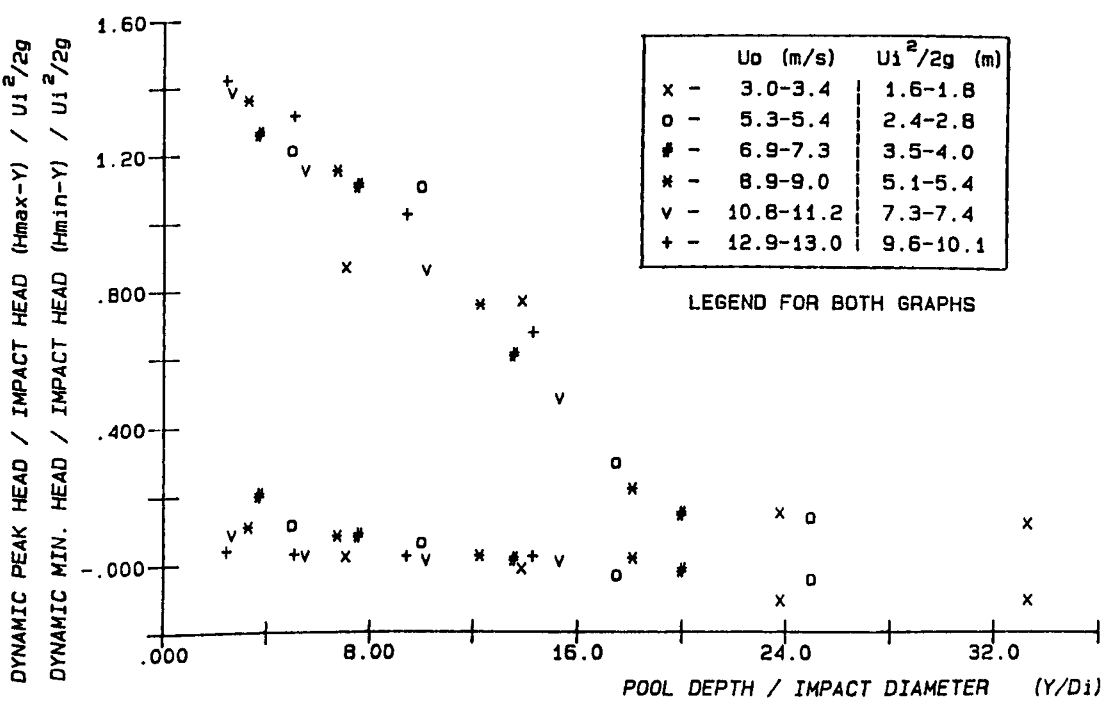

FIG. 5.49(b) CENTRE LINE DYNAMIC PEAK AND MINIMUM PRESSURE HEAD RATIO WITH (Y/Di). (ORIFICE : Do = 25 mm , L = 1020 - 1420 mm)

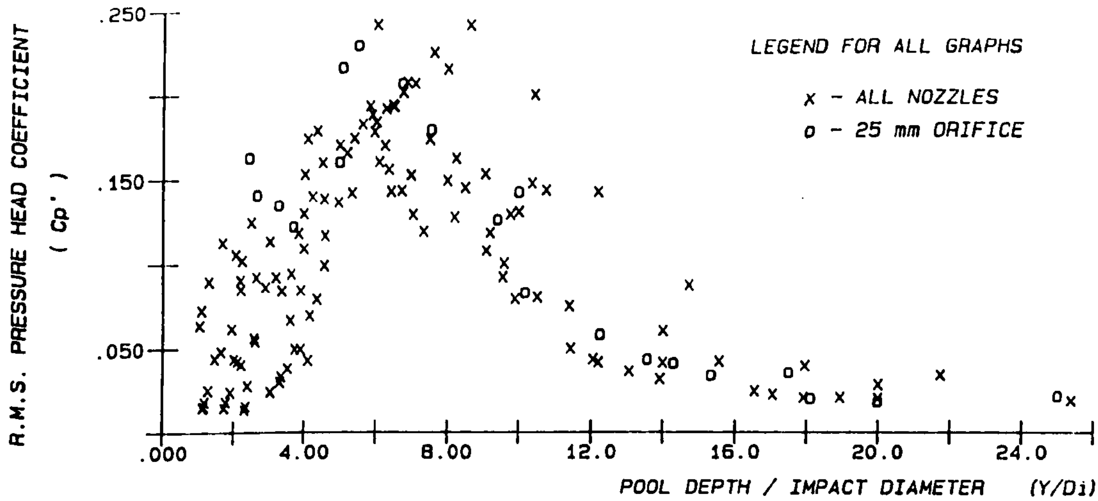

FIG. 5.50(a) COMPARISON OF R.M.S. PRESSURE HEAD COEFFICIENT AGAINST PLUNGE POOL DEPTH FOR ALL NOZZLES AND 25 mm ORIFICE

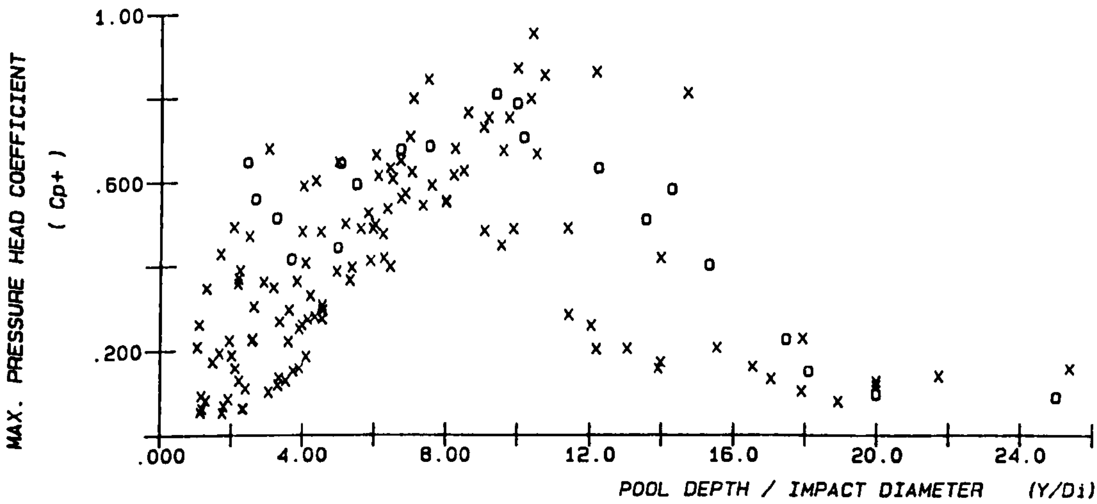

FIG. 5.50(b) COMPARISON OF MAX. PRESSURE HEAD COEFFICIENT AGAINST PLUNGE POOL DEPTH FOR ALL NOZZLES AND 25 mm ORIFICE

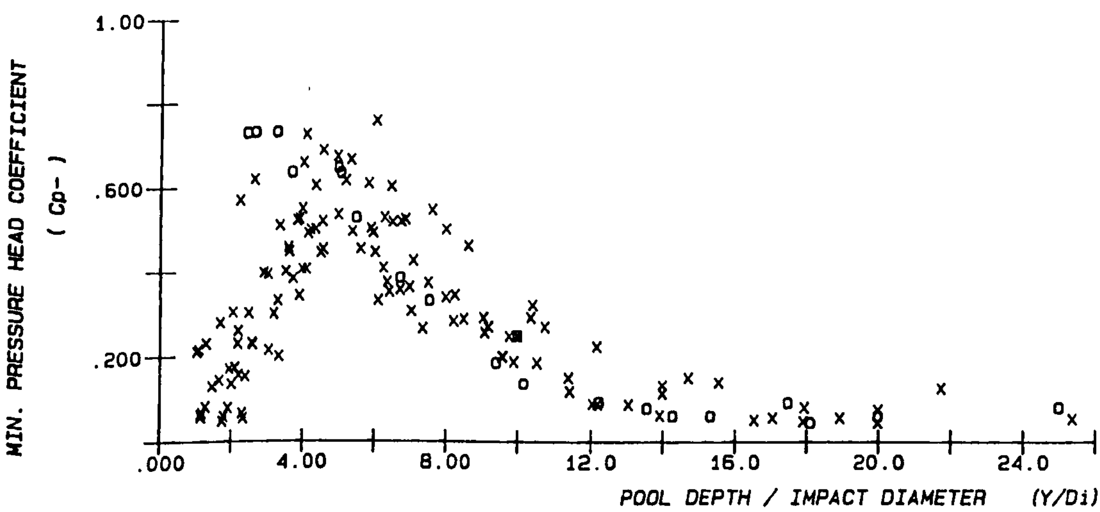

FIG. 5.50(c) COMPARISON OF MIN. PRESSURE HEAD COEFFICIENT AGAINST PLUNGE POOL DEPTH FOR ALL NOZZLES AND 25 mm ORIFICE

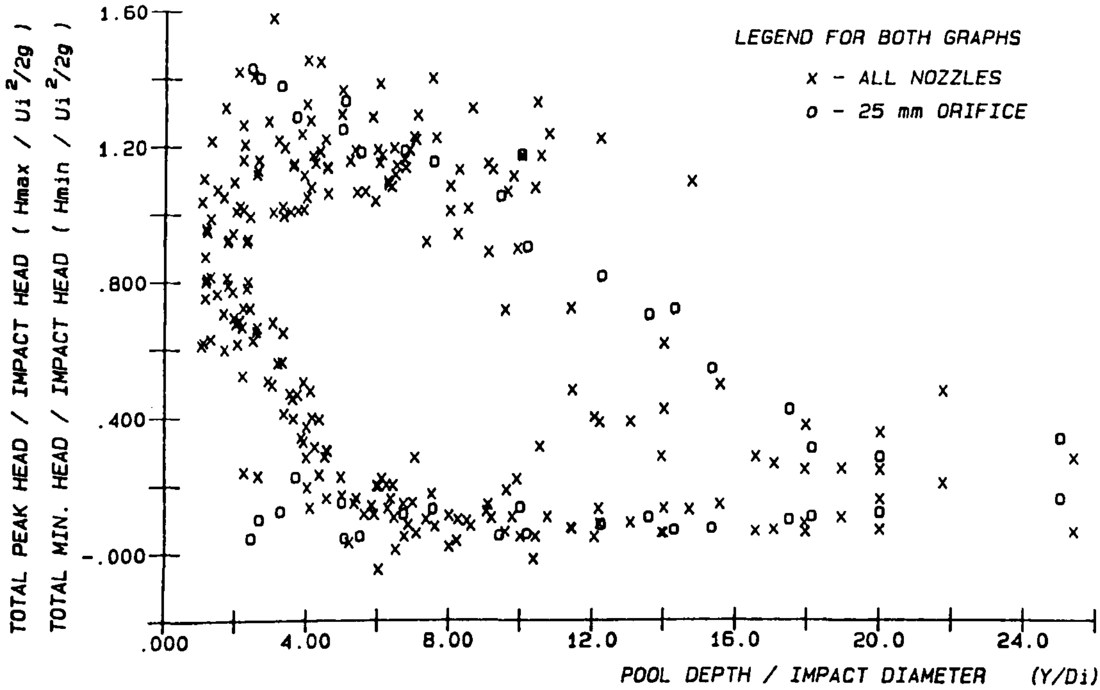

FIG. 5.51 (a) COMPARISON OF TOTAL PEAK AND MINIMUM HEAD AGAINST PLUNGE POOL DEPTH FOR ALL NOZZLES AND 25 mm ORIFICE

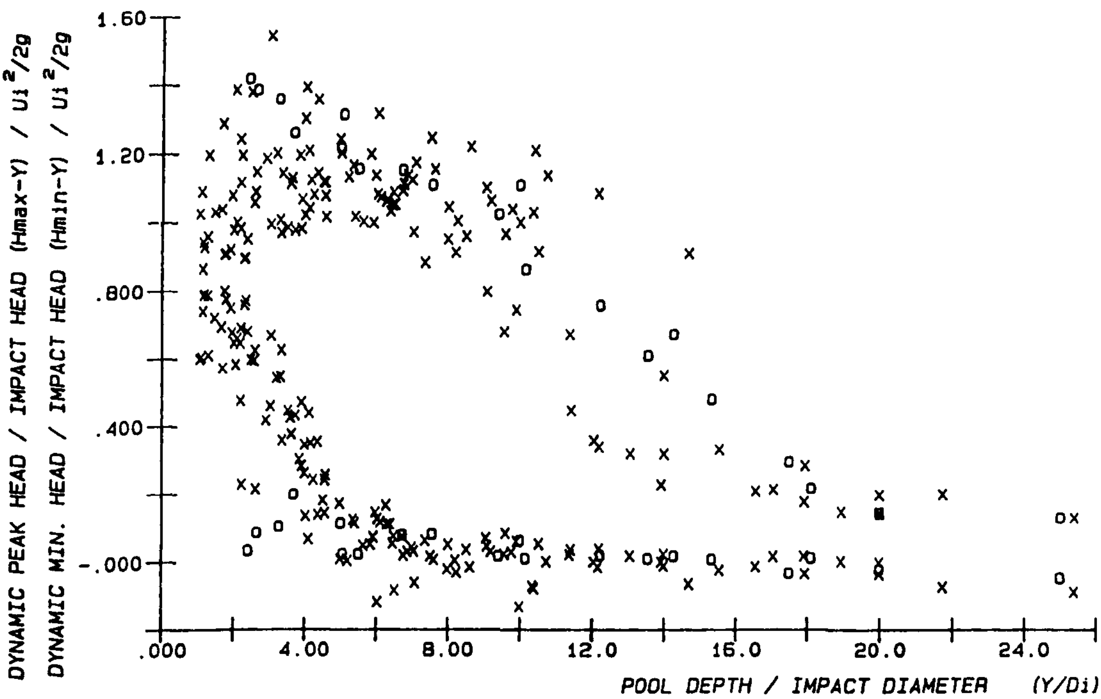

FIG. 5.51 (b) COMPARISON OF DYNAMIC PEAK AND MINIMUM HEAD AGAINST PLUNGE POOL DEPTH FOR ALL NOZZLES AND 25 mm ORIFICE

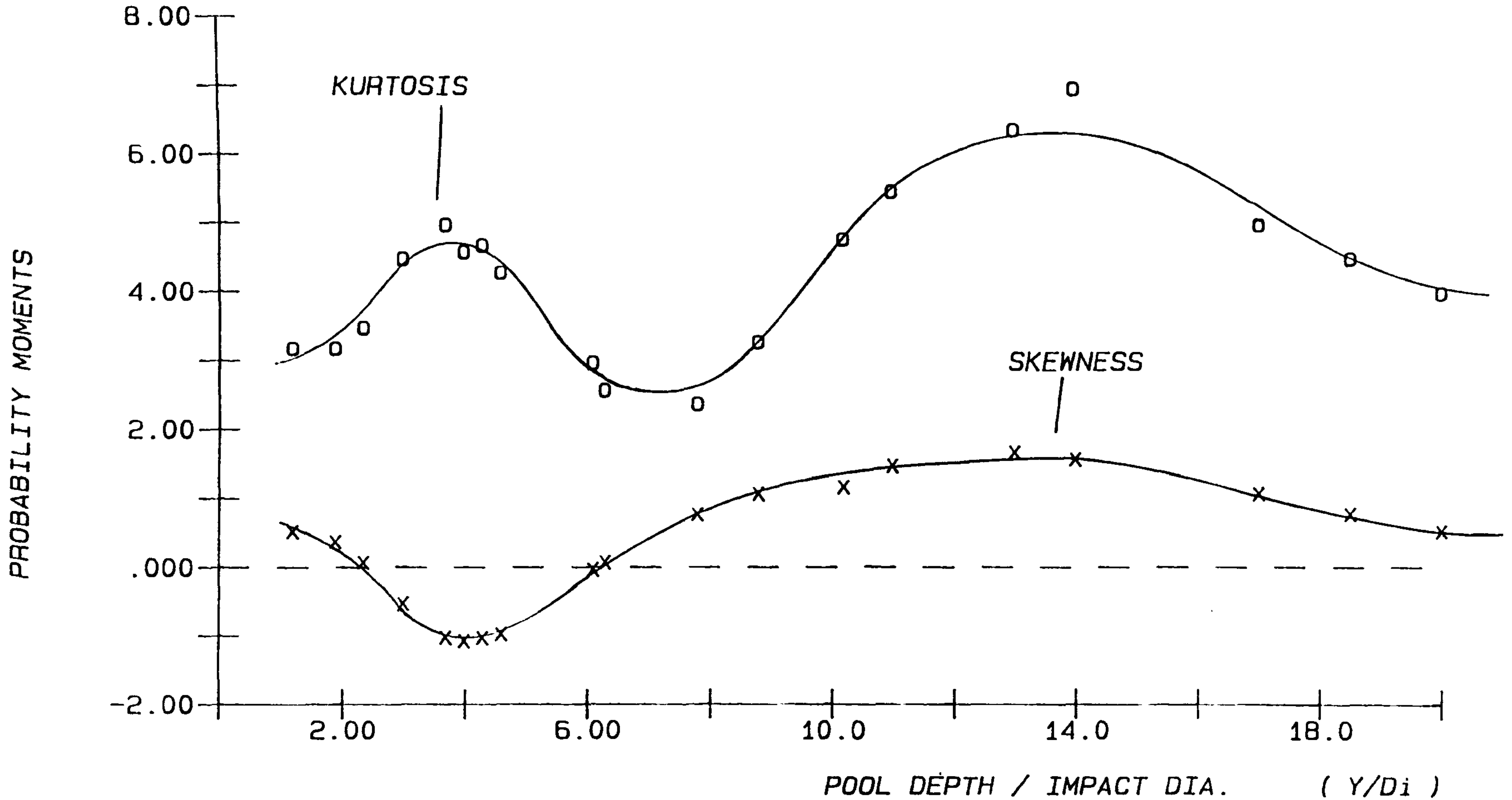

Fig. 5.52 SKEWNESS AND KURTOSIS WITH PLUNGE POOL DEPTH ($Ui^2/2g$ = 4.7-5.6)

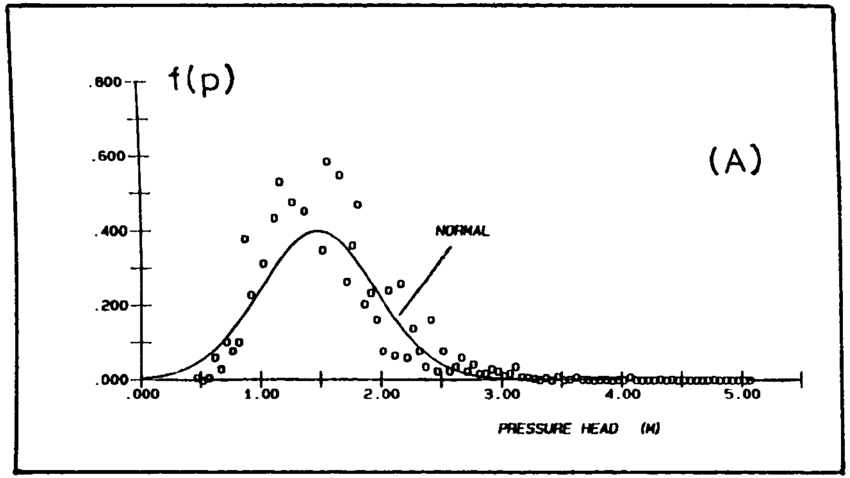

NORMAL DISTRIBUTION

$$f(P) = \frac{1}{\sqrt{2\pi}} e - \frac{(h-\bar{H}m)^2}{2\sigma^2}$$

$Ui^2/2g$ = 6.35 m

Y/Di = 11.4

$\bar{H}m$ = 1.4810 m

Cp' = 0.0755

SKEWNESS = 1.2117

KURTOSIS = 5.8017

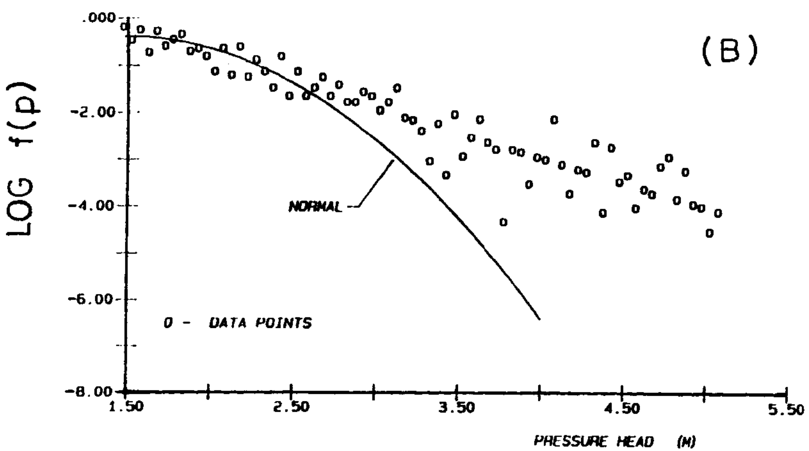

Fig. 5.53 PROBABILITY DENSITY FUNCTION OF PRESSURE FLUCTUATIONS AT CENTRAL MEASUREMENT POINT COMPARED WITH NORMAL DISTRIBUTION

TABLES & FIGURES FOR CHAPTER 6

L/LB

Do (mm)	L (mm)	Uo 3 m/s	Uo 5 m/s	Uo 7 m/s	Uo 9 m/s	Uo 11 m/s	Uo 13 m/s
78	725-1125	0.09-0.14	0.06-0.10	0.05-0.8	0.04-0.07	0.04-0.06	0.035-0.055
78	2230-2630	0.27-0.32	0.20-0.23	0.16-0.19	0.14-0.16	0.12-0.14	0.11-0.13
52.5	620-1020	0.11-0.18	0.08-0.13	0.06-0.10	0.05-0.09	0.05-0.08	0.04-0.07
52.5	2126-2526	0.37-0.44	0.27-0.32	0.22-0.26	0.18-0.22	0.16-0.19	0.15-0.175
25	513-913	0.17-0.31	0.13-0.22	0.10-0.18	0.09-0.16	0.08-0.14	0.07-0.12
25	2018-2418	0.68-0.82	0.49-0.59	0.4-0.48	0.34-0.41	0.3-0.36	0.27-0.33
orifice 25	970-1370*	0.42-0.59	0.36-0.51	0.32-0.46	0.3-0.42	0.28-0.40	0.27-0.38

Notes : (i) $LB = 41.2\ Uo^{0.625}\ Do^{0.9}$ - Nozzles

(ii) $LB = 16.1\ Uo^{0.31}\ Do^{0.62}$ - Orifice

(McKeogh, 3% Tu)

(iii) * - Droplength from Vena Contracta.

Table 6.1 Estimated ratios of L/LB for nozzles and orifice.

Ci (Initial mean air concentration)

Do (mm)	L (mm)	Uo 3 m/s	Uo 5 m/s	Uo 7 m/s	Uo 9 m/s	Uo 11 m/s	Uo 13 m/s
78	725-1125	0.19-0.26	0.24-0.30	0.27-0.33	0.296-0.35	0.31-0.36	0.32-0.37
78	2230-2630	0.39-0.42	0.40-0.43	0.425-0.45	0.44-0.46	0.45-0.47	0.46-0.48
52.5	620-1020	0.19-0.28	0.26-0.33	0.296-0.36	0.32-0.38	0.34-0.40	0.35-0.41
52.5	2126-2526	0.42-0.46	0.45-0.48	0.47-0.49	0.48-0.5	0.49-0.52	0.50-0.525
25	513-913	0.22-0.34	0.31-0.40	0.36-0.43	0.38-0.46	0.40-0.47	0.41-0.48
25	2018-2418	0.53-0.56	0.55-0.58	0.57-0.59	0.58-0.6	0.59-0.61	0.59-0.62
orifice 25	970-1370	0.6-0.65	0.61-0.66	0.62-0.66	0.63-0.67	0.63-0.67	0.63-0.673

Notes : (i) $Ci = \beta i/(1+\beta i)$

(ii) $\beta i = K\ (L/Do)^{1/2}\ (1-Umin/Ui)$

(iii) Umin = 3m/s (nozzles)

Umin = 1m/s (orifice)

(vi) K = 0.2 (nozzles)

K = 0.3 (orifice)

Table 6.2 Initial air concentrations in plunge pool.

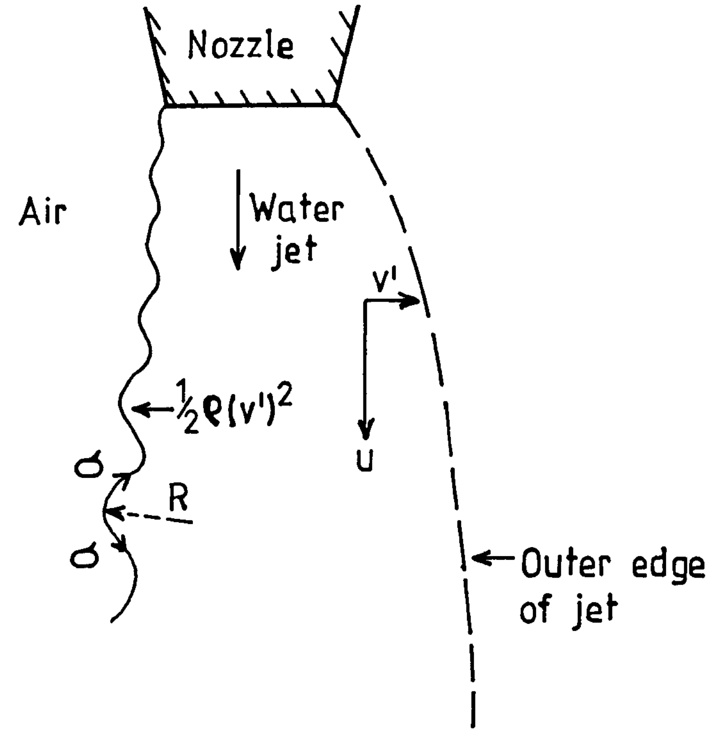

Fig. 6·1 GROWTH OF SURFACE DISTURBANCES (Ervine & Falvey)

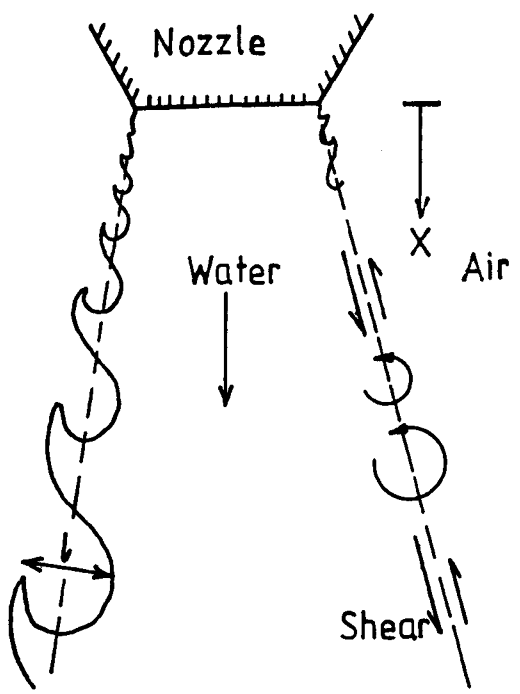

Fig. 6·2 GROWTH OF SURFACE DISTURBANCES. (Hecker)

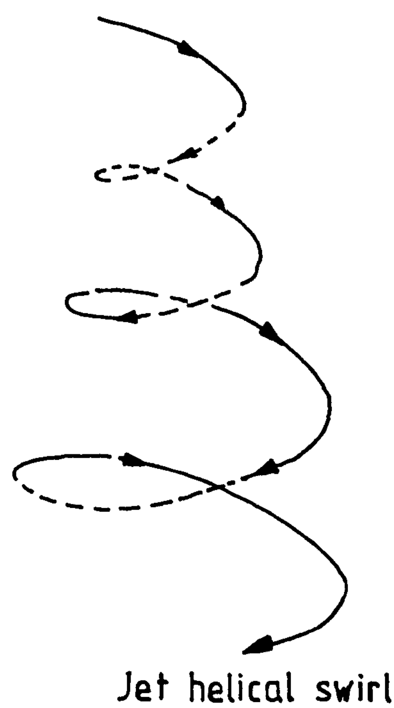

Fig. 6·3 GROWTH OF SURFACE DISTURBANCES. (Hoyt)

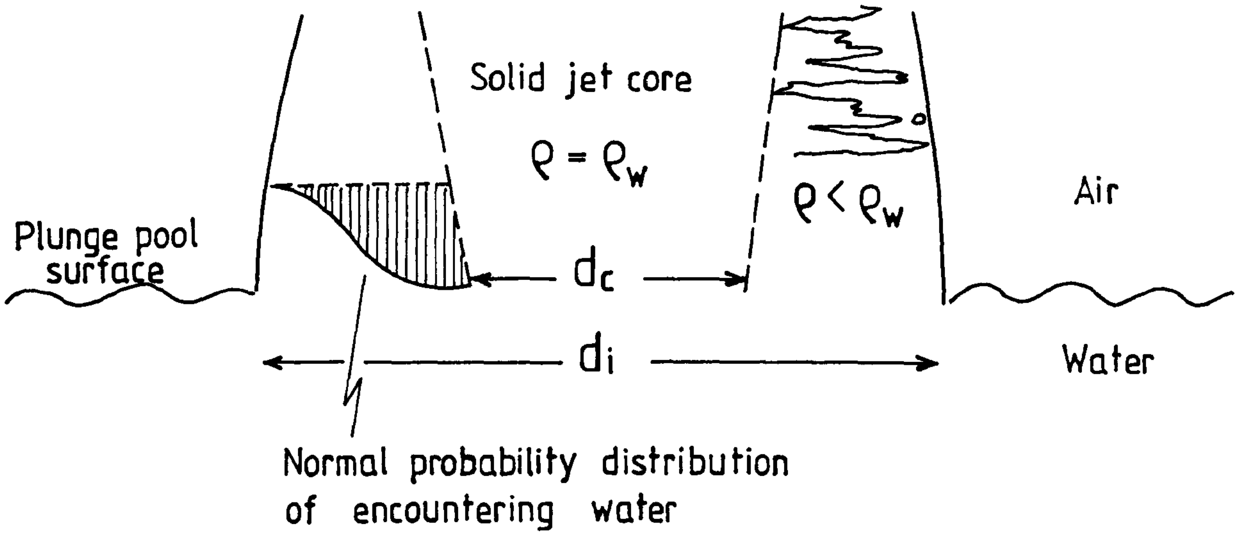

Fig. 6·4 IDEALISATION OF JET CONDITION AT IMPACT

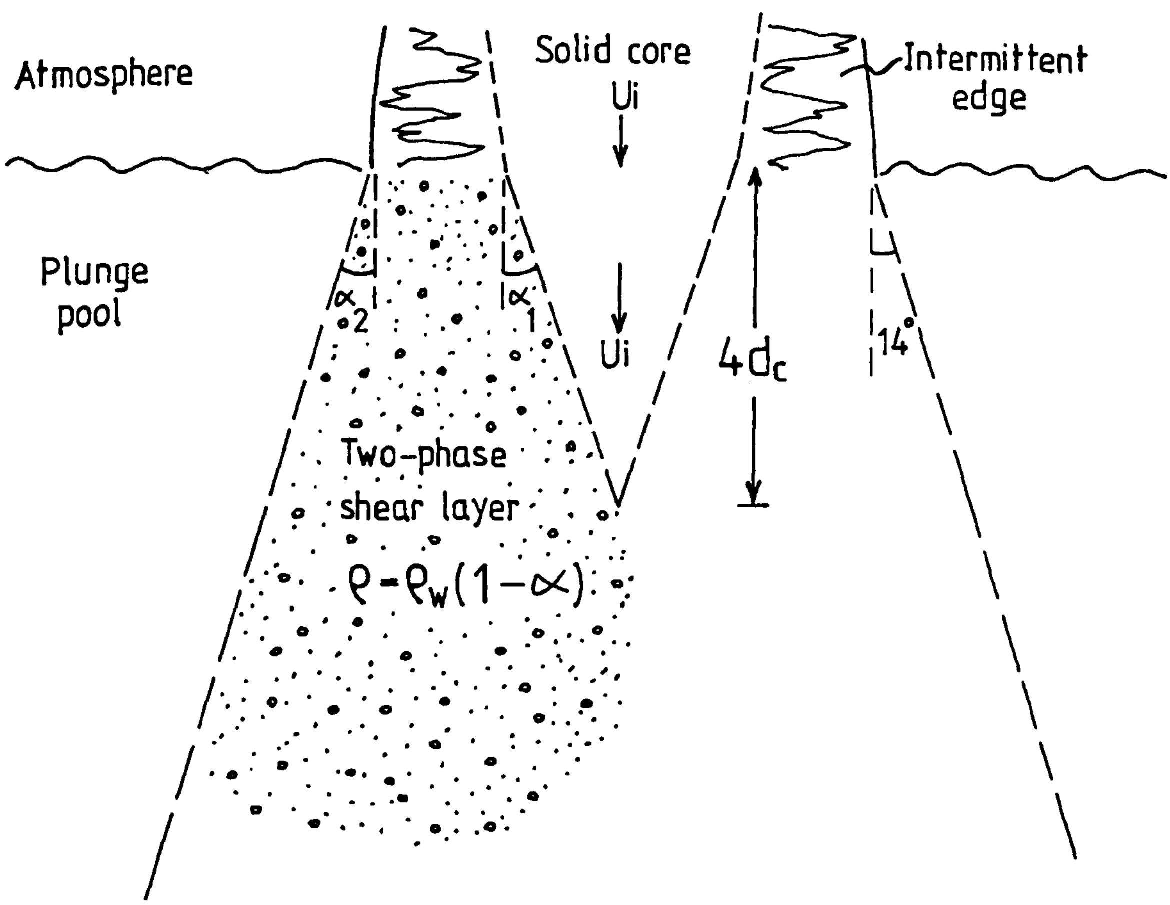

Fig. 6·5 CONDITIONS IN PLUNGE POOL FOR IMPINGING TURBULENT JET

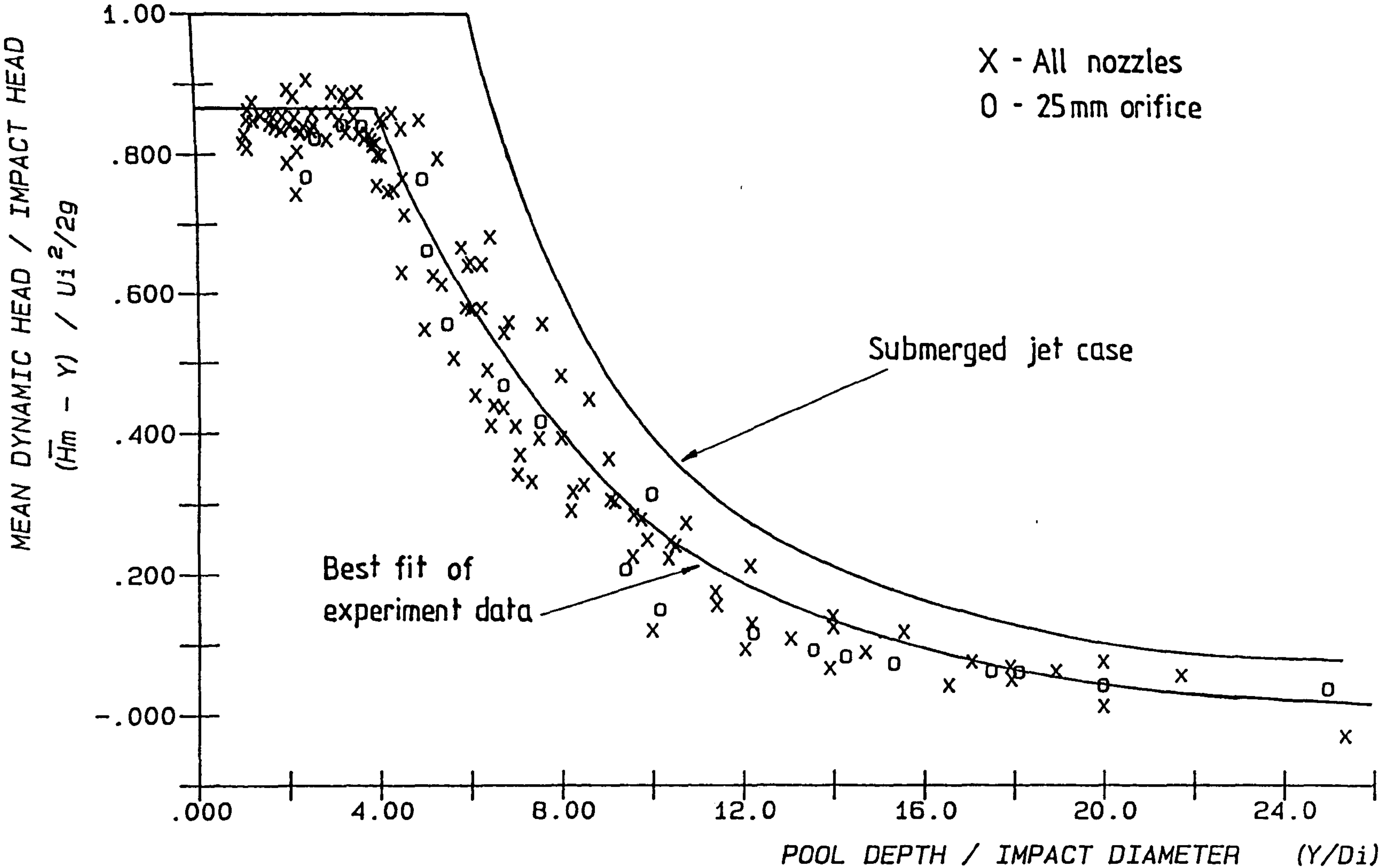

Fig.6·6 COMPARISON OF MEAN DYNAMIC HEAD VALUES WITH SUBMERGED JET CASE

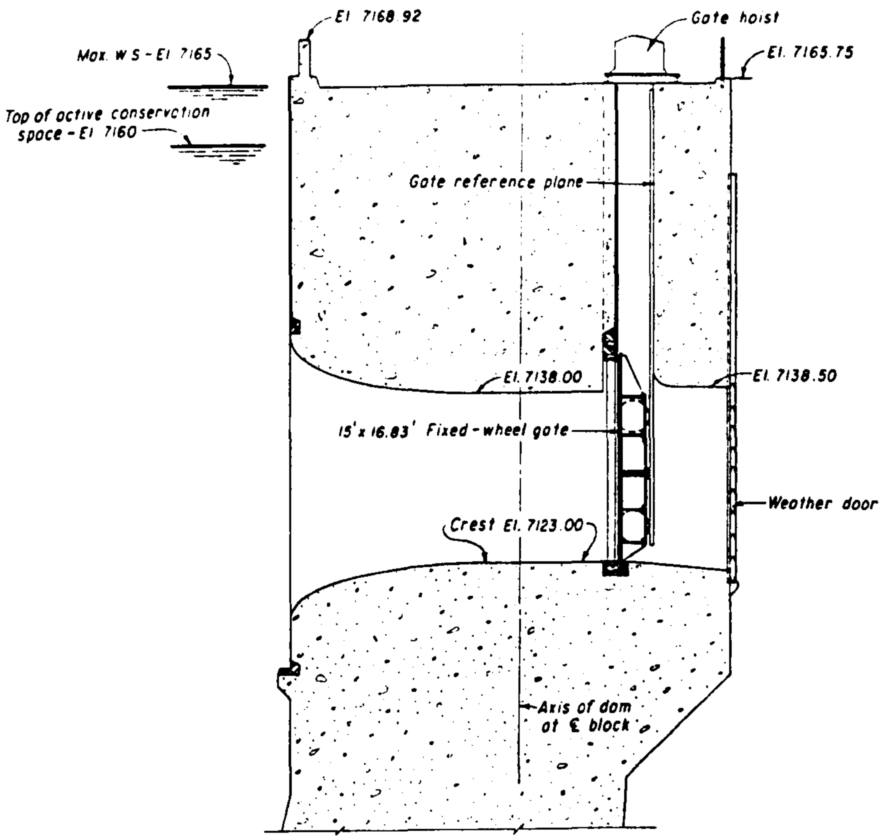

Fig.6·7 DETAIL OF MORROW POINT OUTLET STRUCTURE

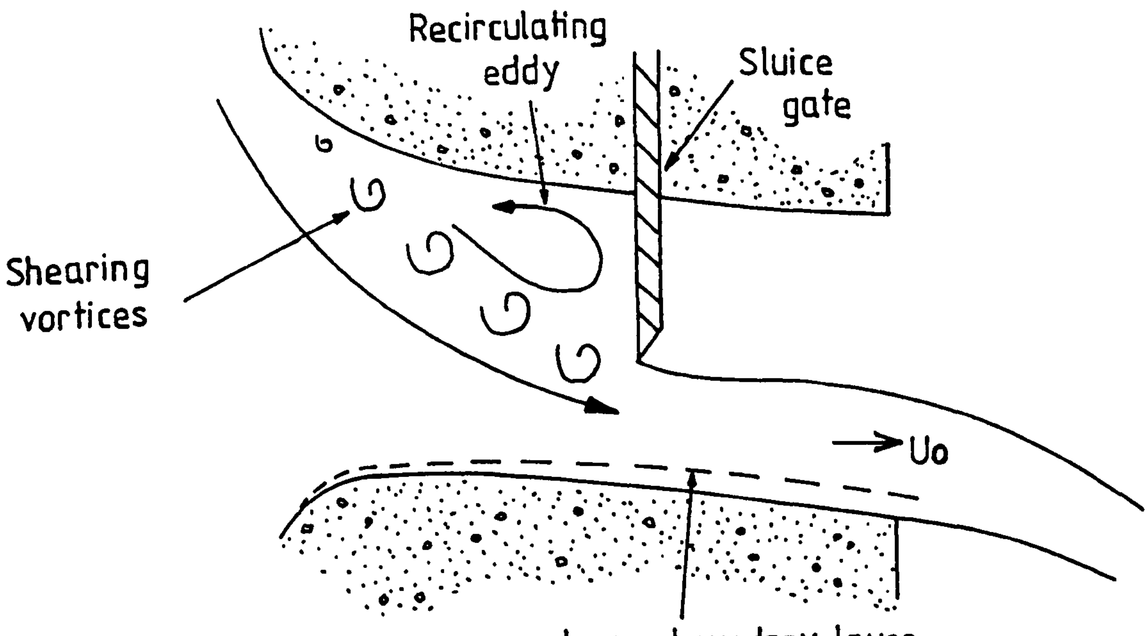

Fig.6·8 EFFECT OF PARTIALLY OPEN SLUICE GATE

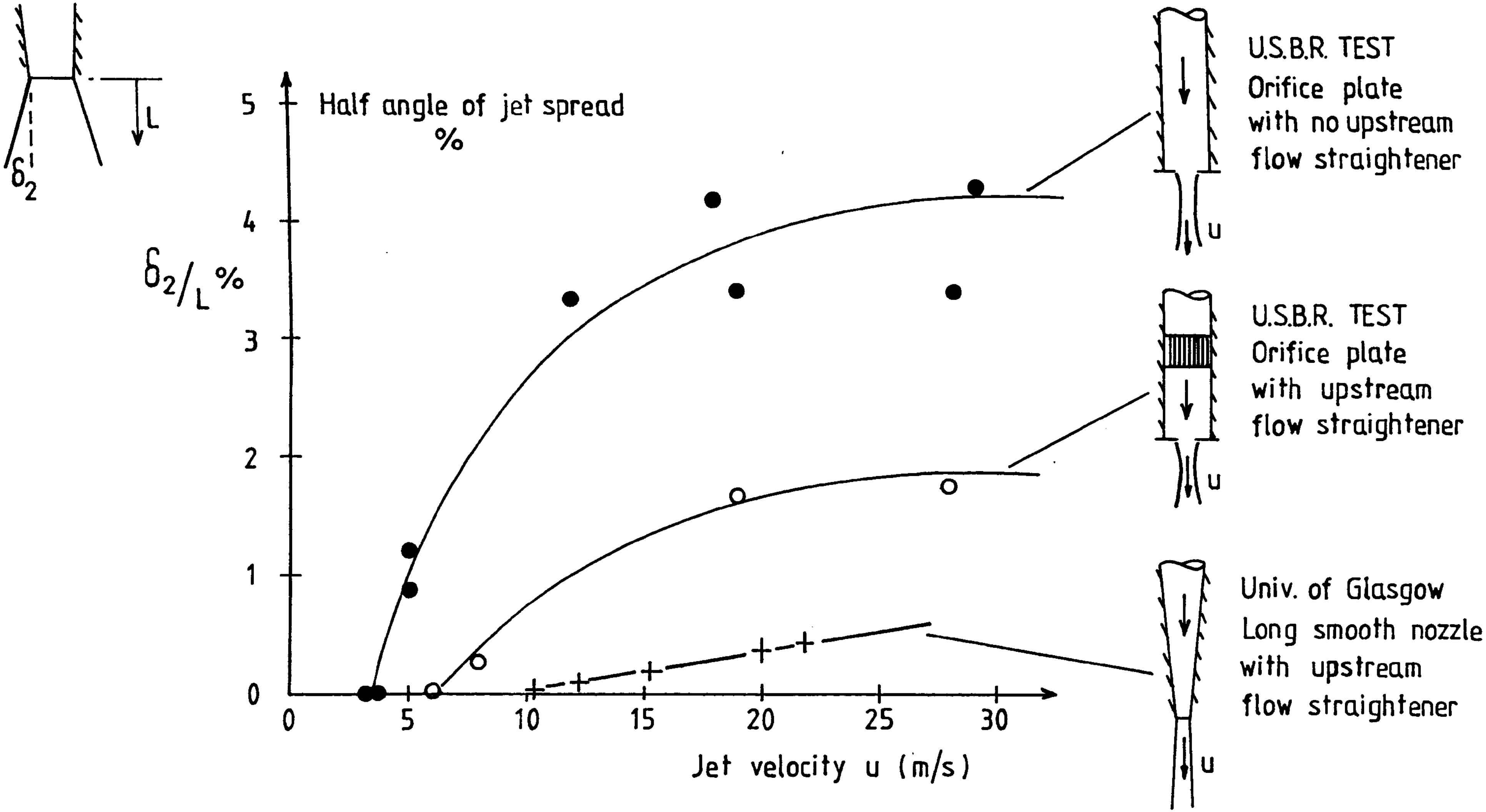

Fig.6·9 Degree of jet spread in the atmosphere with outlet condition

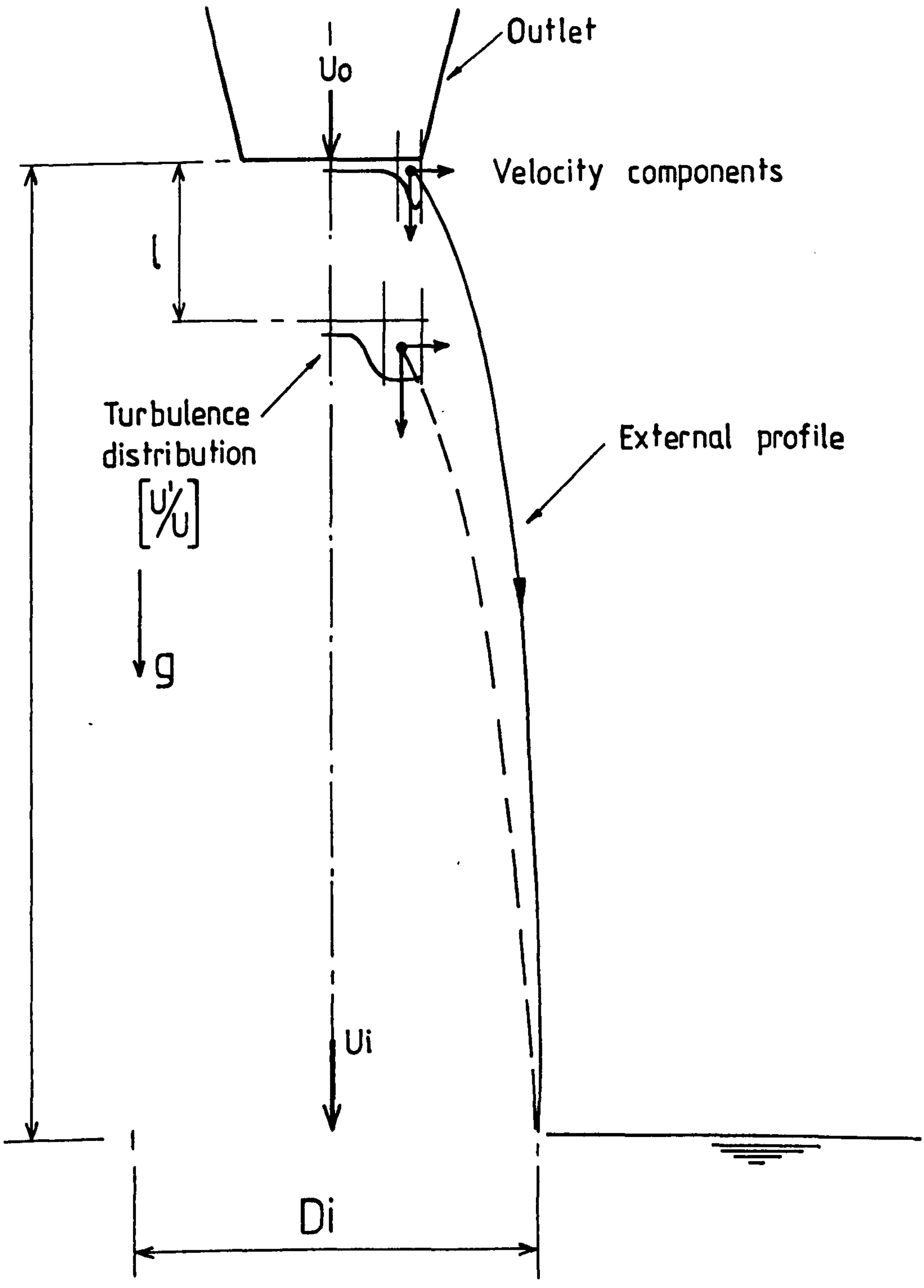

Fig. 6·10 JET SPREADING CONCEPT (Basis of calculations)

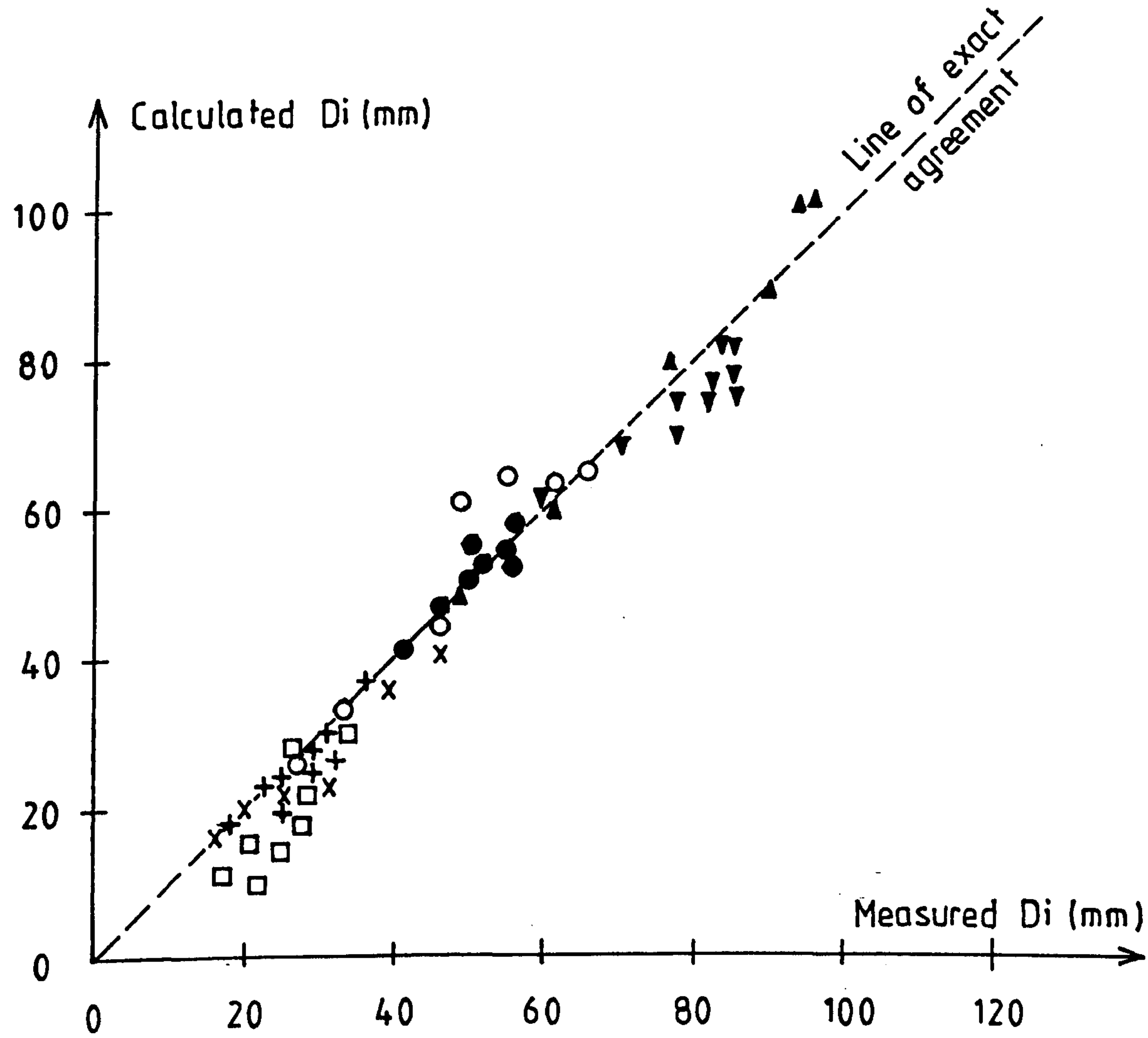

▼ – Do=78mm, L=725–1125 mm

▲ – Do=78 mm, L=2230–2630 mm

● – Do=52·5mm, L=620–1020 mm

○ – Do=52·5mm, L=2126–2526 mm

+ – Do=25 mm, L=513–913 mm

X – Do=25 mm, L=2018–2418 mm

□ – Orifice, L=1020–1420 mm

Fig. 6·11 Comparison of measured and calculated jet diameter at impact.

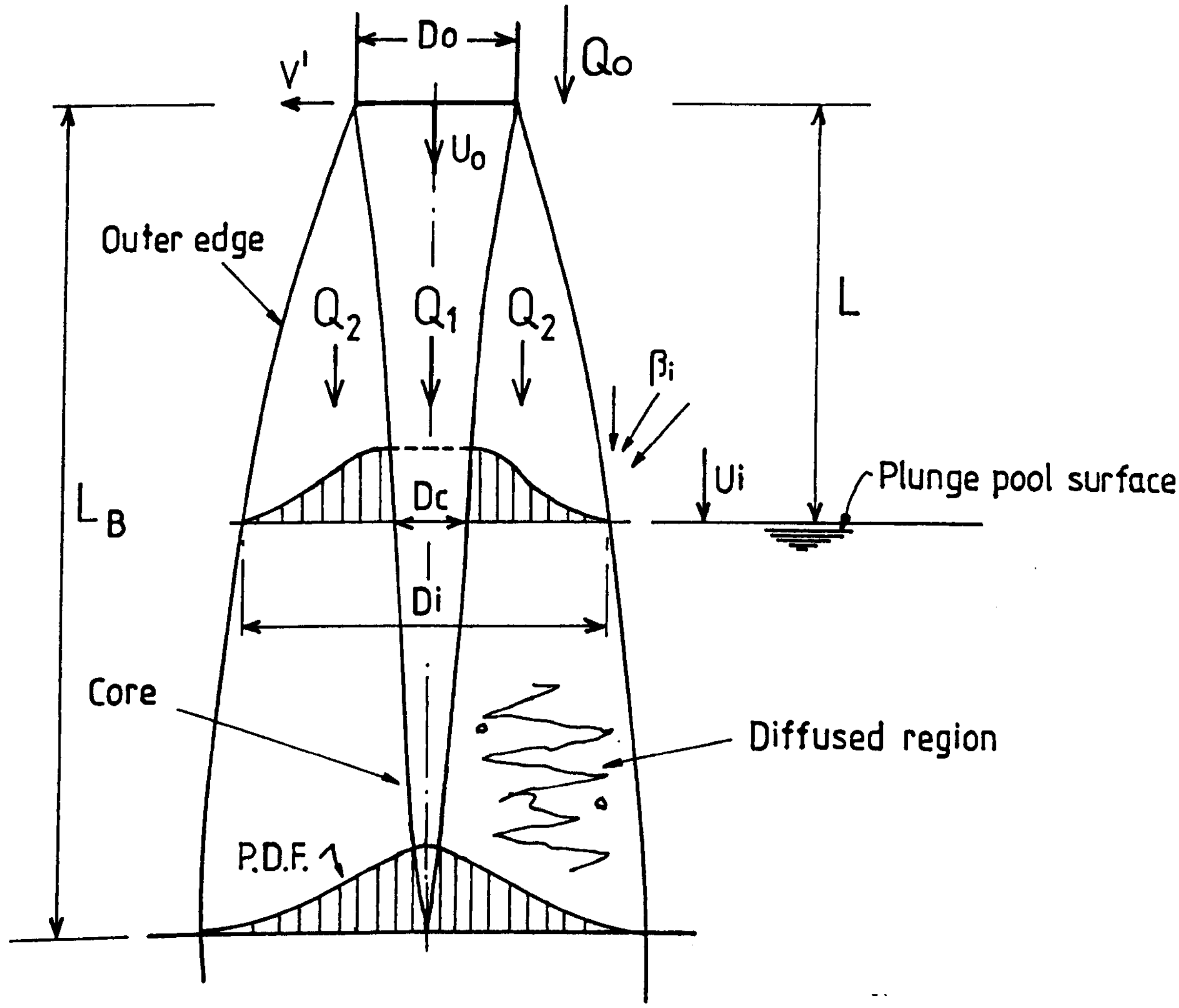

Fig. 6·12 Spreading jet condition at various cross sections.

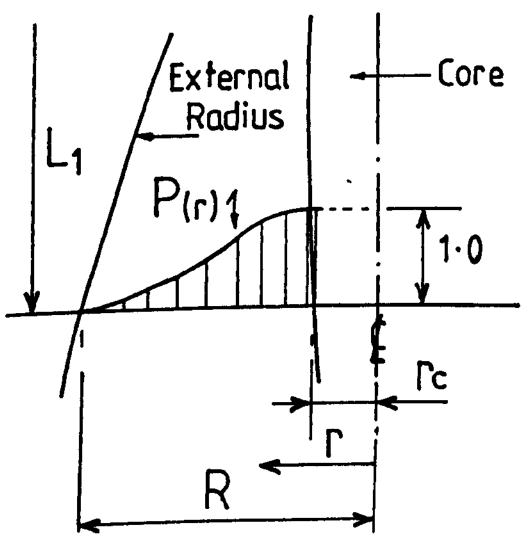

$$P(r) = e^{-\left[\frac{(r-r_c)^2}{2\sigma^2}\right]}$$

Fig. 6·13 Probability of encountering water outwith solid core and notation.

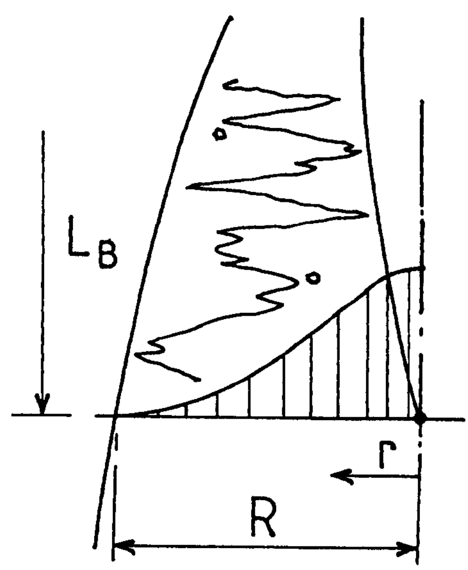

Fig. 6·14 Condition of plunging jet once core has diminished.

Picture of profile
Flow = 0·00245 m^3/s
Dia. = 0·025 m
Tu_o = 1 %

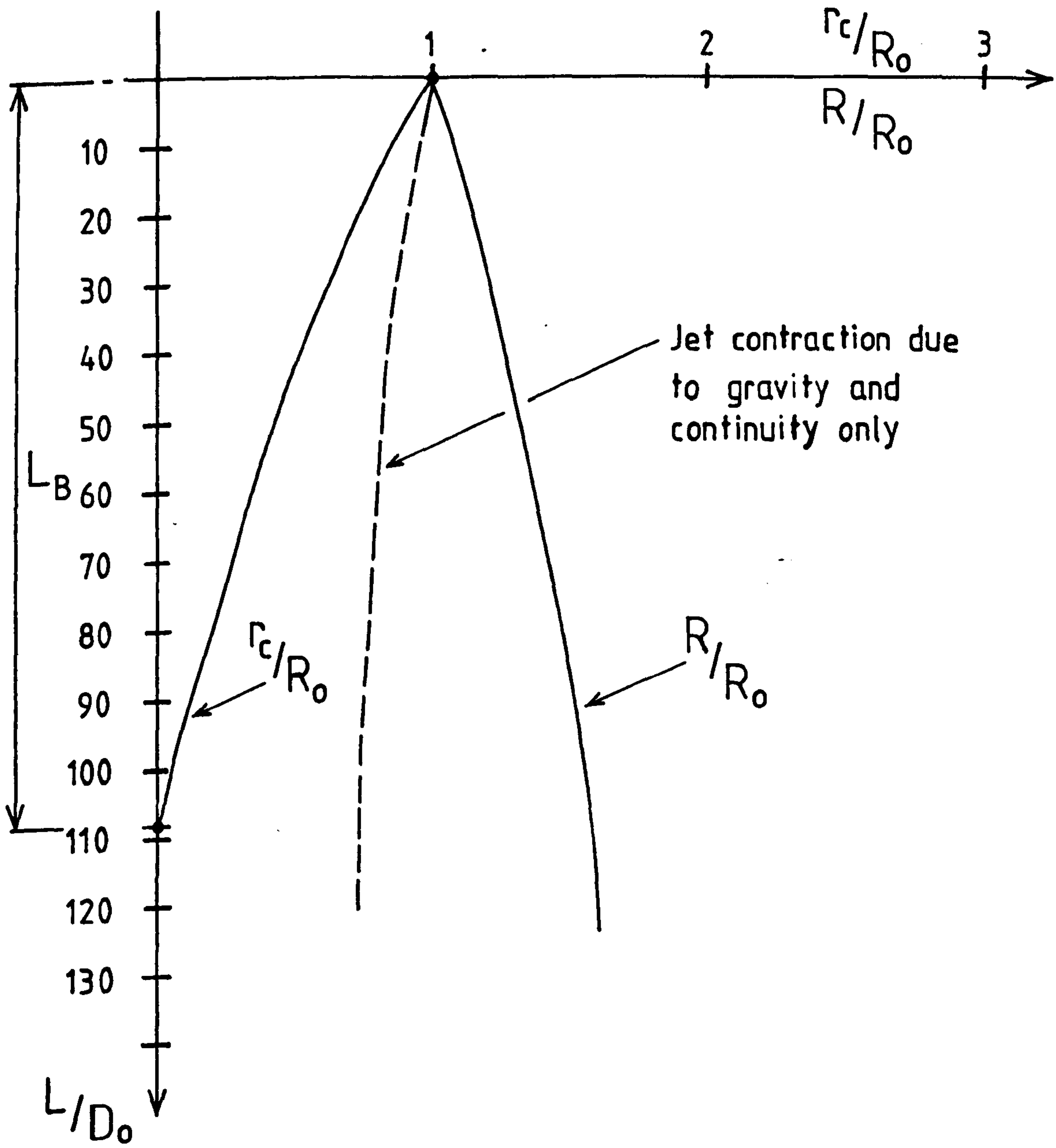

Fig. 6·15 GRAPHICAL REPRESENTATION OF CORE DIAMETER CALCULATION.

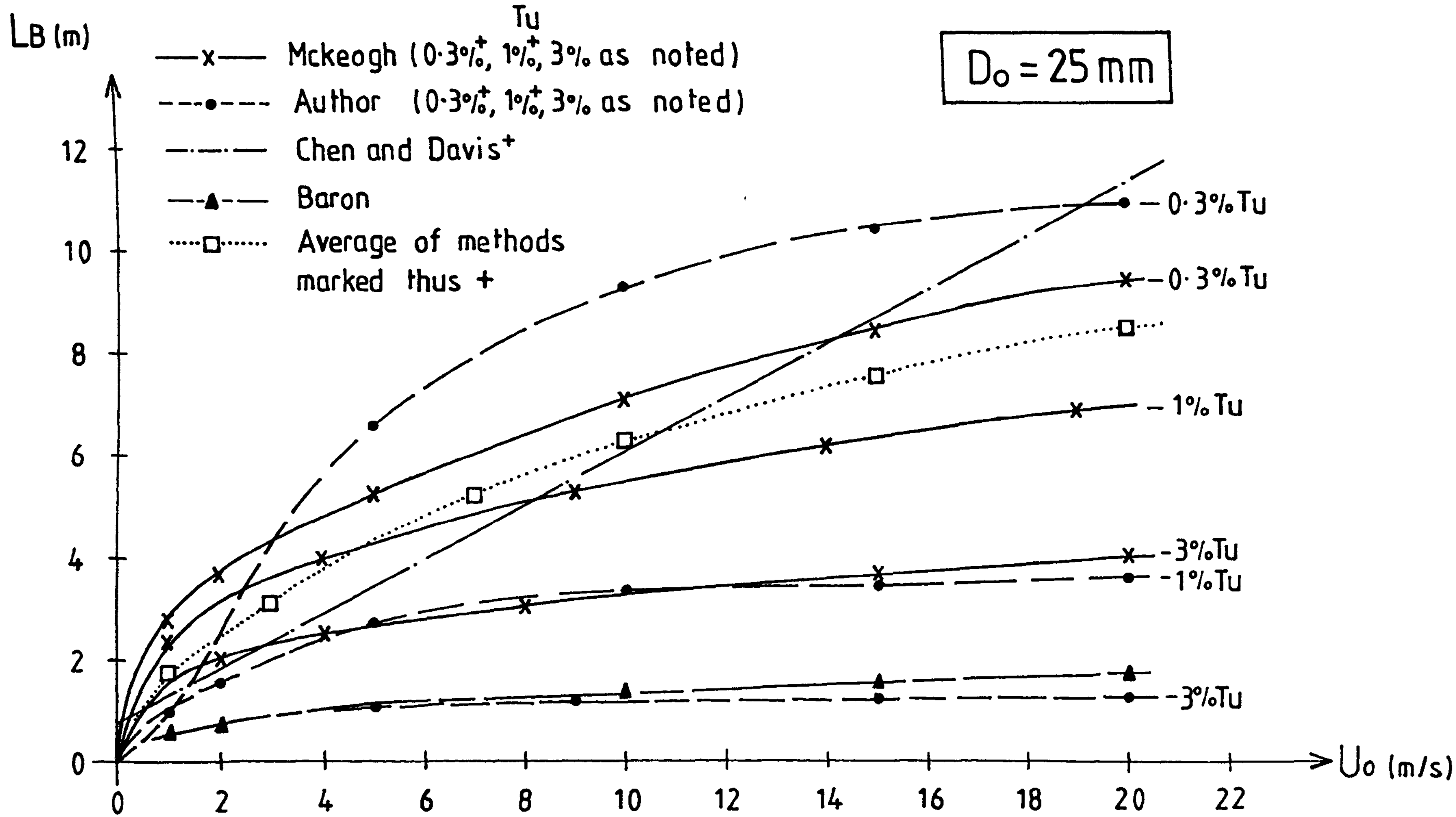

Fig. 6·16 Comparison of jet break-up lengths.

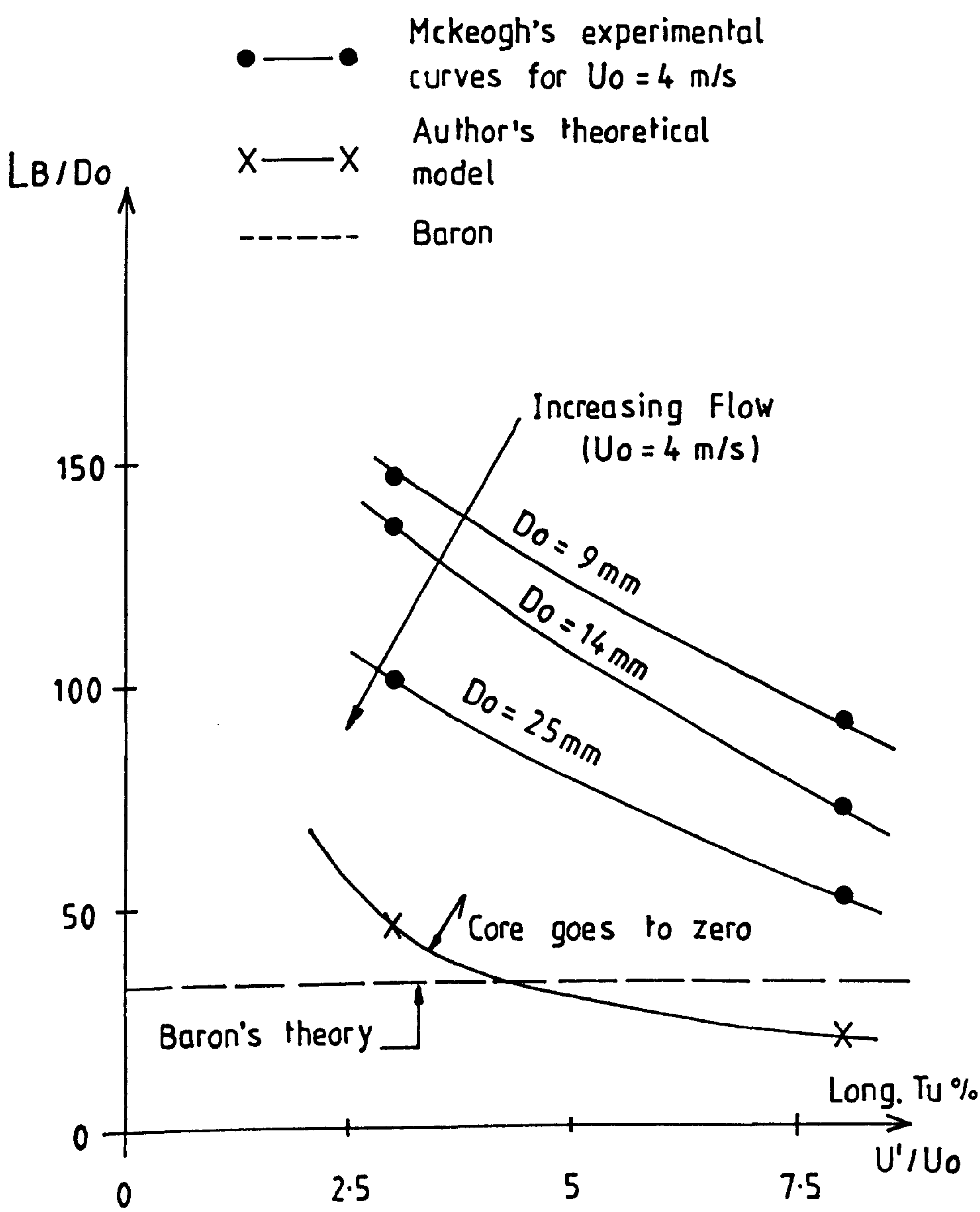

Fig. 6·17 Jet break-up length with turbulence intensity

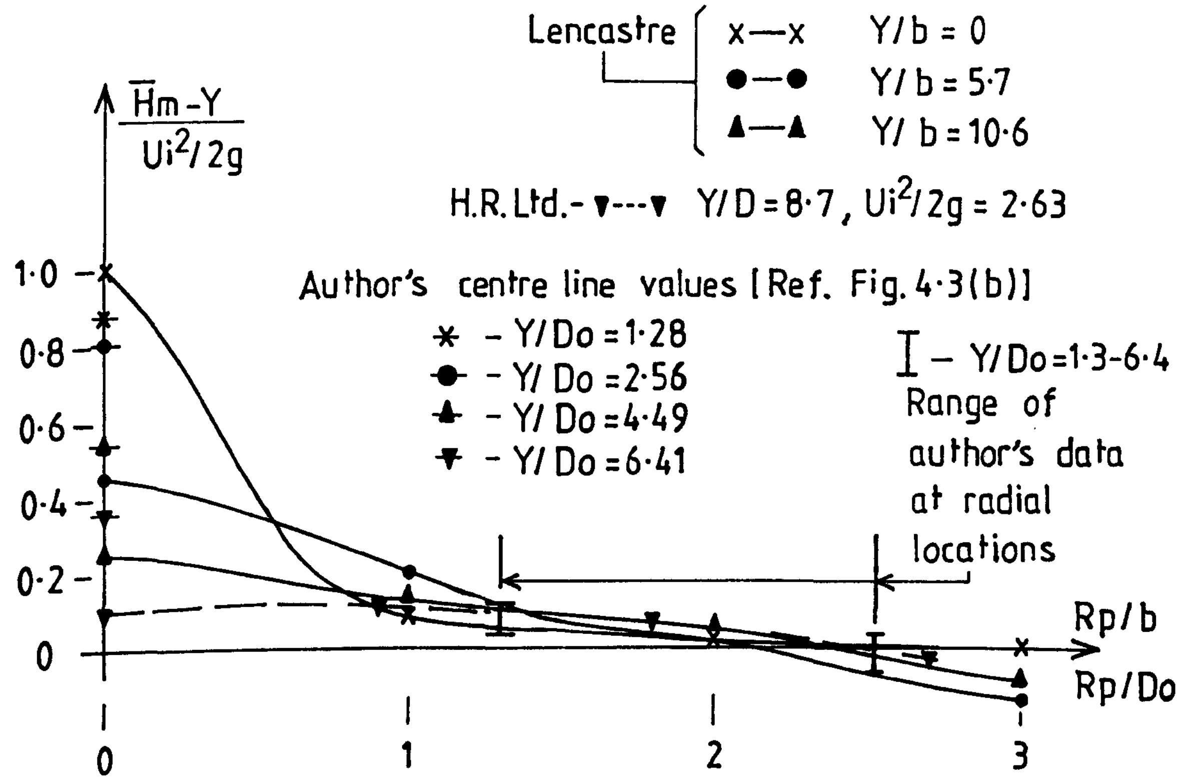

Fig. 6·18 Comparison of radial variation of mean dynamic pressures for plunging jet impingement.

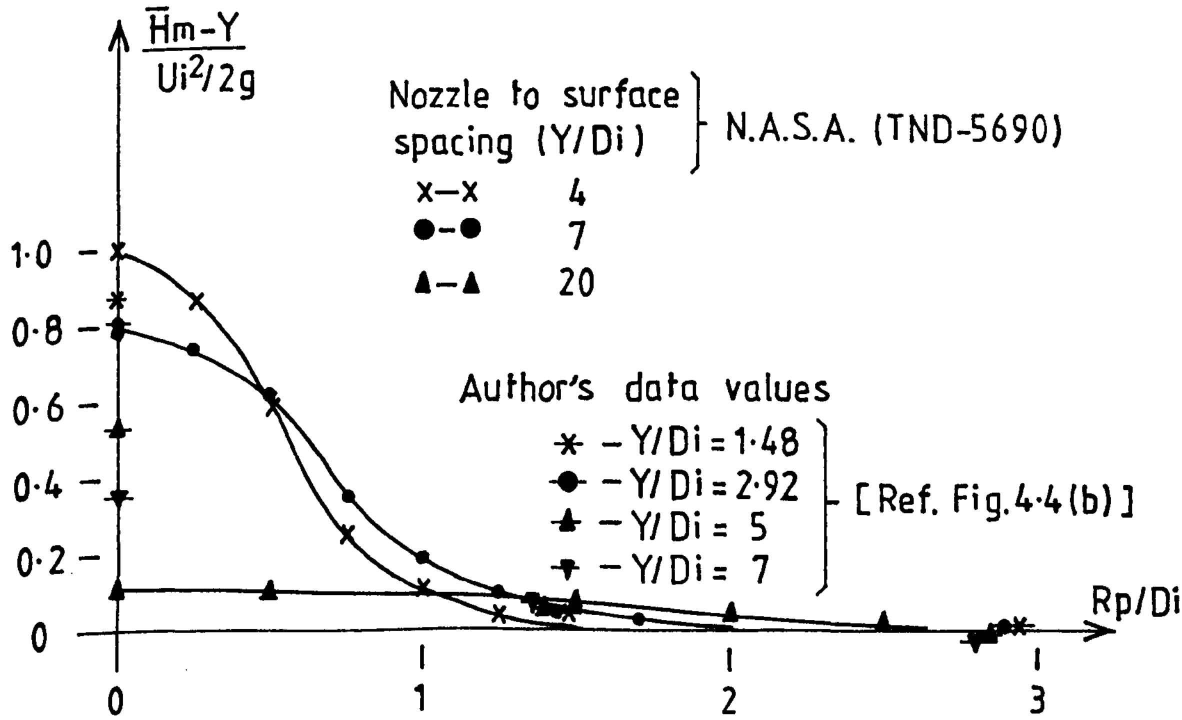

Fig. 6·19 Mean dynamic pressure head variation with radius compared with submerged jet values.

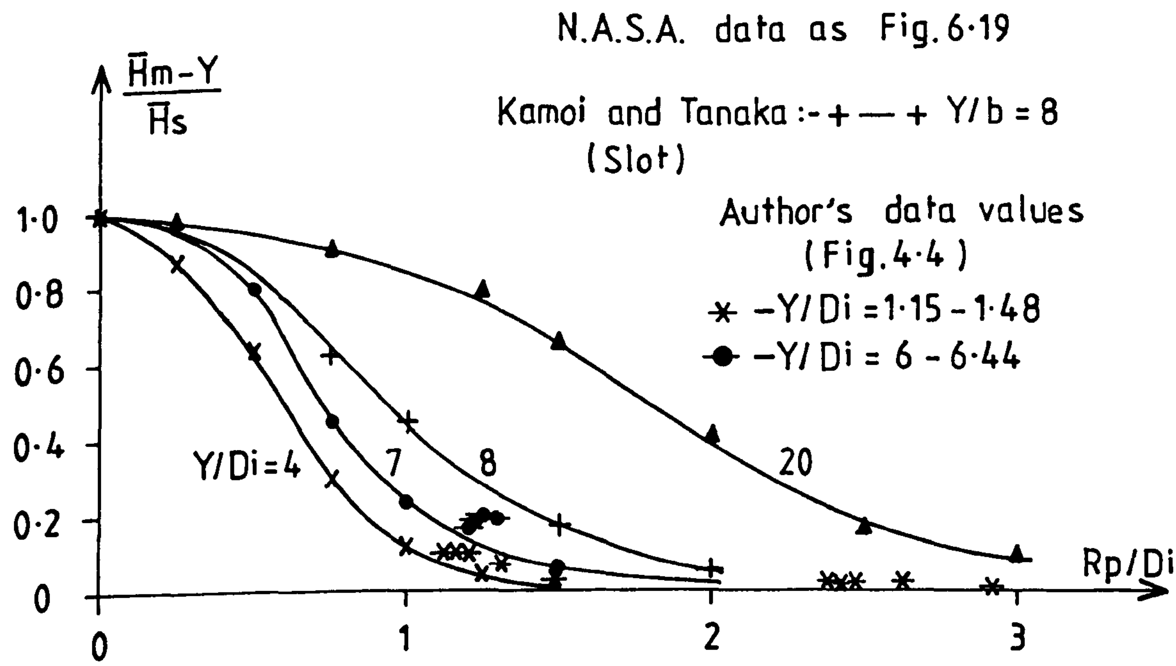

Fig. 6·20(a) Mean dynamic pressure head relative to centre line value with Rp/Di.

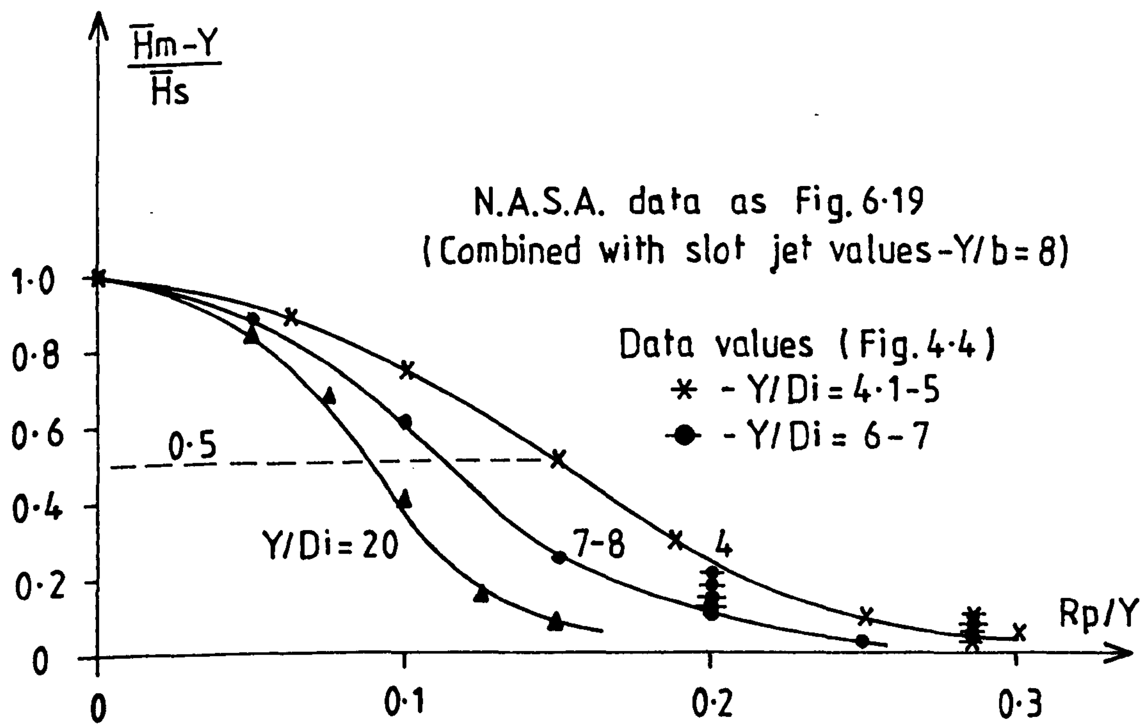

Fig. 6·20(b) Mean dynamic pressure head relative to centre line value with Rp/Y.

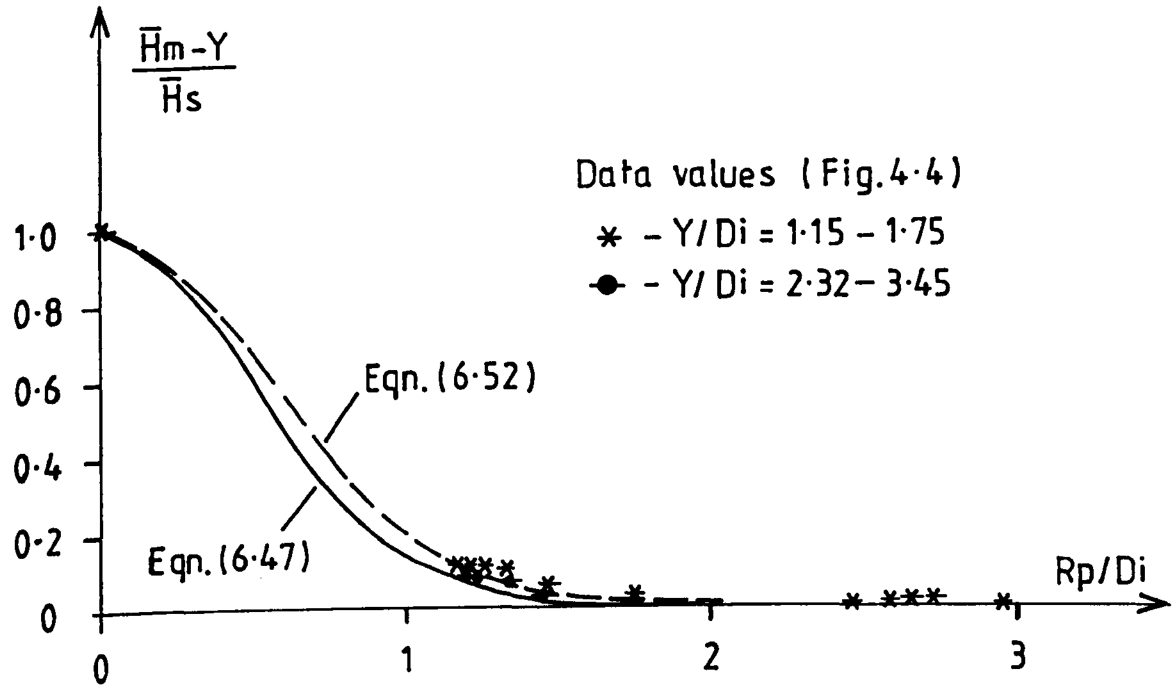

Fig.6·21(a) Expressions for radial distribution of mean dynamic pressure head. (Y=100 and 200 mm)

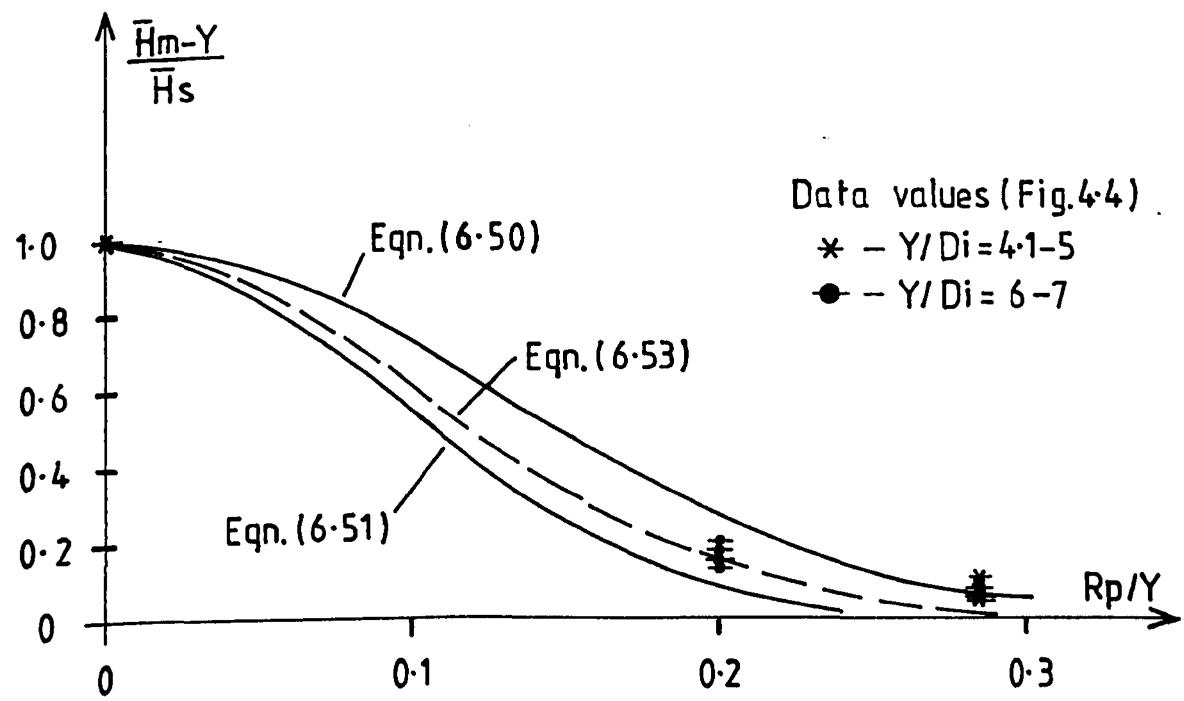

Fig. 6·21(b) Expressions for radial distribution of mean dynamic pressure head. (Y=350 and 500 mm)

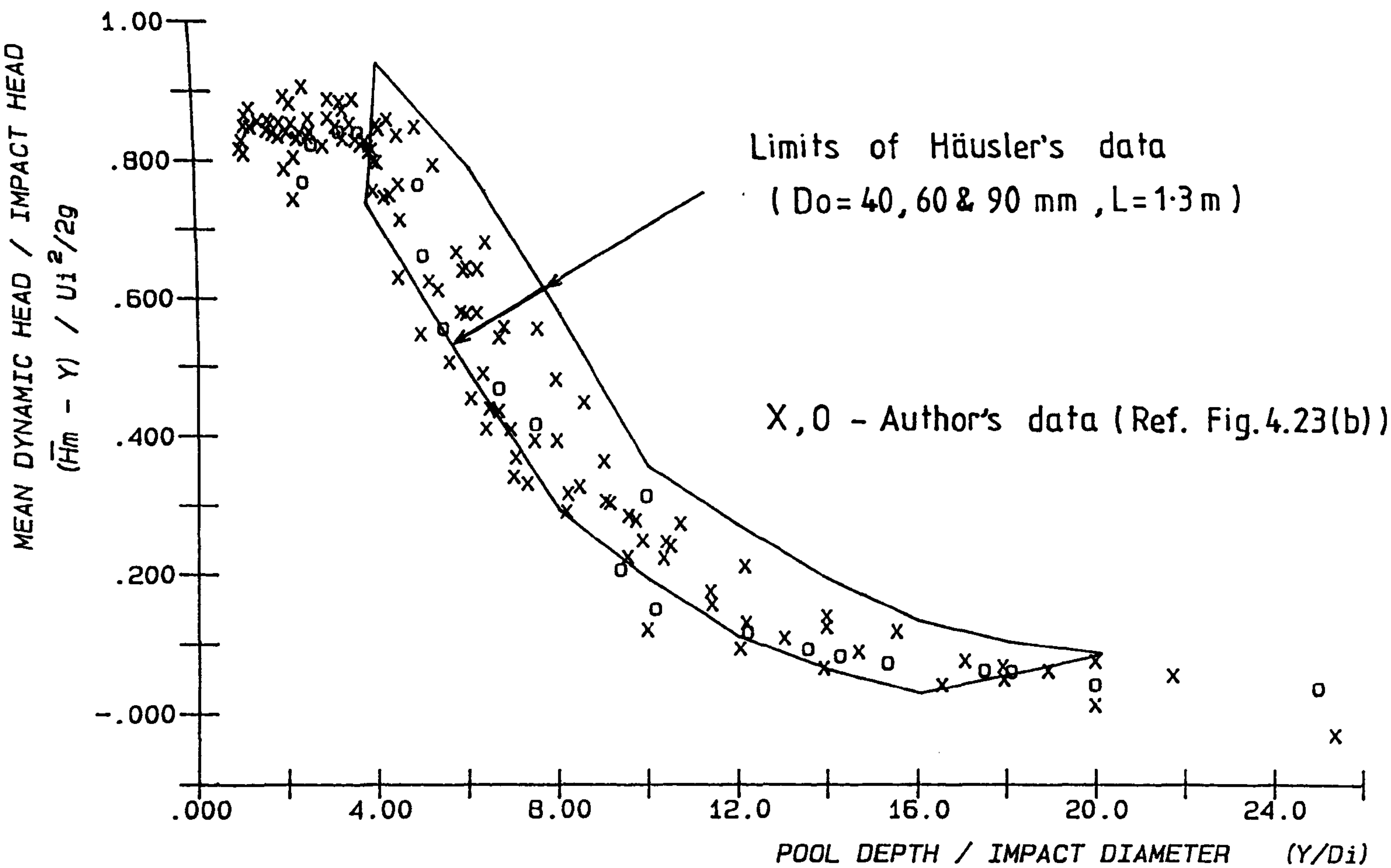

Fig. 6·22 Comparison of centre line mean dynamic pressure head results with Häusler's data.

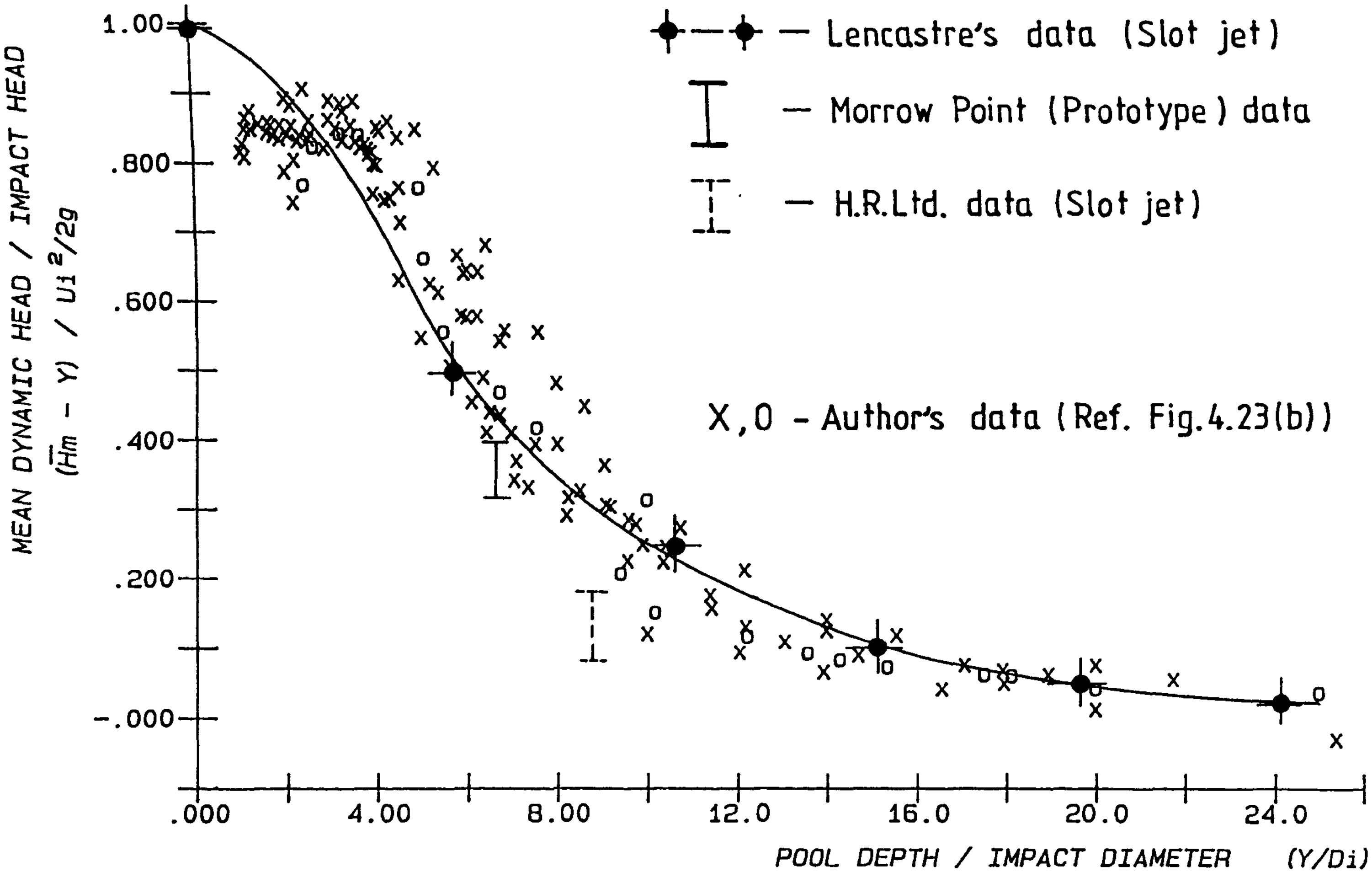

Fig. 6·23 Comparison of centre line mean dynamic pressure head results with Lencastre's data etc.

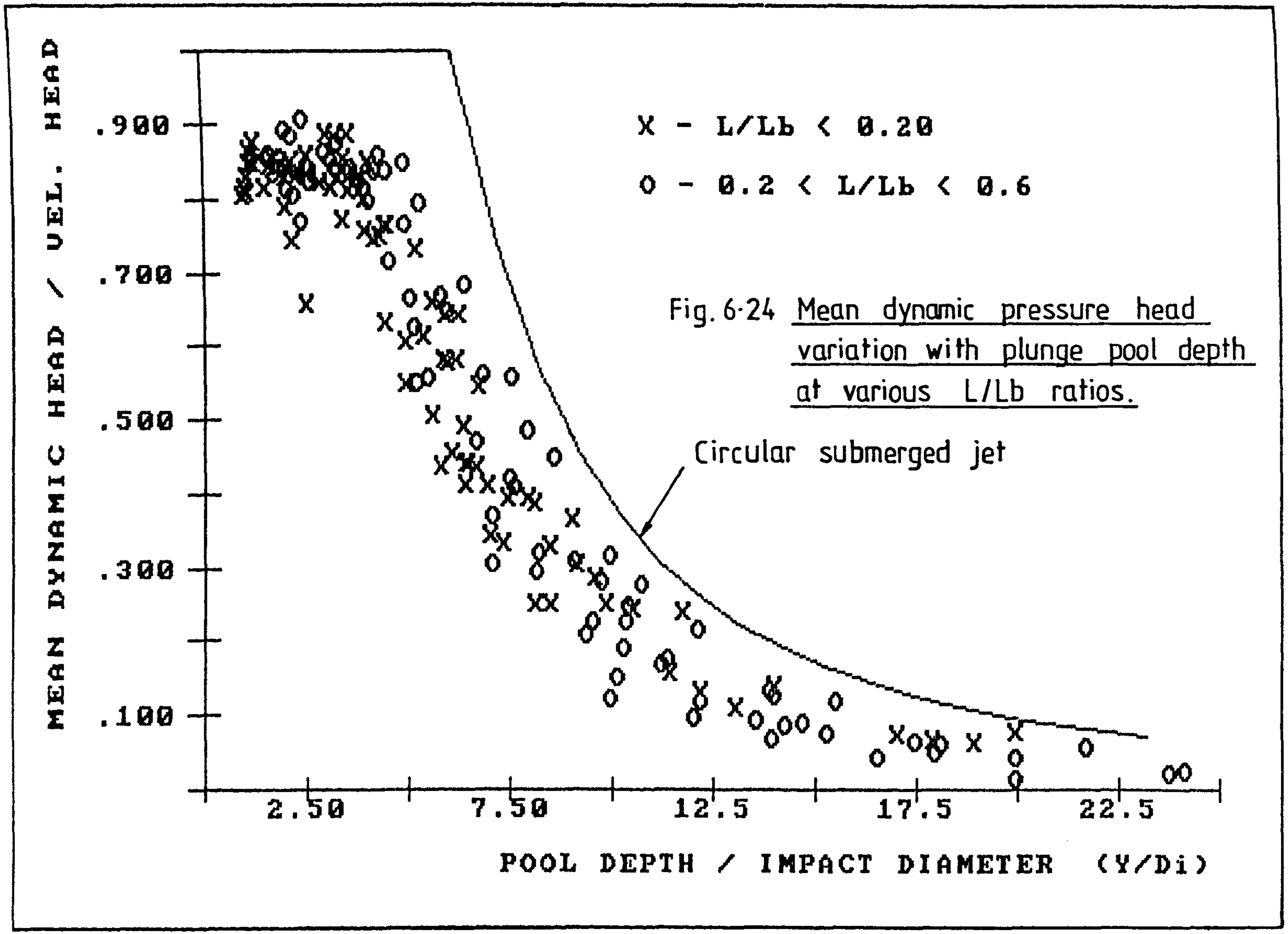

Fig. 6·24 Mean dynamic pressure head variation with plunge pool depth at various L/Lb ratios.

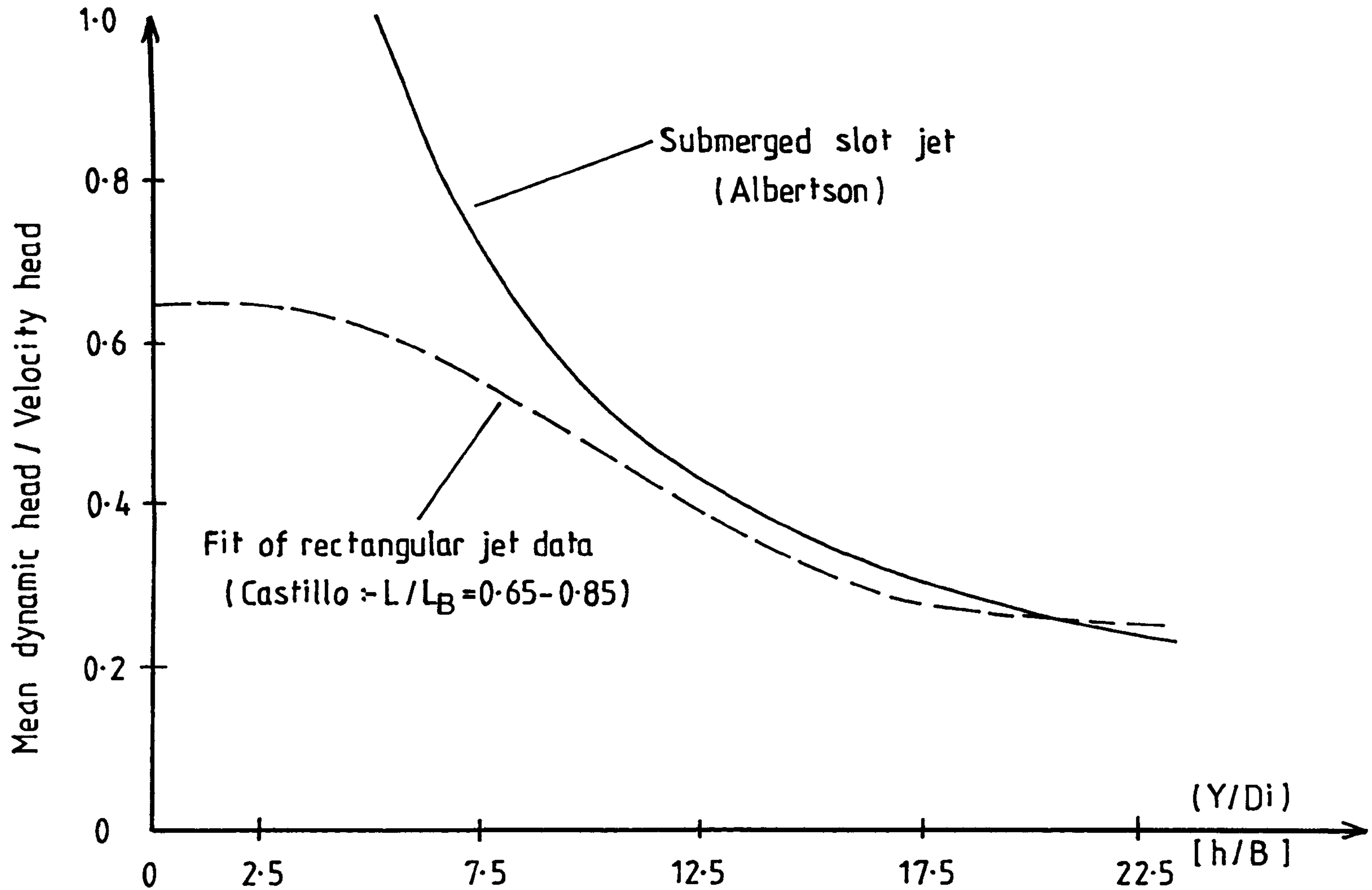

· Fig. 6·25 Comparison of mean dynamic head for rectangular jet (L/L_B = 0·65 – 0·85) with submerged slot jet case.

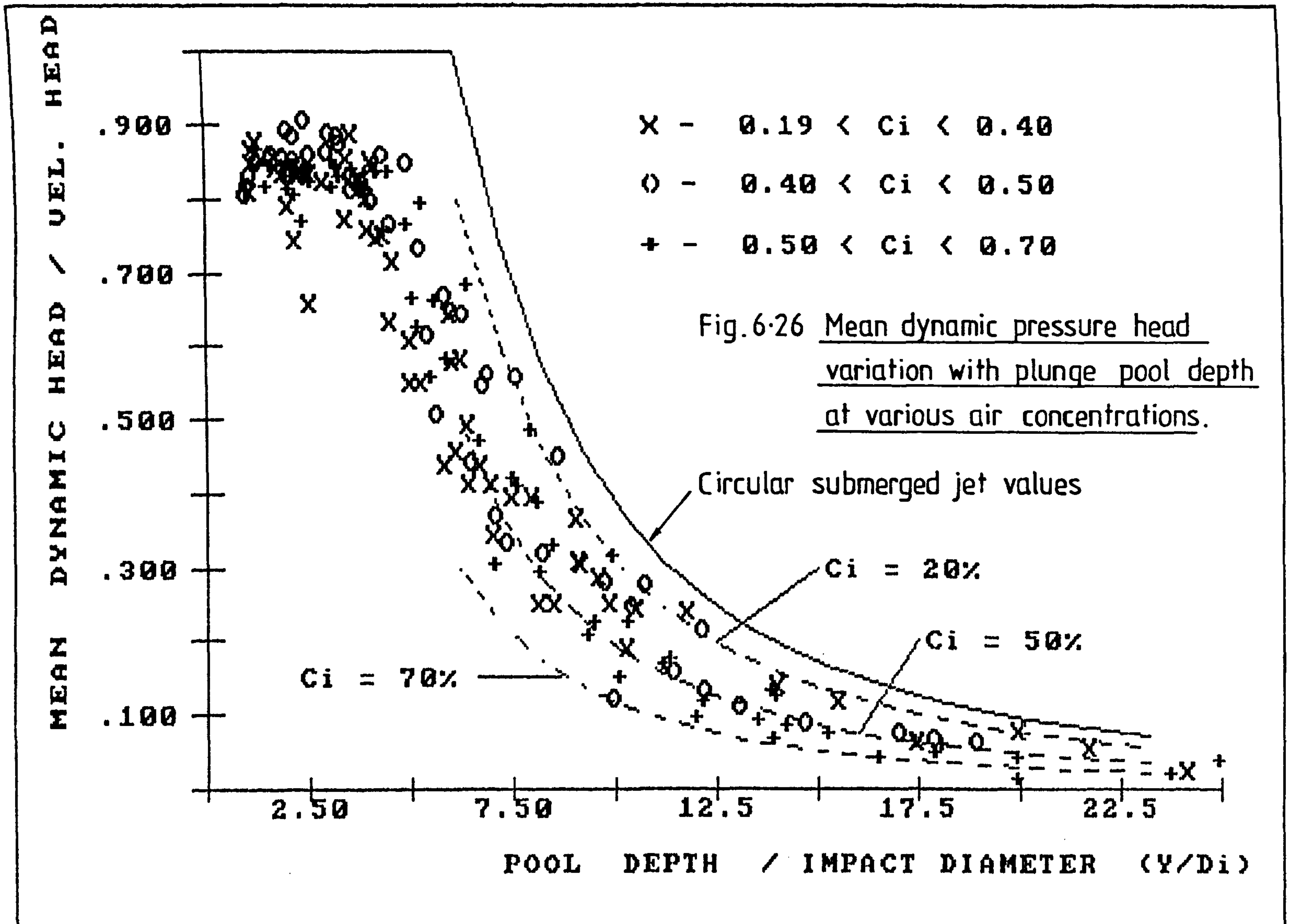

Fig. 6·26 Mean dynamic pressure head variation with plunge pool depth at various air concentrations.

FIGURES FOR CHAPTER 7

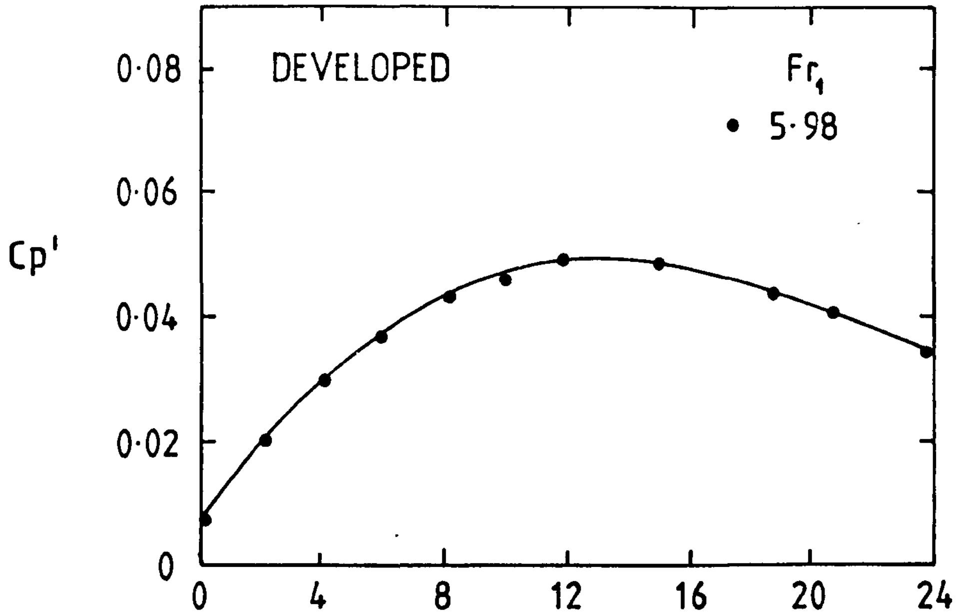

Fig. 7·1 RMS pressure fluctuation (Cp') versus position in the hydraulic jump [Toso].

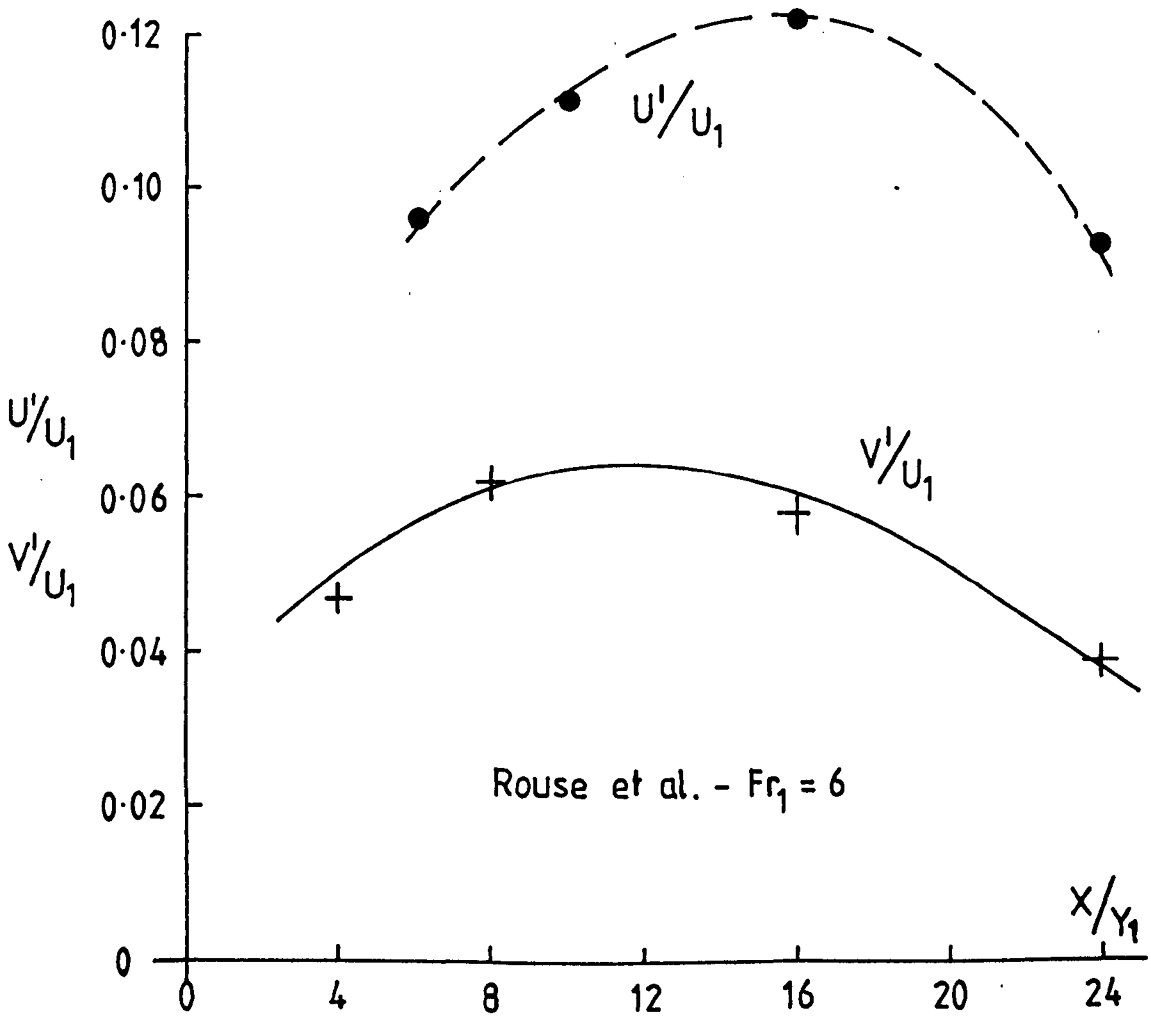

Fig. 7·2 Components of turbulent velocity in hydraulic jump [Rouse]

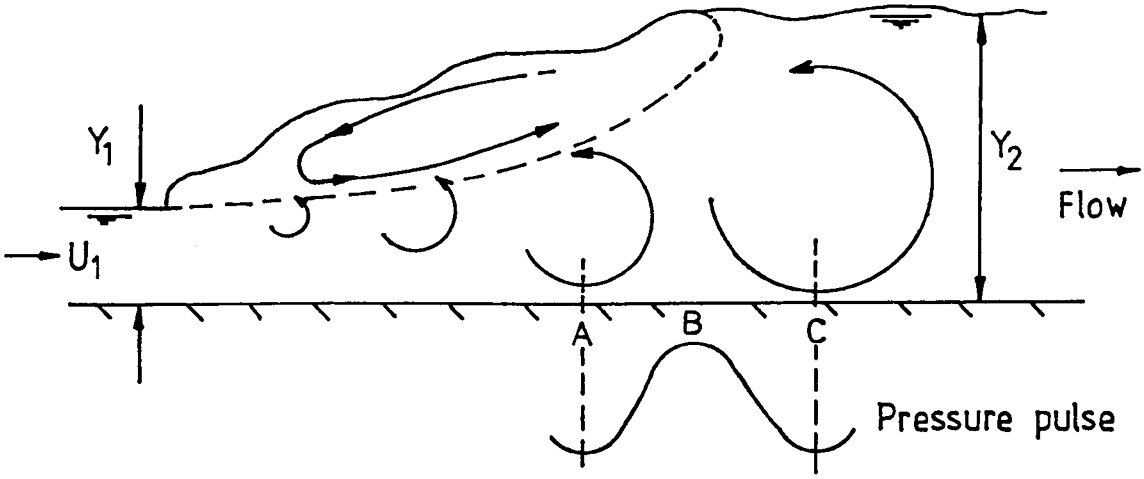

Fig.7·3 Large scale flow structures in the hydraulic jump.

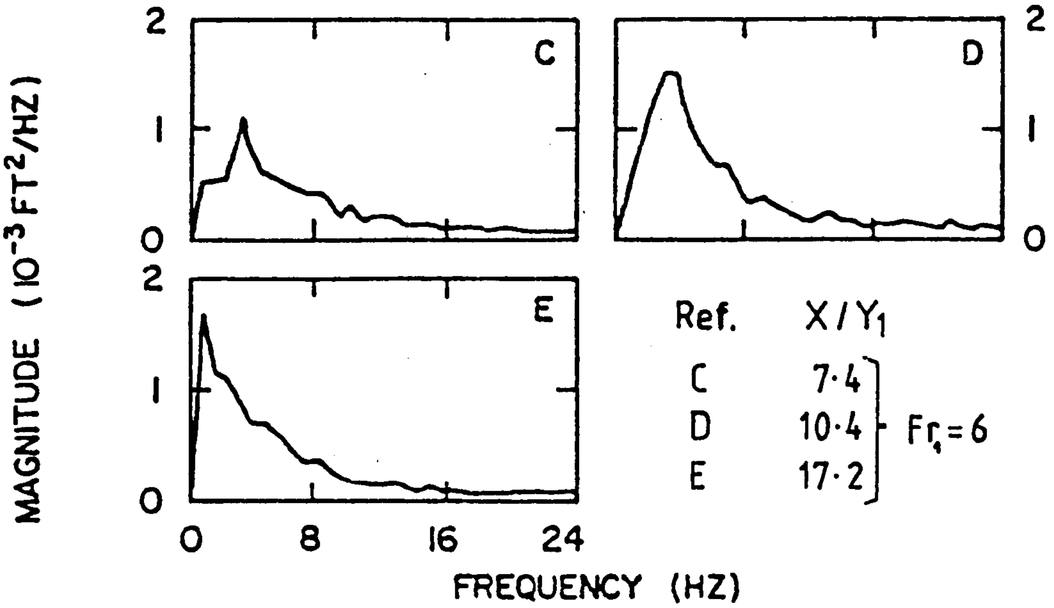

Fig.7·4 Power Spectra versus location in hydraulic jump. [Toso]

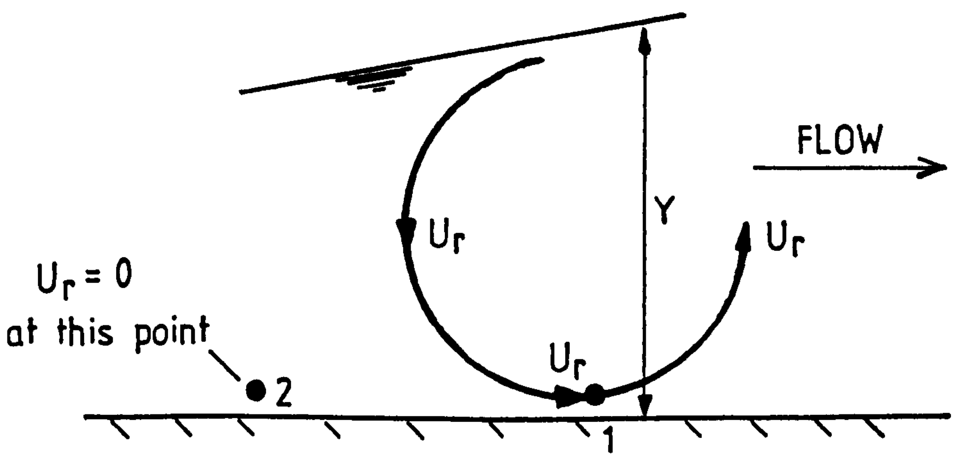

Fig.7·5 Recirculation Velocity (U_r).

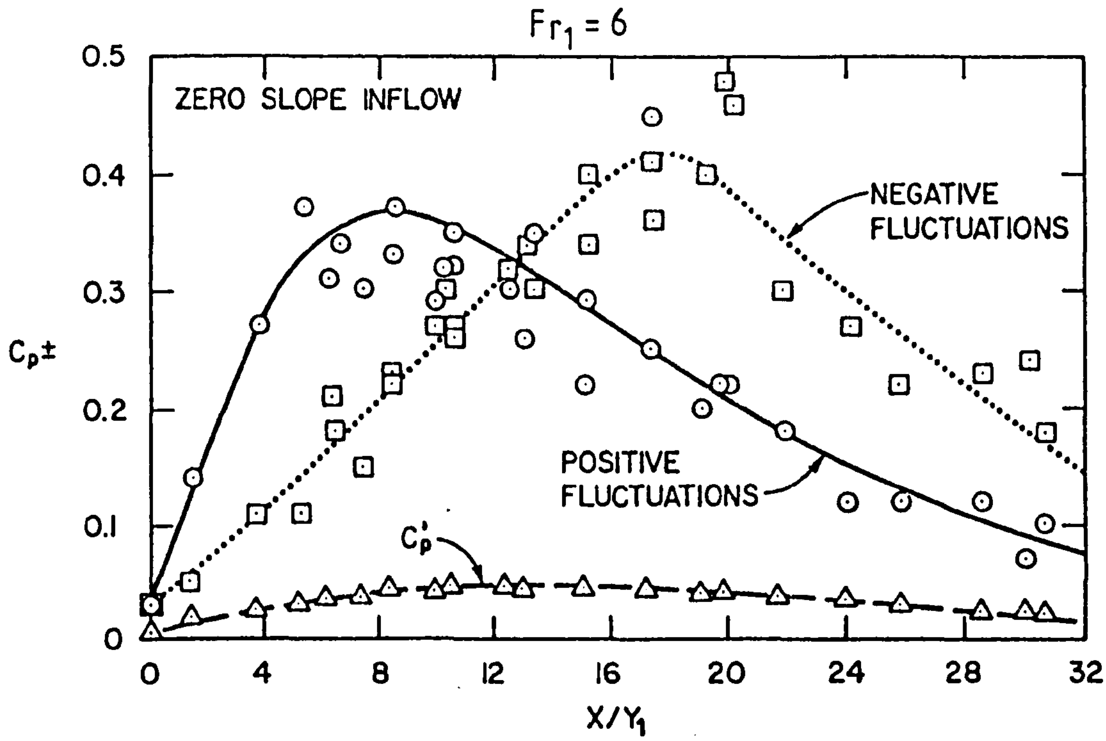

Fig.7·6 Maximum pressure fluctuations beneath hydraulic jump. [Toso]

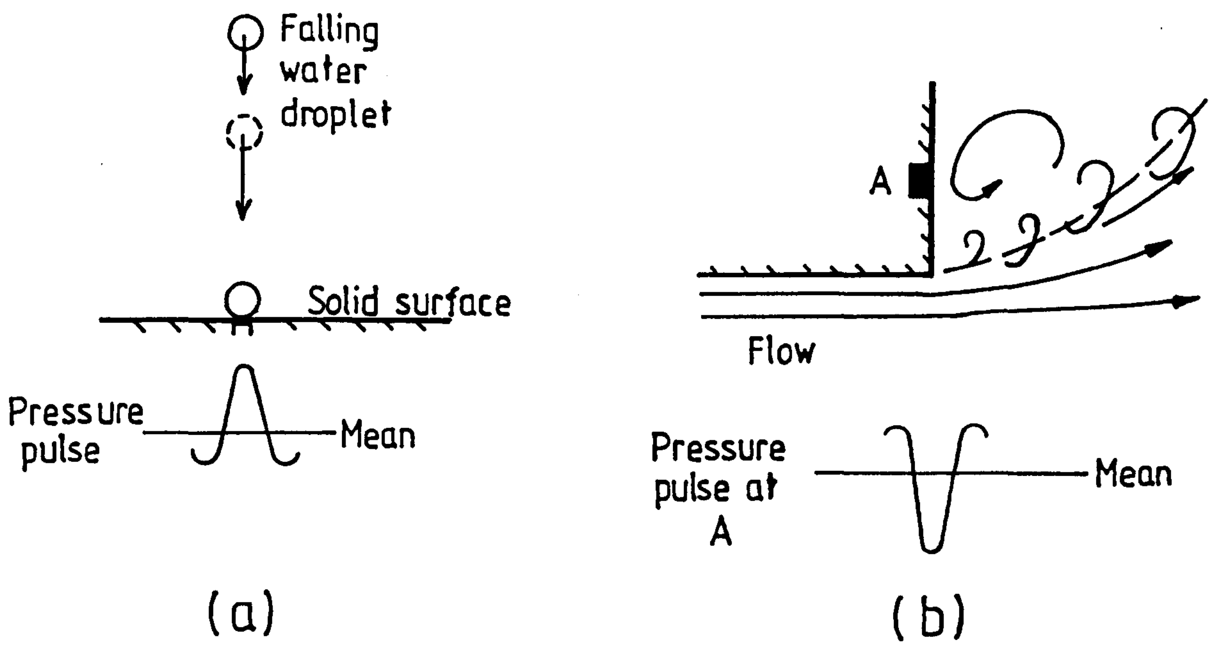

Fig.7·7 Situations for cause of pressure fluctuations.

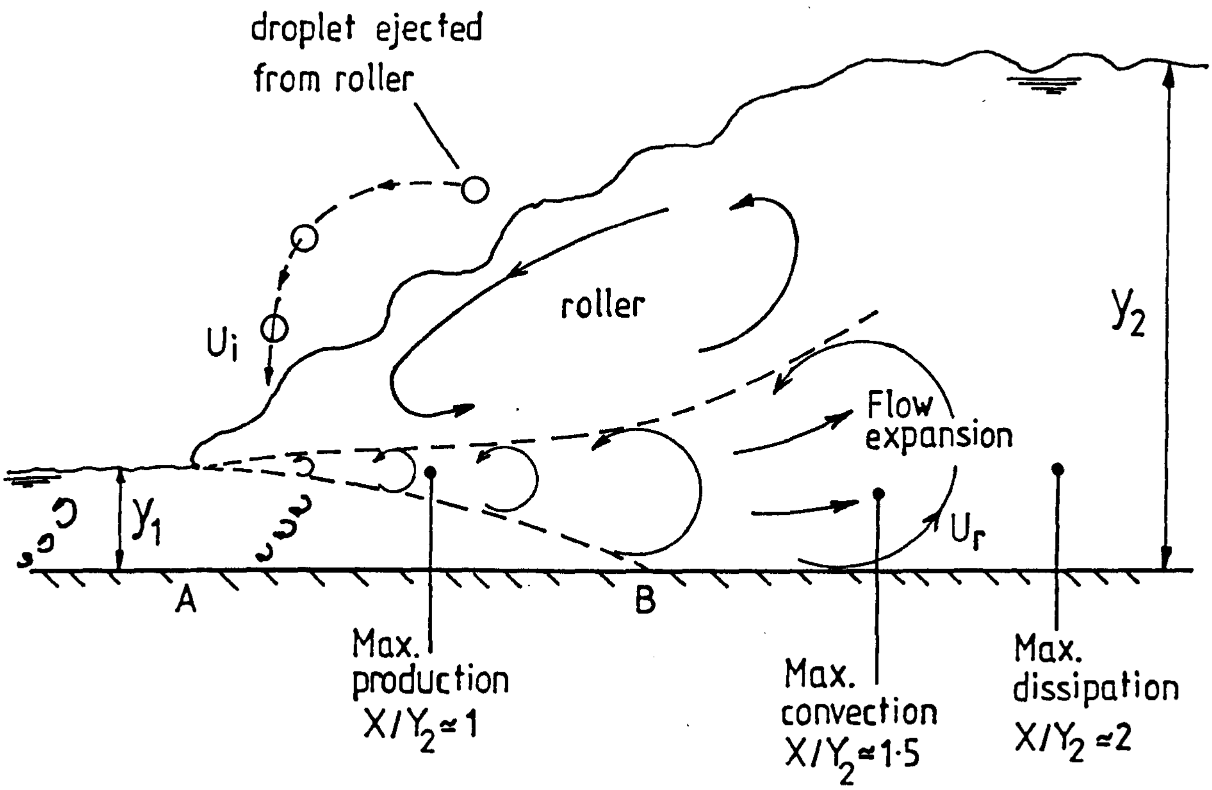

Fig.7·8 Mechanisms for fluctuations in hydraulic jumps.

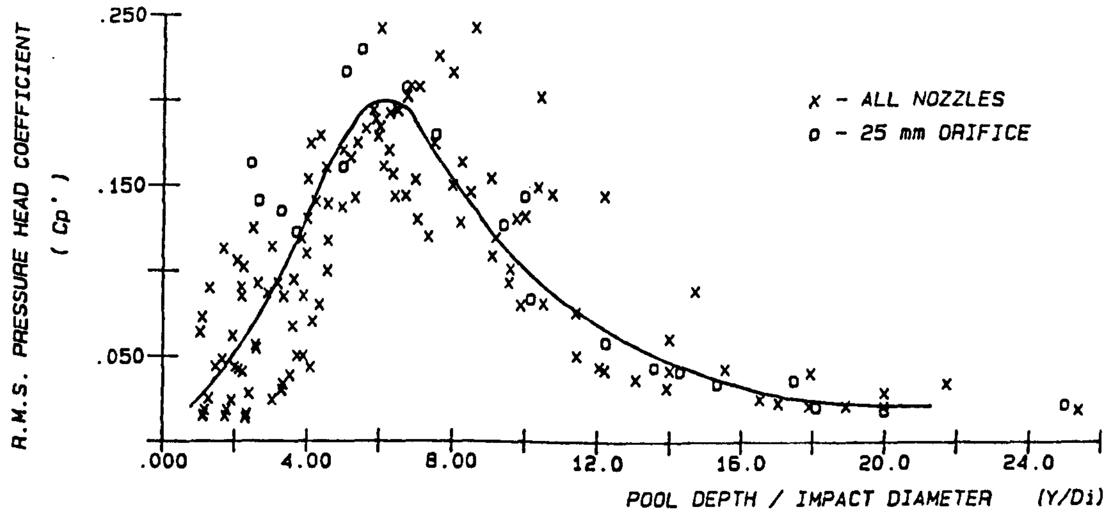

Fig. 7·9 Mean value of jet centre line r.m.s. pressure fluctuations.

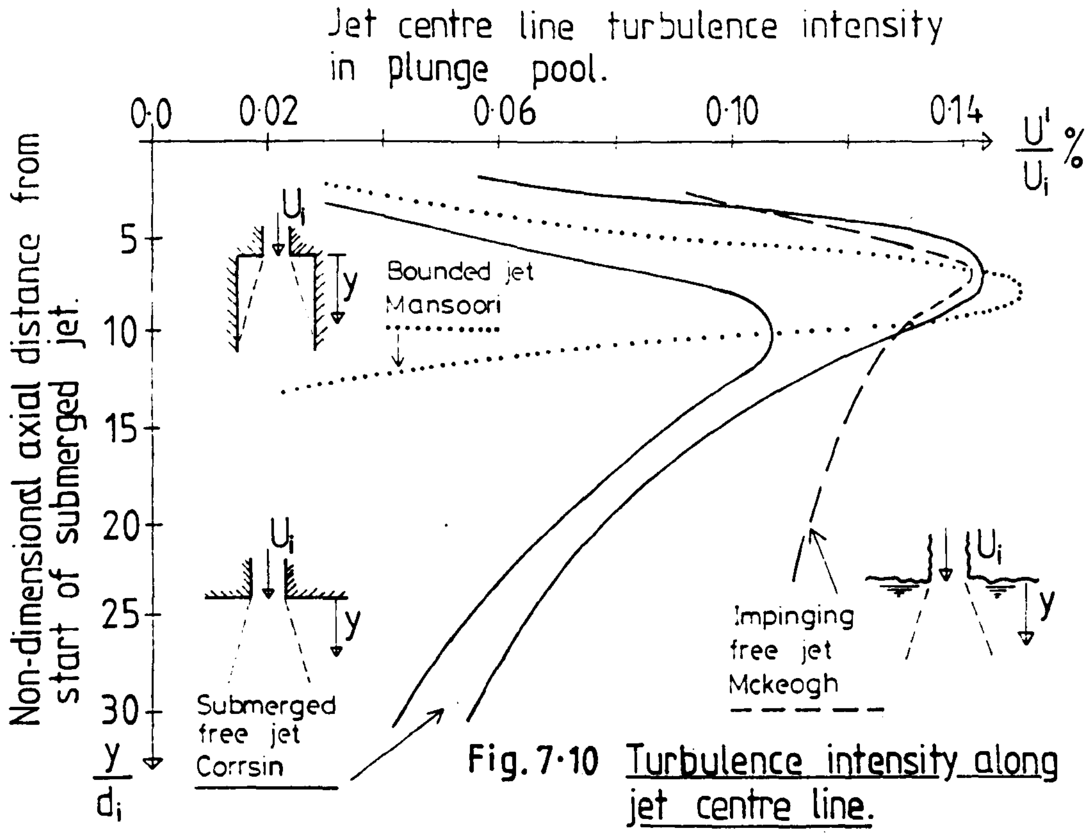

Fig. 7·10 Turbulence intensity along jet centre line.

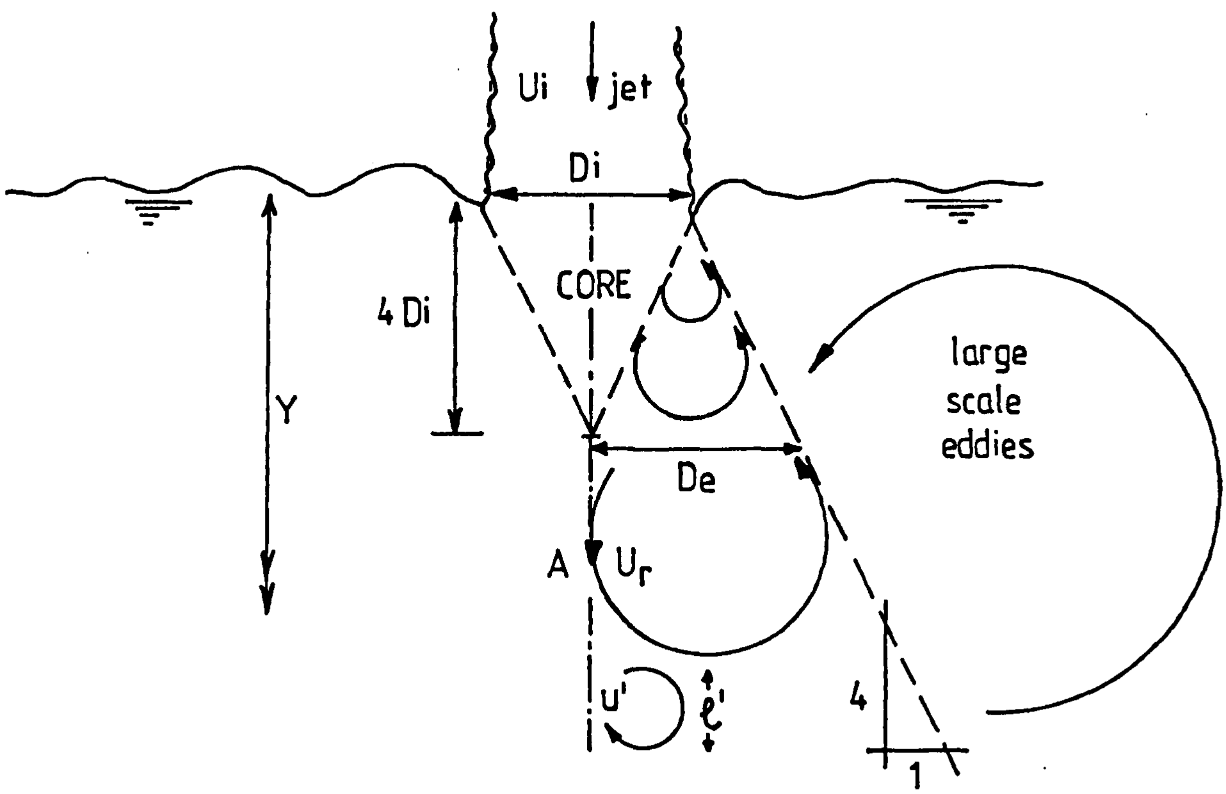

Fig. 7·11 Vortex structures in plunge pool.

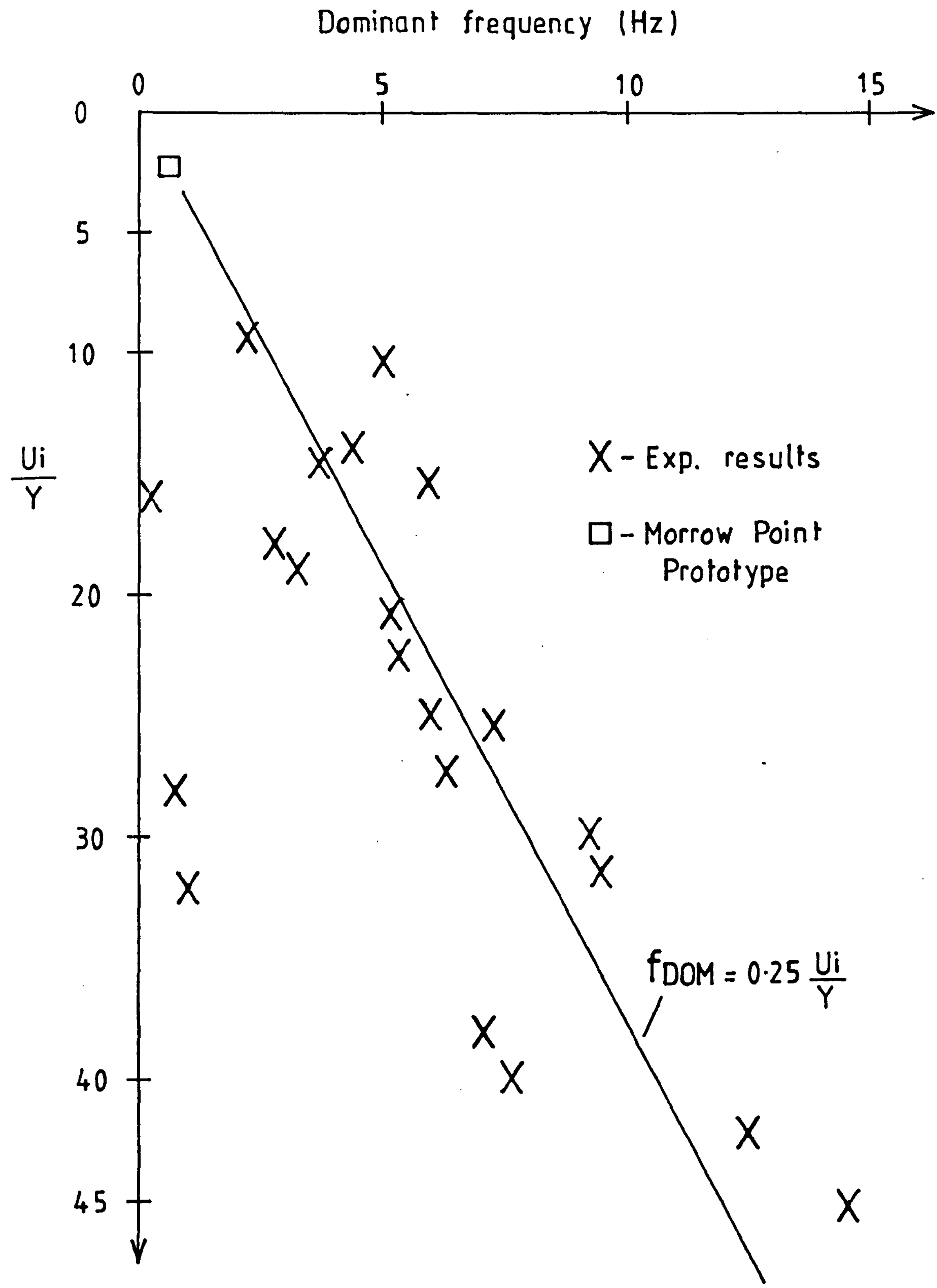

Fig. 7·12 Relation of dominant frequency with Ui/Y

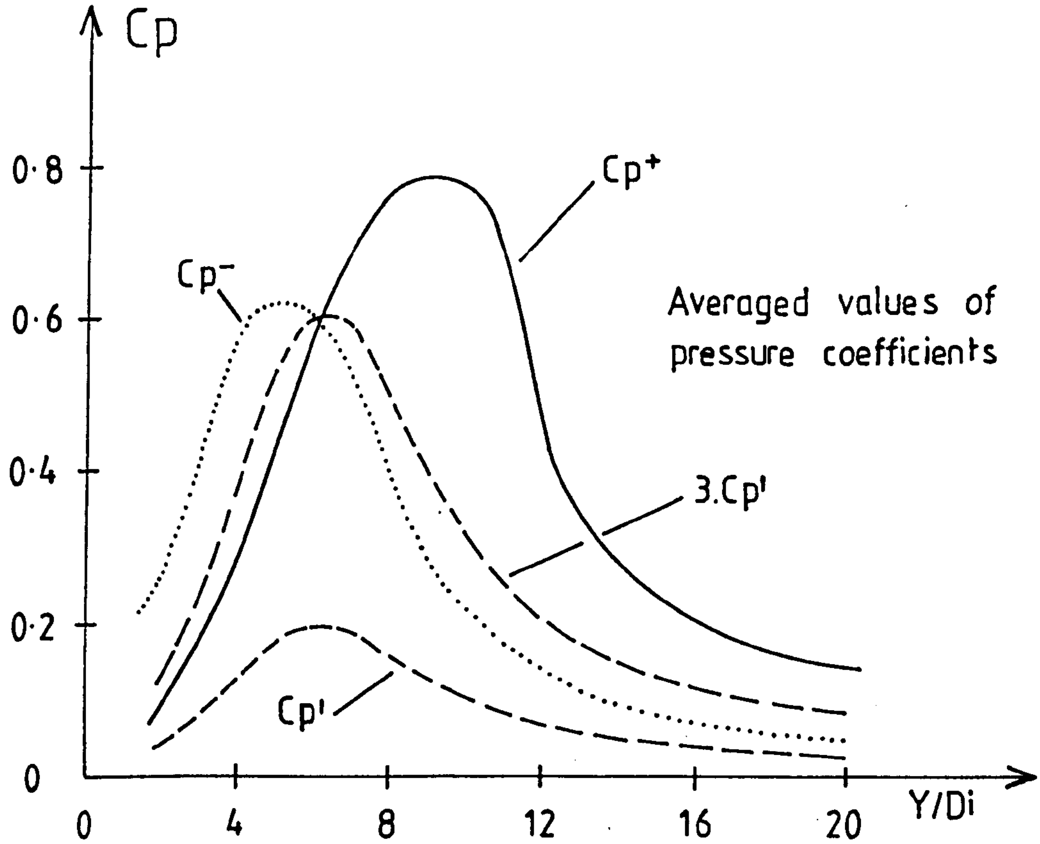

Fig.7·13 Comparison of maximum and minimum instantaneous fluctuations in plunge pool with Cp'.

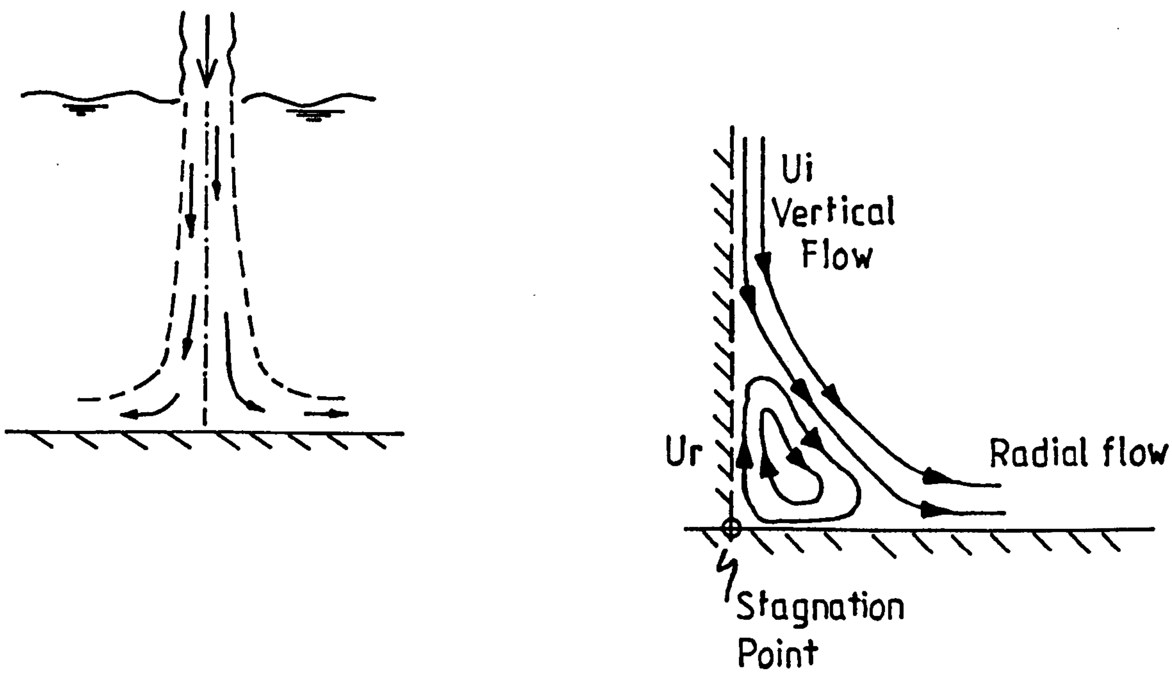

Fig.7·14 Recirculating eddy at boundary.

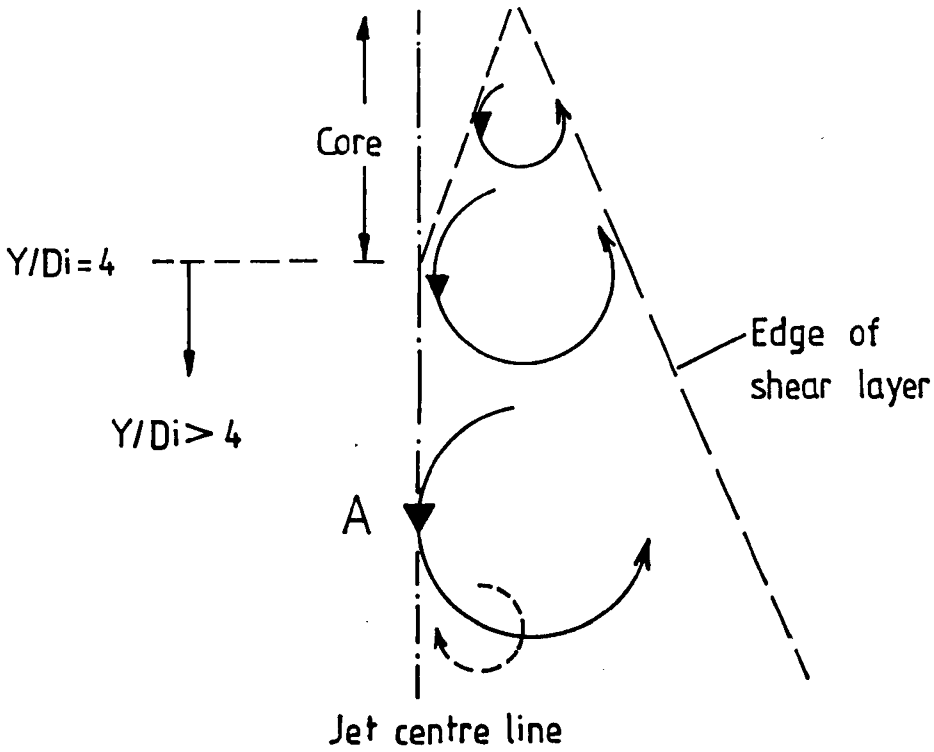

Fig.7·15 Predominant anti-clockwise eddies in plunge pool.

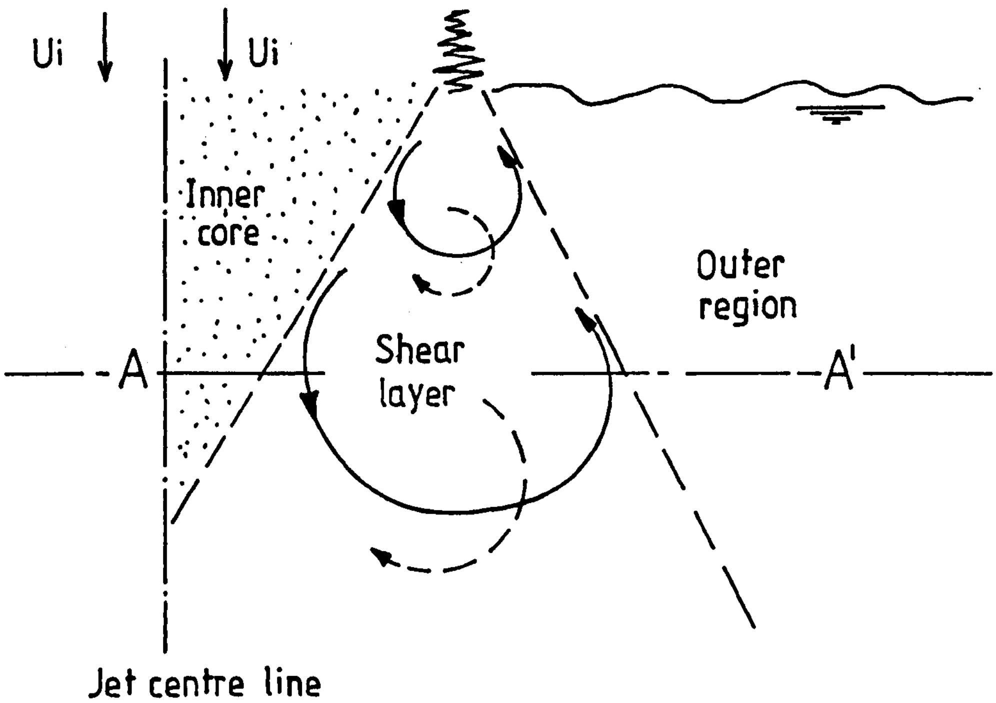

Fig.7·16 Likely flow structures in plunge pool.

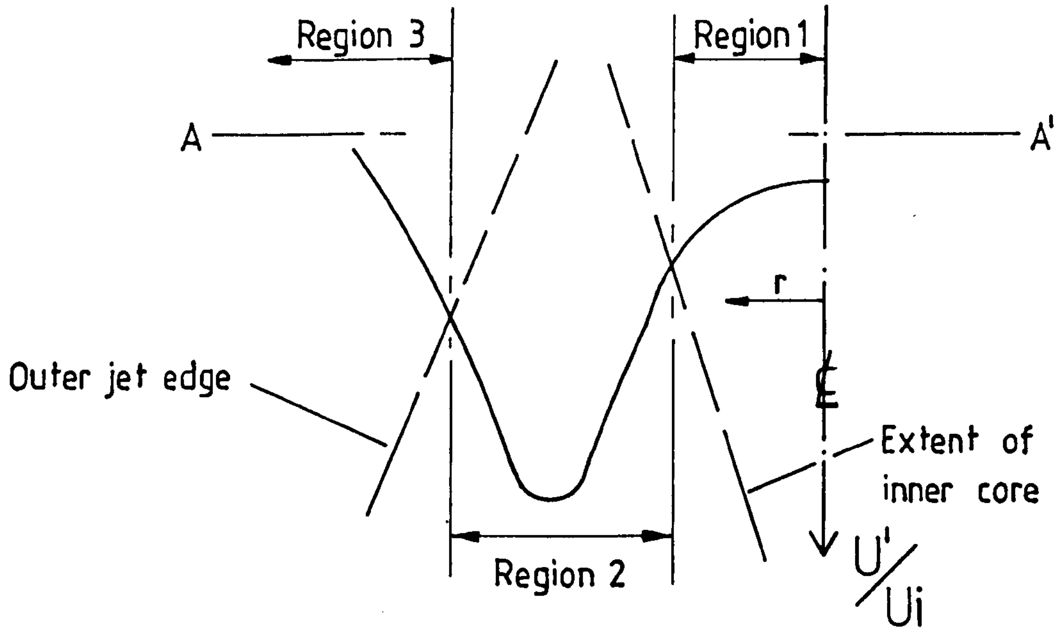

Fig. 7·17 Radial distribution of axial turbulence intensity

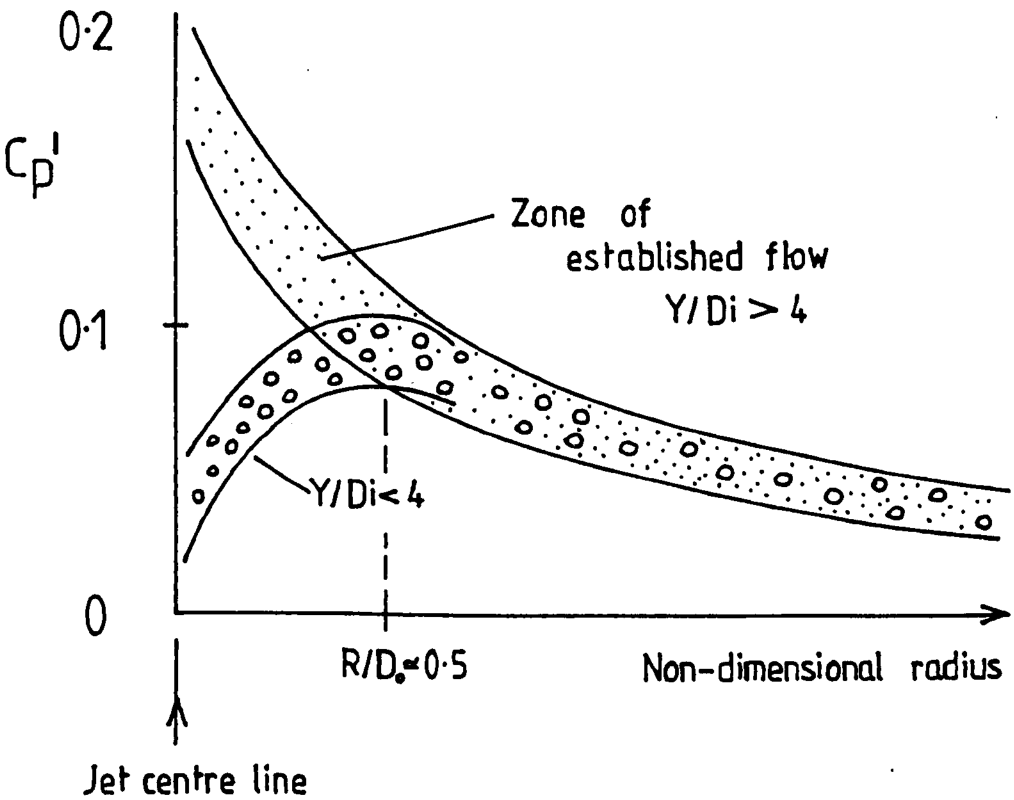

Fig. 7·18 Radial pattern of pressure head fluctuations.

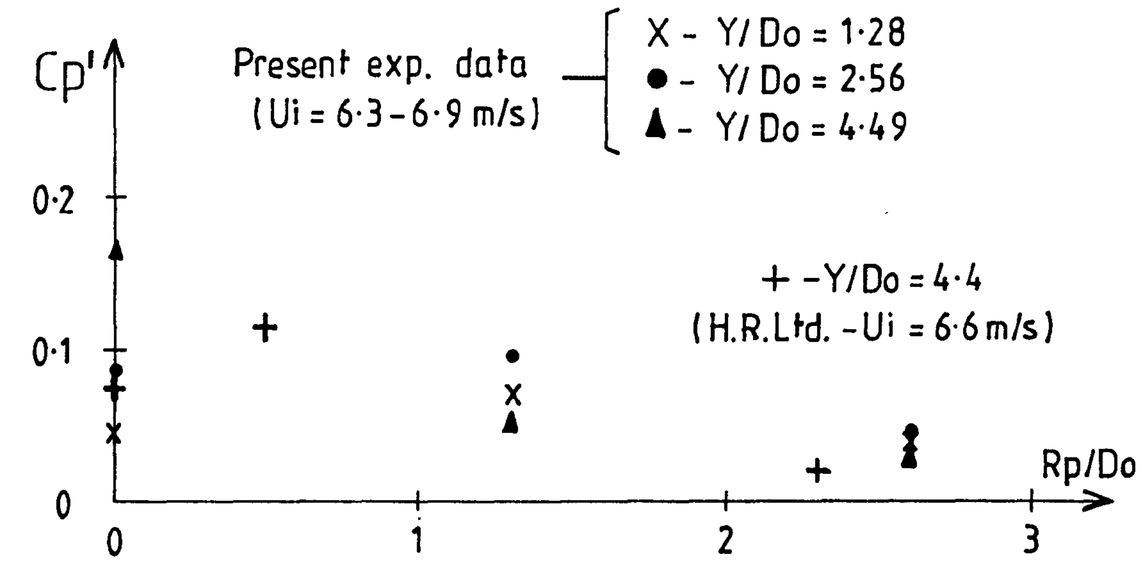

Fig. 7·19 Comparison of radial distribution of Cp' with H.R.Ltd. data

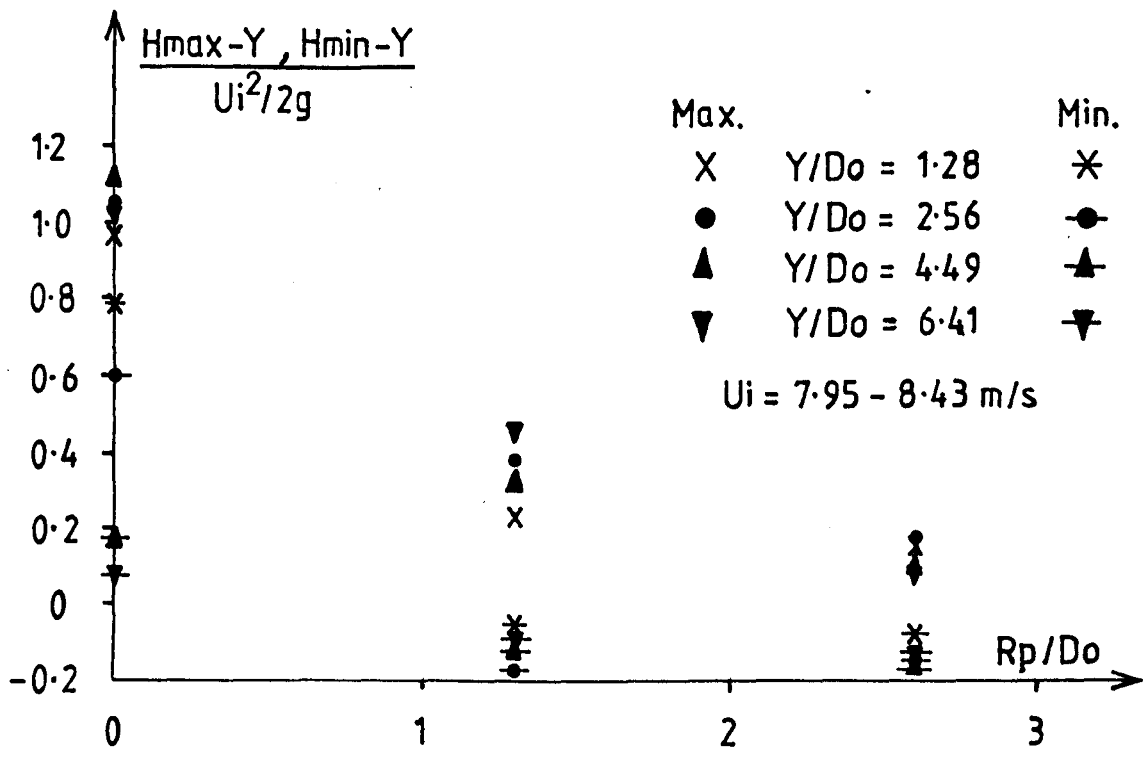

Fig. 7·20 Distribution of dynamic peak and minimum head at plunge pool floor.

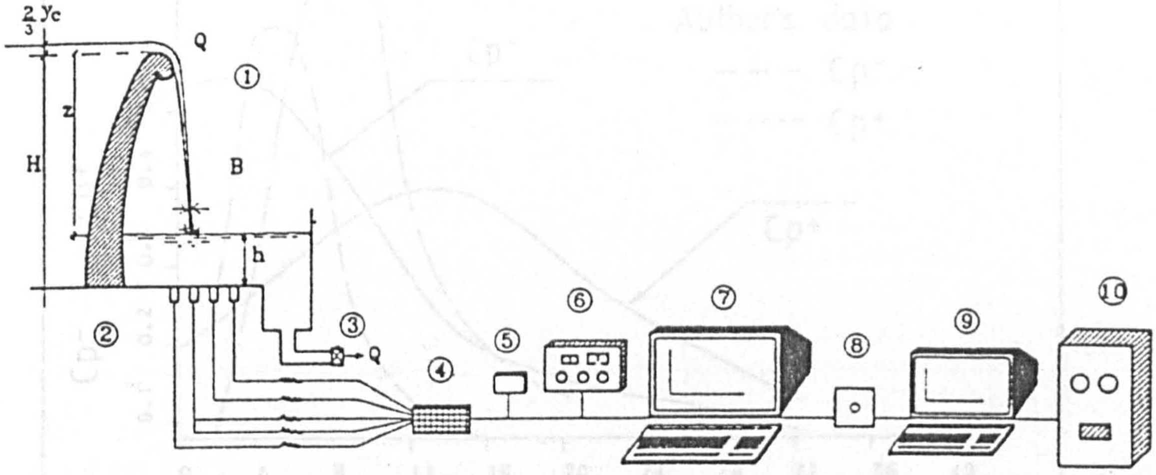

Fig. 7·21 Experimental set-up and acquisition system [Castillo].

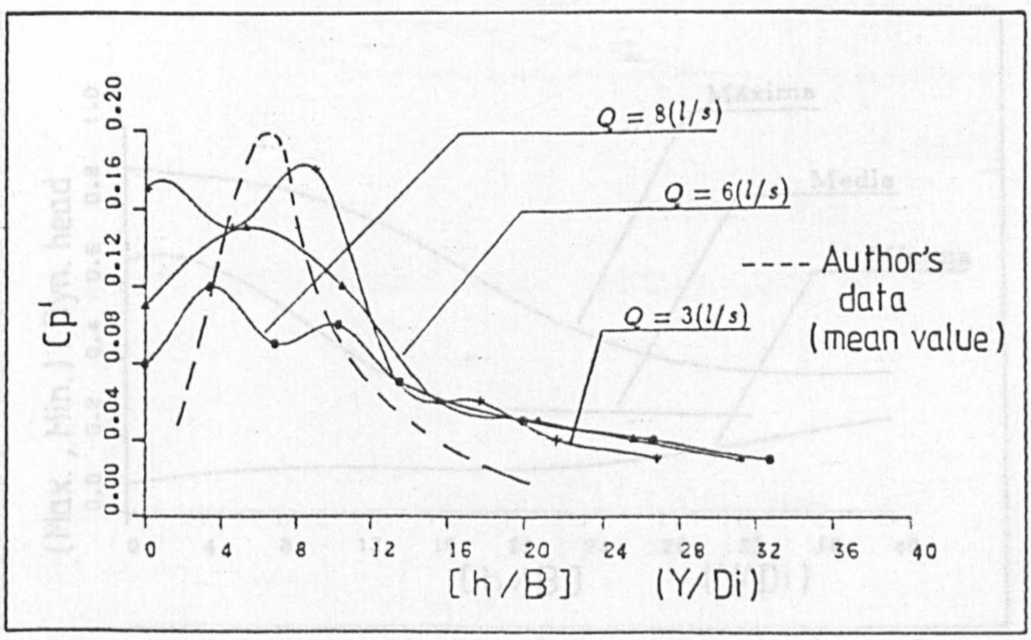

Fig. 7·22 Variation of Cp' with pool depth [Castillo].

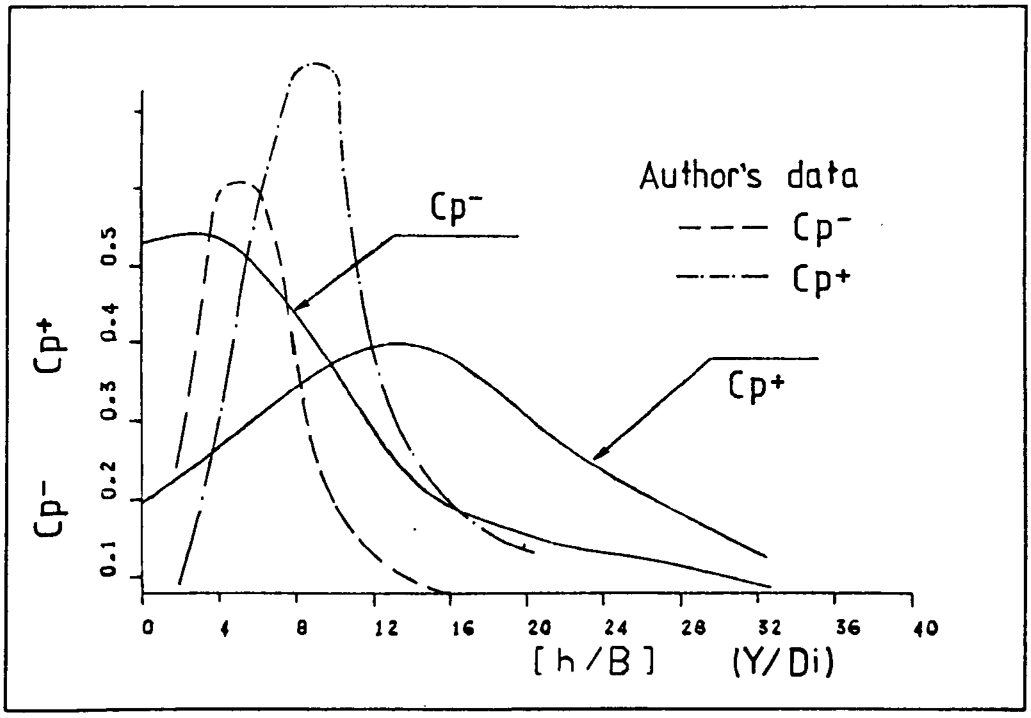

Fig.7·23 Variation of Cp^+ and Cp^- with pool depth [Castillo].

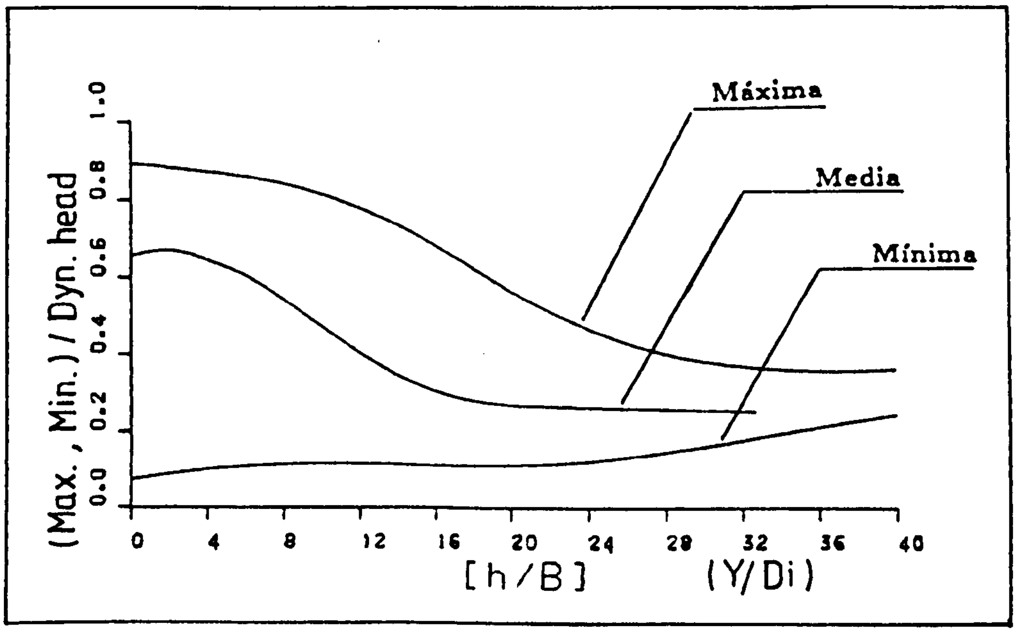

Fig.7·24 Maximum, minimum and mean dynamic pressure envelope. [Castillo]

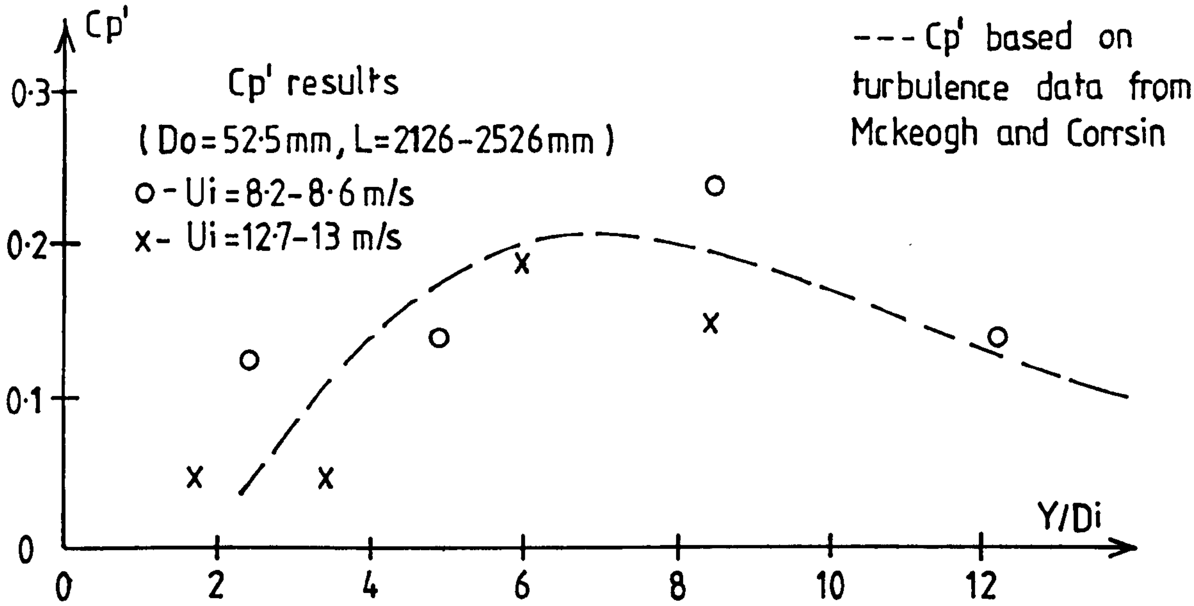

Fig.7·25 Comparison of centre line Cp' results with values computed from jet turbulence data.

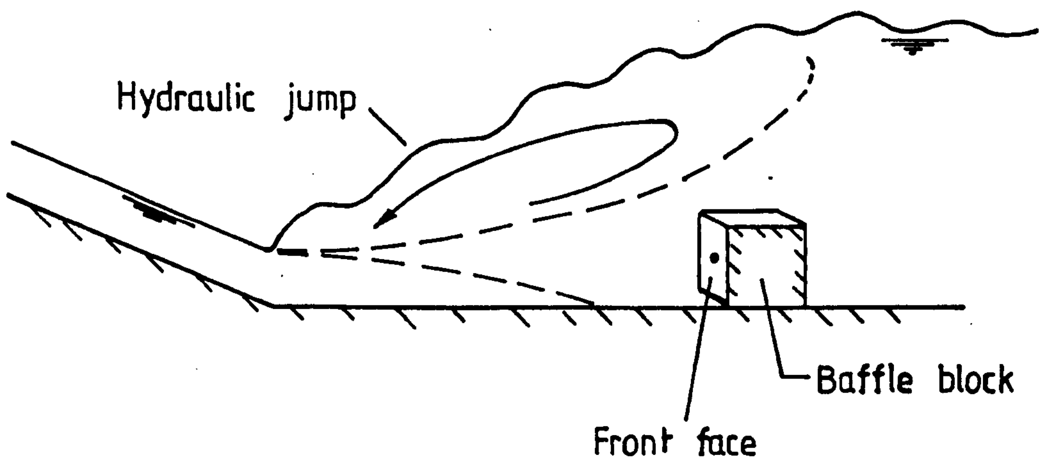

Fig.7·26 Baffle block within hydraulic jump.

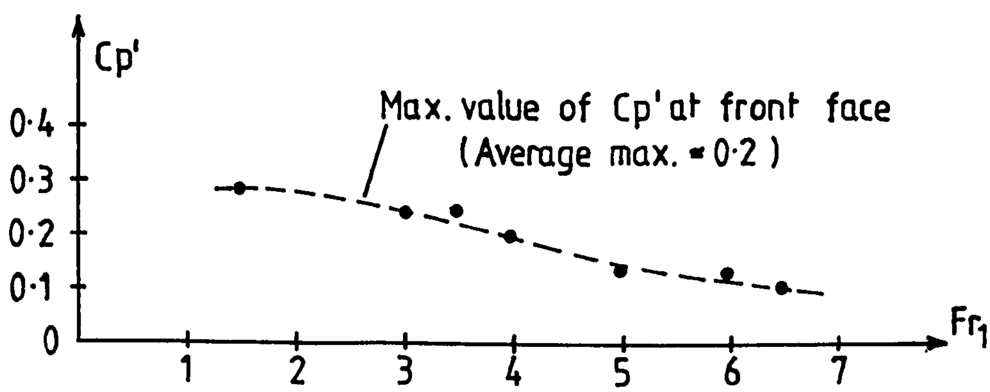

Fig.7·27 Cp' values at front face of baffle block

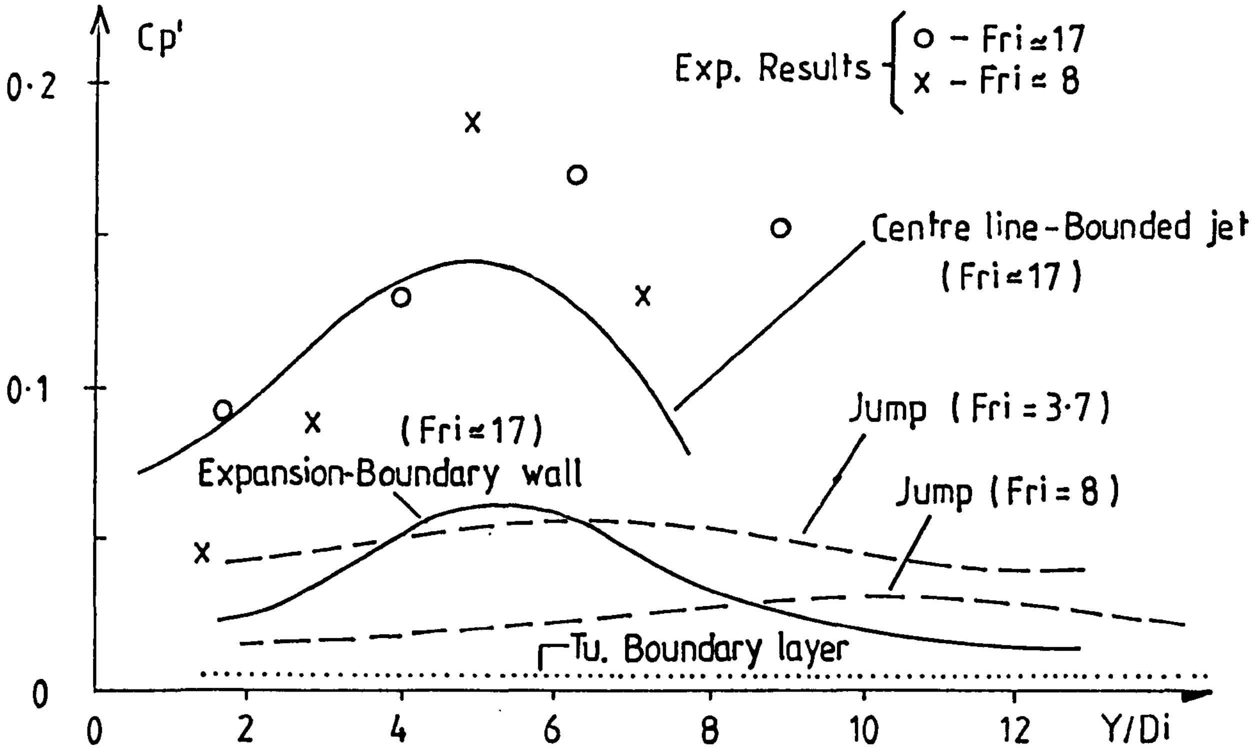

Fig. 7·28 Comparison of centre line Cp' results with values obtained at other hydraulic structures.

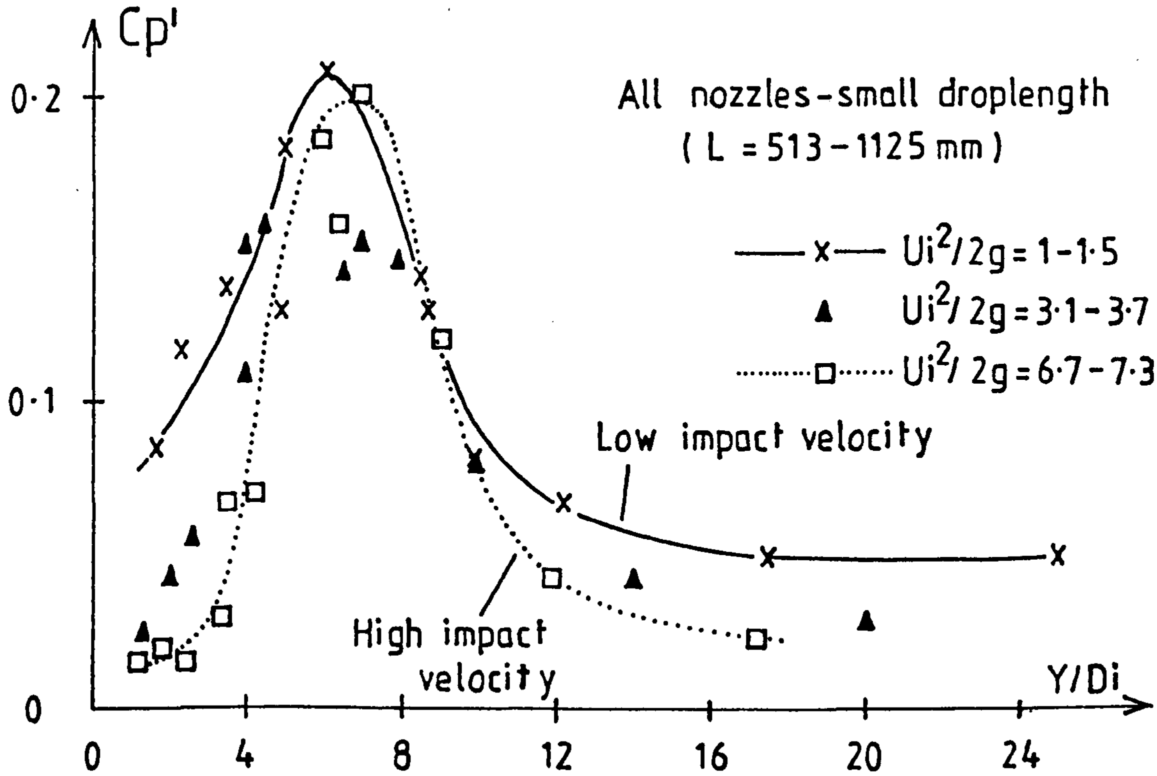

Fig. 7·29 Comparison of Cp' results at low droplength.

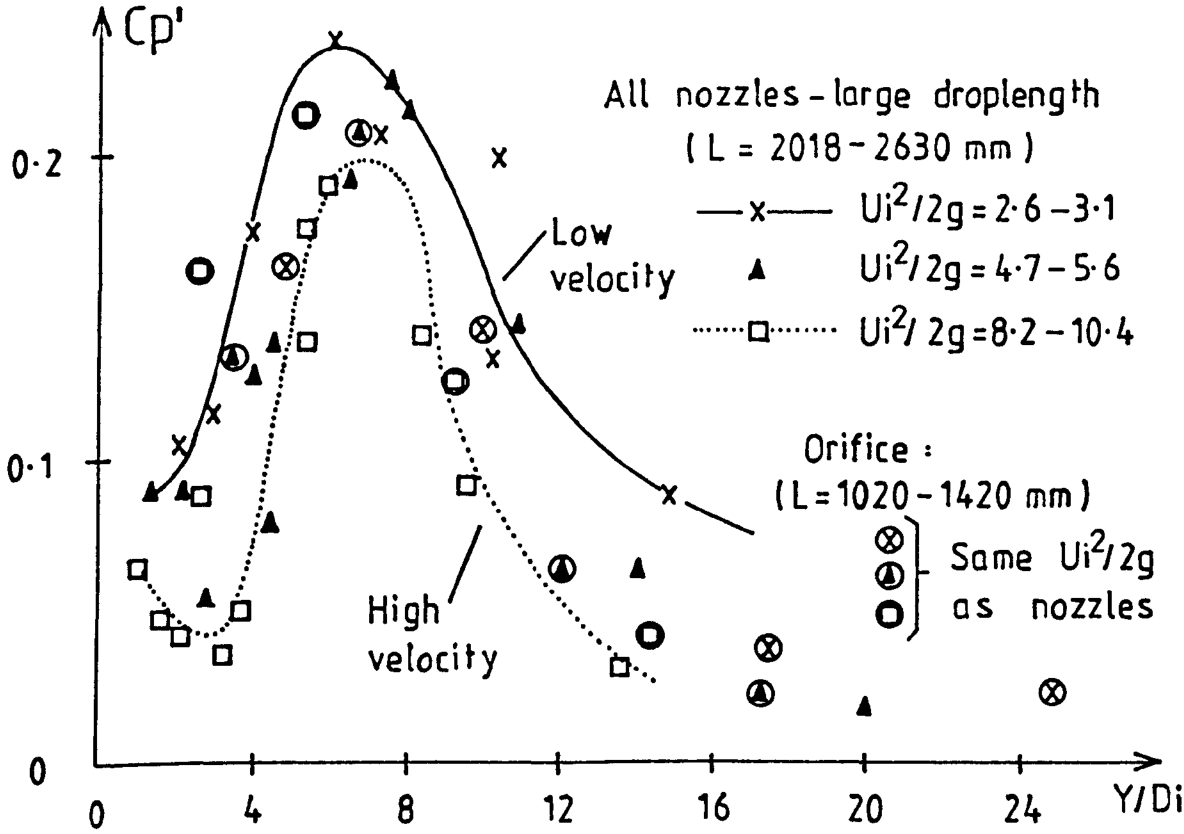

Fig. 7·30 Comparison of Cp' results at larger droplength.

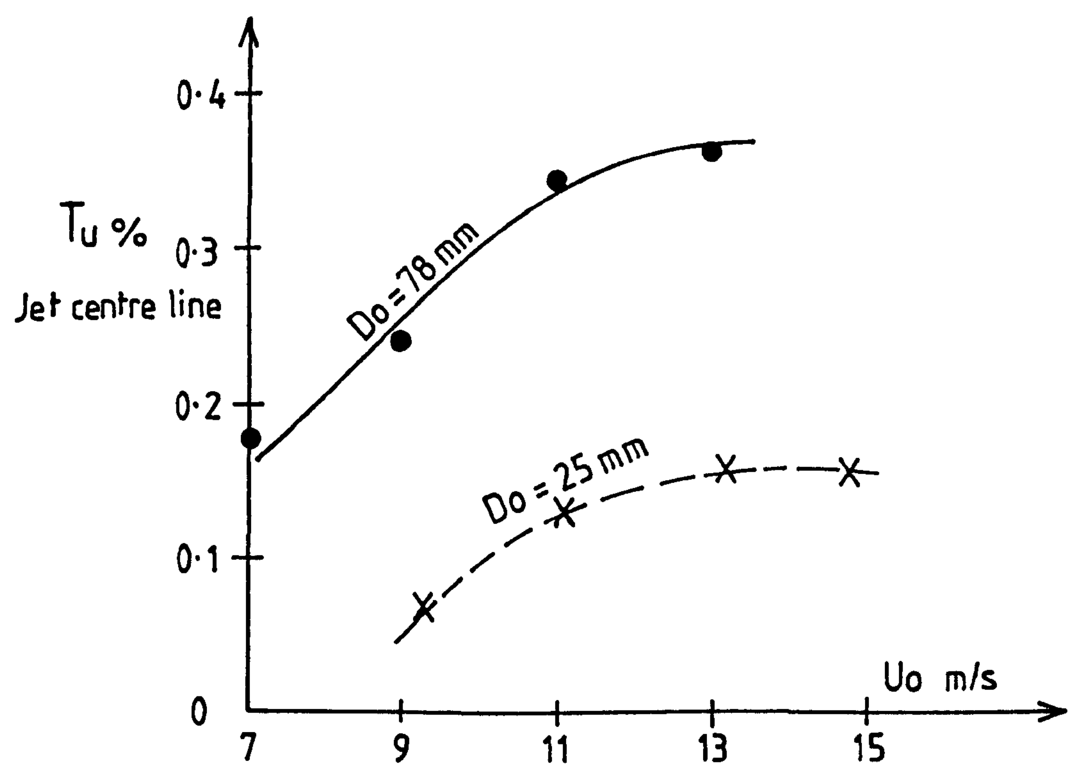

Fig. 7·31 (a) Jet centre line turbulence near nozzle outlet.

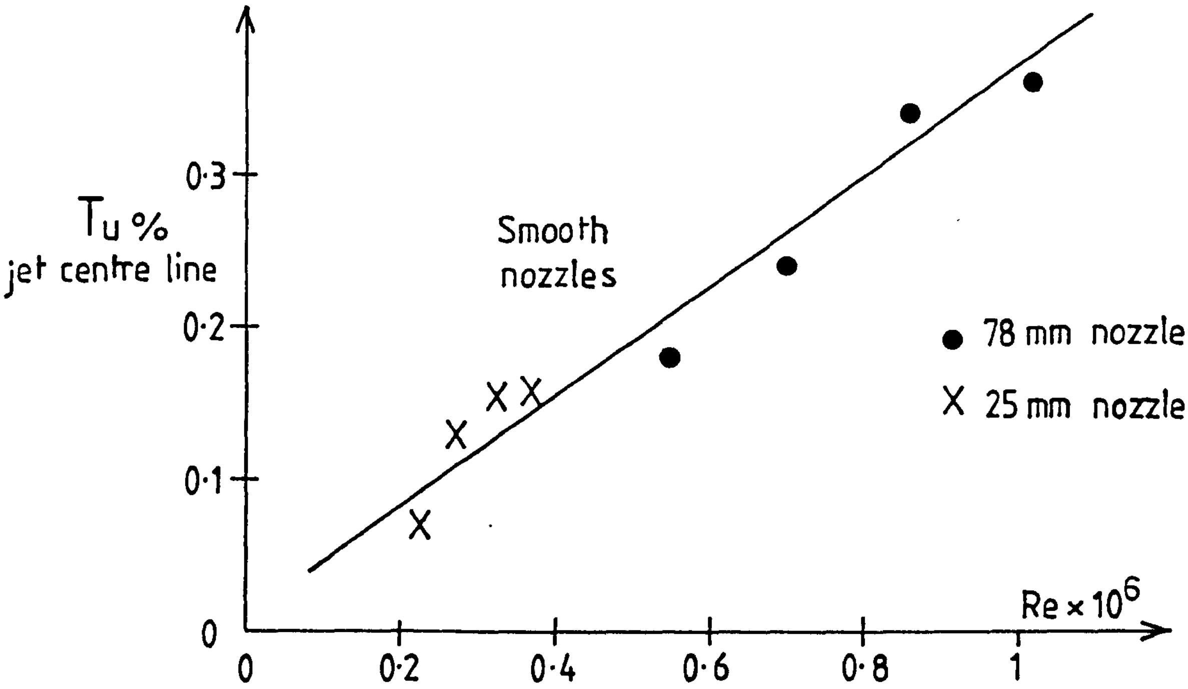

Fig.7·31 (b) Jet centre line turbulence near nozzle outlet.

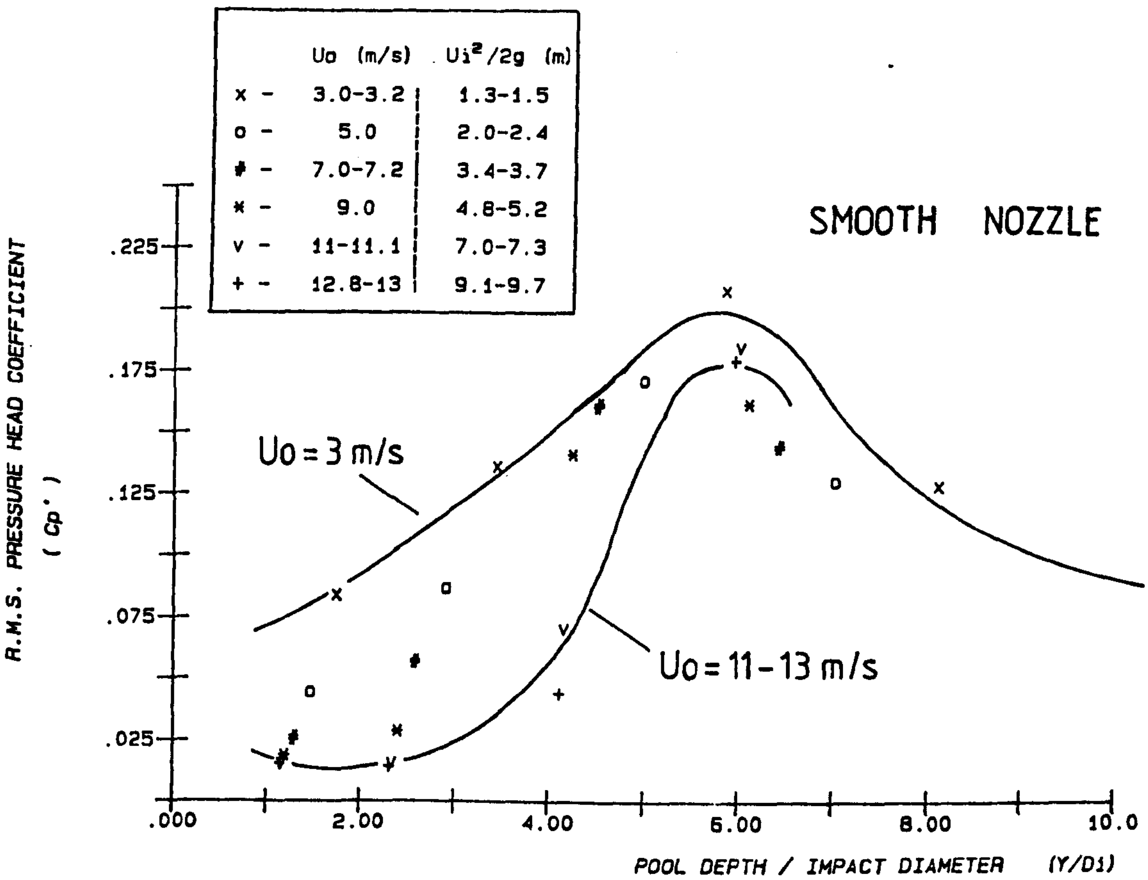

Fig.7·32 Cp' with Y/Di (Do=78 mm , L=725 - 1125 mm)

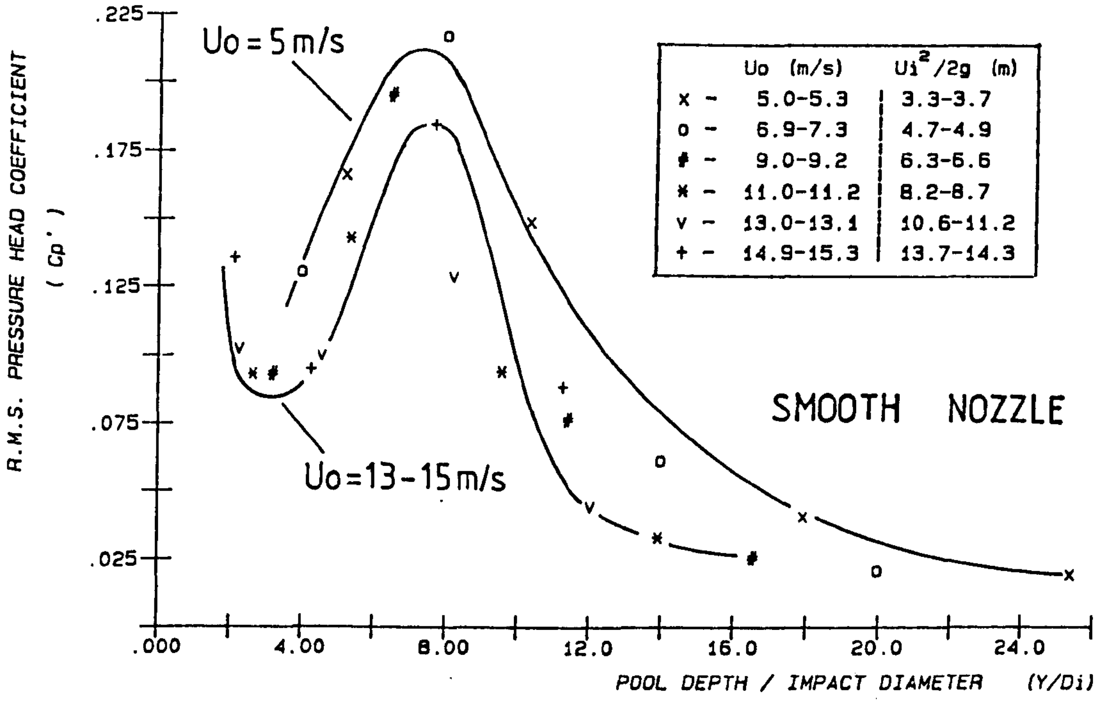

Fig.7·33 Cp' with Y/Di (Do= 25mm, L= 2018 - 2418 mm)

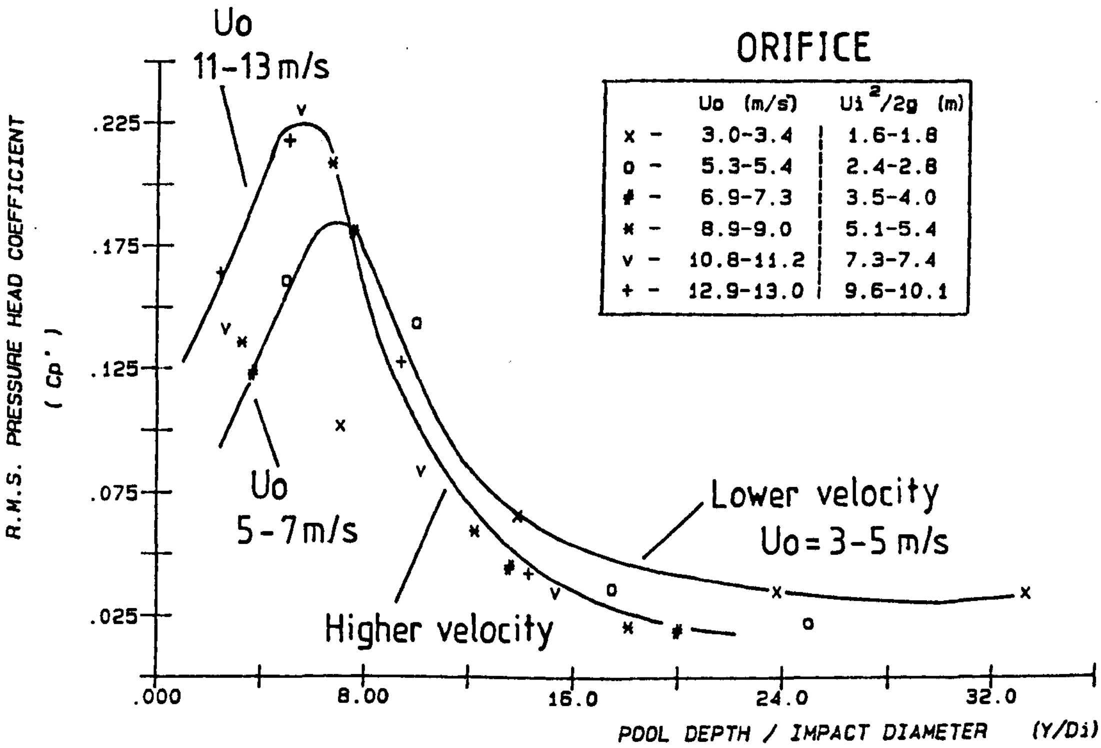

Fig.7·34 Cp' with Y/Di (Orifice: Do= 25mm, L=1020 - 1420 mm)

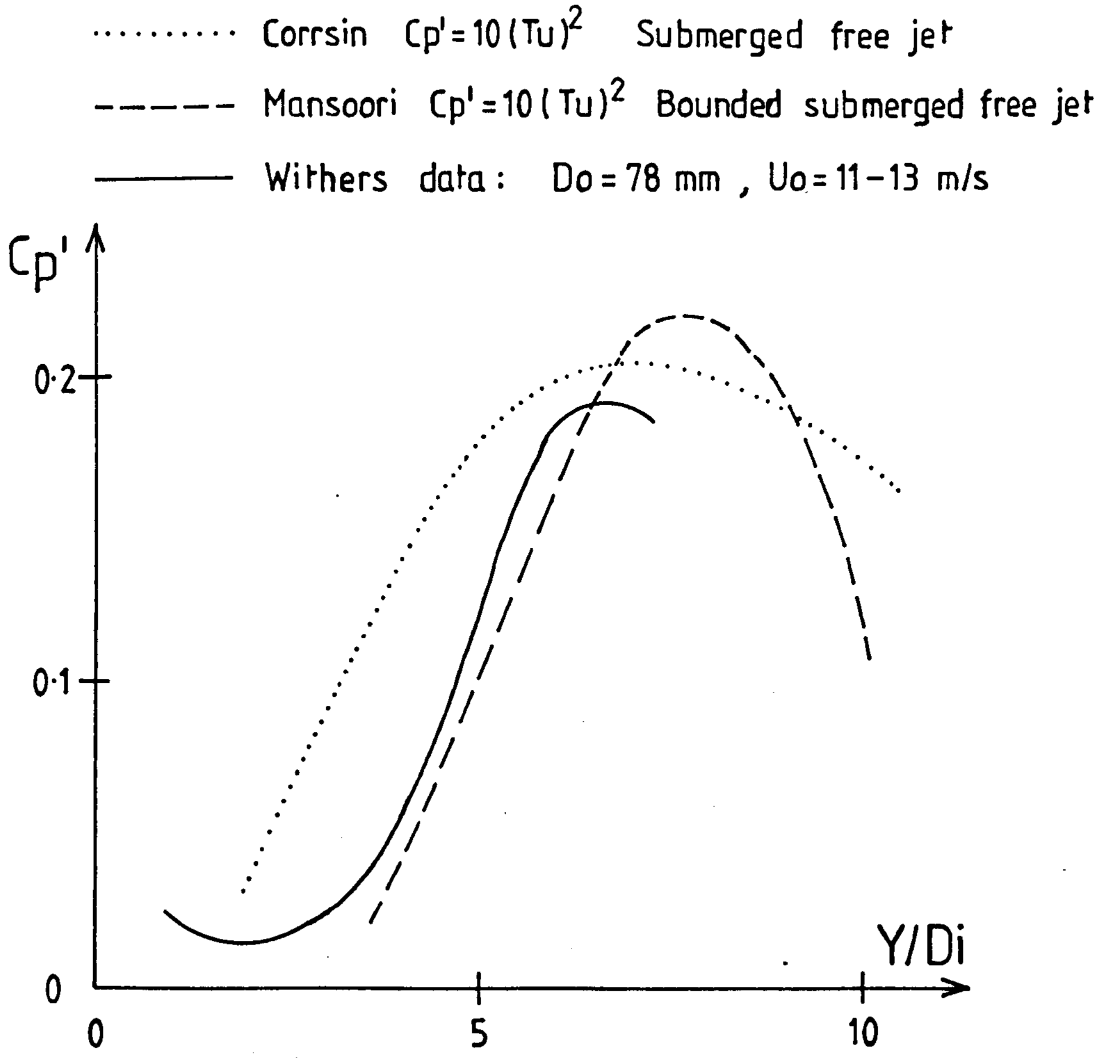

Fig.7·35 Comparison of fluctuations for intact plunging jet with submerged jets.

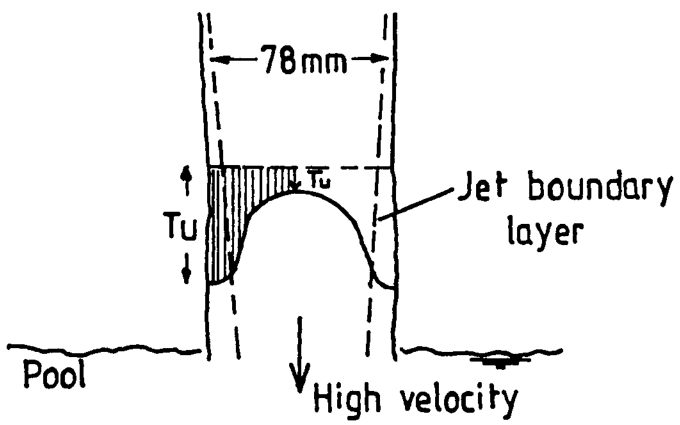

Fig.7·36 Growth of boundary layer and jet condition at impact for high velocity jet (Do = 78mm).

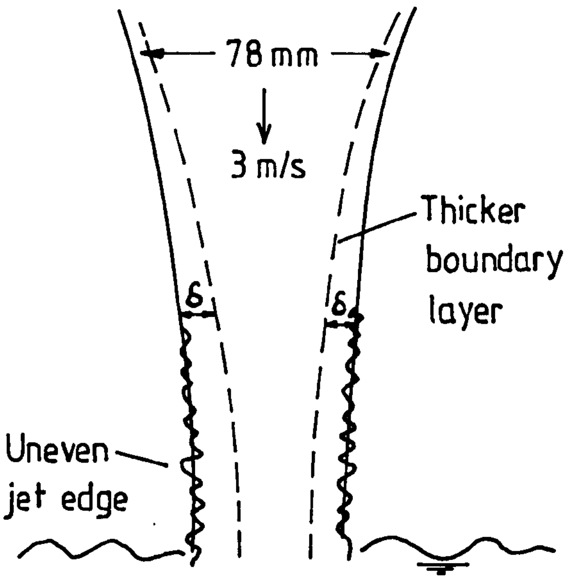

Fig.7·37 Growth of boundary layer and jet condition at impact for low velocity jet (Do = 78 mm)

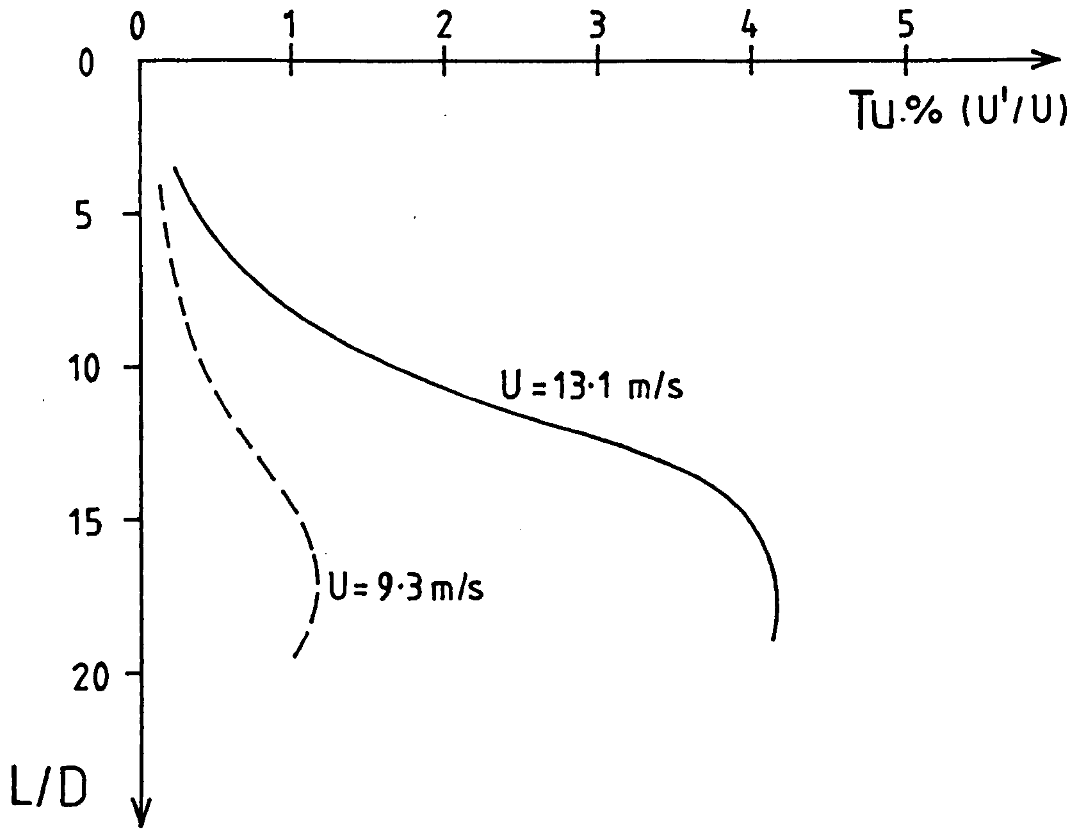

Fig.7·38 Turbulence intensity along centre line of orifice jet.

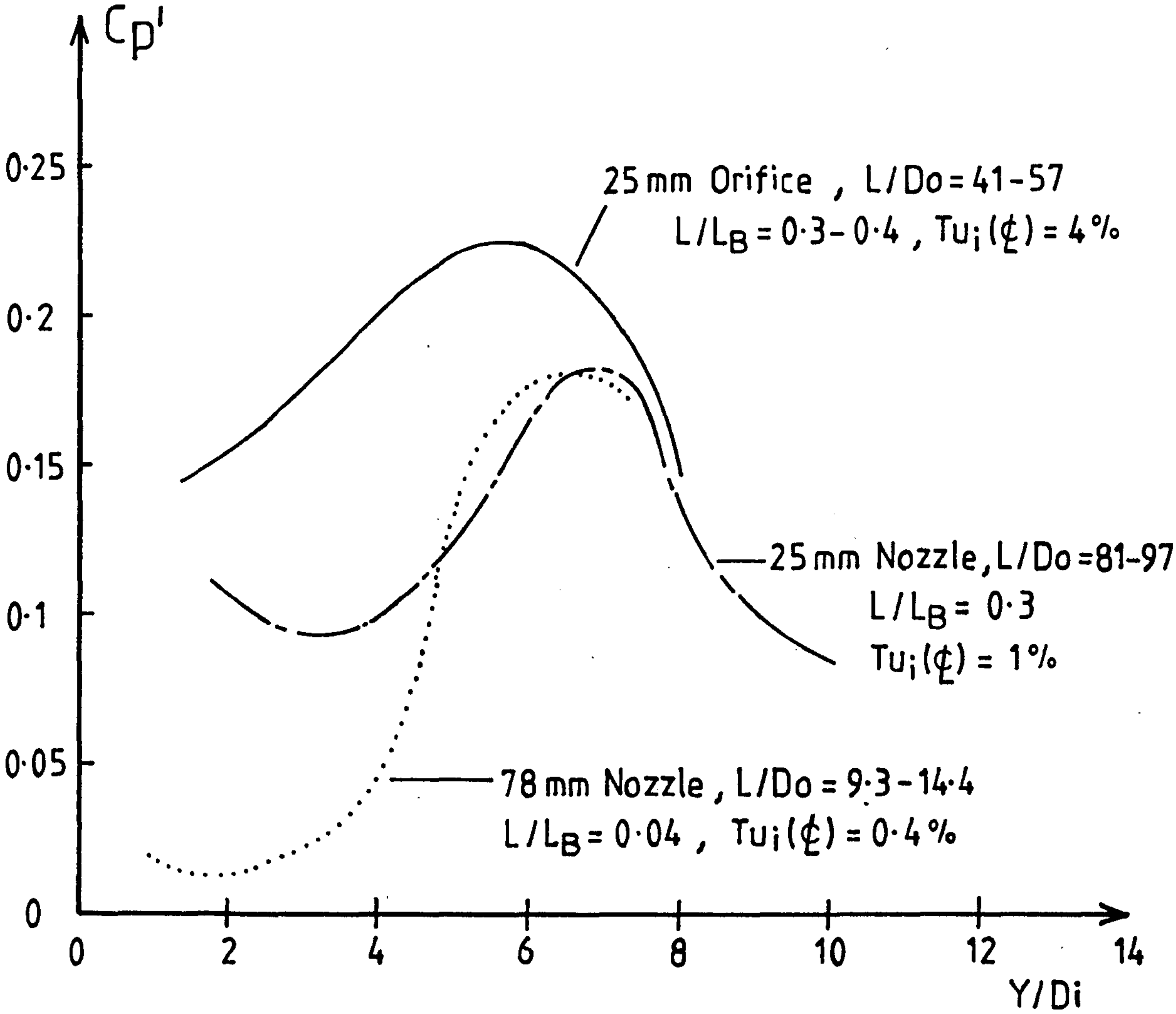

Fig. 7·39 Variation of Cp' for constant high impact velocity ($Ui^2/2g$=9–10) for 78mm nozzle, 25mm nozzle and 25mm orifice.

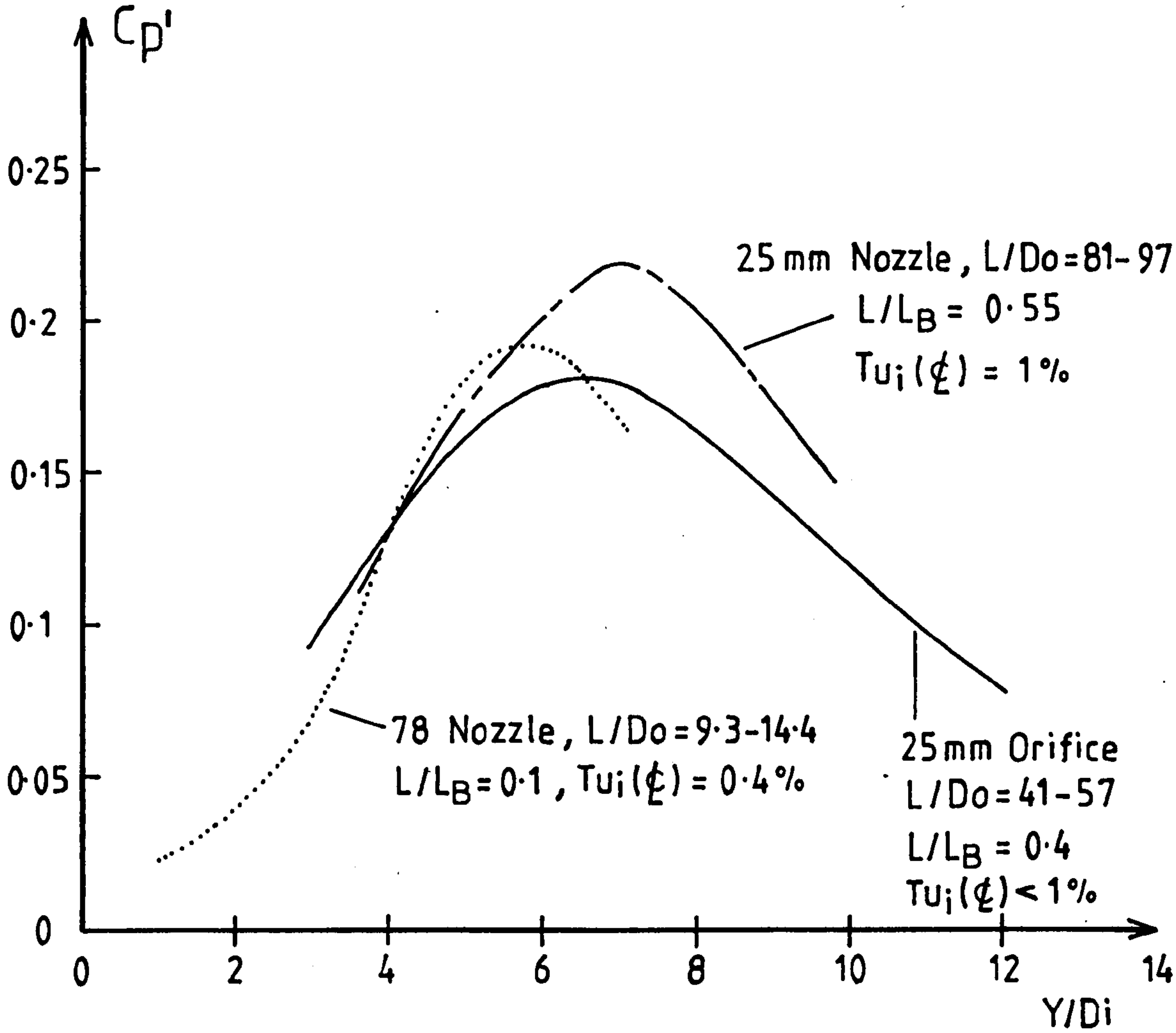

Fig. 7·40 Variation of Cp' for a constant lower impact velocity ($Ui^2/2g = 3{\cdot}3-4$) for 78 mm nozzle, 25 mm nozzle and 25 mm orifice.

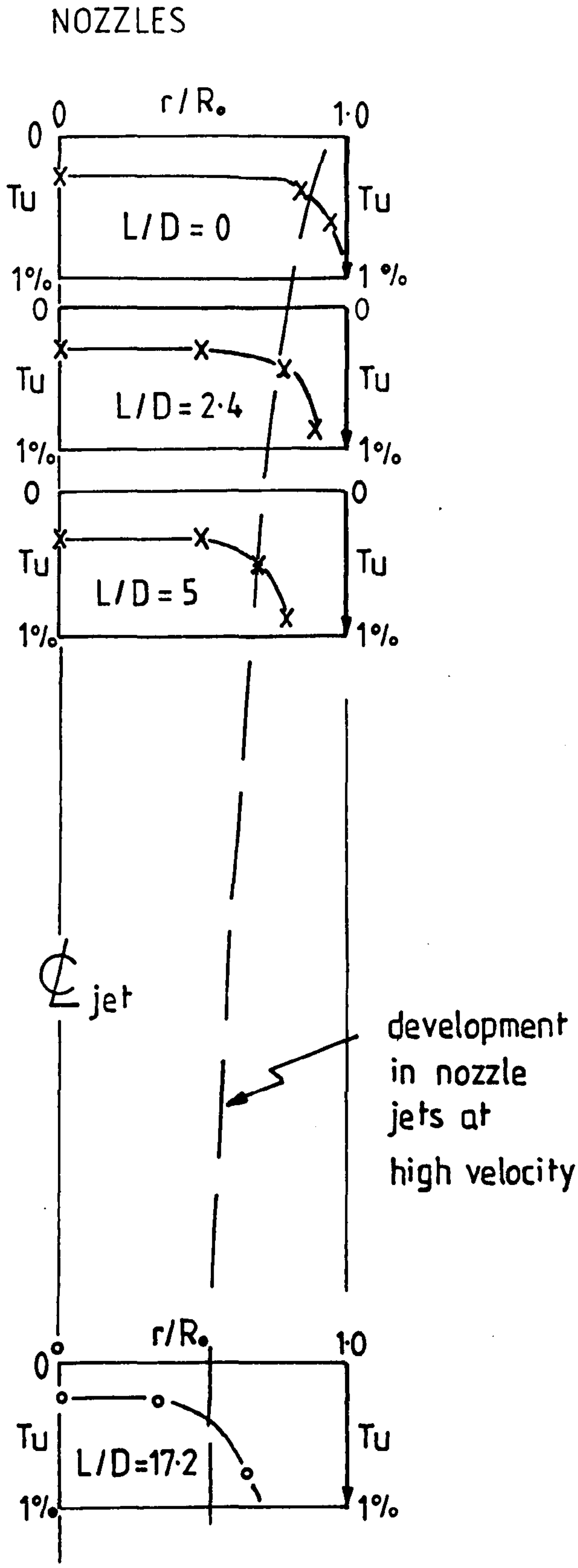

Fig. 7·41 (a)
Typical growth in boundary layer in smooth nozzle jets plunging through atmosphere.

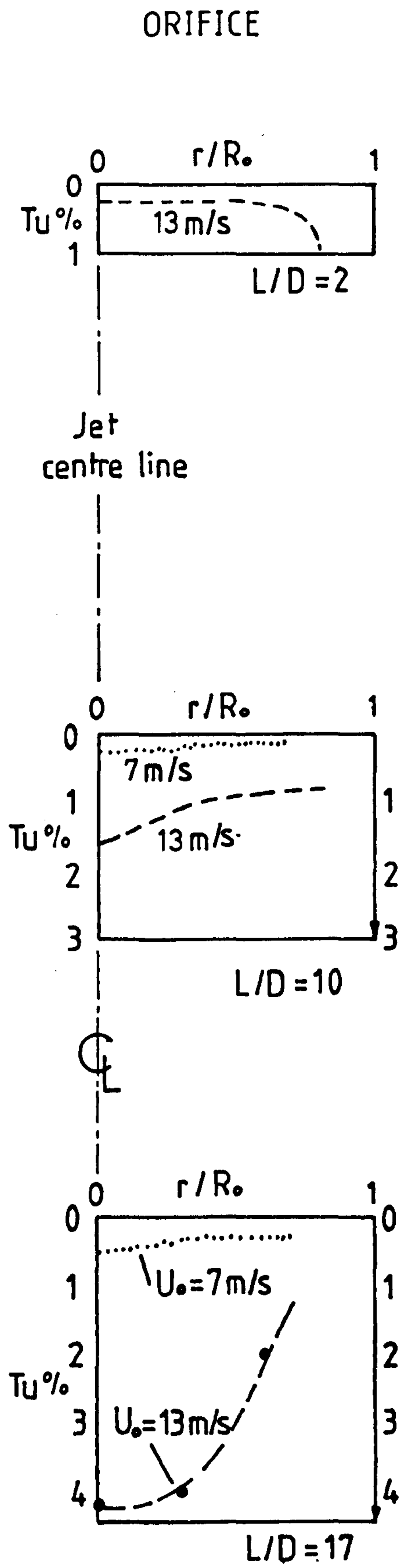

Fig.7·41(b) Turbulence levels in plunging orifice jet at two velocities.

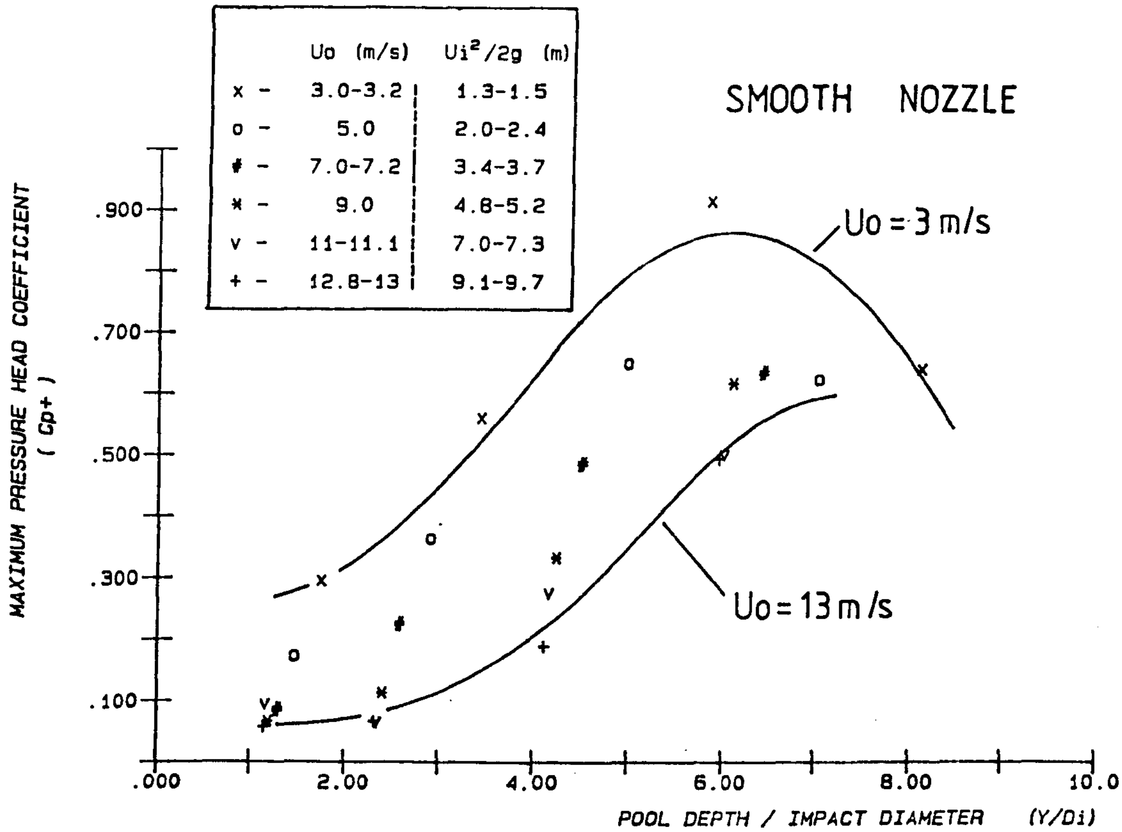

Fig.7·42 Cp+ with Y/Di (Do=78 mm, L=725 - 1125 mm)

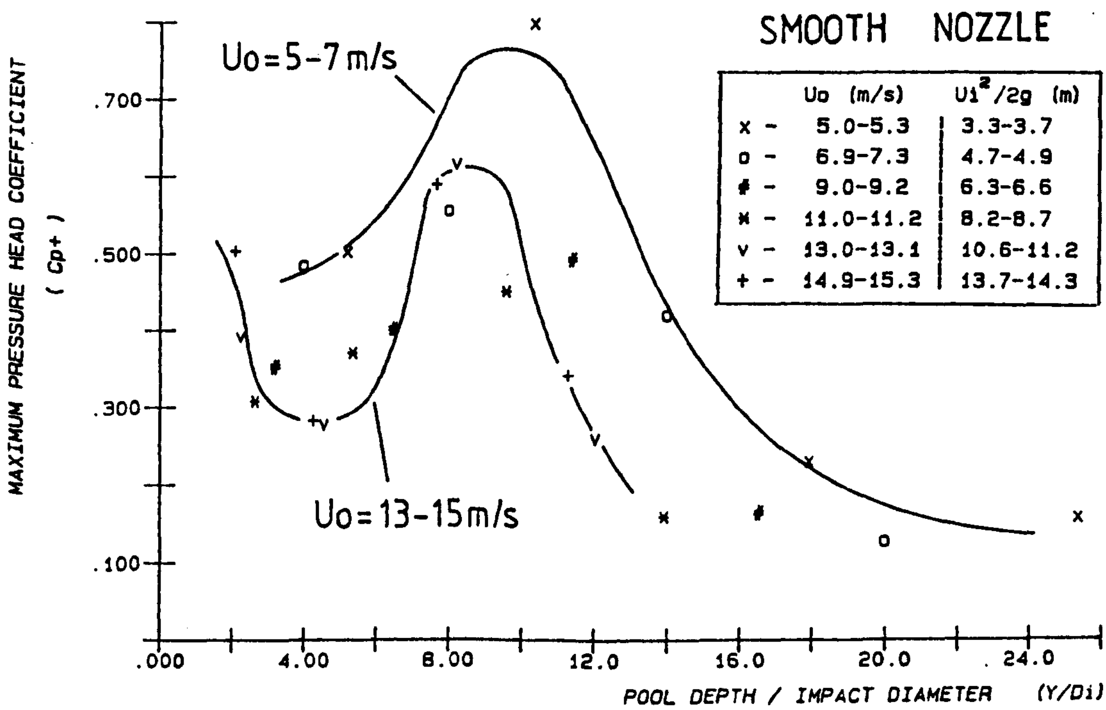

Fig.7·43 Cp+ with Y/Di (Do=25 mm, L= 2018 - 2418 mm)

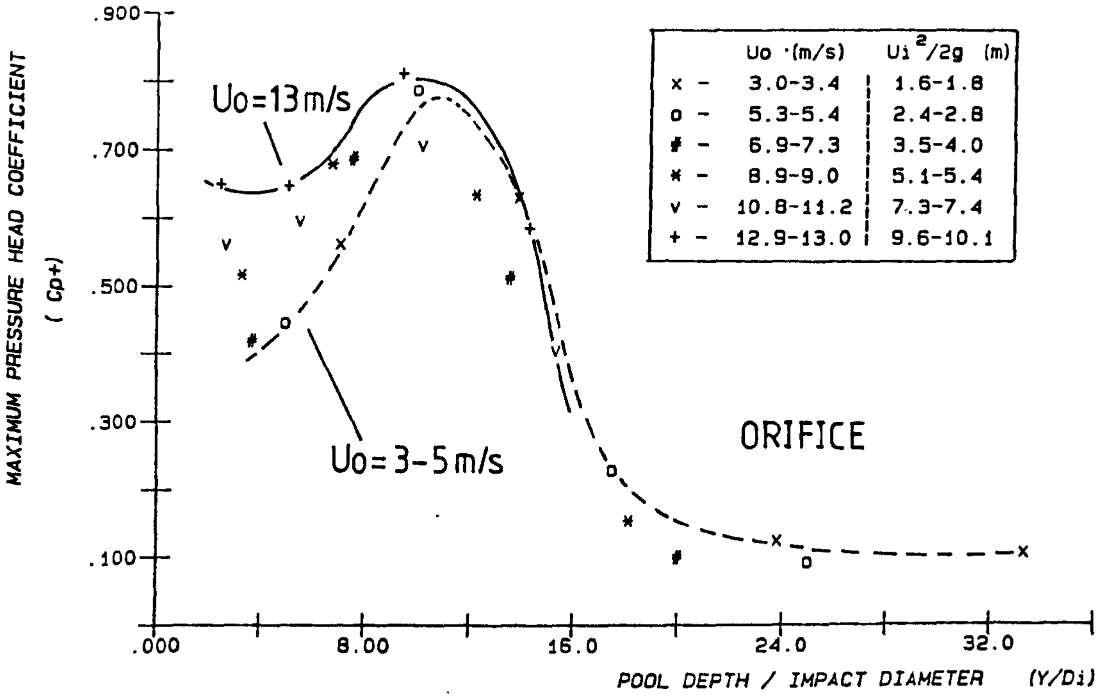

Fig.7·44 Cp+ with Y/Di (Orifice: Do=25mm, L=1020-1420 mm)

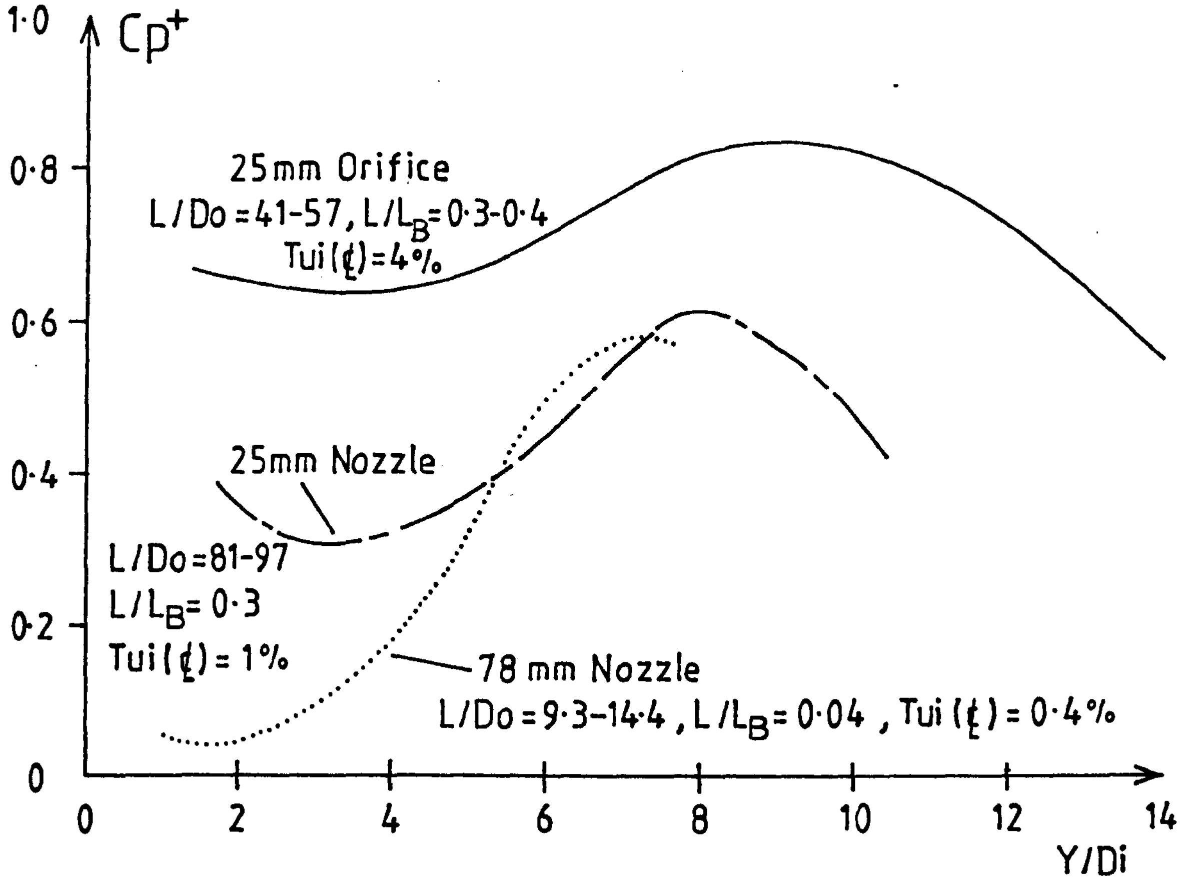

Fig.7·45 Variation of Cp+ for a fixed high impact velocity (Ui²/2g 9-10) for 78mm nozzle, 25mm nozzle and orifice.

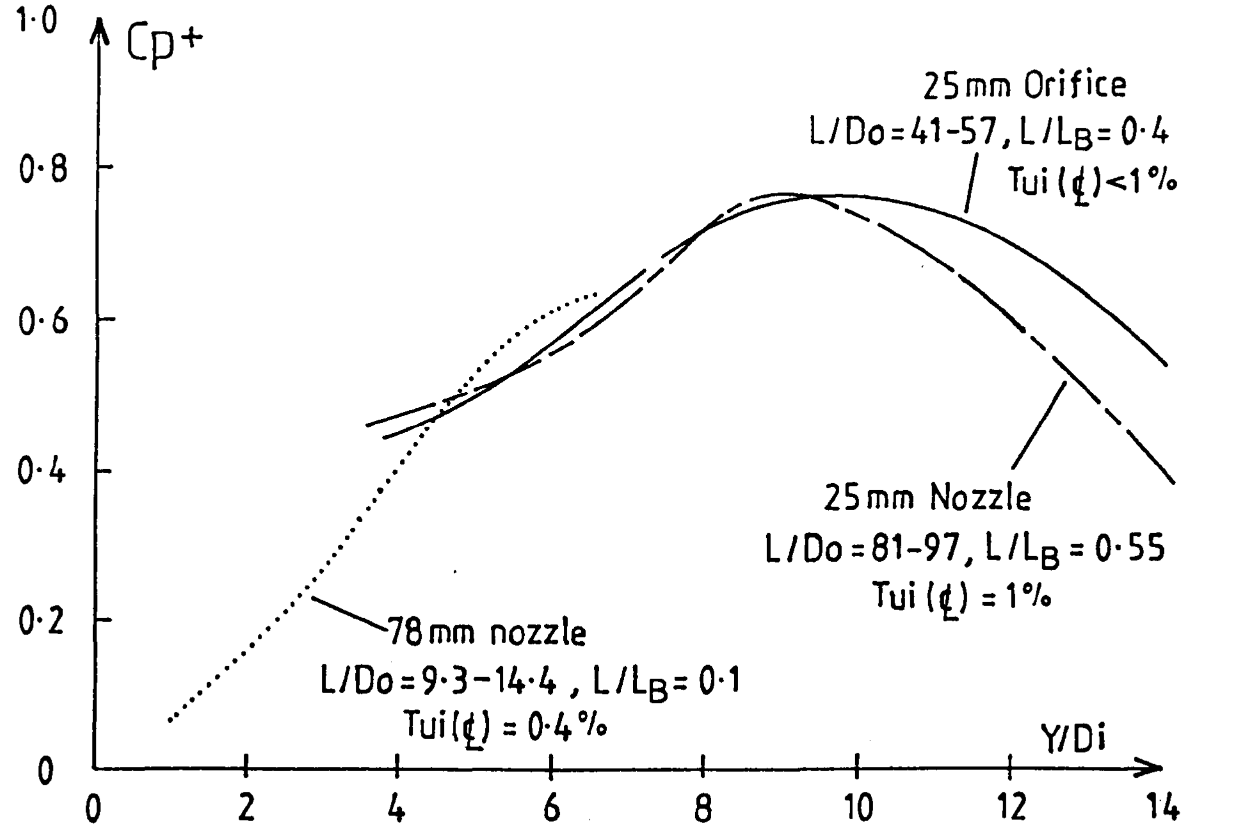

Fig.7·46 Variation of Cp+ for a fixed lower impact velocity ($Ui^2/2g$= 3·3-4) for 78mm nozzle, 25mm nozzle and orifice.

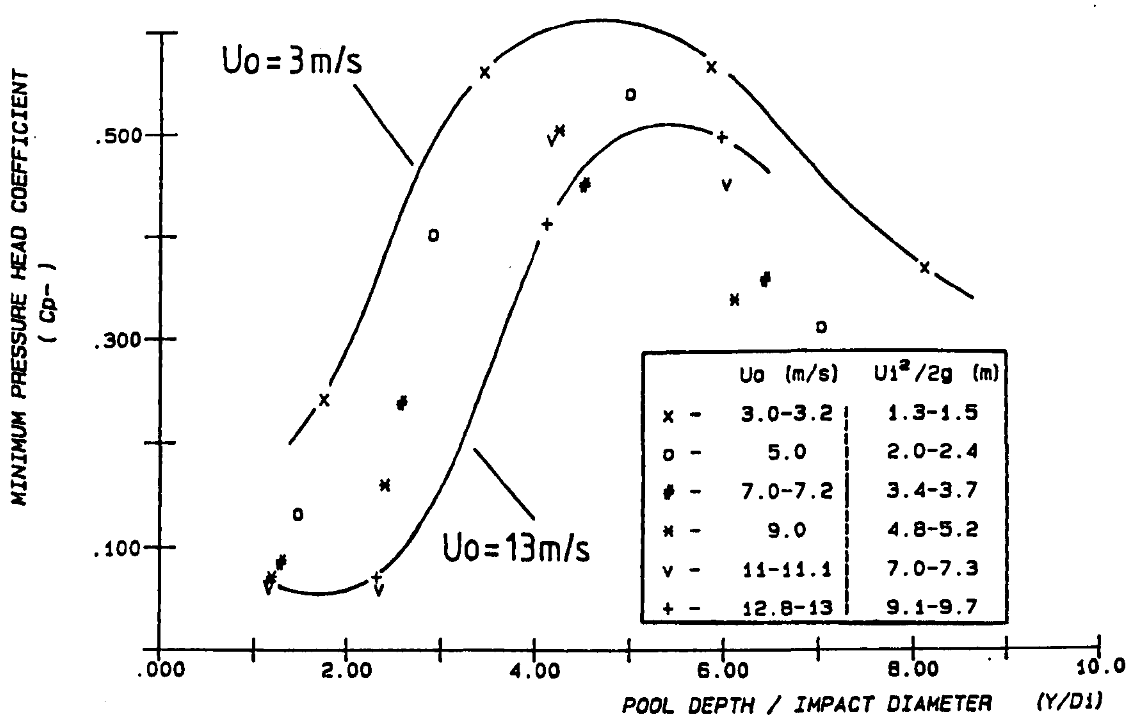

Fig.7·47 Cp- with Y/Di (Do=78mm, L=725-1125mm)

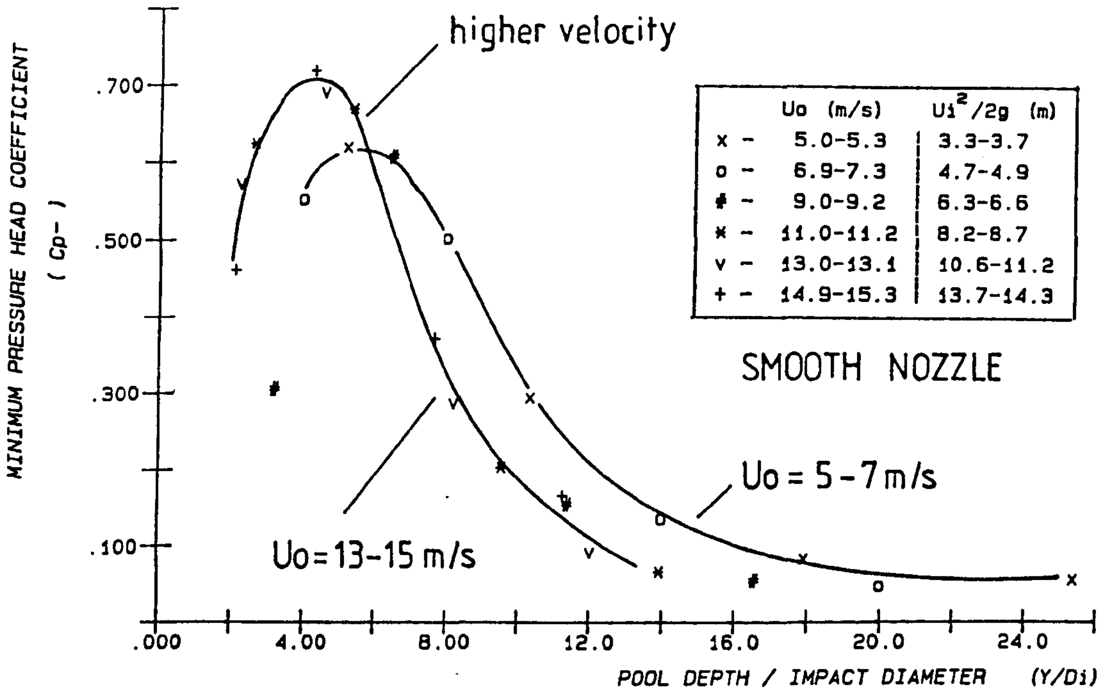

Fig.7·48 Cp⁻ with Y/Di (Do=25 mm, L= 2018-2418 mm)

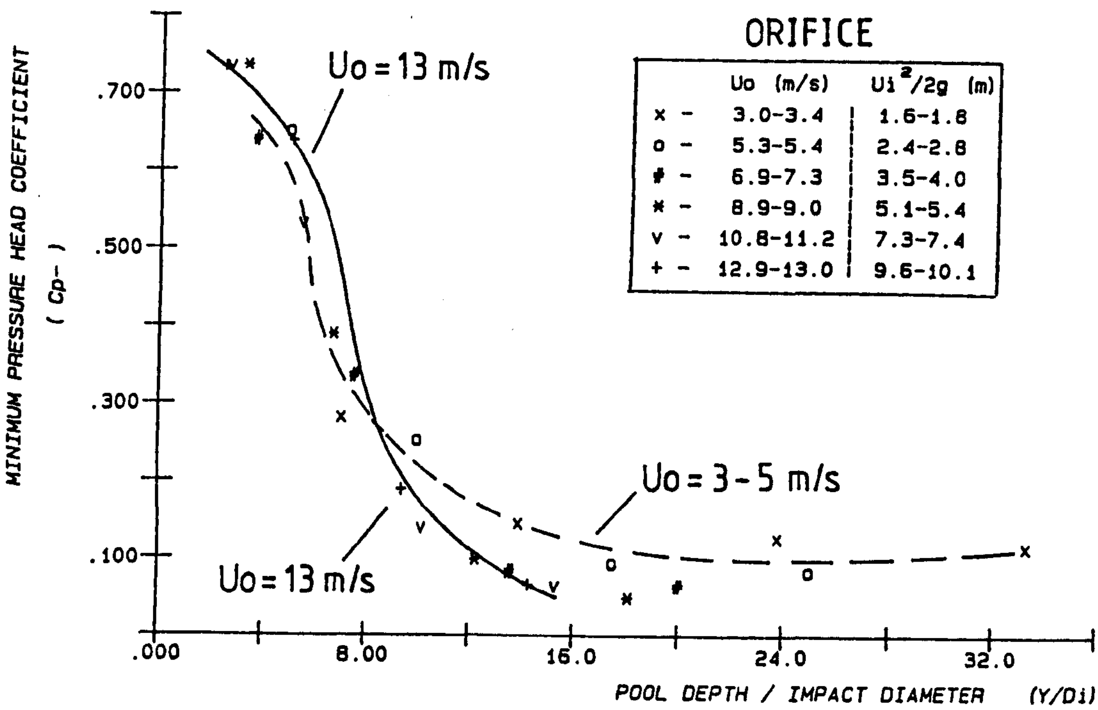

Fig.7·49 Cp⁻ with Y/Di (Orifice : Do=25 mm, L = 1020 - 1420 mm)

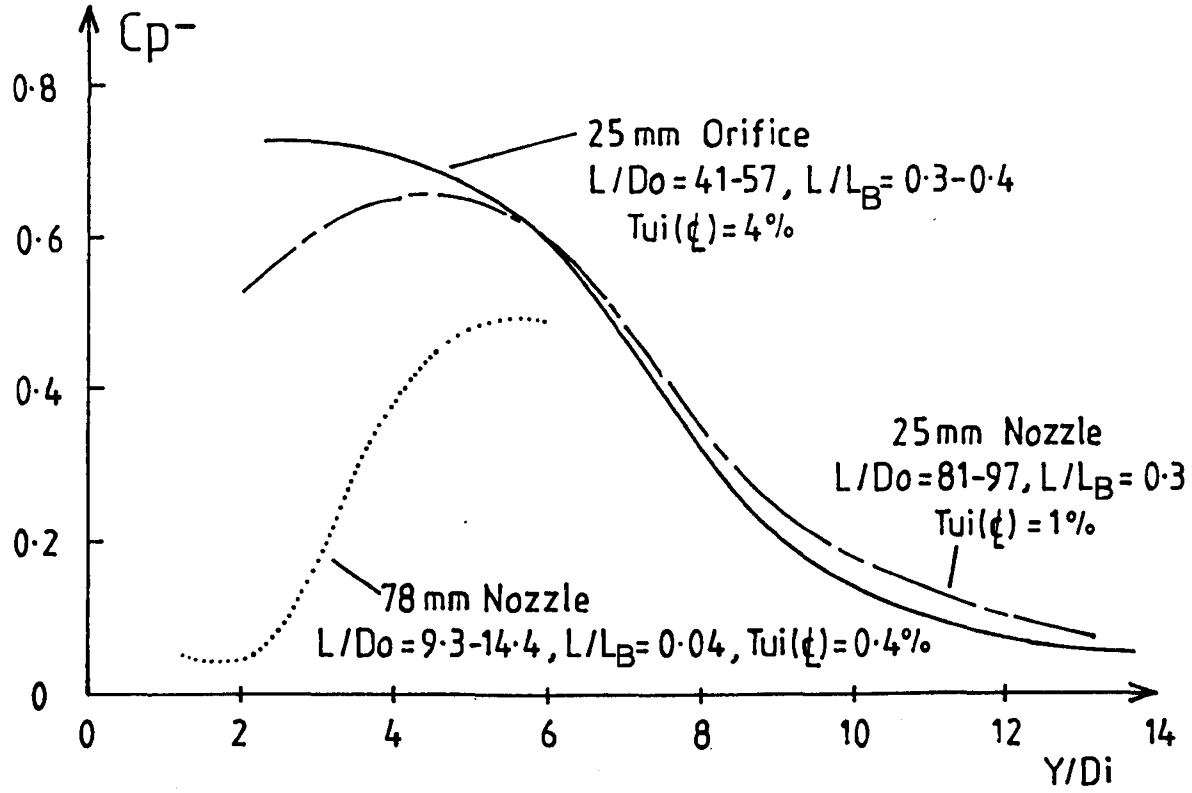

Fig.7·50 Variation of Cp^- for a fixed high impact velocity ($Ui^2/2g$ = 9-10) for 78 mm nozzle, 25 mm nozzle and orifice.

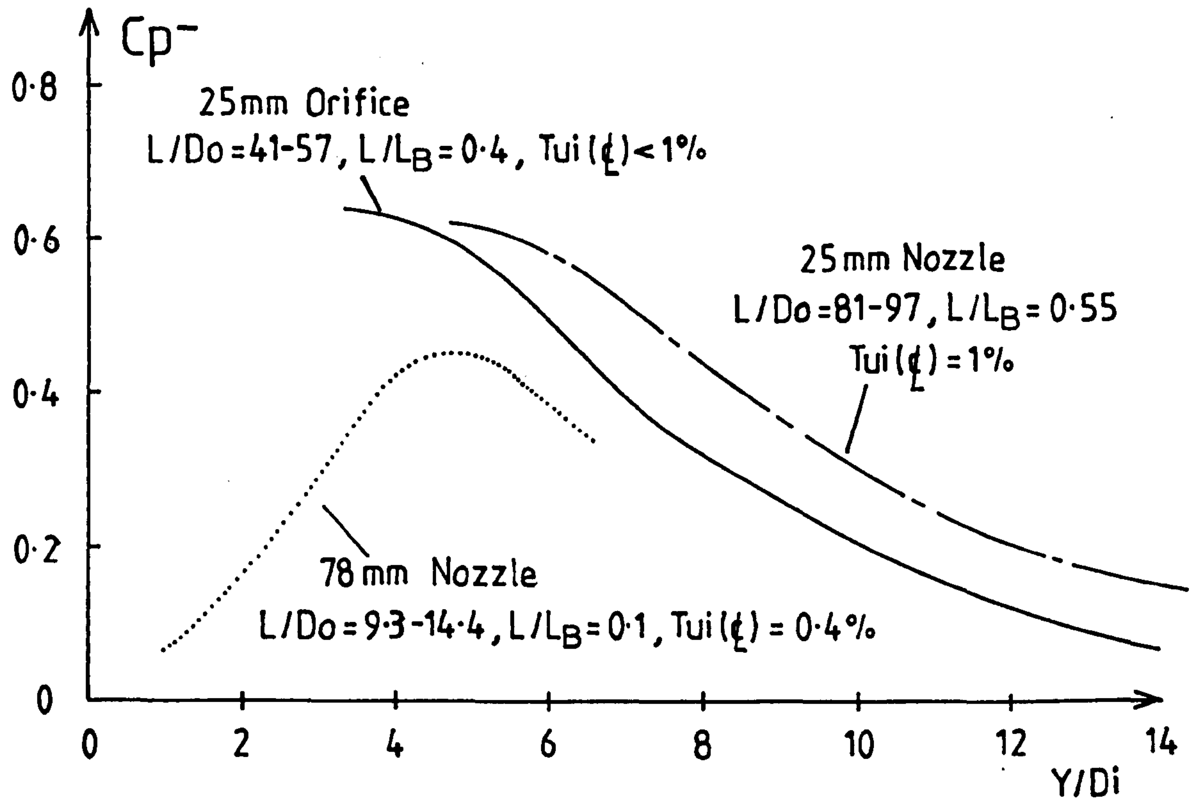

Fig. 7·51 Variation of Cp^- for a fixed lower impact velocity ($Ui^2/2g$ = 3·3-4) for 78 mm nozzle, 25 mm nozzle and orifice.

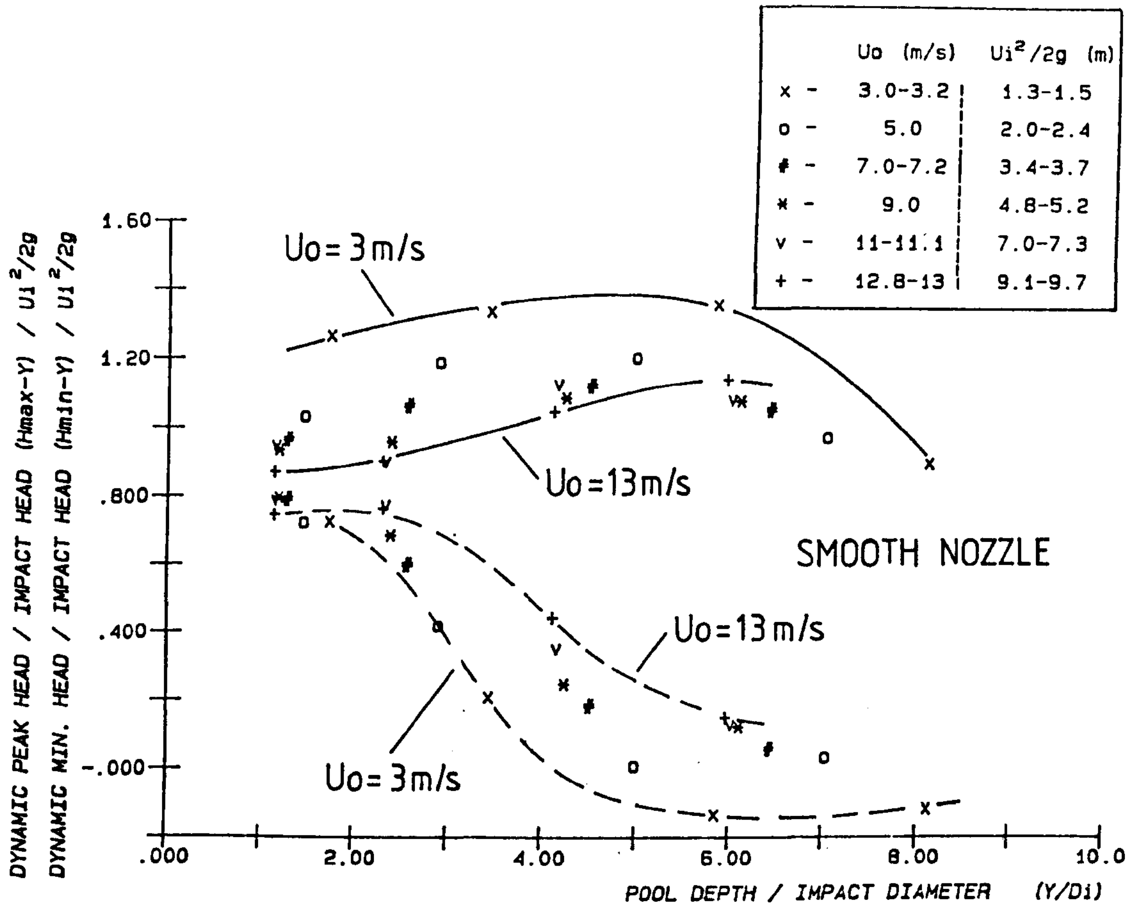

Fig.7·52 Extreme pressures with Y/Di (Do=78 mm, L=725-1125 mm)

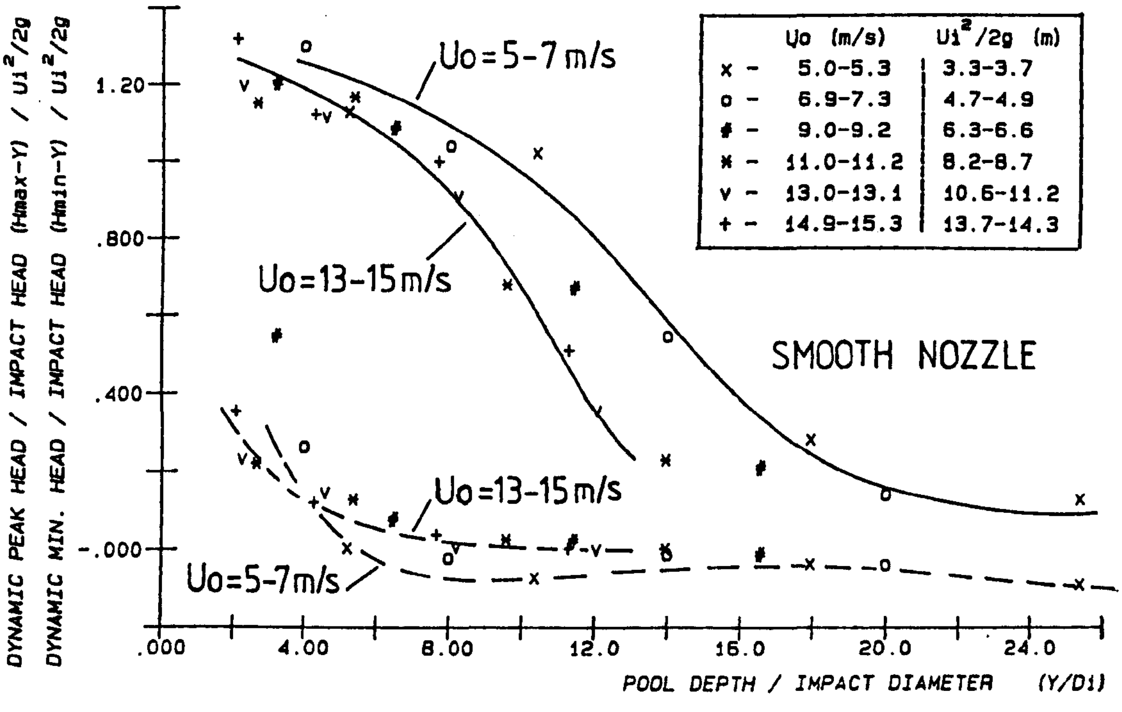

Fig.7·53 Extreme pressures with Y/Di (Do=25mm, L=2018-2418 mm)

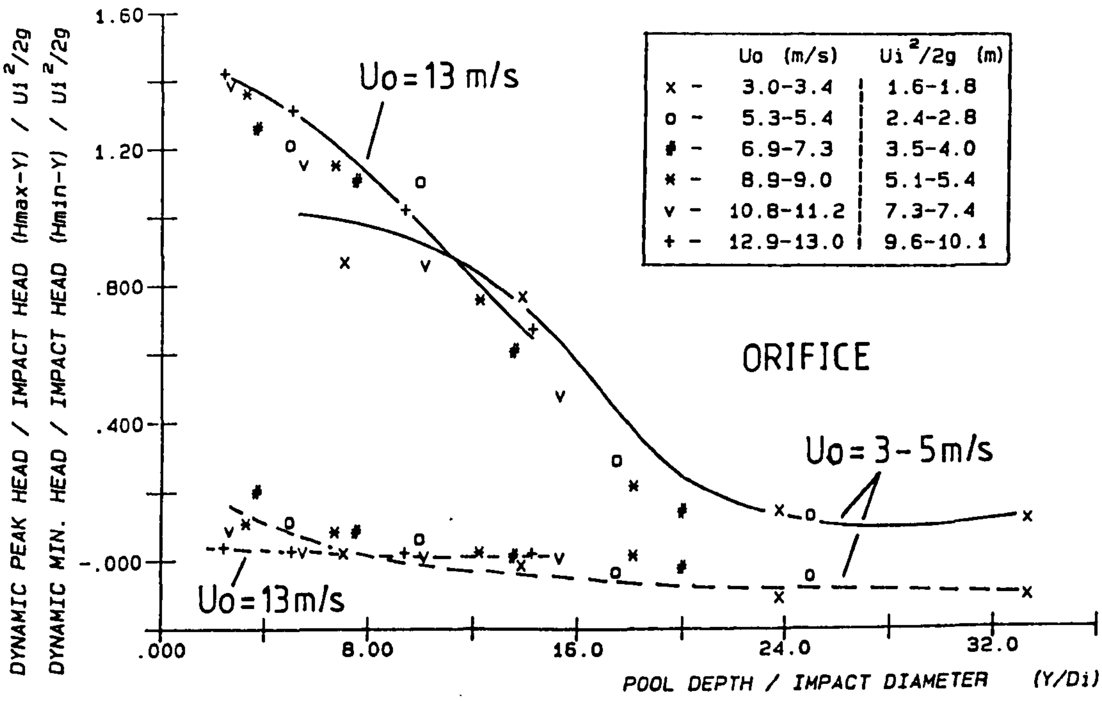

Fig.7·54 Extreme pressures with Y/Di (Orifice, L=1020-1420 mm)

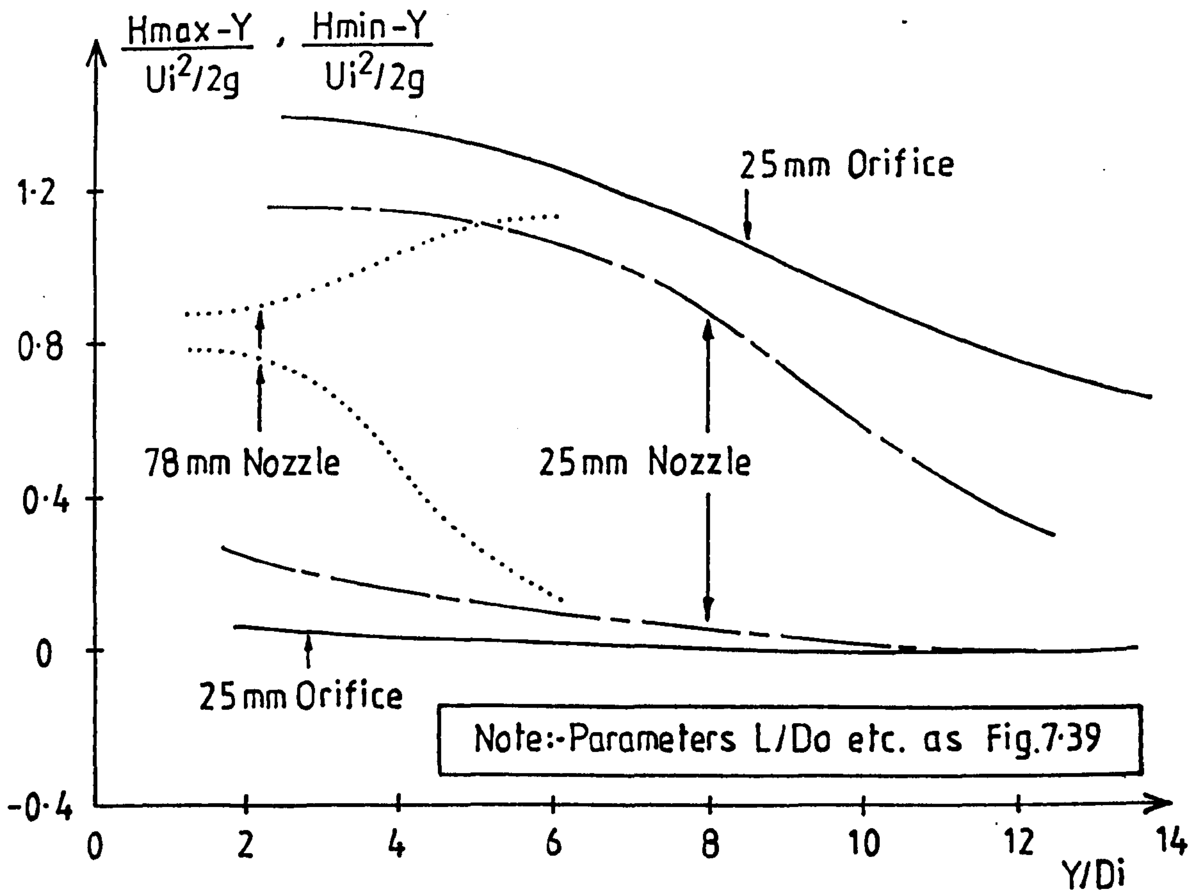

Fig. 7·55 Variation of extreme pressures for a fixed high impact vel. ($Ui^2/2g$=9-10) for 78mm nozzle, 25mm nozzle and orifice.

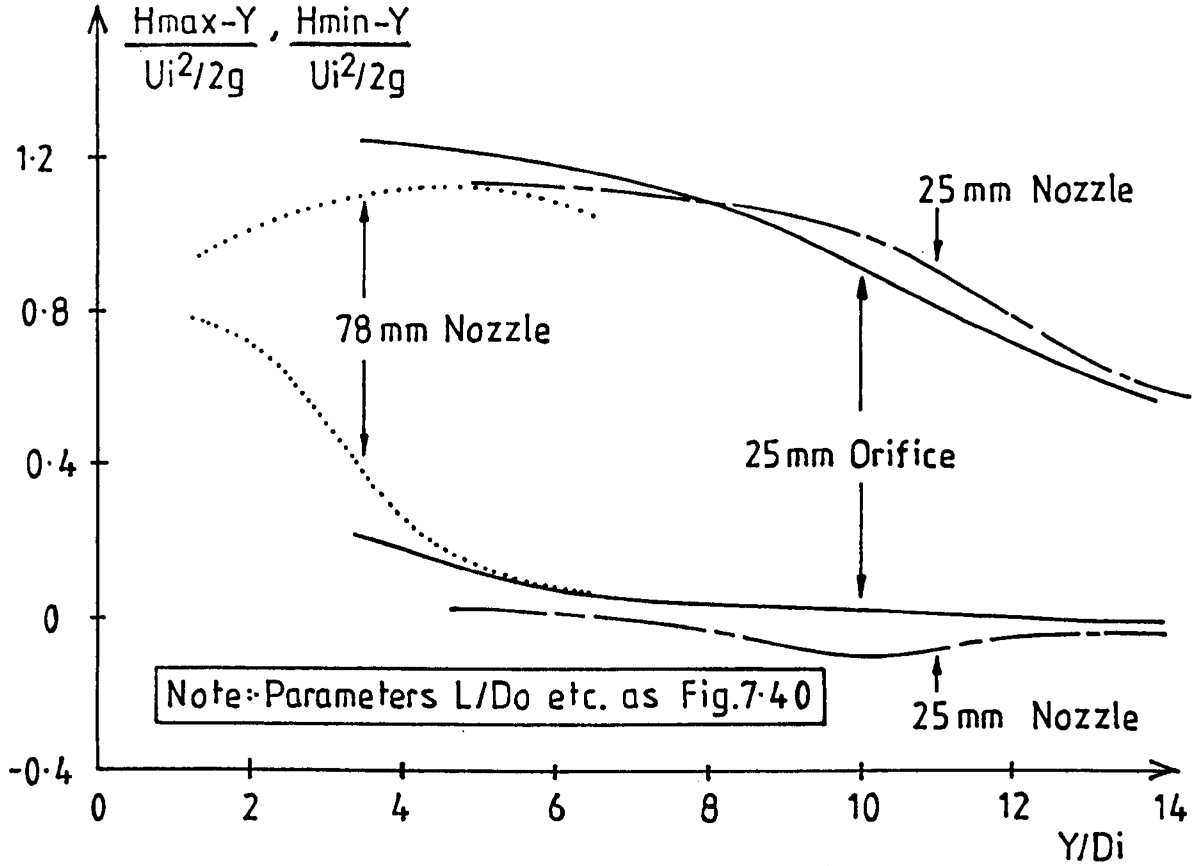

Fig. 7·56 Variation of extreme pressures for a fixed lower impact vel. (Ui /2g = 3·3–4) for 78 mm nozzle, 25 mm nozzle and orifice.

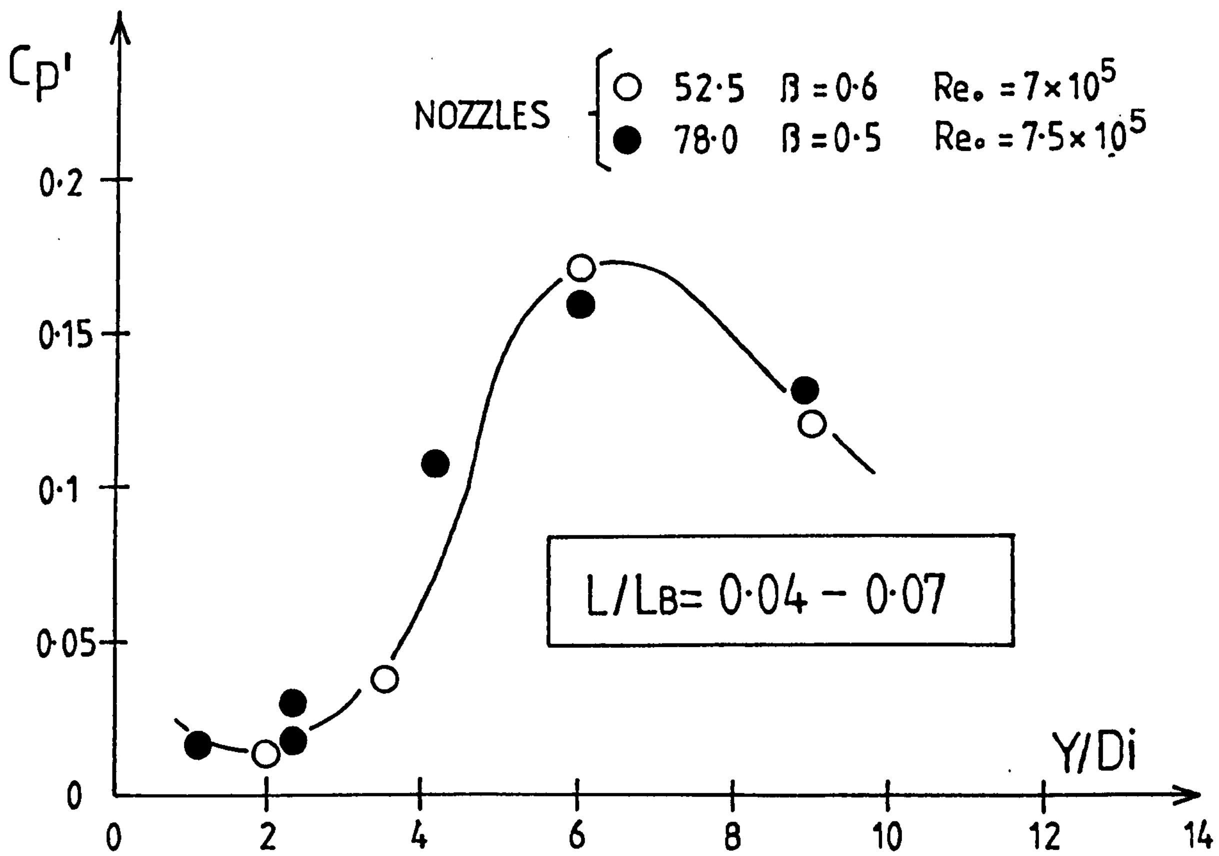

Fig. 7·57 Pressure fluctuations (Cp') for L/LB = 0·04 – 0·07

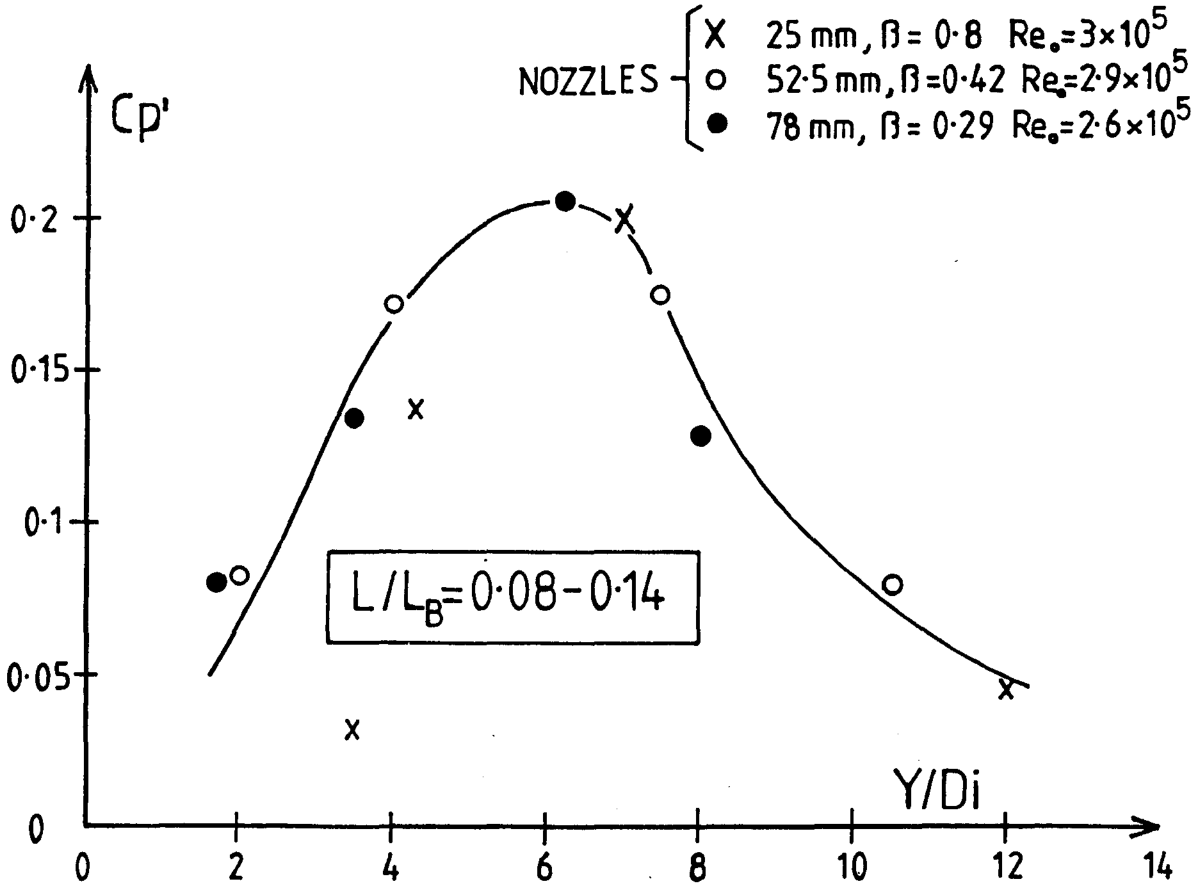

Fig. 7·58 Pressure fluctuations (Cp') for $L/L_B = 0{\cdot}08 - 0{\cdot}14$

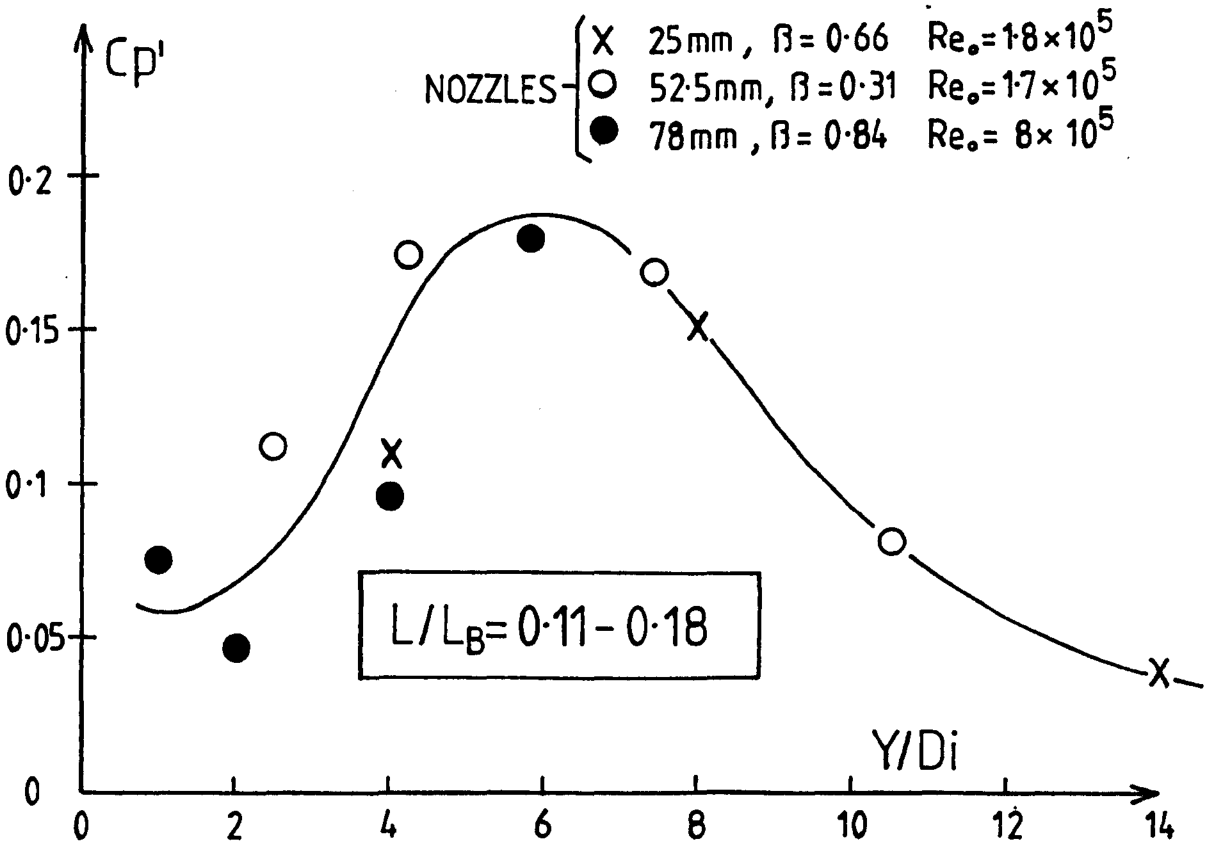

Fig. 7·59 Pressure fluctuations (Cp') for $L/L_B = 0{\cdot}11 - 0{\cdot}18$

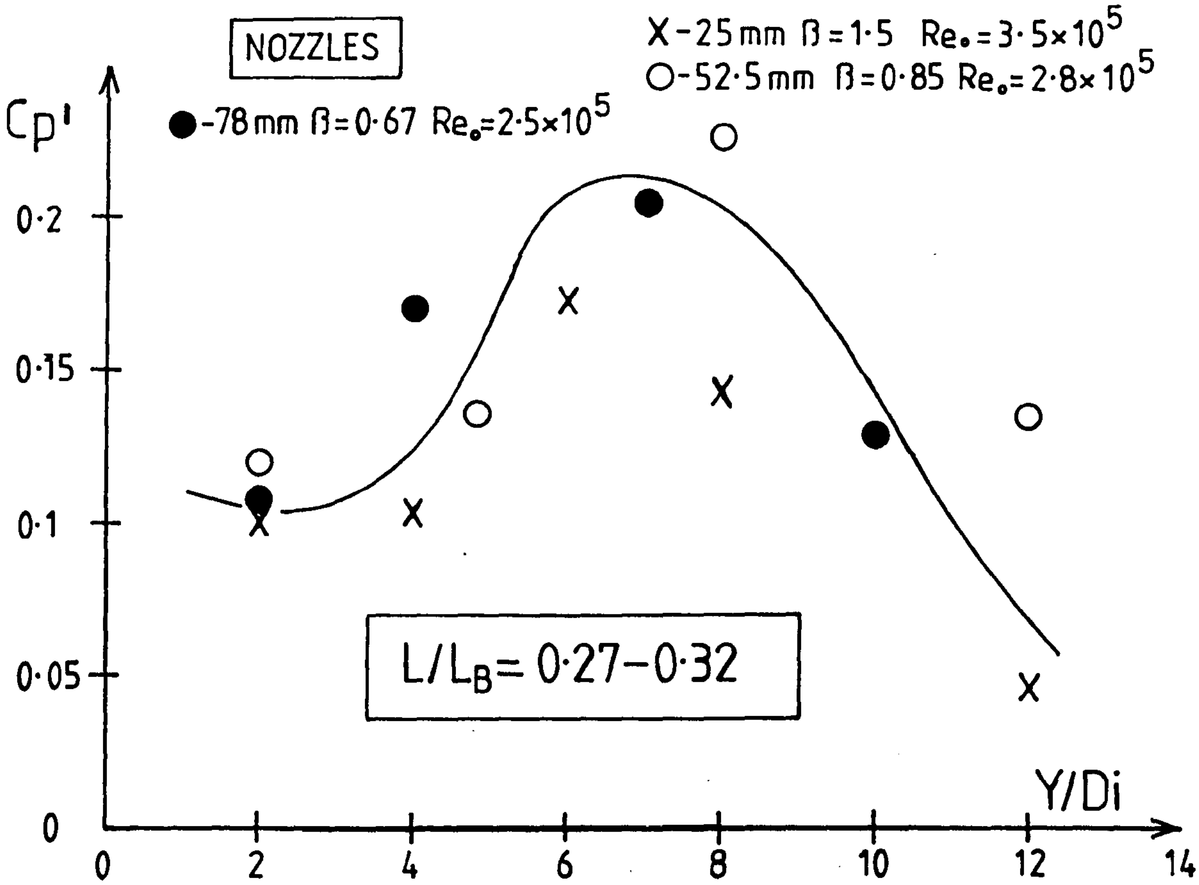

Fig.7·60 Pressure fluctuations (Cp') for $L/L_B = 0{\cdot}27 - 0{\cdot}32$

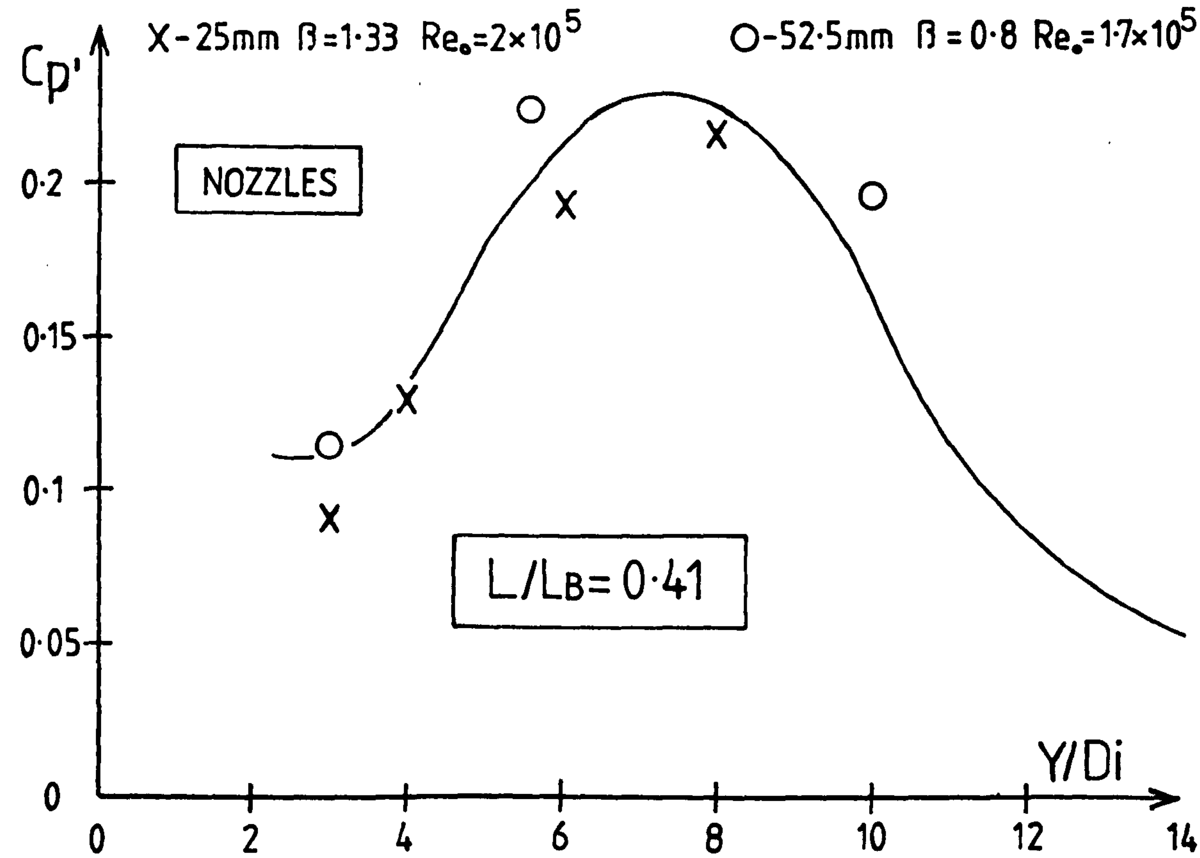

Fig.7·61 Pressure fluctuations (Cp') for $L/L_B = 0{\cdot}41$

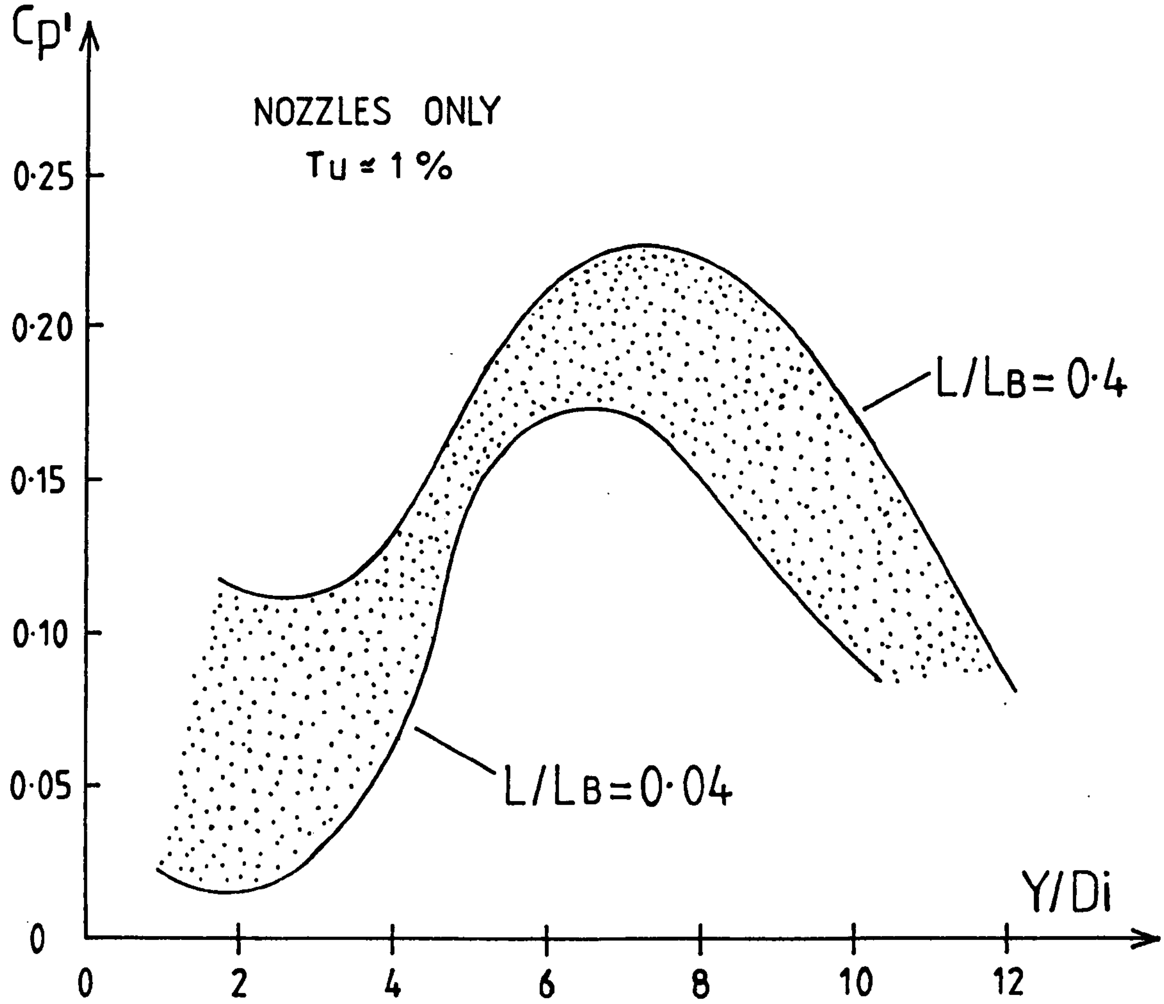

Fig.7·62 The influence of jet break-up (L/L_B) on pressure fluctuations in a plunge pool.

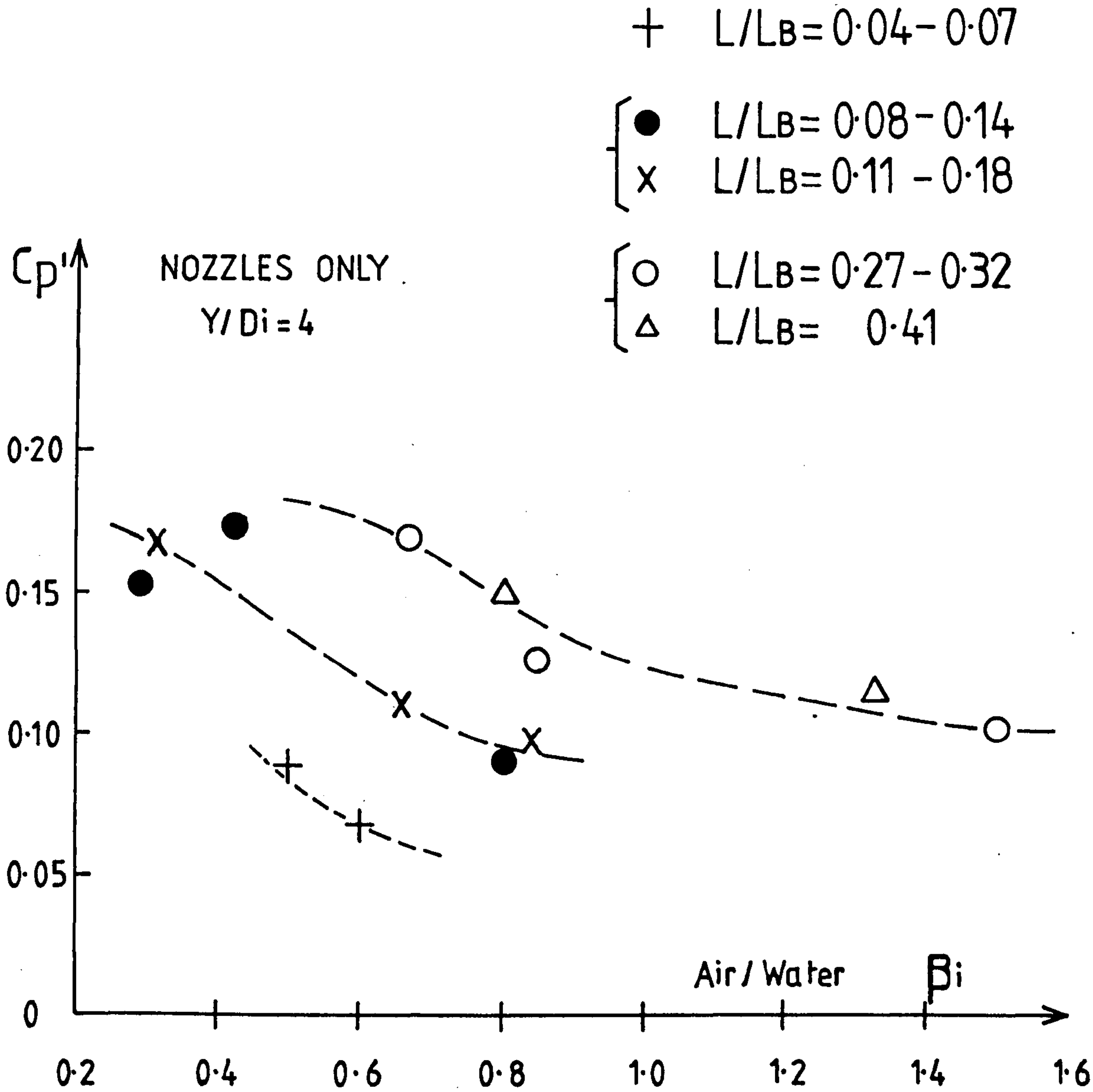

Fig.7·63 Variation of Cp' with air/water ratio (βi) for a pool depth of Y/Di = 4

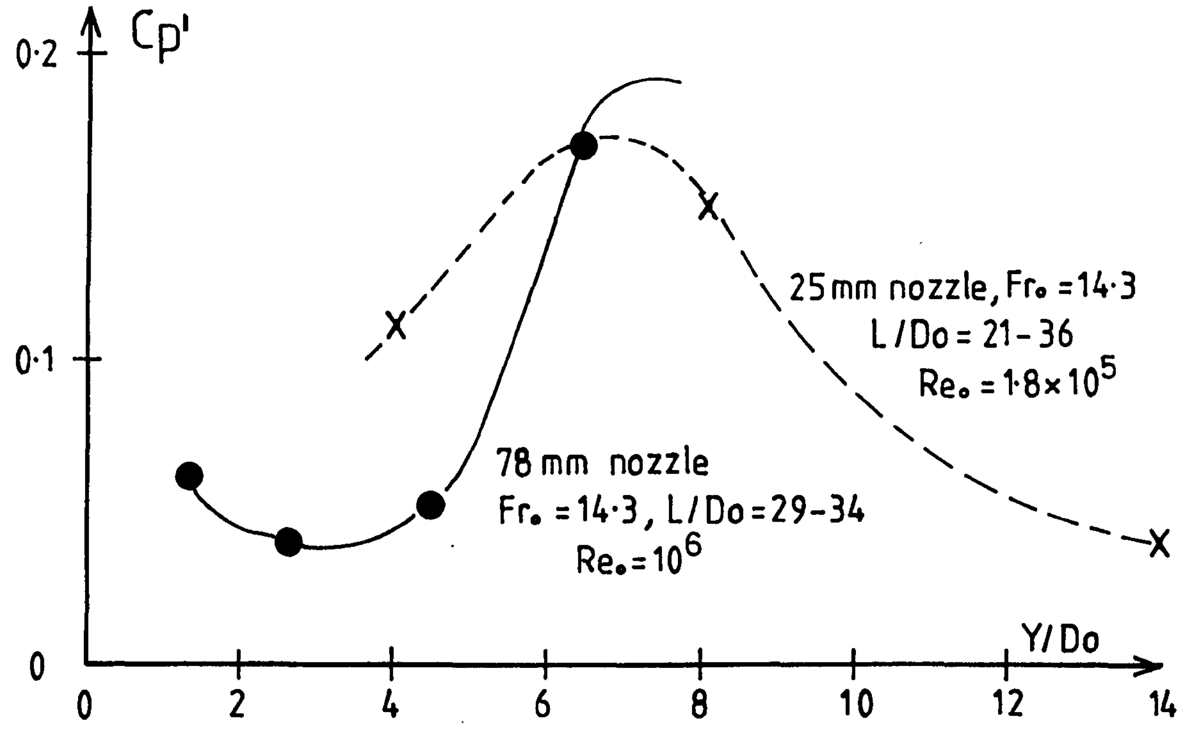

Fig. 7·64 An impinging jet Froude comparison $\boxed{Fr_0 = 14{\cdot}3}$

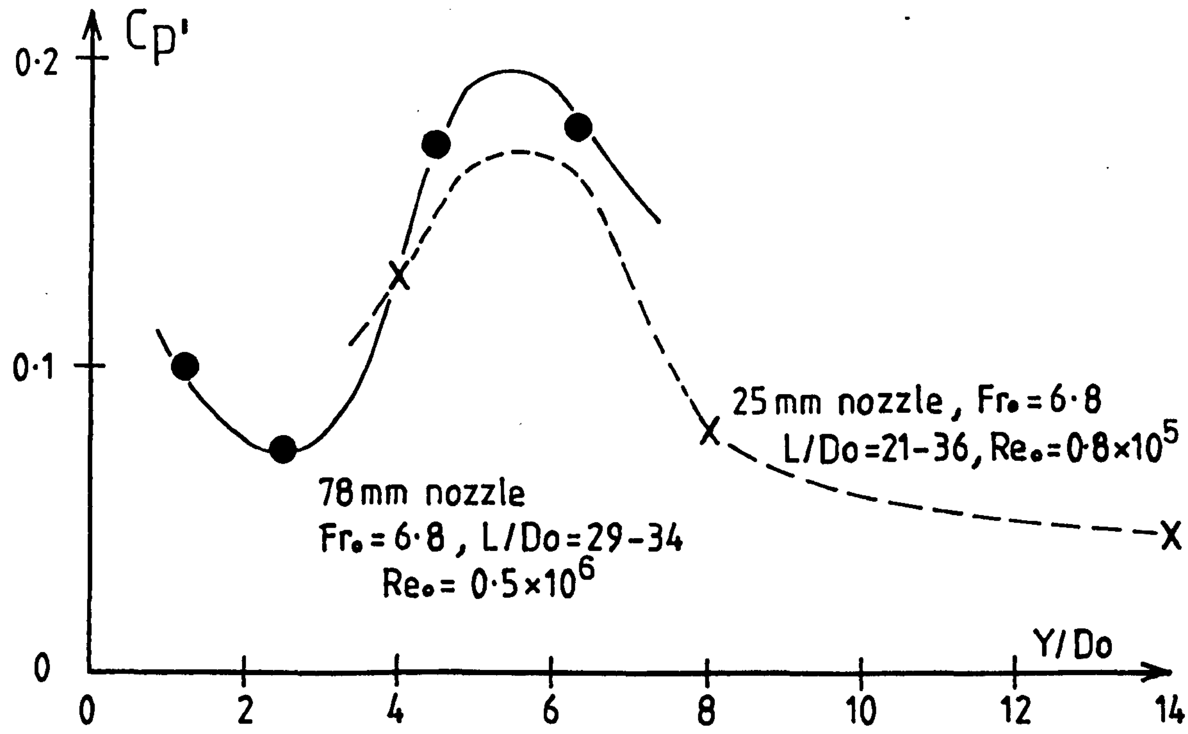

Fig. 7·65 An impinging jet Froude comparison $\boxed{Fr_0 = 6{\cdot}8}$

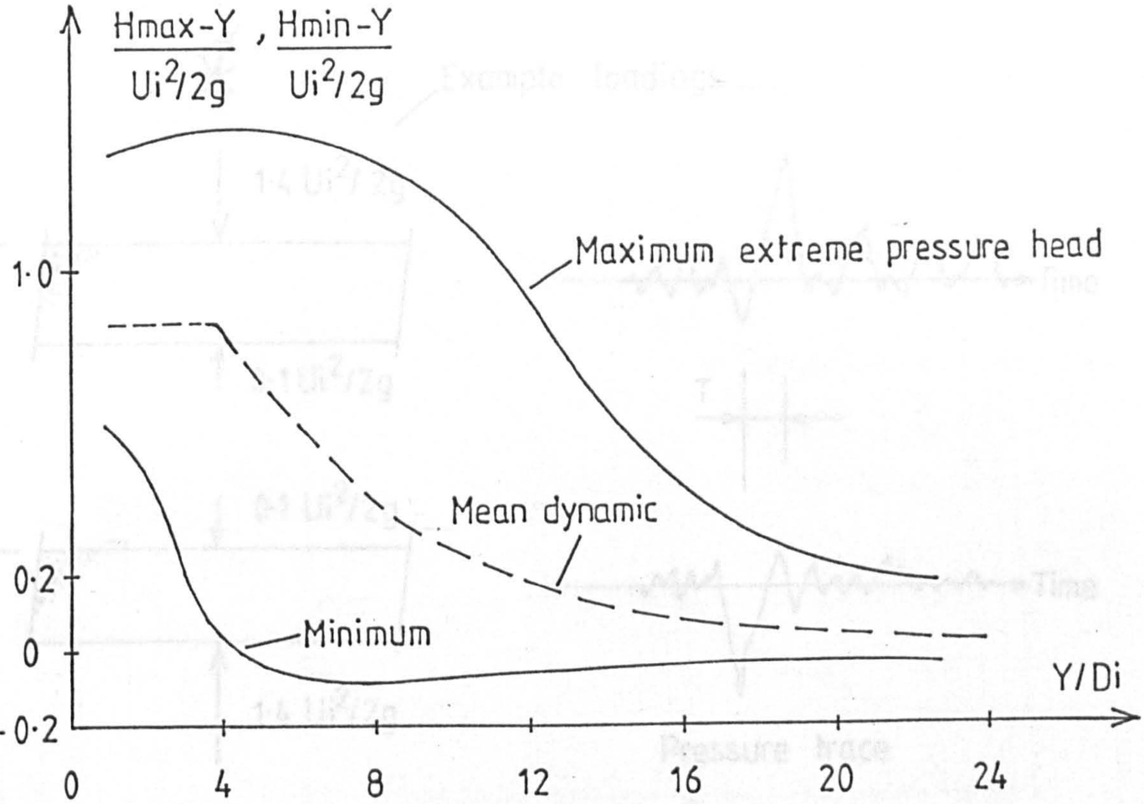

Fig.7·66 Envelope of maximum and minimum dynamic head.

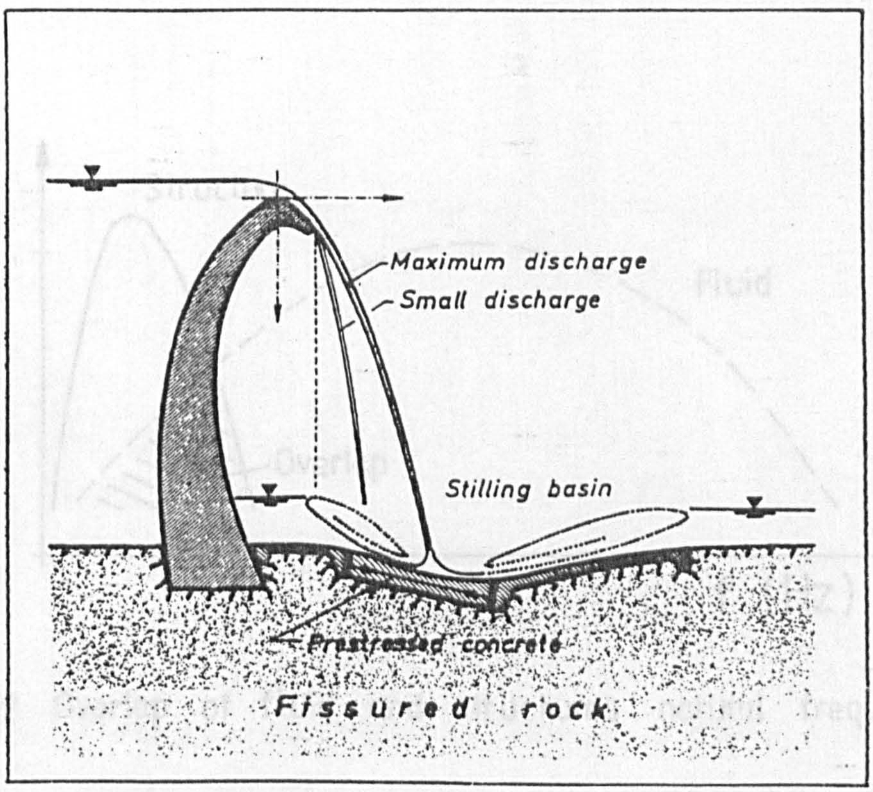

Fig.7·67 Proposed stilling basin design below free-falling jets. (Hartung and Häusler)

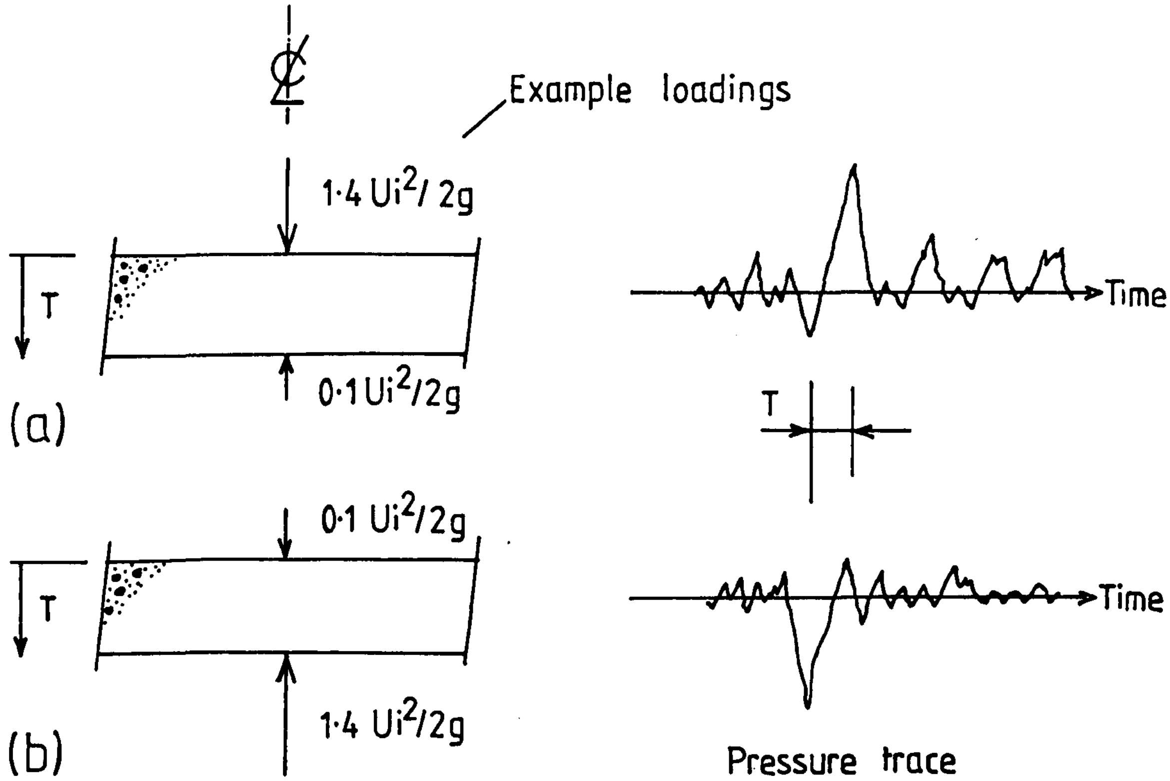

Fig.7·68 Load combinations for downward and upward pressure application.

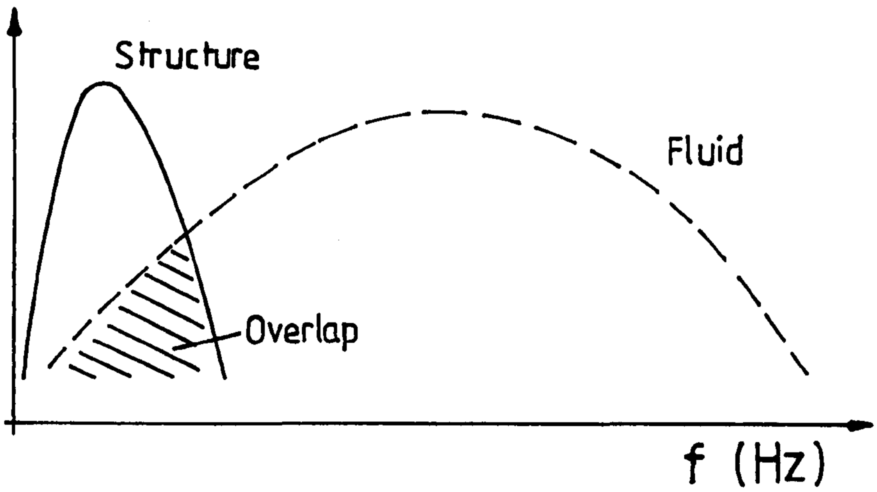

Fig. 7·69 Overlap of fluid and structures natural frequency.

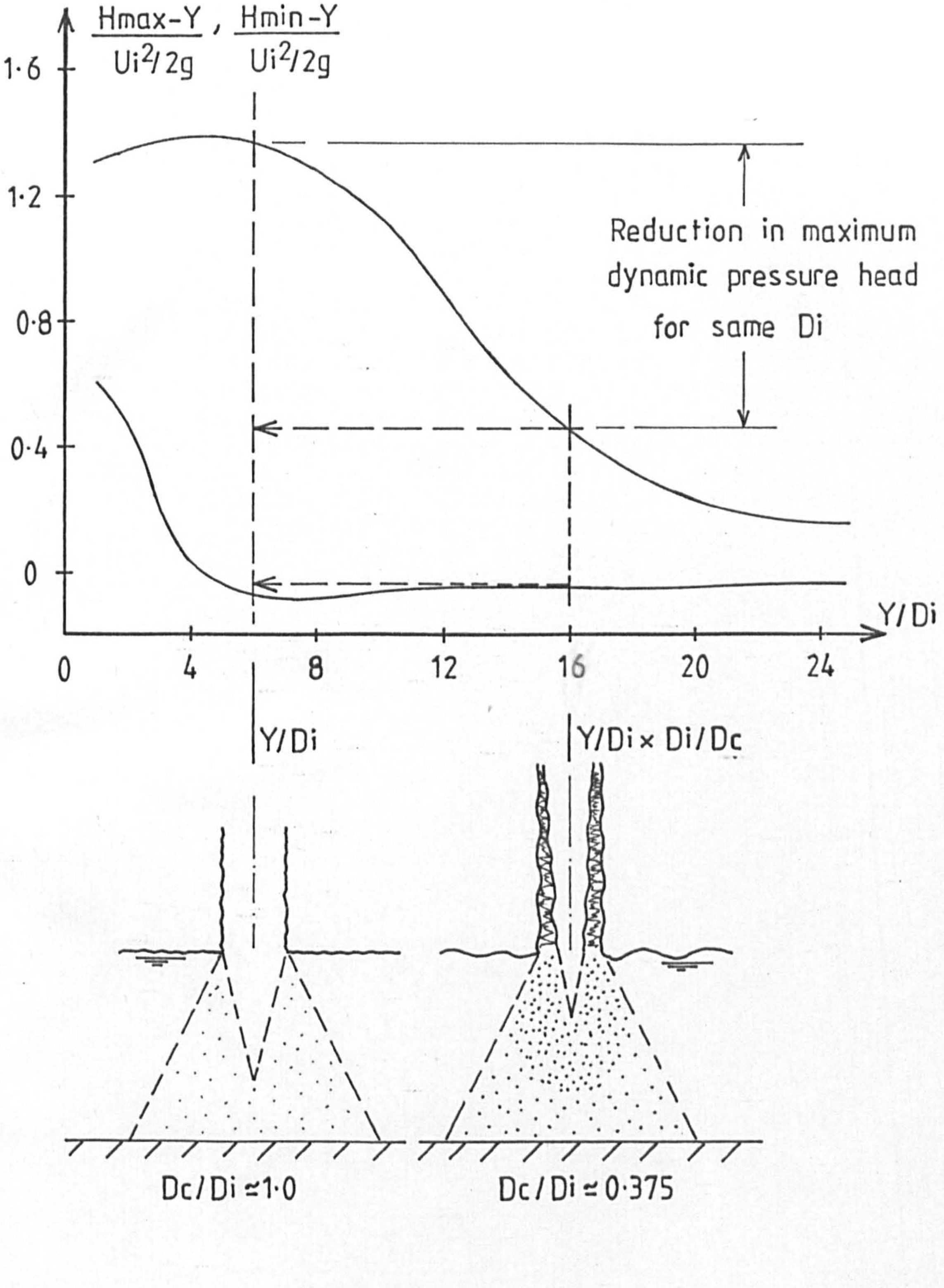

Fig.7·70 Pressure reduction at same pool depth due to highly diffused jet in the atmosphere.